Trinity College Dublin
Coláiste na Tríonóide, Baile Átha Cliath
The University of Dublin

Ph.D. Surgery and Philosophy

March 2022

Investigating the applicability of immune checkpoint blockade in upper gastrointestinal cancers

Maria Davern, Irish Research Council Ph.D. candidate
Student number: 12300553

Supervisor: Associate Professor Dr. Joanne Lysaght.
Departmental Head: Professor John V. Reynolds.

DECLARATION

I declare that this thesis has not been submitted as an exercise for a degree at this or any other university and it is entirely my own work. I agree to deposit this thesis in the University's open access institutional repository or allow the library to do so on my behalf, subject to Irish Copyright Legislation and Trinity College Library conditions of use and acknowledgement.

Summary

Oesophagogastric junctional adenocarcinoma (OGJ) is an aggressive malignancy with a high propensity to metastasise. Response rates to first-line chemo(radio)therapy regimens remain poor therefore, better treatment options are required to improve clinical outcomes for OGJ patients. Combining ICB with immunostimulatory chemotherapies to boost response rates is an attractive approach for converting 'cold non-inflamed' tumours into 'hot inflamed' tumours, which typically respond better to ICB. This body of work highlighted the cooperation between ICB and first-line chemotherapy regimens to boost anti-tumour immunity and decrease the survival of OGJ cells via immune-independent and immune dependent mechanisms.

FLOT (5-FU, oxaliplatin, docetaxel) and CROSS chemotherapies (CT) (paclitaxel, carboplatin) regimens induced immunogneic cell death in OGJ cells and icnreaed the cytotoxic potential of healthy donor T cells. Post-FLOT and post-CROSS CT tumour cell secretome enhanced lymphocyte-mediated killing of OGJ cells highlighting the immunostimulatory potentail of first-line chemtoherapy regimens. Pro-inflammatory T cell cytokine profiles were enhanced by first-line chemotherapy regimens. This body of work demonstrated that FLOT and CROSS CT regimens decreased co-stimulatory marker CD27 expression and increased co-stimulatory markers CD69 and ICOS expression on the surface of T cells. However, ICB attenuated chemotherapy-induced downregulation of CD27 on T cells and promoted differentiation of effector memory T cells into a terminally differentiated state. Importantly, dual nivolumab-ipilimumab treatment enhanced OGJ lymphocyte-mediated cytolysis of OE33 cells. This study also profiled immune checkpoint (IC) expression to help guide design of rational ICB and chemotherapy combinations in the first-line setting. Expression of ICs on T cells positively correlated with a subsequent poor response to neoadjuvant treatment and more advanced tumours. First-line chemotherapy regimens substantially altered IC expression profiles of T cells increasing PD-1, A2aR, KLRG-1, PD-L1, PD-L2 and CD160 and decreasing TIM-3 and LAG-3 on OGJ donor T cells. These findings highlight a link between chemotherapy and the development of immune-resistance, reaffirming the rationale to administer ICBs concurrently with first-line chemotherapies to prevent potential IC-mediated suppression of chemotherapy-induced anti-tumour immunity.

Interestingly, this study also identified that PD-1, PD-L1, A2aR and TIGIT ICs expressed on the surface of OGJ cells possessed novel immune-independent functions and could

promote a range of hallmarks of cancer including proliferation, DNA repair, metabolism, pre-survival signalling and chemoresistance. Blockade of PD-1, PD-L1 or A2aR enhanced the toxicity of FLOT chemotherapy in OGJ cells. In addition, this body of work identified that blockade of PD-1 signalling in OGJ cells decreased tumour cell survival however, under glucose deprived or hypoxic conditions PD-1 blockade provided OGJ cells with a survival advantage. Given that PD-1 blockade enhanced basal respiration and glycolytic reserve it may be the case that under these conditions PD-1 blockade promoted a metabolic phenotype that was more adaptable. Collectively, this highlighted an immune-independent explanation for resistance to PD-1 ICBs in hypoxic tumours other than suppression of immune responses. In contrast, TIGIT blockade decreased survival of OGJ cells under full nutrient and normoxic conditions as well as hypoxic and nutrient deprived conditions suggesting that TIGIT blockade may be a more suitable ICB to target OGJ cells in hypoxic tumours.

Hostile features of the tumour microenvironment including glucose deprivation, serum deprivation, hypoxia and acidosis all had profound effects on the IC expression profile of OGJ patient-derived T cells. A range of ICs were significantly upregulated on the surface of T cells which may contribute to T cell dysfunction. LAG-3, TIGIT and A2aR have been implicated in promoting a regulatory T cell phenotype and pre-clinical studies have demonstrated that blockade of these ICs promoted tumour regression in murine studies. This body of work demonstrates that hostile features of the tumour microenvironment create exploitable targets that could be harnessed with the use of novel ICBs targeting A2aR, TIGIT and LAG-3 in combination with conventional ICBs that target the PD-1 and CTLA-4 axes. ICB increased IFN-γ production by T cells under moderately acidic conditions this effect was abrogated under severe acidic conditions highlighting the ability of acidosis to potentially limit ICB efficacy. A rationale for administering oral neutralizing buffers in conjunction with ICB in OGJ patients to limit the immunosuppressive effects of tumour acidosis on the efficacy of ICB is highlighted.

Visceral adipose tissue plays a significant role in tumour initiation, development and progression via generation of chronic systemic low-grade inflammation via release of pro-inflammatory factors into circulation. Therefore, this study investigated the effect of the visceral adipose secretome on T cell activation status and IC expression profiles. These findings demonstrated that adipose conditioned media (ACM) from both early and late stage OGJ patients enhanced T cell activation status and upregulated CTLA-4 on the surface of Th1-like cells and Treg cells and increased PD-L1 on the surface of Treg cells.

Thus, creating a therapeutic niche for harnessing anti-cancer immunity with the use of ICB targeting CTLA-4 and PD-L1. Importantly, the addition of ICB in the presence of ACM decreased the production of pro-inflammatory tumour-promoting cytokines IL-17 and TNF-α which have been reported to drive malignant progression.

Acknowledgements

Foremost, I wish to sincerely thank my supervisor Dr. Joanne Lysaght for her support over the past 5 years; from my early days as a master's student in the M.Sc. Translational Oncology, for her support and guidance through applying for funding to carry out a Ph.D right up to the time of submitting this thesis. Dr. Lysaght has been a source of guidance and sound advice all delivered with patience. Thank you for the endless valuable feedback on presentations, posters and papers and training you have provided me with throughout my Ph.D. studies. I am also very grateful for the opportunities afforded to me in Dr. Lysaght's group to pursue my own research interests through various side projects and design and supervision of student laboratory projects.

I would like to thank the Irish Research Council and C.R.O.S.S Charity for affording me the opportunity to carry out this research. I wish to thank Dr. Margaret Dunne for training me into the lab in the Department of Surgery during my M.Sc. laboratory project which I carried out under Dr. Dunne's supervision before I began my Ph.D. The research techniques, experimental knowledge of planning and design of experiments, time management, organisation skills, scientific writing and preparation of oral presentations that I learned during my M.Sc. project prepared me well to carry out my Ph.D. studies in the Cancer Immunology and Immunotherapy group and I am very grateful for everything that I have learnt from Dr. Dunne during that period. Thank you to the course coordinators and PIs who run the M.Sc. in Translational Oncology in the Department of Surgery which include Professor Jacintha O' Sullivan, Dr. Joanne Lysaght, Dr. Graham Pidgeon, Dr Stephen Maher, Dr. Melissa Conroy, Dr. Niamh Lynam-Lennon and Dr. Margaret Dunne. This M.Sc. gave me a strong foundation and broad fundamental understanding of cancer biology and immune biology including practical laboratory research skills which eased my transition from my Master's studies into my Ph.D. studies and greatly helped prepare me to carry out my Ph.D. studies.

A sincere thank you to the other PIs within the Department of Surgery; Professor Jacintha O' Sullivan, Dr. Stephen Maher, Dr. Niamh Lynam-Lennon and Dr. Melissa Conroy. The invaluable and encouraging advice and feedback I have received at our weekly departmental lab meetings on my data and presentations including feedback on papers has been greatly appreciated and has undoubtedly enhanced and improved my research, presentation, communication and writing skills.

I would also like to thank Professor John Reynolds for his intellectual advice, guidance and feedback in my academic writing and preparation of presentations for conferences given with encouragement and patience.

It has been a genuine pleasure to work alongside such talented peers who have not just been an invaluable source of insight for designing 'sensible' experiments and troubleshooting failed experiments or making sense of 'weird' data but have truly provided me with life-long friendships. The Ph.D. journey brings with it challenging experiences and the last couple of years have undoubtedly been stressful, but I have always had a very strong support system in the department through these friendships so a very special thank you to Noel Donlon, Andrew Sheppard, Croí Buckley, Fiona O' Connell, Aisling Heeran, Rebecca O' Brien, Jason McGrath, Eimear Mylod, Klaudia Majcher, Laura Kane, Christine Butler and Marina Zaki.

I would also like to thank all of the undergraduate and masters students and clinical researchers that I have worked with throughout my Ph.D., I certainly have learnt a lot from working with each of you and am very grateful to have been given the opportunity which certainly fostered my love for teaching in academia. Thank you, Aoife Nolan, Caoimhe Neville, Liam Dwyer, Malika Grant, Malvika Desphpande, Ellen McKenna, Parinav Swaroop, Katelynn Cahill, Caoimhe Gaughan, Cillian O' Donovan, Mohammed Habash, Conall Hayes, Ross King and Dr. Dara Bracken-Clarke. I wish to thank Claire Fitzgerald and Dr. Brona Murphy from the Department of Physiology RCSI for their valuable collaborations. And a special thank you to Fiona O' Connell for all of her time spent doing correlations for me which I greatly appreciated. I would also like to thank the post-doctoral researchers within the Department of Surgery; Dr. Aoife Cannon and Dr. Simone Marconi, thank you so much for your encouraging words which were always really appreciated.

A huge thank you to my best friends Anto, Siobhan and Miriam. Without you I would have certainly gone insane 😊 your everlasting and undying friendship which has always been a strong source of laughter, encouragement, praise, loyalty and empathy with amazing advice. I will be forever grateful to you for getting me through the last few years <3.

I am eternally grateful to Mam, Dad, Eamon and Grandma. I have been truly privileged to have such a strong support system. Their love, constant encouragement, support, advice and guidance and the strong work ethic they instilled in me has allowed me to achieve many

things in my life which would have never been possible without them, and I always endeavour to make them proud.

Publications

Reviews

Published first author reviews (2)

- **The tumour immune microenvironment in oesophageal cancer.** Authors: **Maria Davern***, Noel E. Donlon*, Robert Power, Conall Hayes, Ross King, Margaret R. Dunne*, John V. Reynolds. *denotes equal contribution. *British Journal of Cancer 2021.*
- **Cooperation between chemotherapy and immunotherapy in gastroesophageal cancers.** Authors: **Maria Davern**, Joanne Lysaght. *Cancer Letters 2020.*

Published authored reviews (4)

- **Radiotherapy in upper gastrointestinal cancers: the current state of play.** Authors: Noel E. Donlon, Robert Power, Conall Hayes, **Maria Davern**, John V. Reynolds, Joanne Lysaght. *International Journal of Molecular Sciences 2021.*
- **Hypoxia and its Impact on the Tumour Microenvironment of Gastroesophageal Cancers.** Authors: Conall Hayes, Claire Donohue, **Maria Davern** and Noel E. Donlon. *BPG 2021.*
- **The immunosuppressive role of lactate within the tumour microenvironment and its clinical implications.** Authors: Conall Hayes, Claire Donohue, **Maria Davern** and Noel E. Donlon. *Cancer Letters 2020.*
- **Chemokine-targeted therapies: An opportunity to remodel immune profiles in gastro-oesophageal tumours.** Authors: Cillian O' Donovan, **M Davern**, NE Donlon, J Lysaght, Melissa J. Conroy. *Cancer Letters 2021.*

Research articles

Published First author/Co-First authored research articles (6)

- **The prognostic value of the lymph node in Oesophageal adenocarcinoma; Incorporating ClinicoPathological, Immunological profiling of tumour and Lymph node into the multimodal paradigm.** Authors: N.E Donlon*, **M Davern***, A Sheppard, R Power, F O Connell, A Heeran, R King, C Hayes, A Bhardwaj, N Ravi, CL Donohoe, J O' Sullivan, JV Reynolds, J Lysaght. *denotes equal contribution. *Cancers 2021.*

- **Chemotherapy regimens induce inhibitory immune checkpoint protein expression on stem-like and senescent-like oesophageal adenocarcinoma cells.** Authors: **Maria Davern**, Noel E. Donlon, Andrew Sheppard, Fiona O' Connell, Conall Hayes, Anshul Bhardwaj, Emma Foley, Dermot O' Toole, Niamh Lynam-Lennon, Narayanasamy Ravi, John V. Reynolds, Stephen G. Maher, Joanne Lysaght. *Translational Oncology 2021.*
- **PD-1 and TIGIT blockade differentially affect tumour cell survival under hypoxia and glucose deprived conditions in oesophageal adenocarcinoma; implications for overcoming resistance to PD-1 blockade in hypoxic tumours.** Authors: **Maria Davern**, Croí Buckley, Claire Fitzgerald, Aisling B. Heeran, Noel E. Donlon, Andrew S. Sheppard, Malvika Dreshpande, Fiona O' Connell, John V. Reynolds, Stephen G. Maher, Joanne Lysaght. *Translational Oncology 2022.*
- **The Impact of Esophageal Oncological Surgery on Perioperative Immune Function; Implications for Adjuvant Immune Checkpoint Inhibition.** Authors: NE Donlon*, **M Davern***, A Sheppard*, R Power, Conall Hayes, N Ravi, CL Donohoe, J V Reynolds, J Lysaght. *Frontiers in Immunology 2022. *denotes equal contribution.*
- **PD-1 immune checkpoint blockade enhances FLOT chemotherapy toxicity in oesophageal adenocarcinoma.** Authors: **Maria Davern**, Noel E. Donlon, Andrew Sheppard, Gillian Cotter, Michael MacLean, Hugo Temperley, Melissa J. Conroy, Christine Butler, Fiona O' Connell, Anshul Bhardwaj, N Ravi, Dara Bracken-Clarke, Claire L. Donohoe, John V. Reynolds, Margaret Dunne, Joanne Lysaght. *Scientific Reports 2022.*
- **The impact of conventional and hypofractionated radiotherapy on the immune landscape in oesophageal adenocarcinoma.** Noel E Donlon*, **Maria Davern***, Andrew Sheppard, Fiona O' Connell, Aisling B Heeran, Anshul Bhardwaj, Christine Butler, Narayanasamy Ravi, Claire L Donohoe, Niamh Lynam Lennon, Margaret R Dunne, Stephen G Maher, Jacintha O' Sullivan, John V Reynolds, Joanne Lysaght. *denotes equal contribution. *Accepted to World Journal of Gastroenterology 2022.*

Published authored research articles (7)

- **The impact of COVID-19 on the diagnosis and surgical treatment of Colorectal Cancer; A National perspective.** Authors: Noel E Donlon, Conall Hayes, Tim S Nugent, **Maria Davern**, Brendan Moran, Shane Irwin, Ryan Roopnarinesingh, Deborah A Mc Namara, Ken Mealy. *Accepted to Diseases of the Colon & Rectum, August 2021.*
- **Fractalkine elicits chemotactic and phenotypic effects on CX3CR1^{+}CD27^{-} natural killer cells in obesity-associated cancer.** Authors: Eimear Mylod, Ashanty Melo, Noel E. Donlon, **Maria Davern**, Niamh Kerslake, Aoife Cannon, Anshul Bhardwaj, John V. Reynolds, Joanne Lysaght, Melissa J. Conroy. *Journal of Immunology 2021.*
- **FLOT in Esophageal Adenocarcinoma Patients undergoing Transthoracic en bloc Resection: An analysis of operative and oncologic outcomes, and impact on pulmonary physiology and body composition.** Authors: Noel E Donlon, Anitha Kammili, Ryan Roopnarinesingh, **Maria Davern**, Robert Power, Sinead King, Claire L Donohoe, Narayanasamy Ravi, Carmen L. Mueller, Jonathan Cools-Lartigue, Lorenzo E. Ferri, John V Reynolds. *Annals of Surgery 2021.*
- **Linking Circulating Serum Proteins with Clinical Outcomes in Esophageal Adenocarcinoma-An Emerging Role for Chemokines.** Noel E Donlon, Andrew Sheppard, **Maria Davern**, Fiona O'Connell, James J Phelan, Robert Power, Timothy Nugent, Kate Dinneen, John Aird, John Greene, Paul Nevins Selvadurai, Anshul Bhardwaj, Emma K Foley, Narayanasamy Ravi, Claire L Donohoe, John V Reynolds, Joanne Lysaght, Jacintha O'Sullivan, Margaret R Dunne. *Cancers 2020.*
- **Negative appendicectomy rates as a quality measure in a regional surgical unit: a retrospective review.** Authors: Noel E Donlon, Michael E. Kelly, Andrew Sheppard, **Maria Davern**, Tim S. Nugent, Patrick A. Boland, Kevin Corless, Waqar Khan, Iqbal Khan, Ronan Waldron, Kevin Barry. *Irish Journal of Medical Sciences 2020.*
- **Real time metabolic profiling in human oesophageal tumours reveals an altered and adaptive metabolic phenotype under different oxygen tensions and following treatment with the anti-metabolic compound Pyrazinib (P3).** Authors: Amy M. Buckley, Margaret R. Dunne, Maria A. Morrissey, Susan A. Kennedy, Aoife Nolan, **Maria Davern**, Emma K. Foley, Niamh Clarke, Joanne

Lysaght, Narayanasamy Ravi, Dermot O'Toole, Finbar MacCarty, John V. Reynolds, Breandán N. Kennedy, Jacintha O'Sullivan. *Scientific Reports July 2020.*

- **Characterisation of an isogenic model of cisplatin resistance in oesophageal adenocarcinoma cells.** Authors: Amy M. Buckley, Becky AS. Bibby, Margaret R. Dunne, Susan A. Kennedy, **Maria B. Davern**, Breandán N. Kennedy, Stephen G. Maher, Jacintha O'Sullivan. *Pharmaceuticals journal January 2019.*

Research articles under revisions/preparation (8)

- **FLOT and CROSS chemotherapy regimens alter the frequency of $CD27^+$ and $CD69^+$ T cells in oesophagogastric adenocarcinomas; implications for combination with immunotherapy.** Authors: **Maria Davern**, Noel E. Donlon, Andrew S. Sheppard, Klaudia Majcher, Fiona O' Connell, Aisling B. Heeran, Malika Grant, Robert A. Farrell, Conall Hayes, Melissa J. Conroy, Emma Foley, Dermot O' Toole, Anshul Bhardwaj, Narayanasamy Ravi, John V. Reynolds, Stephen G. Maher, Joanne Lysaght. *Submitted to Medical Oncology November 2021.*
- **Investigating the susceptibility of treatment-resistant oesophageal tumours to Natural Killer cell-mediated responses.** Ellen McKenna, Eimear Mylod, **Maria Davern**, Martin Barr, Noel Donlon, Becky A.S. Bibby, Anshul Bhardwaj, John V. Reynolds, Joanne Lysaght, Stephen G. Maher, and Melissa J. Conroy. *Submitted to Cancer Immunology and Immunotherapy August 2021.*
- **Cooperation between chemotherapy and immune checkpoint blockade to enhance anti-tumour T cell immunity in oesophageal adenocarcinoma.** Authors: **Maria Davern**, Noel E. Donlon, Andrew S. Sheppard, Fiona O' Connell, Conall Hayes, Melissa J. Conroy, Emma Foley, Dermot O' Toole, Anshul Bhardwaj, Narayanasamy Ravi, John V. Reynolds, Stephen G. Maher, Joanne Lysaght. *Submitted to Translational Oncology January2022.*
- **Acidosis significantly alters immune checkpoint expression profiles of T cells.** Authors: **Maria Davern***, Noel E. Donlon*, Conall Hayes, Ross King, Robert Power, Andrew Sheppard, Gillian Cotter, Michael MacLean, Hugo Temperley, Melissa J. Conroy, Christine Butler, Fiona O' Connell, Anshul Bhardwaj, N Ravi, Dara Bracken-Clarke, Claire L. Donohoe, John V. Reynolds, Margaret Dunne,

Joanne Lysaght. *Submitted to Cancer Immunology and Immunotherapy January 2021. *denotes equal contribution.*

- **Nutrient deprivation and hypoxia alter T cell immune checkpoint expression; potential impact for immunotherapy.** Authors: **Maria Davern**, Noel E. Donlon, Conall Hayes, Ross King, Andrew Sheppard, Gillian Cotter, Hugo Temperley, Melissa J. Conroy, Christine Butler, Fiona O' Connell, Anshul Bhardwaj, N Ravi, Claire L. Donohoe, John V. Reynolds, Joanne Lysaght. *Submitted to Cancer Immunology and Immunotherapy October 2021.*
- **Visceral adipose tissue secretome from early and late stage oesophageal cancer patients differentially affects effector and regulatory T cells.** Authors: **Maria Davern,** Dara Bracken-Clarke, Noel E. Donlon, Andrew D. Sheppard, Fiona O' Connell, Klaudia Majcher, Melissa J. Conroy, Eimear Mylod, Christine Butler, Claire Donohoe, Anshul Bhardwaj, Narayanasamy Ravi, Ashanty Melo, John V. Reynolds, Joanne Lysaght. *Submitted to Carcinogenesis October 2021.*
- **The secretome of tumour-draining lymph nodes, omentum and liver promote a metastatic phenotype in oesophageal adenocarcinoma cells via chemokine receptor signalling axes; a role for CXCR4, CCR1 and CX_3CR1 to target metastasis.** Authors: **Maria Davern***, Katelynn Cahill*, Noel E. Donlon, Caoimhe Guaghan, Andrew Sheppard, Christine Butler, Fiona O' Connell, Eimear Mylod, Ashanty Melo, Klaudia Majcher, Maria Kavanagh, Anshul Bhardwaj, N Ravi, Dara Bracken-Clarke, Claire L. Donohoe, John V. Reynolds, Melissa J. Conroy, Joanne Lysaght. *Manuscript under preparation*denotes equal contribution.*
- **Radiation alters chemokine receptor signalling which alters migration and anti-tumour phenotypes of T cells in oesophageal adenocarcinoma.** Authors: **Maria Davern**, Cillian O' Donovan, Noel E. Donlon, Caoimhe Guaghan, Eimear Mylod, Andrew Sheppard, Christine Butler, Fiona O' Connell, Anshul Bhardwaj, N Ravi, Dara Bracken-Clarke, Claire L. Donohoe, John V. Reynolds, Joanne Lysaght, Melissa J. Conroy. *Manuscript under preparation*denotes equal contribution.*

Oral presentations at conferences

International conferences- presenting author (3)

- **6th European Congress of Immunology, 1st-4th September 2021. Title:** Cooperation between chemotherapy and immunotherapy to enhance anti-tumour T-cell mediated immunity in oesophageal adenocarcinoma; implications for synergistic combination regimens.
- **Cancer Immunotherapy Early-Career Researcher Meeting 29th April 2021. Title:** The impact of major oncologic surgery on immune responses in the immediate post-operative setting in oesophageal adenocarcinoma patients; a guide to harnessing the double-edged sword of cancer surgery.
- **The 11th International Cancer Conference "Advances and Future Directions in Personalised Medicine", Trinity Translational Medicine Institute, Trinity College Dublin, Ireland, 24th-25th September 2019. Title:** A potential role for immune checkpoint inhibitors in combination with chemotherapy for treating oesophageal adenocarcinoma patients.

National conferences - presenting author (15)

- **Invited speaker to present at the 'President's Medal Presentation Session' during the Charter Meeting April 22nd 2022 in Royal College of Surgeons Ireland.** *(all medal winners from the Freyer, Sylvester O'Halloran and Waterford surgical meetings in 2021 were invited to give talks at this session).*
- **Sir Peter Freyer memorial lecture & surgical virtual symposium, 4th-5th September 2021. Title:** Immune checkpoint blockade limits the immunosuppressive effects of the oesophageal adenocarcinoma tumour microenvironment on T-cells (Plenary, Awards Session).
- **The Irish Association for Cancer Research Annual Conference, (oral poster presentation session) virtual conference, 24th-26th March 2021. Title:** Cooperation Between Chemotherapy and Immunotherapy to Enhance Anti-tumour T-cell Mediated Immunity in Oesophageal Adenocarcinoma: Implications for Synergistic Combination Regimens.
- **The Irish Association for Cancer Research Annual Conference, (EACR session) virtual conference, 24th-26th March 2021. Title:** Novel Insights into Immune-independent Functions of Immune Checkpoint Inhibitors in Oesophageal Adenocarcinoma; Potential Implications for Overcoming Chemoresistance to First-line Chemotherapy Regimens.

- **Sylvester O' Halloran Virtual Perioperative Symposium, Ireland, 5th-6th March 2021 (Plenary, Awards Session). Title:** Cooperation Between Chemotherapy and Immunotherapy to Enhance Anti-tumour T-cell Mediated Immunity in Oesophageal Adenocarcinoma: Implications for Synergistic Combination Regimens.
- **Sylvester O' Halloran Virtual Perioperative Symposium, Ireland, 5th-6th March 2021 (Plenary, Awards Session). Title:** Novel Insights into Immune-independent Functions of Immune Checkpoint Inhibitors in Oesophageal Adenocarcinoma; Potential Implications for Overcoming Chemoresistance to First-line Chemotherapy Regimens.
- **Sir Peter Freyer memorial lecture & surgical virtual symposium, 4th-5th September 2020. Title:** The immunostimulatory and immunoinhibitory effects of chemotherapies in oesophageal adenocarcinoma; a double-edged sword.
- **Sylvester O' Halloran Perioperative Symposium, Limerick, Ireland, 28th February- 2nd March 2020 (Plenary, Awards Session). Title:** First line chemotherapy regimens used in oesophageal adenocarcinoma promote immune dysfunction and enhance a cancer stem-like phenotype; potential implications for chemoimmune-resistance and novel multi-modal treatment regimens.
- **The Irish Association for Cancer Research Annual Conference, (Breakthrough Cancer Research Session, poor survival rate cancers) Galway Bay Hotel, Ireland, 26th-28th February 2020. Title:** The double-edged sword of chemotherapy in oesophageal adenocarcinoma.
- **Irish Association of Pharmacology 20th Annual Meeting, National University of Galway, Ireland, 30th November 2019. Title:** A rationale for combining immune checkpoint inhibitors with chemotherapy in oesophageal adenocarcinoma.
- **Sylvester O' Halloran Perioperative Symposium, Limerick, Ireland, 28th February- 2nd March 2019 (Plenary, Awards Session). Title:** Clinically relevant chemotherapies promote immune resistance via upregulation of inhibitory immune checkpoints on T cells and oesophageal adenocarcinoma cells.
- **Sylvester O' Halloran Perioperative Symposium, Limerick, Ireland, 28th February- 2nd March 2019. Title:** Characteristics of the tumour microenvironment affect the expression of inhibitory immune checkpoints on T cells and oesophageal adenocarcinoma cells.

- **Trinity Translational Medicine Institute Precision Medicine Cancer Symposium, Dublin, Ireland, 15th February 2019 3-minute flash presentation. Title:** The effect of clinically relevant chemotherapies on the expression of inhibitory immune checkpoints in oesophageal adenocarcinoma.
- **Young Cancer Researchers Networking Conference, Cork, Ireland, 21st – 22nd June 2018. Title:** The effect of clinically relevant chemotherapies on the expression of immune checkpoints in oesophageal adenocarcinoma.
- **Trinity Translational Medicine Institute Annual Scientific Conference, Dublin, Ireland, 23rd March 2018 3-minute flash presentation. Title:** The effect of clinically relevant chemotherapies on the expression of immune checkpoints in oesophageal adenocarcinoma.

Poster presentations at conferences

International conferences - presenting author **(11)**

- **8th ImmunoTherapy of Cancer Conference (iTOC8), 8th-9th October 2021. Title:** Novel insights into immune-independent functions of immune checkpoint inhibitors in oesophageal adenocarcinoma; potential implications for designing combination immuno-chemotherapy regimens to achieve synergistic responses.
- **6th European Congress of Immunology, 1st-4th September 2021. Title:** Immune checkpoint blockade limits the immunosuppressive effects exerted by key features of the hostile tumour microenvironment on T cells in oesophageal adenocarcinoma.
- **6th European Congress of Immunology, 1st-4th September 2021. Title:** The secretome of visceral adipose tissue from advanced stage oesophageal adenocarcinoma patients dampened anti-tumour immunity ex vivo; implications for the potential use of immune checkpoint blockade to abrogate these immune inhibitory effects.
- **6th European Congress of Immunology, 1st-4th September 2021. Title:** Novel insights into immune-independent functions of immune checkpoint inhibitors in oesophageal adenocarcinoma; potential implications for overcoming chemoresistance to first-line chemotherapy regimens.
- **EACR 2021 Virtual Congress, 9th-12th June 2021. Title:** Chemotherapy-altered tumour microenvironment enhances T-cell mediated immunity in oesophageal

adenocarcinoma; implications for synergistic combination regimens with immune checkpoint blockade.

- **EACR 2021 Virtual Congress, 9th-12th June 2021. Title:** Novel insights into immune-independent functions of immune checkpoint inhibitors in oesophageal adenocarcinoma; potential implications for overcoming chemoresistance to chemotherapy regimens.
- **EACR Defence is the Best Attack 2021, virtual conference, 16th-17th February 2021. Title:** Immune checkpoints promote the hallmarks of cancer in oesophageal adenocarcinoma; therapeutic implications for combination chemoimmunotherapy combinations.
- **Society for Immunotherapy of cancer, virtual conference, November 2020. Title:** A role for immune checkpoint blockade to enhance T cell-mediated responses in combination with chemotherapy in oesophageal adenocarcinoma.
- **Breaking Through: Research to Transform Cancer Treatment, Cork Cancer Research Centre, University College, Cork 5th-6th September 2019. Title:** Immunostimulatory and immune-inhibitory effects of conventional chemotherapy regimens in oesophageal adenocarcinoma.
- **Defence is the Best Attack: Immuno-Oncology Breakthroughs, Barcelona, Spain, 11th-13th March 2019. Title:** The effect of clinically relevant chemotherapies and the tumour microenvironment on inhibitory immune checkpoint expression on T-cells and oesophageal adenocarcinoma cells.
- **30th EORTC/AACR/NCI symposium, Dublin, 13-16th November 2018; late breaking poster presentation. Title:** The effect of current standards of care on immune checkpoint expression in oesophageal adenocarcinoma.

National conferences - presenting author **(6)**

- **Irish Society for Immunology Conference, Royal College of Surgeons, Dublin Ireland, 19th-20th September 2019. Title:** Alterations in inhibitory immune checkpoint expression following chemotherapy treatment.
- **Annual Irish Association for Cancer Research Conference, Belfast, Ireland, 20th-22nd February 2019. Title:** Clinically relevant chemotherapies promote immune resistance via upregulation of inhibitory immune checkpoints on T-cells and oesophageal adenocarcinoma cells.

- **Annual Irish Association for Cancer Research Conference, Belfast, Ireland, 20th-22nd February 2019. Title:** Characteristics of the tumour microenvironment affects the expression of inhibitory immune checkpoints on both T-cells and oesophageal adenocarcinoma cells.
- **Annual Meeting of the Irish Association of Pharmacologists, Belfast, Ireland, 30th November 2018. Title:** The effect of current standards of care on immune checkpoint expression in oesophageal adenocarcinoma.
- **Irish Society for Immunology Conference, Dublin, Ireland, 30-31st August 2018. Title:** The effect of clinically relevant chemotherapies on the expression of immune checkpoints in oesophageal adenocarcinoma.
- **University College Dublin St. Vincent's Healthcare Group Translational Medicine Symposium, Dublin, Ireland, 8th June 2018. Title:** The effect of clinically relevant chemotherapies on the expression of immune checkpoints in oesophageal adenocarcinoma.

Awards

- ISI-EFIS travel bursary to attend the virtual 6th European Congress of Immunology conference (1st–4th September 2021).
- Plenary Prize Sylvester O' Halloran medal for best oral presentation at the Plenary Session, Sylvester O' Halloran Virtual Perioperative Symposium, Ireland, 5th-6th March 2021. Title: Cooperation Between Chemotherapy and Immunotherapy to Enhance Anti-tumour T-cell Mediated Immunity in Oesophageal Adenocarcinoma: Implications for Synergistic Combination Regimens *(2021).*
- EACR Junior Investigator Award 2020 (Junior category- less than 3 years post-doc experience) for highest scoring abstract entitled: "Novel Insights into Immune-independent Functions of Immune Checkpoint Inhibitors in Oesophageal Adenocarcinoma; Potential Implications for Overcoming Chemoresistance to First-line Chemotherapy Regimens", awarded by the IACR *(2020).*
- EMBO Travel Grant for the EMBO Practical Course: The Fundamentals of High-End Cell Sorting *(2019).*
- IACR AOIFA Conference Travel Award *(2019).*

- Eurolife Summer School Scholarship to attend ‘Molecular Mechanisms in Cancer; Translating Discoveries into Personalized Therapies’ Leiden University Medical Centre *(2018).*
- Immunotools Special Award *(2018).*
- Government of Ireland Postgraduate Scholarship *(2017).*

Table of Contents

List of Figures

Figure A6.5: Gating strategy for assessing effect of conditioned media from post-FLOT and post-CROSS CT tumour cell conditioned media on cytokine production by T cells by flow cytometry.

Figure A6.6: Gating strategy for assessing direct effects of FLOT and CROSS CT on the expression of ICs on T cells surfaces by flow cytometry.

List of Tables

Table 6.3. The frequency of $CD3^{+}CTLA\text{-}4^{+}$ circulating peripheral blood T cells positively correlates with a subsequent poor pathologic treatment response in the neoadjuvant setting in OGJ patients.

List of Abbreviations

A2aR	A2A receptor, also known as ADORA2A
ABCB1	ATP-Binding Cassette sub-family B member 1
cRPMI	complete Roswell Parks Memorial Institute
Cap	capecitabine
Cis	cisplatin
CTLs	Cytotoxic T Lymphocytes
CTLA-4	Cytotoxic T-lymphocyte-associated antigen-4
Doc	Docetaxel
Epi	Epirubicin
FBS	Foetal Bovine Serum
5-FU	5-Fluorouracil
GITR-L	glucocorticoid-induced tumour necrosis factor-related gene (GITR) ligand
GrB	Granzyme B
ICOS-L	Inducible T-cell costimulatory-ligand
IFN-γ	Interferon-gamma
LAG-3	Lymphocyte Activation Gene-3
OGJ	Oesophagogastric junctional adenocarcinoma
PBS	Phosphate Buffered Saline
PD-1	Programmed cell Death protein-1
PD-L1	Programmed Death-Ligand 1
TCR	T Cell Receptor
TIM-3	T-cell immunoglobulin and mucin-domain containing-3
TIGIT	T cell immunoreceptor with Ig and ITIM domains

Chapter 1 - Introduction

1.1 Introduction

Gastroesophageal cancers (GOCs) are comprised of oesophageal cancer (OC) and gastric cancer (GC) and collectively have one of the highest incidence rates of all cancers, causing more than one million annual deaths globally[2]. Despite new therapies, OC has a dismal prognosis with a 5-year survival rate of 10-20%[3]. Five-year survival rates for GC vary from 70-95% in early stage patients and 20-30% in patients with advanced disease[4].

The two major histological subtypes of OC are oesophageal adenocarcinoma (OGJ) and oesophageal squamous cell carcinoma (OSCC), which differ greatly in terms of risk factors, epidemiology, incidence and geographic distribution[3]. The main histological subtype of OC is OSCC, however OGJ is the predominant subtype in Western countries[3]. The main histological subtype of GC is gastric adenocarcinoma and comprises 90-95% of GC cases[5]. OGJ is more prevalent in males than females likely due to central obesity affecting more men than women[6]. Adipose tissue is deposited subcutaneously and below the waste in most women contributing to a 'pear-shaped body'[7]. While in men and some women, fat tissue is deposited viscerally and above the waste resulting in central or visceral obesity and an 'apple-shaped' body[7]. Visceral fat is more metabolically active than subcutaneous fat and secretes a range of cytokines and adipokines generating systemic chronic low grade inflammation and a pro-coagulant insulin-resistant state which promote tumour development and growth[8].

1.2 Current treatments for OGJ patients

The standard of care for patients with resectable advanced oesophagogastric junctional adenocarcinoma (OGJ) includes the peri-operative FLOT chemotherapy-based regimen[9]. The FLOT regimen includes 4 biweekly cycles of a cocktail of chemotherapies neoadjuvantly followed by a 6 week break prior to surgery to allow the body to recover from the toxic side effects associated with these chemotherapies. Six weeks post-surgery patients receive a further 4 biweekly cycles of FLOT[10]. However, only 35% of OGJ patients prescribed the FLOT regimen complete the entire 8 cycles of perioperative FLOT chemotherapy as a result of severe toxic side associated with chemotherapy treatment and due to the invasive oesophagectomy surgery to remove the tumour the majority of patients are not 'fit' enough to receive further chemotherapy adjuvantly[10]. FLOT comprises of 5-fluorouracil (5-FU), leucovorin, oxaliplatin and a taxane (such as the anti-microtubule agent docetaxel). Leucovorin enhances the binding of 5-FU to thymidylate synthetase and

prolongs the half-life of 5-FU *in vivo*[11]. 5-FU is an anti-metabolite which inhibits thymidylate synthetase an enzyme that creates new strands of DNA.

A multimodal approach involving combined chemoradiotherapy is also an option for OSCC and OGJ patients; the CROSS regimen (paclitaxel and carboplatin with a cumulative radiation dose of 41.4 Gy over 23 fractions) followed by surgery[12]. CROSS regimen involves 5 weekly cycles of a combination of chemotherapy and radiation neoadjuvantly only followed by a 6 week rest period prior to surgery to allow the body to recover[12]. 5-FU is a fluorinated pyrimidine which is an analogue of pyrimidine[13]. 5-FU is phosphorylated to fluorouridine triphosphate, a fraudulent nucleotide (analogue), which is incorporated into RNA by RNA polymerase, inhibiting RNA synthesis and function generating genotoxic stress in the cell activating programmed cell death pathways[14]. Oxaliplatin and carboplatin are platinum is an alkylating cytotoxic agent, which inhibits DNA replication by forming adducts between two adjacent guanines or guanine plus adenine[15,16]. Docetaxel and paclitaxel are taxanes which target microtubule polymerisation during the mitotic phase of the cell cycle[17,18]. Docetaxel inhibits microtubular depolymerization and paclitaxel stabilizes microtubule formation which both ultimately prevent transition of the tumour cell from the metaphase-anaphase stages of the cell cycle collectively causing cell cycle arrest in tumour cells[17,18]. GOC patients with $HER2^+$ tumours (~20%) receive trastuzumab (anti-HER2 monoclonal antibody) in combination with a cisplatin and fluoropyrimidine-based chemotherapy regimen in the first-line setting[19].

Unfortunately, a significant proportion of GOC patients fail to benefit from the current standards of care, with only ~30% of OSCC and OGJ patients achieving a complete pathological response[20]. However, immunotherapy which targets the body's own immune system to mediate tumour eradication via an army of licensed and mobilised anti-tumour immune cells is now considered by many as the fifth pillar of cancer therapy along with surgery, chemotherapy, radiotherapy and molecular targeted therapies[21].

1.3 Immune evasion and cancer development

In 1909 Paul Ehrlich postulated for the first time that the immune system could suppress tumour growth by recognising tumour cells as foreign and eradicating transformed cells, thus initiating a century long quarrelsome debate over the role of the immune system in cancer[22]. Burnet and Lewis proposed the hypothesis of cancer immunosurveillance 50 years later, which stated that mutations in cancer cells generate neoantigens enabling immune

cells that constantly survey host tissues to recognise and kill these malignant cells before growing into a clinically detectable tumour mass[23]. In the 1990s Schreiber and colleagues refined this theory to produce the cancer immunoediting hypothesis, which was a more nuanced concept based on the knowledge that the immune system can influence the fate of a developing cancer through either supressing or promoting tumour growth, essentially acting as a 'double-edged sword'[24]. The immune system not only suppresses tumour development but it also functions to promote tumour growth by sculpting tumour cell immunogenicity and facilitating cellular transformation by selecting for less immunogenic tumour clones and establishing immunosuppressive conditions conducive for tumour outgrowth[25]. This hypothesis is divided into three phases: (1) elimination (or immunosurveillance), (2) equilibrium and (3) escape[26]. In the elimination phase innate and adaptive immune cells recognise and kill malignant cells. If the innate or adaptive arms of the immune system fail to eradicate all neoplastic cells the tumour cells progress to the equilibrium phase. During the temporary and dynamic equilibrium phase the immune system exerts a selective pressure by killing susceptible tumour cells. However, in this phase the tumour cells can evolve acquiring further mutations that enable neoplastic cells to either evade immune destruction or suppress anti-tumour immunity allowing the tumour cells to progress to the escape phase and grow into a clinically detectable tumour mass. Transformed cells express an array of mutated and non-mutated antigens which have the potential to elicit an anti-tumour T cell immune response. However, through the loss or mutation of immunogenic tumour antigens or acquisition of defects in antigen presentation machinery (dysregulation of antigen processing machinery or loss of major histocompatibility complex (MHC) expression) neoplastic cells can reduce their antigenicity evading immune destruction and facilitating immune escape[27]. Tumour cells have acquired multiple mechanisms to facilitate immune escape through direct inhibition of anti-tumour $CD4^+$ and $CD8^+$ T cells or indirectly via inhibition of DC maturation and antigen presentation preventing T cell differentiation into IFNy-secreting T cells[28].

Neoplastic cells secrete a range of immunosuppressive factors such as interleukin-10 (IL-10), transforming growth factor-beta (TGF-β), VEGF[29], indoleamine-2,3-dehydrogenase (IDO)[30], prostaglandins, adenosine and macrophage colony-stimulating factor that inhibit DC maturation, antigen presentation and cytolytic T cell activity[31]. These immunosuppressive molecules decrease the expression of costimulatory molecules and MHC, inhibit the cytotoxic function of CTLs and NK cells, prevent T cell activation and catabolize nutrients essential for T cell activation, ultimately impairing T cell expansion

and differentiation into IFN-γ-producing T cells[31–33]. IDO catalyzes the degradation of l-tryptophan to N-formylkynurenine, an essential amino acid required for T cell function, its depletion halts the growth of T cells[34]. VEGF reduces the expression of adhesion molecules on the endothelium required by T cells to extravasate from blood vessels into neoplastic tissue thereby inhibiting T cells from infiltrating the tumour site[35,36]. IL-10, VEGF and prostaglandin E2 stimulate Fas ligand expression on endothelial cells inducing Fas receptor-mediated apoptosis of cytotoxic T lymphocytes (CTLs)[37]. Additionally, tumour cells express surface FasL and induce T cell and NK cell apoptosis[38,39]. A recent study conducted in mouse models demonstrated that polymorphonuclear myeloid-derived suppressor cells (PMN-MDSC) present in the induced tumour expressed high levels of Fas Ligand and induced apoptosis in infiltrating adoptively transferred T cells via Fas-Fas-ligand binding to the Fas receptor expressed on T cell surfaces[40]. Blocking this Fas-Fas-ligand interaction restored the effectiveness of the T cells to kill malignant cells suggesting that the effect of immunotherapy could be improved through the inhibition of the Fas-Fas-Ligand interaction.

Modification of damage-associated molecular patterns (DAMPs) such as adenosine triphosphate (ATP) and high mobility group box 1 (HMGB1) protein by tumour cells prevents DC maturation thereby, inhibiting T cell priming and activation[31]. Such modifications are mediated through enzymatic degradation of ATP to its subsequent non-stimulatory products adenosine and adenosine monophosphate (AMP) and post-translational modification of HMGB1[31,41]. Cancer cells evade NK cell-mediated killing through the secretion or cleavage of NKG2D ligands (an activating receptor expressed by NK cells)[42]. Tumours decrease MHC I expression to avoid destruction by CTLs however, downregulated MHC I expression stimulates NK cell mediated killing[43]. Collectively, NKG2D ligand release and decreased MHC I expression may enable tumour cells to escape both NK cell and T cell detection. Immunosuppressive factors present in the TME promote the polarization of tumour-associated macrophages (TAMs) into tumour-promoting M-2 like macrophages which secrete more immunosuppressive molecules[44]. Additionally, myeloid derived suppressor cells (MDSCs) recruited by tumours inhibit effector T cells and induce polarization into regulatory T cells (Tregs)[45]. MDSCs mediate their immunosuppressive effects through the secretion of inducible nitric oxide synthase (iNOS), TGF-β and arginase[46]. Therefore, it is now widely accepted that the immune system plays a central role in tumour development, progression and therapeutic resistance. In 2011 Hanahan and Weinberg published an updated version of the hallmarks of cancer to include

the important role of the immune system in cancer[47]. The hallmarks of cancer describe the key characteristics that work in tandem to initiate cancer development, progression and therapeutic progression and include sustaining proliferative signalling, evading growth suppressors, resisting cell death, enabling replicative immortality, inducing angiogenesis, and activating invasion and metastasis[47]. These hallmarks of cancer were updated in 2011 to include genomic instability which is responsible for generating the genetic diversity in tumour cells and inflammation which fosters and promotes several hallmarks of cancer[47]. In the last decade two additional emerging hallmarks of cancer have been added which include reprogramming of energy metabolism and evading immune destruction. Furthermore, the role of the tumour microenvironment is increasingly recognised for supporting and promoting each of these hallmarks of cancer and together all the hallmarks of cancer along with the tumour microenvironment work in tandem to promote tumour initiation, progression, dissemination, and therapy resistance. An increased understanding of these factors to enable careful development of therapeutics to target a multitude of these factors embodies the fundamental design of emerging and future anti-cancer therapies[47]. A paradigm-shifting therapeutic is that of immunotherapy in particular immune checkpoint blockers (ICBs) which block inhibitory immune checkpoints (ICs) on immune cells and cancer cells and reinvigorate anti-tumour immune responses. These therapies have induced durable responses in lung cancer patients as single agents but also when combined with the current standards of chemotherapeutic care. Therefore, a significant area of research is investigating how best to combine ICBs with first-line chemotherapy regimens in OGJ and which ICs would represent the most fruitful targets in boosting response rates in OGJ. One of the most important cell types that ICBs act on are T cells, reinvigorating exhausted T cells and promoting robust Th1 responses.

1.3.1 T cell phenotypes

T cells are important players in eliminating neoplastic cells[48]. T cells are activated by their cognate tumour antigens which are presented to them by either MHC-I for CD8 cells or MHC-II for CD4 cells on the surface of antigen presenting cells (macrophages, dendritic cells)[49]. If the T cell also receives appropriate co-stimulatory signals via CD28 signalling expressed on the surface of T cells via binding with its cognate receptor CD80 and CD86 on the surface of a DC, then the T cell receptor will engage intracellular signalling pathways that induces T cell proliferation and activation[50]. The type of polarising cytokines present in the TME at the time of antigen recognition will dictate what type of T cell the T cell

differentiates into i.e. IL-12 polarising cytokines induce T helper 1 (Th1) differentiation, IL-4 and IL-13 induce Th2 differentiation and IL-10 induces regulatory T cell (Treg) differentiation[51]. Th1 cells are anti-tumour and secrete pro-inflammatory cytokines such as IFN-γ, TNF-α and IL-2[51]. Both IFN-γ and TNF-α directly induce tumour cell death and IL-2 is an important proliferative cytokine necessary for T cell activation, proliferation, and function[5152]. However, an overabundance of IL-2 can drive Treg development. Tregs promote tumour progression and development by dampening anti-tumour immune responses via secretion of IL-10 - an immunosuppressive anti-inflammatory cytokine[52]. In addition, Th2 cells secrete IL-10, IL-4 and IL-5 which are also anti-inflammatory cells that dampen anti-tumour Th1 immune responses[51]. Other T helper cells include Th17 cells, which have contradictory roles in tumorigenesis, conflicting research exists which claims that Th17 cells can inhibit tumour development and other research demonstrates that Th17 cells can promote tumourigenesis via stimulating pro-inflammatory responses which can facilitate tumour progression[53]. Overall, the role of Th17 cells remains to be fully elucidated in the context of OGJ as to whether this cell type is a poor or good prognostic factor, however it will likely be very context dependent and really depend on the overall composition of the tumour microenvironment.

1.4 Immune checkpoint blockers

The activation of naïve T cells requires two signals: T cell receptor (TCR) signalling upon recognition of cognate peptide antigen presented by an MHC molecule and costimulatory signalling. Co-stimulatory interactions between dendritic cells (DCs) and T cells include: GITRL:GITR (glucocorticoid-induced tumour necrosis factor-related gene (GITR) ligand (GITRL)), OX40L:OX40, CD80/CD86:CD28, CD70:CD27 and 4-1BBL:4-1B[54]. Tumour-derived immunosuppressive factors downregulate the expression of costimulatory molecules[31]. TCR activation in the absence of appropriate co-stimulation results in excessive calcium and nuclear factor of activated T cell (NFAT) signalling which renders T cells unresponsive and induces T cell anergy[55]. Immune checkpoint (IC) molecules tightly regulate T cell responses to antigens by either upregulating or downregulating coinhibitory or ICs that maintain tolerance to prevent autoimmunity and promote protective immunity. Inhibitory ICs such as the well-known Cytotoxic T-lymphocyte-associated antigen-4 (CTLA-4) and programmed death-1 (PD-1) restrict the strength and duration of immune responses thereby regulating inflammation resolution, limiting immune-mediated tissue damage and maintaining tolerance to prevent the development of autoimmune

diseases[56]. However, tumour cells exploit these inhibitory pathways to evade immune destruction through the upregulation of inhibitory IC ligands on the surface of tumour cells such as PD-L1 and PD-L2, the ligands for PD-1[57]. Therefore, immune checkpoint blockers (ICBs) were developed as an anti-cancer therapeutic option for treating a range of malignancies demonstrating remarkable responses in a subset of patients are a promising new therapeutic for treating GOCs[21].

ICBs block immune checkpoint (IC) pathways, reinvigorating anti-tumour immunity[21]. ICs control the magnitude and duration of the immune response, preventing overactivation of the immune system, which could lead to the development of autoimmunity[58]. ICs include cytotoxic T lymphocyte-associated antigen-4 (CTLA-4), programmed death-1 (PD-1), lymphocyte activation gene-3 (LAG-3), T cell immunoglobulin-mucin domain-3 (TIM-3), T cell immunoglobulin and ITIM domain (TIGIT), V-domain immunoglobulin-containing domain suppressor of T cell activation (VISTA), HHLA2, butyrophilin-like 2, B and T lymphocyte attenuator, 2B4, B7-H3, B7-H4 and adenosine A2a receptor (A2aR)[21]. The receptors for ICs are predominantly expressed on activated T cells. IC ligands, such as PD-L1 and PD-L2 (ligands for PD-1), CD160 (ligand for herpes virus entry mediator), galectin-9 and carcinoembryonic antigen-related cell adhesion molecule 1 (ligands for TIM-3), and CD112 and CD155 (ligands for TIGIT), are found on the surface of antigen presenting cells (APCs)[21]. However, tumour cells exploit IC pathways to evade immune destruction through the upregulation of IC ligands, such as PD-L1 and PD-L2 on their surfaces[57]. Tumour cells also secrete adenosine, which binds A2aR on T cells dampening anti-tumour T cell function[21].

Despite the vast array of ICs expressed on the surfaces of immune cells, to date the majority of related clinical trials in GOCs and other cancer types have largely focussed on testing the efficacy of blocking PD-1 and CTLA-4 IC pathways (**Table 1.1**). Anti-CTLA-4, anti-PD-1 and anti-PD-L1 ICBs have been FDA approved in first-, second- and third-line settings, spanning a wide range of malignancies, including melanoma, lymphoma, renal cell carcinoma, lung cancer and microsatellite instability-high (MSI-H) cancers[59–62]. They have been approved as monotherapies, as a dual anti-PD-1/anti-CTLA-4 cocktail or in combination with chemotherapy or anti-angiogenic drugs (receptor tyrosine kinase inhibitors against vascular endothelial growth factor receptor 1, 2 and 3)[59–62].

Two ICBs have been FDA approved as part of second and third-line settings for treating GOCs. In 2017, single agent pembrolizumab (Keytruda), an anti-PD-1 monoclonal antibody, was FDA-approved for the treatment of advanced or recurrent GC or OGJ cancers

in the third-line setting for tumours expressing PD-L1 (combined positive score (CPS) ≥1)[63]. In 2019, single agent pembrolizumab was also granted FDA approval in the second-line setting for the treatment of OSCC patients with recurrent, locally-advanced, or metastatic disease, whose tumours express PD-L1 (CPS ≥10%)[64].

Chen *et al*., performed a meta-analysis for clinical trials testing the efficacy of anti-PD1, anti-PD-L1 and anti-CTLA-4 ICBs in advanced GCs and OGJs, which demonstrated that the addition of ICBs to the second- and third-line setting for treating GOCs improves some, but not all survival endpoints[65]. The objective response rates were 9.9%, 12.0% and 2.1%, respectively and the disease control ratios were 33.3%, 34.7% and 30.1%, respectively[65]. The median progression-free survival (mPFS) was 1.6, 1.6 and 2.9 months, respectively and the median overall survival (mOS) of the three groups was 6.0, 5.4 and 7.7 months, respectively[65]. ICBs targeting the PD-1 pathway were more effective in GC patients who were PD-L1^{+}, MSI-H, Epstein-Barr virus positive or have a high tumour mutational burden (TMB)[65]. These features have demonstrated the greatest success for distinguishing responders from non-responders, acting as surrogate markers of pre-existing anti-tumour immunity[65].

Immunogenic 'hot' tumours are characterised by T cell infiltration, the presence of effector mediators, such as granzyme B, in addition to interferon-gamma (IFN-γ)-induced PD-L1 expression[66]. However, ICBs are thought to be largely ineffective in non-immunogenic 'cold' tumours, where there is an absence of pre-existing anti-tumour immunity and therefore no immune response to reinvigorate[67]. Thus, it is crucial to elucidate the underlying cellular and molecular mechanisms that contribute to the generation of non-immunogenic tumours in order to enable the design of rational therapeutic approaches to convert 'cold' tumours to 'hot' tumours, or alternatively be able to stratify these patients to receive treatments other than circumstantially ineffective ICBs. Immunogenic cytotoxic chemotherapies are emerging as a valuable tool to convert 'cold' tumours to 'hot' tumours, widening the therapeutic window and benefits of ICBs to a greater spectrum of patients[68]. Furthermore, resistance to PD-1 ICBs can be mediated through upregulation of other ICs including TIM-3 in lung cancer[69]. Therefore, co-blockade of multiple ICs has been suggested as a method to overcome/prevent IC blockade resistance and enhance the efficacy of ICBs targeting the PD-1 pathway.

.

Table 1.1: Ongoing clinical trials in GOCs testing the efficacy of ICBs as monotherapies or combination therapies.

Trial		Treatment regimen	ICB(s) tested	Cancer-type	Clinical outcomes
NCT02730546	I/II	pembrolizumab + neoadjuvant chemotherapy, and radiation therapy	anti-PD-1	resectable OGJ or GC	recruiting, data pending.
NCT02735239	I/II	durvalumab alone followed by capecitabine and oxaliplatin or combination durvalumab + tremelimumab + oxaliplatin and capecitabine or durvalumab + paclitaxel + carboplatin + radiation or durvalumab + FLOT (5-FU, leucovorin, oxaliplatin and docetaxel)	anti-PD-L1 and anti-CTLA-4	OC	active, data pending.

NCT02559687 (KEYNOTE-180)	II	pembrolizumab	anti-PD-1	OC, OGJ	mPFS: 2 months and mOS: 5.8 months[70] .
NCT02564263 (KEYNOTE-181)	III	pembrolizumab versus paclitaxel + docetaxel + irinotecan	anti-PD-1	OGJ and OSCC	mOS for OGJ cohort: 7.1 months (pembrolizumab) versus 7.1 months (chemotherapy), OSCC cohort: 8.2 months (pembrolizumab) versus 7.1 months (chemotherapy), OGJ/OSCC cohort with PD-L1 expression CPS ≥10: 9.3 months (pembrolizumab) versus 6.7 months (chemotherapy). 12-month OS rates for OGJ cohort: 32% (pembrolizumab) versus 24% (chemotherapy), OSCC cohort: 39% (pembrolizumab) versus 25% (chemotherapy) and for OGJ/OSCC with PD-L1 expression CPS ≥10: 42% (pembrolizumab) versus 20% (chemotherapy), (n=628)[71].
NCT02340975	Ib/II	tremelimumab versus durvalumab versus	anti-CTLA-4, anti-PD-L1	OGJ, GC	data pending.

		tremelimumab + durvalumab			
NCT02370498 (KEYNOTE-061)	III	pembrolizumab versus paclitaxel	anti-PD-1	OGJ, GC	mOS: 9.1 months (pembrolizumab) versus 8.3 months (paclitaxel) and mPFS: 1.5 months (pembrolizumab) versus 4.1 months (paclitaxel)[72].
NCT02589496	II	pembrolizumab	anti-PD-1	OGJ, GC	overall response rate: 24.6%. 85.7% of patients with MSI-H responded and 100% patients with Epstein-Barr virus^{+} responded[73].
NCT02901301	Ib/II	triplet pembrolizumab + trastuzumab + chemotherapy (capecitabine + cisplatin)	anti-PD-1	HER2^{+} GC HER2^{+} OC, OGJ, GC	mPFS: 8.6 months, mOS: 18.4 months and objective response rate of 76.7%, n=43[74].
NCT02494583 (KEYNOTE-062)	III	pembrolizumab versus pembrolizumab + cisplatin + 5-FU/capecitabine or cisplatin + 5-FU/capecitabine	anti-PD-1	OGJ, GC	mOS: 10.6 months (pembrolizumab) versus 11.1 months (chemotherapy) and 12.5 months (combined pembrolizumab and chemotherapy). mPFS: 2 months (pembrolizumab) versus 6.4 months

					(chemotherapy) and 6.9 months (pembrolizumab and chemotherapy)[75].
NCT02625610 (JAVELIN Gastric 100)	III	avelumab versus oxaliplatin + capecitabine/5-FU	anti-PD-L1	OGJ, GC	mOS: 10.4 months (avelumab) versus 10.9 months (chemotherapy), objective response rate: 13.3% (avelumab) versus 14.4% (chemotherapy). mPFS: similar between arms (HR 1.04 [95% CI 0.85-1.28]) for n=499[76].
NCT02625623 (JAVELIN Gastric 300)	III	avelumab versus irinotecan + paclitaxel	anti-PD-L1	OGJ, GC	mOS: 4.6 months (avelumab) versus 5.0 months (chemotherapy) and mPFS: 1.4 months (avelumab) versus 2.7 months (chemotherapy) (n=371)[77].
NCT02872116	III	nivolumab + ipilimumab versus nivolumab + oxaliplatin + 5-FU/capecitabine (FOLFOX/XELOX) versus FOLFOX/XELOX	anti-PD-1, anti-CTLA-4	OGJ, GC	data unavailable[78]. Trial ended due to toxicities and death.
NCT02864381	II	nivolumab versus nivolumab + GS-5745	anti-PD-1, MMP-9 inhibitor	OGJ, GC	data pending[79].

NCT02340975	Ib/II	second-line patients received durvalumab + tremelimumab (arm A), or durvalumab (arm B) or tremelimumab monotherapy (arm C), and third-line patients received durvalumab + tremelimumab (arm D).	anti-PD-1, anti-CTLA-4	OGJ, GC	overall response rates were 7.4%, 0%, 8.3% and 4.0% in the four arms, respectively. PFS rates at 6 months were 6.1%, 0%, 20% and 15% and 12-month OS rates were 37.0%, 4.6%, 22.9%, 38.8%, respectively[80]. n=6 in phase Ib and n=107 in phase II (arm A: 27; arm B, 24; arm C, 12; arm D, 25) in phase II.

BSC, best supportive care; CPS, combined positive score; CI, confidence interval; HR, hazard ratio; MSI-H, microsatellite instability-high; mOS, median overall survival; mPFS, median progression free survival; OS, overall survival

1.5 Visceral adiposity promotes immune dysfunction

OGJ is more prevalent in males than females likely due to central obesity affecting more men than women[6]. Adipose tissue is deposited subcutaneously and below the waste in most women contributing to a 'pear-shaped body'[7]. While in men and some women, fat tissue is deposited viscerally and above the waste resulting in central or visceral obesity and an 'apple-shaped' body[7]. Visceral fat is more metabolically active than subcutaneous fat and secretes a range of cytokines and adipokines generating systemic chronic low grade inflammation and a pro-coagulant insulin-resistant state which promote tumour development and growth[8]. It is well-established that visceral adipose tissue in OGJ patients contributes to tumour development, progression and treatment resistance via secretion of proinflammatory cytokines, insulin, fatty acids and leptin, which favours tumour initiation and progression[81,82]. Visceral obesity plays an important role in driving cancer development via the pro-inflammatory secretions interleukin (IL)-6 and tumour necrosis factor (TNF)-from adipocytes and infiltrating immune cells that reside in the visceral adipose tissue which leak into systemic circulation creating low grade systemic inflammation increasing the risk of cancer development and progression (**Figure 1.1**). An increase in visceral adiposity due to obesity also increases intra-abdominal pressure, forcing caustic stomach and bile acids into the distal part of the oesophagus giving rise to the pro-inflammatory condition gastroesophageal reflux disease, which many obese individuals suffer with and carries an increased risk of developing OGJ[83]. Approximately 5% of individuals suffering with gastroesophageal reflux disease progress to the pre-malignant condition of Barret's oesophagus which carries an overall 0.05% risk of progressing to OGJ[84]. Furthermore, visceral adipose tissue also contributes to the generation of systemic low-grade inflammation which promotes tumour development, progression and resistance to current standards of care[85]. In contrast to lean individuals, adipocytes in obese individuals become hypertrophic to handle increased lipid storage[86]. An expansion of adipocytes leads to hypoxic areas within adipose tissue, which leads macrophage recruitment and activation, and results in the generation of a pro-inflammatory environment within adipose tissues[87,88]. These hypertrophic adipocytes can also burst, releasing their contents into the extracellular environment. Immune cells such as macrophages are recruited to remove the debris, however lipids can be toxic to immune cells which causes cell death[87,88]. More immune cells are then recruited, perpetuating this state of chronic systemic inflammation by secretion of IL-6 and TNF-α[89] into the circulation and affecting distal organs. IL-6 promotes anti-apoptotic pathways

and TNF-α activates the transcription of oncogenes contributing to the survival of transformed cells and development of cancerous lesions[90]. OGJ patients have higher levels of circulating IL-6 in their serum compared with healthy controls[91]. Increased serum levels of IL-6 positively correlated with progression from Barret's oesophagus to OGJ[91]. IL-6 is one of the key pro-inflammatory factors that is produced by viscerally obese adipose tissue, playing an important role in the development of obesity-related systemic low-grade inflammation[92]. Receptors for leptin and adiponectin have been shown to be upregulated in OGJ and correlate with the stage of the tumour and nodal involvement[93]. Leptin promotes tumour development and progression through promotion cell proliferation and inhibition of apoptotic pathways mediated through Akt, mitogen-activated protein kinase, and signal transducer and activator of transcription pathways[94,95]

Resistance to first-line chemo(radio)therapy regimens is high across all solid malignancies including OGJ[96] Despite the unprecedented efficacy of ICBs the majority of the patients do not respond[97]. High tumour mutational burden and a 'hot' T cell-inflamed tumour microenvironment correlate with better responses to ICB therapies[98]. However, the role of other factors, such as body mass index is now emerging as a favourable indicator of response to ICB[99]. In a recent study, Wang *et al*[100]., have found that obesity impairs T cell function characterized by increased expression of PD-1 in mice, nonhuman primates, and humans. In addition, obesity resulted in impaired antitumor immunity and subsequently increased growth of melanoma, lung, and breast tumours in mice. Leptin also upregulated the expression of PD-1 on the surface of T cells, causally linking obesity with T cell dysfunction[100]. These elegant studies highlight how obesity-induced T cell dysfunction can be exploited for cancer treatment where the authors demonstrate that the use of ICB improved response rates in melanoma and lung tumours in obese mice and patients. The development of obesity-associated cancers such as OGJ also occurs in a background of inflammation acquiring several mutations overtime which eventually leads to neoplastic transformation[101]. Therefore, it's plausible that obesity-associated cancers may have a higher level of non-synonymous and immunogenic neo-epitopes resulting in a more immunologically hot tumour compared to OGJ cancers that did not develop as a result of obesity-associated inflammation[98]. Collectively these observations and findings highlight how the negative effect of obesity creates a vulnerability that can be harnessed for cancer treatment by ICB.

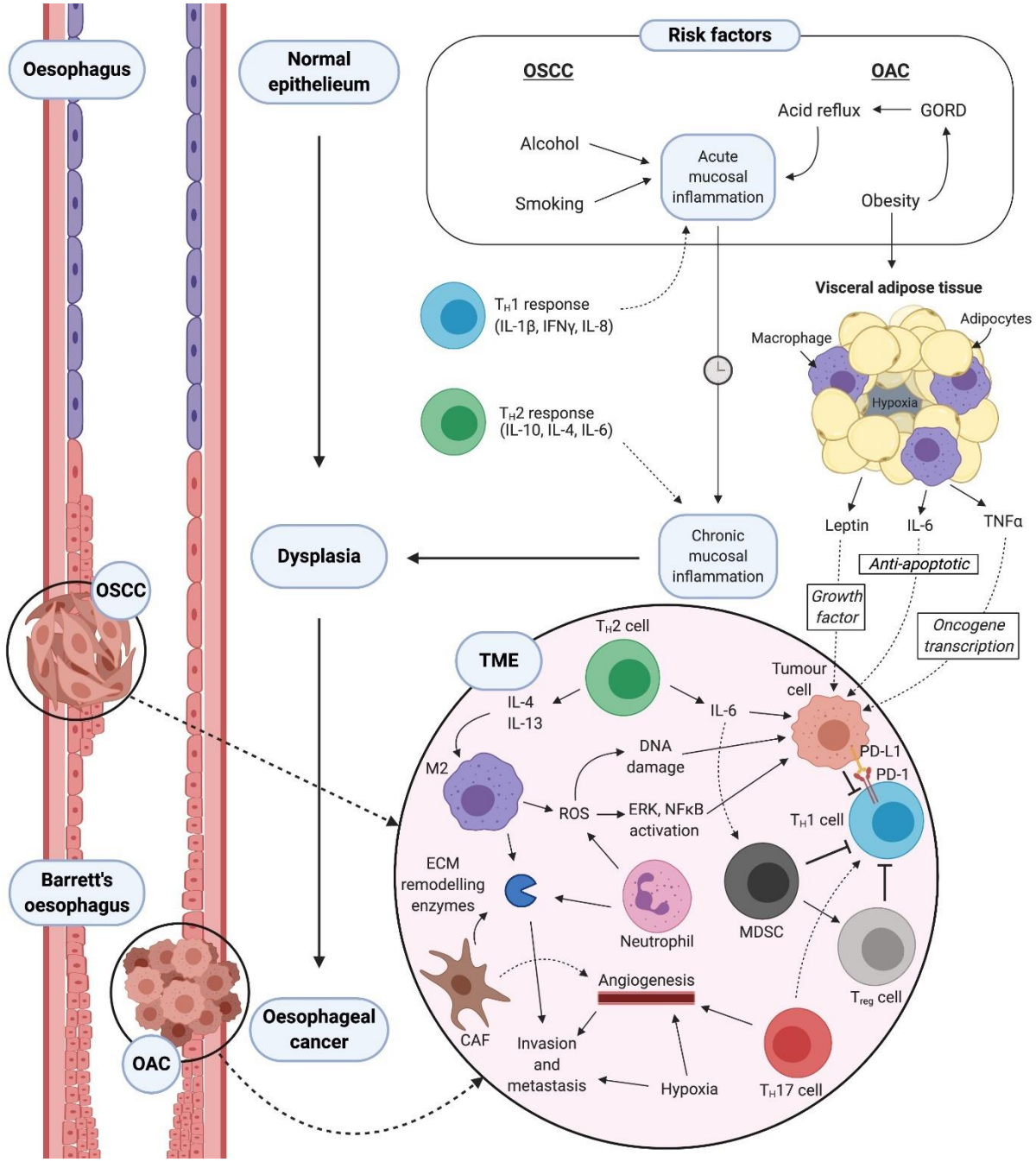

Figure 1.1: Summary of cell types, soluble mediators and pathways that promote OC initiation/development and progression. Chronic inflammation is the central driver of dysplasia. Acid reflux resulting from GORD is the major risk factor for OGJ while smoking and alcohol consumption underpins much of the aetiology for OSCC. OGJ originates from a precursor lesion known as BO in the lower two thirds of the oesophagus while OSCC most often arises in the upper third. Anti-inflammatory Th2 responses thought to dominate chronically inflamed, dysplastic tissue whereas Th1 cells are associated with a normal acute resolving inflammatory response to epithelial injury. Progression of normal cells to dysplasia and malignancy is further promoted by the TME. Resident Th2 cells promote M2

macrophage polarisation leading to ROS accumulation. ROS are genotoxic and can promote genomic instability, engendering dysplasia as well as tumour progression. Furthermore, ROS activate a plethora of pro-survival signalling pathways such as ERK, NF-κB and PI3K/Akt dysregulating key cellular controls and advancing cells towards transformation. Th2 cells also encourage MDSC activity which suppress Th1 cells. Treg cells have a similar effect and can be recruited to the tumour by M2 macrophages. Tumour cells themselves can further dampen immune surveillance by expressing co-inhibitory molecules such as PD-L1 which repress cytotoxicity following ligation with their cognate receptor PD-1 on T cells. Th17 cells can counterbalance these inhibitory effects by promoting Th1 polarisation; however, they can also facilitate angiogenesis, a key tumour hallmark. Angiogenesis is primarily driven by hypoxia as well as by the pro-angiogenic molecule VEGF. Additionally, release of extracellular matrix (ECM) remodelling enzymes by CAFs and M2 macrophages contributes to tumour invasion and metastasis. In the case of OGJ, factors outside of the TME are also central in tumour initiation and progression; expansion of adipose tissue in obese patients creates hypoxic regions recruiting and activating macrophages which release pro-inflammatory cytokines such as IL-6 and TNF-α into systemic circulation. Adipocytes complement this pro-tumour cocktail by secreting a range of growth factors such as leptin. Combined, these signalling molecules exert a powerful stimulus promoting abnormal cellular growth and transformation. Adapted from[83]

1.6 The tumour microenvironment induces immune suppression

It is well-known that the tumour microenvironment (TME) has profound effects on tumou progression and response to treatments by mediating immune suppression[102]. The TME consists of a complex array of immunosuppressive stromal cells including cancer-associated fibroblasts, tumour-associated macrophages, neutrophils, myeloid-derived suppressor cells, regulatory T (Tregs) cells, T helper (Th) 17 cells, extracellular matrix, tumour vasculature and soluble immunosuppressive mediators including transforming growth factor-β, IL-10, indoleamine 2,3-dioxygenase, arginase, vascular endothelial growth factor and prostaglandins (**Figure 1.2**)[101]. These TME factors work in tandem promoting pro-tumourigenic processes such as angiogenesis, hypoxia to generate and propagate an immunosuppressive milieu facilitating immune escape and tumour progression[103].

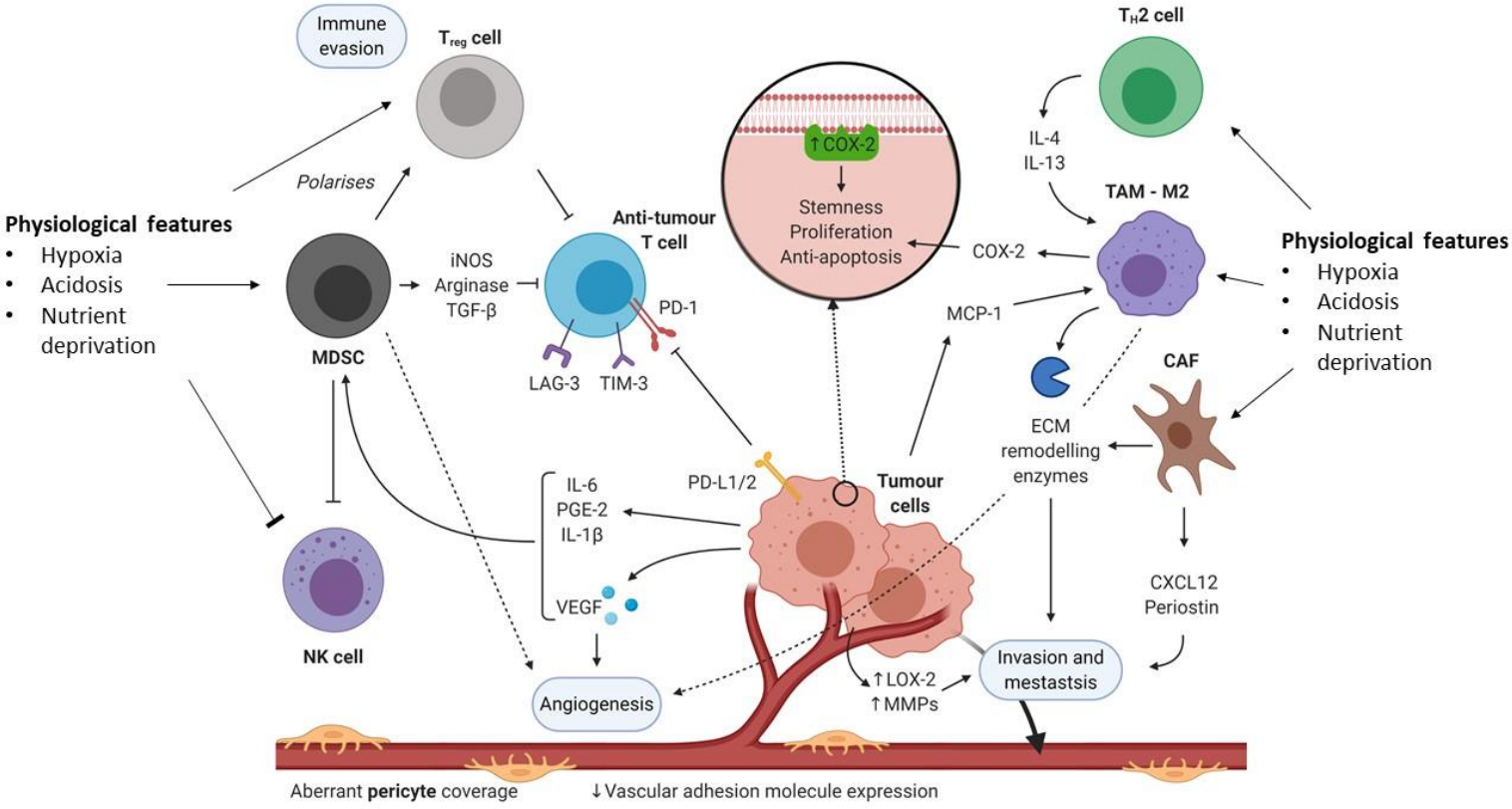

Figure 1.2: Overview of the TME in OC. Inhibition of anti-tumour immune responses (immune evasion), chiefly mediated by Th1 cells, is critical to tumour development and progression. Immunosuppressive cells such as regulatory T cells (Treg cells) and myeloid-derived suppressor cells (MDSCs) work in tandem with co-inhibitory immune checkpoint molecules including cytotoxic T-lymphocyte-associated protein 4 (CTLA-4) and programmed cell death protein 1 (PD-1) to repress effector T cell activity. PD-1 ligates with programmed death-ligand 1 (PD-L1) or PD-L2 expressed on tumour cells while the cognate ligand for CTLA-4 is CD80/86 expressed on dendritic cells (DCs). Additional immune checkpoint molecules such as TIM-3 and LAG-3 have been reported on Th1 cells in OC. Tumour-associated macrophages (TAMs) can be polarised to a pro-tumour M2 phenotype by Th2 cell-derived IL-4 and IL-13. T_H2 cells also release IL-6 which has notable pro-tumour properties. TAMs along with cancer-associated fibroblasts (CAFs) release factors such as extracellular matrix (ECM) remodelling enzymes, transforming growth factor-β (TGFβ), CXCL12 and periostin to promote cancer cell invasion and metastatic dissemination to distant sites via the blood and lymphatic vessels (latter not shown). Angiogenesis, the induction of new vasculature, is critical to this process as well as for tumour growth. Vascular endothelial growth

factor (VEGF) released by tumour cells is integral to this process. Th17 cells also promote angiogenesis, despite boosting anti-tumour Th1 cell activity. Physiological features of the TME including hypoxia, acidosis and nutrient deprivation promote pro-tumourigenic immune cells including TAMs, CAFs Th2 cells and Treg cells and inhibit anti-tumour immune cells including NK cells and Th1 cells. Adapted from[83].

1.6.1 Nutrient depletion

The TME imposes profound metabolic restrictions on antitumour T cells, understanding these insights is important for informing immunotherapeutic anticancer strategies[104]. Therapeutic approaches such as those targeting metabolic restrictions, including low glucose levels and hypoxia have shown promise as combination therapies for different types of cancer[105]. Both nutrient deprivation and hypoxia have a profound impact on the cellular composition of the TME - subsequently promoting or hindering anti-tumour immune responses. The glucose deprived environment is exacerbated by the poorly-vascularised TME and cancer cells sequestering glucose for glycolysis to facilitate tumour progression[106]. A nutrient depleted milieu arises as a result of rapidly growing tumour cells, which outcompete anti-tumour immune cells for essential nutrients required for their optimal function[107]. The well-known Warburg effect depicts the metabolic hard-wiring of tumour cells to carry out aerobic glycolysis providing tumour cells with an immediate source of fuel but in parallel contributes to rapid depletion of essential nutrients such as glucose, which is essential for effector T cell function[108]. Similarly, arginase and indoleamine 2,3-dioxygenase selectively deplete arginine and tryptophan which are essential amino acids required by effector T cells[109]. These distinct metabolic pathways in tumour cells cause functional impairment in immune cells and contribute to immune evasion[106]. Glucose is also an essential nutrient for the metabolic demands and function of anti-tumour immune cells, particularly effector T cells[110]. Glucose is an essential nutrient which plays an important role during the early stages of T cell activation in regulating T cell differentiation and maintaining activation states[110]. T cell activation involves a dramatic increase in nutrient uptake. Depletion of glucose or glutamine in cell culture media during the early stages of T cell activation inhibits T cell expansion, cytokine production and suppresses pro-inflammatory T cell differentiation[111]. Conversely, regulatory T cells thrive in a glucose depleted environment as these cell types predominantly rely on fatty acid oxidation to fulfil their energy demands[112]. Metabolic

reprogramming in T cells during their activation and differentiation have led to an emerging concept of "immunometabolism"[113]. Considering the recent success of cancer immunotherapy in the treatment of several cancer types, increasing research efforts are elucidating alterations in metabolic profiles of cancer and immune cells in the setting of cancer progression and immunotherapy[114]. Therefore, immunometabolism is a key factor in regulating immune responses in the tumour. Immune checkpoint blockade (ICB), in particular programmed death-1 (PD-1) blockade, promotes the metabolic fitness of exhausted immune cells, reinvigorating and enhancing anti-tumour effector T cell responses[115].

1.6.2 Hypoxia

Tumour vasculature is characterised as a chaotic network of tortuous and leaky blood vessels comprising dysfunctional endothelial cells with decreased expression of adhesion molecules required for immune cell extravasation to the tumour and aberrant pericyte coverage[116]. Oxygen is also consumed by rapidly growing tumour cells generating hypoxic 'pockets' within the tumour and in conjunction with nutrient depletion. Tumour hypoxia profoundly impacts the TME, in part via hypoxia-inducible factor 1-α (HIF1-α). Hypoxia increases the expression of HIF1-α which promotes carcinogenesis and tumour growth via the regulation of genes involved in angiogenesis, glycolytic metabolism and other biological mechanisms[101]. Under normoxia HIF remains in an inactivated form by prolyl hydroxylase enzymes 1-3 using oxygen as a substrate[101]. Once HIF is hydroxylated it binds to a protein called Von Hippel Lindau protein for its degradation, whereas under hypoxia HIF is stabilized and HIF translocates to the nucleus to carry out transcription of oncogenes to promote angiogenesis, metastasis and glycolytic metabolism by transcribing mediators such as VEGF, HGF and Met[101]. HIF-1 which is a heterodimer comprising of two forms, the form α is expressed in manner oxygen dependent, the form β is expressed constitutively[101]. Hypoxia profoundly alters immune cell phenotypes, in particular the myeloid compartment, which comprises of macrophages and myeloid-derived suppressor cells that cooperatively promote immune evasion, tumour cell survival and metastatic dissemination[101]. Tumour hypoxia promotes the recruitment of regulatory T cells through induction of the chemokine CC-chemokine ligand 28 which, in turn, promotes tumour tolerance and angiogenesis[117]. Pro-angiogenic processes and hypoxia have profound effects

on the metabolism of not just cancer cells but also stromal and tumour-infiltrating immune cells, this subsequent metabolic reprogramming in immune cells ultimately promotes pro-tumourigenic immune cell phenotypes[107].

1.6.3 Acidosis

Solid tumours possess regions of acute and chronic hypoxia that can select for metabolic transformations in cells[118,119]. Tumour cells exposed to chronic or intermittent hypoxia can transiently express a glycolytic phenotype, which can eventually become hard-wired even under aerobic conditions[120]. A rapid rate of glycolysis coupled with poor tumour perfusion leads to acidification of the extracellular tumour microenvironment, which can be cytotoxic to both immune cells and tumour cells[120]. However, these harsh conditions select for a phenotype that enables cancer cells to survive, proliferate, and eventually metastasize to secondary sites as demonstrated by Moellering *et al*[121]. In that study Moellering *et al.*, acclimatised human melanoma cells to low pH growth conditions, which resulted in a substantial amount of cell mortality. However, re-acclimatisation of the surviving cells to a physiological pH gave rise to stable populations with an increased invasive phenotype[121]. Furthermore, tumoural acidity induces tumour cell and stromal cell autophagy, tumour cell genome instability as well conferring resistance to chemo(radio)therapy[120,122]. Administering systemic buffer therapies to neutralize tumour acidity has been shown to inhibit local invasion and metastasis and improve immune surveillance in a variety of cancer model systems, underlining the prominent and important role of tumoural acidosis in driving malignant progression and dampening anti-tumour immunity[120,122]. A large body of evidence in the literature indicates that protons present in the tumour microenvironment as a result of tumour acidification are recognised as a damage-associated molecular pattern by DCs and subsequently enhance DC maturation and function[123]. However, the opposite has been proven for the effect of acidosis on lymphocyte function, which has been shown to suppress IFN-γ production by Th1 cells and $CD8^+$ T cell cytolytic ability[124], inducing an anergic state[125].

1.7 Overcoming ICB resistance using conventional chemotherapy regimens

Emerging studies demonstrate that the presence of tumour-associated antigens and neoantigens is a superior biomarker of response to ICBs compared with the presence of tumoural PD-L1 expression[126]. Studies from The Cancer Genome Atlas reveal that only 22% of GCs are MSI-

H, suggesting that a significant proportion of GC patients are unlikely to respond to ICBs, thus requiring additional therapeutics to sensitise their tumours to ICBs[127,128]. As such, chemotherapies that induce DNA damage in cancer cells, consequently increasing their immunogenicity through the generation of neoantigen-yielding nonsynonymous mutations, are emerging as an attractive tool to sensitise TMB-low tumours to ICBs[129]. However, chemotherapy also exerts a range of effects on the immune system depending on the agent and dose given, either leading to an augmentation of anti-tumour immunity or the induction of immunosuppression[130]. The ability of chemotherapy to induce immunogenic tumour cell death (ICD) determines how the dying tumour cell interacts with the immune system and whether an anti-tumour immune response will be triggered[131]. Chemotherapy-induced DNA-damage is associated with increased antigen presentation and the recruitment of APCs to the tumour microenvironment (TME)[132–134]. Therefore, chemotherapy is a potentially useful strategy to overcome low TMB and enhance anti-tumour immunity. Conventional chemotherapy regimens are administered using a maximal tolerated dosing schedule, typically resulting in lymphodepletion and destruction of both anti-tumour and immunosuppressive immune cells[135]. In response to chemotherapy-induced lymphodepletion, homeostatic T cell reconstitution occurs, generating new populations of T cells, which are subsequently educated in the thymus[135]. This temporal therapeutic window offers an opportunity to shape the T cell repertoire towards tumour antigens released from tumour cells that have died via chemotherapy-induced ICD. To support the synergy between chemotherapy and ICB combinations in OGJ the phase III CheckMate 649 trial demonstrated that combining nivolumab with first-line chemotherapy (FOLFOX and XELOX) in previously untreated OGJ patients (n=1,581), significantly improved overall survival in patients with a PD-L1 combined positive score of 5 or greater (14.4 months (nivolumab + chemotherapy arm) vs. 11.1 months (chemotherapy arm))19. Furthermore, the nivolumab + chemotherapy arm also reduced the risk of death by 29% (HR, 0.71; 98.4% CI, 0.59-0.86; $p<0.0001$)[136]. The findings from this trial highlight the potential therapeutic synergy that can be exploited between chemotherapy and ICB. Several supporting studies have demonstrated that the clinical efficacy of chemotherapy is not solely due to the direct killing of tumour cells but also results from the restoration of immunosurveillance[137]. Individual chemotherapies have a range of effects on the immune system; the immunomodulatory mechanisms of each chemotherapy used in the treatment of GOCs is summarized in **Table 1.2**.

Table 1.2: Immunomodulatory mechanisms of chemotherapies used in the treatment of GOCs.

Chemotherapy	Chemotherapeutic class	Mechanism of immunomodulation
5-FU	anti-metabolite	increases the frequency of tumour-infiltrating CTLs[138], depletes tumour-associated MDSCs[139], release of HSPs[140], enhances DC maturation and cross-presentation of tumour antigens to T cells[140].
oxaliplatin	alkylating agent	increases T cell recognition, induces CRT expression, HMGB1 and ATP release, increases the CTLs/regulatory T cell ratio, depletes MDSCs, improves the activity of neutrophils and macrophages[141].
docetaxel	taxane	regulatory T cell and MDSC depletion[142], DC maturation[143].
carboplatin	alkylating agent	single agent effects unknown.
paclitaxel	taxane	depletes regulatory T cells[144] and MDSCs[145], induces DC maturation[143].

ATP, adenosine triphosphate; CRT, calreticulin; CTLs, cytotoxic T lymphocytes; DC, dendritic cell; 5-FU, 5-fluorouracil; HMGB1, high mobility group box protein 1; HSP, heat shock protein; MDSCs, myeloid-derived suppressor cells.

Immunostimulatory chemotherapies induce ICD via the release of damage-associated molecular patterns (DAMPs). ICD is characterized by the induction of tumour cell apoptosis and concurrent appearance of DAMPs on the cell surface or by the release of DAMPs into the extracellular TME[146]. DAMPs indirectly trigger anti-tumour immunity via binding to pattern recognition receptors, such as CD91 and toll-like receptor-4 on APCs, inducing maturation and activation of DCs and subsequent activation and mobilisation of anti-tumour T cells to the tumour site[147]. Studies highlighting the different mechanisms of ICD induced by specific chemotherapies used for treating GOCs are outlined below. **Figure 1.3** summarises the mechanisms that mediate ICD.

1) Calreticulin (CRT) is a pre-apoptotic marker which translocates from the endoplasmic reticulum to the cell surface as a result of endoplasmic reticulum stress[148]. Membrane exposure of CRT acts as a phagocytic 'eat me' signal and attracts APCs to the tumour site. Binding of CRT to CD91 on the surface of DCs and macrophages mediates phagocytosis of the dying tumour cell and subsequent antigen processing and presentation to T cells[148]. Binding and activation of CD91 also induces the production of pro-inflammatory tumour necrosis factor-alpha (TNF-α) and interleukin (IL)-6[149]. Oxaliplatin has been shown to induce cell surface CRT expression in colorectal cancer[141] and murine lung carcinoma[150], while docetaxel induced CRT cell surface expression in breast, prostate and colorectal cancer cell lines *in vitro*[151].
2) Following, exposure of pre-apoptotic CRT on the cell surface, adenosine triphosphate (ATP) is released from lysosomes during the blebbing phase of apoptosis into the extracellular TME[152]. ATP acts through the ATP-purinergic P2Y2 ligand-receptor axis, functioning as a chemotactic signal attracting DCs and macrophages, leading to their maturation[152]. Oxaliplatin has been shown to induce ATP secretion in colorectal cancer[141] and murine lung carcinoma[150].
3) The release of high mobility group box protein 1 (HMGB1) from dying cancer cells binds toll-like receptor (TLR)-4 on the surface of APCs, stimulating their activation and maturation[153]. Studies have demonstrated that HMGB1 is important for ensuring optimal processing and phagocytosis of tumour peptides[153]. HMGB1 also binds the receptor for advanced glycation end products resulting in downstream activation of NF-κB and MAPK, promoting DC maturation and subsequent migration to the lymph node[153]. Docetaxel (lung adenocarcinoma[154]), oxaliplatin (colorectal cancer[141] and lung carcinoma[151]) and 5-FU (colon carcinoma cells[155]) all induce tumour cell secretion of HMGB1. Paclitaxel, but not carboplatin, was found to induce ICD through the release of HMGB1 and activation of TLR-4-dependent and -independent pathways in ovarian cancer[156].
4) ICD results in the increased production and release of inducible heat shock proteins (HSPs), part of the adaptive stress response, namely HSP70 and HSP90, which enhance DC maturation via binding to CD91 on their surface[157]. HSPs bind tumour antigens and guide antigen presentation for T cell activation[158]. HSPs are also known as chaperone proteins due to their regular function in mediating the refolding of misfolded proteins or in the degradation of damaged proteins[157]. 5-FU induces production of HSP70 in GC[140].

5) Additionally, chemotherapy can also activate the stimulator of IFN genes (STING) pathway, which is critical in generating an effective anti-tumour immune response[159,]. Cyclic GMP-AMP synthase detects cytosolic double-stranded DNA, another DAMP, resulting in the production of cyclic GMP-AMP, which activates STING and induces the expression of type I interferons[159]. Type I interferons induce the release of CXCL10, an effector T cell chemoattractant that binds CXCR3 on effector T cells[160]. Paclitaxel has been shown to induce the activation of STING in breast cancer cells *in vitro*[161], while oxaliplatin induces the production of type I interferons in ovarian cancer *in vitro*[162].

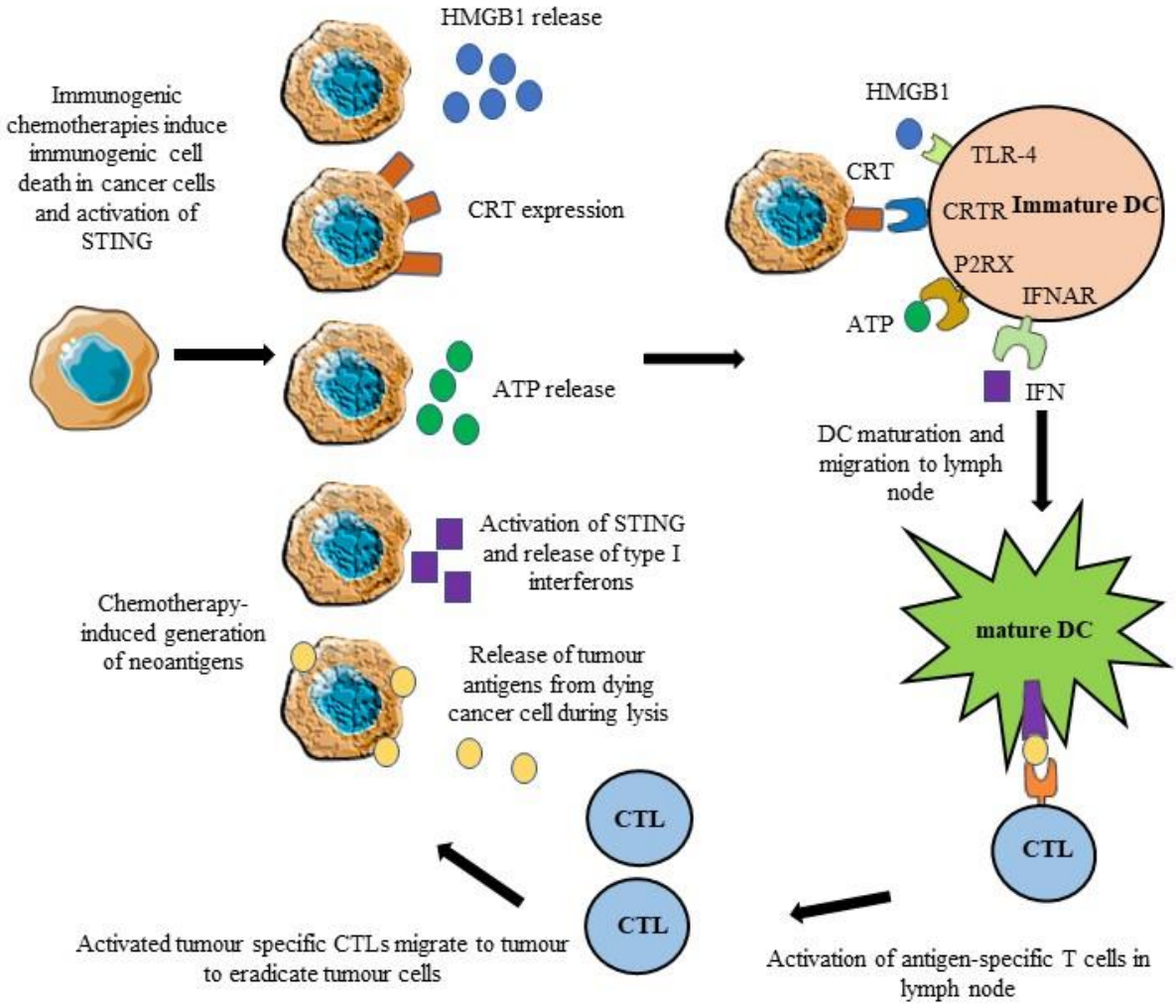

Figure 1.3: Immunogenic chemotherapies stimulate anti-tumour immunity via induction of ICD. Mechanisms of ICD induced by chemotherapies used to treat gastroesophageal malignancies. Different chemotherapies induce ICD through diverse pathways and include the release of tumour antigens from dying cancer cells, translocation of CRT to the tumour cell surface and the secretion of DAMPs, such as HMGB1 and ATP. CRT, HMGB1 and ATP bind

their respective receptors calreticulin receptor (CRTR), toll-like receptor-4 (TLR-4), and the P2RX7 receptor on immature DCs, respectively. The binding of DAMPs to their receptors on immature DCs results in their maturation and subsequent migration to lymph nodes. In the lymph nodes, mature DCs activate antigen-specific cytotoxic $CD8^+$ T cells (CTLs). Activated CTLs then migrate to the tumour and kill tumour cells expressing their cognate tumour antigens. Certain chemotherapies result in the activation of STING and subsequent production of type I interferons further enhancing anti-tumour immunity. Adapted from[163].

GOCs are highly heterogeneous cancers and emerging evidence suggests that they can be stratified into unique immune-based subtypes[164,165]. In a study of 1,524 GC patients, distinct TME phenotypes were identified and associated with prognosis. The high TME score subtype was characterized by immune activation and was an independent prognostic biomarker in predicting response to immunotherapy. Immune activation was defined by enrichment for genes involved in response to viruses (IFNG, TRIM22, CXCL10, CXCL9, and CD8A), response to IFN-γ (HLA-DPB1, CCL4, CCL5, and IFNG) and T-cell activation (TRBC1, IDO1, CD2, NLRP3, and CD8A). The low TME score subtype was enriched for genes involved in extracellular matrix remodelling (DCN, TIMP2, FOXF2, and MYH11), epithelial mesenchymal transition (EMT) (ACTA2, TGFB1L1, and SFRP1), cell adhesion and angiogenesis (PDGFRA, GREM1, and TMEM100), which are considered suppressive factors for T cells and may be responsible for significantly worsening prognosis in GC patients[164].

Relative to other tumour types, OGJ has a relatively high TMB and ranked 5th of 30 tumour types in terms of TMB[166,167]. A study of 129 OGJ patients identified 3 subgroups based on mutational signatures. The “mutagenic” subgroup displayed the highest TMB, neoantigen burden and $CD8^+$ tumour infiltrating lymphocyte density, which may lead to an increased response to ICBs[168].

An additional study of 551 OGJ patients demonstrated a three-way association between hypermutation, activation of the Wnt pathway and loss of immune signalling genes, such as β2 microglobulin, a component of the major histocompatibility complex-I, which is associated with T cell exclusion from the tumour[169]. Hypermutation is associated with higher immune activity, while Wnt dysregulation and loss of β2 microglobulin is associated with immune escape[170]. This provides an acquired mechanism through which OGJ may prevent immune surveillance induced by a high TMB, potentially contributing to the lack of response to ICBs in OGJ.

Contextually, a “one size fits all” approach will unlikely be suitable for treating GOCs with ICB, chemotherapy and their combinations. The available evidence to date supports the premise that certain tumours will likely respond better to ICBs, whereas tailored combination approaches will be required to sensitise other tumours.

1.8 The double-edged sword of chemotherapy provides a therapeutic niche for ICBs

1.8.1 Chemotherapy upregulates immune checkpoints on the surface of cancer cells

Chemotherapy may be a double-edged sword in cancer, tumour-promoting or tumour-inhibiting, depending upon the circumstances. Several studies have highlighted a role for the immune system in the development of chemoresistance. In particular, chemotherapy-induced PD-L1 upregulation on the surface of breast cancer cells results in immune evasion via ligation of PD-L1 to PD-1 on T cells, thereby inducing T cell apoptosis[171]. Additionally, *in vitro* and *in vivo* murine model studies[172] demonstrate that cisplatin upregulates PD-L1 on head and neck squamous cell carcinoma cells[172] and ovarian cancer cells[173]. It has been demonstrated that 5-FU increases PD-L1 expression on the surface of colorectal and OGJ cancer cells *in vitro*[174]. However, the post-treatment expression levels of PD-L1 on OGJ cells from *ex vivo* tumour tissue that received 5-FU, cisplatin and radiation, was not significantly different compared with matched treatment-naïve tumour tissue (n=10)[174]. Several studies have demonstrated that DNA damage signalling upregulates PD-L1 expression on the surface of cancer cells[175,176,] and that PD-L1 cancer cell-intrinsic signalling mediates DNA repair, including base excision repair in osteosarcoma, breast and colorectal cancer[176]. This suggests that the 5-FU-induced PD-L1 upregulation on cancer cells *in vitro* may be as a result of the 5-FU-induced DNA damage, which would be repaired by the time the biopsy is taken post-treatment[174]. In a study by Ng *et al.,* PD-L1 was expressed in 21% of OSCC tumours, as determined by immunohistochemistry (n=84)[177]. PD-L1 staining positively correlated with advanced stage III and IV disease and lymph node metastasis[177]. Combination cisplatin and 5-FU and combination carboplatin and paclitaxel significantly upregulated PD-L1 on OSCC cells *in vitro* via the EGFR/ERK and MAPK/MEK pathways. The chemotherapy-induced PD-L1 upregulation may be a pro-survival strategy to protect against chemotherapy-induced cell death and/or the chemotherapy may be selecting for a more aggressive and resistant clone, highlighting the double-edged sword of

chemotherapy[177]. A study by Fournel *et al.*, reported significantly increased PD-L1 expression on both lung cancer cells and tumour-infiltrating immune cells following cisplatin-based chemotherapy (n=22)[178]. Cisplatin treatment also significantly increased PD-L1 expression on tumour cells in nude and immunocompetent mice bearing lung carcinoma tumours[178]. Combined anti-PD-L1 antibody and cisplatin significantly reduced tumour growth compared to single agent treatment and controls in Lewis lung murine models[178].

Overall, the chemotherapy-induced upregulation of PD-L1 on the surface of tumour cells is presenting a therapeutic target. It is unclear what mechanisms are regulating the chemotherapy-induced upregulation of PD-L1; be it in response to chemotherapy-induced cancer cell secretion of cytokines known to upregulate PD-L1, such as IFN-γ[174] and transforming growth factor-β[179], or DNA damage signalling[175,176]. Emerging studies have demonstrated that cancer cell-intrinsic signalling of PD-L1 and other ICs promote various immune-independent hallmarks of cancer and that blockade of these pathways may have additional benefits in terms of reducing overall tumour burden[180–183].

1.9 Immune checkpoint signalling promotes cancer hallmarks in addition to immune evasion

Several studies have identified PD-1[182,184–186], TIM-3[187,188], VISTA[189,190] and TIGIT[191] IC receptors on the surface of cancer cells across a range of malignancies. Tumour-expressed IC receptors have novel immune-independent functions associated with various hallmarks of cancer via cancer cell-intrinsic signalling including glycolysis[180], DNA repair[181], proliferation[182], invasion and migration (**Figure 1.4**)[187,183].

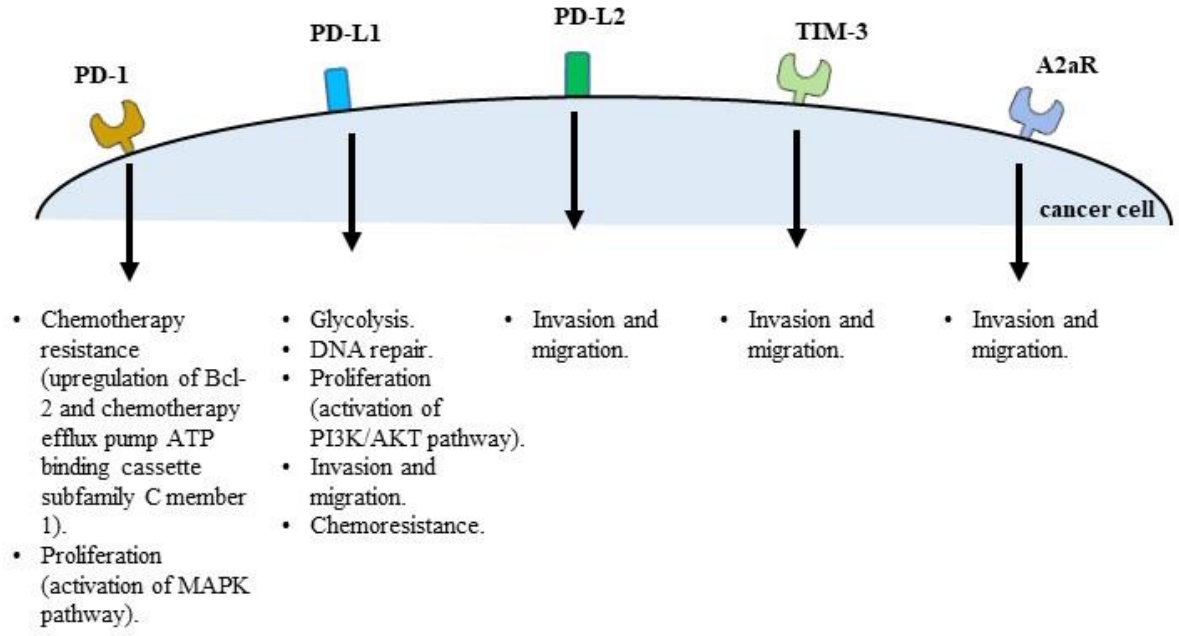

Figure 1.4: Cancer cell-intrinsic signalling of IC ligands and cognate receptors promotes a range of immune-independent hallmarks of cancer. Several studies in a range of cancer types including lung, melanoma, head and neck, colorectal, gastric and oesophageal cancers have demonstrated that cancer cell-intrinsic signalling of various IC ligands and receptors promotes a range of hallmarks of cancer other than immune evasion. This figure summarises the results from a range of studies demonstrating that activation of these pathways promotes proliferation, invasion, migration, metabolism, DNA repair and confers chemoresistance. Adapted from[163].

Sustained proliferative signalling is another hallmark of cancer and is mediated by oncogenic signalling in tumour cells including RAS, MYC, RAF and MAPK signalling pathway[47]. Studies in other cancers, including pancreatic ductal adenocarcinoma have demonstrated that activation of PD-1 signalling *in vitro* using recombinant PD-L1 promotes proliferation via MAPK signalling[185]. Similarly, PD-1 overexpressing murine melanoma tumours demonstrate increased tumourigenICBty compared with PD-1 knockdown murine melanoma tumours in NOD SCID gamma mice (IL-2R γ-chain (-/-)), identifying an immune-independent role for cancer cell-intrinsic PD-1 signalling in tumourigenesis[192].

Cancer cells also possess increased migratory and invasiveness characteristics to promote metastatic dissemination and is a key hallmark of cancer[47] and one of the principal causes of mortality in OGJ patients[193]. Interestingly, it has been shown that the levels of TIM-3 in GC

tissue are higher in adjacent normal gastric tissue[188]. Decreased galectin-9 and increased TIM-3 correlated with poor prognosis in GC[188]. Similarly, TIM-3 was also identified on the surface of HeLa cervical cancer cells *in vitro* and high expression of TIM-3 on cervical tumour cells correlated with advanced cancer grade and decreased OS compared with patients who had lower tumour cell TIM-3 expression[187]. Downregulating TIM-3 using adenoviral mutants encoding anti-sense TIM-3 significantly decreased the *in vitro* invasive capacity of HeLa cells, highlighting an immune-independent role for this IC[187].

It has been shown that the A2aR IC receptor is also expressed on the surface of GC cells. Activation of A2aR by adenosine promotes GC cell metastasis by enhancing PI3K-AKT-mTOR signalling[194]. The expression of A2aR positively correlates with TNM stage and is associated with poor outcomes[194]. Binding of adenosine to A2aR induces migration and invasion, increases pseudofoot and ciliary growth and increases expression of matrix metalloproteases, such as MMP-9 and MMP-13, which are required for invasion and migration in GC cells[194], among others. Adenosine was shown to upregulate stemness-associated and EMT-like proteins, including SOX2 (SRY-box 2), OCT4 (POU class 5 homeobox 1), Nanog, CD44, and CD133 via A2aR receptor axis[194]. PI3K inhibition significantly inhibited adenosine-induced EMT, stemness and migration in GC cell lines *in vitro*[194]. Human GC tumour xenograft mice injected with A2aR knockout GC cells had significantly reduced numbers and size of micrometastatic lung lesions compared to mice injected with GC cells expressing A2aR[194].

Cancer stem-like cells (CSCs) play important roles in tumour initiation, treatment resistance, tumour recurrence and are thought to play a key role in mediating metastatic dissemination a hallmark of cancer[195]. Cancer stem-like cells are typically resistant to conventional cytotoxic regimens which selectively target rapidly growing cells, however cancer stem-like cells have a low proliferative index and often survive chemo(radio)therapy regimens and following treatment these treatment resistant cancer stem-like cells proliferate giving rise to a treatment resistant tumour[196]. Kollmann *et al*., recently reported that PD-1 is expressed on 77% of OGJ patient tumours (n=168) at levels greater than 5%, as determined by immunohistochemical analysis[184]. Additionally, PD-1 has been found to be preferentially expressed on melanoma CSCs in melanoma xenografts and melanoma patient biopsies, as characterised by the expression of tumour-initiating cell determinant ABCB5[197]. CSCs exist as a small sub-population of cells within a tumour, which are more resistant to therapies and persist following conventional chemoradiotherapy[198]. CSCs are thought to be primarily responsible for tumour

initiation, treatment resistance and disease recurrence[198] and destruction or complete removal of CSCs is essential for complete tumour eradication[199]. It remains to be determined if blocking PD-1 on the surface of CSCs can render them more sensitive to chemotherapy-induced cell death, or whether this may contribute to the striking clinical efficacy of PD-1 ICBs in melanoma - a question that certainly warrants further investigation.

A study by Hsu *et al.*, demonstrated that the process of EMT upregulates PD-L1 on CSCs via the EMT/β-catenin/STT3/PD-L1 signalling axis[200]. Induction of EMT promotes N-glycosyltransferase STT3 transcription through β-catenin and subsequent STT3-dependent N-glycosylation inducing PD-L1 upregulation[200]. The enrichment of PD-L1 on CSCs may enable this aggressive subpopulation of cancer cells.

Collectively, these studies highlight the inhibitory effects of ICBs on the various hallmarks of cancer (other than immune evasion), including cancer cell metabolism, proliferation, metastasis and invasion. It is possible that chemotherapy drugs may indirectly activate these immune-independent pathways via upregulation of IC ligands and receptors on cancer cells and immune cells. Chemotherapy may predispose patients to respond to ICBs as a result of higher IC expression and ultimately enhance response rates. However, recent studies have also shown that IC cancer cell-intrinsic signalling can confer chemoresistance via immune-independent mechanisms[180–183].

1.10 Immune checkpoint signalling can confer chemoresistance via immune-independent mechanisms

Several studies have demonstrated that IC cancer cell-intrinsic signalling offers protection to cancer cells against chemotherapy-induced cell death[201]. One study showed that a 5-FU resistant GC cell line SGC7901/5-FU expressed significantly higher levels of cell surface PD-1 than 5-FU sensitive SGC7901 cells[202]. Upregulation of PD-1 in SGC7901 cells protected against 5-FU chemotherapy-induced cell death, increased proliferation and upregulated the expression of the Bcl-2 anti-apoptotic protein and chemotherapy efflux pump, ATP binding cassette subfamily C member 1[202]. Downregulating PD-1 expression in SGC7901/5-FU cells reduced 5-FU resistance demonstrated by a decrease in proliferation and increase in apoptosis[202].

Other studies have reported a higher expression of PD-1 and PD-L1 on tumour cells that are more resistant to cisplatin in small cell lung cancer[186] and GC[202] *in vitro* and *ex vivo*. PD-1 and

PD-L1 were expressed at significantly higher levels on cisplatin resistant (H69R and H82R) compared to cisplatin sensitive small cell lung cancer cells (H69P and H82P) *in vitro*[186]. Additionally, small cell lung cancer tumour tissue in the treatment-naïve setting had lower expression of PD-1 and PD-L1 than resistant tumours[186]. Of significant clinical relevance, blockade of PD-1 and PD-L1 resensitised cisplatin resistant small cell lung cancer cells to cisplatin[186]. Several studies have demonstrated that DNA damage signalling upregulates PD-L1 expression on the surface of cancer cells[175,176,203] and that PD-L1 cancer cell-intrinsic signalling mediates DNA repair[203], including base excision repair in osteosarcoma, breast and colorectal cancer[176]. Therefore, blockade of PD-L1 on the surface of GOC cells could prevent repair of chemotherapy-induced DNA damage, thereby enhancing chemotherapy toxICBty.

1.11 Clinical trials assessing ICB-chemotherapy combinations

There is minimal clinical data available to determine if the addition of ICBs to chemotherapy regimens will enhance the efficacy of chemotherapy in GOCs. However, a range of clinical trials are ongoing to answer this clinically relevant question.

Results from the phase III keynote-062 trial with 763 OGJ/GC patients show the objective response rate is higher in the combined pembrolizumab and chemotherapy arm (cisplatin + 5-FU/capecitabine) versus the chemotherapy alone arm. The mOS was 10.6 months (pembrolizumab) versus 11.1 months (chemotherapy) and 12.5 months (combined pembrolizumab and chemotherapy). The mPFS was 2 months (pembrolizumab) versus 6.4 months (chemotherapy) and 6.9 months (pembrolizumab-chemotherapy)[75].

The addition of ICBs to chemotherapy for the treatment of lung cancer patients substantially enhanced the efficacy of chemotherapy inducing synergistic effects with improved and durable clinical responses[204]. A phase II study in non-squamous non-small cell lung cancer (n=123) demonstrated that the addition of pembrolizumab significantly enhanced response rates to carboplatin and pemetrexed, which led to accelerated FDA approval (overall response rate: 55% for pembrolizumab-chemotherapy arm versus 29% for chemotherapy only arm)[205]. The PFS was 19 months for the pembrolizumab-chemotherapy arm versus 8.9 months for the chemotherapy only arm (median follow-up of 18.7 months)[205]. This is encouraging data for the use of ICBs to enhance response rates to chemotherapy regimens.

An ongoing phase II trial demonstrated that 39% of OSCC patients (9/31) achieved a pathological complete response to combination atezolizumab and CROSS treatment[206]. However, no CROSS only arm was included in the trial design so it is not possible to determine

if adding atezolizumab to the CROSS regimen enhanced efficacy[206]. However, the authors suggest that despite the small cohort, this was a promising result as the CROSS trial demonstrated that 23% of OC patients (47/161) receiving CROSS achieved a pathological complete response rate compared with 39% of OSCC patients in this phase II trial (9/31)[20].

An ongoing phase II study (KEYNOTE-059, NCT02335411) in GC and OGJ patients is investigating pembrolizumab in three different arms, which include: (1) pembrolizumab, 5-FU and cisplatin in treatment-naïve patients, (2) single agent pembrolizumab in previously treated patients and (3) treatment-naïve patients. Preliminary safety data from the pembrolizumab, 5-FU and cisplatin arm reported that grade 3-4 treatment related adverse effects were documented in 37% of patients (n=18, median follow-up was 5.5 months). This trial is forecast to reach completion in May 2022[207].

1.12 Co-blockade of multiple immune checkpoints in GOCs to enhance response rates

The vast array of IC receptors and ligands expressed on immune cells and cancer cells suggests non-redundant functions with unique roles in immunological tolerance in cancer but ultimately synergise to inhibit T cell function. Co-expression of PD-1 with other ICs characterizes a more dysfunctional population of tumour-infiltrating lymphocytes (TILs) compared with TILs expressing PD-1 alone in GOC patients[208]. Dual blockade of CTLA-4 and PD-1 can achieve a more effective anti-tumour immune response as both the CTLA-4 and PD-1 pathways inhibit T cell activation and function using non-redundant mechanisms[209].

PD-1 regulates primed T cells in lymphoid organs, peripheral tissues and tumours where PD-L1 and PD-L2 are expressed. PD-1 blockade reinvigorates exhausted T cells enhancing their anti-tumour effector function. CTLA-4 blockade increases the level of IFN-y-producing TILs which subsequently upregulates IFN-y-driven expression of PD-L1 on immune cells and tumour cells.

CTLA-4 attenuates initial T cell priming in secondary lymphoid organs inhibiting the activation of naïve and memory T cells[210]. In Treg cells PKC-n kinase is constitutively bound to the cytoplasmic domain of CTLA-4 and it is believed that this interaction plays a key role in the function of CTLA-4 in Tregs[210]. The second mechanism involves CTLA-4 expressing T cells inhibiting activation of neighbouring T cells in a cell-extrinsic fashion[210]. CTLA-4 binding to CD80/CD86 on the surface of DCs stimulates DCs to secrete the

immunosuppressive tryptophan-degrading enzyme IDO, thereby suppressing the function of neighbouring T cells[210]. Additionally, CTLA-4 binding to CD80/CD86 induces transendocytosis of CD80/CD86 and intracellular degradation of the ligands by the CTLA-4 expressing cell thereby, reducing the availability of CD80/86 for binding to CD28 required in T cell activation[211]. The precise mechanisms in which anti-CTLA-4 therapy enhances anti-tumour immunity have yet to be fully elucidated. It is likely a combination of factors including an enabling of T cell priming, reduced level of Tregs facilitated by Treg depletion in the TME via antibody-dependent cell mediated cytotoxicity and decreased level of secreted-immunosuppressive molecules such as IDO, lowering of the threshold required for T-cell activation and a broadening of the T cell repertoire in the periphery[212,213]. In contrast, PD-1 negatively regulates T cell activation in the periphery maintaining peripheral tolerance[214]. Engagement of PD-1 receptor by its ligands PD-L1 or PD-L2 reduces phosphorylation of TCR signalling molecules leading to decreased T cell activation and cytokine production. Overall, PD-1 activation inhibits the phosphatidylinositol-3-kinase (PI3K)/akt signalling pathway resulting in decreased expression of transcription factors necessary for effector function (T-bet, Gata3 and Eomes)[215]. Signalling through PD-1 impairs proliferation and cytokine production[216].

Combined use of nivolumab and ipilimumab has been FDA-approved in melanoma, MSI-H and DNA mismatch repair-deficient metastatic colorectal cancer and kidney cancer[217]. Unfortunately, the majority of patients still fail to benefit from CTLA-4, PD-1 and PD-L1 ICBs. Therefore, co-blockade of novel ICs, such as TIM-3, TIGIT and LAG-3 are being investigated in clinical trials. These novel IC receptors regulate T cell function, maintain self-tolerance, regulate ongoing T cell responses at peripheral tissues, and synergistically regulate autoimmunity and antitumor responses[218].Tim-3, TIGIT and LAG-3 pathways specifically inhibit pro-inflammatory responses and promote regulatory T cells and DCs responses[218].It remains to be determined if specific ICs may be co-opted by specific cancer types to evade anti-tumour immunity depending on the tissue site. A greater fundamental understanding of the specialized functions of the array of ICs that exist will inform the rational design of therapeutic strategies for GOC patients.

A study by Zong *et al.*, demonstrated that TILs in GC patients have increased expression of CTLA-4, TIGIT, TIM-3 and PD-1 and the percentage of peripheral blood PD-1^{+}TIM-3^{+} and PD-1^{+}TIM-3^{-} T cells was significantly higher than circulating levels in healthy donors[208]. Furthermore, the predominant fraction of TILs was comprised of PD-1^{+} TIM-3^{+} double positive

cells[208]. PD-1 inhibition enhanced cytokine production *in vitro* and co-blockade of PD-1 and TIM-3 synergistically enhanced cytokine production (IFN-γ, TNF-α and IL-2) *in vitro*[208]. Additionally, the percentage of $CD3^+$ TILs expressing PD-1 positively correlated with tumour size and lymph node metastasis in GC patients[208]. The presence of lymph node metastasis and larger tumour sizes in patients with a higher percentage of $CD3^+PD\text{-}1^+$ TILs may indicate immune escape due to immune exhaustion.

Wilms' tumour 1 (WT1) is often overexpressed in cancer cells and knockdown of WT1 induces mitochondrial damage and inhibits cancer cell growth[219]. WT1 antigen is a promising target for DC-based vaccines in several malignancies, including GC[219]. The expression of TIGIT, PD-1 and TIM-3 was upregulated in GC patients with limited WT1-specific $CD8^+$ T cell proliferation and function following administration of a WT1-targeted DC-based vaccine[220]. TIGIT-expressing $PD1^+Tim3^-$ $CD8^+$ T cells comprised the predominant subset of TILs, however, $TIGIT^+PD1^+Tim3^+$ represented the most dysfunctional subset of WT1-specific $CD8^+$ T cells. Co-blockade of PD-1, TIGIT and TIM-3 enhanced the growth, proliferation and cytokine production (IFN-γ, TNF-α and IL-2) of WT1-specific $CD8^+$ T cells *in vitro*[220]. This may suggest that the co-expression of TIGIT, TIM-3 and PD-1 may identify exhausted tumour-antigen specific T cells. Reinvigoration using TIM-3, TIGIT and PD-1 co-blockade may represent an attractive and tailored therapeutic approach to reinvigorate tumour-antigen specific T cells in this cohort of GC patients.

An additional study demonstrated that the level of $PD\text{-}1^+$, $TIM\text{-}3^+$ and $PD\text{-}1^+TIM\text{-}3^+$ peripheral blood $CD4^+$ and $CD8^+$ T cells was significantly higher in oesophageal cancer patients compared with healthy donors, whereas the expression of TIGIT was significantly lower [221]. While the expression of $PD\text{-}1^+$, $TIM\text{-}3^+$, $TIGIT^+$ and $PD\text{-}1^+TIM\text{-}3^+$ $CD4^+$ T cells was significantly higher in OC tumour tissue compared with 'normal' adjacent oesophageal mucosa[221]. This suggests that single agent blockade of PD-1 alone may not be suffICBent to reinvigorate exhausted T cells and perhaps co-blockade of TIM-3 and PD-1 may be required in these patients.

Studies in other cancers, such as colon carcinoma and fibrosarcoma tumour models have demonstrated that dual blockade of PD-1 and LAG-3 synergistically promotes anti-tumour immunity and reduces tumour growth[222]. Preliminary data from a phase I/IIa clinical trial testing the efficacy of combined PD-1 and LAG-3 blockade in advanced melanoma patients demonstrated an objective response rate of 12.5% (n=48)[223]. This patient cohort was heavily pre-treated and either refractory or had relapsed on anti-PD-1/PD-L1 therapy[223]. Patients who

had LAG-3 expression in at least 1% of immune cells within the tumour margin achieved a higher objective response rate of nearly three-fold compared to those with less than 1% expression (20% (n=25) versus 7.1% (n=14), respectively)[223]. This clinical data suggests that upregulation of other ICs may play a role in immune escape and treatment resistance to other ICBs and that combined blockade of LAG-3 and PD-1 in PD-1/PD-L1 refractory patients may help overcome resistance.

Collectively, these studies suggest that co-blockade of multiple ICs, such as TIGIT, PD-1, LAG-3 and TIM-3, could achieve better reinvigoration of anti-tumour immunity than monotherapy, which warrants further investigation through clinical trials in GOC patients. However, the level of immune-related adverse events (irAEs) that accompanies co-blockade of multiple ICs is an important consideration.

1.13 Administration and timing of chemotherapy-ICB combinations for GOC patients

The effect of chemotherapy on IC expression on T cells is an important factor that requires consideration. This information will enable rational design of chemotherapy-ICB combinations and help guide the appropriate timing of these treatments for trial design in GOC patients. A study by Zhang *et al.*, demonstrate that following neoadjuvant chemotherapy in GC patients the majority demonstrated a significant increase in the expression levels of CD4, CD8, PD-1, PD-L1 and TIM-3, as determined by immunohistochemical analysis (n=60 paired)[224]. This increase in tumour-infiltrating lymphocytes (TILs) further supports the immunogenic properties of chemotherapies in GC patients[224]. Additionally, the increase in ICs suggests potential exhaustion of the induced anti-tumour immune response and highlights a role for ICBs in combination with chemotherapy in the neoadjuvant and the adjuvant setting for GC patients[224]. Interestingly, in this study a small percentage of patients demonstrated a significant decrease in CD4, CD8, PD-1, PD-L1 and TIM-3 expression following neoadjuvant chemotherapy treatment, suggesting a subset of patients with a distinct tumour biology resistant to the immunomodulatory effects of chemotherapies and unlikely to achieve benefit from ICBs[224]. Changes in the expression of PD-1, PD-L1 and TIM-3 revealed strong pairwise correlation, further supporting the rationale for co-blockade of multiple ICs[224]. Furthermore, high expression levels of CD8, PD-1 and PD-L1 following neoadjuvant chemotherapy were positive prognostic factors of OS[224]. The increase in cytotoxic T lymphocytes and ICs may

likely be surrogate markers of ongoing anti-tumour immunity and may stratify patients who could benefit from ICBs.

IC blockade is a promising therapeutic strategy in GOCs, however, a substantial proportion of tumours lack TILs or a pre-existing anti-tumour immune response[67]. Therefore, the timing of delivery of ICBs with other treatment modalities is critical. The addition of adjunct therapies, such as conventional chemotherapy regimens, offers an opportunity to stimulate anti-tumour immunity, whereby ICBs can prevent exhaustion of the subsequent induced anti-tumour immunity. Administering ICBs prior to chemotherapy would therefore be less effective as concurrent or potentially administration of immunogenic chemotherapy with subsequent IC blockade.

1.14 Immune related Adverse Events (irAEs)

Emerging evidence suggests that ICB-induced irAEs are associated with improved responses[225]. However, enhancing the efficacy of ICBs by the addition of chemotherapy may subsequently escalate irAE profiles and may ultimately represent a barrier to advancing dual ICB combinations and ICB-chemotherapy combinations in the clinic. It is recognised that the frequency of irAEs increases with the duration and dose of ICB administered[226]. Additionally, agents targeting CTLA-4 are associated with more frequent irAEs compared to agents targeting PD-1 and PD-L1, and combinations of both anti-CTLA-4 and anti-PD-1/PD-L1 agents results in higher incidences of irAEs[227]. Thus, the choice of ICB has a considerable impact on irAE frequency and intensity. To date, trials in GOCs combining chemotherapy with ICBs indicate a manageable safety profile, although higher incidences of irAEs in the ICB-chemotherapy arm compared with ICB alone arm is often reported. In a phase I/IIb trial of GC patients testing the efficacy of anti-PD-1 alone versus combination anti-PD-1-oxaliplatin, 77.6% experienced at least one irAE and 22.4% experienced a grade 3 or higher irAE in the anti-PD-1 arm. However, in the anti-PD-1-oxaliplatin arm 94.4% of patients experienced at least one irAE and 38.9% experienced at least one grade 3 or higher irAE. In the phase III keynote-062 trial with 763 OGJ and GC patients, the incidence of grade 3-5 drug-related adverse events was 17% for the pembrolizumab arm, 69% for the chemotherapy arm and 73% for the combination pembrolizumab-chemotherapy arm[75]. However, although an increase in irAEs was observed with the addition of chemotherapy, the safety profile reported was clinically manageable highlighting combination chemotherapy-ICB regimens as a clinically feasible option for OGJ patients[128].

1.15 Concluding remarks

Research to date highlight both an immune- and non-immune-based rationale for blocking ICs on cancer cells, either alone or as part of a multimodal chemotherapy regimen. ICBs could potentially limit immune resistance, but also block the various tumour-promoting functions of IC cancer cell-intrinsic signalling. Further studies are required to investigate which ICs are expressed by cancer cells in GOCs and to elucidate the immune-dependent and -independent functions of these ICs. This will inform the rational design of clinical trials testing ICB combinations with conventional cytotoxic regimens to achieve better response rates for GOC patients. Development of clinically applicable prognostic and predictive tools will be crucial in stratifying patients into suitable treatment arms, such as those likely to benefit from ICB monotherapy and those who are unlikely to respond. For non-responders, the development of clinically applicable methods to identify what specific therapeutic combinations, if any, are required and capable of sensitising immunologically 'cold' tumours to ICBs are needed. Combination chemotherapy and ICB regimens offer a potential strategy to alter the TME sufficiently to convert 'cold' tumours to 'hot' tumours with the ultimate outcome of converting non-responders to responders. Furthermore, understanding the direct effects of features of the TME on IC expression profiles and T cell function in GOCs will be important for designing effective immunotherapy regimens to attenuate the immunosuppressive effects of the TME.

1.16 Hypothesis and aims

The specific hypotheses and aims of the research are as follows:

Hypothesis 1: Features of the TME such as nutrient deprivaiton, hypoxia and acidosis upregulate ICs on the surface of OGJ cells and T cells. Blockade of tumour cell-expressed ICs will reduce the survival of OGJ cells under these conditions. Blockade of ICs on the surface of T cells under these conditions will enhance anti-tumour T cell acitivity however, these harsh conditions will likely reduce the efficacy of ICB.

Aim 1: Investigate the effect of features of the TME including nutrient deprivation, hypoxia and acidosis on IC expression profiles of OGJ cells and T cells derived from OGJ patients and the effect of features of the TME on the efficacy of ICB - assessing immune-independent and immune-dependent mechanisms.

Hypothesis 2: The visceral adipose tissue secretome enhances T cell activation and upregulates inhibitory immune checkpoints on the surface of T cells which may promote T cell dysfunction.

Aim 2: Investigate the effect of the secretome from visceral adipose tissue derived from OGJ patients on IC expression profiles of T cells and the effect of this secretome on the efficacy of ICB to boost anti-tumour T cell function.

Hypothesis 3: First-line chemotherapy regimens signficantly alter IC expression profiles of OGJ cells. Tumour-expressed immune checkpoint ligands and receptors provide OGJ cells with a survivial advantage and blockade of immune checkpoints enhances chemotherapy toxICBty.

Aim 3: Assess IC expression profiles of OGJ cells and the effect of chemotherapy. Determine the effect of ICB on OGJ cell viability alone and in combination with first-line chemotherapy regimens.

Hypothesis 4: First-line chemotherapy regimens significantly alter T cell phenotypes and immune checkpoint expression profiles and combining immune checkpoint blockade with first-line chemotherapy regimens will achieve synergistic responses

Aim 4: Profile IC expression on the surface of T cells from OGJ patients in the neoadjuvant and adjuvant setting. Assess the direct effects of first-line chemotherapy regimens on anti-tumour T cell phenotypes and the effect of chemotherapy on the efficacy of ICB.

Chapter 2: Materials and methods

2.1 Ethical approval

Ethical approval was granted from the St. James's Hospital Ethics Committee. All patient samples were collected with prior informed written consent for sample and data acquisition from patients attending St. James's Hospital or from healthy donors. This study was carried out in accordance with the World Medical Association's Declaration of Helsinki guidelines on medical research involving human subjects. Patient samples were pseudonymised in line with GDPR and data protection policies to protect the privacy and rights of the patients.

2.2 Prospective specimen collection

All patients involved in this study were enrolled from 2018-2020. Whole blood and tumour tissue biopsies were obtained from oesophagogastric junctional adenocarcinoma (OGJ) patients undergoing endoscopy at St. James's hospital at time of diagnosis prior to initiation of any chemotherapy or radiotherapy. Post-FLOT chemotherapy-treated and post-CROSS chemoradiotherapy-treated whole blood and tumour tissue biopsies were obtained at time of surgical tumour resection.

2.3 Cell culture

2.3.1 Cell lines

Human normal oesophageal cells (HET-1A), BO cells (QH), OGJ cells (OE33, SK-GT-4 and OE19 cells) used in this study were obtained from the European Collection of Cell Cultures. The HET-1A cell line was derived in 1986 from human esophageal autopsy. The BO QH cell line was derived from an endoscopic biopsy specimen obtained from a region of non-dysplastic metaplasia. The OE33 cell line was established from a 73-year old female patient from the adenocarcinoma of the lower oesophagus. The tumour was poorly differentiated and characterised as stage IIA. SK-GT-4 cell line originated from a well differentiated oesophageal adenocarcinoma arising in Barrett's epithelium from an 89-year-old Caucasian male. The OE19 cell lines was established in 1993 from an adenocarcinoma of gastric cardia/oesophageal gastric junction of a 72 year old male patient. The tumour was identified as pathological stage III (UICC) and showed moderate differentiation. The Jurkat cell line is an IL-2-prodcing immortalized human T lymphocyte cell line commonly used to study T cell signalling. Jurkat cells were purchased from the European Collection of Cell Cultures.

2.3.2 Culture of cell lines

Cells were cultured as monolayers in 75 cm^2 filtered culture flasks (Thermo Scientific). Cells were incubated at 37˚C at 5% CO_2 in a 95% humidified atmosphere in a FORMA water jacketed CO_2 incubator (Thermo Forma, Steri-cycle, CO_2, incubator, Hepafilter. Sub-culture was performed when cells reached a confluency of 70-80%. HET-1A cells were grown in flasks precoated with a solution of fibronectin (0.01 mg/ml, Merck, Germany), collagen type I (0.03 mg/ml, Corning, USA) and bovine serum albumin (0.01 mg/ml, Sigma, USA) dissolved in PBS and cultured in serum free Bronchia/Trachea Epithelial Cell Growth Medium (511-500, Merck, Germany). HET-1A cells were detached from flask using accutase (Sigma, USA) diluted 1:15 in PBS. QH cells were grown in Bronchia/Trachea Epithelial Cell Growth Medium supplemented with 1% (v/v) penicillin-streptomycin (50 U/ml penicillin 100µg/ml streptomycin) and 10% (v/v) foetal bovine serum (ThermoFisher Scientific, Ireland) and detached from flask using trypsin-EDTA solution (Sigma, USA). OE33 cells, SK-GT-4 cells and OE19 cells were grown in RPMI 1640 medium with 2 mM L-glutamine (ThermoFisher Scientific, Ireland) and supplemented with 1% (v/v) penicillin-streptomycin (50 U/ml penicillin 100µg/ml streptomycin (P/S)) and 10% (v/v) foetal bovine serum (FBS) (ThermoFisher Scientific, Ireland) and detached using trypsin-EDTA solution. Jurkat cells were cultured in suspension in a 75 cm^2 filtered culture flasks (Thermo Scientific) and 25 ml of cRPMI at 37˚C at 5% CO_2. Sub-culture was performed using a 1 in 15 splitting density when cells reached a confluency of 70-80%. All cell lines were maintained in a humidified chamber at 37°C 5% CO_2 and were tested regularly to ensure mycoplasma negativity using qPCR. Cell waste was decontaminated with a 24 h treatment with Haztab chlorine tablets (Guest Medical).

2.3.3 Cell Counting

Trypan blue (0.4%, Sigma-Aldrich) was used to determine cell viability and number. Live cells with an intact membrane remain impermeable to the trypan blue dye. However, dead cells lack an intact membrane and are permeable to the dye. This results in dead cells staining blue and viable cells not staining. The vortexed cell pellet was resuspended in 1 ml cRPMI and 10 µl of cell suspension was diluted 1 in 20 in 190 µl of diluted trypan blue solution (1:1 ratio of Trypan blue:PBS). 10 µl of trypan blue/cell suspension was added to a glass hemocytometer, (Neubauer glass hemocytometer 0.01 mm depth, Marienfeld-Superior) and visualised at X20 magnification under a light microscope (Nikon Eclipse E200). A 9 square, 3 x 3 hemocytometer was used (**Figure 2.1**). The number of cells in the outer four corner squares was counted. Cells touching the outer sides of the squares were included and cells touching the

inner sides of the squares were excluded from the count. The cell count was always performed immediately because trypan blue is toxic to cells. The total number of viable cells was determined using the equation. The average number of cells per square was multiplied by the dilution factor (20) and by 10^4 (takes into account the volume of the hemocytometer) using the following formula: average no. cells X dilution factor X 10^4 = number of cells/ ml. The optimised seeding densities for cell lines are listed in **Table 2.1**.

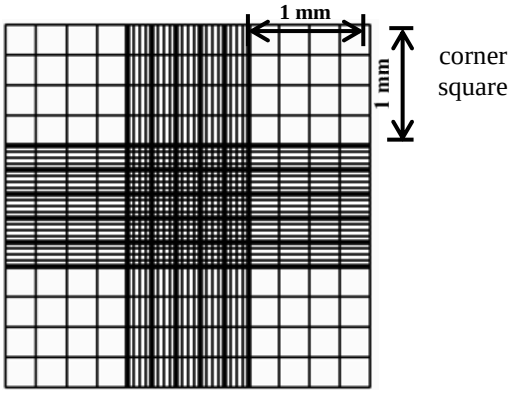

Figure 2.1: Schematic representation of a chamber on a glass hemocytometer. 9 squares (3 x 3) with a dimension of 1 mm x 1 mm (Taken from[1]).

Table 2.1 Seeding densities used for cell lines

Cells	plate size	Seeding density
HET-1A, QH, OE33, SK-GT-4, OE19 cells, Jurkat cells, Jurkat cells.	Flat 96 well plate	5 x 10^3 cells/ml
HET-1A, QH, OE33, SK-GT-4, OE19 cells, Jurkat cells.	Flat 12 well plate	0.1 x 10^6 cells/ml

2.4 PBMC isolation by density gradient centrifugation

Peripheral blood mononuclear cell (PBMC) isolation was carried out by density gradient centrifugation using lymphoprep solution (Axis-Shield) at room temperature. The procedure was carried out under sterile conditions in a laminar flow cabinet (Microflow Biological Safety

Cabinet) which was turned on 10 mins prior to use to achieve a sterile atmosphere. Blood was diluted 1:1 in PBS solution (Gibco). The diluted blood solution was carefully layered on top of lymphoprep solution (Axis-Shield) so as to not break the lymphoprep-blood interface (1:2 ratio of lymphoprep:diluted blood). The sample was centrifuged at 2000 RPM for 25 mins with the brake off (centrifuge, Thermo Scientific Heraeus Megafuge 40). Following centrifugation, the different blood cells separated into distinct layers based on their relative densities (**Figure 2.2**). The layer containing the PBMCs was a white cloudy layer (buffy layer) and contained monocytes and lymphocytes. The buffy layer was removed and washed twice with PBS. The supernatant was discarded and the resulting cell pellet was vortexed and resuspended in 1 ml of cRPMI. PBMCs were then counted as described in section 2.5.2. and plated at 1 x 10^6 cells in 1 ml of cRPMI per well in a 24 well plate (Sarstedt) or at 2 x 10^5 cells in 200 µl of cRPMI per well in a 96 well plate (Sarstedt) and incubated overnight to rest the cells at 37˚C, 5% CO_2 (ESCO cell culture, CO_2 incubator, Medical Supply Company).

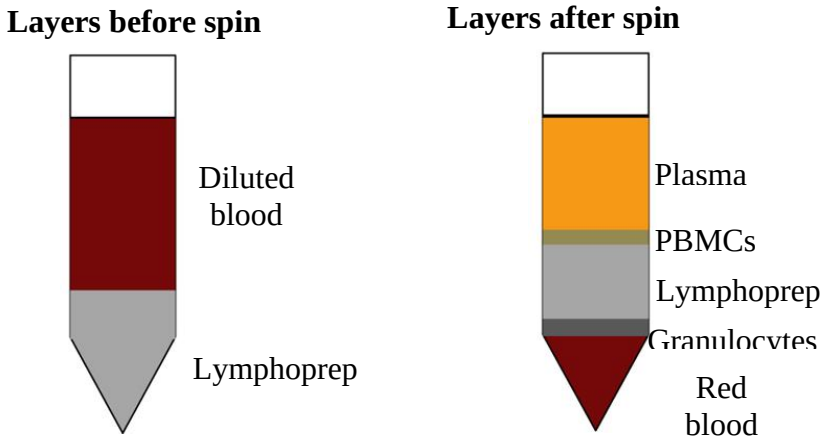

Figure 2.2: PBMC isolation by density gradient centrifugation. Schematic representation of PBMC isolation using Lymphoprep solution, before and after centrifugation. The different blood cells separate into distinct layers based on their relative densities (Taken from[1]).

2.5 Anti-CD3 and anti-CD28 antibody T cell activation

The base of a 96-well flat bottomed plate or 12-well plate was coated with 50 µl and 200 µl, respectively of goat anti-mouse IgG (5 µg/ml in PBS) and incubated overnight at 4°C. The well was washed twice with PBS and coated with 200 µl of anti-CD3/anti-CD28 antibody solution (anti-CD3 5µg/ml BioLegend and anti-CD28 Ancell diluted 1 in 1000 dilution) and incubated for 2h at 37°C. Wells were washed with PBS and cells were seeded in 100 µl of cRPMI with IL-2 (100 units/ml, ImmunoTools, Germany) at a density of 1 x 10^6 cells/ml.

2.6 Chemotherapy treatment

2.6.1 Identification of IC_{50} doses for treating OGJ cells and T cells

2.6.1.1 Preparation of chemotherapeutic drugs

Chemotherapies used in FLOT (5-FU, oxaliplatin, docetaxel), CROSS (paclitaxel and carboplatin) and MAGIC (epirubicin, cisplatin and 5-FU (ECF) and epirubicin, cisplatin and capecitabine (ECX)) regimens were purchased from Sigma Aldrich (country) and were reconstituted in appropriate vehicles (**Table 2.2**) and stored at -20°C in the dark. For use in cell culture chemotherapies were diluted in cRPMI immediately prior to use.

Table 2.2 Single agent chemotherapies and concentration ranges.

Chemotherapy	Concentration Range	Stock conc.	Working stock conc.	Vehicle
5-fluorouracil (sigma Aldrich)	0, 0.01, 1, 10, 50, 100, 200 μM	200 mM	0, 0.1, 10, 100, 500, 1000, 2000 μM	DMSO (0.1%)
Cisplatin (sigma Aldrich)	0, 0.01, 1, 10 50, 100, 200 μM	3.3 mM	0, 0.1, 10, 100, 500, 1000, 2000 μM	0.15 M sodium chloride
Capecitabine (sigma Aldrich)	0, 0.01, 1.0, 10, 100, 500, 1,000, 2,000 μM	25 mM	0, 0.1, 10, 100, 1000, 5000, 1,0000, 2,0000 μM	Deionised water (6%)
Oxaliplatin (sigma Aldrich)	0, 0.01, 1.0, 10, 50, 100, 200 μM	12 mM	0, 0.1, 10, 100, 500, 1000, 2000 μM	Deionised water (6%)
Docetaxel (sigma Aldrich)	0, 0.000001, 0.00001, 0.0001, 0.001, 0.01, 10 μM	16 mM	0, 0.00001, 0.0001, 0.001, 0.01, 0.1, 100 μM	DMSO (0.1%)
Epirubicin (sigma Aldrich)	0, 0.0001, 0.001, 0.01, 0.5, 1, 20, 100 μM	170 mM	0, 0.001, 0.01, 0.1, 5, 10, 200, 1000 μM	DMSO (0.1%)
Carboplatin (sigma Aldrich)	0, 0.0001, 0.001, 0.01, 0.5, 1, 20, 100 uM	26.9 mM	0, 0.001, 0.01, 0.1, 5, 10, 200, 1000 uM	Deionised water (6%)
Paclitaxel (sigma Aldrich)	0, 0.0001, 0.001, 0.01, 0.5, 1, 20, 100 uM	120 mM	0, 0.001, 0.01, 0.1, 5, 10, 200, 1000 uM	DMSO (0.1%)

2.6.1.2 CCK-8 assay to identify IC_{50} values of chemotherapies for OGJ cells and T cells

OE33 cells were seeded at 5 x 10^3 cells/200 ul in cRPMI in a 96-well flat-bottomed plate and incubated at 37°C, 5% CO_2 overnight. Media was replaced with 180 µl of fresh cRPMI and cells were treated with 20 ul of single agent chemotherapy at a range of increasing concentrations. **Table 2.3** shows the chemotherapies and drug concentrations that were used to treat OE33 cells and Jurkat cells. Vehicle control treated cells were included and cells were treated with 20 µl of appropriate vehicle depending on the chemotherapy (**Table 2.3**).

Jurkat cells were used as a T cell model and were seeded at 2.5 x 10^3 cells/180 ul of cRPMI in a 96-well flat-bottomed plate. Jurkat cells were treated with 20 µl of single agent chemotherapy at a range of increasing concentrations (**Table 2.3**). Vehicle control treated cells were included and cells were treated with 20 µl of appropriate vehicle depending on the chemotherapy. 20 µl of cRPMI were added to untreated control cells.

Cells were incubated for 24, 48 or 72h at 37°C, 5% CO_2. 10 µl of cell counting kit-8 (CCK-8) assay solution (Sigma-Aldrich) was added to each well after 24, 48 or 72h. Cells were incubated at 37°C, 5% CO_2 for 1.5 to 2h until appropriate pink to orange colour development was observed. Colour development was carefully observed so that the colour development of the untreated wells did not become saturated. The absorbance was measured at 450 nm and 650 nm (reference wavelength) using a microplate reader (Versa max Medical Devices). **Table 2.4** contains the IC_{50} values for OE33 and Jurkat cells at 24, 48 and 72h. Experiments were repeated n=3 times in triplicate.

Table 2.3 IC_{50} values for single agent chemotherapies for Jurkat cells and OE33 cells at 24, 48 and 72h time points, determined by CCK-8 assay.

Chemotherapy	Time point	IC_{50} jurkat cells	IC_{50} OE33 cells
5-FU	24h	Not determined	Not toxic
	48h	0.04223 µM	0.3511 µM
	72h	Not determined	0.8982 µM
Capecitabine	24h	Not toxic	Not toxic
	48h	Not toxic	1,000 µM
	72h	1,500 µM	224.7 µM
cisplatin	24h	30.16 µM	10 µM
	48h	2.573 µM	2.39 µM
	72h	1.663 µM	1.295 µM
Oxaliplatin	24h	36.44 µM	200 µM

	48h	2.562 µM	4.18 µM
	72h	0.2313 µM	1.705 µM
Docetaxel	24h	Not determined	Not toxic
	48h	0.0001 µM	0.0016 µM
	72h	Not determined	0.0000653 µM
Epirubicin	24h	Not determined	0.5018 µM
	48h	0.09559 µM	0.8629 µM
	72h	Not determined	0.0896 µM
Paclitaxel	24h	Not determined	Not determined
	48h	**0.001196 µM**	0.0007645 µM
	72h	Not determined	Not determined
Carboplatin	24h	Not determined	Not determined
	48h	150 µM	300 µM
	72h	Not determined	Not determined

2.6.1.3 Identification of IC_{50} values for combination chemotherapy regimens (FLOT, CROSS CT, MAGIC) for OGJ cells and T cells using CCK-8 assay

OE33 and SK-GT-4 cells were seeded at 5 x 10^3 cells/200 ul in cRPMI in a 96-well flat-bottomed plate and incubated at 37°C, 5% CO_2 overnight. Media was replaced with 140 µl of fresh cRPMI (for cells receiving FLOT, ECF or EXC regimens) or 160 µl of CRPMI (for cells receiving CROSS CT regimen). Jurkat cells were seeded at 5 x 10^3 cells/200 ul in cRPMI in a 96-well flat-bottomed plate and left rest for 2h at 37°C, 5% CO_2. OE33, SK-GT-4 or Jurkat cells were treated with a combination of FLOT (5-FU, oxaliplatin, docetaxel), CROSS CT (paclitaxel and carboplatin), ECF (epirubicin, cisplatin and 5-FU) and ECX (epirubicin, cisplatin and capecitabine) chemotherapies at a range of concentrations (IC_5, IC_{10}, IC_{20}, IC_{25}, IC_{50}) as listed in **Table 2.4, Table 2.5 and Table 2.6**, respectively.

Table 2.4: Concentration of drug combinations FLOT, CROSS CT, ECF and ECX used to treat OE33 cells for 48h to identify IC_{50} concentration of combination regimen using CCK-8 assay.

	IC value	5-FU	Oxaliplatin	Docetaxel
FLOT	IC_5	0.1303 µM	0.01 µM	0.00001 µM
	IC_{10}	0.2750 µM	0.05 µM	0.00005 µM
	IC_{15}	0.4367 µM	0.1 µM	0.0001 µM
	IC_{20}	0.6187 µM	1 µM	0.0005 µM

	IC_{25}	0.8249 µM	2 µM	0.001 µM
	IC_{50}	2.475 µM	3.948 µM	0.005 µM
CROSS CT	**IC value**	**paclitaxel**	**Carboplatin**	
	IC_{5}	0.000001 µM	10 µM	
	IC_{10}	0.00001 µM	50 µM	
	IC_{15}	0.0001 µM	100 µM	
	IC_{20}	0.0005 µM	500 µM	
	IC_{25}	0.001 µM	1000 µM	
	IC_{50}	0.005 µM	2000 µM	
ECF	**IC value**	**epirubicin**	**Cisplatin**	**5-FU**
	IC_{5}	0.2357 µM	0.01 µM	0.1303 µM
	IC_{10}	0.4977 µM	0.05 µM	0.2750 µM
	IC_{15}	0.7904 µM	0.1 µM	0.4367 µM
	IC_{20}	1.120 µM	1 µM	0.6187 µM
	IC_{25}	1.493 µM	1.5 µM	0.8249 µM
	IC_{50}	4.479 µM	2.39 µM	2.475 µM
ECX	**IC value**	**epirubicin**	**Cisplatin**	**Capecitabine**
	IC_{5}	0.2357 µM	0.01 µM	1 µM
	IC_{10}	0.4977 µM	0.05 µM	10 µM
	IC_{15}	0.7904 µM	0.1 µM	50 µM
	IC_{25}	1.493 µM	1.5 µM	100 µM
	IC_{50}	4.479 µM	2.39 µM	1,500 µM

Table 2.5: Concentration of drug combinations FLOT, CROSS CT and ECF used to treat SK-GT-4 cells for 48h to identify IC_{50} concentration of combination regimen using CCK-8 assay. Following chemotherapy treatment 50% of OGJ cells were alive.

FLOT	IC value	5-FU	oxaliplatin	docetaxel
	IC_{10}	2 uM	0.1 uM	0.0000001 uM
	IC_{25}	6 uM	1 uM	0.00001 uM
	IC_{50}	50 uM	10 uM	0.01 uM
CROSS CT	IC value	paclitaxel	Carboplatin	
	IC_{10}	0.00001 uM	100 uM	
	IC_{25}	0.001 uM	250 uM	
	IC_{50}	0.005 uM	500 uM	
MAGIC (ECF)	IC value	epirubicin	Cisplatin	5-FU
	IC_{10}	0.001 uM	1 uM	2 uM
	IC_{25}	0.1 uM	3 uM	6 uM
	IC_{50}	0.25 uM	6 uM	50 uM

Table 2.6: Concentration of drug combinations FLOT, CROSS CT and ECF used to treat Jurkat cells and PBMCs for 48h to identify IC_{50} concentration of combination regimen using CCK-8 assay or AV PI assay. Following chemotherapy treatment 50% of the T cells were alive.

FLOT	IC value	5-FU	oxaliplatin	docetaxel
	IC_{10}	0.001 uM	0.001 uM	0.000001 uM
	IC_{25}	0.01 uM	0.01 uM	0.00001 uM
	IC_{50}	0.04 uM	2.862 uM	0.0001 uM
CROSS CT	IC value	paclitaxel	Carboplatin	
	IC_{10}	0.0001 uM	100 uM	
	IC_{25}	0.00055 uM	120 uM	
	IC_{50}	0.001196 uM	150 uM	
MAGIC (ECF)	IC value	epirubicin	Cisplatin	5-FU

	IC_{10}	0.09399 uM	0.01 uM	0.001 uM
	IC_{25}	0.1461 uM	1 uM	0.01 uM
	IC_{50}	0.2277 uM	2.573 uM	0.04 uM

Table 2.7 contains the optimised IC_{50} combination doses for FLOT, CROSS CT and ECF chemotherapy treatment for OE33, SK-GT-4 and PBMCs used throughout this thesis for examining the effects of chemotherapy on cellular phenotype.

Table 2.7: Determined IC_{50} drug combinations for FLOT, CROSS CT and ECF used to treat OE33, SK-GT-4 and PBMCs for 48h for all experiments in this thesis.

FLOT	Cell type	5-FU	oxaliplatin	docetaxel
	OE33	0.8249 µM	2 µM	0.001 µM
	SK-GT-4	50 uM	10 uM	0.01 uM
	PBMCs	0.01 uM	0.01 uM	0.0001 uM
CROSS CT	**Cell type**	**paclitaxel**	**Carboplatin**	
	OE33	0.001 µM	1000 µM	
	SK-GT-4	0.001 uM	250 uM	
	PBMCs	0.0001 uM	50 uM	
MAGIC (ECF)	**Cell type**	**epirubicin**	**Cisplatin**	**5-FU**
	OE33	1.493 µM	1.5 µM	0.8249 µM
	SK-GT-4	0.1 uM	3 uM	6 uM
	PBMCs	Not determined	Not determined	Not determined

2.7 Nutrient deprivation and hypoxia treatment

2.7.1 Nutrient deprivation and hypoxia treatment of OGJ cells

OE33 cells and OE19 cells were cultured in complete RPMI (cRPMI, 10% FBS, 1% P/S), serum-free RPMI (0% FBS, 1% P/S), glucose-free RPMI (Gibco (11560406), 10% FBS, 1% P/S), dual glucose-free and serum deprived RPMI (Gibco (11560406), 0% FBS, 1% P/S) under normoxic conditions (37°C, 5% CO_2, 21% atmospheric O_2) or hypoxic conditions (37°C, 5% CO_2, 0.5% O_2) for 48h using the H35 Don Whitley hypoxia station.

2.7.2 Nutrient deprivation and hypoxia treatment of OGJ donor PBMCs

5-day anti-CD3/CD28 expanded PBMCs were seeded at a density of 1 x 10^6 cells/ml in 100 µl of media in a 96 well round bottomed plate (not pre-coated with anti-CD3/28) for an additional 24h in complete RPMI (cRPMI, 10% FBS, 1% P/S), serum-free RPMI (0% FBS, 1% P/S), glucose-free RPMI (Gibco, 10% FBS, 1% P/S), dual glucose-free and serum deprived RPMI (Gibco, 0% FBS, 1% P/S) under normoxic conditions (37°C, 5% CO_2, 21% atmospheric O_2) or hypoxic conditions (37°C, 5% CO_2, 0.5% O_2) using the H35 Don Whitley hypoxia station. PBMCs were then harvested for flow cytometry staining.

2.8 Acidosis treatment

2.8.1 Acidosis treatment of PBMCs

PBMCs were isolated from whole blood using density gradient centrifugation and expanded for 7 days with plate bound anti-CD3 (10 µg/ml, Biolegend, USA), anti-CD28 (10 µg/ml, Ancell, USA) and recombinant human IL-2 (100 units/ml, Immunotools, Germany) for 7 days in complete RPMI 1640 medium (cRPMI) (containing 2 mM L-glutamine (Gibco) and supplemented with 1% (v/v) penicillin-streptomycin ((P/S) 50 U/ml penicillin 100µg/ml streptomycin) and 10% (v/v) foetal bovine serum (Gibco)). Following a 7 day T cell activation PBMCs were seeded in cRPMI in a 96 well round bottom plate (not pre-coated with anti-CD3/28 antibodies) at a density of 0.2 x 10^6 cells/ml at increasing levels of acidity (pH 7.4, 6.6 and 5.5) in the absence or presence of nivolumab (10 µg/ml), ipilimumab (10 µg/ml) or dual nivolumab and ipilimumab (10 µg/ml and 10 µg/ml, respectively) at 37°C 5% CO_2 for an additionally 48h. The acidity was altered using a pH meter and concentrated hydrochloric acid. Wu *et al*[228]., demonstrated that the acidic pH present in lymph nodes does not hinder initial activation of naïve T cells. Typically, T cells spend 5-7 days in the lymph node undergoing activation before travelling to the tumour site therefore, in this study a 7 day T cell activation timepoint was chosen followed by an additional 48h culture in acidic conditions to recapitulate the timing of biological processes in human.

2.8.2 Acidosis treatment of OGJ cell lines

OE33 or OE19 cells were seeded at a density of 0.1 x 10^6 cells/ml at increasing levels of acidity (pH 7.4, 6.6 and 5.5) for 48h at 37°C 5% CO_2.

2.9 Co-culture of OGJ donor PBMCs with OE33 cells

OE33 cells were seeded at a density of 1 x 10^4 cells/100 µl in cRPMI in a flat bottomed 96 well plate and left adhere overnight. Following 24h, 5-day expanded OGJ patient-derived PBMCs were cultured alone or co-cultured with OE33 cells at a ratio of 5:1 (PBMCs:OE33 cells) for 48h at 37°C 5% CO_2. PBMCs were then harvested for flow cytometry staining.

2.10 Generation of conditioned media

2.10.1 Generation of OGJ patient-derived PBMC conditioned media under nutrient deprivation and hypoxia

Treatment-naïve PBMCs were isolated from whole blood using density gradient centrifugation and expanded for 7 days with plate bound anti-CD3 (10 µg/ml, Biolegend, USA), anti-CD28 (10 µg/ml, Ancell, USA) and recombinant human IL-2 (Immunotools, Germany) for 5 days in complete RPMI 1640 medium (cRPMI) (containing 2 mM L-glutamine (Gibco) and supplemented with 1% (v/v) penicillin-streptomycin ((P/S) 50 U/ml penicillin 100µg/ml streptomycin) and 10% (v/v) foetal bovine serum (Gibco)). Following 5-day T cell activation PBMCs were cultured for an additional 24h under nutrient deprivation +/- normoxic/hypoxic conditions in a separate 96 round bottom plate (not pre-coated with anti-CD3/28 (as described in **Section 2.7.2**). The supernatant was harvested and stored at -80°C for later use.

2.10.2 Generation of chemotherapy-treated OGJ cell conditioned media

OE33 or SK-GT-4 cells were seeded at a density of 1 x 10^6 cells/flask in T25 flasks and the media was changed the following day. When the flasks reached 40-50% confluency the cells were treated with a combination of chemotherapies that comprise the FLOT regimen (5-FU, oxaliplatin and docetaxel), the CROSS chemotherapy (CT) regimen (paclitaxel and carboplatin) or MAGIC chemotherapy regimen (epirubicin, cisplatin and 5-FU) or a vehicle control for 48h (0.0001% DMSO, 0.001% H_2O and 0.0001% NaCl (0.8% v/v)). These combination doses were pre-optimised using a CCK8 assay to achieve 50% cell death (as carried out in[229]). The conditioned media was harvested and stored at -80°C.

2.10.3 Generation of tumour biopsy conditioned media

Resected post-FLOT or post-CROSS OGJ tumour explants of ~2–3 mm^3 were transferred into 1 ml of serum-free M199 media (Gibco), supplemented with gentamicin and cultured for 24 h

at 37˚C, 5% CO_2. The resulting tumour conditioned media (TCM) was harvested and stored at −80˚C until required for experimentation (**Table 2.8**). Protein content was assessed by BCA assay for normalisation.

Table 2.8 Patient Demographic Table for generating tumour biopsy conditioned media.

Age (years)	**65.5**
Sex ratio (M:F)	6:4
Diagnosis (no. patients)	
OGJ	10
Clinical tumour stage[a] (no. patients)	
T0	1
T1	1
T2	1
T3	7
T4	1
Clinical nodal status[a] (no. patients)	
Positive	6
Negative	5
Received neoadjuvant FLOT	45.5%
Received neoadjuvant CROSS CRT	54.5%
Did not receive neoadjuvant treatment	0%

2.10.4 Generation of conditioned media for OE33-OGJ PBMC co-culture cytolysis assay

OE33 cells were treated for 48h with vehicle (0.0001% DMSO and 0.0001% H_2O), FLOT or CROSS CT chemotherapy regimens (IC_{50} doses as previously described in[229]), washed twice to remove the chemotherapy drugs and replaced with fresh media and the subsequent OE33 conditioned media was collected 48h later and stored at −80˚C until required for experimentation

2.11 Co-culture with conditioned media

2.11.1 Co-culture of PBMCs with post-FLOT or post-CROSS CRT tumour biopsy conditioned media

Healthy donor PBMCs were prepared from whole blood collected in EDTA Vacutainer tubes (BD Biosciences) by density gradient centrifugation over Lymphoprep^{TM} (Stemcell Technologies). PBMCs were seeded at a concentration of 1×10^6 cells per ml in complete RPMI media (10% FBS, 1% penstrep) and activated using plate bound anti-CD3 (10 μg/ml, Biolegend, USA) and anti-CD28 (10 μg/ml, Ancell, USA) in the absence or presence of 50% post-FLOT or post-CROSS CRT tumour biopsy conditioned media for 48h. PBMCs were then harvested and stained for flow cytometry.

2.11.2 Co-culture of PBMCs with post-FLOT, post-CROSS CT or post-MAGIC OGJ cell line conditioned media

Healthy donor PBMCs were prepared from whole blood collected in EDTA Vacutainer tubes (BD Biosciences) by density gradient centrifugation over Lymphoprep^{TM} (Stemcell Technologies). PBMCs were plated at a concentration of 1×10^6 cells per ml in complete RPMI media (10% FBS, 1% penstrep) and activated using plate bound anti-CD3 (10 μg/ml, Biolegend, USA) and anti-CD28 (10 μg/ml, Ancell, USA). PBMCs were concomitantly activated in the absence or presence of 50% OGJ cell conditioned media from 48h vehicle-treated OE33/SK-GT-4 cells or FLOT, CROSS CT or MAGIC chemotherapy-treated OE33/SK-GT-4 cells) for 48h. PBMCs were then harvested and stained for flow cytometry.

2.11.3 Co-culture of OE33 cells with supernatants from OGJ patient-derived PBMCs cultured under nutrient deprivation with or without hypoxia for 24h

OE33 cells were seeded at a density of 1 x 10^4 cells/100 μl in cRPMI in a flat bottomed 96 well plate and left adhere overnight. The media was replaced with 100 μl of cRPMI or 100 μl of 1 in 2 diluted supernatant that was collected from OGJ donor PBMCs that had been cultured under hypoxia +/- nutrient deprivation and cultured for 24h at 37°C 5% CO_2.

2.12 OGJ tumour tissue dissociation

Tumour tissue was cut into small 2-3 mm^3 pieces. Tumour tissue biopsy was digested in 5 ml of collagenase type IV solution (50 μl type IV collagenase (1 mg/ml, Sigma-Aldrich) in 5 ml of HBSS buffer at 37ºC on a shaker for 20-30 mins maximum agitation. The digested biopsy

solution was filtered using 70 µm nylon mesh filter into a 50 ml tube (Fisher Scientific) to separate released cells from tissue debris. Filter was washed with 5 ml of HBSS buffer. Cells were washed twice with FACs buffer at room temperature. 100 µl of vortexed cell pellet was transferred to a FACs tube and cells were stained according to the flow cytometry staining protocol.

2.13 Visceral adipose tissue culture

2.13.1 Generation of adipose conditioned media

Visceral adipose tissue was obtained from OGJ patients undergoing surgical resection of tumour post-neoadjuvant treatment at St. James's between 2014 and 2021. The group consisted of 25 males and 6 females, with an average age of 66.4 years. The patient demographics are detailed in **Table 2.9**. Visceral adipose tissue was minced using a scalpel and cultured in M199 (Gibco) with 0.01% gentamicin for 72h at 37°C 5% CO_2 (1 gram of adipose tissue per 2 ml of media). Following 72h incubation the adipose conditioned media (ACM) was filtered using a 70 µM nylon mesh filter (ThermoScientific) and stored at -80°C until required for experimentation.

Table 2.9 Patient demographic table for ACM cohort.

Mean age (years)	**63.9**
Sex ratio (M:F)	25:6
Diagnosis (no. patients)	
OGJ	31
Pathological tumour stage (no. patients)	
T0	3
T1	7
T2	2
T3	19
T4	0
Pathological nodal status (no. patients)	
Positive	12
Negative	19

2.13.2 Culturing of PBMCs with ACM

Healthy donor PBMCs were isolated from whole blood using density gradient centrifugation and expanded with plate bound anti-CD3 (10 µg/ml, Biolegend, USA), anti-CD28 (10 µg/ml,

Ancell, USA) and recombinant human IL-2 (100 units/ml, Immunotools, Germany) for 2 days in the absence and presence of ACM (diluted 1 in 2 using M199 media (Gibco) supplemented with 0.01% gentamicin with or without nivolumab (10 μg/ml), atezolizumab (10 μg/ml), ipilimumab (10 μg/ml), dual nivolumab-atezolizumab (10 μg/ml and 10 μg/ml, respectively), or dual nivolumab-ipilimumab (10 μg/ml and 10 μg/ml, respectively). PBMCs were grown in RPMI 1640 medium with 2 mM L-glutamine (Gibco) and supplemented with 1% (v/v) penicillin-streptomycin (50 U/ml penicillin 100μg/ml streptomycin) and 10% (v/v) foetal bovine serum (Gibco) and maintained in a humidified chamber at 37°C 5% CO_2.

2.14 Flow cytometry staining

2.14.1 Whole blood staining

100 μl of whole blood was added to two FACs tubes with extracellular fluorochrome-conjugated antibodies and incubated for 15 min at room temperature in the dark. Without washing off the antibodies, red cells were lysed using red blood cell lysing solution (Biolegend, USA), according to manufacturer's recommendations: 500 μl of red blood cell lysing solution was added to stained and unstained blood at a concentration of 1X and vortexed well (BD Biosciences, USA, 10X concentration). Red blood cell lysing solution was diluted using distilled water to diluted a 10X solution down to a 1X solution. Tubes were incubated in the dark for an additional 15 mins at room temperature. Cells were washed twice with FACs buffer. Cells were washed with FACs buffer at room temperature. Cells were washed with PBS and stained with zombie aqua viability dye (BioLegend, USA) for 20 mins (1 in 1000 dilution using PBS). Cells were washed with FACs buffer at room temperature and resuspended in 300 μl of FACs buffer. Cells were fixed for 15 min in 1% paraformaldehyde solution (Santa Cruz Biotechnology, USA) and resuspended in FACs buffer and acquired using BD LSR Fortessa flow cytometer (BD Biosciences) using BD FACs Diva Software. Data was analysed using FlowJo v10 software (TreeStar Inc.).

2.14.2 Cell line and PBMC flow cytometry staining

Trypsinised cells, PBMCs, or digested tumour biopsies were transferred to FACs tubes (BD Biosciences, USA) and washed twice with PBS and stained with Zombie aqua, NIR or violet viability dye (BioLegend, USA using an overall 1 in 1000 dilution of Zombie viability dye using PBS) for 15 minutes in the dark at room temperature. Cells were then sequentially stained with appropriate antibodies for 15 minutes in the dark at room temperature: calreticulin-AF488

(Bio-techne, USA), HMGB-1-PE, MIC-A/B-APC, CD45RA-PE/Cy7, CD45RO-BV510, CD3-APC, CD3-PerCP, CD4-BV510, CD4-APC, CD69-BV605, TIGIT-BV605, PD-L2-BV421 (Biolegend, USA), CD69-PE, CD62L-FITC, CD8-BV421, CD3-PEefluor610 (BD Biosciences, USA) or CD4-PerCpCy5.5, CD27-APEefluor780 (eBioscience, USA), A2aR-PE, β-galactosidase-AF405 (Novus Biologics, USA) (**Table 2.10**). Cells were washed with FACs buffer and fixed with 1% paraformaldehyde solution (diluted with PBS), washed with FACs buffer, resuspended in FACs buffer and acquired using BD LSR Fortessa flow cytometer (BD Biosciences) or Cells using the BD FACs CANTO II flow cytometer and BD FACs Diva Software. Data was analysed using FlowJo v10 software (TreeStar Inc.).

Table 2.10 Volume of extracellular fluorochrome-conjugated antibodies added per sample.

Antibody	Company	Antibody Clone	Volume per well/tube
PD-L1-FITC	BD Biosciences (USA)	MIH4	2 µl
PD-L2-PE	Biosciences (USA)	MIH37	2 µl
TIM-3-ViobrightFITC	Miltenyi (Germany)	F38-2E2	2 µl
LAG-3-FITC	BioLegend (USA)	11C3C65	2 µl
PD-1-PE/Cy7	BioLegend (USA)	EH12.2H7	2 µl
TIGIT-PE/Cy7 or TIGIT-BV650	BioLegend (USA)	A15153G	2 µl
CD160-PerCpC5.5	BioLegend (USA)	BY55	2 µl
CTLA-4-PECy5.5	BioLegend (USA)	BNI3	2 µl
KLRG1-APC	Miltenyi (Germany)	REA261	2 µl
CD8-BV421	BioLegend (USA)	SK1	1 µl
CD3-PerCpCy5.5 or CD3-APC or CD3-FITC or CD3-PEeluor610	BioLegend (USA)	OKT3	1 µl
CD4-APC or CD4-BV510	BioLegend (USA)	OKT4	1 µl
CD4-PercPCy5.5	eBiosciences (USA)	RPA-T4	1 µl
CD62L-FITC	BD Biosciences (USA)	SK11	1 µl
CD69-PE	BD Biosciences (USA)	RUO	1 µl
CD69-BV605	BioLegend (USA)	FN50	1 µl
PD-L2-BV421	BioLegend (USA)	MIH18	2 µl
HMGB1-PE	BioLegend (USA)	3E8	2 µl
MIC-A/B-APC	BioLegend (USA)	6D4	2 µl

HLA-DR-FITC	BD Biosciences (USA)	L243	2 µl
Calreticulin-AF405	BioLegend (USA)	SK11	2 µl
CD45RA-PE/Cy7	BioLegend (USA)	HI100	1 µl
CD45RO-BV510	BioLegend (USA)	UCHL1	1 µl
CD27-APCefluor780	eBiosciences (USA)	MIH18	1 µl
A2aR-PE	Novus Biologics (USA)	BY55	2 µl
β-galactosidase-AF405	Novus Biologics (USA)	MIH4	1 µl
CD107a-PE	BD Biosciences (USA)	11C3C65	2 µl

2.14.3 Intracellular flow cytometry staining

For intracellular cytokine staining PBMCs were treated with PMA (10 ng/ml, Sigma Aldrich, USA) and ionomycin (1 µg/ml, Sigma Aldrich, USA) for the last 4h of the incubation. 2 µl of anti-CD107a-PE (BD Biosciences, USA) was added during stimulation. For the last 3h of the incubation PBMCs were treated with brefeldin A (10 µg/ml, eBiosciences). Cells were harvested, washed in FACs buffer and intracellular cytokines were assessed using a Fixation/Permeabilisation kit (BD Biosciences), as per manufacturer's recommendations. Cells were stained with cell surface antibodies first (CD8-BV421, CD3-APC or CD3-PerCP, CD4-PerCP, CD4-APC or CD4-BV510 (Biolegend, USA)) washed, permeabilised, and then stained for intracellular cytokines: IFN-γ-BV510, IL-17A-FITC, IL-4-PE/Cy7, IL-10-PE, IL-2-FITC (Biolegend, USA) and TNF-α-APC (BD Biosciences, USA) (**Table 2.11**). Cells were washed with FACs buffer and fixed with 1% paraformaldehyde solution, washed with FACs buffer, resuspended in FACs buffer and acquired using the BD FACs CANTO II flow cytometer and BD FACs Diva Software. Data was analysed using FlowJo v10 software (TreeStar Inc.).

Table 2.11 Volume of intracellular fluorochrome-conjugated antibodies added per sample.

Antibody	Company	Antibody Clone	Volume per well/tube
IL-17A/F-FITC	BD Biosciences (USA)	9B10	2 µl
TNF-α-APC	BD Biosciences (USA)	MAb11	2 µl
IL-2-FITC	BioLegend (USA)	MQ1-17H12	2 µl
IFN-γ-BV510	BioLegend (USA)	4S.B3	2 µl
IL-10-PE	BioLegend (USA)	JES3-19F1	2 µl
IL-4-PE/Cy7	BioLegend (USA)	8D4-8	2 µl

2.14.4 Annexin V and propidium iodide assay

Apoptosis was measured using annexin V (AV)-FITC (BioLegend, USA) and propidium iodide (PI, BioLegend, USA) staining and was assessed by flow cytometry. Cells were washed with of 1X binding buffer (diluted in PBS from 10X stock: 11.92 g (0.1 M) HEPES pH 7.4, 40.91 g (1.4 M) NaCl, 1.39 g (25 mM) CaCl2 (Fluka), up to 500 ml in dH2O) and then stained with 0.5 µl of Annexin V-FITC (Biolegend, USA) for 15 minutes at room temperature. Cells are washed and resuspended in 50 µl of 1X binding buffer. Immediately before acquisition 50 µl of 1:4000 PI is added to each tube resulting in an overall 1:8000 dilution of PI (diluted in AV binding buffer, Invitrogen, CA, USA). Samples were acquired using BD FACs CANTO II (BD Biosciences) using Diva software and analysed using FlowJo v10 software (TreeStar, Inc., Ashland, Oregon). AV-FITC and PI are excited by the 488 nm laser and AV-FITC emission spectrum is detected using a 530/30 nm filter and PI is detected by a 670-735 nm filter. The annexin V and PI dead cell staining assay identifies viable cells and differentiates between cells which are undergoing early stage apoptosis, late stage apoptosis and necrosis (**Figure 2.3**).

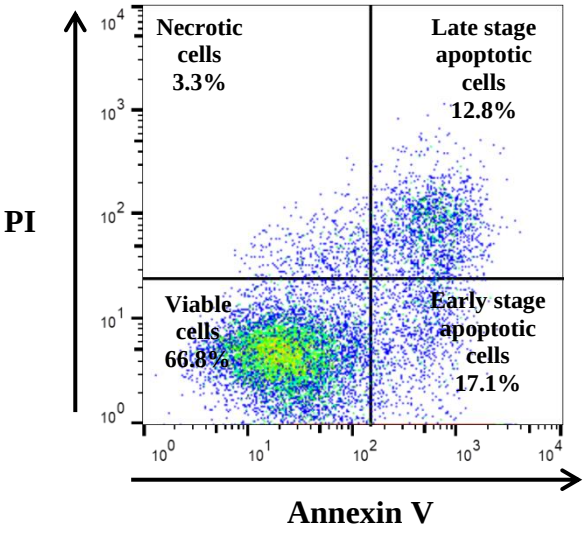

Figure 2.3: Representative dot plot illustrating annexin V and PI staining on the OE33 cancer cell line.

2.14.5 Detection of Ki67 staining by flow cytometry

Cells were collected by trypsinization, fixed in 2.5 ml of ice-cold 70% ethanol (Merck, Darmstadt, Germany) and incubated at room temperature for 30 minutes. The fixative was decanted after centrifugation at 1,300 RPM for 3 mins and cells were resuspended in 100 µl of FACs buffer and stained with 1 µl of Ki67-AF647 (BioLegend). OGJ cells were washed and

resuspended in FACs buffer and acquired using BD FACs CANTO II (BD Biosciences) using Diva software and analysed using FlowJo v10 software (TreeStar Inc.).

2.14.6 Detection of γH2AX by flow cytometry

After treatment, cells were collected by trypsinization, fixed in 2.5 ml of ice-cold 70% ethanol (Merck, Darmstadt, Germany), and incubated at room temperature for 30 minutes. The fixative was decanted after centrifugation at 1,300 RPM for 3 mins with 2 ml of PBS containing 2% FBS. Cells were resuspended in 100 µl γH2AX-FITC staining (BioLegend, 1:100 dilution of antibody using FACs buffer) solution [Triton X100 (0.1%), FBS (2%)] for 2h at room temperature. Cells were washed and resuspended in 100 µl of FACs buffer and acquired using BD FACs CANTO II (BD Biosciences) using Diva software and analysed using FlowJo v10 software (TreeStar Inc.).

2.14.7 Aldehyde dehydrogenase (ALDH) assay

Aldehyde dehydrogenase (ALDH) enzyme activity was assessed using the Aldefluor® assay (Stem Cell Technologies), according to the manufacturer's instructions. Briefly, cells were trypsinised and resuspended at a density of 1 x 10^6 cells/mL in Aldefluor® assay buffer containing ALDH substrate (bodipy-aminOGJetaldehyde) (5 µl/ml). ALDH is excited by the 488 nm laser. Immediately following this, half of the resuspended cells were added to a tube containing the ALDH inhibitor diethylaminobenzaldehyde (DEAB) to provide a negative control. Cells were acquired using BD FACs CANTO II (BD Biosciences) using Diva software and analysed using FlowJo v10 software (TreeStar Inc.).

2.15 Cytolysis assay for assessing lymphocyte-mediated killing of OGJ cells

Cytolysis assay was carried out as previously demonstrated in[230]. Treatment naïve OGJ patient-derived PBMCs were isolated using density gradient centrifugation and expanded using plate bound anti-CD3 (10 µg/ml, Biolegend, USA) and anti-CD28 (10 µg/ml, Ancell, USA) and recombinant human IL-2 (100 units/ml, Immunotools, Germany) for 5 days, (n=6, duplicate technical replicates). OE33 cells were seeded at a density of 5 x 10^3 cells/100 µl of media in a flat 96 well plate and incubated overnight at 37°C, 5% CO_2. The media was replaced and PBMCs were co-cultured with OE33 cells in an effector:target ratio of 5:1 and 10:1 for 48h in the absence or presence of post-vehicle, post-FLOT or post-CROSS CT OE33 conditioned

media (overall 1 in 2 dilution). PBMCs were also cultured alone to use as a control to account for an increase in viability due to their presence in the well. OE33 cells were also cultured alone. Following a 48h co-culture 5 ul of CCK8 (Sigma, USA) was added to each well and the optical density at 450 nm and 650 nm (reference wavelength) was measured using the Versa Max microplate reader (Molecular Devices, Sunnyvale, CA, USA) to determine a viable cell number. Formula: (viability OE33 cell-lymphocyte co-culture)-(viability PBMCs alone)/ (viability untreated OE33 cells alone) x 100 = % live cells[230].

2.16 Human normal, BO and OGJ datasets

Normalized mRNA expression and associated metadata data were obtained and assessed from the Broad Institute, The Cancer Genome Atlas (TCGA) study of normal oesophageal epithelium, Barrett's metaplasia, and oesophageal adenocarcinomas as previously described[231].

2.17 Collection of serum

Whole blood was collected using vacutainer tubes suitable for collecting serum (BD Biosciences). Tubes were centrifuged at 3,000 RPM for 10 minutes at room temperature and serum was collected and stored at -80°C to be used later for experimentation.

2.18 Lactate assay

Lactate concentration was assessed in OGJ donor serum samples (n=41) using the lactate colorimetric/fluorometric assay kit purchased from BioVision (Catalog#K607-100). The assay was carried out as per Manufacturer’s instructions. In brief, 10 µl of each serum sample was added to a flat bottomed 96-well plate in duplicate and 40 µl of Lactate Assay Buffer was added to each sample. To prepare the standard curve the Lactate Standard (MW 90.08) was diluted to 1 nmol/µl by adding 10 µl of the 100 nmol/µl Lactate Standard to 990 µl of Lactate Assay Buffer and 0, 2, 4, 6, 8 and 10 µl of the diluted lactate standard was added to a series of wells in duplicate. The standard curve wells were adjusted to a total volume to 50 µl/well with Lactate Assay Buffer to generate 0, 2, 4, 6, 8 and 10 nmol/well of the L(+)-Lactate Standard. 50 µl Reaction Mix was added to each well and mixed well. To prepare the reaction mix each well should receive 46 µl of lactate assay buffer, 2 ul of lactate enzyme mix and 2 ul of the probe totalling 50 µl of reaction mix per well. A background control was also prepared which contained 98 µl of lactate assay buffer and 2 µl of probe in duplicate. The plate was incubated for 30 minutes at room temperature, protected from light and the absorbance was measure

absorbance at 570 nm using the Versa Max microplate reader (Molecular Devices, Sunnyvale, CA, USA).

2.19 Quantification of serum immune proteins

Serum was prepared according to the manufacturer's instructions (Meso Scale Diagnostics, USA). To assess angiogenic, vascular injury, pro-inflammatory, cytokine, chemokine and soluble checkpoint secretions from the serum, a 54-plex ELISA kit was used (Meso Scale Diagnostics, USA). The multiplex kit was used to quantify the secretions of CRP, Eotaxin, Eotaxin-3, FGF(basic), Flt-1, GM-CSF, ICAM-1, IFN-γ, IL-10, IL-12/IL-23p40, IL-12p70, IL-13, IL-15, IL-16, IL-17A, IL-17A/F, IL-17B, IL-17C, IL-17D, IL-1RA, IL-1α, IL-1β, IL-2, IL-21, IL-22, IL-23, IL-27, IL-3, IL-31, IL-4, IL-5, IL-6, IL-7, IL-8, IL-8 (High Abundance), IL-9, IP-10, MCP-1, MCP-4, MDC, MIP-1α, MIP-1β, MIP-3α, PlGF, SAA, TARC, Tie-2, TNF-α, TNF-β, TSLP, VCAM-1, VEGF-A, VEGF-C and VEGF-D and immune checkpoints PD-1, PD-L1, TIGIT, TIM-3, CD276 and CD80 from TCM. All assays were run as per manufacturer's instructions, with an overnight supernatant incubation protocol used for all assays except Angiogenesis Panel 1 and Vascular Injury Panel 2, which were run according to the same day protocol. This was carried out by Fiona O' Connell and Dr. Margaret Dunne in the Department of Surgery, TCD.

2.20 BrdU assay

Cells were seeded at 5 x 10^3 in 100 µl/ well in a flat 96 well plate in complete RPMI (10% FBS) and were allowed adhere overnight at 37 °C, 5% CO_2. The media was removed, and cells were cultured for 24h in complete RPMI or nutrient deprived media or under hypoxia in the absence or presence of PD-1 blockade or TIGIT blockade. The cell proliferation was then assessed using a BrdU cell proliferation ELISA (Roche Diagnostics Ltd., Sussex, UK) according to the manufacturer's guidelines. The optical density at 450 nm and 690 nm (reference wavelength) was measured using the Versa Max microplate reader (Molecular Devices, Sunnyvale, CA, USA) to determine a viable cell number. Wells containing cells but no BrdU label were used to subtract the background absorbances and the percentage increase/decrease in proliferation was calculated relative to the untreated cells. All of the data were analysed from three independent experiments.

2.21 Western Blot Analysis for Bcl-2 and Bcl-xL

OE33 and OE19 cells were homogenized in RIPA lysis buffer (150 mM NaCl, 0.1% Triton X-100, 0.5% sodium deoxycholate, 0.1% sodium dodecyl sulfate, 50 mM Tris), with added protease/phosphatase inhibitor cocktails (Sigma-Aldrich, Arklow, Ireland). Protein concentration of samples was determined using a BCA protein assay (Pierce, Rockford, IL, USA), and 20 μg samples were boiled in Laemmli buffer and separated on 12 % SDS-PAGE gels. Proteins were transferred to nitrocellulose membranes using wet transfer. The membranes were blocked in 5% non-fat milk TBS, 0.1% Tween 20 detergent (TBST) for 1 h at room temperature prior to being incubated with primary antibodies overnight at 4 °C. The following primary antibodies were used: rabbit anti-Bcl-xL (1:1,000) (Cat #2764S, Cell Signalling, Danvers, MA, US); mouse anti-Bcl-2 (1:500) (Cat #sc-7382, Santa Cruz Biotechnology, Santa Cruz, CA, US); mouse anti-GAPDH (1:1,000) (Cat #MAB374, Sigma-Aldrich) mouse anti-β-actin (1:1,000) (Cat #A5441, Sigma-Aldrich). Membranes were then washed three times with TBST for 5 min prior to being incubated with goat anti-mouse IgG (1:15,000) (#AP124P, Merck KGaA, Darmstadt, Germany) or goat anti-rabbit IgG (1:5,000) (#AP132P, Merck KGaA, Darmstadt, Germany) peroxidase-conjugated secondary antibodies for 1 h at room temperature. Protein bands were visualized using the Immobilon western chemiluminescent HRP substrate (Millipore Sigma) and images were captured using a LAS-3000 imager equipped with a cooled 12 bit digital CCD camera (Fujifilm UK Ltd, Bedfordshire, UK). To guarantee accurate quantifications, special care was taken not to over-expose the protein bands. Densitometry was carried out on 12-bit raw images using Image Studio Lite v5.2 (LI-COR Biosciences Ltd., UK). This was carried out by Marie-Claire Fitzgerald in the Department of Physiology, RCSI.

2.22 Real-time Metabolic analysis

OE33 and OE19 cells were seeded in five wells per treatment group at a density of 10,000 cells/well, in 24-well cell culture XFe24 microplates (Agilent Technologies, Santa Clara, CA, USA) at a volume of 100 μL and allowed to adhere at 37 °C in 5% CO2/95% air. Five hours later, an additional 150 μL/well complete cell culture RPMI medium was added. Following 48 h of incubation, media was removed and cells were washed with unbuffered Dulbecco's Modified Eagle's medium (DMEM) supplemented with 10 mM of glucose and 10 mM of sodium pyruvate, (pH 7.4) and incubated for one hour at 37 °C in a CO2-free incubator. The oxygen consumption rate (OCR) and extracellular acidification rate (ECAR) were measured

using a Seahorse Biosciences XFe24 Extracellular Flux Analyser (Agilent Technologies, Santa Clara, CA, USA). Three basal measurements of OCR and ECAR were taken over 24 min consisting of three repeats of mix (three min)/wait (2 min)/measurement (3 min) to establish basal respiration. Three additional measurements were obtained following the injection of three mitochondrial inhibitors including oligomycin (Sigma Aldrich, Missouri, USA), antimycin-A (Sigma Aldrich, Missouri, USA) and an uncoupling agent Carbonyl cyanide 4-(trifluoromethoxy) phenylhydrazone (FCCP) (Sigma Aldrich, Missouri, USA). ATP turnover was calculated by subtracting the OCR post oligomycin injection from baseline OCR prior to oligomycin addition. Proton leak was calculated by subtracting OCR post antimycin-A addition from OCR post oligomycin addition. Maximal respiration was calculated by subtracting OCR post antimycin addition from OCR post FCCP addition. Non-mitochondrial respiration was determined as the OCR value post antimycin-A addition. All the measurements were normalised to cell number using the crystal violet assay, transferring the eluted stain to a 96-well plate before reading.

2.23 Crystal violet assay

Cells were fixed with 1% glutaraldehyde (Sigma-Aldrich, Missouri, USA) for 15 min at room temperature. The fixative was removed, and cells were washed with PBS and stained with 0.1% crystal violet for 30 min at room temperature. Plates were left to air dry and incubated with 50 µL of 1% Triton X-100 in PBS on a plate shaker for 30 min at room temperature. Absorbance was read at 595 nm on a VersaMax microplate reader (Molecular Devices, Sunnyvale, CA, USA).

2.24 qPCR

2.24.1 RNA isolation and quantification

Cells were seeded at a density of 3×10^6 cells in a T75 flask in 11 ml of cRPMI and allowed to adhere overnight. Following drug treatment RNA was isolated from cell lines using the TRI Reagent® method (**Table 2.12**). The RNA pellet was re-suspended in 30 µl RNAase free molecular grade H_20 and stored at −80 °C. RNA quantification was determined spectrophotometrically, using a Nanodrop 1000 spectrophotometer (version 3.1.0, Nanodrop technologies, DE, USA). 1 µl RNase-free water was used to blank the instrument prior to RNA analysis. 1 µl of each sample of isolated RNA was loaded onto the instrument and concentration was measured in ng/µl.

Table 2.12 Reagents required for RNA isolation.

Reagent		Volume per sample
Trizol	Inhibits RNase activity Lyses cells	0.5 mL
Bromochloropropane	Separates the mixture into 3 phases. Upper aqueous phase (Colourless) Middle DNA phase (white) Lower organic protein phase	50 µl
Isopropanol	Precipitates RNA	250 µl

2.24.2 cDNA synthesis

For cell line samples, total RNA (1 µg total RNA) was reverse transcribed to cDNA using the manufacturer's instructions for the cDNA Reverse Transcription Kit from eBioscienes (4368814). In brief, to anneal the primers to the RNA, a master mix containing RNaseOUT 25X dNTP Mix 10 mm, (10 mM, prepared as a 1:1:1:1 ratio of dATP, dGTP, dTTP and dCTP), 10x rt random primers, Bioscript reverse transcriptase (200units/µl) and 10X Bioscript Reaction Buffer in RNase-free water was added to each sample (**Table 2.12**) and the samples were incubated for 10 mins at 25 ℃, for 120 mins at 37 ℃ then for 5 mins at 85℃ and held at 4 ℃. The resulting cDNA was stored at -20 ℃.

Table 2.13 Preparation of reverse transcriptase master mix.

Component	Volume per sample	Vol per master mix (22 samples per plate)
10 X Reaction Buffer	2 µl	44 µl
25X dNTP Mix 10 mm	0.8 µl	17.6 µl
RNase Out	1 µl	22 µl
multiscribe Reverse Transcriptase enzyme	1 µl	22 µl
Molecular Grade Water	3.2 µl	70.4 µl
10x rt random primers	2 µl	44 µl

		Total of 10 µl per sample

2.24.3 Quantitative real time PCR and analysis

qPCR was performed using TaqMan primer probes (MLH1, SMUG1, PARP1, MMS19 (Roche)) and a Quant Studio 5 real-time thermal cycler (Thermo Fisher Scientific). 18S (eBioscienes) was used as an endogenous control for data normalization. To prepare the gene master mix: use 10 µl of Taq man, 8 ul of molecular grade water and 1 µl of primer probe per sample. Add 19 µl of gene mix to the bottom of each well. Add 1 µl of cDNA-sample to the top corner of each well. For no template control do in single with 19 µl of gene mix and 1 µl of molecular grade water instead of the cDNA-sample. Centrifuge for 1 minute to pool contents. Data analysis was performed using Thermofisher Scientific Connect qPCR application software.

2.24 Statistical Analysis

Data were analysed using GraphPad Prism 5 software (GraphPad Prism, San Diego, CA, USA) and was expressed as mean ± SEM. Statistical differences between two treatments in a particular cell line were analysed using a paired parametric Student's t-test. To compare the statistical differences between two different cell lines an unpaired parametric t-test was conducted. To compare differences between patients and different treatments an unpaired non-parametric t-test was conducted. Statistical differences between treatments within cancer donors or within healthy donors were analysed using paired non-parametric t-test and statistical differences between treatments between healthy donors and cancer donors were analysed using unpaired non-parametric t-tests. Statistical significance was determined as $p \leq 0.05$. Spearman correlations were performed to analyse correlation data between clinical characteristics and flow data and visualised using the R package 'corrplot'. Correlations analysis was carried out by Fiona O' Connell, department of Surgery, TCD.

Chapter 3 – The effect of features of the tumour microenvironment on the efficacy of immune checkpoint blockade; assessing both immune-independent and -dependent effects

Hypothesis

Features of the TME such as nutrient deprivaiton, hypoxia and acidosis upregulate ICs on the surface of OGJ cells and T cells. Blockade of tumour cell-expressed ICs will reduce the survival of OGJ cells under these conditions. Blockade of ICs on the surface of T cells under these conditions will enhance anti-tumour T cell acitivity however, these harsh conditions will likely reduce the efficacy of ICB.

3.1.1 Highlights

- Glucose deprivation and hypoxia upregulate PD-1 and TIGIT on the surface of OGJ cells *in vitro*.
- PD-1 blockade in OGJ cells enhances basal respiration and glycolytic reserve and upregulates GLUT1 on the surface of OGJ cells.
- PD-1 inhibition confers a survival advantage to OGJ cells under glucose deprivaiton and hypoxia.
- TIGIT blockade decreases OGJ cell proliferation and induces OGJ cell death under normoxia, hypoxia and nutrient deprivation.
- TIGIT blockade increases ECAR yet decreases a range of metabolic parameters in OGJ cells.
- Culturing OGJ patient-derived PBMCs under dual hypoxia and glucose deprivation, reflective of the conditions within the hostile TME upregulated an array of ICs on the surface of T cells including PD-1, CTLA-4, A2aR, PD-L1 and PD-L2 and decreased production of IFN-γ by T cells.
- Importantly, addition of nivolumab under these hostile conditions decreased the production of pro-tumourigenic cytokine IL-10.
- Acidic conditions substantially altered immune checkpoint expression profiles of OGJ-derived T cells upregulating TIM-3, LAG-3 and CTLA-4.
- Severe acidic conditions (pH 5.5) significantly decrease the percentage of OGJ-derived central memory $CD4^+$ T cells, an effect that was attenuated by ICB treatment.
- ICB increases T cell production of IFN-γ under moderately acidic conditions (pH 6.6) but not severe acidic conditions (pH 5.5) and decreases IL-10 production by T cells under severe acidic conditions only.

- Our findings establish that features of the TME induce upregulation of immune checkpoints on OGJ cells and T cells which may potentially contribute to immune evasion in OGJ.
- The use of ICB to suppress pro-tumourigenic processes in OGJ cells and enhance anti-tumour T cell immunity under conditions that recapitulate the harsh TME are highlighted supporting a rationale for the use of ICB to boost response rates in OGJ.

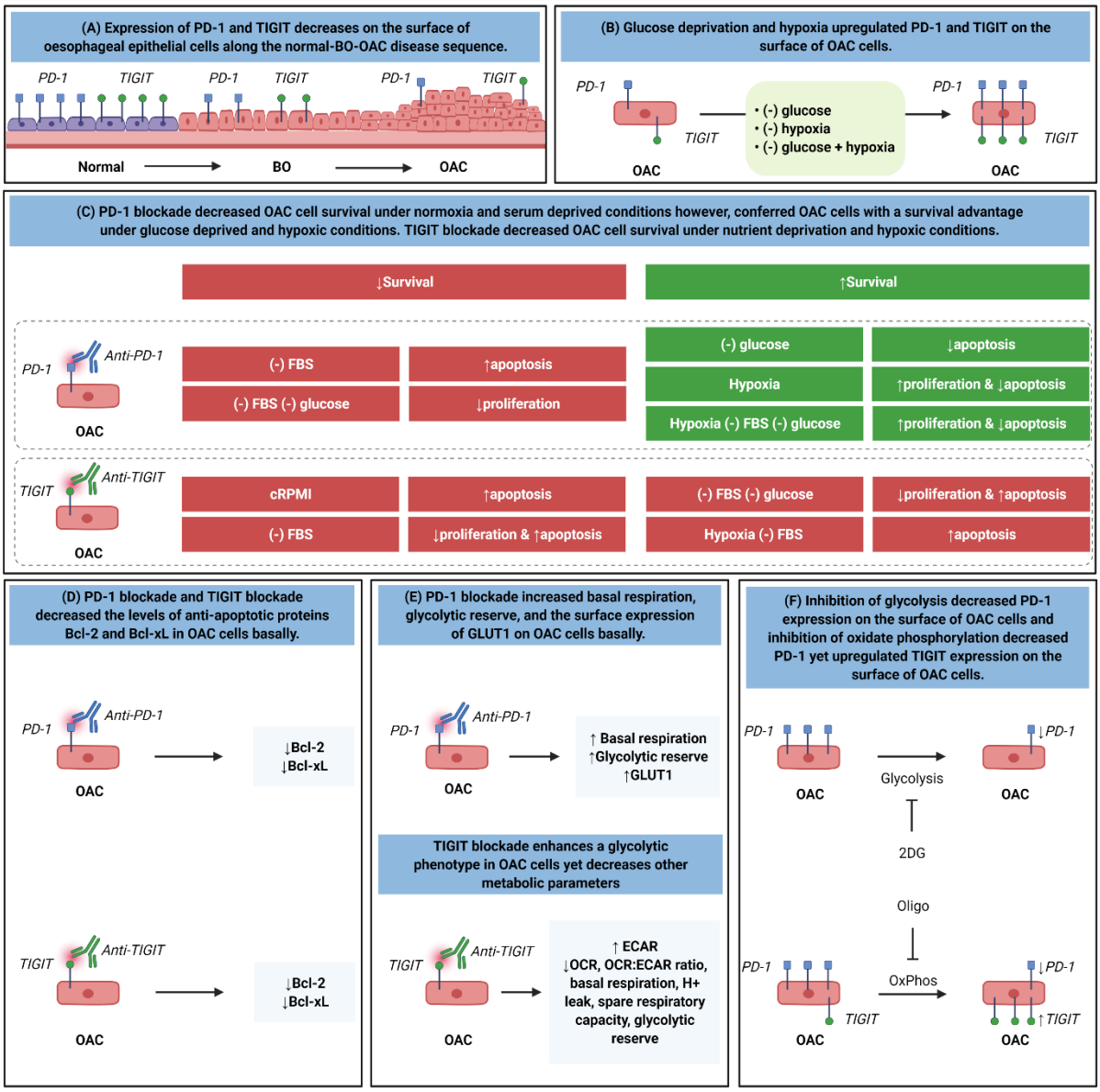

Graphical abstract 1: (A) Expression of PD-1 and TIGIT decreases on the surface of oesophageal epithelial cells along the normal-BO-OAC disease sequence. (B) Glucose deprivation and hypoxia upregulated PD-1 and TIGIT on the surface of OAC cells. (C) PD-1 blockade decreased OAC cell survival under normoxia and serum deprived conditions however, conferred OAC cells with a survival

advantage under glucose deprived and hypoxic conditions. TIGIT blockade decreased OAC cell survival under nutrient deprivation and hypoxic conditions. (D) PD-1 blockade and TIGIT blockade decreased the levels of anti-apoptotic proteins Bcl-2 and Bcl-xL in OAC cells basally. E. PD-1 blockade increased basal respiration, glycolytic reserve, and the surface expression of GLUT1 on the surface of a subpopulation of OAC cells basally. TIGIT blockade enhanced a glycolytic phenotype in OAC cells yet decreased other metabolic parameters basally. (F) Inhibition of glycolysis decreased PD-1 expression on the surface of a subpopulation of OAC cells and inhibition of oxidate phosphorylation decreased PD-1 yet upregulated TIGIT expression on the surface of a subpopulation of OAC cells.

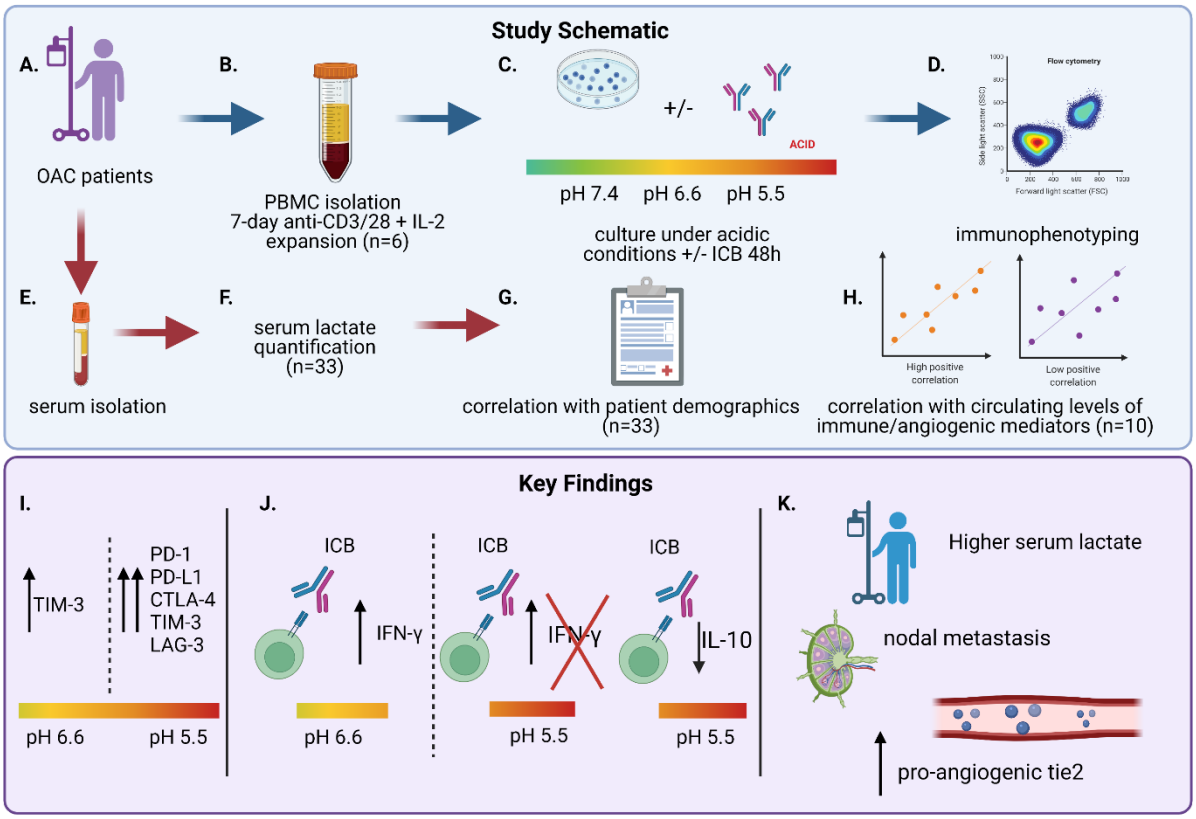

Graphical abstract 2: Study schematic – PBMCs were isolated from OAC patients (A) and expanded ex vivo for 7 days using anti-CD3/28+IL-2 T cell activation protocol (B) and further cultured for 48h under increasing acidic conditions in the absence or presence of immune checkpoint blockade (nivolumab, ipilimumab or dual nivolumab + ipilimumab) (C). Immunophenotyping was then carried out to assess immune checkpoint expression profiles and anti-tumour T cell phenotypes (D). Serum lactate was assessed in OAC patients (E-F) and levels were correlated with patient demographics (G) and the levels of circulating immune/pro-angiogenic cytokines that were determined by multiplex ELISA (H). Key Findings – severe acidic conditions upregulated multiple immune checkpoints on T cells (I). Efficacy of ICB was curtailed under severe acidic conditions (J). Circulating lactate levels positively correlated with circulating levels of pro-angiogenic factor tie-2 and higher serum lactate levels were found in patients who had nodal metastasis (K).

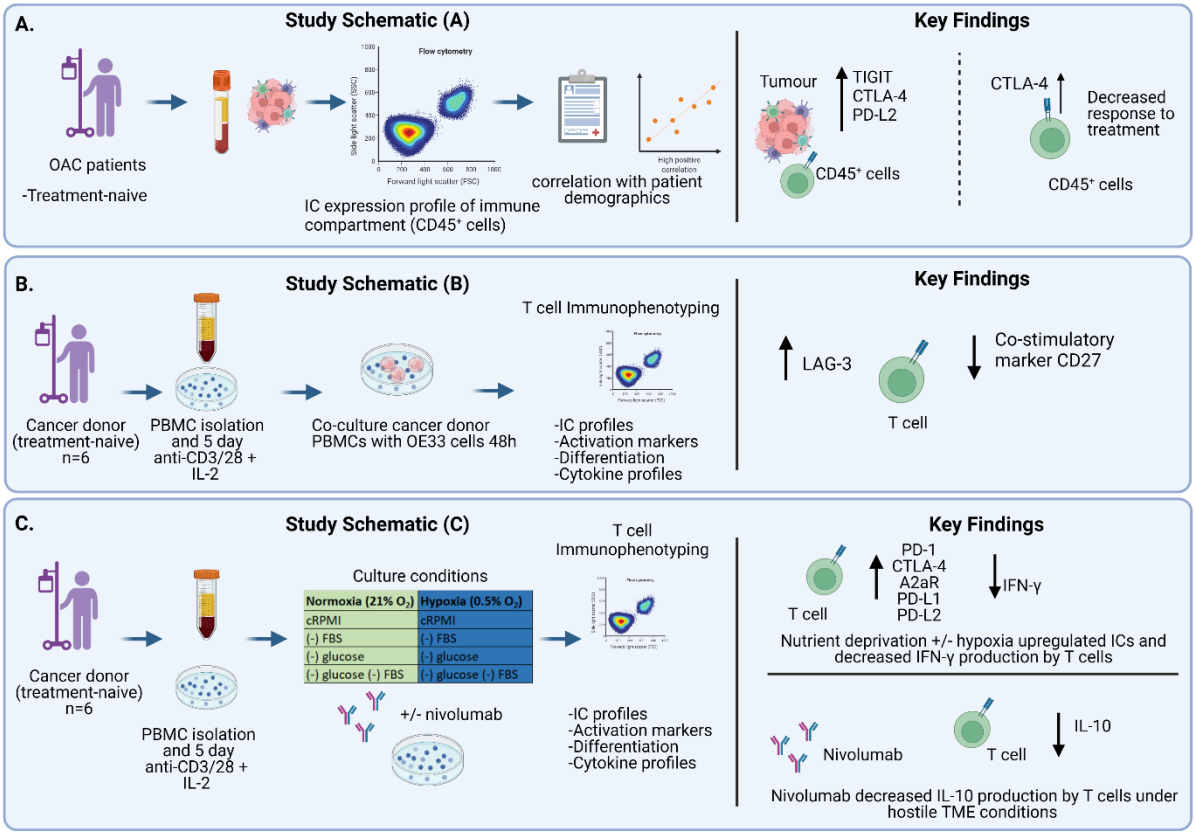

Graphical abstract 3: Study schematic – (A) IC expression profiles were assessed on CD45$^+$ cells in peripheral whole blood and infiltrating tumour tissue from OGJ patients in the treatment-naïve setting. (B) PBMCs were isolated from OAC patients and expanded *ex vivo* for 5 days using anti-CD3/28+IL-2 T cell activation protocol and then co-cultured for 48h with OE33 cells. T cell phenotypes were then assessed by flow cytometry. (C) PBMCs were isolated from OAC patients and expanded ex vivo for 5 days using anti-CD3/28+IL-2 T cell activation protocol and then further cultured under conditions of nutrient deprivation or hypoxia for 48h and T cell phenotypes were then assessed by flow cytometry. Key findings – (A) TIGIT, CTLA-4 and PD-L2 were upregulated on stromal immune cells and CTLA-4 expression on CD45$^+$ cells correlated with a subsequent decreased response to neoadjuvant regimen. (B) Following a 48h co-culture with OE33 cells, T cells upregulated LAG-3 and decreased CD27 co-stimulatory marker. (C) Nutrient deprivation and hypoxia upregulated a range of ICs on T cells and decreased IFN-γ production by T cells. Nivolumab decreased IL-10 production by T cells under nutrient deprivation-hypoxic conditions.

3.1.2 Introduction

The cellular composition of the TME plays a pivotal role in the development and progression of oesophagogastric junctional cancer (OGJ), including dictating response to the current standards of care[83]. Targeting inhibitory immune checkpoints (ICs) is an attractive therapeutic

strategy to reinvigorate exhausted anti-tumour immunity in OGJ. Interestingly, recent studies have demonstrated that IC ligands and receptors are expressed on the surface of tumour cells in a range of malignancies such as melanoma, lung, head and neck and colorectal cancer[182,184–186,188–191,232]. In addition IC tumour cell intrinsic signalling has been shown to promote various hallmarks of cancer including glycolysis[180], DNA repair[181], proliferation[182] invasion and migration[233,183]. Liu *et al*., have demonstrated that PD-1 intrinisc signalling in gastric tumour cells protects against 5-FU induced cell death[202]. However, it remains to be investigated if IC-intrinsic signalling in OGJ cells might confer a survival advantage under the harsh physiological conditions of the tumour microenvironment (TME). Therefore, we investigated the effect of characteristic features of the hostile TME, such as nutrient deprivation and hypoxia on IC expression by OGJ cells. Importantly, we assessed if ICB under these TME conditions might promote or inhibit the surival of OGJ cells. The effect of ICB on the metabolic phenotype of OGJ cells was also assessed as nutrient deprivation and hypoxia have profound effects on metabolism in OGJ cells[234] and PD-L1 intrinsic signalling in melanoma cells has been shown to enhance a glycolytic phenotype in renal cancer cells[235] and non-small cell lung cancer[236]. Importantly, this current study also investigated the expression of a range of inhibitory ICs on the surface of oesophageal cells along the normal-BO-OGJ disease sequence to determine if expression is altered as disease progresses. Previous studies have demonstrated that TIM-3[232] and PD-1[237] IC receptors were significantly upregulated along the normal-pre-malignant-carcinoma disease sequence in cervical cancer and pancreatic cancer, respectively. Therefore, gaining a deeper insight into the changes in IC expression across the malignant progression sequence could identify appropriate ICs to target to block disease progression from BO to OGJ. In addition, the TME imposes profound metabolic restrictions on antitumour T cells, understanding these insights is important for informing immunotherapeutic anticancer strategies[104]. Therapeutic approaches such as those that target metabolic restrictions, including low glucose levels and hypoxia, have shown promise as combination therapies for different types of cancer[105]. Firstly, nutrient deprivation and hypoxia, have a profound impact on the cellular composition of the TME, subsequently promoting or hindering anti-tumour immune responses. Tumour hypoxia promotes the recruitment of regulatory T cells through induction of expression of the chemokine CC-chemokine ligand 28 which, in turn, promotes tumour tolerance and angiogenesis[117]. In addition, cancer cells grow rapidly outcompeting anti-tumour immune cells for essential nutrients subsequently producing metabolic by-products that are

toxic to immune cells, such as lactate, resulting in a both a nutrient starved and acidic hostile environment for the anti-tumour immune cells[238].

The TME is often described as a glucose deprived environment, attributed to a poorly-vascularised TME and cancer cells sequestering glucose for glycolysis to facilitate tumour progression[106]. These distinct metabolic pathways in tumour cells cause functional impairment of immune cells and contribute to immune evasion by cancer[106]. Glucose is also an essential nutrient for the metabolic demands and function of anti-tumour immune cells, particularly effector T cells[110]. Glucose is an essential nutrient which plays an important role during the early stages of T cell activation in regulating T cell differentiation and maintaining activation states[110]. T cell activation involves a dramatic increase in nutrient uptake. Depletion of glucose in cell culture media during the early stages of T cell activation inhibits T cell expansion, cytokine production and suppresses pro-inflammatory T cell differentiation[111]. Conversely, regulatory T cells thrive in a glucose depleted environment as these cell types predominantly rely on fatty acid oxidation to fulfil their energy demands[112]. Moreover, the TME is often depleted in amino acids, which are also an important fuel for many cellular processes for both tumour cells and immune cells[239]. The amino acid consumption of tumour cells and pro-tumour immune cells is increased compared with normal cells, creating a nutrient-depleted microenvironment, which negatively hinders anti-tumour immune cells[240].

Metabolic reprogramming in T cells during their activation and differentiation have led to an emerging concept of "immunometabolism"[113]. Considering the recent success of cancer immunotherapy in the treatment of several cancer types, increasing research efforts are being made to elucidate alterations in metabolic profiles of cancer and immune cells during their interplays in the setting of cancer progression and immunotherapy[114]. Therefore, immunometabolism is a key factor in regulating immune responses in the tumour. ICB in particular PD-1 blockade, promotes the metabolic fitness of exhausted immune cells, reinvigorating an exhausted phenotype and enhancing anti-tumour effector T cell responses[115]. However, a substantial number of OGJ patients possess tumours refractory to ICB[98]. It is thought that concurrent targeting of ICs and targeting immunometabolism pathways may have a greater effect in restoring effector functions to exhausted T cells[115]. However, more in-depth research is required to study how the nutrient depleted and hypoxic TME might shape immune T cell function and alter responses to ICB in the context of OGJ.

Furthermore, tissue acidosis (pH 6.0 to 7.0) is typically accompanied with inflammatory processes in peripheral tissues, where the pH can decrease as low as 5.5[123]. Moreover, acidosis

is a hallmark feature of solid tumours ranging from a pH of 5.7 to 7.0[241,242]. A combination of poor tissue perfusion and high rates of lactic acid due to fermentative glycolytic metabolism contribute to the generation of an acidic tumour microenvironment[243]. This acidity also contributes to tumour progression by substantially altering both the innate and adaptive immune responses. Overall a low pH has been shown to suppress anti-tumour immunity and promote the pro-tumourigenic arm of the immune system[244]. However, extracellular acidosis can either stimulate or suppress innate immune responses depending on both the cell type involved and the particular response analysed[244]. However, it has been suggested that a high concentration of protons as a consequence of a low pH might be recognized by innate immune cells as a danger-associated molecular pattern[123]. Extracellular acidosis (pH 6.5) increased the endocytic activity of DCs and the expression of MHC class II, CD40, and CD86[245]. Moreover, DCs pulsed with antigens at low pH values showed an improved efficacy to induce specific cytotoxic responses mediated by $CD8^+$ T cells as well as specific antibody responses *in vivo*[245]. DCs derived from monocytes cultured with IL-4 and GM-CSF, transient exposure of DCs to pH 6.5 markedly increases the expression of HLA-DR, CD40, CD80, CD86, CD83, and CCR7, improves the T cell priming ability of DCs, and increases the production of IL-12, stimulating the synthesis of IFN-γ, but not IL-4, by Ag-specific $CD4^+$ T cells[246]. Similarly, Tong *et al*. further confirmed the ability of extracellular acidosis to induce the phenotypic maturation of human DCs via activation of acid sensing ion channels, a family of proton receptors[247].

In contrast, a large body of evidence indicates that low pH has been shown to suppress the cytotoxic response mediated by $CD8^+$ T cells as well as the production of IFN-γ by Th1 cells[124]. Calcinotto *et al*.,[125] have shown that lowering the environmental pH to values of 6.0-6.5 induced an anergic state in human and mouse tumour-specific $CD8^+$ T cells, characterized by impaired cytotoxic activity, inhibition of cytokine production, reduced expression of the alpha chain of the IL-2R (CD25), and a diminished activation of extracellular signal-regulated kinase (ERK) and STAT5 upon T cell activation[125]. However, buffering the pH to neutral values restored T cell function[125,248]. Moreover, systemic treatment of tumour-bearing mice with proton pump inhibitors improved the therapeutic efficacy of immunotherapy, suggesting that proton pump inhibitors might represent useful therapeutic tools to reverse the anergy of tumour-infiltrating T cells and to improve the performance of immunotherapy approaches used in cancer[249].

Glucose deprivation and hypoxia inhibit anti-tumour immune responses in several solid tumour types which has yet to be investigated in OGJ. Effective anti-tumour immunity is a pre-requisite

for successful chemotherapy treatment as well not just immunotherapy treatment. Furthermore, hypoxia treatment promotes more resistant tumour cell types to emerge that are more aggressive and pro-metastatic[250]. Hypoxia has several knock on effects in promoting other key hallmarks of cancer such as angiogenesis in an attempt to reoxygenate the poorly vascularised tumour that is contributing to the hypoxic state[250]. For this reason escape of pro-metastatic tumour cell clones is facilitated by these new blood vessels, allowing them to migrate to distal sites in the body to form micrometastatic niches in secondary sites[250]. Hypoxia has also been described as a key cause of radiation resistance in several tumour types including OGJ[251]. Therefore, understanding the effects of hypoxia on T cell phenotypes and how ICBs work under these hostile TME conditions is important for designing more successful treatments for OGJ patients that could include ICBs.

Importantly, this study also investigates the direct effect of nutrient deprivation (serum deprivation and glucose deprivation), hypoxia and acidosis on the IC expression profiles of T cells and T cell function using OGJ patient-derived T cells. Importantly, the ability of nivolumab to promote anti-tumour T cell-mediated immunity under conditions reflective of the hostile TME is also explored. Collectively, these findings will help guide the clinical development of rationale immunotherapeutic strategies to improve immune responses within the inhospitable TME for treating OGJ patients. We also assess systemic lactate levels in OGJ patients post-treatment and correlate these levels with clinical characteristics to provide a deeper insight into how serum lactate levels may be used as a clinical indicator of treatment response and prognosis. Importantly systemic lactate levels are also correlated with circulating levels of pro-tumourigenic and anti-tumourigenic immune mediators as well as pro-angiogenic factors to shed light on potential pro-tumourigenic processes that may be interlinked with the lactate axis.

3.1.3 Specific aims

1. Investigate IC expression profiles on the surface of oesophageal cells along the normal-BO-OGJ disease sequence to determine if expression is altered as disease progresses.
2. Investigate the effect of characteristic features of the hostile TME such as nutrient deprivation (serum deprivation and glucose deprivation) and hypoxia on IC expression on OGJ cells and if ICB under these conditions might promote or inhibit the surival of OGJ cells.
3. Determine the effect of ICB on the metabolic phenotype of OGJ cells.

4. Assess the direct effect of nutrient deprivation (serum deprivation and glucose deprivation) and hypoxia on the function of T cells in particular the expression profile of ICs and the ability of nivolumab to promote anti-tumour T cell-mediated immunity under these conditions.
5. Examine the direct effects of acidosis on T cell function and the ability of ICB to enhance T cell immunity under these conditions.

3.2 Results

3.2.1 PD-1 and TIGIT expression on the surface of oesophageal epithelial cells decreases along the normal-BO-OGJ disease sequence

This study investigated the expression profile of a range of inhibitory ICs along the normal-BO-OGJ disease sequence. IC expression was assessed at the mRNA level in normal, BO and OGJ tissue using online RNA sequencing databases obtained from the Broad Institute, The Cancer Genome Atlas (TCGA) study of normal oesophageal epithelium, Barrett's metaplasia, and oesophageal adenocarcinomas as previously described[231]. RNA-sequenced data was only available for PD-L2 and CD160 IC ligands and PD-1, LAG-3 and A2aR IC receptors across the normal-BO-OGJ disease sequence (**Figure 3.1A**). These tissue samples comprised all the cells within the TME that might contribute to IC expression in the tissue. Levels of PD-L2 mRNA were significantly reduced in BO tissue compared with normal oesophageal tissue and trended toward a significant increase in the mRNA levels of PD-L2 in OGJ tissue compared with BO tissue (normal:14.31 ± 1.6% vs. BO:9.6 ± 0.9%, OGJ:13.53 ± 0.9% p=0.02 and p=0.06, respectively) (**Figure 3.1A**). In addition, mRNA levels of LAG-3 were significantly reduced in BO tissue compared with normal oesophageal tissue (normal:139.3 ± 21.6% vs. BO:61.38 ± 13.7%, p=0.01), (**Figure 3.1A**). There were no significant alterations in A2aR, CD160 or PD-1 across the disease sequence at the mRNA level (**Figure 3.1A**).

To determine if IC expression profiles on just the oesophageal epithelial cells was altered across the normal-BO-OGJ disease sequence, cell line models of normal oesophageal epithelial cells (HET-1A cells), metaplastic BO cells (QH cells) and OGJ cells (OE33 cells and OE19 cells) were screened by flow cytometry for the surface expression of a range of ICs (**Figure 3.1B**). Interestingly, the surface expression of PD-1 on oesophageal epithelial cells significantly decreased across the normal-BO-OGJ disease sequence. OE33 cells expressed significantly less PD-1 compared with the HET-1A cells (8.30 ± 3.0% vs. 27.8 ± 5.5%, p=0.02) (**Figure 3.1B**). Similar trends were observed in the OE19 cells, in which PD-1 was expressed at significantly lower levels on OE19 cells compared with the HET-1A cells (5.80 ± 0.5% vs.

27.8 ± 5.5%, p=0.008) (**Figure 3.1B**). Similarly, TIGIT protein expression significantly decreased on the surface of epithelial cells across the normal-BO-OGJ disease sequence with a reduction in TIGIT expression on the surface of QH cells compared with HET-1A cells (14.69 ± 2.5% vs. 30.00 ± 5.1%, p=0.05). A significantly lower percentage of OE33 cells expressed TIGIT compared with the HET-1A cells (7.29 ± 1.9% vs. 30.00 ± 5.1%, p=0.01), as was the case for OE19 cells compared with HET-1A cells (3.20 ± 0.4% vs. 30.00 ± 5.1%, p=0.001) (**Figure 3.1B**). Furthermore, significantly less OE19 cells expressed TIGIT compared with QH cells (3.20 ± 0.4% vs. 14.69 ± 2.5%, p=0.02). Low levels of the IC ligands PD-L1, PD-L2, CD160, LAG-3, TIM-3 and A2aR were detected on the surface of HET-1A cells, QH cells, OE33 cells and OE19 cells, however, there was no significant difference in the expression of these ICs between the different cell types across the normal-BO-OGJ disease sequence (**Figure 3.1B**).

Overall, these findings demonstrated that IC expression is significantly altered in oesophageal tissue across the normal-BO-OGJ disease sequence at the mRNA level. Reductions in PD-L2 and LAG-3 mRNA were found specifically in BO tissue compared with normal tissue however, the levels of PD-L2 and LAG-3 mRNA were comparable between normal tissue and OGJ tissue. Interestingly, specific alterations in IC expression profiles on the surface of epithelial cells was observed, in which PD-1 and TIGIT were significantly decreased across the disease sequence from normal-BO-OGJ.

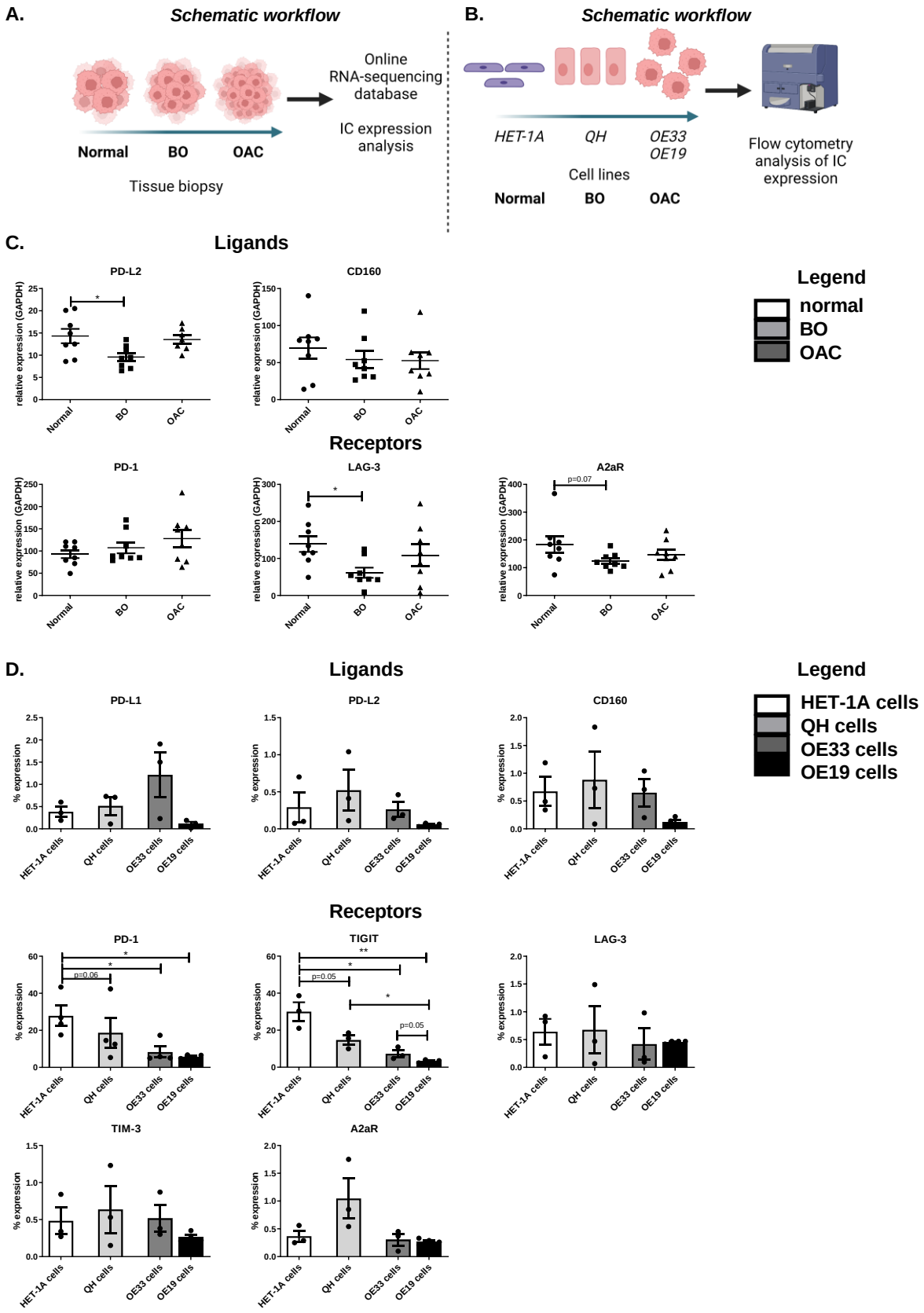

Figure 3.1: The expression of PD-1 and TIGIT on the surface of oesophageal epithelial cells decreases along the normal-BO-OGJ disease sequence. (A) Schematic workflow for assessing

mRNA levels of inhibitory IC ligands and receptors were assessed in 8 normal oesophageal tissue samples, 8 BO tissue samples and 8 OAC tissue samples from online RNA-sequenced databases[231]. The inhibitory IC ligands available in the database included: PD-L2 and CD160 and the IC receptors available included: PD-1, LAG-3 and A2aR (C) (PD-L1 and TIGIT were not sequenced so the data was unavailable). Kruskal-Wallis with uncorrected Dunn's test. Expression presented relative to GAPDH ± SEM. (B) Schematic workflow for analysing the IC ligand and IC receptor expression on the surface of HET-1A, QH, OE33 and OE19 cells by flow cytometry. The inhibitory ligands assessed include PD-L1, PD-L2 and CD160 and the inhibitory IC receptors include PD-1, TIGIT, LAG-3, TIM-3 and A2aR (D). Pooled analysis of 4 independent biological replicates that were carried out using singlet technical replicates. Mixed-effects analysis, Tukey's multiple comparison. *p<0.05 and **p<0.01. Data expressed as ± SEM.

3.2.2 Glucose deprivation and hypoxia upregulate PD-1 and TIGIT on the surface of OGJ cells

As OGJ cells express significantly less PD-1 and TIGIT compared with normal oesophageal cells, we sought to investigate if features of the hostile TME including hypoxia and nutrient deprivation might alter the expression of PD-1 and TIGIT on the surface of viable OGJ cells *in vitro* (**Figure 3.2**). Glucose deprivation for 24h significantly upregulated PD-1 on the surface of viable OE33 cells compared with cells cultured in cRPMI *in vitro* (cRPMI:4.86 ± 1.5% vs. glucose-deprivation:24.9 ± 3.2%, p=0.008), (**Figure 3.2**). In addition, 24h hypoxia and combined glucose-deprivation with hypoxia significantly upregulated PD-1 on the surface of viable OE19 cells *in vitro* (cRPMI:2.46 ± 0.1% vs. hypoxia:4.63 ± 0.4%, combined glucose-deprivation with hypoxia:17.03 ± 2.2%, p=0.04 and p=0.01, respectively), (**Figure 3.2**). Similarly, 48h combined glucose-deprivation with hypoxia significantly upregulated PD-1 on the surface of viable OE19 cells compared with cells cultured in cRPMI (cRPMI:5.18 ± 0.7% vs. combined glucose-deprivation with hypoxia:13.77 ± 2.0%, p=0.02).

Furthermore, 24h glucose deprivation and combined glucose-deprivation with hypoxia significantly upregulated TIGIT on the surface of viable OE33 cells compared with cells cultured in cRPMI *in vitro* (cRPMI:5.43 ± 1.6% vs. hypoxia:24.9 ± 3.2, combined glucose-deprivation with hypoxia:27.50 ± 2.0%, p=0.007 and p=0.003, respectively), (**Figure 3.2**). Similarly, 24h hypoxia and combined glucose-deprivation with hypoxia significantly upregulated TIGIT on the surface of viable OE19 cells compared with cells cultured in cRPMI *in vitro* (cRPMI:2.2 ± 0.1% vs. hypoxia:7.23 ± 0.5%, combined glucose-deprivation with hypoxia:15.93 ± 1.0%, p=0.001 and p=0005, respectively), (**Figure 3.2**). Similarly, 48h

combined glucose-deprivation with hypoxia significantly upregulated TIGIT on the surface of viable OE19 cells compared with cells cultured in cRPMI *in vitro* (cRPMI:6.38 ± 0.7% vs. combined glucose-deprivation with hypoxia:12.50 ± 1.3%, p=0.01), (**Figure 3.2**).

In addition, we also assessed whether the levels of mutated HIF-1α in a cohort of OGJ patients available from TCGA database correlated with survival outcomes, and we found that there was no significant difference in the survival of OGJ patients who had a mutated HIF-1α gene compared with wild-type (Figure 3.2L).

Overall, glucose-deprivation, hypoxia, or combined glucose-deprivation with hypoxia significantly upregulated PD-1 and TIGIT on the surface of OGJ cells *in vitro*.

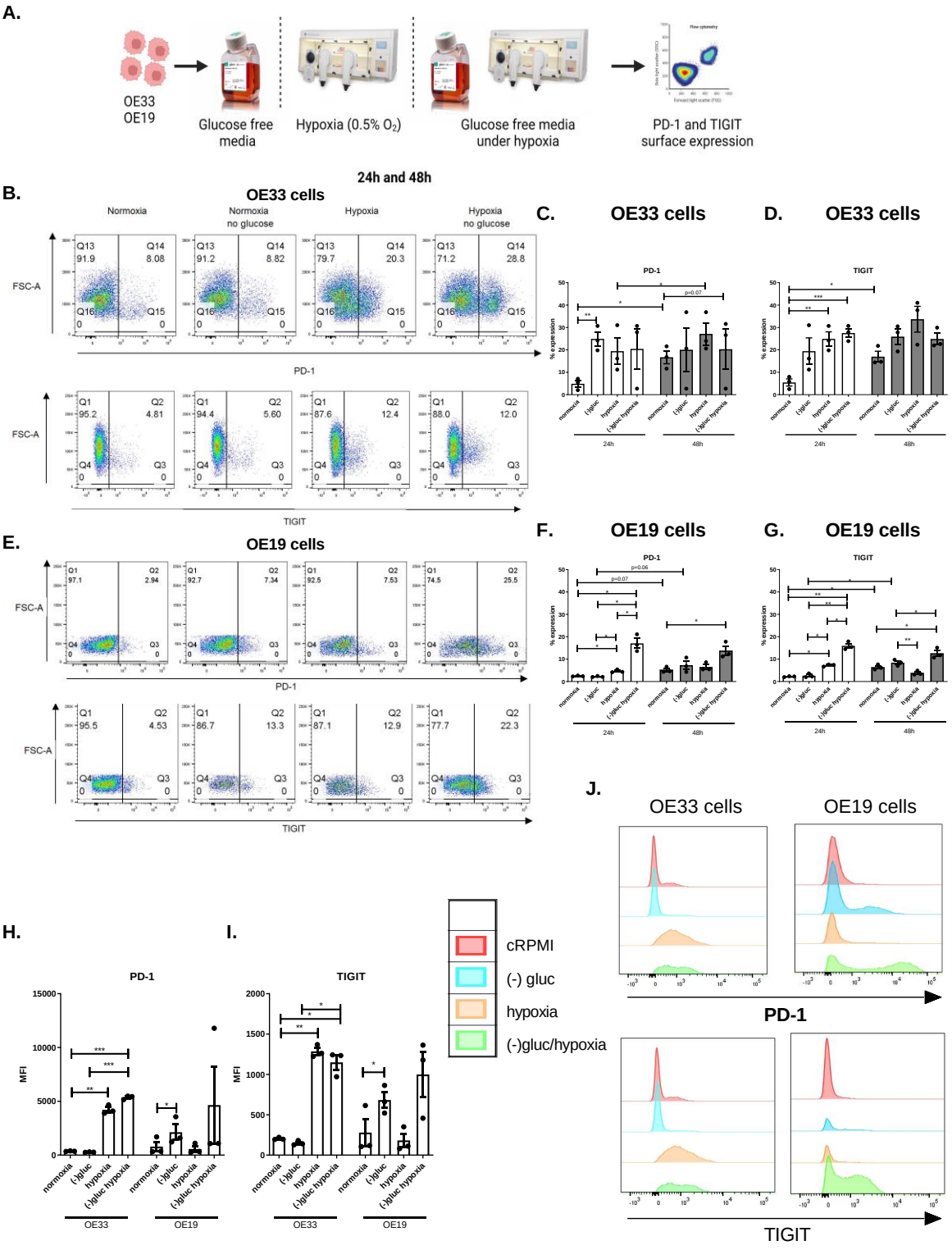
A.
OE33
OE19
Glucose free media
Hypoxia (0.5% O2)
Glucose free media under hypoxia
PD-1 and TIGIT surface expression
24h and 48h
B.
OE33 cells
Normoxia
Normoxia no glucose
Hypoxia
Hypoxia no glucose
FSC-A
PD-1
TIGIT
C.
OE33 cells
PD-1
D.
OE33 cells
TIGIT
E.
OE19 cells
F.
OE19 cells
PD-1
G.
OE19 cells
TIGIT
H.
PD-1
MFI
OE33
OE19
I.
TIGIT
cRPMI
(-) gluc
hypoxia
(-)gluc/hypoxia
J.
OE33 cells
OE19 cells
PD-1
TIGIT

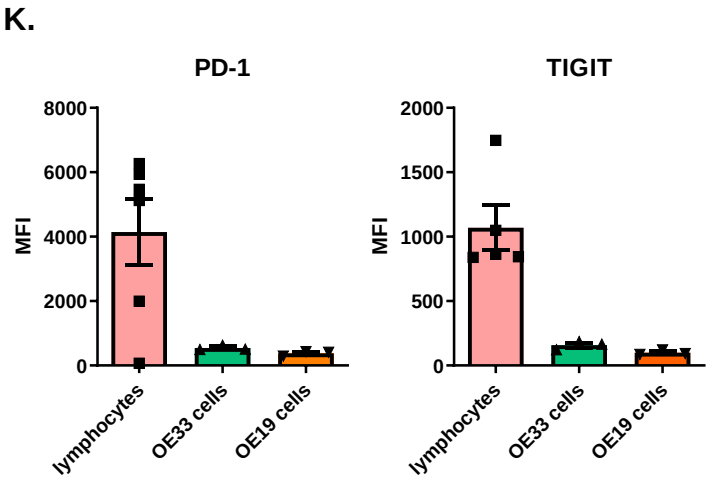

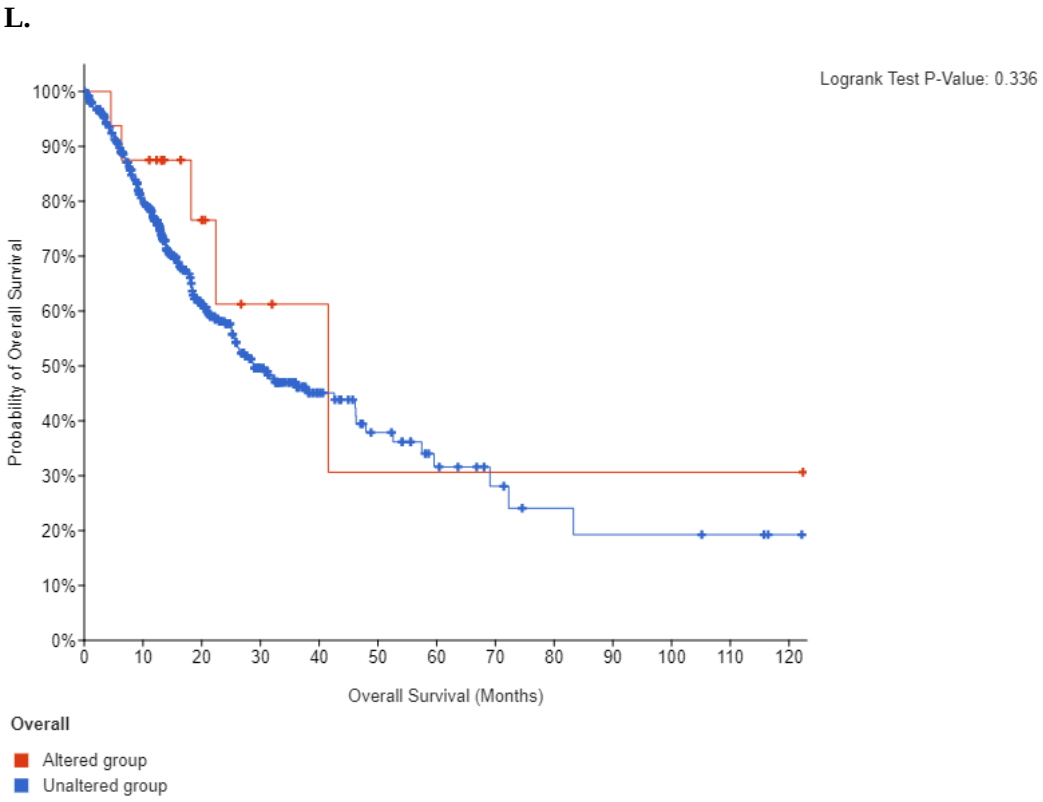

Figure 3.2: Glucose deprivation and hypoxia significantly increase the percentage of viable OGJ cells expressing PD-1 and TIGIT. (A) Schematic workflow. OE33 and OE19 cells were cultured in normoxia (white bars), with glucose deprivation, hypoxia (0.5% O_2) (grey bars) and combined glucose deprived hypoxic conditions for 24h and 48h. The surface expression of inhibitory IC receptors PD-1 and TIGIT on viable OAC cells was assessed by flow cytometry. Representative dot plots displayed showing effect of each condition following 24h treatment on PD-1 and TIGIT expression on the surface of viable OE33 cells (B) and OE19 cells (E). (C) and (D) depicts PD-1 and TIGIT percentage expression on OE33 cells and (F) and (G) depicts PD-1 and TIGIT percentage expression on OE19 cells. Median fluorescence intensity (MFI) for PD-1 (H) and TIGIT (I) expression in OE33 and OE19 cells following

24h under each condition. (J) Representative histograms showing MFI levels for PD-1 and TIGIT in OE33 and OE19 cells under each condition. (K) Displays the MFI levels for PD-1 and TIGIT in peripheral blood lymphocytes (isolated from n=6 treatment-naïve OGJ donor peripheral blood samples) vs. OE33 (n=3) and OE19 (n=3) cells. Pooled analysis for 3 independent biological replicates carried out using singlet technical replicates. *p<0.05, **p<0.01 and ***p<0.001. Paired, parametric t-test. Data expressed as ± SEM. (L) details the overall survival of OGJ patients with a mutated copy of the HIF-1α gene compared with patients who had unaltered HIF-1α using data from TCGA.

3.2.3 PD-1 blockade increases OGJ cell proliferation under hypoxia and TIGIT blockade reduces OGJ cell proliferation under dual glucose and serum deprivation

Given that hostile features of the TME such as hypoxia and nutrient deprivation upregulated PD-1 and TIGIT on the surface of OGJ cells, we aimed to investigate if PD-1 or TIGIT upregulation might provide OGJ cells with a survival advantage under these unfavourable conditions. Therefore, the effect of single agent PD-1 blockade and TIGIT blockade on the viability of OGJ cells was assessed under complete RPMI conditions, nutrient deprivation, hypoxia and combined nutrient deprivation-hypoxia following 24h culture (**Figure 3.3A and Figure 3.3B,** respectively).

PD-1 blockade decreased the proliferation of OE33 cells under dual serum deprivation-glucose deprivation compared with untreated cells cultured in dual serum deprivation-glucose deprivation (84.8 ± 1.1% vs. 102.0 ± 1.2%, respectively p=0.02), (**Figure 3.3A**). Contrastingly, PD-1 blockade increased the proliferation of OE33 cells under hypoxia compared with untreated cells cultured under hypoxia (100.7 ± 5.6% vs. 93.21 ± 4.5%, p=0.04), (**Figure 3.3A**). PD-1 blockade did not have a significant effect on the proliferation of OE19 cells cultured in complete RPMI conditions, nutrient deprivation, hypoxia, or dual nutrient deprivation-hypoxia (**Figure 3.3A**).

Interestingly, TIGIT blockade significantly decreased the proliferation of OE33 cells under serum deprivation compared with untreated cells cultured in serum deprived media (84.84 ± 0.8% vs. 94.06 ± 2.4%, p=0.008), (**Figure 3.3B**). Similarly, TIGIT blockade significantly decreased the proliferation of OE33 cells under dual serum-glucose deprivation compared with untreated cells cultured in dual serum-glucose deprivation (90.25 ± 0.7% vs. 102.0 ± 1.2%, p=0.0007), (**Figure 3.3B**). In addition, TIGIT blockade significantly reduced OE19 cell proliferation under glucose deprivation compared with untreated cells cultured under glucose deprivation (73.33 ± 2.3% vs. 90.68 ± 1.4%, p=0.002), (**Figure 3.3B**). TIGIT blockade did not

significantly affect OE33 or OE19 cell proliferation under hypoxia or combined nutrient deprivation-hypoxic conditions (**Figure 3.3B**).

Overall, TIGIT blockade had the greatest effect in reducing OGJ cell proliferation under glucose deprivation and serum deprivation. PD-1 blockade had similar effects in reducing proliferation of OE33 cells under dual serum-glucose deprivation however, PD-1 blockade increased OE33 cell proliferation under hypoxia.

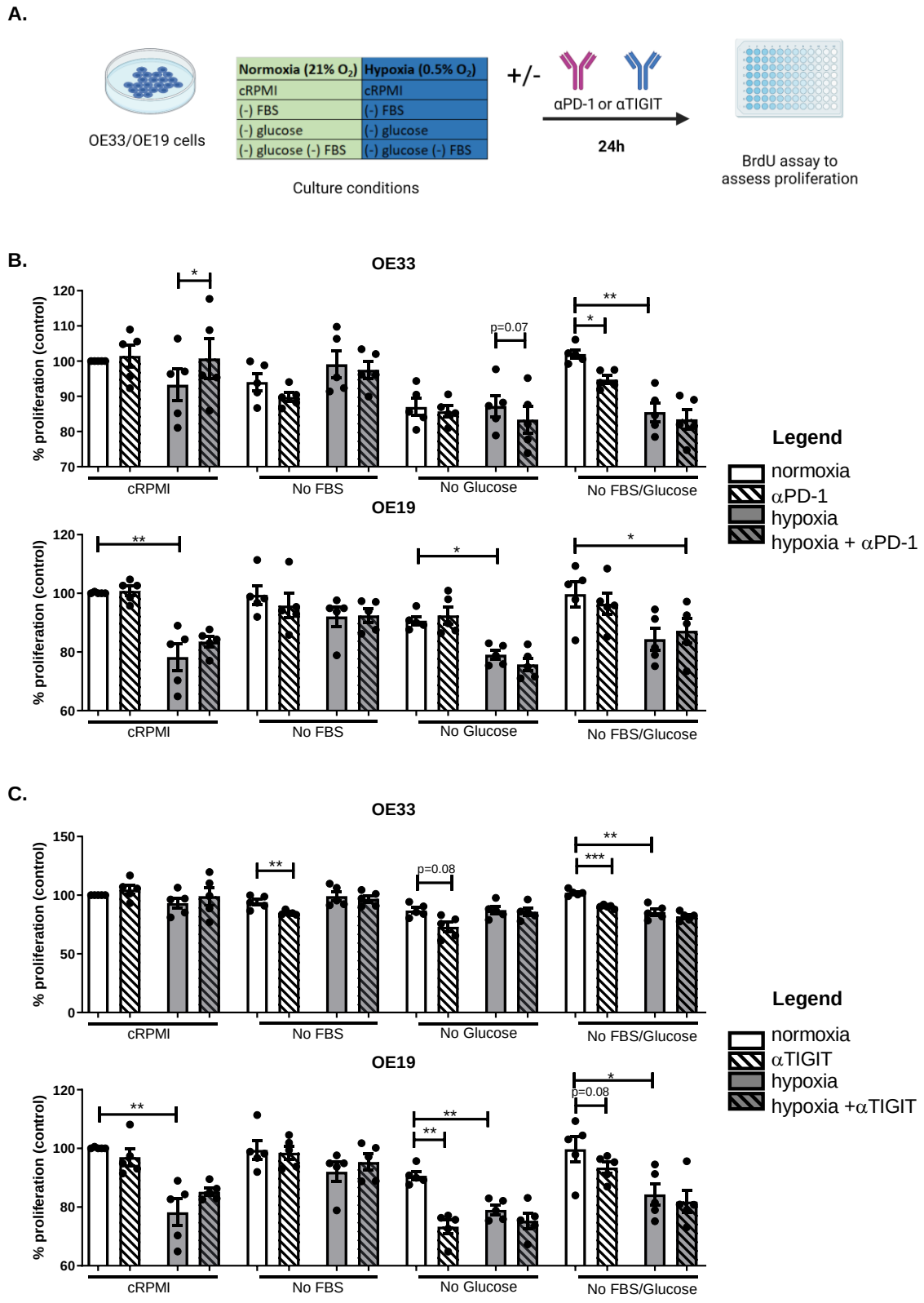

Figure 3.3: PD-1 blockade increases OGJ cell proliferation under hypoxia whereas, TIGIT blockade decreases proliferation in OGJ cells under glucose deprivation and serum deprivation. (A) Schematic workflow. OE33 and OE19 cells were cultured under cRPMI (complete media), serum

deprivation (no FBS), glucose deprivation, cRPMI under hypoxia and combined serum deprivation-hypoxia and combined glucose deprivation-hypoxia for 24 in the absence or presence of αPD-1 (pembrolizumab, 10 μg/ml) (B) or αTIGIT monoclonal antibody (C). Pooled analysis for 5 independent biological replicates carried out in duplicate technical replicates were used for both the OE33 and OE19 cell line. A BrdU assay was used to determine the percentage of proliferating cells. Paired parametric t-test *p<0.05 and **p<0.01 and ***p<0.001. Data expressed as ± SEM.

3.2.4 PD-1 blockade decreases, whereas TIGIT blockade increases OGJ cell death under hypoxia

To further interrogate the effects of PD-1 blockade and TIGIT blockade on OGJ cell viability under nutrient deprivation and hypoxia, OE33 and OE19 cells were treated with PD-1 and TIGIT immune checkpoint inhibitors and OGJ cell death was assessed by AV PI assay.

PD-1 blockade significantly decreased the percentage of early-stage apoptotic OE33 cells under hypoxia compared with untreated cells cultured under hypoxia (23.82 ± 3.2% vs. 28.02 ± 4.1%, p=0.04), (**Figure 3.4A**). In addition, PD-1 blockade significantly decreased the percentage of early-stage apoptotic OE33 cells cultured under combined serum-deprivation with hypoxia compared with untreated OE33 cells cultured under these conditions (56.23 ± 2.9% vs. 60.27 ± 3.4%, p=0.02), (**Figure 3.4A**). However, PD-1 blockade did not significantly affect the percentage of late-stage apoptotic OE33 cells cultured in cRPMI, nutrient-deprived conditions or hypoxia (**Figure 3.4A**).

Interestingly, PD-1 blockade under serum-deprivation significantly increased the percentage of early-stage apoptotic OE19 cells compared with untreated cells cultured under those conditions (40.20 ± 4.5% vs. 24.18 ± 3.8%, p=0.003), (**Figure 3.4A**). However, under glucose-deprivation PD-1 blockade significantly decreased the percentage of early-stage apoptotic OE19 cells compared with untreated cells cultured under those conditions (28.14 ± 1.9% vs. 33.22 ± 1.2%, p=0.01), (**Figure 3.4A**). Interestingly, under combined glucose and serum-deprivation in combination with hypoxia, PD-1 blockade significantly decreased the percentage of late-stage apoptotic OE19 cells compared with untreated cells cultured under those conditions (27.53 ± 1.3% vs. 53.48 ± 11.11%, p=0.05), (**Figure 3.4A**).

Interestingly, TIGIT blockade significantly increased the percentage of late-stage apoptotic OE33 cells cultured under serum-deprivation compared with untreated cells cultured under those conditions (28.24 ± 6.0% vs. 17.9 ± 2.8%, p=0.03), (**Figure 3.4B**). Similarly, TIGIT blockade significantly increased the percentage of late-stage apoptotic OE33 cells under glucose-deprived conditions compared with untreated cells cultured under those conditions

(47.10 ± 1,4% vs. 31.72 ± 1.8%, p=0.008), (**Figure 3.4B**). In contrast, TIGIT blockade under combined serum-deprivation in combination with hypoxia significantly decreased the percentage of early-stage apoptotic OE33 cells compared with untreated cells cultured under those conditions (40.38 ± 4.2% vs. 60.27 ± 3.4%, p=0.001), (**Figure 3.4B**). Subsequently, TIGIT blockade significantly increased the percentage of late-stage apoptotic OE33 cells cultured under combined serum-deprivation in combination with hypoxia compared with untreated cells cultured under those conditions (26.02 ± 2.5% vs. 22.52 ± 2.0%, p=0.02), (**Figure 3.4B**).

Complementary findings were observed with the OE19 cell line. TIGIT blockade significantly increased the percentage of early-stage apoptotic OE19 cells under cRPMI conditions compared with untreated cells cultured under those conditions (29.32 ± 3.3% vs. 25.70 ± 2.6%, p=0.05), (**Figure 3.4B**). TIGIT blockade significantly increased the percentage of early-stage apoptotic OE19 cells under serum-deprivation compared with untreated cells cultured under those conditions (40.20 ± 4.5% vs. 24.18 ± 3.8%, p=0.003), (**Figure 3.4B**). TIGIT blockade significantly decreased the percentage of early-stage apoptotic OE19 cells and subsequently increased the percentage of late-stage apoptotic cells under glucose-deprivation compared with untreated cells cultured under those conditions (early-stage apoptotic cells:28.14 ± 1.9% vs. 33.22 ± 1.2%, p=0.01, late-stage apoptotic cells: 43.60 ± 8.9% vs. 16.11 ± 2.7%, p=0.04), (**Figure 3.4B**). TIGIT blockade also induced OE19 cell death under complete RPMI conditions demonstrated by a significant increase in the percentage of late-stage apoptotic cells (21.63 ± 0.8% vs. 15.75 ± 0.8%, p<0.0001), (**Figure 3.4B**). Similarly, TIGIT blockade significantly increased the percentage of late-stage apoptotic cells cultured under serum-deprivation, (26.17 ± 3.2% vs. 17.65 ± 3.3%, p=0.02), (**Figure 3.4B**). TIGIT blockade significantly increased the percentage of late-stage apoptotic cells cultured under dual serum- and glucose-deprived conditions compared with untreated cells cultured under those conditions (39.3 ± 4.5% vs. 25.35 ± 2.7%, p=0.004), (**Figure 3.4B**). Moreover, there was no significant effect of TIGIT blockade on the percentage of late-stage apoptotic OE19 cells cultured under hypoxia or combined hypoxia-nutrient deprivation (**Figure 3.4B**).

Overall, PD-1 blockade induced apoptosis under serum- and glucose-deprivation however, under hypoxia or combined serum- and glucose-deprivation with hypoxia, PD-1 blockade conferred OGJ cells with a survival advantage and decreased apoptosis and OGJ cell death. Whereas, TIGIT blockade induced apoptosis and OGJ cell death under nutrient-deprivation and hypoxia.

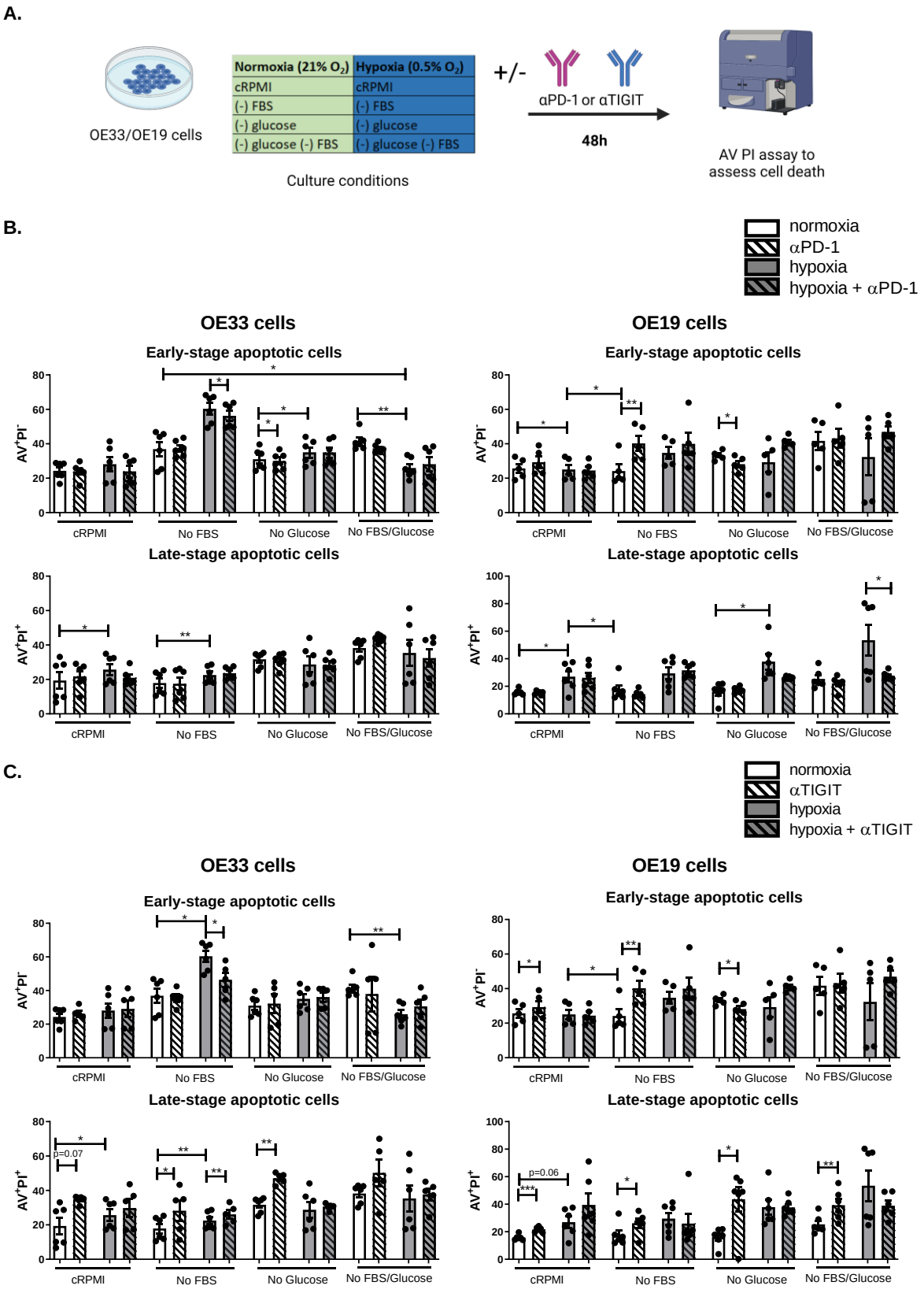
A.
OE33/OE19 cells
Normoxia (21% O2)
Hypoxia (0.5% O2)
cRPMI
cRPMI
(-) FBS
(-) FBS
(-) glucose
(-) glucose
(-) glucose (-) FBS
(-) glucose (-) FBS
Culture conditions
+/-
αPD-1 or αTIGIT
48h
AV PI assay to assess cell death
B.
normoxia
αPD-1
hypoxia
hypoxia + αPD-1
OE33 cells
OE19 cells
Early-stage apoptotic cells
Late-stage apoptotic cells
AV+PI-
AV+PI+
cRPMI
No FBS
No Glucose
No FBS/Glucose
C.
normoxia
αTIGIT
hypoxia
hypoxia + αTIGIT
OE33 cells
OE19 cells
Early-stage apoptotic cells
Late-stage apoptotic cells
p=0.07
p=0.06

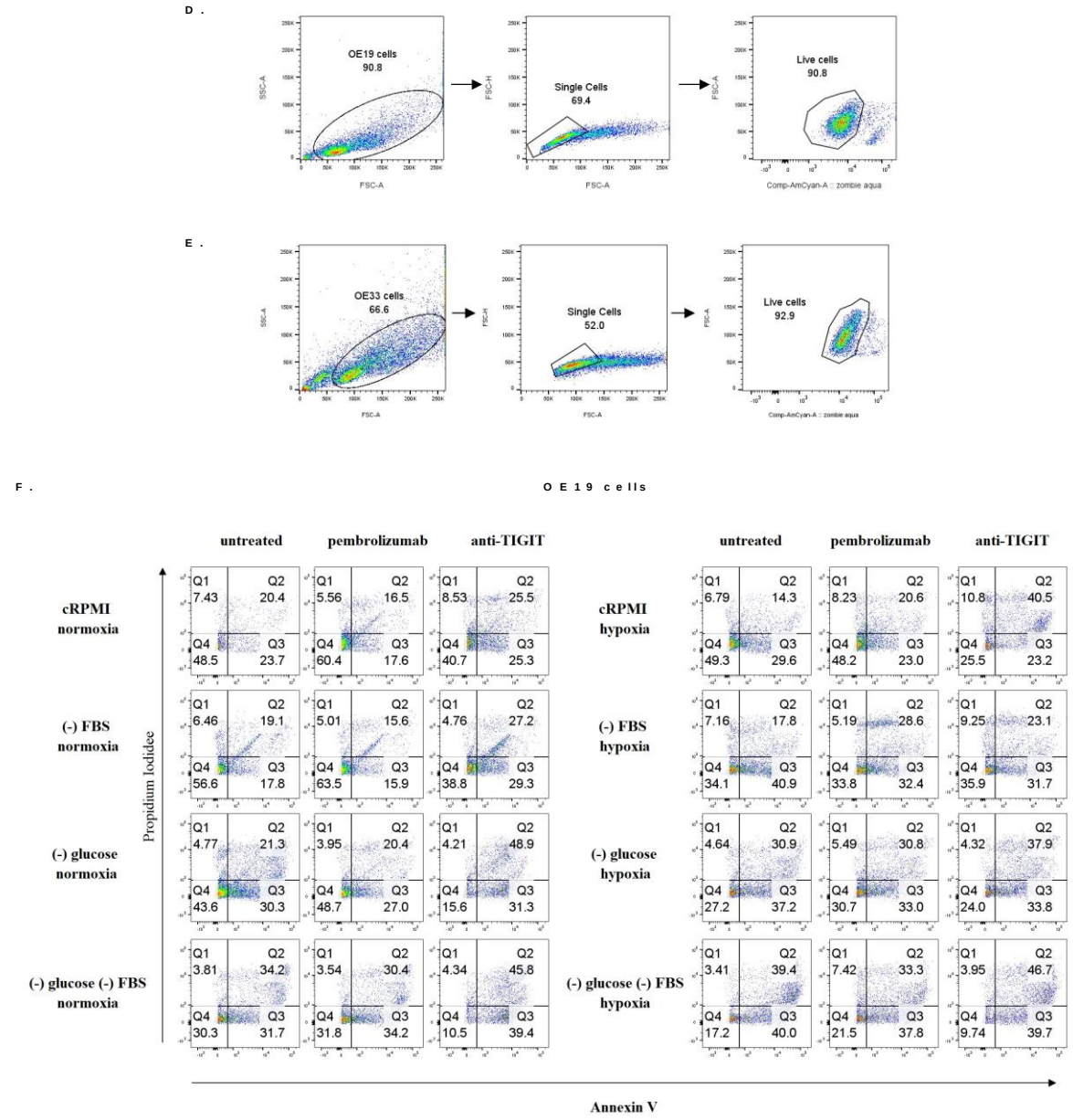

Figure 3.4: PD-1 blockade decreases OGJ cell death under hypoxia and TIGIT blockade induces OGJ cell death basally and under nutrient deprivation. (A) Schematic workflow. OE33 cells and OE19 cells were cultured under in complete media (cRPMI), serum deprived (no FBS), glucose deprived, combined serum deprived-glucose deprived, hypoxia and combined serum deprived-hypoxia, combined glucose deprived-hypoxia and combined serum deprived-glucose deprived-hypoxia for 48h in the absence or presence of αPD-1 (B) or αTIGIT monoclonal antibody (C). Viability was determined by annexin V propidium iodide assay by flow cytometry. Viable cells (AV^-PI^-), early-stage apoptotic cells (AV^+PI^-), late-stage apoptotic cells (AV^+PI^+) and necrotic cells (AV^-PI^+) were characterised, only data for early-stage apoptotic and late-stage apoptotic cells shown. Pooled analysis for 5 independent biological replicates that were carried out in singlet. White bars denote normoxic conditions, grey bars

denote hypoxic conditions. White bars with dashes denote normoxic conditions with addition of αPD-1 (B) or αTIGIT (C) and grey bars with dashes denote hypoxic conditions with αPD-1 (B) or αTIGIT (C). *p<0.05, **p<0.01, ***p<0.001, paired parametric t-test. (D) and (E) display gating strategies for OE33 and OE19 cells and (F) shows representative dot plots in the OE19 cell line.

3.2.5 PD-1 blockade and TIGIT blockade decreases the levels of anti-apoptotic proteins Bcl-2 and Bcl-xL in OGJ cells

To further elucidate the effect of inhibiting PD-1 and TIGIT tumour cell intrinsic signalling on pro-survival pathways in OGJ cells, the levels of anti-apoptotic proteins Bcl-2 and Bcl-xL were assessed following single agent PD-1 and TIGIT blockade in OE33 and OE19 cells (**Figure 3.5**). PD-1 and TIGIT blockade significantly decreased the levels of Bcl-2 in OE33 cells compared with untreated cells (αPD-1:0.77 ± 0.1%, αTIGIT:0.58 ± 0.1% vs. veh:1.0 ± 0.0%, p=0.03 and p=0.02, respectively) (**Figure 3.5**). In addition, there were trends toward a significant decrease in Bcl-2 levels following single agent PD-1 blockade and TIGIT blockade in OE19 cells (αPD-1:0.60 ± 0.1%, αTIGIT:0.80 ± 0.05% vs. veh:1.0 ± 0.0%, p=0.07 and p=0.05, respectively), (**Figure 3.5**).

Similarly, single agent PD-1 blockade and TIGIT blockade significantly decreased the levels of Bcl-xL in OE33 cells compared with untreated cells (αPD-1:0.51 ± 0.1%, αTIGIT:0.54 ± 0.1% vs. veh:1.0 ± 0.0%, p=0.04 and p=0.02, respectively), (**Figure 3.5**). In addition, there was a decrease in Bcl-xL levels following single agent PD-1 blockade and TIGIT blockade in OE19 cells (αPD-1:0.77 ± 0.1%, αTIGIT:0.62 ± 0.1% vs. veh:1.0 ± 0.0%, p=0.06 and p=0.05, respectively), (**Figure 3.5**).

Overall, both PD-1 and TIGIT blockade significantly decreased levels of two anti-apoptotic factors Bcl-2 and Bcl-xL in OGJ cells *in vitro*.

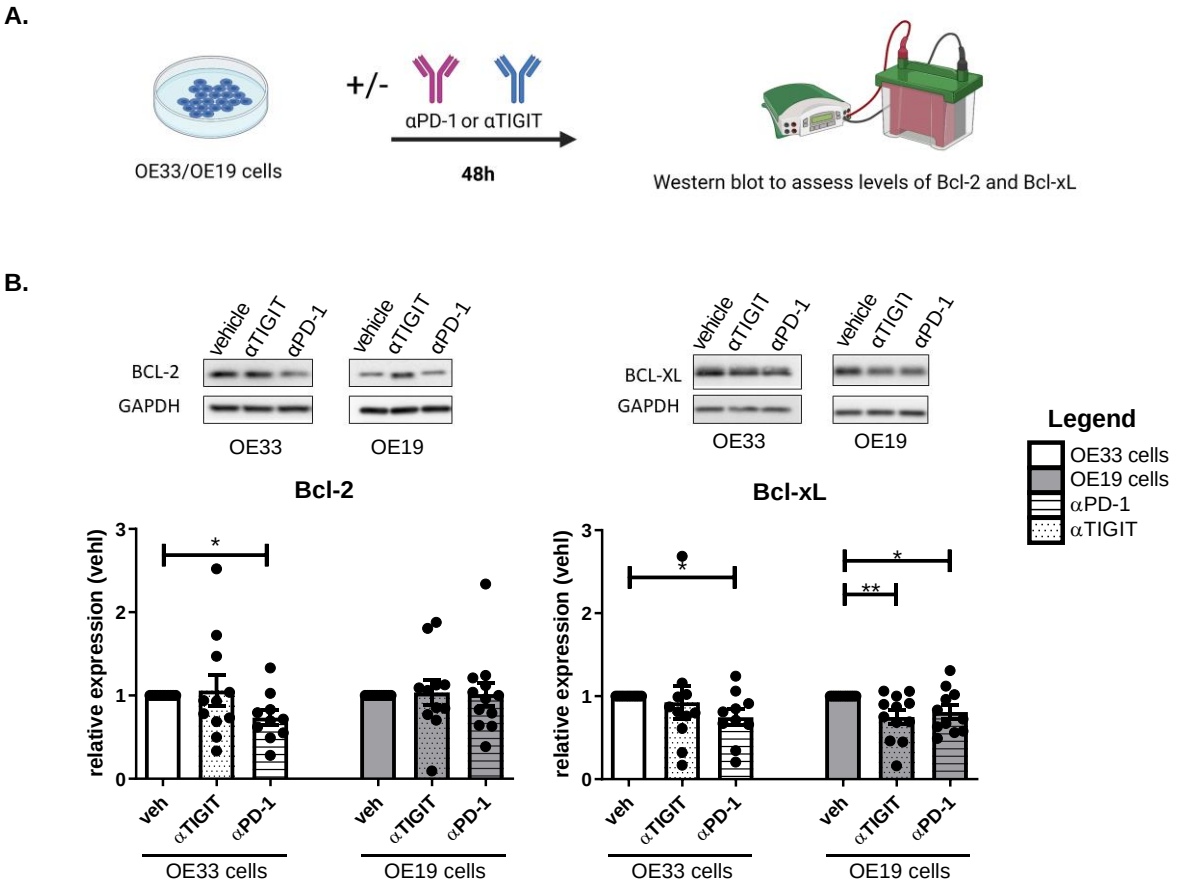

Figure 3.5: TIGIT blockade decreases the expression of anti-apoptotic factor Bcl-xL in OGJ cells *in vitro*. (A) Schematic workflow. OE33 cells and OE19 cells were treated with αPD-1 (pembrolizumab, 10 μg/ml) or αTIGIT (10 μg/ml) for 48h. (B) Expression levels of Bcl-2 and Bcl-xL were determined by western blot. β-actin or GAPDH were used as housekeeping controls to normalise protein expression. Representative blot images of OE19 cell line. Data expressed as ± SEM relative to vehicle (veh) control. Pooled analysis for 11 independent biological replicates carried out in singlet technical replicates for the OE33 cell line and pooled analysis for 12 independent biological replicates carried out in singlet technical replicates for the OE19 cell line. *p<0.05, paired parametric t-test.

3.2.6 Single agent PD-1 blockade and TIGIT blockade in OGJ cells differentially alters tumour cell metabolism

Given that the findings from this study demonstrated that glucose deprivation and hypoxia significantly upregulate PD-1 and TIGIT on the surface of OGJ cells *in vitro* and that these conditions have substantial effects on the metabolism of cancer cells, we sought to investigate if PD-1 blockade or TIGIT blockade might alter the metabolism of OGJ cells. Seahorse

Biosciences XFe24 Extracellular Flux Analyser was used to measure changes in metabolism in real time (**Figure 3.6A**).

TIGIT blockade significantly increased ECAR a measure of glycolysis in OE33 cells compared with vehicle control (veh:100.8 ± 0.7% vs. αTIGIT:131.7 ± 5.3%, p=0.03, respectively), (**Figure 3.6B**). In contrast, TIGIT blockade significantly decreased OCR a measure of oxidative phosphorylation in OE33 cells and OE19 cells compared with vehicle control (OE33 cells: veh:100 ± 0.0% vs. αTIGIT:56.79 ± 6.7% and OE19 cells:veh:100.0 ± 0.0% vs. αTIGIT:7.88 ± 0.22%, p=0.02 and p<0.0001, respectively), (**Figure 3.6B**). TIGIT blockade also significantly decreased the OCR:ECAR ratio in OE19 cells compared with the vehicle control (veh:3.25 ± 0.14 vs. αTIGIT:0.26 ± 0.1, p=0.001), (**Figure 3.6D**). PD-1 blockade significantly increased basal respiration in OE33 cells compared with the vehicle control (veh:100 ± 0.0% vs. αPD-1:111.0 ± 1.9%, p=0.02), (**Figure 3.6E**). Contrastingly, TIGIT blockade significantly reduced basal respiration in OE33 cells (veh:100 ± 0.0% vs. αTIGIT:54.93 ± 7.7%, p=0.02), (**Figure 3.6E**). Similarly, TIGIT blockade significantly reduced the basal respiration in OE19 cells compared with the vehicle control (veh:100 ± 0.0% vs. αTIGIT:6.37 ± 1.0%, p<0.0001). Furthermore, TIGIT blockade significantly decreased OCR-linked ATP turnover in OE33 cells and OE19 cells compared with vehicle control (OE33 cells: veh:100 ± 0.0% vs. αTIGIT:59.6 ± 9.5% and OE19 cells:veh:100.0 ± 0.0% vs. αTIGIT:5.9 ± 1.8%, p=0.05 and p=0.0004, respectively), (**Figure 3.6F**). Maximal respiration is also significantly reduced following TIGIT blockade compared with vehicle control in both OE19 cells and OE33 cells (OE33 cells: veh:100 ± 0.0% vs αTIGIT 57.57 ± 5.9%. OE19 cells: veh:100 ± 0.0% vs. αTIGIT:2.76 ± 0.45%, p=0.01 and p=0.003, respectively), (**Figure 3.6G**). TIGIT blockade significantly decreased proton leak in both OE33 and OE19 cells compared with vehicle control (OE33 cells: veh:100 ± 0.0% vs. αTIGIT:46.63 ± 5.5% and OE19 cells:veh:100.0 ± 0.0% vs. αTIGIT:9.9 ± 1.3%, p=0.01 and p=0.009, respectively), (**Figure 3.6H**). Furthermore, TIGIT blockade significantly reduced the spare respiratory capacity in OE33 cells and OE19 cells compared with the vehicle control (OE33 cells: veh:100 ± 0.0% vs. αTIGIT: 62.35 ± 4.6% and OE19 cells: veh:100.0 ± 0.0% vs. αTIGIT: 8.65 ± 3.3%, p=0.01 and p=0.02, respectively), (**Figure 3.6I**). PD-1 blockade and TIGIT blockade significantly increased and decreased the glycolytic reserve in OE33 cells compared with vehicle control, respectively (veh:100 ± 0.0% vs. αPD-1: 112.1 ± 2.6%, αTIGIT: 55.6 ± 6.6%, p=0.04 and p=0.02 respectively), (**Figure 3.6J**).

Overall, PD-1 blockade enhanced basal respiration and glycolytic reserve in OGJ cells compared with the vehicle control. Whereas, TIGIT blockade increases ECAR yet decreased several metabolic parameters in OGJ cells including oxidative phosphorylation, basal respiration, OCR-linked ATP turnover, maximal respiration, proton leak, spare respiratory capacity and glycolytic reserve.

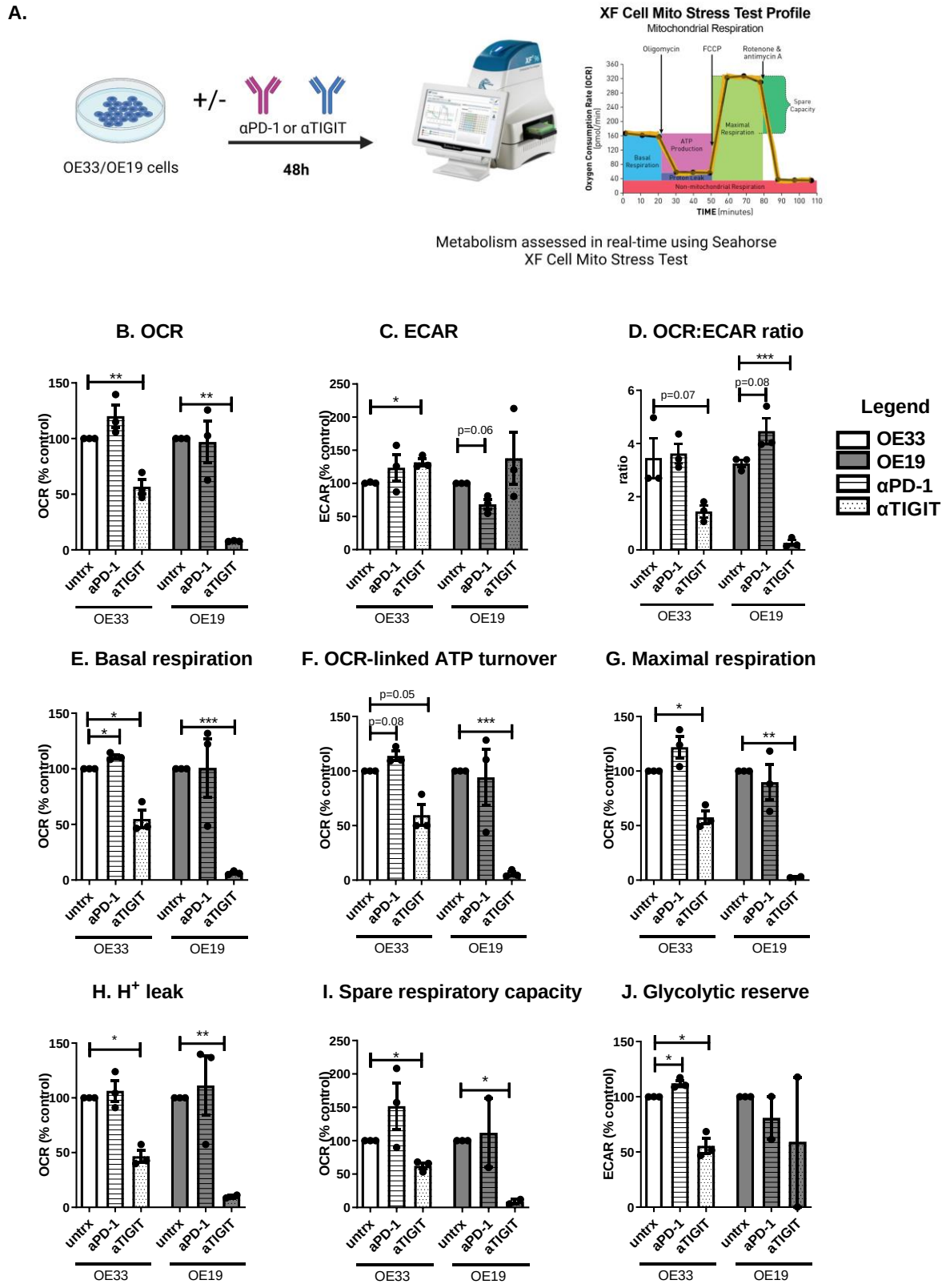

Figure 3.6: PD-1 blockade increases basal respiration and glycolytic reserve whereas TIGIT blockade increases ECAR and decreases OCR in OGJ cells.

OE33 and OE19 cells were treated with and without αPD-1 (pembrolizumab, 10 μg/ml) or αTIGIT monoclonal antibody (10 μg/ml) for 48h. OCR, a measure of oxidative phosphorylation and ECAR, a measure of glycolysis was assessed in real-time using the Seahorse Biosciences XFe24 Analyser. (A) Schematic workflow showing the Seahorse XF Mito Stress Test that was used. A range of metabolic parameters were then calculated from the mito stress test profile using Seahorse technology including: OCR (B.), ECAR (C.), OCR:ECAR ratio (D.), basal respiration (E.), OCR-linked ATP turnover (F.), maximal respiration (G.), H^+ leak (H.), spare respiratory capacity (I.) and glycolytic reserve (J.) All data expressed as mean ± SEM. Data expressed relative to untreated cells set to 100% (B-J). Pooled analysis for 3 independent biological replicates conducted using triplicate technical replicates. Paired parametric t-test, *$p<0.05$, **$p<0.01$.

The findings from this study demonstrated that PD-1 blockade significantly enhanced glycolytic reserve in OGJ cells whereas, TIGIT blockade significantly enhanced a glycolytic phenotype yet decreased glycolytic reserve in OGJ cells. Therefore, we sought to investigate if PD-1 blockade or TIGIT blockade affected the surface expression of GLUT1 by OGJ cells, which is an important transporter of glucose from the external TME into OGJ cells (**Figure 3.7**). Interestingly, PD-1 blockade significantly upregulated the surface expression of GLUT1 on the surface of OE33 cells and OE19 cells compared with untreated cells (OE33 cells: 5.76 ± 0.5% vs. 4.23 ± 0.5%, p=0.008 and OE19 cells: 9.65 ± 0.3% vs. 5.39 ± 0.2, p=0.0003), (**Figure 3.7**). There was a trend toward an increase in the surface expression of GLUT1 on the surface of OE19 cells following TIGIT blockade compared with untreated cells (6.84 ± 0.6% vs. 5.39 ± 0.2, p=0.08) (**Figure 3.7**). Overall, PD-1 blockade had the greatest effect at upregulating GLUT1 on the surface of OGJ cells *in vitro*.

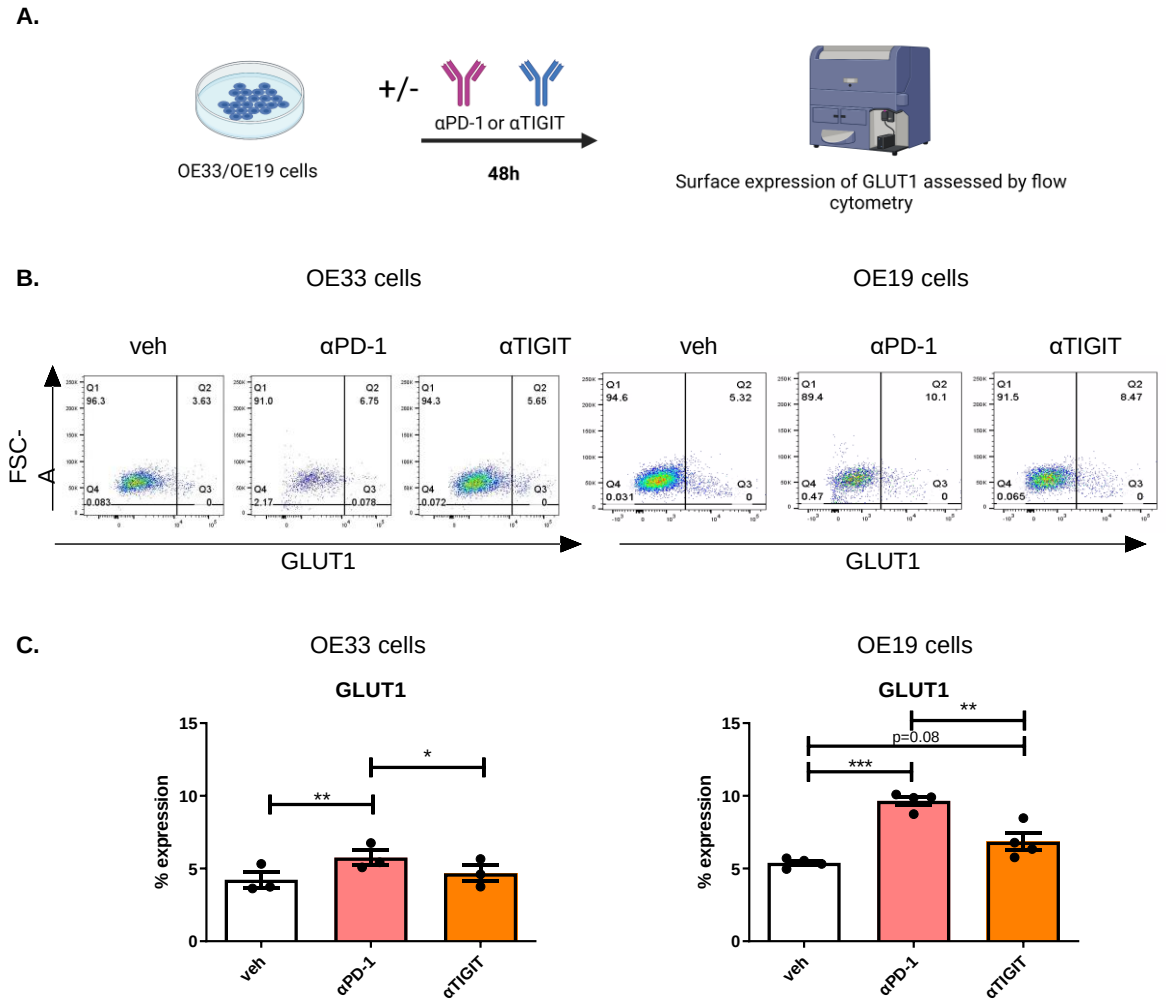

Figure 3.7: Pembrolizumab and αTIGIT significantly increase the percentage of OE19 cells expressing GLUT1. OE33 and OE19 cells were treated with vehicle (veh) control, αPD-1 (pembrolizumab, 10 μg/ml) or αTIGIT monoclonal antibody (10 μg/ml) for 48h. The percentage of live OGJ cells expressing GLUT1 was determined by flow cytometry (n=4). Representative dot plots showing effect of vehicle control, PD-1 blockade or TIGIT blockade on the percentage of GLUT1 positive OE19 cells. Paired parametric t-test. *p<0.05, **p<0.01 and ***p<0.001. Data expressed as ± SEM.

3.2.7 Inhibition of oxidative phosphorylation and glycolysis in OGJ cells differentially alters the surface expression of tumour-intrinsic PD-1 and TIGIT

The findings from this study have demonstrated that both PD-1 and TIGIT blockade significantly alter OGJ cell metabolism, we therefore sought to investigate if inhibiting oxidative phosphorylation and glycolysis in OGJ cells might affect the expression of PD-1 or TIGIT on the surface of OGJ cells *in vitro* (**Figure 3.8**). Inhibition of glycolysis or oxidative

metabolism had no significant effect on the expression of PD-1 in OE33 cells compared with the vehicle control (**Figure 3.8**). However, inhibition of glycolysis with a low dose of 2DG significantly reduced PD-1 expression on the surface of OE19 cells (8.06 ± 2.7 vs. 15.05 ± 3.2%, p=0.03), (**Figure 3.8**). Additionally, inhibition of oxidative phosphorylation using a low dose of oligomycin significantly reduced the expression of PD-1 on the surface of OE19 cells (7.21 ± 1.7 vs. 15.05 ± 3.2%, p=0.02), (**Figure 3.8**). In contrast, inhibition of oxidative phosphorylation significantly upregulated TIGIT on the surface of OE33 cells compared with the vehicle control (17.26 ± 3.7 vs. 8.33 ± 0.1%, p=0.04), (**Figure 3.8**). Inhibition of glycolysis or oxidative phosphorylation had no significant effect on the surface expression of TIGIT in OE19 cells (**Figure 3.8**).

Overall, inhibition of oxidative phosphorylation and glycolysis decreased the surface expression of PD-1 on OGJ cells and inhibition of oxidative phosphorylation significantly upregulated TIGIT on the surface of OGJ cells.

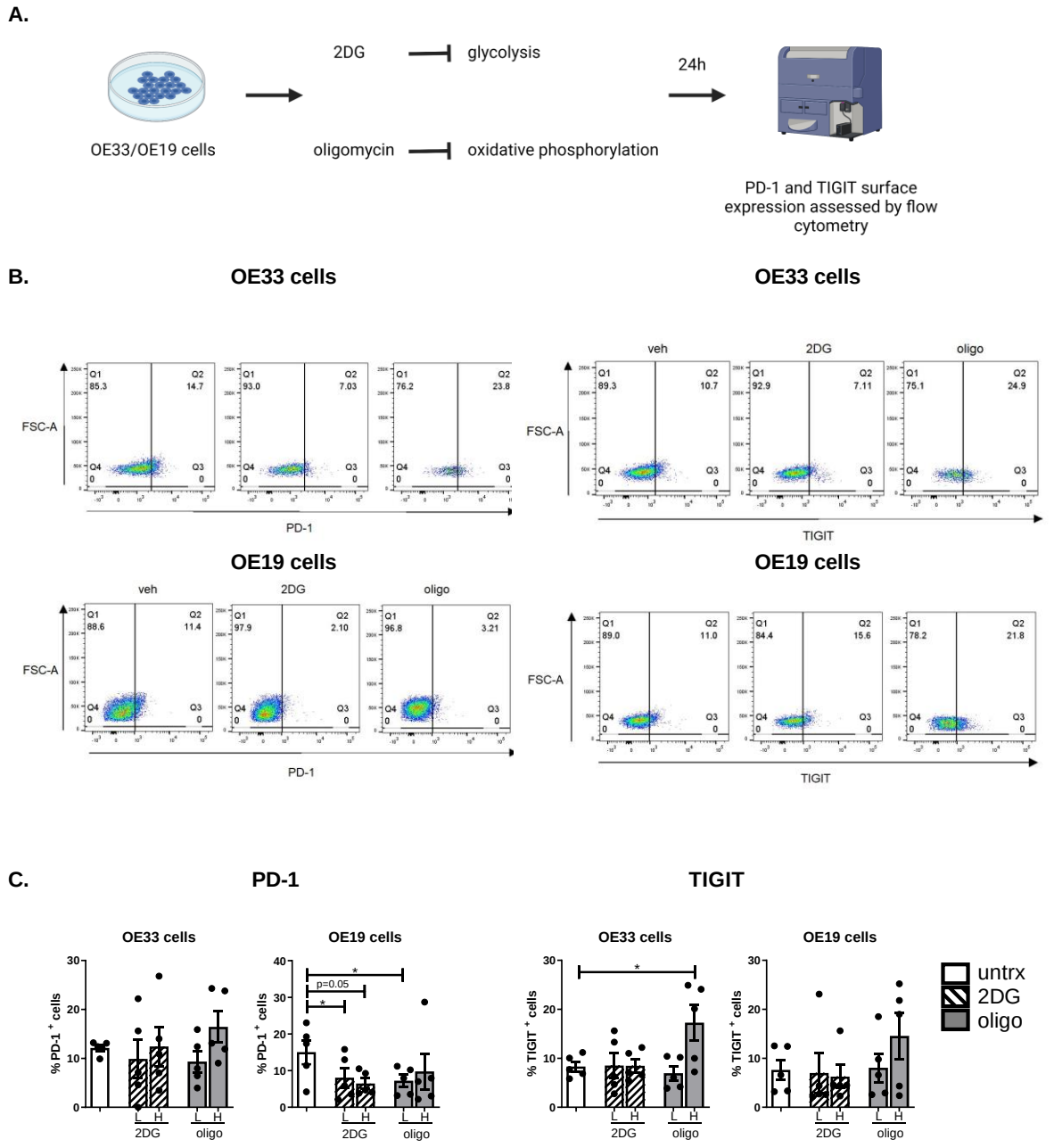

Figure 3.8: Inhibition of glycolysis and oxidative phosphorylation decreases PD-1 on the surface of OE19 cells whereas, inhibition of oxidative phosphorylation increases TIGIT on OE33 cells. (A) Schematic workflow. OE33 and OE19 cells were treated with vehicle control or 2DG (low dose (L): 10 mM and high dose (H): 20 mM) or oligomycin (low dose: 3 μM and high dose: 6 μM) for 24h and the percentage of viable cells expressing PD-1 and TIGIT was determined by flow cytometry (C). Pooled analysis for 5 independent biological replicates carried out in technical singlets were conducted. (B) Representative dot plots showing effect of vehicle, high dose 2DG and high dose oligomycin on PD-1 and TIGIT expression on the surface of OE19 cells and OE33 cells, respectively. Paired parametric t-test. *p<0.05. Abbreviations: 2DG, 2-deoxy-D-glucose; H, high dose; L, low dose; oligo, oligomycin.

3.2.8 TIGIT, CTLA-4 and PD-L2 immune checkpoints were upregulated on stromal cells within the OGJ TME

The TME is a well-characterised inhospitable environment for immune cells, frequently nutrient deprived and hypoxic, which has a profound effect on the immune infiltrate typically promoting an immunosuppressive phenotype. To provide insight into the direct effects of the OGJ TME on immune checkpoint (IC) expression, a range of IC proteins was assessed on the surface of $CD45^+$ cells in the tumour tissue and in circulation (**Figure 3.9**).

There was a significantly higher percentage of $CD45^+$ cells within the tumour tissue expressing TIGIT compared with circulating $CD45^+$ cells (tumour: 29.65 ± 6.5 vs. blood: 10.24 ± 2.1%, p=0.02) (**Figure 3.9A**). Similarly, CTLA-4 was expressed on a significantly higher percentage of $CD45^+$ cells in the tumour tissue compared with circulation (tumour: 44.55 ± 8.9 vs. blood: 12.27 ± 4.9%, p=0.008) (**Figure 3.9A**). In addition, there was a significantly higher percentage of $CD45^+$ cells within the tumour tissue expressing PD-L2 compared with circulating $CD45^+$ cells (tumour: 5.78 ± 0.3% vs. blood: 1.27 ± 0.3%, p=0.05) (**Figure 3.9A**).

IC expression on circulating and tumour-infiltrating immune cells in has been shown to possess prognostic and predictive value of treatment response in several cancer types including OGJ. Therefore, we investigated if the frequency of circulating or tumour-infiltrating $CD45^+$ cells expressing ICs correlated with patient demographics or clinical features of the tumour, including treatment response, tumour stage and adverse features of the tumour which have been shown to predict poor responses to current standards of care and survival in OGJ patients in a study by Donlon *et al*[252]., and include perineural invasion and lymphovascular invasion (**Figure 3.9B**).

The frequency of circulating $CD45^+CTLA\text{-}4^+$ cells positively correlated with a subsequent poor response to neoadjuvant treatment determined by the Mandard tumour regression grade scoring system (r=0.85 and p=0.007) (**Figure 3.9B**). In addition, the frequency of circulating $CD45^+PD\text{-}1^+$ cells negatively correlated with advanced tumour stage determined by PET/CT (r=0.73 and p=0.02) (**Figure 3.9B**). Moreover, the frequency of circulating $CD45^+ICOS^+$ cells negatively correlated with adverse tumour features such as lymphovascular invasion which is indicative of more advanced stage tumours (r= -0.73 and p=0.03) (**Figure 3.9B**).

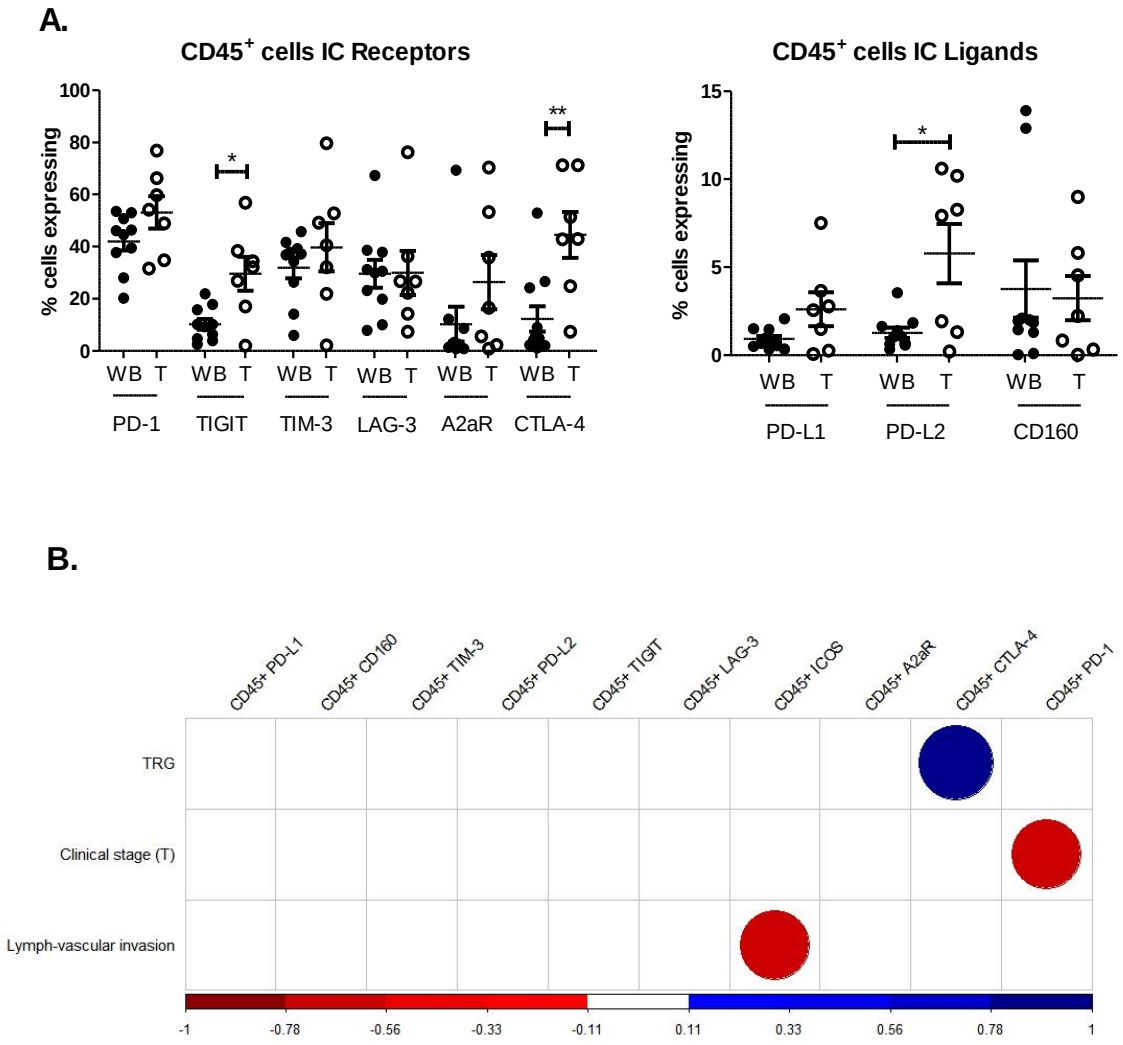

Figure 3.9: TIGIT, CTLA-4 and PD-L2 are expressed at significantly higher levels on the surface of CD45$^+$ cells infiltrating tumour tissue compared with peripheral circulation and frequencies of CD45$^+$CTLA-4$^+$ circulating cells positively correlated with a subsequent poor pathological response to treatment. (A.) CD45$^+$ cells were screened for the surface expression of IC receptors PD-1, TIGIT, TIM-3, LAG-3, A2aR and CTLA-4 and ligands PD-L1, PD-L2 and CD160 in circulating whole blood (WB) (n=10) and infiltrating OGJ pre-treatment tumour biopsies (T) (n=7) by flow cytometry. Mann Whitney test *p<0.05. (B.) The percentage of CD45$^+$ cells expressing inhibitory ICs in peripheral blood circulation and infiltrating OGJ tumour tissue in the treatment-naïve setting were correlated with patient demographics and clinical features. Only significant correlations shown in the corrogram for peripheral circulating CD45$^+$ cells expressing ICs versus pathologic response to neoadjuvant treatment determined by the Mandard tumour regression grade (TRG) scoring system,

clinical tumour (T) stage determined by PET/CT and adverse tumour features such as perineural invasion and lymphovascular invasion. Spearman correlation *p≤0.05. Only significant correlations shown; red circle: negative correlation and blue circle: positive correlation.

3.2.9 OGJ patient lymphocytes co-cultured with OE33 cells significantly upregulated LAG-3, altered T cell activation and cytokine profiles

Cancer cells grow rapidly within the TME producing waste by-products such as lactate, which adversely affects anti-tumour T cell function and can skew T cell phenotypes to a pro-tumour regulatory T cell. In addition, rapidly dividing cancer cells outcompete anti-tumour immune cells within the TME for essential nutrients such as glucose, amino acids and glutamine which also significantly hinders the function of anti-tumour immune populations. Therefore, to ascertain the direct effect of cancer cell competition on T cell function, OE33 OGJ cells were co-cultured with OGJ donor PBMCs, and T cell phenotypes were subsequently assessed.

LAG-3 was significantly upregulated on $CD8^+$ T cells co-cultured with OE33 cells compared with PBMCs cultured alone for 48h (11.05 ± 3.4 vs. 6.50 ± 2.1%, p=0.03) (**Figure 3.10**). There was no significant alteration to the expression profile of PD-1, TIGIT, TIM-3, A2aR, CTLA-4, PD-L1, PD-L2 or CD160 on the surface of T cells following a 48h co-culture with OE33 cells compared with PBMCs cultured alone (**Figure 3.10**).

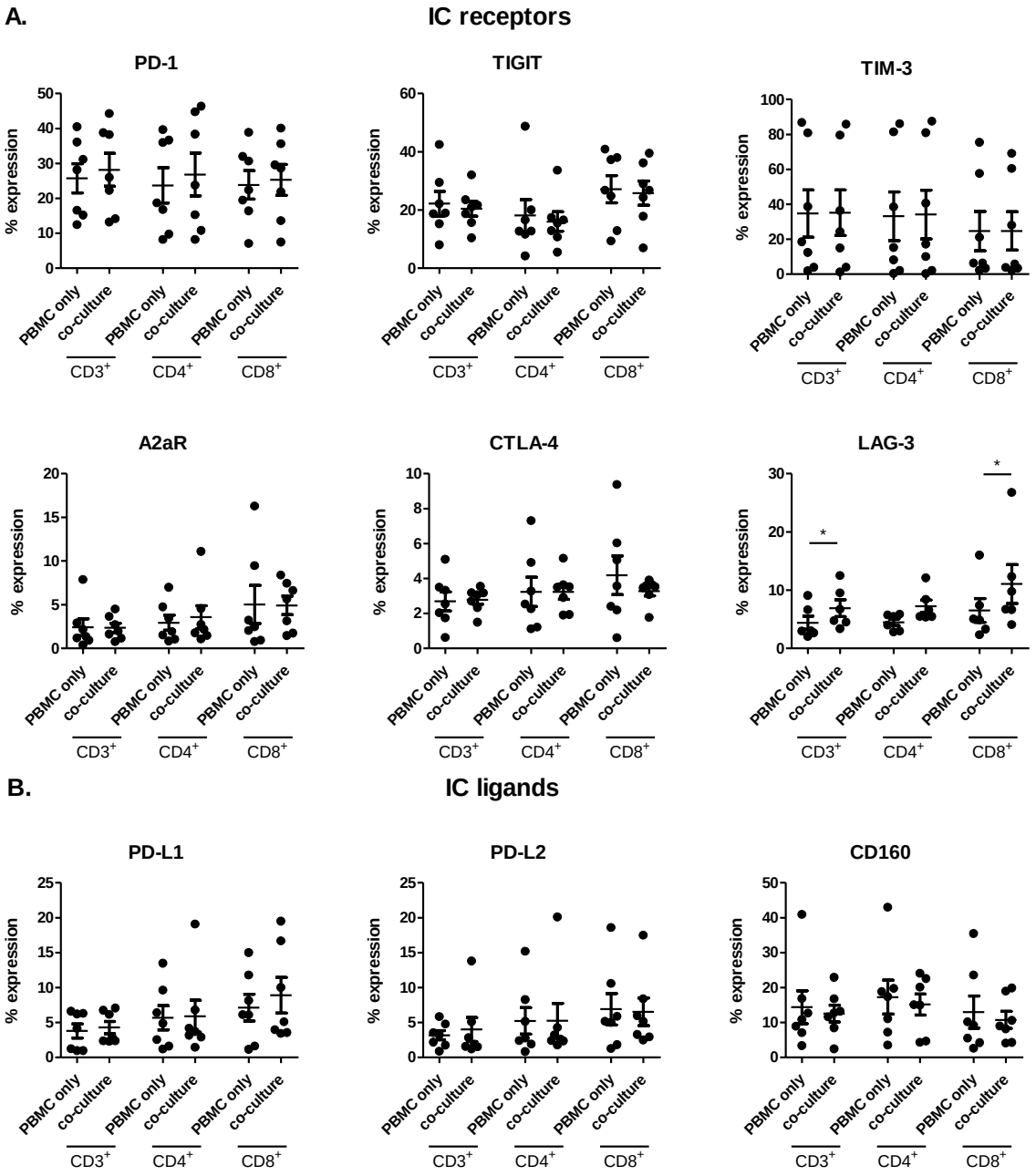

Figure 3.10: Co-culturing OE33 OGJ cells with OGJ donor PBMCs significantly upregulates LAG-3 on the surface of T cells. OE33 cells were cultured for 24h in the absence or presence of PBMCs (OE33: PBMCs, 1:2) isolated from OGJ patients (n=7) that were pre-activated for 5 days with plate bound anti-CD3/28 and IL-2 prior to culture. $CD3^+$, $CD3^+CD4^+$ and $CD3^+CD8^+$ cells were then stained with a zombie viability dye and the expression of inhibitory immune checkpoint receptors including PD-1, TIGIT, TIM-3, LAG-3, A2aR, CTLA-4 and KLRG-1 (A) and IC ligands including PD-L1, PD-L2 and CD160) (B). Paired, non-parametric t test. Expression presented as percentage ± SEM on live cells. *$p<0.05$.

Furthermore, CD69 was significantly upregulated on $CD8^+$ T cells co-cultured with OE33 cells compared with PBMCs cultured alone for 48h (40.32 ± 9.8 vs. 21.45 ± 3.9%, p=0.03) (**Figure 3.11**). However, CD27 were significantly decreased on $CD4^+$ T cells and $CD8^+$ T cells co-cultured with OE33 cells compared with PBMCs cultured alone for 48h ($CD4^+$ T cells: 29.09 ± 12.8 vs. 38.51 ± 12.4%, p=0.01 and $CD8^+$ T cells: 23.06 ± 10.49 vs. 39.38 ± 11.4%, p=0.03) (**Figure 3.11**). Similarly, CD45RA was significantly decreased on the surface of $CD8^+$ T cells following co-culture with OE33 cells compared with PBMCs cultured alone (30.87 ± 8.9 vs. 41.17 ± 10.1%, p=0.03) (**Figure 3.11**). There was no significant change in the expression of CD62L or CD45RO (**Figure 3.11.**).

Interestingly, changes in T cell differentiation state were also observed following co-culture with OE33 cells (**Figure 3.11**). There was a significant increase in the percentage of effector memory $CD4^+$ T cells compared with PBMCs cultured alone for 48h (62.50 ± 14.07 vs. 54.65 ± 13.65%, p=0.03) (**Figure 3.11**). Furthermore, there was a significant decrease in the percentage of central memory $CD8^+$ T cells and a significant increase in the frequency of terminally differentiated effector memory $CD8^+$ T cells following co-culture with OE33 cells compared with PBMCs that were cultured alone for 48h (central memory $CD8^+$ T cells: 22.76 ± 11.13 vs. 31.48 ± 13.18%, p=0.03 and terminally differentiated effector memory $CD8^+$ T cells: 64.23 ± 9.5 vs. 49.00 ± 9.7%, p=0.01) (**Figure 3.11**).

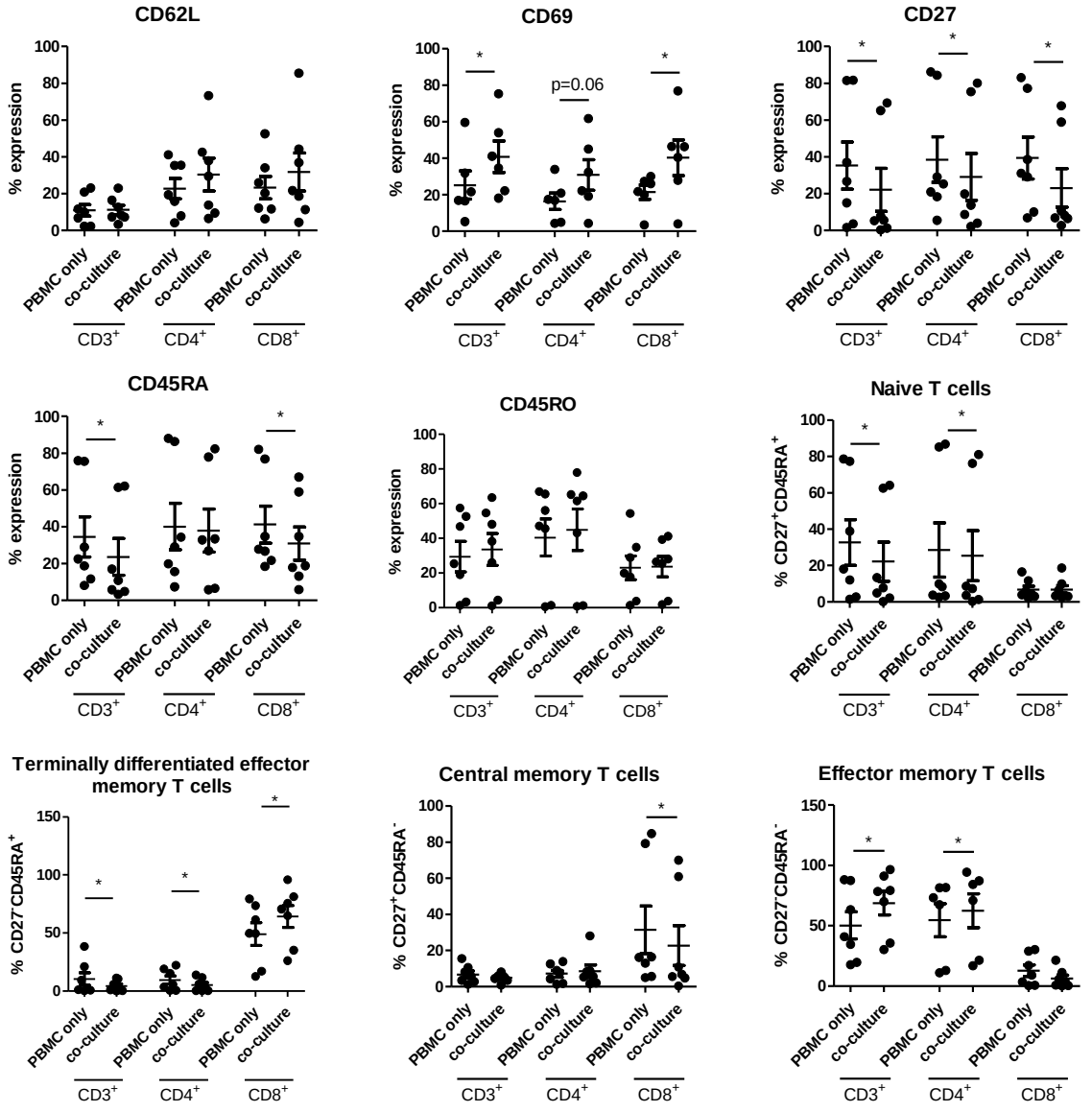

Figure 3.11: Co-culturing OE33 OGJ cells with OGJ donor PBMCs significantly alters the activation status of T cells. OE33 cells were cultured for 24h in the absence or presence of PBMCs (OE33: PBMCs, 1:2) isolated from OGJ patients (n=7) that were pre-activated for 5 days with plate bound anti-CD3/28 and IL-2 prior to culture. $CD3^+$, $CD3^+CD4^+$ and $CD3^+CD8^+$ cells were then stained with a zombie viability dye and the expression of T cell activation markers (CD62L, CD69, CD27 and CD45RA on the surface of T cells and the frequency of naïve ($CD45RA^+CD27^+$), central memory ($CD45RA^-CD27^+$), effector memory ($CD45RA^-CD27^-$) and terminally differentiated effector memory ($CD45RA^+CD27^-$) T cells was assessed via flow cytometry. Paired, non-parametric t test. Expression presented as percentage ± SEM on live cells. *$p<0.05$.

There was no significant difference in the frequency of T cells producing of IL-17A/F, IFN-γ, TNF-α, IL-4 and IL-10 cytokines following a 48h co-culture with OE33 cells compared with PBMCs cultured alone (**Figure 3.12**).

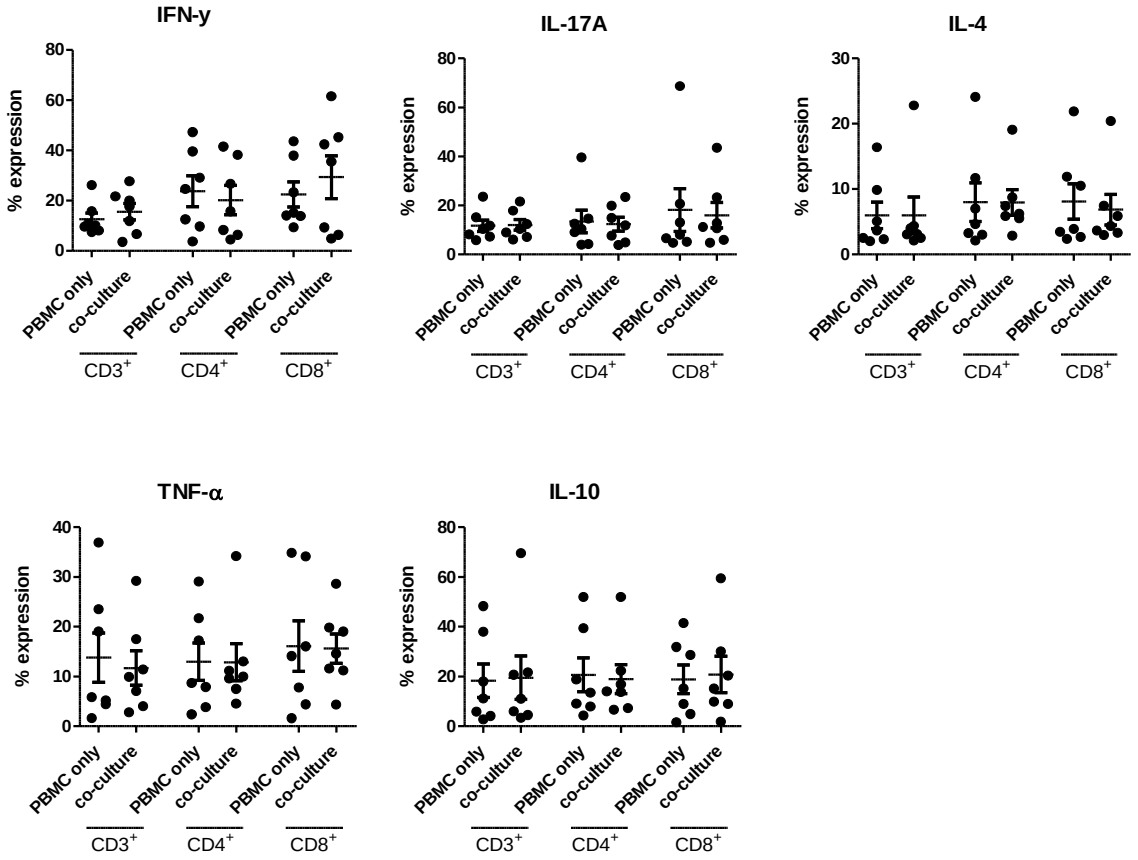

Figure 3.12: Co-culturing OE33 OGJ cells with OGJ donor PBMCs does not significantly alter the activation status of T cells. OE33 cells were cultured for 24h in the absence or presence of PBMCs (OE33: PBMCs, 1:2) isolated from OGJ patients (n=7) that were pre-activated for 5 days with plate bound anti-CD3/28 and IL-2 prior to culture. $CD3^+$, $CD3^+CD4^+$ and $CD3^+CD8^+$ cells were then stained with a zombie viability dye and the expression of IFN-γ, IL-17A/F, IL-4, IL-10 and TNF-α was assessed by flow cytometry. Paired, non-parametric t test. Expression presented as percentage ± SEM on live cells.

3.2.10 The secretome from OGJ PBMCs upregulates PD-L1 and PD-L2 on the surface of OE33 cells *in vitro*

The nutrient deprived and hypoxic TME has a substantial effect not only on the phenotype of T cells but also on the T cell secretome, which could in turn alter IC expression by cancer cells and facilitate IC-mediated immune escape.

The secretome from OGJ patient-derived T cells cultured in cRPMI significantly upregulated PD-L1 on the surface of OE33 cells *in vitro* compared with untreated OE33 cells (11.33 ± 4.4 vs. 1.71 ± 0.4%, p=0.03) (**Figure 3.13A**). There was a trend toward a significant increase in the upregulation of PD-L1 on the surface of OE33 cells following treatment with the secretome of T cells that had been cultured in serum deprived conditions (5.98 ± 2.9 vs. 1.71 ± 0.4%, p=0.06) (**Figure 3.13A**).

In addition, the secretome from OGJ patient-derived PBMCs that had been cultured in cRPMI, serum deprivation, dual serum deprivation and hypoxia, glucose deprivation, dual glucose deprivation and hypoxia and dual glucose and serum deprivation in combination with hypoxia significantly upregulated PD-L2 on the surface of OE33 cells *in vitro* compared with untreated OE33 cells (17.26 ± 6.5 vs. 10.9 ± 4.1, 13.84 ± 6.1, 11.41 ± 3.7, 16.70 ± 8.1, 18.20 ± 8.2 and 1.43 ± 0.5%, p=0.03, p=0.03, p=0.03, p=0.03, p=0.03 and p=0.03, respectively) (**Figure 3.13A**). There was a trend toward a significant increase in the upregulation of PD-L2 on the surface of OE33 cells following treatment with the secretome of PBMCs cells that had been cultured under hypoxic conditions compared with untreated OE33 cells (11.95 ± 5.2 vs. 1.47 ± 0.5%, p=0.06) (**Figure 3.13A**).

CD160 and PD-1 expression increased on the surface of OE33 cells following treatment with the secretome of PBMCs cultured in cRPMI compared with untreated OE33 cells (3.82 ± 1.3 vs. 1.58 ± 0.1%, p=0.06, **Figure 3.13A** and 15.00 ± 2.4 vs. 7.51 ± 1.6%, p=0.06, **Figure 3.13B,** respectively). TIGIT expression was increased on the surface of OE33 cells following treatment with the secretome of PBMCs cultured under combined serum deprived hypoxic conditions compared with untreated OE33 cells (27.2 ± 6.8 vs. 18.52 ± 8.8%, p=0.06) (**Figure 3.13B**). TIM-3 and LAG-3 expression decreased on the surface of OE33 cells following treatment with the secretome of PBMCs that had been cultured under dual glucose and serum deprived hypoxic conditions compared with untreated OE33 cells (TIM-3: 1.12 ± 0.2 vs. 1.86 ± 0.1%, p=0.06 and LAG-3: 1.14 ± 0.2 vs. 1.86 ± 0.3%, p=0.06) (**Figure 3.13B**).

Overall, the secretome from OGJ patient-derived PBMCs cultured in cRPMI normoxic conditions had the greatest effect in upregulating PD-L1 and PD-L2 on the surface of OE33 cells *in vitro*.

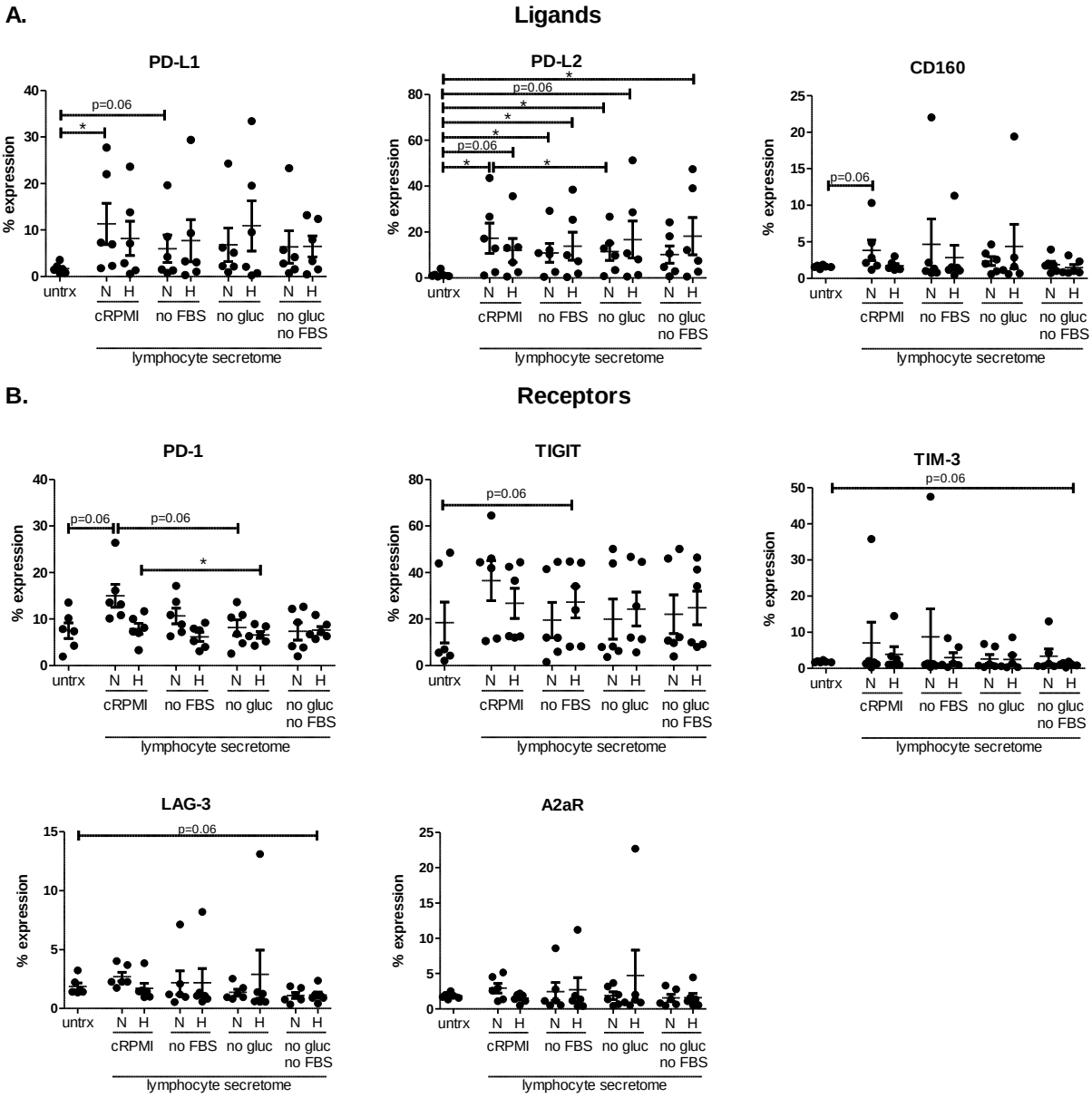

Figure 3.13: OGJ patient-derived PBMC secretome significantly increased the expression of PD-L1 and PD-L2 on OE33 OGJ cells under full nutrient and normoxic conditions. PBMCs were isolated from peripheral blood of treatment-naïve OGJ patients (n=6) and expanded for 5 days in the presence of plate bound anti-CD3/anti-CD28 and recombinant human IL-2. Following a 5-day expansion, PBMCs were cultured for an additional 24h under nutrient deprivation (FBS deprived or glucose deprived), hypoxia (0.5% O_2) and combined nutrient deprivation hypoxic conditions and the soluble secretome was harvested and cultured with OE33 cells using a 1 in 2 dilution for 24h. OE33 cells were then stained with a zombie viability dye and antibodies specific for a range of ligands (PD-L1, PD-L2 and CD160) and IC receptors (PD-1, TIGIT, TIM-3, LAG-3 and A2aR) and expression was assessed by flow cytometry. Paired, non-parametric t test. Expression presented as percentage ± SEM

on live cells. Zombie dye was used to exclude dead cells from analysis. Abbreviations: N: normoxia, H: hypoxia.

3.2.11 Combination hypoxia and glucose deprivation upregulates PD-1, CTLA-4, PD-L1 and PD-L2 on the surface of OGJ patient-derived T cells

Given the findings demonstrating that OGJ donor lymphocytes co-cultured with OE33 cells significantly upregulated LAG-3 on the surface of T cells, we sought to investigate the direct effect of nutrient deprivation, including glucose deprivation and serum deprivation, and hypoxia on the IC expression profile of OGJ donor lymphocytes. Cancer cells outcompete T cells for nutrients and oxygen within the TME resulting in a nutrient-deprived, hypoxic inhospitable microenvironment for T cells. Studies have demonstrated that hypoxia upregulates PD-L1 on the surface of tumour cells. As there is a wide range of immune checkpoint inhibitors (ICIs) currently under clinical development that target a wide spectrum of ICs, it is therefore important to elucidate the effects of the OGJ TME on T cell IC expression. However, little is known about the effect of nutrient deprivation or hypoxia on the IC expression profile of OGJ derived T cells. These findings will help guide the rationale selection of ICIs to reinvigorate T cells within this inhospitable environment.

Hypoxia treatment alone did not significantly affect the expression of ICs on the surface of OGJ patient-derived T cells (**Figure 3.14**). However, glucose deprivation significantly increased the expression of PD-1 on the surface of $CD4^+$ T cells compared with cells cultured in cRPMI (24.93 ± 4.3 vs. 22.40 ± 4.25%, p=0.03) (**Figure 3.14B**). In contrast, serum deprivation significantly decreased A2aR, CTLA-4 and PD-L2 expression on the surface of $CD4^+$ T cells compared with cells cultured in cRPMI (A2aR: 1.58 ± 0.4 vs. 7.43 ± 3.0%, p=0.03, CTLA-4: 2.19 ± 0.2 vs. 4.5 ± 1.0%, p=0.03 and PD-L2: 1.17 ± 0.4 vs. 4.07 ± 1.5%, p=0.03) (**Figure 3.14A**). Similarly, serum deprivation significantly decreased A2aR, CTLA-4, KLRG-1 and PD-L2 expression on the surface of $CD8^+$ T cells compared with cells cultured in cRPMI (A2aR: 1.75 ± 0.3 vs. 8.34 ± 2.6%, p=0.03, CTLA-4: 1.74 ± 0.2 vs. 4.54 ± 1.2%, p=0.03, KLRG-1: 27.41 ± 8.3 vs. 30.45 ± 8.8%, p=0.03, and PD-L2: 1.08 ± 0.2 vs. 5.28 ± 1.8%, p=0.03) (**Figure 3.14B**).

Dual hypoxia and serum deprivation significantly decreased LAG-3, A2aR and CD160 on the surface of $CD4^+$ T cells compared with cells cultured in cRPMI (LAG-3: 2.99 ± 0.8 vs. 9.54 ± 2.0%, p=0.03, A2aR: 1.97 ± 0.6 vs. 7.42 ± 3.0%, p=0.03 and CD160: 2.13 ± 0.3 vs. 8.18 ± 1.15%, p=0.03) (**Figure 3.14A**). Furthermore, dual hypoxia and serum deprivation significantly decreased LAG-3, A2aR and CD160 on the surface of $CD8^+$ T cells compared

with cells cultured in cRPMI (LAG-3: 2.87 ± 0.7 vs. 11.69 ± 3.0%, p=0.03 and PD-L2: 1.49 ± 0.4 vs. 5.29 ± 1.8%, p=0.03) (**Figure 3.14B**).

Interestingly, dual hypoxia and glucose deprivation significantly increased A2aR, CTLA-4, PD-L1 on the surface of $CD4^+$ T cells compared with cells cultured in cRPMI (A2aR: 14.88 ± 6.4 vs. 7.42 ± 3.0%, p=0.03, CTLA-4: 11.85 ± 2.6 vs. 4.50 ± 1.0%, p=0.03 and PD-L1: 17.99 ± 6.8 vs. 6.67 ± 2.1%, p=0.03) (**Figure 3.14A**). Similarly, dual hypoxia and glucose deprivation significantly increased A2aR, CTLA-4, PD-L1 and PD-L2 on the surface of $CD8^+$ T cells compared with cells cultured in cRPMI (A2aR: 20.73 ± 6.0 vs. 8.33 ± 2.50%, p=0.03, CTLA-4: 15.18 ± 3.6 vs. 4.50 ± 1.2%, p=0.03, PD-L1: 27.63 ± 8.3 vs. 8.84 ± 2.5%, p=0.03 and PD-L2: 17.42 ± 7.1 vs. 5.28 ± 1.8%, p=0.03) (**Figure 3.14B**). In contrast, dual hypoxia and glucose deprivation significantly decreased TIGIT expression on the surface of $CD8^+$ T cells compared with cells cultured in cRPMI (36.08 ± 2.8 vs. 47.33 ± 5.7%, p=0.03) (**Figure 3.14B**).

Additionally, dual glucose and serum deprivation significantly increased PD-1 and decreased KLRG-1 and CD160 on the surface of $CD4^+$ T cells compared with cells cultured in cRPMI (PD-1: 27.65 ± 4.3 vs. 22.40 ± 4.3%, p=0.03, KLRG-1: 12.84 ± 5.6 vs. 18.82 ± 7.1%, p=0.03 and CD160: 4.65 ± 1.07 vs. 8.18 ± 1.1%, p=0.03) (**Figure 3.14A**). Similarly, dual glucose and serum deprivation significantly decreased KLRG-1 and CD160 on the surface of $CD8^+$ T cells compared with cells cultured in cRPMI (KLRG-1: 20.67 ± 5.7 vs. 30.45 ± 8.7%, p=0.03 and CD160: 4.08 ± 0.6 vs. 7.75 ± 0.8%, p=0.03) (**Figure 3.14A**).

Combined hypoxia with both glucose and serum deprivation significantly increased PD-1 and CTLA-4 on the surface of $CD4^+$ T cells compared with cells cultured in cRPMI (PD-1: 26.87 ± 3.8 vs. 22.40 ± 4.3%, p=0.03 and CTLA-4: 8.02 ± 1.3 vs. 4.50 ± 1.0%, p=0.03) (**Figure 3.14A**). Contrastingly, combined hypoxia with both glucose and serum deprivation significantly decreased CD160 on the surface of $CD4^+$ T cells compared with cells cultured in cRPMI (3.79 ± 0.7 vs. 8.18 ± 1.2%, p=0.03) (**Figure 3.14A**). Moreover, combined hypoxia with both glucose and serum deprivation significantly increased CTLA-4 and PD-L2 on the surface of $CD8^+$ T cells compared with cells cultured in cRPMI (CTLA-4: 8.45 ± 1.0 vs. 4.55 ± 1.2%, p=0.03 and PD-L2: 5.96 ± 1.7 vs. 5.29 ± 1.7%, p=0.03) (**Figure 3.14B**).

Overall, nutrient deprivation and hypoxia had a profound effect on the IC expression profiles T cells, overall decreasing CD160, TIGIT, LAG-3 and KLRG-1 expression and increasing PD-1 and PD-L1 expression on T cells. Interestingly, depending on the specific combination of conditions of nutrient deprivation and hypoxia the expression of PD-L2, A2aR and CTLA-4 were differentially expressed on T cell surfaces.

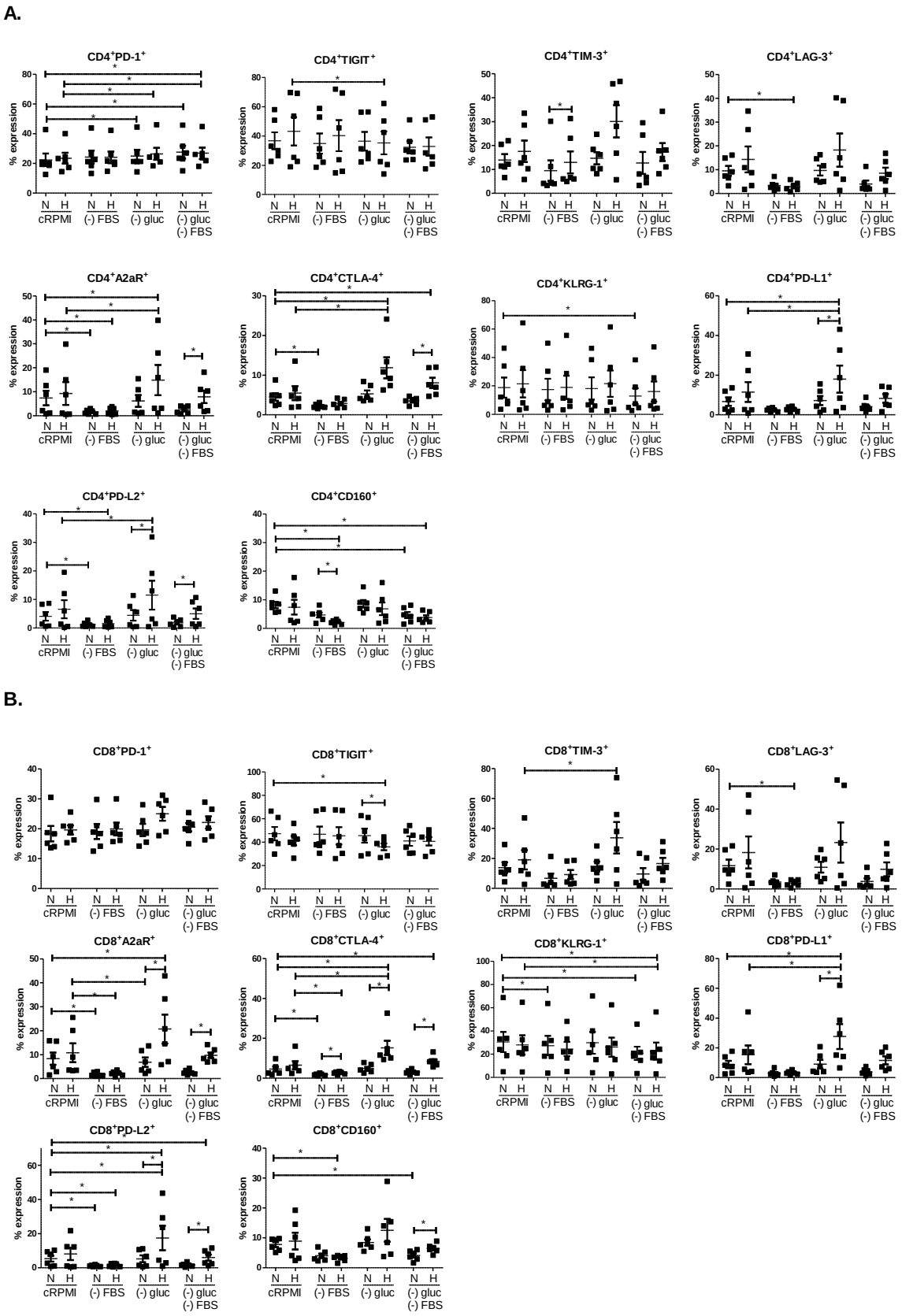

Figure 3.14: Combination hypoxia and glucose deprivation upregulated PD-1, CTLA-4, A2aR, PD-L1 and PD-L2 on the surface of OGJ patient-derived T cells. PBMCs were isolated from

peripheral blood of treatment-naïve OGJ patients (n=6) and expanded for 5 days in the presence of plate bound anti-CD3/anti-CD28 and recombinant human IL-2. Following a 5-day expansion, PBMCs were cultured for 24h under nutrient deprivation (FBS deprived or glucose deprived), hypoxia (0.5% O_2) and combined nutrient deprivation and hypoxic conditions. $CD3^+CD4^+$ (A) and $CD3^+CD8^+$ (B) cells were stained with a zombie viability dye and antibodies specific for a range of inhibitory immune checkpoint receptors (PD-1, TIGIT, TIM-3, LAG-3, A2aR, CTLA-4 and KLRG-1) and inhibitory immune checkpoint ligands (PD-L1, PD-L2 and CD160) and expression was assessed by flow cytometry. Paired, non-parametric t test. Expression presented as percentage ± SEM on live cells. Zombie dye was used to exclude dead cells from analysis. Abbreviations: N, normoxia; H, hypoxia. Gating strategy and representative dot plots are shown in Appendix **Figure A3.1**.

3.2.12 Hypoxia treatment decreases the frequency of central memory and effector memory T cells and promotes a terminally differentiated state

To provide further insight into the effect of nutrient deprivation and hypoxia on T cell phenotype, we investigated the effect of nutrient deprivation and hypoxia on T cell differentiation states using OGJ patient-derived T cells (**Figure 3.15**).

Hypoxia treatment significantly decreased CD27 and CD62L expression on the surface of $CD4^+$ T cells compared with cells cultured under normoxic conditions (CD27: 14.41 ± 2.9 vs. 20.83 ± 3.4%, p=0.03 and CD62L: 45.93 ± 7.5 vs. 61.78 ± 6.7%, p=0.03) (**Figure 3.15A**). Similarly, hypoxia treatment significantly decreased CD27 and CD62L expression on the surface of $CD8^+$ T cells compared with cells cultured under normoxic conditions (CD27: 11.94 ± 2.5 vs. 17.01 ± 3.6%, p=0.03 and CD62L: 33.14 ± 6.9 vs.50.52 ± 8.09%, p=0.03) (**Figure 3.15B**). Furthermore, hypoxia treatment significantly decreased the frequency of central memory $CD4^+$ T cells and significantly increased the frequency of effector memory $CD4^+$ T cells compared with cells cultured under normoxic conditions (central memory $CD4^+$ T cells: 13.57 ± 3.9 vs. 18.33 ± 3.7%, p=0.03 and effector memory $CD4^+$ T cells: 78.60 ± 6.9 vs. 72.95 ± 7.3%, p=0.03) (**Figure 3.15A**). Similarly, hypoxia treatment significantly decreased the frequency of naïve $CD8^+$ T cells and central memory $CD8^+$ T cells and significantly increased the frequency of effector memory $CD8^+$ T cells compared with cells cultured under normoxic conditions (naive $CD8^+$ T cells: 1.95 ± 0.6 vs. 3.20 ± 1.0%, p=0.03, central memory $CD8^+$ T cells: 13.07 ± 3.31 vs. 17.15 ± 4.2%, p=0.03 and effector memory $CD8^+$ T cells: 81.72 ± 3.2 vs. 75.45 ± 4.3%, p=0.03) (**Figure 3.15B**).

Serum deprivation significantly decreased CD62L and CD45RA expression on the surface of $CD4^+$ T cells compared with cells cultured in cRPMI (CD62L: 32.46 ± 10.7 vs. 61.78 ± 6.7%,

p=0.03 and CD45RA: 5.37 ± 2.3 vs. 8.45 ± 4.37%, p=0.03) (**Figure 3.15A**). However, serum deprivation did not significantly alter $CD4^+$ T cell differentiation states compared with cells cultured in cRPMI (**Figure 3.15A**). Similarly, serum deprivation significantly decreased CD27, CD69 and CD62L expression on the surface of $CD8^+$ T cells compared with cells cultured in cRPMI (CD27: 12.59 ± 3.1 vs. 17.01 ± 3.6%, p=0.03, CD69: 5.32 ± 1.5 vs. 10.19 ± 1.3%, p=0.03 and CD62L: 31.12 ± 9.7 vs. 50.52 ± 8.1%, p=0.03) (**Figure 3.15B**). In addition, serum deprivation decreased the frequency of naïve $CD8^+$ T cells compared with cells cultured in cRPMI (2.06 ± 0.8 vs. 3.19 ± 1.0%, p=0.03) (**Figure 3.15B**).

Interestingly, glucose deprivation alone did not significantly alter the expression of T cell activation markers or frequency of T cell differentiation states compared with cells cultured in cRPMI (**Figure 3.15**).

Dual serum deprivation and glucose deprivation significantly decreased CD62L expression on the surface of $CD4^+$ T cells and $CD8^+$ T cells compared with cells cultured under cRPMI ($CD4^+$ T cells: 35.40 ± 12.54 vs. 61.78 ± 6.6%, p=0.03 and $CD8^+$ T cells: 35.66 ± 10.9 vs. 50.52 ± 8.1%, p=0.03) (**Figure 3.15**). Furthermore, dual serum deprivation and glucose deprivation significantly decreased CD69 expression on the surface of $CD8^+$ T cells compared with cells cultured in cRPMI (5.82 ± 1.2 vs. 10.19 ± 1.3%, p=0.03) (**Figure 3.15B**). Dual serum deprivation and glucose deprivation also significantly decreased the frequency of naïve $CD8^+$ T cells compared with cells cultured in cRPMI (2.25 ± 0.7 vs. 3.19 ± 0.1%, p=0.03) (**Figure 3.15B**).

Combined serum deprivation and hypoxia treatment significantly decreased CD27 and CD62L expression on the surface of $CD4^+$ T cells compared with cells cultured in normoxic cRPMI conditions (CD27: 10.06 ± 1.1 vs. 20.83 ± 3.6%, p=0.03 and CD62L: 22.21 ± 5.9 vs. 61.78 ± 6.7%, p=0.03) (**Figure 3.15A**). Similarly, combined serum deprivation and hypoxia treatment significantly decreased CD27, CD62L and CD45RA expression on the surface of $CD8^+$ T cells compared with cells cultured in normoxic cRPMI conditions (CD27: 10.07 ± 2.4 vs. 17.01 ± 3.6%, p=0.03, CD62L: 18.07 ± 4.5 vs. 50.52 ± 8.1%, p=0.03 and CD45RA: 4.41 ± 1.2 vs. 7.15 ± 1.7%, p=0.03) (**Figure 3.15B**). Furthermore, combined serum deprivation and hypoxia treatment significantly decreased the frequency of central memory $CD4^+$ T cells and subsequently increased the frequency of effector memory $CD4^+$ T cells compared with cells cultured in normoxic cRPMI conditions (central memory $CD4^+$ T cells: 10.94 ± 1.5 vs. 18.33 ± 3.7%, p=0.03 and effector memory $CD4^+$ T cells: 84.02 ± 3.5 vs. 72.95 ± 7.2%, p=0.03) (**Figure 3.15A**). Similarly combined serum deprivation and hypoxia treatment significantly

decreased the frequency of naïve $CD8^+$ T cells and central memory $CD8^+$ T cells and increased the frequency of effector memory $CD8^+$ T cells compared with cells cultured in normoxic cRPMI conditions (naive $CD8^+$ T cells: 1.50 ± 0.6 vs. 3.19 ± 0.9%, p=0.03, central memory $CD8^+$ T cells: 11.12 ± 2.9 vs.17.15 ± 4.2%, p=0.03 and effector memory $CD8^+$ T cells: 84.30 ± 3.1 vs. 75.45 ± 4.3%, p=0.03) (**Figure 3.15B**).

Combined glucose deprivation and hypoxia treatment significantly decreased CD27 and CD62L expression on the surface of $CD4^+$ T cells compared with cells cultured in normoxic cRPMI conditions (CD27: 9.32 ± 1.6 vs. 20.83 ± 3.7%, p=0.03 and CD62L: 32.53 ± 7.6 vs. 61.78 ± 6.7%, p=0.03) (**Figure 3.15A**). Combined glucose deprivation and hypoxia treatment significantly decreased the frequency of central memory $CD4^+$ T cells and subsequently increased the frequency of effector memory $CD4^+$ T cells compared with cells cultured in normoxic cRPMI conditions (central memory $CD4^+$ T cells: 8.49 ± 1.5 vs. 18.33 ± 3.6%, p=0.03 and effector memory $CD4^+$ T cells: 82.37 ± 5.3 vs. 72.95 ± 7.3%, p=0.03) (**Figure 3.15A**). Similar effects were observed in the $CD8^+$ T cell compartment, where combined glucose deprivation and hypoxia treatment significantly decreased CD27 and CD62L expression on the surface of $CD8^+$ T cells compared with cells cultured in normoxic cRPMI conditions (CD27: 8.12 ± 1.9 vs. 17.01 ± 3.6%, p=0.03 and CD62L: 25.21 ± 6.6 vs. 50.52 ± 8.1%, p=0.03) (**Figure 3.15B**). Furthermore, combined glucose deprivation and hypoxia treatment significantly decreased the frequency of central memory $CD8^+$ T cells and subsequently increased the frequency of effector memory $CD8^+$ T cells compared with cells cultured in normoxic cRPMI conditions (central memory $CD8^+$ T cells: 9.35 ± 2.9 vs. 17.15 ± 4.2%, p=0.03 and effector memory $CD8^+$ T cells: 84.72 ± 2.3 vs. 75.45 ± 4.3%, p=0.03) (**Figure 3.15B**).

All three treatments combined, hypoxia with both glucose and serum deprivation significantly decreased CD62L expression on the surface of $CD4^+$ T cells compared with cells cultured in normoxic cRPMI conditions (CD27: 36.01 ± 8.8 vs. 61.78 ± 6.7%, p=0.03) **Figure 3.15A**). Similarly, combined hypoxia with both glucose and serum deprivation significantly decreased CD27 and CD62L expression on the surface of $CD8^+$ T cells compared with cells cultured in normoxic cRPMI conditions (CD27: 10.90 ± 2.3 vs. 17.01 ± 3.6%, p=0.03 and CD62L: 28.42 ± 6.8 vs. 50.52 ± 8.1%, p=0.03) (**Figure 3.15B**). Although combined hypoxia with both glucose and serum deprivation did not significantly affect $CD4^+$ T cell differentiation state (**Figure 3.15A**). Combined hypoxia with both glucose and serum deprivation significantly decreased the frequency of naive $CD8^+$ T cells and subsequently increased the frequency of effector

memory $CD8^+$ T cells compared with cells cultured in normoxic cRPMI conditions (naive $CD8^+$ T cells: 1.89 ± 0.5 vs. 3.19 ± 1.0%, p=0.03 and effector memory $CD8^+$ T cells: 81.47 ± 2.6 vs. 75.45 ± 4.3%, p=0.03) (**Figure 3.15B**).

Overall, nutrient deprivation and hypoxia treatment decreased CD27, CD62L and CD45RA expression on T cells and promoted differentiation of $CD4^+$ and $CD8^+$ T cells into an effector memory-like state, whilst subsequently decreasing the frequencies of naïve and central memory $CD4^+$ and $CD8^+$ OGJ patient-derived T cells.

To provide further insight into the effect of nutrient deprivation and hypoxia on T cell phenotype, we investigated the effect of nutrient deprivation and hypoxia on T cell differentiation states using OGJ patient-derived T cells (**Figure 3.15**).

Hypoxia treatment significantly decreased CD27 and CD62L expression on the surface of $CD4^+$ T cells compared with cells cultured under normoxic conditions (CD27: 14.41 ± 2.9 vs. 20.83 ± 3.4%, p=0.03 and CD62L: 45.93 ± 7.5 vs. 61.78 ± 6.7%, p=0.03) (**Figure 3.15A**). Similarly, hypoxia treatment significantly decreased CD27 and CD62L expression on the surface of $CD8^+$ T cells compared with cells cultured under normoxic conditions (CD27: 11.94 ± 2.5 vs. 17.01 ± 3.6%, p=0.03 and CD62L: 33.14 ± 6.9 vs.50.52 ± 8.09%, p=0.03) (**Figure 3.15B**). Furthermore, hypoxia treatment significantly decreased the frequency of central memory $CD4^+$ T cells and significantly increased the frequency of effector memory $CD4^+$ T cells compared with cells cultured under normoxic conditions (central memory $CD4^+$ T cells: 13.57 ± 3.9 vs. 18.33 ± 3.7%, p=0.03 and effector memory $CD4^+$ T cells: 78.60 ± 6.9 vs. 72.95 ± 7.3%, p=0.03) (**Figure 3.15A**). Similarly, hypoxia treatment significantly decreased the frequency of naïve $CD8^+$ T cells and central memory $CD8^+$ T cells and significantly increased the frequency of effector memory $CD8^+$ T cells compared with cells cultured under normoxic conditions (naive $CD8^+$ T cells: 1.95 ± 0.6 vs. 3.20 ± 1.0%, p=0.03, central memory $CD8^+$ T cells: 13.07 ± 3.31 vs. 17.15 ± 4.2%, p=0.03 and effector memory $CD8^+$ T cells: 81.72 ± 3.2 vs. 75.45 ± 4.3%, p=0.03) (**Figure 3.15B**).

Serum deprivation significantly decreased CD62L and CD45RA expression on the surface of $CD4^+$ T cells compared with cells cultured in cRPMI (CD62L: 32.46 ± 10.7 vs. 61.78 ± 6.7%, p=0.03 and CD45RA: 5.37 ± 2.3 vs. 8.45 ± 4.37%, p=0.03) (**Figure 3.15A**). However, serum deprivation did not significantly alter $CD4^+$ T cell differentiation states compared with cells cultured in cRPMI (**Figure 3.15A**). Similarly, serum deprivation significantly decreased CD27, CD69 and CD62L expression on the surface of $CD8^+$ T cells compared with cells cultured in cRPMI (CD27: 12.59 ± 3.1 vs. 17.01 ± 3.6%, p=0.03, CD69: 5.32 ± 1.5 vs. 10.19 ± 1.3%,

p=0.03 and CD62L: 31.12 ± 9.7 vs. 50.52 ± 8.1%, p=0.03) (**Figure 3.15B**). In addition, serum deprivation decreased the frequency of naïve $CD8^+$ T cells compared with cells cultured in cRPMI (2.06 ± 0.8 vs. 3.19 ± 1.0%, p=0.03) (**Figure 3.15B**).

Interestingly, glucose deprivation alone did not significantly alter the expression of T cell activation markers or frequency of T cell differentiation states compared with cells cultured in cRPMI (**Figure 3.15**).

Dual serum deprivation and glucose deprivation significantly decreased CD62L expression on the surface of $CD4^+$ T cells and $CD8^+$ T cells compared with cells cultured under cRPMI ($CD4^+$ T cells: 35.40 ± 12.54 vs. 61.78 ± 6.6%, p=0.03 and $CD8^+$ T cells: 35.66 ± 10.9 vs. 50.52 ± 8.1%, p=0.03) (**Figure 3.15**). Furthermore, dual serum deprivation and glucose deprivation significantly decreased CD69 expression on the surface of $CD8^+$ T cells compared with cells cultured in cRPMI (5.82 ± 1.2 vs. 10.19 ± 1.3%, p=0.03) (**Figure 3.15B**). Dual serum deprivation and glucose deprivation also significantly decreased the frequency of naïve $CD8^+$ T cells compared with cells cultured in cRPMI (2.25 ± 0.7 vs. 3.19 ± 0.1%, p=0.03) (**Figure 3.15B**).

Combined serum deprivation and hypoxia treatment significantly decreased CD27 and CD62L expression on the surface of $CD4^+$ T cells compared with cells cultured in normoxic cRPMI conditions (CD27: 10.06 ± 1.1 vs. 20.83 ± 3.6%, p=0.03 and CD62L: 22.21 ± 5.9 vs. 61.78 ± 6.7%, p=0.03) (**Figure 3.15A**). Similarly, combined serum deprivation and hypoxia treatment significantly decreased CD27, CD62L and CD45RA expression on the surface of $CD8^+$ T cells compared with cells cultured in normoxic cRPMI conditions (CD27: 10.07 ± 2.4 vs. 17.01 ± 3.6%, p=0.03, CD62L: 18.07 ± 4.5 vs. 50.52 ± 8.1%, p=0.03 and CD45RA: 4.41 ± 1.2 vs. 7.15 ± 1.7%, p=0.03) (**Figure 3.15B**). Furthermore, combined serum deprivation and hypoxia treatment significantly decreased the frequency of central memory $CD4^+$ T cells and subsequently increased the frequency of effector memory $CD4^+$ T cells compared with cells cultured in normoxic cRPMI conditions (central memory $CD4^+$ T cells: 10.94 ± 1.5 vs. 18.33 ± 3.7%, p=0.03 and effector memory $CD4^+$ T cells: 84.02 ± 3.5 vs. 72.95 ± 7.2%, p=0.03) (**Figure 3.15A**). Similarly combined serum deprivation and hypoxia treatment significantly decreased the frequency of naïve $CD8^+$ T cells and central memory $CD8^+$ T cells and increased the frequency of effector memory $CD8^+$ T cells compared with cells cultured in normoxic cRPMI conditions (naive $CD8^+$ T cells: 1.50 ± 0.6 vs. 3.19 ± 0.9%, p=0.03, central memory $CD8^+$ T cells: 11.12 ± 2.9 vs.17.15 ± 4.2%, p=0.03 and effector memory $CD8^+$ T cells: 84.30 ± 3.1 vs. 75.45 ± 4.3%, p=0.03) (**Figure 3.15B**).

Combined glucose deprivation and hypoxia treatment significantly decreased CD27 and CD62L expression on the surface of $CD4^+$ T cells compared with cells cultured in normoxic cRPMI conditions (CD27: 9.32 ± 1.6 vs. 20.83 ± 3.7%, p=0.03 and CD62L: 32.53 ± 7.6 vs. 61.78 ± 6.7%, p=0.03) (**Figure 3.15A**). Combined glucose deprivation and hypoxia treatment significantly decreased the frequency of central memory $CD4^+$ T cells and subsequently increased the frequency of effector memory $CD4^+$ T cells compared with cells cultured in normoxic cRPMI conditions (central memory $CD4^+$ T cells: 8.49 ± 1.5 vs. 18.33 ± 3.6%, p=0.03 and effector memory $CD4^+$ T cells: 82.37 ± 5.3 vs. 72.95 ± 7.3%, p=0.03) (**Figure 3.15A**). Similar effects were observed in the $CD8^+$ T cell compartment, where combined glucose deprivation and hypoxia treatment significantly decreased CD27 and CD62L expression on the surface of $CD8^+$ T cells compared with cells cultured in normoxic cRPMI conditions (CD27: 8.12 ± 1.9 vs. 17.01 ± 3.6%, p=0.03 and CD62L: 25.21 ± 6.6 vs. 50.52 ± 8.1%, p=0.03) (**Figure 3.15B**). Furthermore, combined glucose deprivation and hypoxia treatment significantly decreased the frequency of central memory $CD8^+$ T cells and subsequently increased the frequency of effector memory $CD8^+$ T cells compared with cells cultured in normoxic cRPMI conditions (central memory $CD8^+$ T cells: 9.35 ± 2.9 vs. 17.15 ± 4.2%, p=0.03 and effector memory $CD8^+$ T cells: 84.72 ± 2.3 vs. 75.45 ± 4.3%, p=0.03) (**Figure 3.15B**).

All three treatments combined, hypoxia with both glucose and serum deprivation significantly decreased CD62L expression on the surface of $CD4^+$ T cells compared with cells cultured in normoxic cRPMI conditions (CD27: 36.01 ± 8.8 vs. 61.78 ± 6.7%, p=0.03) **Figure 3.15A**). Similarly, combined hypoxia with both glucose and serum deprivation significantly decreased CD27 and CD62L expression on the surface of $CD8^+$ T cells compared with cells cultured in normoxic cRPMI conditions (CD27: 10.90 ± 2.3 vs. 17.01 ± 3.6%, p=0.03 and CD62L: 28.42 ± 6.8 vs. 50.52 ± 8.1%, p=0.03) (**Figure 3.15B**). Although combined hypoxia with both glucose and serum deprivation did not significantly affect $CD4^+$ T cell differentiation state (**Figure 3.15A**). Combined hypoxia with both glucose and serum deprivation significantly decreased the frequency of naive $CD8^+$ T cells and subsequently increased the frequency of effector memory $CD8^+$ T cells compared with cells cultured in normoxic cRPMI conditions (naive $CD8^+$ T cells: 1.89 ± 0.5 vs. 3.19 ± 1.0%, p=0.03 and effector memory $CD8^+$ T cells: 81.47 ± 2.6 vs. 75.45 ± 4.3%, p=0.03) (**Figure 3.15B**).

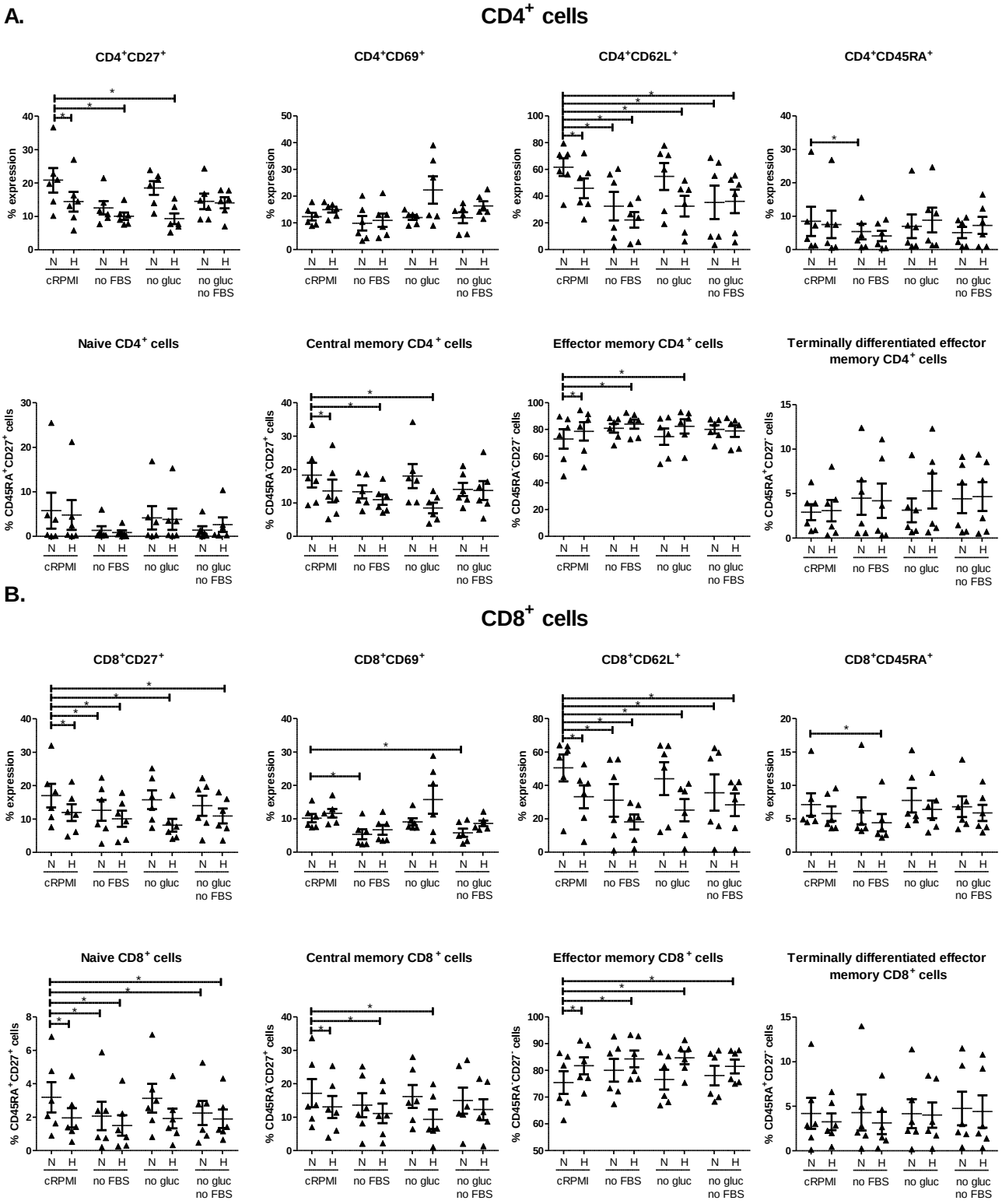

Figure 3.15: Combination hypoxia and glucose deprivation decreases the frequency of CD27$^+$ T cells and central memory T cells while increasing the frequency of effector memory T cells. PBMCs were isolated from peripheral blood of treatment-naïve OGJ patients (n=6) and expanded for 5 days in the presence of plate bound anti-CD3/anti-CD28 and recombinant human IL-2. Following a 5-

day expansion, PBMCs were cultured for an additional 24h under nutrient deprivation (FBS deprived or glucose deprived), hypoxia (0.5% O_2) and combined nutrient deprivation hypoxic conditions. Expression of a range of markers reflective of T cell activation status was assessed on viable $CD3^+CD4^+$ (A) and $CD3^+CD8^+$ (B) cells by flow cytometry. Markers assessed included: CD62L, CD69, CD27 and CD45RA. The percentage of viable naïve ($CD45RA^+CD27^+$), central memory ($CDRA^-CD27^+$), effector memory ($CD45RA^-CD27^-$) and terminally differentiated effector memory ($CD45RA^+CD27^-$) $CD3^+CD4^+$ (A) and $CD3^+CD8^+$ (B) cells was also determined by flow cytometry. Dead cells were excluded using a zombie viability dye. Paired, non-parametric t test. Expression presented as percentages ± SEM on live cells, *p<0.05. Zombie dye was used to exclude dead cells from analysis. Abbreviations: no gluc: no glucose, N: normoxia, H: hypoxia. Gating strategy and representative dot plots are shown in Appendix **Figure A3.2**.

Nivolumab has induced durable response rates in only a subpopulation of OGJ patients and studies have implicated a role of nutrient depletion and hypoxia for driving resistance to ICB[98,253]. Therefore, the ability of nivolumab to enhance T cell activation status or T cell differentiation status was also assessed. However, nivolumab had a minimal effect on the expression of T cell activation markers, under glucose deprivation under normoxic conditions nivolumab significantly decreased the expression of CD69 on the surface of $CD4^+$ T cells compared with untreated cells under those condition (9.75 ± 0.8 vs. 12.03 ± 0.9%, p=0.03) (**Figure 3.16).** Nivolumab did not significantly affect the differentiation status of T cells (**Figure 3.17)** under nutrient deprivation or hypoxia.

Overall, nutrient deprivation and hypoxia treatment decreased CD27, CD62L and CD45RA expression on T cells and promoted differentiation of $CD4^+$ and $CD8^+$ T cells into an effector memory-like state, whilst subsequently decreasing the frequencies of naïve and central memory $CD4^+$ and $CD8^+$ OGJ patient-derived T cells.

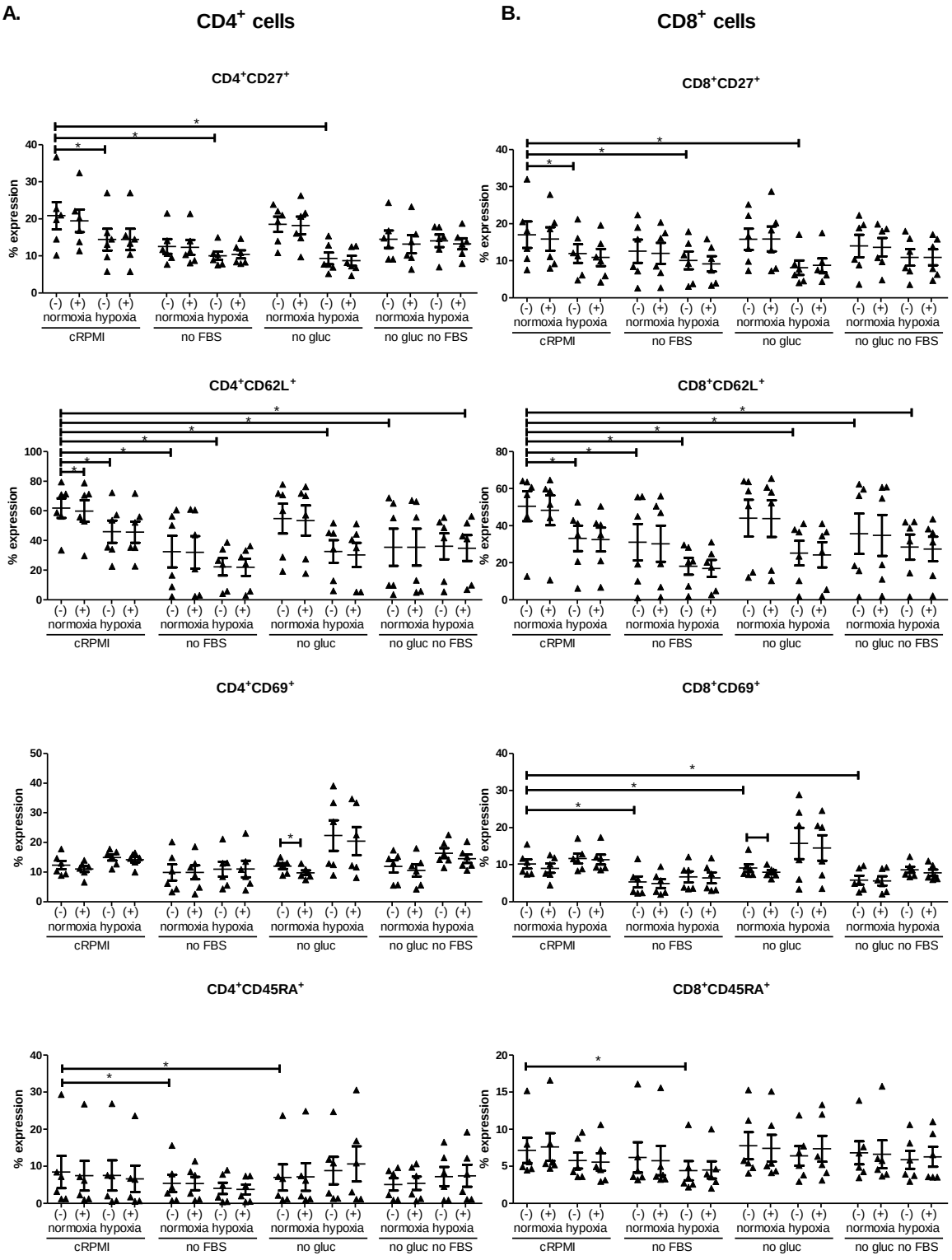

Figure 3.16: Nivolumab significantly decreased CD69 expression on T cells under nutrient deprivation. PBMCs were isolated from peripheral blood of treatment-naïve OGJ patients (n=6) and expanded for 5 days in the presence of plate bound anti-CD3/anti-CD28 and recombinant human IL-2. Following a 5-day expansion, PBMCs were cultured for 24h under nutrient deprivation (FBS deprived or glucose deprived), hypoxia (0.5% O_2) and combined nutrient deprivation hypoxic conditions in the

absence or presence of nivolumab (niv). Expression of a range of markers reflective of T cell activation status was assessed on viable $CD3^+CD4^+$ (A) and $CD3^+CD8^+$ (B) cells by flow cytometry (n=3). Markers assessed included: CD62L, CD69, CD27 and CD45RA. Dead cells were excluded using a zombie viability dye. Paired, non-parametric t test. Expression presented as percentages ± SEM on live cells. Abbreviations: (-): no nivolumab, (+): nivolumab (10 μg/ml), no gluc: no glucose, N: normoxia, H: hypoxia.

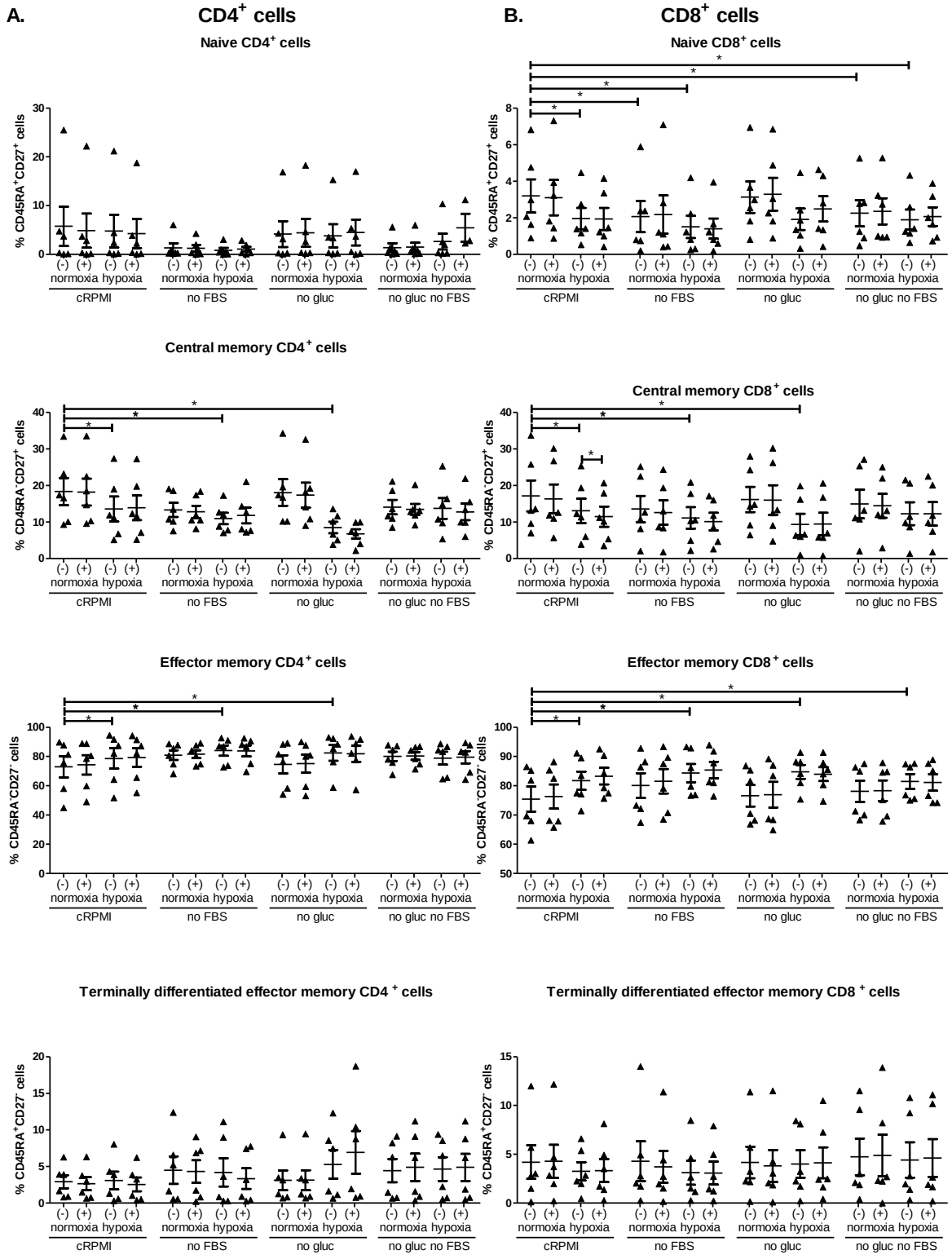

Figure 3.17: Nutrient deprivation and hypoxia substantially alter T cell differentiation status, however addition of nivolumab did not significantly affect T cell differentiation state under these conditions. PBMCs were isolated from peripheral blood of treatment-naïve OGJ patients (n=6) and expanded for 5 days in the presence of plate bound anti-CD3/anti-CD28 and recombinant human IL-2. Following a 5-day expansion, PBMCs were cultured for 24h under nutrient deprivation (FBS deprived

or glucose deprived), hypoxia (0.5% O_2) and combined nutrient deprivation hypoxic conditions in the absence or presence of nivolumab (niv). The percentage of viable naïve ($CD45RA^+CD27^+$), central memory ($CDRA^-CD27^+$), effector memory ($CD45RA^-CD27^-$) and terminally differentiated effector memory ($CD45RA^+CD27^-$) $CD3^+CD4^+$ (A) and $CD3^+CD8^+$ (B) cells was determined by flow cytometry. Dead cells were excluded using a zombie viability dye. Paired, non-parametric t test, *$p<0.05$. Expression presented as percentages ± SEM on live cells. Abbreviations: (-): no nivolumab, (+): nivolumab (10 μg/ml), no gluc: no glucose, N: normoxia, H: hypoxia.

3.3.13 Serum deprivation and hypoxia treatment decreased both IL-10 and IFN-γ expression by T cells

To determine the effect of nutrient deprivation and hypoxia on OGJ T cell phenotypes the expression of Th1-like and Th2-like cytokines were assessed following culture of OGJ patient-derived T cells under nutrient deprived and hypoxic conditions for 24h (**Figure 3.18**).

Hypoxia or nutrient deprivation did not significantly alter the production of TNF-α, IL-4 or IFN-γ by $CD4^+$ T cells (**Figure 3.18A**). However, the frequency of IL-10 producing $CD4^+$ T cells was significantly decreased following 24h culture under serum deprivation, dual serum deprivation combined with hypoxia, glucose deprivation, dual glucose deprivation and serum deprivation and dual glucose and serum deprivation in combination with hypoxia compared with cells cultured in cRPMI under normoxic conditions (4.89 ± 1.7 vs. 4.23 ± 1.6, 6.82 ± 2.3, 4.89 ± 1.6, 3.62 ± 1.2 and 10.62 ± 3.4%, p=0.03, p=0.03, p=0.03, p=0.03, p=0.03 and p=0.03, respectively) (**Figure 3.18A**).

Furthermore, hypoxia or nutrient deprivation did not significantly alter the production of TNF-α or IL-4 by $CD8^+$ T cells (**Figure 3.18B**). However, the frequency of IL-10 producing $CD8^+$ T cells was significantly decreased following 24h culture under serum deprivation, dual serum deprivation combined with hypoxia, glucose deprivation and dual glucose deprivation and serum deprivation compared with cells cultured in cRPMI under normoxic conditions (7.19 ± 2.4 vs. 5.63 ± 1.7, 10.47 ± 2.5, 7.59 ± 2.2 and 15.42 ± 3.6%, p=0.03, p=0.03, p=0.03, p=0.03 and p=0.03, respectively) (**Figure 3.18B**). In addition, the frequency of IFN-γ producing $CD8^+$ T cells was significantly decreased following 24h culture under dual glucose and serum deprivation and dual glucose and serum deprivation in combination with hypoxia compared with cells cultured in cRPMI under normoxic conditions (11.50 ± 3.9 vs. 9.46 ± 1.3 and 30.00 ± 5.2%, p=0.03 and p=0.03) (**Figure 3.18B**).

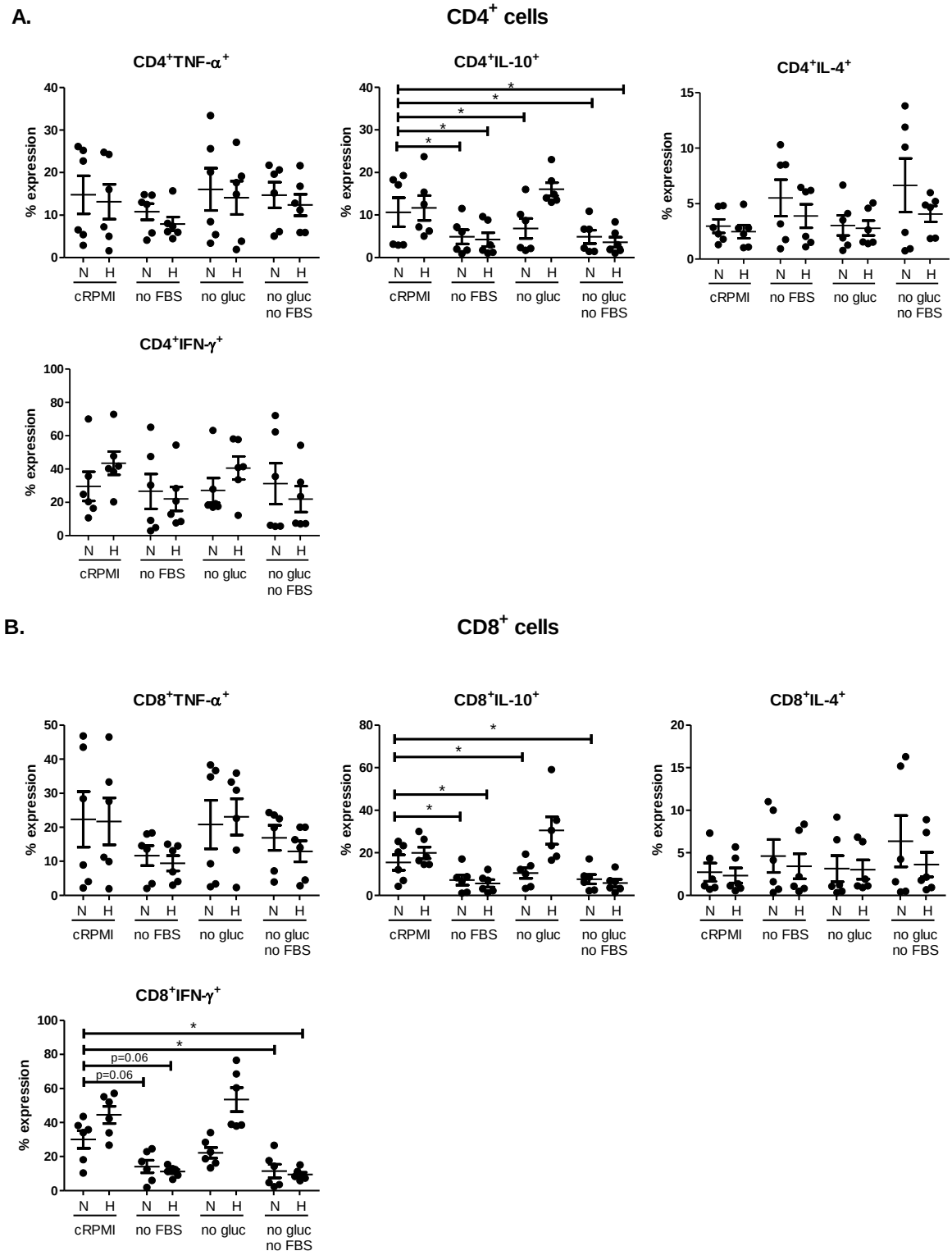

Figure 3.18: Combination serum deprivation and hypoxia treatment decreases the production of IL-10 and IFN-γ by T cells. PBMCs were isolated from peripheral blood of treatment-naïve OGJ patients (n=6) and expanded for 5 days in the presence of plate bound anti-CD3/anti-CD28 and recombinant human IL-2. Following a 5-day expansion, PBMCs were cultured for an additional 24h under nutrient deprivation (FBS deprived or glucose deprived), hypoxia (0.5% O_2) and combined

nutrient deprivation hypoxic conditions. Intracellular staining was conducted to assess $CD3^+CD4^+$ (A) and $CD3^+CD8^+$ (B) cell expression of TNF-α, IL-10, IL-4 and IFN-γ by flow cytometry. Paired, non-parametric t test. Expression presented as percentages ± SEM on viable cells. Abbreviations: no gluc: no glucose, N: normoxia, H: hypoxia. Gating strategy and representative dot plots are shown in Appendix **Figure A3.3**.

In addition, the effect of nivolumab on T cell cytokine profiles was also assessed under nutrient deprivation and hypoxia to determine if PD-1 blockade might enhance an anti-tumour phenotype in OGJ patient-derived T cells under conditions reflective of a hostile TME.
Interestingly, nivolumab significantly decreased the frequency of IL-10-producing $CD4^+$ T cells under combined glucose deprivation and hypoxic conditions compared with untreated cells cultured under those conditions (13.08 ± 1.3 vs. 16.07 ± 1.6%, p=0.03) (**Figure 3.19A**). Nivolumab did not significantly affect the frequency of IL-10-producing $CD4^+$ T cells under cRPMI conditions, nutrient deprivation alone or hypoxia treatment alone (**Figure 3.19A**). Similarly, nivolumab significantly decreased the frequency of IL-10-producing $CD8^+$ T cells under combined glucose deprivation and hypoxic conditions compared with untreated cells cultured under those conditions (27.12 ± 6.9 vs. 30.53 ± 6.4%, p=0.03) (**Figure 3.19B**). Nivolumab also significantly decreased the frequency of IL-10-producing $CD8^+$ T cells under combined glucose and serum deprivation under hypoxic conditions compared with untreated cells cultured under those conditions (4.80 ± 1.6 vs. 5.79 ± 1.7%, p=0.03) (**Figure 3.19B**). Nivolumab did not significantly affect the frequency of IL-10-producing $CD8^+$ T cells under cRPMI conditions, nutrient deprivation alone or hypoxia treatment alone (**Figure 3.19B**).
Moreover, nivolumab significantly decreased the frequency of IL-4-producing $CD8^+$ T cells cultured in cRPMI compared with untreated cells cultured under those conditions (2.23 ± 0.9 vs. 2.72 ± 1.1%, p=0.03) (**Figure 3.19B**). However, nivolumab did not significantly affect the frequency of IL-4-producing $CD8^+$ T cells under nutrient deprivation or hypoxia treatment alone or combined (**Figure 3.19B**). In addition, nivolumab treatment did not significantly affect the frequency of IFN-γ or TNF-α expressing T cells cultured in cRPMI, nutrient deprivation, hypoxia treatment or a combination of nutrient deprivation or hypoxia treatment (**Figure A3.4**).
Overall, nivolumab decreased the production of IL-10 by T cells under combined glucose deprivation and hypoxia treatment. In addition, nivolumab marginally but significantly decreased the production of IL-4 by T cells cultured in cRPMI but not nutrient deprived or hypoxic conditions.

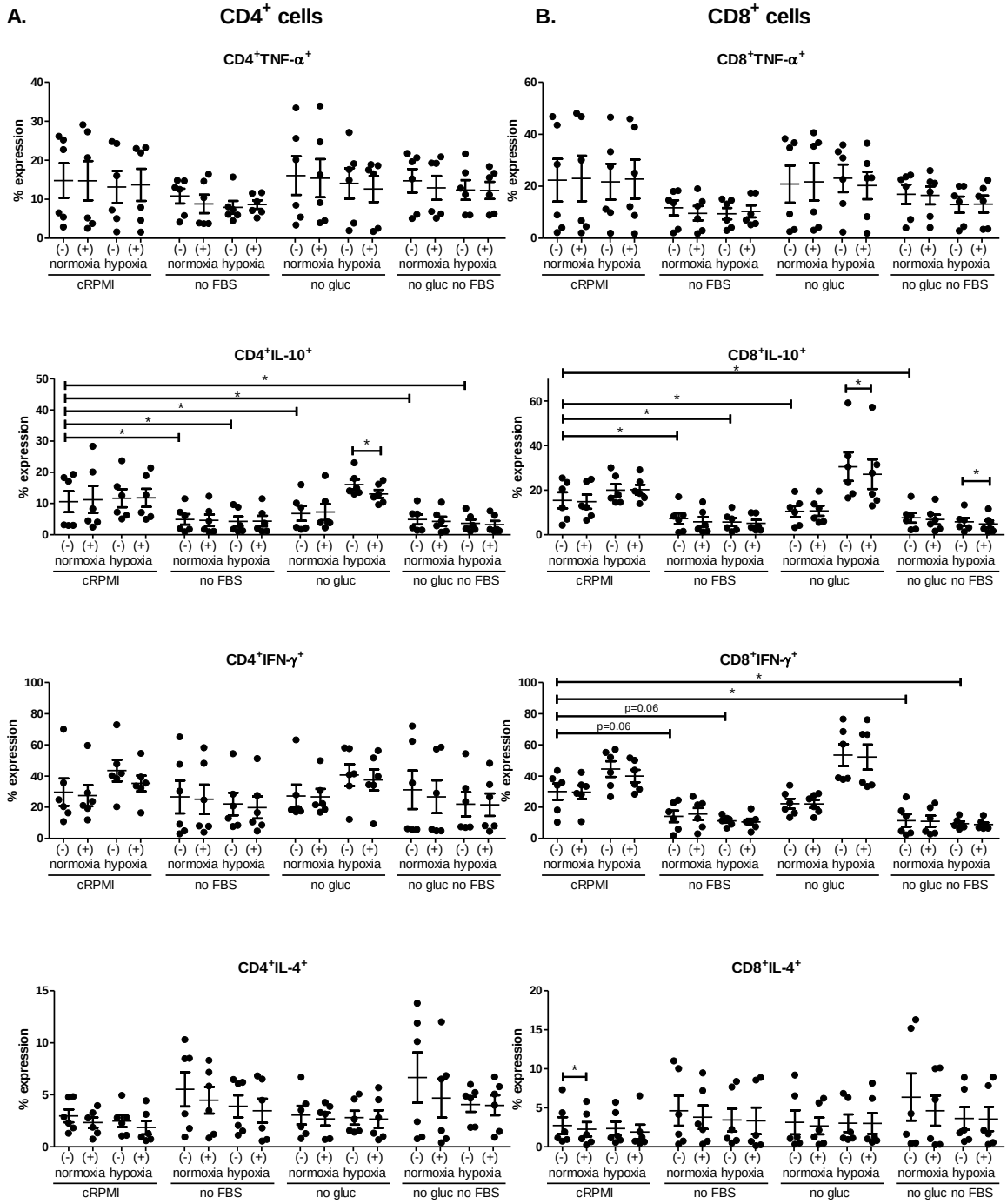

Figure 3.19: Nivolumab decreases the production of IL-10 by T cells under combined glucose deprived and hypoxic conditions and IL-4 production by T cells under normoxic conditions only. PBMCs were isolated from peripheral blood of treatment-naïve OGJ patients (n=6) and expanded for 5 days in the presence of plate bound anti-CD3/anti-CD28 and recombinant human IL-2. Following a 5-day expansion, PBMCs were cultured for an additional 24h under nutrient deprivation (FBS deprived or glucose deprived) and/or hypoxia (0.5% O_2) and combined nutrient deprivation hypoxic conditions in the absence or presence of nivolumab. Intracellular staining was conducted to assess $CD3^+CD4^+$ (A) and $CD3^+CD8^+$ (B) T cell production of TNF-α, IL-10, IL-4 and IFN-γ by flow cytometry. Paired, non-

parametric t test. Expression presented as percentages ± SEM on viable cells. Abbreviations: (-): no nivolumab, (+): nivolumab (10 μg/ml), no gluc: no glucose, N: normoxia, H: hypoxia. *p<0.05.

3.2.14 Acidic conditions substantially alter IC expression profiles of T cells but have minimal effect on IC expression profiles of OGJ cells

Investigating the effect of acidosis on IC expression on OGJ-derived T cells and OGJ cells will help guide identification of rational and novel ICs to target within the tumour microenvironment for OGJ patients.

There was a trend toward a significant increase in the expression of PD-1 on the surface of $CD8^+$ T cells cultured in pH 5.5 cRPMI compared with cells cultured in pH 7.4 cRPMI (8.25 ± 0.9 vs. 7.07 ± 1.2%, p=0.06) (**Figure 3.20D**). However, the expression of PD-1 was not significantly altered on $CD4^+$ T cells or on the surface of OE33 cells when cultured in acidic cRPMI compared with non-acidic cRPMI (**Figure 3.20D**). Additionally, there was a trend toward a significant decrease in the expression of TIGIT on the surface of $CD4^+$ T cells cultured in pH 5.5 cRPMI compared with cells cultured in pH 6.6 cRPMI (22.10 ± 1.9 vs. 26.72 ± 1.2%, p=0.06) (**Figure 3.20E**). However, the expression of TIGIT was not significantly altered on $CD8^+$ T cells or on the surface of OE33 cells when cultured in acidic cRPMI compared with non-acidic cRPMI (**Figure 3.20E**). Interestingly, the expression of TIM-3 was significantly increased on the surface of $CD4^+$ T cells (6.02 ± 0.8 vs. 2.90 ± 0.7%, p=0.03) and $CD8^+$ T cells (8.09 ± 1.5 vs. 3.45 ± 0.5%, p=0.03) when cultured in pH 5.5 cRPMI compared with pH 7.4 cRPMI (**Figure 3.20F**). In addition, there was a trend toward a significant increase in the expression of TIM-3 on the surface of OE33 cells when cultured in pH 5.5 cRPMI compared with pH 7.4 cRPMI (1.54 ± 0.1 vs. 1.12 ± 0.1%, p=0.07) (**Figure 3.20F**). Furthermore, the expression of LAG-3 was significantly increased on the surface of $CD4^+$ T cells (10.87 ± 1.9 vs. 3.61 ± 0.4%, p=0.03) and $CD8^+$ T cells (23.20 ± 2.7 vs. 5.40 ± 0.3%, p=0.03) when cultured in pH 5.5 cRPMI compared with pH 7.4 cRPMI (**Figure 3.20G**). Similarly, the expression of LAG-3 was significantly increased on the surface of $CD4^+$ T cells (10.87 ± 1.9 vs. 4.05 ± 0.4%, p=0.03) and $CD8^+$ T cells (23.20 ± 2.7 vs. 6.04 ± 0.4%, p=0.03) when cultured in pH 5.5 cRPMI compared with pH 6.6 cRPMI (**Figure 3.20G**). However, the expression of TIM-3 was not significantly altered on the surface of OE33 cells when cultured in acidic cRPMI compared with non-acidic cRPMI (**Figure 3.20G**). In addition, there was a trend toward a significant decrease in the expression of A2aR on the surface of $CD8^+$ T cells when cultured in pH 5.5 cRPMI compared with pH 7.4 cRPMI (5.41 ± 0.8 vs. 7.56 ± 1.3%, p=0.06) (**Figure 3.20H**).

Similarly, there was a trend toward a significant decrease in the expression of A2aR on the surface of $CD8^+$ T cells when cultured in pH 5.5 cRPMI compared with pH 6.6 cRPMI (5.41 ± 0.8 vs. 6.98 ± 1.1%, p=0.06) (**Figure 3.20H**). However, the expression of A2aR was not significantly altered on the surface of OE33 cells when cultured in acidic cRPMI compared with non-acidic cRPMI (**Figure 3.20H**).

In addition, KLRG-1 was significantly decreased on the surface of $CD8^+$ T cells when cultured in pH 5.5 cRPMI compared with pH 7.4 cRPMI (3.99 ± 0.7 vs. 11.40 ± 2.6%, p=0.03) (**Figure 3.20I**). Similarly, there was a trend toward a significant decrease in the expression of KLRG-1 on the surface of $CD8^+$ T cells when cultured in pH 5.5 cRPMI compared with pH 6.6 cRPMI (3.99 ± 0.7 vs. 10.76 ± 2.2%, p=0.06) (**Figure 3.20I**). Moreover, CTLA-4 was significantly increased on the surface of $CD4^+$ T cells (7.93 ± 0.6 vs. 5.23 ± 0.4%, p=0.03) and $CD8^+$ T cells (13.65 ± 0.6 vs. 9.75 ± 0.7%, p=0.03) when cultured in pH 5.5 cRPMI compared with pH 7.4 cRPMI (**Figure 3.20J**). Similarly, there was a trend toward a significant increase in the expression of CTLA-4 on the surface of $CD4^+$ T cells (7.93 ± 0.6 vs. 5.75 ± 0.5%, p=0.06) when cultured in pH 5.5 cRPMI compared with pH 6.6 cRPMI (p=0.06) (**Figure 3.20J**). In addition, CTLA-4 was significantly increased on the surface of $CD8^+$ T cells when cultured in pH 5.5 cRPMI compared with pH 6.6 cRPMI (13.65 ± 0.6 vs. 9.97 ± 0.8%, p=0.03) (**Figure 3.20J**).

There was a trend toward a significant increase in the expression of PD-L1 on the surface of $CD4^+$ T cells when cultured in pH 5.5 cRPMI compared with pH 7.4 cRPMI (1.76 ± 0.1 vs. 1.21 ± 0.1%, p=0.06) (**Figure 3.20K**). However, the expression of PD-L1 was not significantly altered on the surface of $CD8^+$ T cells or OE33 cells when cultured in acidic cRPMI compared with non-acidic cRPMI (**Figure 3.20K**). The expression of PD-L2 was not significantly altered on the surface of $CD4^+$ T cells or $CD8^+$ T cells by acidosis. However, there was a trend toward a significant increase in the expression of PD-L2 on the surface of OE33 cells when cultured in pH 5.5 cRPMI compared with pH 6.6 cRPMI and pH 7.4 cRPMI (1.05 ± 0.1 vs. 0.83 ± 0.1 and 0.84 ± 0.2%, p=0.06 and p=0.07, respectively) (**Figure 3.20L**). Additionally, the expression of CD160 significantly decreased on the surface of $CD4^+$ T cells when cultured in pH 5.5 cRPMI compared with pH 6.6 cRPMI and pH 7.4 cRPMI (2.94 ± 1.1 vs. 10.91 ± 2.8 and 11.67 ± 2.7%, p=0.03 and p=0.03, respectively) (**Figure 3.20M**). Similarly, the expression of CD160 significantly decreased on the surface of $CD8^+$ T cells when cultured in pH 5.5 cRPMI compared with pH 7.4 cRPMI (2.77 ± 0.4 vs. 5.70 ± 0.5%, p=0.03) (**Figure 3.20M**). In contrast, the expression of CD160 was significantly increased on the surface of OE33 cells

when cultured in pH 5.5 cRPMI compared with pH 7.4 cRPMI (1.59 ± 0.3 vs. 1.30 ± 0.1%, p=0.03) (**Figure 3.20M**).

We also assessed if mutated levels of the LDHA gene which converts pyruvate into lactate and if levels of the mutate lactate gene corelated with overall survival in OGJ patients and we found that they did not (**Figure 3.20P** and Figure **3.20Q**).

Overall, while acidosis significantly altered expression profiles of ICs on both the surface of OGJ-derived T cells and OE33 cells, acidosis had a much greater effect on the T cells. LAG-3, TIM-3 and CTLA-4 were significantly increased and KLRG-1 and CD160 were significantly decreased on the surface of T cells under acidic conditions.

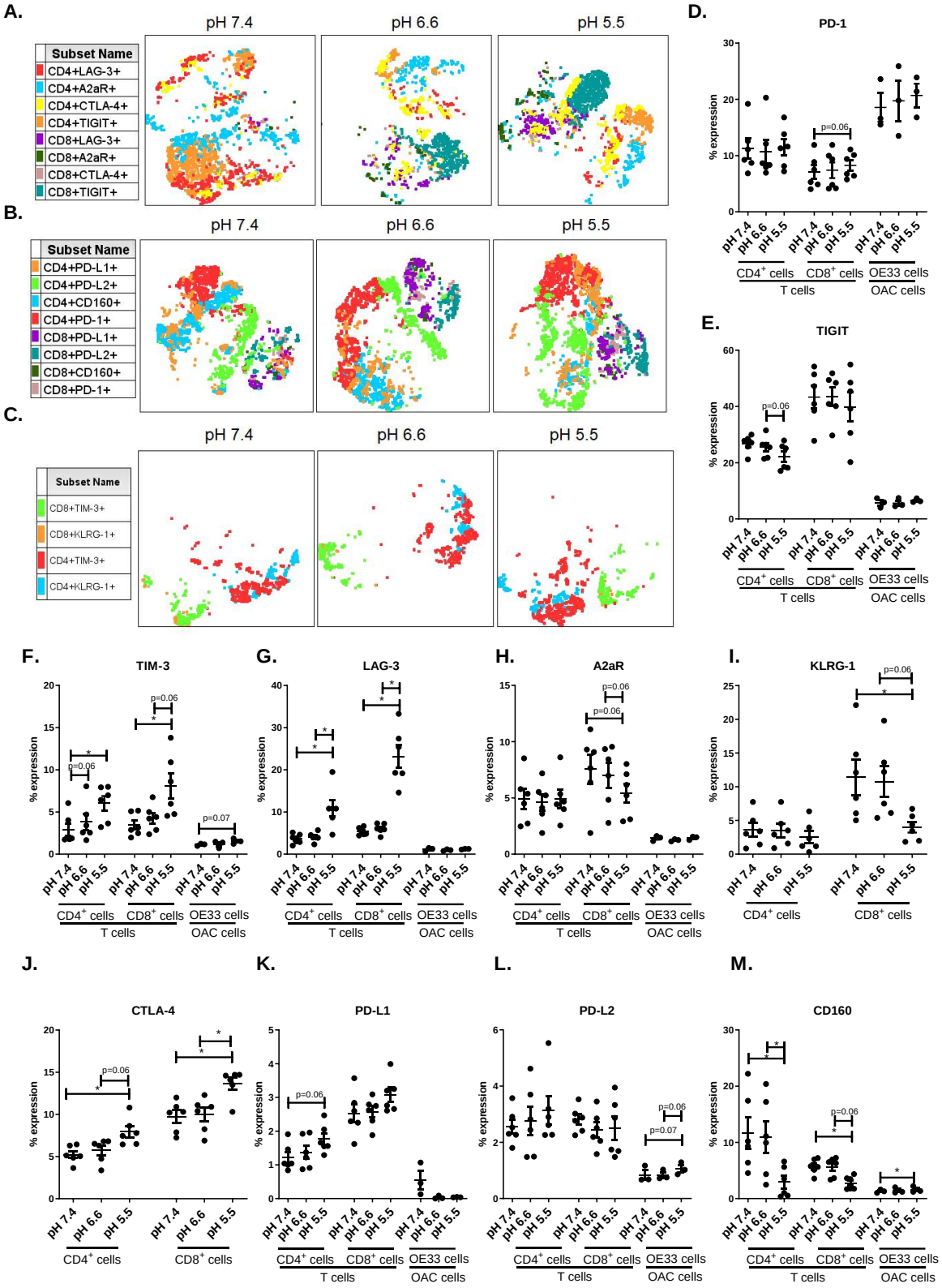
A.
pH 7.4
pH 6.6
pH 5.5
Subset Name
CD4+LAG-3+
CD4+A2aR+
CD4+CTLA-4+
CD4+TIGIT+
CD8+LAG-3+
CD8+A2aR+
CD8+CTLA-4+
CD8+TIGIT+
B.
Subset Name
CD4+PD-L1+
CD4+PD-L2+
CD4+CD160+
CD4+PD-1+
CD8+PD-L1+
CD8+PD-L2+
CD8+CD160+
CD8+PD-1+
C.
Subset Name
CD8+TIM-3+
CD8+KLRG-1+
CD4+TIM-3+
CD4+KLRG-1+
D.
PD-1
% expression
p=0.06
CD4+ cells
CD8+ cells
OE33 cells
T cells
OAC cells
E.
TIGIT
F.
TIM-3
p=0.07
G.
LAG-3
H.
A2aR
I.
KLRG-1
J.
CTLA-4
K.
PD-L1
L.
PD-L2
M.
CD160

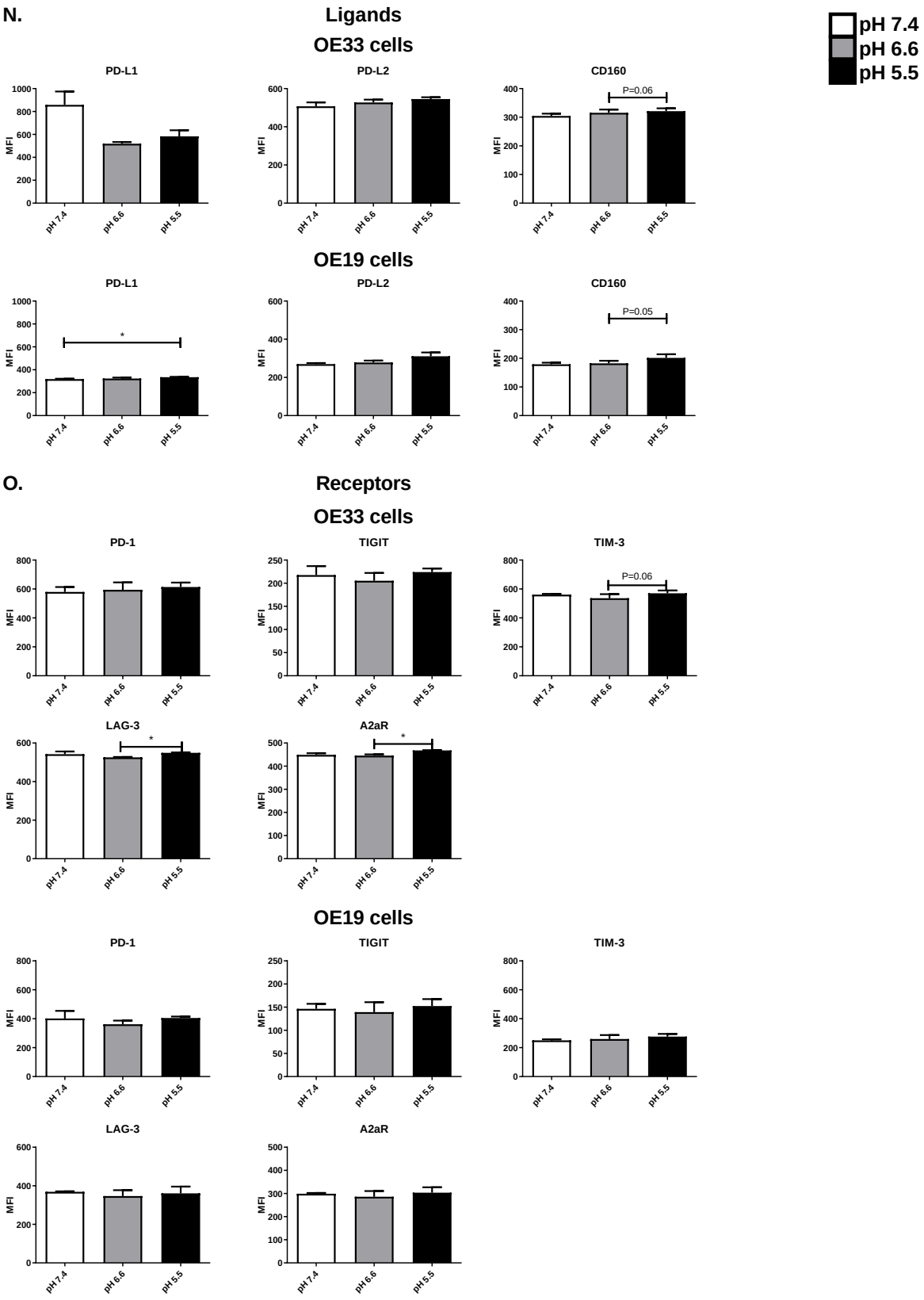
N.
Ligands
OE33 cells
pH 7.4
pH 6.6
pH 5.5
PD-L1
PD-L2
CD160
P=0.06
MFI
pH 7.4
pH 6.6
pH 5.5
OE19 cells
PD-L1
PD-L2
CD160
*
P=0.05
O.
Receptors
OE33 cells
PD-1
TIGIT
TIM-3
P=0.06
LAG-3
A2aR
*
*
OE19 cells
PD-1
TIGIT
TIM-3
LAG-3
A2aR

P. LDHA

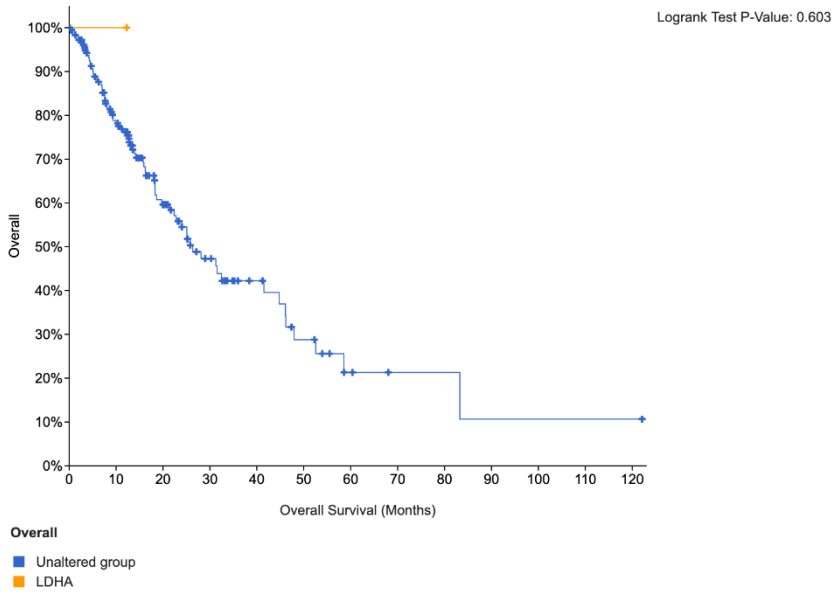

Q. Lactate

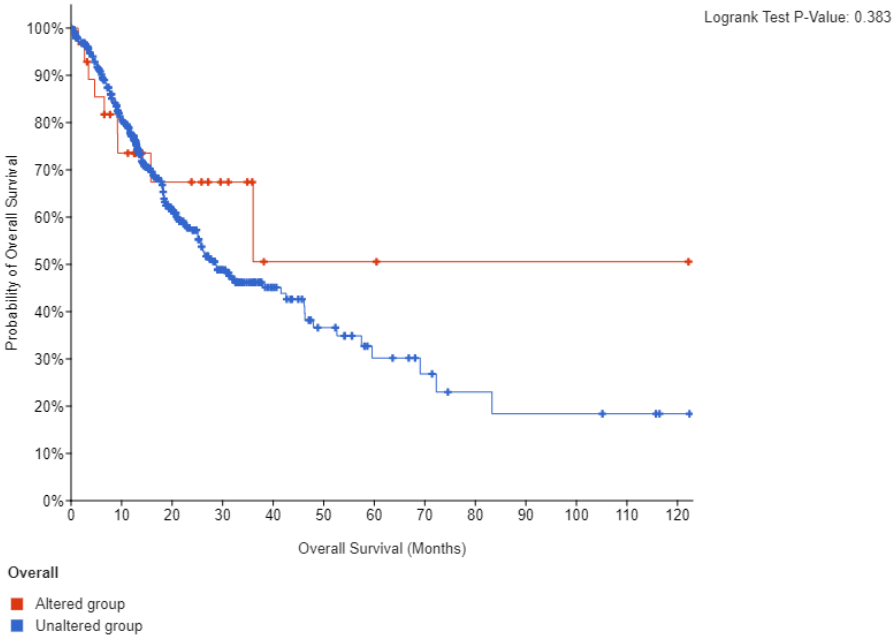

Figure 3.20: Acidic conditions upregulated TIM-3, LAG-3 and CTLA-4 and decreased KLRG-1 and CD160 ICs on T cells *ex vivo*. PBMCs were isolated from peripheral blood of treatment-naïve OAC patients (n=6) and expanded ex vivo for 7 days in the presence of plate bound anti-CD3/anti-CD28 and recombinant human IL-2. Following a 7-day expansion, PBMCs were cultured for 48h in media with increasing levels of acidity (pH 7.4, pH 6.6 and pH 5.5). CD3+, CD3+CD4+ and

CD3+CD8+ cells were stained with zombie viability dye and antibodies specific for IC ligands and receptors and expression was assessed by flow cytometry. OE33 cells were cultured for 48h in media with increasing levels of acidity (pH 7.4, pH 6.6 and pH 5.5) and expression of IC ligands and receptors was assessed by flow cytometry. (A-C) tSNE plots showing the effect of acidosis on the frequency of CD4+ and CD8+ cells expressing IC ligands and receptors on viable CD3+ singlet cells. (D-M) graphically displays the effect of acidosis on the frequency of CD4+ and CD8+ cells expressing IC ligands and receptors. CLTA-4 and KLRG-1 are typically expressed on lymphocyte cells so their expression on OE33 cells under acidic conditions was not assessed. Expression presented as percentages ± SEM. Paired, non-parametric t test for PBMCs (n=6) and paired parametric t-test for OE33 cells (n=3), *p<0.05. (N) and (O) display the effects of acidic conditions on the MFI of IC ligand and receptor levels in OE33 and OE19 cells. (P) and (Q) displays the overall survival of OGJ patients who had a mutated version of the LDHA gene and the lactate gene using TCGA database. Gating strategy and representative dot plots are shown in Appendix **Figure A3.4**.

3.2.15 Acidic conditions decrease the frequency of central memory T cells which is abrogated by ICB *ex vivo*

Given that acidosis significantly altered the expression profile of ICs on T cell surfaces we sought to investigate if acidosis might alter the activation status or differentiation status of T cells using OGJ-derived PBMCs (**Figure 3.21**).

There was a trend toward a decrease in the frequency of $CD4^+$ T cells expressing CD62L when cultured in pH 6.6 cRPMI compared with cells cultured in pH 7.4 cRPMI (1.45 ± 0.1 vs. 1.93 ± 0.4%, p=0.06) (**Figure 3.21A**). The frequency of $CD8^+$ T cells expressing CD62L was significantly decreased when cultured in pH 5.5 cRPMI compared with cells cultured in pH 7.4 cRPMI (3.65 ± 0.9 vs. 5.28 ± 1.3%, p=0.03) (**Figure 3.21A**). Although, acidosis did not significantly alter the frequency of $CD4^+$ T cells expressing CD69, there was a trend toward a decrease in the frequency of $CD8^+$ T cells expressing CD69 when cultured in pH 5.5 cRPMI compared with cells cultured in pH 7.4 cRPMI (2.22 ± 0.6 vs. 3.39 ± 1.3%, p=0.06) (**Figure 3.21A**). Moreover, there was a trend toward a significant increase in the frequency of $CD4^+$ T cells expressing CD27 when cultured in pH 6.6 cRPMI compared with cells cultured in pH 7.4 cRPMI (2.11 ± 0.4 vs. 1.45 ± 0.3%, p=0.06) (**Figure 3.21A**). However, acidosis did not significantly alter the frequency of $CD8^+$ T cells expressing CD27 (**Figure 3.21A**). In addition, there was a trend toward an increase in the frequency of $CD3^+$ cells expressing CD45RA when cultured in pH 5.5 cRPMI compared with cells cultured in pH 6.6 cRPMI (8.08 ± 2.4 vs. 5.76

± 1.5%, p=0.06) (**Figure 3.21A**). However, acidosis did not significantly alter the frequency of $CD4^+$ T cells or $CD8^+$ T cells expressing CD45RA (**Figure 3.21A**).

Although, acidosis did not significantly alter the frequency of naïve $CD4^+$ T there was a trend toward an increase in the frequency of naive $CD8^+$ T cells when cultured in pH 5.5 cRPMI compared with cells cultured in pH 7.4 cRPMI (1.34 ± 0.2 vs. 1.00 ± 0.1%, p=0.06) (**Figure 3.21B**). In addition, the frequency of central memory $CD4^+$ T cells was significantly decreased when cultured in pH 5.5 cRPMI compared with cells cultured in pH 6.6 cRPMI (1.94 ± 0.5 vs. 2.70 ± 0.7%, p=0.06) (**Figure 3.21A**). However, acidosis did not significantly alter the frequency of central memory $CD8^+$ T cells (**Figure 3.21B**). In addition, acidosis did not significantly alter the frequency of effector memory $CD4^+$ T cells or $CD8^+$ T cells or terminally differentiated effector memory $CD4^+$ T cells or $CD8^+$ T cells (**Figure 3.21B**).

Overall, acidosis did not have substantial effects on T cell activation status or differentiation state however acidosis did marginally but significantly decrease CD62L expression on the surface of $CD8^+$ T cells and significantly decrease the frequency of $CD4^+$ central memory T cells *ex vivo.*

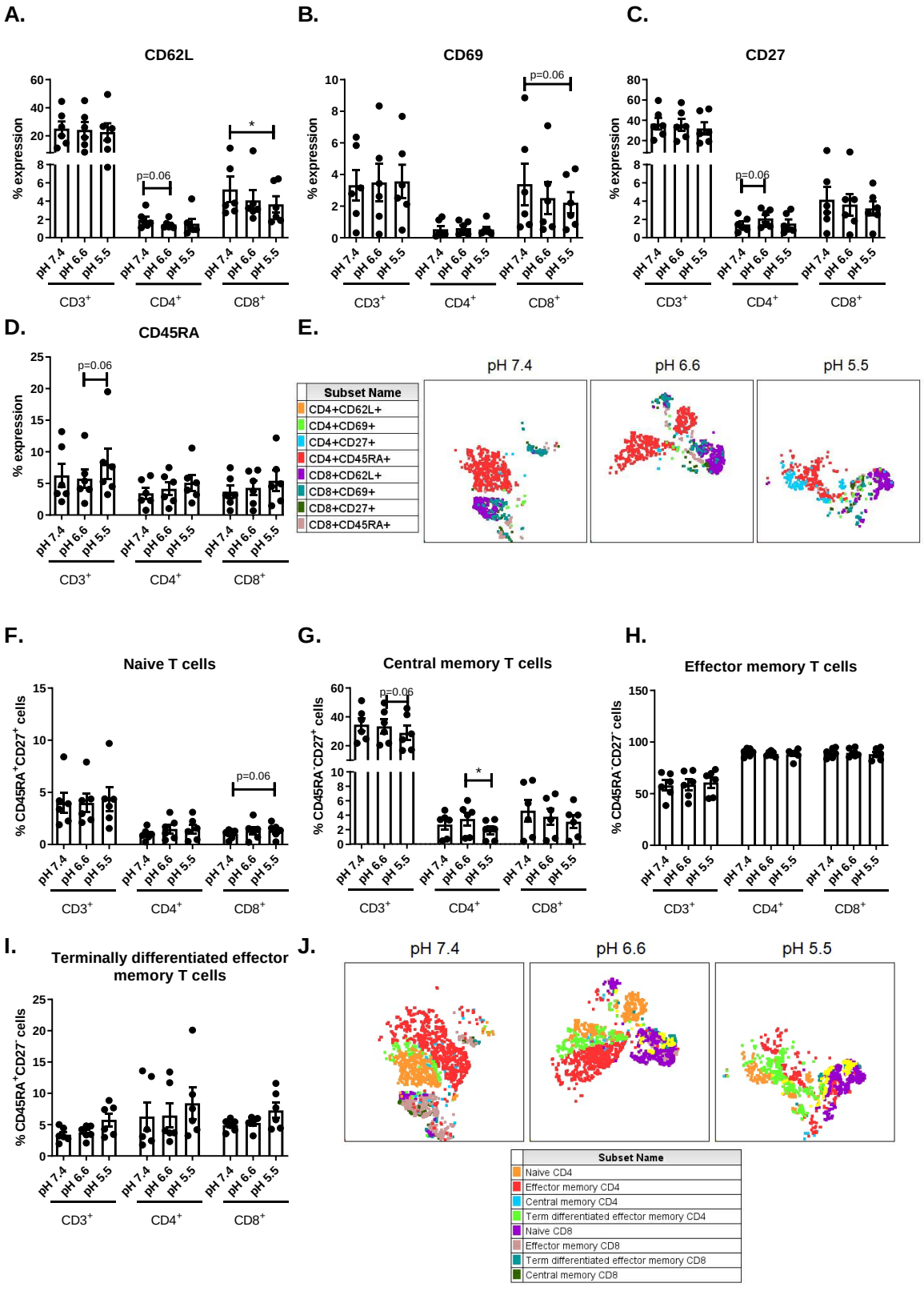

Figure 3.21: The percentage of central memory CD4⁺ T cells decreases under acidic conditions *ex vivo*. PBMCs were isolated from peripheral blood of treatment-naïve OAC patients (n=6) and expanded *ex vivo* for 7 days in the presence of plate bound anti-CD3/anti-CD28 and recombinant human IL-2.

Following a 7-day expansion, PBMCs were cultured for 48h in media with increasing levels of acidity (pH 7.4, pH 6.6 and pH 5.5) in the absence or presence of ICB. ICB included nivolumab (niv), ipilimumab (ipi) or dual nivolumab-ipilimumab (niv + ipi). Expression of markers reflective of T cell activation status was assessed on viable $CD3^+CD4^+$ (A-H) and $CD3^+CD8^+$ (I-P) cells by flow cytometry (n=6). Markers assessed included: CD62L, CD69, CD27 and CD45RA. The percentage of viable naïve ($CD45RA^+CD27^+$), central memory ($CD45RA^-CD27^+$), effector memory ($CD45RA^-CD27^-$) and terminally differentiated effector memory ($CD45RA^+CD27^-$) $CD3^+CD4^+$ (A) and $CD3^+CD8^+$ (B) cells was also determined by flow cytometry. Dead cells were excluded using a zombie viability dye. Paired, non-parametric t test, *$p<0.05$. Expression presented as percentages ± SEM. Gating strategy and representative dot plots are shown in Appendix **Figure A3.5**.

To further understand how ICB might improve T cell function under acidic conditions which are typically found within the tumour microenvironment single agent nivolumab, ipilimumab or dual nivolumab and ipilimumab treatment were added to the acidic *ex vivo* culture system (**Figure 3.22**).

Nivolumab significantly decreased CD62L expression on the surface of $CD4^+$ T cells compared with untreated cells in pH 7.4 cRPMI (1.56 ± 0.4 vs. 1.93 ± 0.4%, p=0.03) (**Figure 3.22A**). Interestingly, in pH 5.5 cRPMI CD62L expression is significantly increased on the surface of $CD4^+$ T cells following nivolumab treatment compared with untreated cells (2.01 ± 0.5 vs. 1.54 ± 0.5%, p=0.03) (**Figure 3.22A**). Moreover, dual nivolumab and ipilimumab treatment significantly decreased CD27 expression on the surface of $CD4^+$ T cells compared with untreated cells in pH 6.6 cRPMI (1.54 ± 0.3 vs. 2.11 ± 0.3%, p=0.03) but not in pH 7.4 or pH 5.5 cRPMI (**Figure 3.22A**). Interestingly, ipilimumab treatment significantly increased the frequency of central memory $CD4^+$ T cells compared with untreated cells in pH 5.5 cRPMI (2.77 ± 0.6 vs. 1.94 ± 0.5%, p=0.03) but not in pH 7.4 or pH 6.6 cRPMI (**Figure 3.22A**). Ipilimumab significantly decreased CD62L expression on the surface of $CD8^+$ T cells compared with untreated cells in pH 7.4 cRPMI (4.15 ± 0.9 vs. 5.28 ± 1.3%, p=0.03) but not in pH 6.6 cRPMI or pH 5.5 cRPMI (**Figure 3.22B**). In contrast, single agent nivolumab and single agent ipilimumab significantly increased CD62L expression on the surface of $CD8^+$ T cells compared with untreated cells in pH 5.5 cRPMI (5.20 ± 1.3 vs. 4.80 ± 1.1 and 3.65 ± 0.8%, p=0.03 and p=0.03) but not in pH 6.6 cRPMI or pH 7.4 cRPMI (**Figure 3.22B**). In addition, ipilimumab significantly decreased CD69 expression on the surface of $CD8^+$ T cells compared with untreated cells in pH 7.4 cRPMI (2.49 ± 0.8 vs. 3.39 ± 1.3%, p=0.03) (**Figure 3.22B**). In contrast, ipilimumab significantly increased CD69 expression on the surface of

$CD8^+$ T cells compared with untreated cells in pH 5.5 cRPMI (3.16 ± 0.9 vs. 2.22 ± 0.6%, p=0.03) (**Figure 3.22B**). ICB did not significantly alter the expression of CD69 in pH 6.6 cRPMI (**Figure 3.22B**). Moreover, there were trends toward a significant increase in the expression of CD27 on the surface of $CD8^+$ T cells in pH 5.5 cRPMI following single agent nivolumab and ipilimumab treatment compared with untreated cells (4.11 ± 1.1 vs. 4.08 ± 1.0 and 3.20 ± 0.7%, p=0.03 and p=0.03) (**Figure 3.22B**).

Single agent ipilimumab significantly decreased the frequency of central memory $CD8^+$ T cells compared with untreated cells in pH 7.4 cRPMI (3.16 ± 0.8 vs. 4.63 ± 1.4%, p=0.03) (**Figure 3.22B**). However, in pH 5.5 cRPMI single agent nivolumab significantly increased the frequency of central memory $CD8^+$ T cells compared with untreated cells (4.52 ± 1.3 vs. 3.11 ± 0.8%, p=0.03) (**Figure 3.22B**). Similarly, in pH 5.5 there were trends toward a significant increase in the frequency of central memory $CD8^+$ T cells compared with untreated cells following single agent ipilimumab treatment (4.61 ± 1.4 vs. 3.11 ± 0.8%, p=0.03) (**Figure 3.22B**).

Overall, nivolumab and ipilimumab single agent treatment marginally but significantly increased the frequency of central memory-like T cells *ex vivo*.

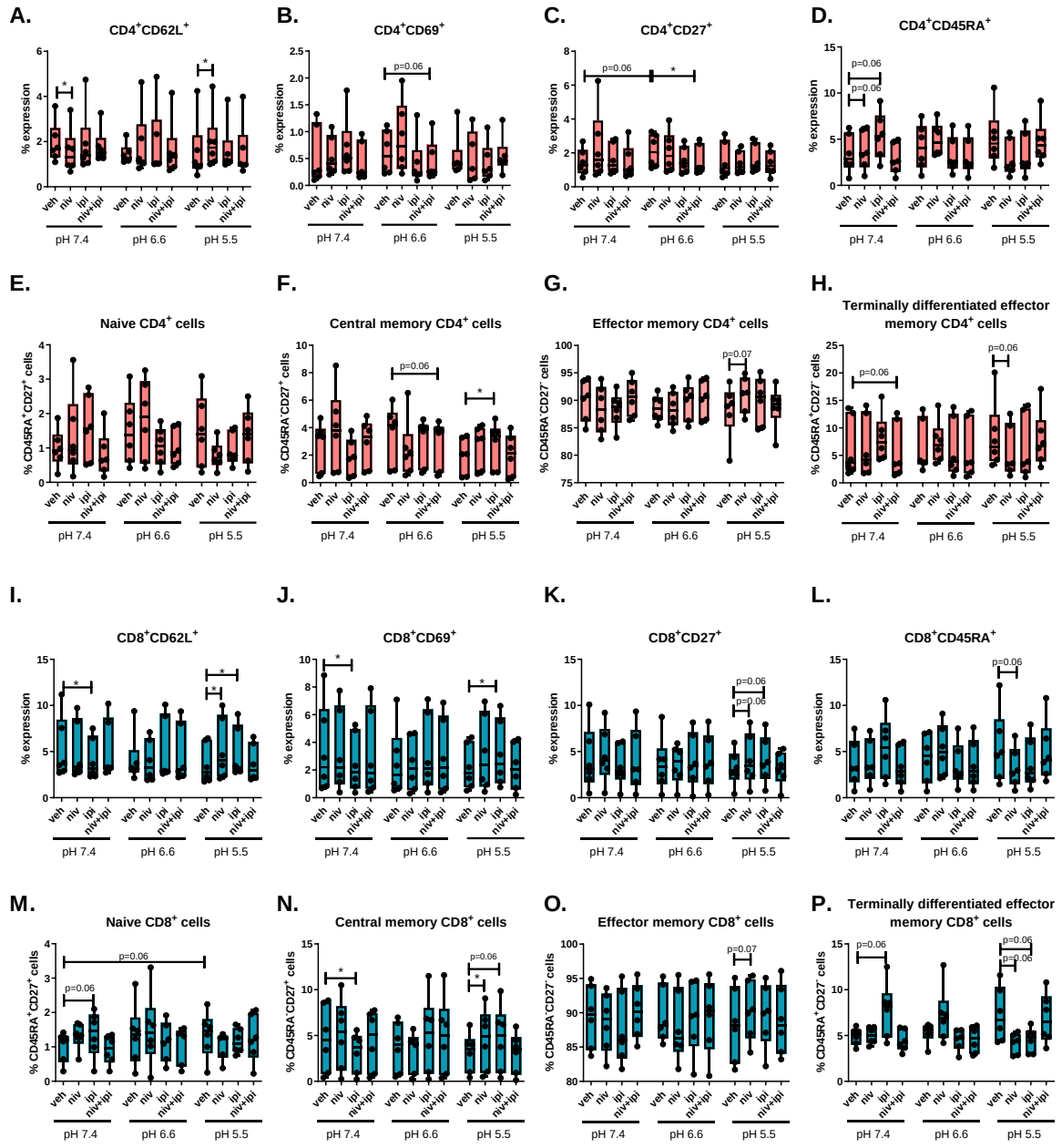

Figure 3.22: ICB increases the percentage of central memory T cells under acidic conditions *ex vivo*. PBMCs were isolated from peripheral blood of treatment-naïve OAC patients (n=6) and expanded *ex vivo* for 7 days in the presence of plate bound anti-CD3/anti-CD28 and recombinant human IL-2. Following a 7-day expansion, PBMCs were cultured for 48h in media with increasing levels of acidity (pH 7.4, pH 6.6 and pH 5.5). Expression of markers reflective of T cell activation status were assessed on viable $CD3^+$ cells, $CD3^+CD4^+$ and $CD3^+CD8^+$ cells by flow cytometry. Activation markers assessed included: CD62L(A), CD69(B), CD27(C) and CD45RA(D). tSNE plots depict the spatial distribution of CD4 and CD8 T cells expressing different activation markers under increasing conditions of acidosis on viable $CD3^+$ singlet cell population (E). T cell differentiation status was also assessed, the percentage of viable naïve ($CD45RA^+CD27^+$)(F), central memory ($CD45RA^-CD27^+$)(G), effector memory

(CD45RA$^-$CD27$^-$)(H) and terminally differentiated effector memory (CD45RA$^+$CD27$^-$)(I) CD3$^+$, CD3$^+$CD4$^+$ and CD3$^+$CD8$^+$ cells were determined by flow cytometry.). tSNE plots presenting the spatial distribution of CD4 and CD8 T cell differentiation states under increasing conditions of acidosis on the viable CD3$^+$ singlet cell population (J). Dead cells were excluded using a zombie viability dye. Paired, non-parametric t test, *p<0.05. Expression presented as percentages ± SEM.Gating strategy and representative dot plots are shown in Appendix **Figure A3.6**.

3.2.16 ICB enhances anti-tumour cytokine profiles of T cells under acidic conditions *ex vivo*

The effect of acidosis on anti-tumour and pro-tumour cytokine profiles of OGJ-derived T cells was investigated to acquire a deeper understanding of the potential immunosuppressive effects of acidosis in the context of OGJ (**Figure 3.23**).

Acidosis did not significantly alter the frequency of IFN-γ-producing T cells, IL-4-producing T cells or IL-10-producing T cells *ex vivo* (**Figure 3.23A**). However, acidosis had substantial effects on the frequency of TNF-α-producing T cells (**Figure 3.23A**). The frequency of TNF-α-producing CD4$^+$ T cells was significantly decreased in pH 5.5 cRPMI compared with cells cultured in pH 6.6 and pH 7.4 cRPMI (1.28 ± 0.3 vs. 31.10 ± 2.5, 36.57 ± 2.5%, p=0.03 and p=0.03) (**Figure 3.23A**). In addition, the frequency of TNF-α-producing CD4$^+$ T cells was significantly decreased in pH 6.6 cRPMI compared with cells cultured in pH 7.4 cRPMI (31.10 ± 2.5 vs. 36.57 ± 2.5%, p=0.03) (**Figure 3.23A**). Similarly, the frequency of TNF-α-producing CD8$^+$ T cells was significantly decreased in pH 5.5 cRPMI compared with cells cultured in pH 6.6 and pH 7.4 cRPMI (2.26 ± 0.5 vs. 23.48 ± 3.6, 25.87 ± 3.65%, p=0.03 and p=0.03) (**Figure 3.23A**). In addition, the frequency of TNF-α-producing CD8$^+$ T cells was significantly decreased in pH 6.6 cRPMI compared with cells cultured in pH 7.4 cRPMI (23.48 ± 3.6 vs. 25.87 ± 3.65%, p=0.03) (**Figure 3.23A**).

Furthermore, acidosis did not significantly alter the cytotoxic potential of CD8$^+$ T cells demonstrated by no significant alteration in the degranulation of CD8$^+$ T cells *ex vivo* (**Figure 3.23B**).

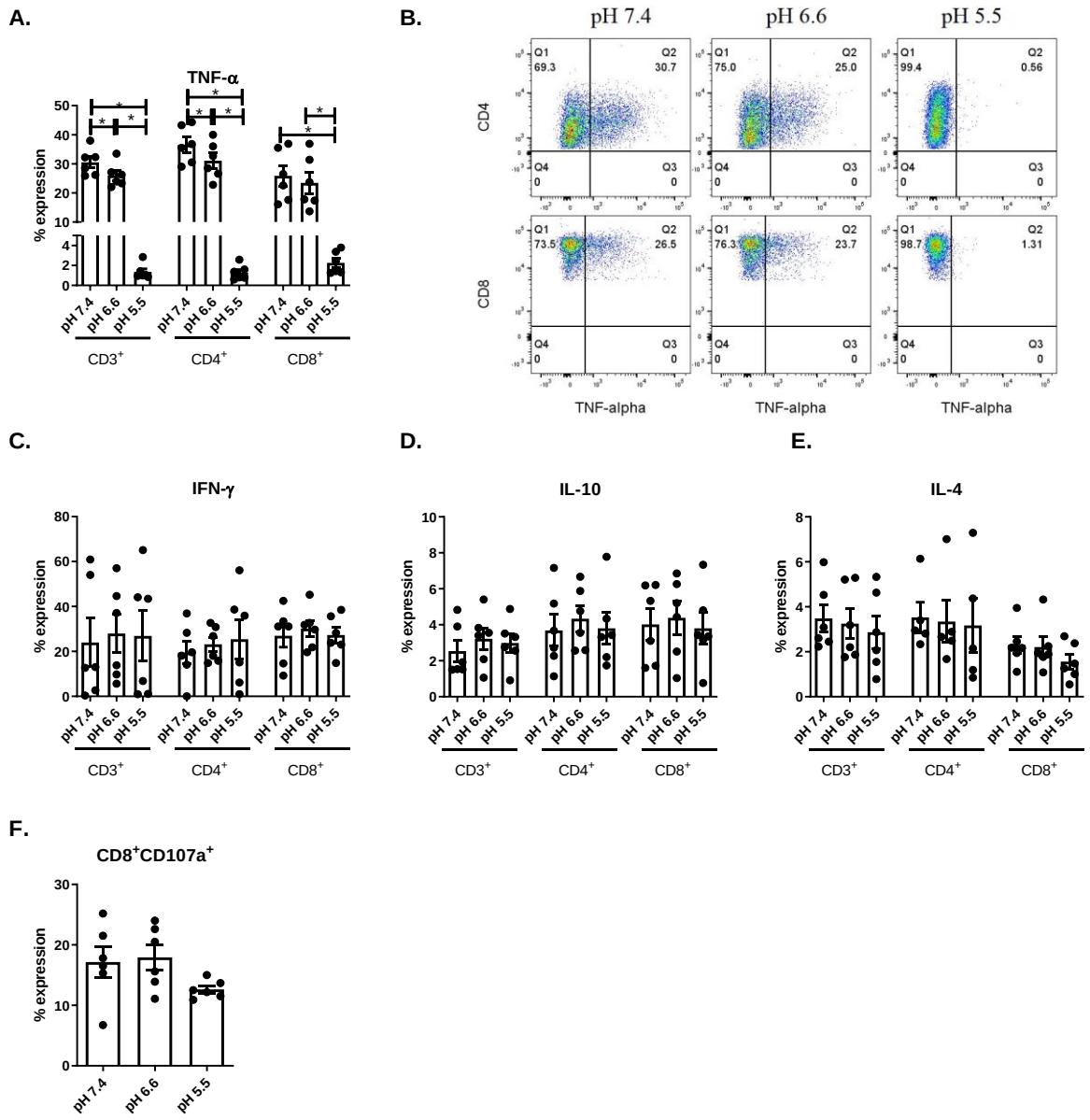

Figure 3.23: The percentage of TNF-α producing T cells is significantly decreased under acidic conditions *ex vivo*. PBMCs were isolated from peripheral blood of treatment-naïve OAC patients (n=6) and expanded *ex vivo* for 7 days in the presence of plate bound anti-CD3/anti-CD28 and recombinant human IL-2. Following a 7-day expansion, PBMCs were cultured for 48h in media with increasing levels of acidity (pH 7.4, pH 6.6 and pH 5.5). Intracellular staining was conducted to assess $CD3^+$, $CD3^+CD4^+$ and $CD3^+CD8^+$ cell production of TNF-α (A-B), IFN-γ (C), IL-10 (D) and IL-4 (E) cytokines by flow cytometry. The cytotoxic potential of $CD3^+CD8^+$ T cells was also assessed using a CD107a degranulation assay by flow cytometry (F). Paired, non-parametric t test, *$p<0.05$. Expression presented as percentages ± SEM.

Use of ICB to enhance anti-tumour cytokine profiles is an attractive therapeutic apprOGJh to boost response rates for OGJ patients however, the ability of ICB to promote anti-tumour cytokine profiles under acidic conditions is of utmost importance. Therefore, the effect of ICB on anti-tumour and pro-tumour cytokine profiles under acidic conditions reflective of the acidic tumour microenvironment was assessed (**Figure 3.24**).

Interestingly, single agent nivolumab significantly increased the production of IFN-γ in $CD4^+$ T cells compared with untreated cells in pH 6.6 cRPMI but not in pH 7.4 cRPMI or pH 5.5 cRPMI (28.97 ± 3.1 vs. 23.15 ± 3.2, p=0.03) (**Figure 3.24A**). Moreover, single agent nivolumab significantly decreased the production of TNF-α in $CD4^+$ T cells compared with untreated cells in pH 6.6 cRPMI (19.70 ± 5.4 vs. 31.10 ± 2.5, p=0.03) and pH 5.5 cRPMI (0.95 ± 0.3 vs. 1.28 ± 0.3, p=0.03) but not in pH 7.4 cRPMI (**Figure 3.24A**). Similarly, single agent ipilimumab significantly decreased the production of TNF-α in $CD4^+$ T cells compared with untreated cells in pH 6.6 cRPMI only but not in pH 5.5 cRPMI or pH 7.4 cRPMI (28.70 ± 2.7 vs. 31.10 ± 2.5, p=0.03) (**Figure 3.24A**). ICB did not significantly alter the frequency of IL-4-producing T cells compared with untreated cells in pH 7.4, pH 6.6 or pH 5.5 cRPMI (**Figure 3.24A**). Furthermore, single agent ipilimumab significantly decreased the production of IL-10 in $CD4^+$ T cells compared with untreated cells in pH 5.5 cRPMI only (2.90 ± 0.5 vs. 3.80 ± 0.8, p=0.03) but not in pH 7.4 or pH 6.6 cRPMI (**Figure 3.24A**). In addition, there were trends toward a significant increase in the production of IFN-γ in $CD8^+$ T cells compared with untreated cells following single agent nivolumab and ipilimumab treatment in pH 6.6 cRPMI only (35.42 ± 3.7 vs. 35.70 ± 3.5 and 30.13 ± 3.7, p=0.06 and p=0.06) but not in pH 7.4 cRPMI or pH 5.5 cRPMI (**Figure 3.24B**). However, dual nivolumab and ipilimumab significantly increased the production of IFN-γ in $CD8^+$ T cells compared with untreated cells in pH 6.6 cRPMI only (36.68 ± 3.6 vs. 30.13 ± 3.7, p=0.03) but not in pH 7.4 cRPMI or pH 5.5 cRPMI (**Figure 3.24B**). ICB did not significantly alter the production of TNF-α, IL-4 or IL-10 in $CD8^+$ T cells *ex vivo* under pH 7.4, 6.6 or 5.5 cRPMI (**Figure 3.24B**). However, single agent ipilimumab treatment significantly deceased the degranulation of $CD8^+$ T cells compared with untreated cells in pH 5.5 cRPMI (8.15 ± 1.5 vs. 12.63 ± 0.6, p=0.03) but had no effect in pH 6.6 cRPMI or pH 7.4 cRPMI (**Figure 3.24B**).

Overall, acidosis significantly decreased the percentage of TNF-α-producing T cells *ex vivo.* ICB increased T cell production of IFN-γ under moderately acidic conditions (pH 6.6) but not

severe acidic conditions (pH 5.5) and decreased IL-10 production by T cells under severe acidic conditions only *ex vivo*.

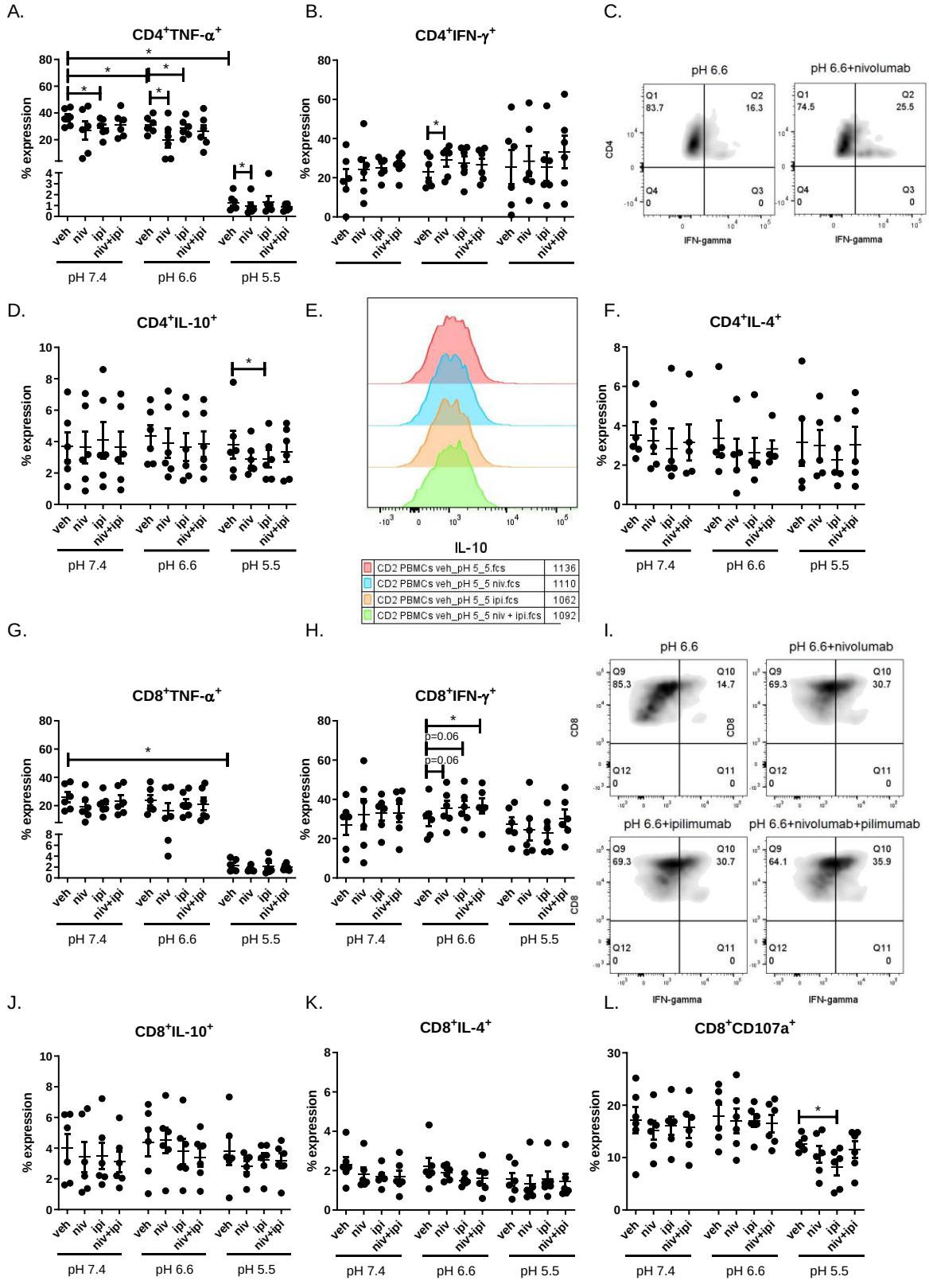

Figure 3.24: ICB increases IFN-γ production under moderately acidic conditions only and decreases IL-10 production by T cells under acidic conditions *ex vivo*. PBMCs were isolated from peripheral blood of treatment-naïve OAC patients (n=6) and expanded *ex vivo* for 7 days in the presence

of plate bound anti-CD3/anti-CD28 and recombinant human IL-2. Following a 7-day expansion, PBMCs were cultured for 48h in media with increasing levels of acidity (pH 7.4, pH 6.6 and pH 5.5) in the absence or presence of ICB. ICB included nivolumab (niv), ipilimumab (ipi) or dual nivolumab-ipilimumab (niv+ipi). Intracellular staining was conducted to assess $CD3^+CD4^+$ and $CD3^+CD8^+$ cell production of TNF-α, (A and G), IFN-γ (B-C and H-I), IL-10 (D-E and J) and IL-4 (F and K) cytokines by flow cytometry. The cytotoxic potential of $CD3^+CD8^+$ T cells was also assessed using a CD107a expression by flow cytometry (L). Paired, non-parametric t test, *$p<0.05$. Expression presented as percentages ± SEM.

3.2.17 Serum lactate levels positively correlate with circulating levels of soluble Lag-3 and soluble Tie-2 in OGJ patients

Studies have shown that serum lactate levels and tumoural expression of lactate dehydrogenase A and B have prognostic value in several cancer types[6]. Therefore, this study assessed the levels of circulating lactate levels in a cohort of 33 OAC patients and interrogated the prognostic value of serum lactate levels in oesophageal cancer. The levels of circulating lactate in the serum of OAC patients ranged from 4.87 to 7.28 mM with a mean value of 5.97 ± 0.08 mM in a cohort of 33 OAC patients post-treatment (**Figure 3.25**). Serum lactate levels were correlated with tumour stage and clinical outcomes in a cohort of 33 OAC patients post-treatment. However, serum lactate levels did not significantly correlate with tumour stage or clinical outcomes (data not shown). Similarly, analysis of a cohort of 80 oesophageal cancer patients available from the TCGA showed that levels of lactate dehydrogenase A and lactate dehydrogenase B were not associated with overall survival or tumour progression-free survival **Figure 3.25D**. A recent publication from our group identified nodal metastasis as a superior prognostic indicator and predictive factor for patient survival compared with pathologic treatment response. Therefore, we assessed if patients who had presence of nodal metastasis had higher levels of circulating serum lactate. Interestingly, patients with nodal metastasis had higher levels of serum lactate compared with patients who's tumours did not metastasise to lymph nodes (p=0.07)(**Figure 3.25A**).

Given the important pleiotropic role of lactate in suppressing T cells, enhancing DC maturation, promoting angiogenesis and tumour progression, serum lactate levels from a subcohort of consecutive OAC patients undergoing oesophagectomy in St. James's Hospital were correlated with circulating levels of a panel of 54 pro-inflammatory, pro-angiogenic, immunostimulatory and immunosuppressive molecules in a cohort of 10 OAC patients[17,18]. Interestingly, serum levels of lactate in OAC patients positively correlated with circulating levels of soluble LAG-

3 (r=0.79 and p=0.006, **Figure 3.25B**) and the pro-angiogenic factor Tie-2 (r=0.68 and p=0.03, **Figure 3.25C**).

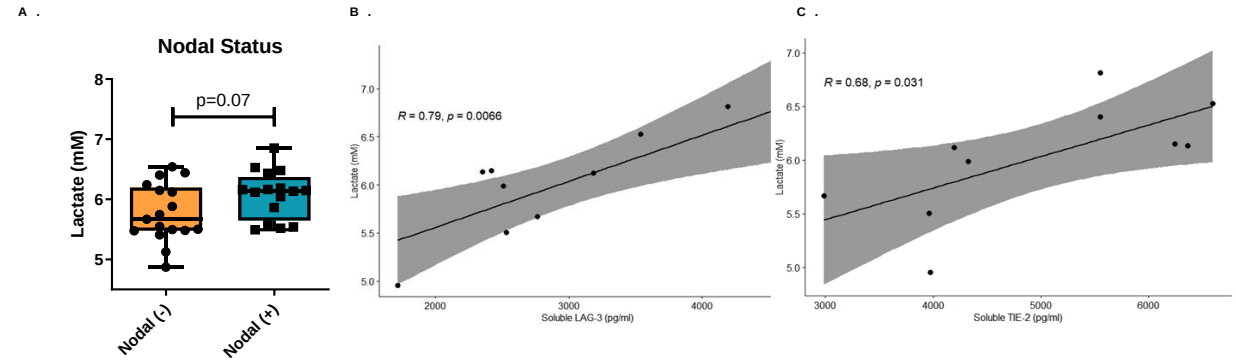

D.

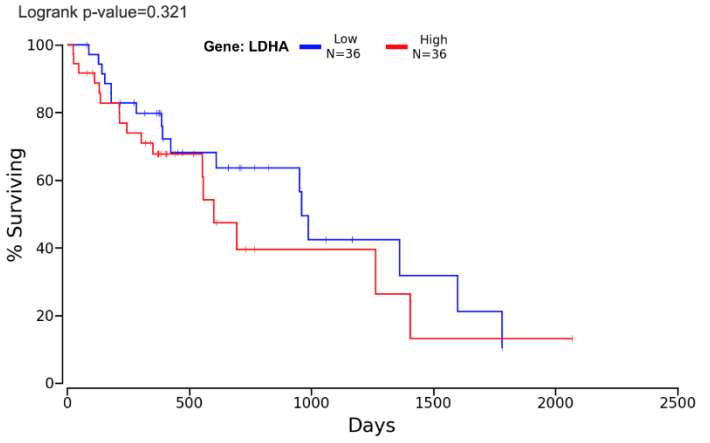

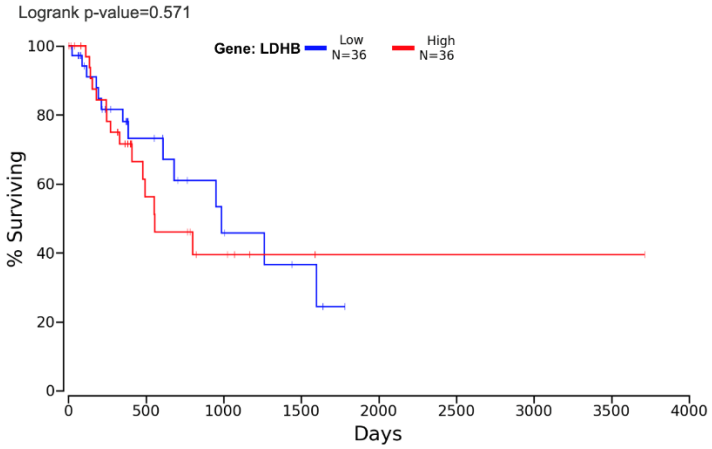

Figure 3.25: Levels of circulating lactate positively correlate with soluble levels of LAG-3 and Tie-2 in the serum of OGJ patients. Serum lactate levels were assessed in OAC patients post-treatment, pre-operatively at time of surgical resection of tumour using a lactate assay in duplicate technical replicates (n=33). Serum lactate levels displayed based on negative (n=17) vs. positive nodal status (n=16) (A) and based on presence of adverse features (nodal metastasis, lymphovascular invasion, perineural invasion and serosal invasion) (B). Correlation plots demonstrating the significant positive

correlations between serum lactate levels and circulating soluble LAG-3 levels (C) and circulating soluble Tie-2 levels (D) (n=10). Mann-Whitney test to compare between 2 groups and Pearson correlation tests were used, *p<0.05. (D) depicts the levels of LDHA and LDHB mRNA in a cohort of OGJ patients and overall survival outcomes from TCGA.

3.3 Discussion

PD-1 has been identified on the surface of OGJ cells and other tumour cell types such as CRC and melanoma. Similarly, TIGIT has been identified on the surface of CRC tumour cells, however its expression in OGJ had not been investigated until this study[191]. Importantly, the expression of these ICs on healthy normal tissues had never been addressed nor had their expression in a pre-malignant condition such as BO. Given the key role of ICs in maintaining immune tolerance and inhibition of autoimmunity[254] the observed decrease in the expression of PD-1 and TIGIT on the surface of oesophageal epithelial cells across the normal-BO-OGJ disease sequence in this study might reflect a loss of homeostasis and immune tolerance with disease development and progression, and implicate a specific role in the oesophagus for PD-1 and TIGIT in maintaining immune tolerance[255]. Loss of PD-1 and TIGIT may play a key role in the uncontrolled amplitude and duration of inflammatory responses in the oesophagus and may facilitate the generation of pathogenic inflammation that plays a key role in promoting the conversion of BO to OGJ. Ligation of PD-1 and TIGIT to their respective ligands PD-L1[256] and poliovirus receptor[257] on the surface of dendritic cells promotes a regulatory dendritic cell or T cell phenotype[258]. In addition, ligation of TIGIT to poliovirus receptor (PVR) on the surface of macrophages induces an M2 anti-inflammatory phenotype which would help resolve pathogenic inflammation[259]. In contrast, PD-1 expression on epithelial cells was significantly upregulated along the normal-pre-cancerous-pancreatic ductal adenocarcinoma disease sequence[237]. These differences may be explained by the distinct differences in cell types and tissue types between oesophageal epithelial cells and pancreatic epithelial cells highlighting tissue specific roles for distinct ICs.

Although PD-1 and TIGIT expression on the surface of OGJ cells decreases along the normal-BO-OGJ disease sequence, stressful conditions that recapitulate characteristic features of the TME such as hypoxia[101] and glucose deprivation[260] upregulated PD-1 and TIGIT on the surface of OGJ cells to similar levels of expression on HET-1A and QH cells. Subsequent inhibition of PD-1 and TIGIT under complete nutrient conditions decreased the levels of anti-apoptotic proteins, decreased cell proliferation and induced apoptosis in OGJ cells. A complementary

study by Liu *et al*, demonstrated that PD-1-intrinsic expression in 5-FU resistant gastric cancer cells promoted resistance via upregulation of Bcl-2[202]. Similar studies in other cancer types highlighted a similar role for PD-1 intrinsic signalling in pancreatic ductal adenocarcinoma[237], melanoma[261], thyroid[262], liver[263], and head and neck cancer cells, whereby PD-1 signalling increased tumour cell proliferation and viability. In contrast, PD-1 blockade in non-small cell lung cancer cells promoted cancer cell proliferation, highlighting the context-dependent role of PD-1-intrinsic signalling in cancer cells as either a tumour promoter or tumour suppressor[264].

Interestingly, PD-1 blockade under glucose deprivation or hypoxia enhanced OGJ cell proliferation and protected against apoptotic-induced cell death. This might be explained by a deeper insight into the mechanistic functions of PD-1 signalling in OGJ cells provided in this study. PD-1 inhibition under glucose deprivation or hypoxia is conferring OGJ cells with a survival advantage and PD-1 inhibition enhanced a range of metabolic parameters in OGJ cells including basal respiration and glycolytic reserve, which may be enhancing a metabolic phenotype in OGJ cells, potentially enabling OGJ cells to better tolerate and adapt to the harsh glucose deprived and hypoxic conditions found within the TME in OGJ. Given that tumour cells rely on glycolysis for the production of ATP under hypoxia the findings from this study demonstrate that inhibition of PD-1 intrinsic signalling in OGJ cells upregulates GLUT1 on the surface of OGJ cells, further supporting the hypothesis that inhibition of PD-1 under glucose-deprivation or hypoxia in OGJ cells is enhancing glycolysis and subsequent survival under these harsh conditions. A complementary study demonstrated that PD-1 inhibition in a mouse model of B16F10 melanoma resulted in an increase in GLUT1 expression and subsequent increase in the uptake of glucose analogue [^{18}F]FDG by cancer cells[265]. Collectively, these findings may suggest that PD-1 inhibitors may promote OGJ cell survival under hypoxia or glucose deprived microenvironments within the tumour. The lack of efficacy of PD-1 inhibitors in hypoxic tumours has been attributed to hypoxia-induced immunosuppression[266] however, these findings suggest an immune-independent mechanistic rationale for the lack of efficacy of PD-1 inhibitors in hypoxic tumours.

However, this phenomenon was specific to the PD-1 IC receptor pathway as inhibition of TIGIT intrinsic signalling in OGJ cells under serum deprivation or glucose deprivation or hypoxic conditions substantially decreased OGJ cell survival. Although TIGIT has been identified on the surface of colorectal cancer cells[191] a role for TIGIT in promoting cancer cell survival via tumour cell intrinsic signalling has not been identified in previous studies. Given that PD-1 and TIGIT inhibition significantly altered metabolism in OGJ cells and that

inhibition of oxidative phosphorylation or glycolysis significantly altered PD-1 and TIGIT expression on the surface of OGJ cells, this further highlights a role for PD-1 and TIGIT tumour cell intrinsic signalling in regulating OGJ cell metabolism and might suggest the existence of a positive/negative feedback loop between the expression of these ICs and regulation of metabolism in OGJ cells.

Collectively the nutrient depleted and hypoxic milieu has profound effects on the metabolism of not just cancer cells but also stromal and tumour-infiltrating immune cells, ultimately promoting pro-tumourigenic immune cell phenotypes[107]. Cham *et al*., demonstrated that glucose deprivation or inhibition of glycolysis by 2-deoxy-D-glucose inhibited the production of IFN-γ by T cells derived from healthy donors[267]. Similarly, dual glucose and serum deprivation under hypoxic conditions significantly decreased IFN-γ production in OGJ patient-derived T cells. In addition to a reduction in IFN-γ production by T cells a decrease in the production of immunosuppressive IL-10 was also observed under nutrient deprivation and hypoxic conditions. This may likely be attributed to the depletion of nutrients which are essential 'building blocks' required by T cells to synthesize proteins and subsequent cytokines. Cohen *et al*., also reported that nutrient depletion significantly reduces T cell cytokine production[268].

In this study several ICs were significantly upregulated on the surface of OGJ patient-derived T cells following dual glucose deprivation and hypoxia treatment, including PD-1, PD-L1, PD-L2 and CTLA-4 ICs. IC intrinsic signalling in T cells has profound effects on T cell metabolism, PD-1 intrinsic signalling in T cells inhibits glycolysis and promotes lipolysis and fatty acid oxidation[269], similarly, CTLA-4 intrinsic signalling in T cells inhibits glycolysis[269]. Glycolysis is essential for effector T cell function therefore, upregulation of PD-1 and CTLA-4 could be detrimental to anti-tumour immunity and may reflect the skewing of T cells toward an altered phenotype facilitated by PD-1 and CTLA-4 metabolic reprogramming. However, a fatty acid oxidative phenotype that could be promoted by PD-1 and CTLA-4 signalling is utilised by both regulatory T cells[270] and tissue resident memory T cells which are known for their anti-tumour functions[271]. CTLA-4 expression by regulatory T cells plays a pivotal role in hindering the anticancer immunity by promoting regulatory T cell function, which suppresses antigen-presenting cells by depleting immune stimulating cytokines, producing immunosuppressive cytokines and constitutively expressing CTLA-4[272]. Preclinical murine models have demonstrated that CTLA-4 blockade promotes cancer regression by increasing

the frequency of effector T cells within the TME and selectively depleting intra-tumoral regulatory T cells via an Fc-dependent mechanism[273].

Glucose consumption by antigenic tumours can metabolically restrict T cells, directly dampening their effector function and allowing tumour progression[274]. ICB therapy may correct this resource imbalance through a direct effect on tumour cells[274]. In particular, PD-L1 blockade on melanoma and lung cancer cells inhibited glycolysis resulting in an increased availability of glucose in the TME and subsequently promoted anti-tumour T cell function[236]. This study demonstrated that nivolumab treatment significantly reduced the production of IL-10 by T cells under glucose deprived hypoxic conditions compared with untreated cells under glucose deprived hypoxic conditions, suggesting that PD-1 blockade may help skew T cells toward an anti-tumour phenotype within the OGJ TME. However, nivolumab did not decrease IL-10 production by T cells under complete nutrient conditions, highlighting that nivolumab was more effective at promoting an anti-tumour T cell phenotype under 'stressful' glucose deprived and hypoxic conditions which are more reflective of the TME than full nutrient conditions. However, it is important to note that emerging research has shown that IL-10 cooperates with granzyme B and IFN-γ stimulating the cytotoxicity of $CD8^+$ T cells to induce tumour rejection in mice[275]. Therefore, it is important to understand the context dependency of these pleiotropic cytokines and further research will be necessary in this regard to further interrogate the effect of ICB on cytokine profiles in humans and how this affects clinical outcomes, as the immune system in mice is very different to that of humans.

However, tumour cells are able to counteract the activity of PD-1 and CTLA-4 ICBs and can commission additional inhibitory pathways via expression of other ICs/ligands within the TME[276]. Of particular clinical relevance regarding mechanisms for development of acquired resistance to therapeutics targeting the conventional PD-1 and CTLA-4 axes, the A2aR IC receptor was also upregulated on the surface of T cells under nutrient deprivation and hypoxic conditions. Furthermore, co-culturing OGJ cells with PBMCs upregulated LAG-3 on the surface of T cells. These novel ICs have been shown to have profound immunosuppressive effects on effector T cells. Therefore, co-blockade of multiple ICs may be a better strategy to enhance effector T cell function in OGJ. Clinical trials are ongoing in other cancer types targeting LAG-3 and A2aR[277]. A2aR elicits profound immunosuppressive effects within the TME. Regulatory T cells secrete adenosine within the TME, which potently inhibits production of anti-tumour cytokines[278]. Increased expression of A2aR on tumour infiltrating immune cells correlated with advanced pathological grade, larger tumour size and positive lymph node status

in head and neck squamous cell carcinoma (HNSCC)[279]. Interestingly, the expression of A2AR was found to significantly correlate with HIF-1α, CD73, CD8 and Foxp3. Furthermore, the increased population of $CD4^+Foxp3^+$ regulatory T cells (Tregs), which partially expressed A2aR, was observed in an immunocompetent mouse model that spontaneously develops HNSCC[279]. Pharmacological blockade of A2aR by SCH58261 delayed the tumour growth in the HNSCC mouse model and significantly decreased the population of $CD4^+Foxp3^+$ Tregs and enhanced the anti-tumour response of $CD8^+$ T cells[279]. These studies highlight the important role A2aR plays in the TME for promoting tumour progression and the pharmacologic impact of A2aR inhibition for promoting anti-tumour responses.

Similarly, Grosso *et al.,* also demonstrated that LAG-3 knockout adoptively transferred antigen-specific CD8 T cells in mice bearing their cognate antigen, as either a self or a tumour antigen, showed enhanced proliferation and cytokine production[280]. Expression of LAG-3 on regulatory CD4 T cells also identified a more immunosuppressive phenotype, which subsequently hindered CD8 T cell function in Hodgkin's lymphoma[281], melanoma and colorectal cancer[282]. Collectively, these studies identify a pivotal role for LAG-3 in dampening anti-tumour immunity and highlight that LAG-3 blockade can induce durable responses in pre-clinical models. Of particular clinical relevance for designing combination ICB therapies, co-targeting LAG-3 in combination with PD-1 inhibition is thought to achieve synergistic responses. In phase I/II study evaluating the safety and efficacy of relatlimab (anti-LAG-3) in combination with nivolumab in patients with advanced melanoma that had progressed during previous anti-PD-1 or anti-PD-L1 immunotherapy (NCT0198609), the combination of relatlimab and nivolumab was well tolerated and the objective response rate (ORR) was 11.5% in 61 patients. ORR was at least 3.5-fold higher in patients with LAG-3 expression in at least 1% of tumour-associated immune cells within the tumor margin (n=33) than that in the patients with less than 1% LAG-3 expression (n=22) (18% and 5%, respectively)[283]. Taken together, these pre-clinical and clinical studies investigating A2aR and LAG-3 demonstrate that targeting these novel ICs to enhance anti-tumour immunity is a viable strategy for boosting the efficacy of conventional PD-1 ICBs.

Our results support the hypothesis that acidity suppresses anti-tumour T lymphocyte function demonstrated by a significant upregulation of inhibitory immune checkpoints TIM-3, LAG-3, and CTLA-4 on the surface of OGJ-derived T cells when cultured under low pH conditions *ex vivo*. Expression of CTLA-4[284], TIM-3[285] and LAG-3[286] immune checkpoints are typically upregulated on dysfunctional and/or exhausted T cells. This further supports the hypothesis

that acidic conditions suppress T lymphocyte function perhaps through immune checkpoint-intrinsic signalling and their blockade may enhance T cell function under acidic conditions. Of note, CTLA-4 has been shown to play a pivotal role in promoting regulatory T cell functions which subsequently suppress antigen-presenting cells by depleting immune stimulating cytokines and producing immunosuppressive cytokines[272]. Ipilimumab treatment significantly decreased production of IL-10 by $CD4^+$ T cells under severe acidic conditions *ex vivo*. Moreover, dual nivolumab and ipilimumab treatment significantly enhanced the production of IFN-γ by $CD8^+$ T cells under moderately acidic conditions (pH 6.6) but this effect was lost under severe acidic conditions (pH 5.5). This suggests that dual nivolumab and ipilimumab treatment might be a promising intervention to limit the immunosuppressive effects of the acidic tumour microenvironment. However, dual nivolumab and ipilimumab treatment failed to enhance the production of IFN-γ by $CD8^+$ T cells under severe acidic conditions (pH 5.5), highlighting that extratumoural acidity might represent a mechanism of resistance to ICB. Combining oral bicarbonate therapy to neutralize tumour acidity in combination with anti-CTLA-4 or anti-PD1 therapy improved antitumor responses in multiple models, including complete remissions in some subjects[248].

However, it is important to note that the efficacy of CTLA-4 blockade is limited to a subpopulation of patients and development of acquired resistance is common[287]. This has prompted the investigation into additional immune checkpoints such as TIM-3 and LAG-3[288] which are highly expressed on Tregs at sites of tissue inflammation and were significantly upregulated on the surface of OGJ-derived T cells cultured under acidic conditions in this study[289]. Findings by Deng *et al*, demonstrated that LAG-3 blockade reduced tumour growth, potentiated anti-tumour responses of $CD8^+$ T cells and decreased the population of immunosuppressive cells in a murine model of head and neck squamous cell carcinoma[286]. Similarly, TIM-3 blockade enhances anti-tumour T cell responses, particularly in conjunction with PD-1 blockade *ex vivo* and in murine models[290–293].

Interestingly, we also found that systemic lactate levels positively correlated with circulating levels of soluble LAG-3 receptor. However, soluble LAG-3 was a good prognostic marker in gastric cancer and positively correlated with $CD8^+$ T cell frequency and secretion of IL-12 and IFN-γ in peripheral blood[294]. Fougeray *et al*[295]., identified soluble LAG-3 protein as an immunopotentiator for therapeutic vaccines via binding to MHC class II on dendritic cells and inducing maturation[295]. Whether lactate might be regulating the cleavage of membrane-bound LAG-3 on the surface of immune cells to enhance DC maturation is unknown. Lactate

stimulates endothelial cell migration and tube formation *in vitro*, as well as the recruitment of circulating vascular progenitor cells and vascular morphogenesis *in vivo*[296]. Our study further highlights a link between lactate and angiogenesis in which systemic lactate levels correlated with an important pro-angiogenic mediator Tie-2. Lactate also binds Tie2 when it is expressed as a cell surface receptor on endothelial cells activating the PI3K/Akt pathway[297].

Overall, these findings suggest that TIGIT blockade may be more effective than PD-1 blockade in reducing the survival of OGJ cells within the nutrient deprived hypoxic TME. A preclinical rationale is highlighted for the use of ICB to improve T lymphocyte function within the nutrient deprived hypoxic and acidic TME. Novel ICs including TIM-3 and LAG-3 are also highlighted as potential therapeutic targets to combine with PD-1 or CTLA-4 ICBs under such conditions to expand the efficacy of ICB for a greater spectrum of patients.

Chapter 4 – The effect of the visceral adipose tissue secretome on anti-tumour T cell immunity and efficacy of immune checkpoint blockade

Hypothesis

The visceral adipose tissue secretome enhances T cell activation and upregulates inhibitory immune checkpoints on the surface of T cells which may promote T cell dysfunction.

4.1.1 Highlights

- Visceral adipose conditioned media (ACM) significantly altered T cell activation status, upregulating co-stimulatory marker CD27 on T cells.
- Immune checkpoint expression profiles of T cells were also significantly altered by the ACM from both early and late stage OGJ patients.
- ACM from OGJ patients enhanced a pro-inflammatory T cell phenotype including a Th1-like, dual Th1/17-like and Th17-like signature.
- Use of immune checkpoint blockade attenuated the ACM-induced increase in IL-17A secretion by T cells.
- ACM from early stage OGJ patients was more pro-inflammatory than ACM from late stage patients, reflected by decreased levels of IL-17A/F, TNF-α, IL-1RA and IL-5.
- This could suggest that inflammation induced by excess visceral adipose tissue is more essential for the early development of cancer rather than sustaining advanced tumours.
- The ACM-induced upregulation of immune checkpoints on T cells also highlights a therapeutic vulnerability that could be exploited by immune checkpoint blockade to harness anti-cancer immunity and attenuate the visceral adipose tissue-induced inflammatory phenotype in OGJ.

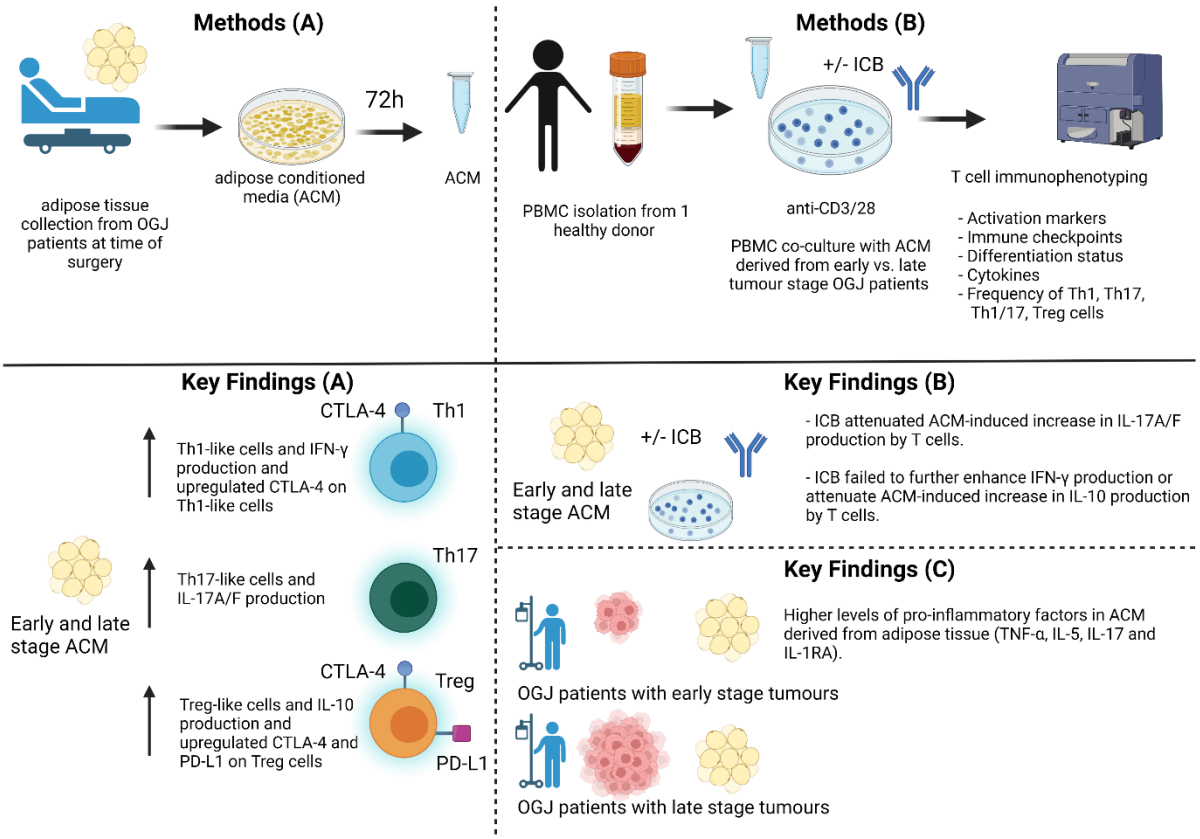

Graphical abstract: Schematic workflow – (A) visceral adipose tissue was taken from OAC patients at time of surgery and cultured for 72h in media. (B) The harvested ACM was co-cultured with healthy donor PBMCs that were concurrently activated with anti-CD3/28 for 48h and T cell immunophenotyping was carried out by flow cytometry. Key findings – (A) Early and late stage ACM enhanced a Th1-like phenotype and upregulated CTLA-4 on Th1-like cells. A Th17-like phenotype was also enhanced in addition with a Treg-like phenotype. CTLA-4 and PD-L1 were upregulated on the surface of Treg-like cells. (B) ICB attenuated IL-17 production by T cells. However, ACM attenuated ICB-mediated reduction in IL-10 production by T cells. Higher levels of pro-inflammatory factors were found in early stage ACM compared with late stage ACM.

4.1.2 Introduction

It is well-established that visceral adipose tissue in oesophageal adenocarcinoma (OGJ) patients contributes to tumour development, progression and treatment resistance via secretion of proinflammatory cytokines, insulin, fatty acids and leptin[81,82]. An increase in visceral adiposity due to obesity also increases intra-abdominal pressure, forces caustic stomach and bile acids into the distal part of the oesophagus giving rise to the pro-inflammatory condition gastroesophageal reflux disease (GORD), which affects many obese individuals and carries an increased risk of developing OGJ[83]. Approximately 5% of individuals suffering with GORD

progress to the pre-malignant condition of Barrett's oesophagus (BO). It has been reported that the presence of BO carries an overall 0.05% risk of progressing to OGJ[84]. However, recent findings highlight that a risk of 0.05% may be gravely underestimating the progression rate of BO to OGJ. Nowicki-Osuch and Zhuang *et al*, recently demonstrated that OGJ likely arises from undifferentiated BO cell types even in the absence of a pathologically identifiable metaplastic precursor, suggesting that the majority of OGJ pre-cursor BO lesions have gone unidentified and undiagnosed[298].

Another factor that plays a key role in driving OGJ tumour initiation, progression and treatment resistance includes visceral adipose tissue via its contribution to the generation of systemic low-grade inflammation[85]. In contrast to lean individuals, adipocytes in obese individuals become hypertrophic and displaying an increase in both size and number, to handle increased lipid storage[86]. An expansion of adipocytes leads to hypoxic areas within adipose tissue, which leads macrophage recruitment and activation, and results in the generation of a pro-inflammatory environment within adipose tissues[87,88]. These hypertrophic adipocytes can burst, releasing their contents into the extracellular environment. Immune cells such as macrophages are recruited to remove the debris, however lipids can be toxic to immune cells which induces cell death[87,88]. More immune cells are then recruited, perpetuating this state of chronic inflammation by secretion of interleukin (IL)-6 and tumour necrosis factor (TNF)-α which are released into the circulation and cause systemic inflammation which is pro-tumourigenic and promotes tumourigenesis in distal sites[89]. IL-6 promotes anti-apoptotic pathways and TNF-α activates the transcription of oncogenes contributing to the survival of transformed cells and development of cancerous lesions[90]. OGJ patients have higher levels of circulating IL-6 in their serum compared with healthy controls[91]. Increased serum levels of IL-6 positively correlated with progression from BO to OGJ[91]. IL-6 is one of the key pro-inflammatory factors that is produced by viscerally obese adipose tissue, playing an important role in the development of obesity-related systemic low-grade inflammation[92]. Receptors for leptin and adiponectin have been shown to be upregulated in OGJ and correlate with the tumour stage and nodal involvement[93]. Leptin promotes tumour development and progression through promotion cell proliferation and inhibition of apoptotic pathways mediated through Akt, mitogen-activated protein kinase, and signal transducer and activator of transcription pathways[94,95]

Resistance to first-line chemo(radio)therapy regimens is high across all solid malignancies including OGJ[96]. However, cancer immunotherapy is revolutionizing the clinical management

of a variety of malignancies. In particular, immune checkpoint blockers (ICB) targeting programmed cell death 1 (PD-1)/programmed death ligand 1 (PD-L1) pathway and targeting the cytotoxic T lymphocyte antigen-4 (CTLA-4) pathway have shown remarkable antitumor activity[299]. Pembrolizumab and nivolumab have been FDA approved for use in OGJ[64,300]. Despite the unprecedented efficacy of ICBs, the majority of the patients do not respond[97]. High tumour mutational burden and a 'hot' T cell-inflamed tumour microenvironment correlate with better responses to ICB therapies[98]. However, the role of other factors, such as body mass is now emerging as an indicator of response to ICB[99]. In a recent study, Wang *et al*[100]., have found that obesity impairs T cell function characterized by increased expression of PD-1 in mice, nonhuman primates, and humans. In addition, obesity resulted in impaired antitumor immunity and subsequently increased growth of melanoma, lung, and breast tumours in mice. Leptin also upregulated the expression of PD-1 on the surface of T cells, causally linking obesity with T cell dysfunction[100]. These studies highlight how obesity-induced T cell dysfunction can be exploited for cancer treatment, where the authors demonstrate that the use of ICB improved response rates in melanoma and lung tumours in obese mice and patients. The development of obesity-associated cancers such as OGJ also occurs in a background of inflammation, acquiring several mutations overtime, which eventually leads to neoplastic transformation[101]. Therefore, it's plausible that obesity-associated cancers may have a higher level of non-synonymous and immunogenic neo-epitopes resulting in a more immunologically hot tumour compared to OGJ cancers that did not develop as a result of obesity-associated inflammation[98]. Collectively these observations and findings highlight how the negative effect of obesity creates a vulnerability that can be harnessed for cancer treatment by ICB.

It is important to note that although obesity plays a significant role in promoting OGJ development and progression, the majority of OGJ patients have lost weight by the time of diagnosis due to considerable disruption to their typical dietary habits and difficulty swallowing attributed to the obstruction of their oesophagus by the tumour mass and are no longer obese however are often still overweight. Furthermore, following first-line chemo(radio)therapy regimens patients continue to lose weight typically muscle mass leading to sarcopenia and cachexia post-treatment and at the time of surgery. Therefore, for the purpose of this study we focussed on the effect of the visceral adipose tissue secretome which is sampled at the time of surgery from OGJ patients based on early versus late stage tumours, on T cell phenotype and investigated whether addition of ICB might enhance the anti-tumour T cell response.

4.1.3 Specific aims

1. Investigate the effect of the secretome from visceral adipose tissue derived from early stage and late stage OGJ patients on T cell activation status, T cell differentiation status and IC expression profiles of T cells.
2. Investigate the effect of the secretome from visceral adipose tissue derived from early stage and late stage OGJ patients on IC expression profiles of Th1-like, Th1/17-like, Th17-like and Treg cells.
3. Assess the effect of the secretome from visceral adipose tissue derived from early stage and late stage OGJ patients on the production of anti-tumour cytokine profiles and tumour-promoting pro-inflammatory cytokine profiles of T cells and whether ICB can enhance anti-tumour cytokine profiles in the presence of early and late stage ACM.
4. Profile the soluble secretome of visceral adipose tissue derived from early stage and late stage OGJ patients for an array of immunomodulatory and pro-metastatic soluble mediators.
5. Determine if the visceral adipose tissue secretome can enhance proliferation of OGJ cells and whether this secretome can counteract the anti-proliferative effects of the first-line FLOT chemotherapy regimen.

4.2 Results

4.2.1 ACM derived from OGJ patients significantly alters the expression of T cell activation and differentiation markers

ACM derived from OGJ patients with late stage tumours significantly increased the expression of CD62L on the surface of $CD4^+$ T cells compared with untreated cells (untrx: 26.73 ± 11.18 vs. and late stage: 37.97 ± 12.9%, p=0.01) (**Figure 4.1A**). ACM derived from OGJ patients with early stage tumours and late stage tumours significantly increased the expression of CD62L on the surface of $CD8^+$ T cells compared with untreated cells (untrx: 23.26 ± 8.2 vs. early stage: 46.05 ± 8.4%, p=0.01 late stage: 47.08 ± 9.3%, p=0.005) (**Figure 4.1A**). ACM derived from OGJ patients with late stage tumours significantly decreased the expression of CD69 on the surface of $CD4^+$ T cells compared with untreated cells (untrx: 7.43 ± 0.8 vs. late stage: 4.29 ± 1.1%, p=0.005) (**Figure 4.1A**). ACM derived from OGJ patients with early stage tumours significantly increased the expression of CD27 on the surface of $CD4^+$ T cells compared with untreated cells (untrx: 41.00 ± 3.5 vs. early stage: 57.55 ± 5.0%, p=0.01)

(**Figure 4.1A**). ACM derived from OGJ patients with early stage tumours and late stage tumours significantly increased the expression of CD27 on the surface of $CD8^+$ T cells compared with untreated cells (untrx: 41.47 ± 2.7 vs. early stage: 64.29 ± 4.8%, p=0.008 and late stage: 60.75 ± 6.7%, p=0.01) (**Figure 4.1A**). ACM derived from OGJ patients did not significantly alter the expression of CD45RA or CD45RO on the surface of T cells compared with untreated cells (**Figure 4.1A**). ACM derived from OGJ patients with early stage tumours significantly increased the frequency of naïve $CD4^+$ T cells compared with untreated cells (untrx: 34.53 ± 2.9 vs. early stage: 43.39 ± 3.1%, p=0.03) (**Figure 4.1B**).

ACM derived from OGJ patients with early stage tumours and late stage tumours increased the frequency of central memory $CD4^+$ T cells compared with untreated cells (untrx: 7.35 ± 0.5 vs. early stage: 11.39 ± 1.0, p=0.07 late stage: 10.66 ± 1.0%, p=0.02) (**Figure 4.1B**). Similarly, ACM derived from OGJ patients with early stage and late stage tumours significantly increased the frequency of central memory $CD8^+$ T cells compared with untreated cells (untrx: 4.86 ± 0.6 vs. early stage: 7.43 ± 0.8% p=0.05, late stage: 9.12 ± 1.8%, p=0.04) (**Figure 4.1B**). ACM derived from OGJ patients with early stage tumours significantly decreased the frequency of effector memory $CD8^+$ T cells compared with untreated cells (untrx: 27.88 ± 2.7 vs. early stage: 19.05 ± 3.0%, p=0.03) (**Figure 4.1B**). ACM derived from OGJ patients with early stage tumours and late stage tumours significantly decreased the frequency of terminally differentiated effector memory $CD4^+$ T cells (untrx: 21.13 ± 2.0 vs. early stage: 13.11 ± 2.2%, p=0.04 and late stage: 12.80 ± 1.6%, p=0.001) and terminally differentiated effector memory $CD8^+$ T cells compared with untreated cells (untrx: 28.15 ± 2.4 vs. late stage: 17.07 ± 1.9%, p=0.05, and late stage: 16.85 ± 1.6%, p=0.01) (**Figure 4.1B**).

Overall ACM from derived from OGJ patients with early or late stage tumours substantially altered T cell activation marker expression and T cell differentiation status. Co-stimulatory marker CD27 was significantly increased on the surface of T cells, and a central memory-like T cell differentiation status was enhanced. However, there was no significant differences on T cell activation status or differentiation status between ACM derived from early versus late stage OGJ patients.

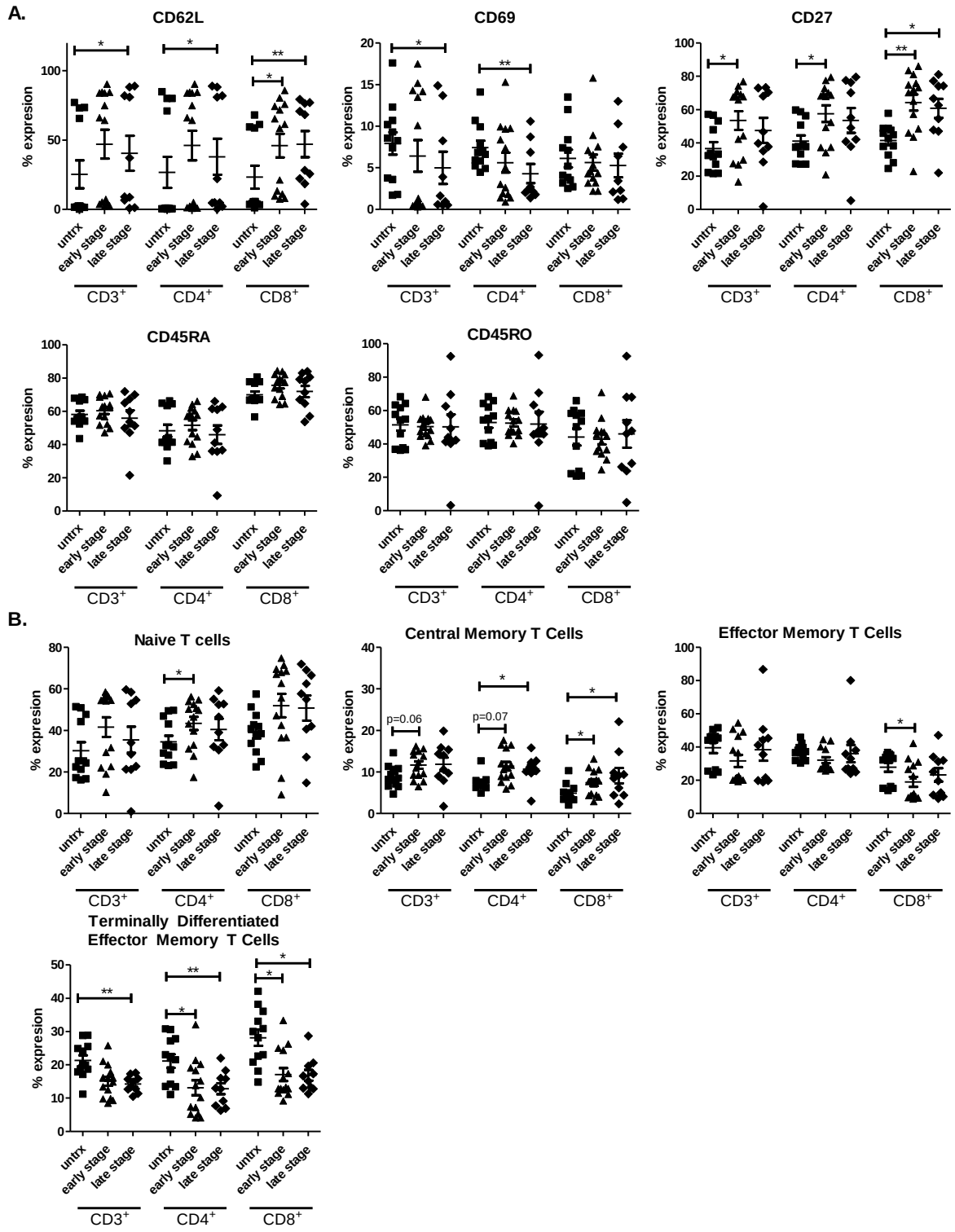

Figure 4.1: ACM derived from OGJ patients upregulates CD27 co-stimulatory maker and promotes differentiation into a central memory-like T cell phenotype. Healthy donor PBMCs were activated for 2 days using plate bound anti-CD3 and anti-CD28 in the absence (n=12) or presence of ACM generated from OGJ patients with early stage tumours (n=14) or late stage tumours (n=14). $CD3^+$, $CD3^+CD4^+$ and $CD3^+CD8^+$ cells were assessed for the

expression of T cell activation markers: CD62L, CD69, CD27, CD45RA and CD45RO by flow cytometry (A). The percentage of naïve ($CD45RA^+CD27^+$), central memory ($CD45RA^-CD27^+$), effector memory ($CD45RA^-CD27^-$) and terminally differentiated effector memory ($CD45RA^+CD27^-$) T cells was also determined by flow cytometry (B). Paired non-parametric t test and data presented as percentages ± SEM *p<0.05, **p<0.01.

4.2.2 ACM derived from OGJ patients significantly alters the IC expression profile of T cells

Given our findings demonstrating that ACM substantially altered the activation status of T cells we sought to investigate if ACM also altered IC expression profiles of T cells as this would help guide identification of appropriate ICs to target in OGJ patients. ACM derived from OGJ patients with late stage tumours decreased the expression of PD-1 on the surface of $CD4^+$ T cells (untrx: 78.63 ± 1.5 vs. late stage: 72.32 ± 3.7%, p=0.06) compared with untreated cells (**Figure 4.2A).** ACM derived from OGJ patients with early stage and late stage tumours significantly increased the expression of TIGIT on the surface of $CD4^+$ T cells (untrx: 11.80 ± 0.5 vs. early stage: 15.86 ± 0.7%, p=0.006, late stage: 17.45 ± 1.0%, p=0.003) and $CD8^+$ T cells (untrx: 8.05 ± 0.3 vs. early stage: 12.19 ± 0.9%, p=0.02, late stage: 13.21 ± 1.5%, p=0.009) compared with untreated cells (**Figure 4.2A).** ACM derived from OGJ patients with early stage and late stage tumours significantly increased the expression of A2aR on the surface of $CD4^+$ T cells (untrx: 0.21 ± 0.03 vs. early stage: 1.24 ± 0.3%, p=0.01, late stage: 2.41 ± 0.6%, p=0.007) and $CD8^+$ T cells (untrx: 0.54 ± 0.07 vs. early stage: 2.33 ± 0.7%, p=0.03, late stage: 4.97 ± 1.6%, p=0.02) compared with untreated cells (**Figure 4.2A**)**.** ACM derived from OGJ patients with early stage and late stage tumours significantly decreased the expression of CTLA-4 on the surface of $CD4^+$ T cells (untrx: 9.12 ± 1.7 vs. early stage: 4.80 ± 0.7%, p=0.04, late stage: 4.34 ± 0.7%, p=0.01) and $CD8^+$ T cells (untrx: 11.70 ± 2.0 vs. early stage: 4.75 ± 1.0%, p=0.04, late stage: 4.33 ± 0.8%, p=0.02) compared with untreated cells (**Figure 4.2A).** ACM derived from OGJ patients with early stage and late stage tumours increased the expression of PD-L2 on the surface of $CD4^+$ T cells (untrx: 0.65 ± 0.08 vs. early stage: 2.38 ± 0.6%, p=0.02, late stage: 3.69 ± 0.9%, p=0.01) and $CD8^+$ T cells (untrx: 0.80 ± 0.1 vs. early stage: 2.73 ± 0.9%, p=0.03, late stage: 4.21 ± 1.7%, p=0.07) compared with untreated cells (**Figure 4.2B**)**.** ACM derived from OGJ patients with early stage and late stage tumours increased the expression of CD160 on the surface of $CD4^+$ T cells (untrx: 1.18 ± 0.2 vs. early stage: 3.30 ± 0.5%, p=0.01, late stage: 4.82 ± 1.1%, p=0.007) and $CD8^+$ T cells (untrx: 0.73 ±

0.1 vs. early stage: 2.51 ± 0.7%, p=0.01, late stage: 3.32 ± 1.2%, p=0.04) compared with untreated cells (**Figure 4.2B**)**.** ACM from early stage of late stage OGJ patients did not alter the expression of TIM-3, LAG-3, KLRG-1 or PD-L1 on the surface of T cells compared with untreated cells (**Figure 4.2**)**.**

Overall, ACM substantially altered the expression profile of ICs on the surface of T cells decreasing PD-1 and CTLA-4 and increasing TIGIT, A2aR, PD-L2 and CD160. However, there was no significant differences on T cell activation status or differentiation status between ACM derived from early versus late stage OGJ patients.

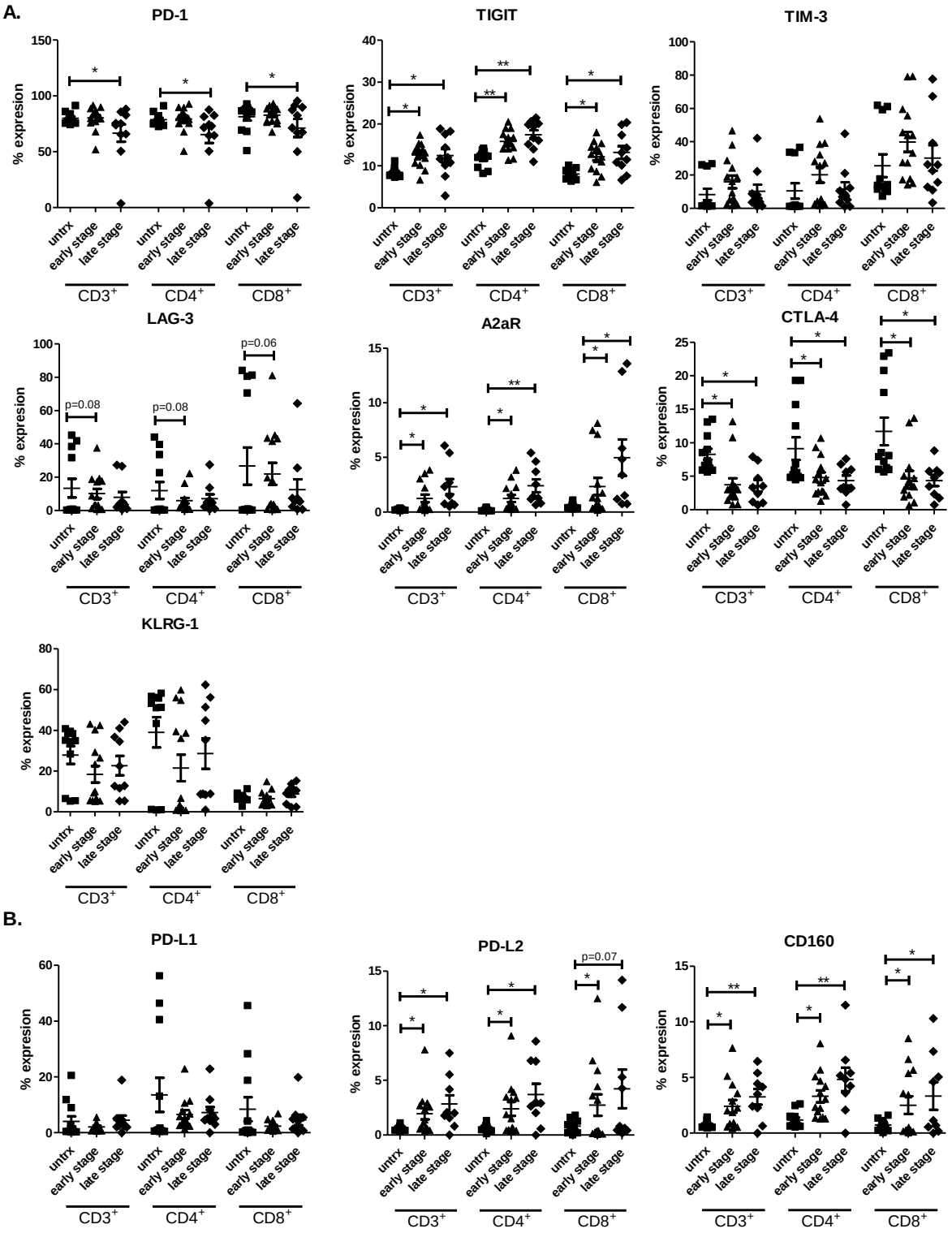

Figure 4.2: ACM derived from OGJ patients significantly upregulates TIGIT on the surface of T cells. Healthy donor PBMCs were activated for 2 days using plate bound anti-CD3 and anti-CD28 in the absence (n=12) or presence of ACM generated from OGJ patients with early stage tumours (n=14) and late stage tumours (n=14). $CD3^+$, $CD3^+CD4^+$ and $CD3^+CD8^+$ cells were assessed for the expression of inhibitory IC receptors including PD-1,

TIGIT, TIM-3, LAG-3, A2aR, CTLA-4 and KLRG-1 (A) and IC ligands including PD-L1, PD-L2 and CD160 (B) by flow cytometry. Paired, non-parametric t-test, *p<0.05, **p<0.01.

4.2.3 ACM derived from OGJ patients promotes a Th1-like phenotype

The findings from this study demonstrated that ACM derived from OGJ patients significantly altered T cell activation status and IC expression profiles. Therefore, we sought to investigate if ACM might alter an anti-tumour Th1-like phenotype which plays a key role orchestrating anti-tumour immunity in OGJ. Th1-like cells were characterised as $CXCR3^{+}CCR6^{-}$ cells[301]. Importantly, the effect of ACM on the expression profile of ICs on Th1-like cells was also assessed to help guide selection of ICs to target. ACM derived from OGJ patients with early stage tumours and late stage tumours significantly increased the frequency of Th1-like $CD8^{+}$ cells compared with untreated cells (untrx: 43.65 ± 1.5 vs. early stage: 52.64 ± 2.8 p=0.01, and late stage: 56.79 ± 2.6%, p=0.003) (**Figure 4.3A).** In addition, ACM significantly altered the IC expression profile of Th1-like cells. ACM derived from late stage OGJ patients significantly decreased PD-1 expression on the surface of $CD4^{+}$ Th1-like cells (untrx: 56.06 ± 3.7 vs. late stage: 31.06 ± 5.0%, p=0.01) compared with untreated cells (**Figure 4.3B).** ACM derived from early stage OGJ patients significantly decreased TIGIT expression on the surface of $CD4^{+}$ Th1-like cells (untrx: 27.57 ± 1.0 vs. late stage: 16.50 ± 3.2%, p=0.01) compared with untreated cells (**Figure 4.3B**)**.** In contrast, ACM derived from early stage and late stage OGJ patients significantly increased CTLA-4 expression on the surface of $CD8^{+}$ Th1-like cells (untrx: 9.47 ± 1.7 vs. early stage: 22.13 ± 3.4%, p=0.003, late stage: 29.56 ± 5.2%, p=0.007) compared with untreated cells (**Figure 4.3B**)**.** Furthermore, ACM derived from early stage OGJ patients increased the frequency of $CD4^{+}IFN\text{-}\gamma^{+}$ cells compared with untreated cells (untrx: 28.88 ± 1.0 vs. early stage: 41.37 ± 2.5%, p=0.03) and $CD8^{+}IFN\text{-}\gamma^{+}$ cells compared with untreated cells (untrx: 48.75 ± 4.6 vs. early stage: 64.43 ± 2.3%, p=0.06) (**Figure 4.3C**)**.**

Overall, early and late stage ACM differentially affected the IC expression profile of Th1-like cells. ACM derived from both early and late stage OGJ patients increased CTLA-4 expression on $CD8^{+}$ cells Th1-like and differentially affected the expression of PD-1, PD-L1 and TIGIT on the surface of Th1-like cells. Late stage ACM and not early stage ACM decreased PD-1 and PD-L1 on the surface of Th1-like cells, however, early stage ACM only decreased TIGIT expression on the surface of Th1-like cells. Although ACM derived from both early and late stage OGJ patients increased the frequency of $CD8^{+}$ Th1-like cells, only ACM derived from

early stage OGJ patients increased IFN-γ production by T cells. However this effect was not observed by ACM derived from late stage OGJ patients.

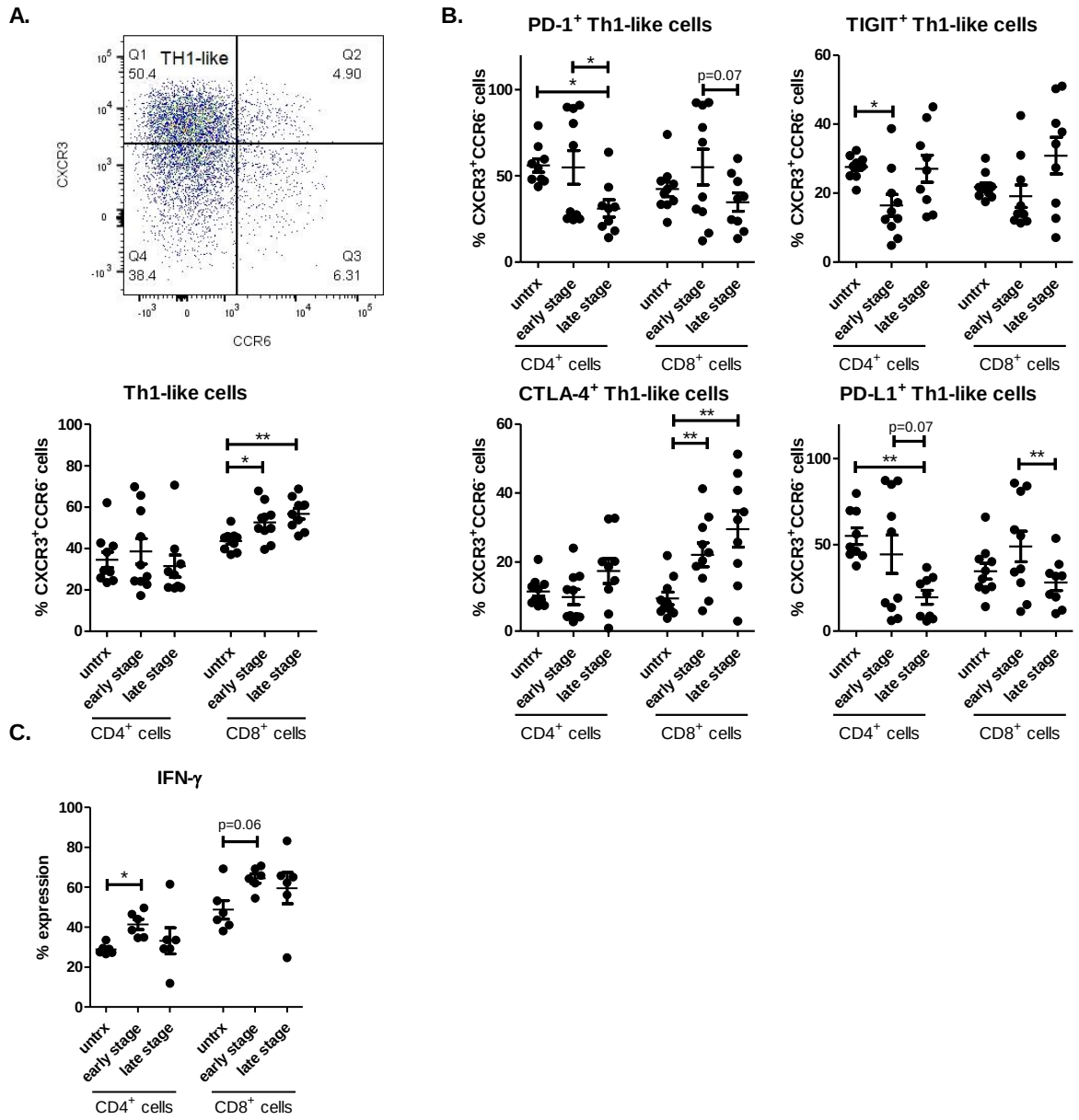

Figure 4.3: ACM derived from OGJ patients promotes a Th1-like phenotype and upregulates CTLA-4 expression on the surface of Th-1 like cells. (A) The effect of early stage ACM (n=9) and late stage ACM (n=8) on the frequency of Th1-like $CD3^+CD4^+$ and $CD3^+$ $CD8^+$ cells was assessed by flow cytometry and compared with untreated cells (n=10). (B) The effect of early stage ACM (n=9) and late stage ACM (n=8) on the expression of TIGIT, CTLA-4, PD-1 and PD-L1 was assessed on the surface of $CD3^+CD4^+$Th1-like and $CD3^+CD8^+$Th1-like cells by flow cytometry. (C) The effect of ACM on the secretion of Th1-

like cytokine IFN-γ was also assessed in $CD3^+CD4^+$ and $CD3^+CD8^+$ cells by flow cytometry. Th1-like cells were characterised as $CXCR3^+CCR6^-$ cells. Representative dot plot shown displaying frequency of $CD4^+$ Th1-like cells (A). Paired, non-parametric t test and data presented as percentages ± SEM. *p<0.05 and **p<0.01.

4.2.4 ACM derived from OGJ patients enhances a Th17-like phenotype; an effect which is abrogated by ICB

Pro-inflammatory Th17 and dual Th1/17 pro-inflammatory cell play an important role in generating tumour promoting inflammation. Their role in either promoting or hindering tumour progression remains conflicting within the literature and whether these cell types help eradicate the tumour or promote its progression is likely dependent on the tumour type and tumour-immune contexture. This study also investigated if ACM derived from OGJ patients had an effect on the frequency of Th1/17-like and Th17-like cells and the expression of pro-inflammatory IL-17A/F and TNF-α. Th1/17-like cells were characterised as $CXCR3^+CCR6^+$ cells and Th17-like cells were characterised as $CXCR3^-CCR6^-$ cells. ACM derived from OGJ patients with early stage tumours and late stage tumours significantly increased the frequency of Th17-like $CD4^+$ cells (untrx: 5.07 ± 0.2 vs. early stage: 7.14 ± 0.7% p=0.01, and late stage: 6.37 ± 0.5%, p=0.05) and the frequency of Th1/17-like $CD4^+$ T cells (untrx: 14.07 ± 0.2 vs. early stage: 16.15 ± 0.9% p=0.02, and late stage: 15.19 ± 0.6%, p=0.007) compared with untreated cells (**Figure 4A**)**.** ACM significantly altered the IC expression profile of Th-17-like and Th1/17-like cells downregulating PD-1, PD-L1, CTLA-4 and TIGIT surface expression (**Figure 4B** and **Figure 4C**). ACM derived from late stage OGJ patients decreased PD-1 expression on the surface of $CD4^+$ Th1/17-like cells (untrx: 64.12 ± 3.9 vs. late stage: 30.49 ± 6.7%, p=0.007) and $CD8^+$ Th1/17-like cells (untrx: 63.51 ± 3.3 vs. late stage: 52.34 ± 6.0%, p=0.07) compared with untreated cells (**Figure 4.4B**)**.** ACM derived from both early stage and late stage OGJ patients significantly decreased TIGIT expression on the surface of $CD4^+$ Th1/17-like cells (untrx: 41.79 ± 1.7 vs. early stage: 23.20 ± 2.9%, p=0.002, late stage: 24.81 ± 1.8%, p=0.003) compared with untreated cells (**Figure 4.4B**)**.** Similarly, ACM derived from both early stage and late stage OGJ patients significantly decreased CTLA-4 expression on the surface of $CD4^+$ Th1/17-like cells (untrx: 21.98 ± 2.5 vs. early stage: 11.28 ± 1.6%, p=0.009, late stage: 9.96 ± 1.4%, p=0.003) compared with untreated cells (**Figure 4.4B**)**.** ACM derived from late stage OGJ patients significantly decreased PD-L1 expression on the surface of $CD4^+$ Th1/17-like cells (untrx: 72.86 ± 3.9 vs. late stage: 21.12 ± 6.5%, p=0.003) and $CD8^+$ Th1/17-

like cells (untrx: 73.52 ± 3.5 vs. late stage: 46.97 ± 6.0%, p=0.003) compared with untreated cells (**Figure 4.4B**)**.** ACM derived from late stage OGJ patients significantly decreased PD-1 expression on the surface of $CD4^+$ Th17-like cells (untrx: 42.19 ± 4.5 vs. late stage: 21.52 ± 4.03%, p=0.02) compared with untreated cells (**Figure 4.4C**)**.** ACM derived from late stage OGJ patients significantly decreased TIGIT expression on the surface of $CD4^+$ Th17-like cells (untrx: 36.00 ± 1.8 vs. late stage: 28.47 ± 1.6%, p=0.01) compared with untreated cells (**Figure 4.4C**)**.** ACM derived from early stage and late stage OGJ patients significantly decreased TIGIT expression on the surface of $CD8^+$ Th17-like cells (untrx: 12.60 ± 13 vs. early stage: 5.37 ± 1.6%, p=0.009, late stage: 6.16 ± 1.4%, p=0.002) compared with untreated cells (**Figure 4.4C**)**.** ACM derived from early stage and late stage OGJ patients significantly decreased CTLA-4 expression on the surface of $CD4^+$ Th17-like cells (untrx: 13.83 ± 1.7 vs. early stage: 3.29 ± 0.9%, p=0.002, late stage: 3.56 ± 1.1%, p=0.003) compared with untreated cells (**Figure 4.4C**)**.** ACM derived from late stage OGJ patients significantly decreased PD-L1 expression on the surface of $CD4^+$ Th17-like cells (untrx: 53.40 ± 5.1 vs. late stage: 14.90 ± 6.0%, p=0.01) and $CD8^+$ Th17-like cells (untrx: 46.66 ± 5.2 vs. late stage: 19.80 ± 2.8%, p=0.003) compared with untreated cells (**Figure 4.4C**)**.**

Overall, both early stage and late stage ACM significantly increased the frequency of $CD4^+$ Th1/17-like cells and Th17-like cells. However, early and late stage ACM differentially affected the IC expression profile of Th1/17-like and Th17-like cells. Both early stage and late stage ACM decreased CTLA-4 and TIGIT on the surface of Th1/17-like and Th17-like cells, however only late stage ACM decreased PD-1 expression on the surface of Th1/17-like and Th17-like cells. Additionally, late stage ACM decreased PD-L1 expression more substantially on the surface of Th1/17-like and Th17-like cells compared with early stage ACM.

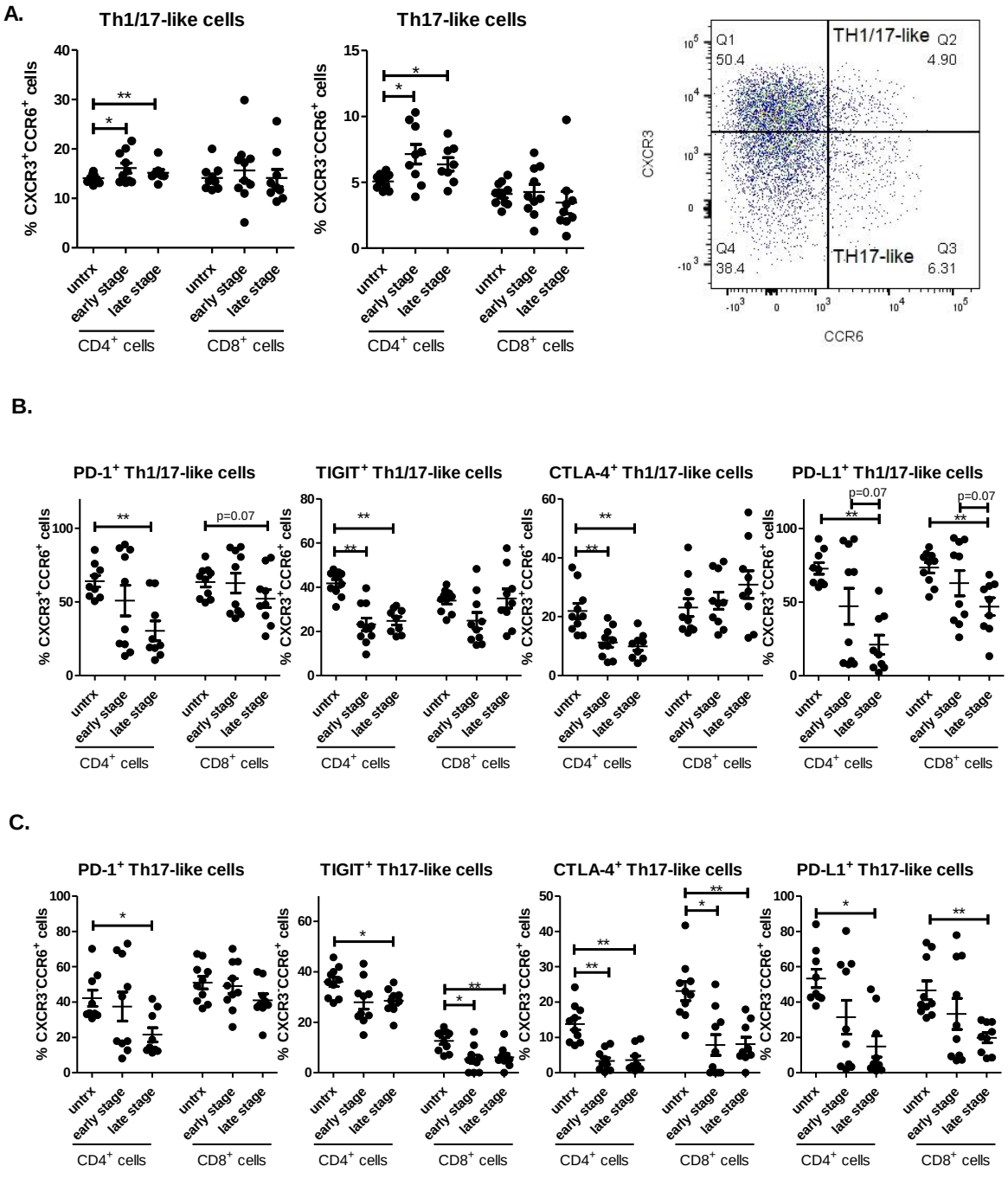

Figure 4.4: ACM derived from OGJ patients increases the frequency of pro-inflammatory-like Th-17 cells and downregulates ICs on their surface. (A) The effect of early stage ACM (n=9) and late stage ACM (n=8) on the frequency of Th1/17-like and Th17-like $CD3^+CD4^+$ and $CD3^+$ $CD8^+$ cells was assessed by flow cytometry and compared with untreated cells (n=10). (B) The effect of early stage ACM (n=9) and late stage ACM (n=8) on the expression of TIGIT, CTLA-4, PD-1 and PD-L1 was assessed on the surface of $CD4^+$Th1/17-like and $CD8^+$Th17-like cells (B) $CD4^+$Th17-like cells and $CD8^+$Th17-like cells

(C) by flow cytometry and compared with untreated cells (n=10). Th1/17-like cells were characterised as $CXCR3^{+}CCR6^{+}$ cells and Th17-like cells were characterised as $CXCR3^{-}CCR6^{-}$ cells. Representative dot plot shown displaying frequency of $CD4^{+}$ Th1/17-like cells and Th17-like cells (A). Paired, non-parametric t test and data presented as percentages ± SEM. *p<0.05 and **p<0.01.

Given that ACM derived from early and late stage OGJ patients significantly altered the frequency of Th-1/17-like and Th17-like cells and their IC expression profile, this study next sought to investigate if the ACM from these patients significantly altered the production of pro-inflammatory cytokines such as IL-17A/F and TNF-α. ACM derived from early stage OGJ patients significantly increased the frequency of IL-17-producing $CD4^{+}$ cells compared with untreated cells (untrx: 9.49 ± 0.7 vs. early stage: 25.95 ± 2.4%, p=0.03) (**Figure 4.5A).** ACM derived from early stage or late stage OGJ patients did not significantly affect the frequency of TNF-α-producing T cells compared with untreated cells (**Figure 4.5A).** Single agent ipilimumab and dual nivolumab-ipilimumab treatment significantly increased the frequency of IL-17-producing $CD4^{+}$ cells compared with untreated cells (untrx: 9.49 ± 0.7 vs. ipilimumab: 11.16 ± 0.5%, p=0.007, nivolumab-ipilimumab: 12.47 ± 1.1%, p=0.01) (**Figure 4.5B).** In contrast, single agent nivolumab, atezolizumab, dual nivolumab-atezolizumab and dual nivolumab-ipilimumab decreased the frequency of IL-17-producing $CD4^{+}$ cells in the presence of early stage ACM compared with cells treated with early stage ACM alone (early ACM: 25.95 ± 2.4 vs. early ACM + nivolumab: 18.87 ± 1.5%, p=0.06, early ACM + atezolumab: 16.95 ± 2.3%, p=0.03, early ACM + nivolumab-atezolziumab: 12.96 ± 2.7%, p=0.03 and early ACM + nivolumab-ipilimumab: 15.48 ± 3.1%, p=0.06) (**Figure 4.5B).** Single agent atezolizumab, dual nivolumab-atezolizumab and dual nivolumab-ipilimumab significantly decreased the frequency of IL-17-producing $CD8^{+}$ cells compared with untreated cells (untrx: 34.83 ± 3.3 vs. atezolizumab: 15.67 ± 5.1%, p=0.03, nivolumab-atezolizumab: 18.05 ± 4.9%, p=0.03 and nivolumab-ipilimumab: 22.48 ± 2.1%, p=0.03) (**Figure 4.5B**). ICB did not significantly affect the frequency of IL-17-producing $CD8^{+}$ T cells in the presence of early stage or late stage ACM compared with untreated cells (**Figure 4.5B**). Dual nivolumab-ipilimumab significantly increased the frequency of TNF-α-producing $CD4^{+}$ cells compared with untreated cells (untrx: 48.29 ± 1.7 vs. nivolumab-ipilimumab: 53.01 ± 3.2%, p=0.04) (**Figure 4.5C**). Single agent nivolumab and dual nivolumab-ipilimumab significantly decreased the frequency of TNF-α-producing $CD4^{+}$ cells in the presence of late stage ACM

compared with cells treated with late stage ACM alone (late ACM: 42.65 ± 10.1 vs. late ACM + nivolumab: 34.26 ± 9.1%, p=0.03, late ACM + nivolumab-ipilimumab: 21.99 ± 4.8%, p=0.03) (**Figure 4.5C**)**.** Single agent nivolumab significantly decreased and dual nivolumab-ipilimumab significantly increased the frequency of TNF-α-producing $CD8^+$ cells compared with untreated cells (untrx: 30.70 ± 2.3 vs. nivolumab: 24.26 ± 1.9%, p=0.04, nivolumab-ipilimumab: 37.88 ± 2.3%, p=0.05) (**Figure 4.5C**)**.** In contrast, dual nivolumab-ipilimumab significantly decreased the frequency of TNF-α-producing $CD8^+$ cells in the presence of late stage ACM compared with cells treated with late stage ACM alone (late ACM: 28.10 ± 7.8 vs. late ACM + nivolumab-ipilimumab: 15.32 ± 4.1%, p=0.03) (**Figure 4.5C**)**.**

Overall, ACM derived from early stage OGJ patients increased the production of IL-17A/F by $CD4^+$ T cells compared with untreated cells, however this effect was not observed by ACM derived from late stage OGJ patients. Single agent ipilimumab and dual nivolumab-ipilimumab significantly increased the production of IL-17-A/F by $CD4^+$ T cells in the absence of ACM however, in the presence of early stage ACM the opposite effect was observed and ICB decreaed IL-17A/F production by $CD4^+$ T cells and in the presence of late stage ACM ICB had not significant effect on the production of IL-17A/F by $CD4^+$ T cells. Dual nivolumab-ipilimumab treatment increased TNF-α production by T cells in the absence of ACM, however, in the presence of early stage ACM this effect was not observed and in the presence of late stage ACM this dual combination of ICB significantly decreased TNF-α production by T cells.

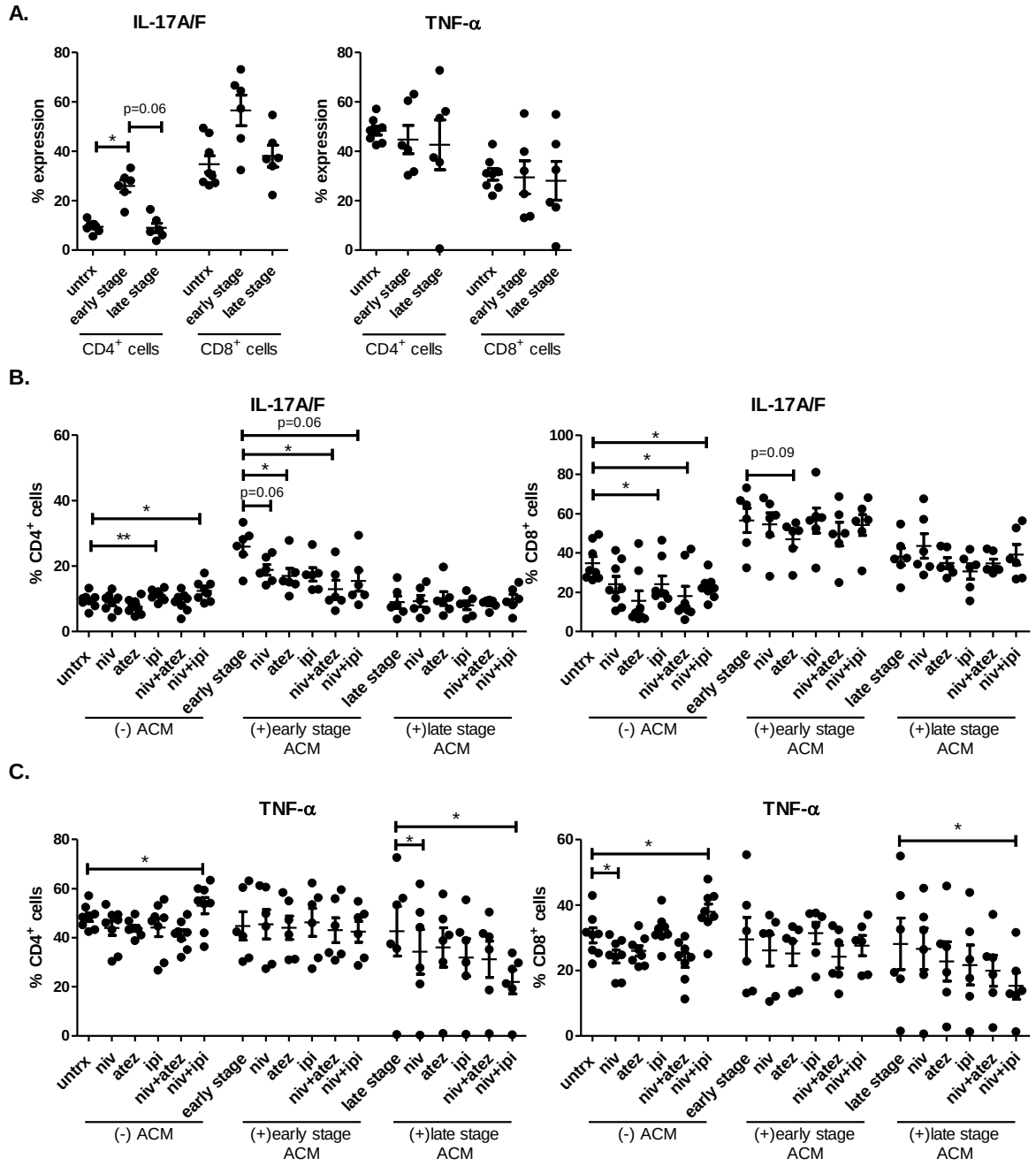

Figure 4.5: ICB attenuates the ACM-enhanced pro-inflammatory T cell cytokine signature. (A) The effect of early stage (n=9) ACM and late stage ACM (n=8) derived from OGJ patients on the secretion of pro-inflammatory cytokines IL-17A/F and TNF-α was assessed in $CD3^+CD4^+$ and $CD3^+CD8^+$ cells by flow cytometry and compared with untreated cells (n=10). The effect of single agent nivolumab, single agent atezolizumab, single agent ipilimumab, dual nivolumab-atezolizumab or dual nivolumab-ipilimumab in the absence (n=6) or presence of early stage ACM (n=6) and late stage ACM (n=6) on the secretion of pro-inflammatory cytokines IL-17A/F (B) and TNF-α (C) was also assessed in $CD3^+CD4^+$ and

$CD3^+CD8^+$ cells by flow cytometry. Paired, non-parametric t test and data presented as percentages ± SEM. *p<0.05 and **p<0.01.

4.2.5 ACM derived from OGJ patients significantly increases the secretion of IL-10 by T cells

Regulatory T cells (Treg) play a vital role in driving tumour progression through dampening anti-tumour immune responses. It is well-established that the visceral adipose tissue is a source of pro-inflammatory mediators however, with immune stimulation immunoregulatory processes are also activated to help maintain homeostasis. Therefore, this study also investigated if ACM derived from OGJ patients had an effect on the Treg compartment. $CD4^+$ Treg cells were characterised as the frequency of $CD4^+CD127^{LOW}CD25^{HIGH}$ that were $FOXP3^+$. ACM derived from OGJ patients with early stage tumours and late stage tumours did not significantly affect the frequency of $CD4^+$ Treg cells compared with untreated cells (**Figure 4.6A**)**.** Early stage and late stage ACM decreased the expression of PD-1 on the surface of Treg cells compared with untreated cells (untrx: 58.57 ± 3.2 vs. early stage: 38.86 ± 6.8%, p=0.06, late stage: 29.47 ± 6.1%, p=0.007) (**Figure 4.6B**)**.** ACM did not significantly affect the expression of TIGIT on the surface of Treg cells compared with untreated cells (**Figure 4.6B**)**.** Early stage and late stage ACM significantly increased the expression of CTLA-4 on the surface of Treg cells compared with untreated cells (untrx: 6.90 ± 0.7 vs. early stage: 21.98 ± 3.0%, p=0.005, late stage: 14.86 ± 2.4%, p=0.01) (**Figure 4.6B**)**,** and similarly, increased the expression of PD-L1 on the surface of Treg cells compared with untreated cells (untrx: 17.07 ± 1.5 vs. early stage: 24.29 ± 2.6%, p=0.06, late stage: 39.93 ± 4.2%, p=0.003) (**Figure 4.6B**)**.** Early stage and late stage ACM significantly increased the frequency of IL-10-producing $CD4^+$ T cells compared with untreated cells (untrx: 1.28 ± 0.2 vs. early stage: 5.37 ± 1.2%, p=0.03, late stage: 3.47 ± 0.3%, p=0.03) (**Figure 4.6C**)**.** Similarly, early stage ACM increased the frequency of IL-10-producing $CD8^+$ T cells compared with untreated cells (untrx: 34.21 ± 3.2 vs. early stage: 47.72 ± 6.6%, p=0.06) (**Figure 4.6C**)**.** ICB did not significantly affect the frequency of IL-10-producing $CD4^+$ T cells in the presence of ACM compared with cells treated with ACM alone (**Figure 4.6C**)**.**

Single agent atezolizumab, ipilimumab, dual nivolumab-atezolizumab and dual nivolumab-ipilimumab significantly decreased the frequency of IL-10-producing $CD8^+$ T cells compared with untreated cells (untrx: 34.21 ± 3.2 vs. atezolizumab: 14.82 ± 4.9%, p=0.03, ipilimumab: 21.64 ± 4.42%, p=0.05, nivolumab-atezolizumab: 16.29 ± 5.1%, p=0.03 and nivolumab-

ipilimumab: 18.47 ± 2.4%, p=0.01) (**Figure 4.6C**)**.** However, ICB did not significantly decrease the frequency of IL-10-producing $CD8^+$ T cells in the presence of ACM compared with cells treated with ACM alone (**Figure 4.6C**)**.**

Overall, both early stage ACM and late stage ACM increased the production of IL-10 by T cells. ACM derived from both early and late stage OGJ patients decreased PD-1 expression and increased the expression of CTLA-4 and PD-L1 on the surface of T cells compared with untreated cells. However, late stage ACM increased PD-L1 on the surface of Treg cells more substantially than early stage ACM. ICB decreased the production of IL-10 from $CD8^+$ T cells in the absence of ACM compared with untreated cells. However, this effect was not observed in the presence of early stage or late stage ACM.

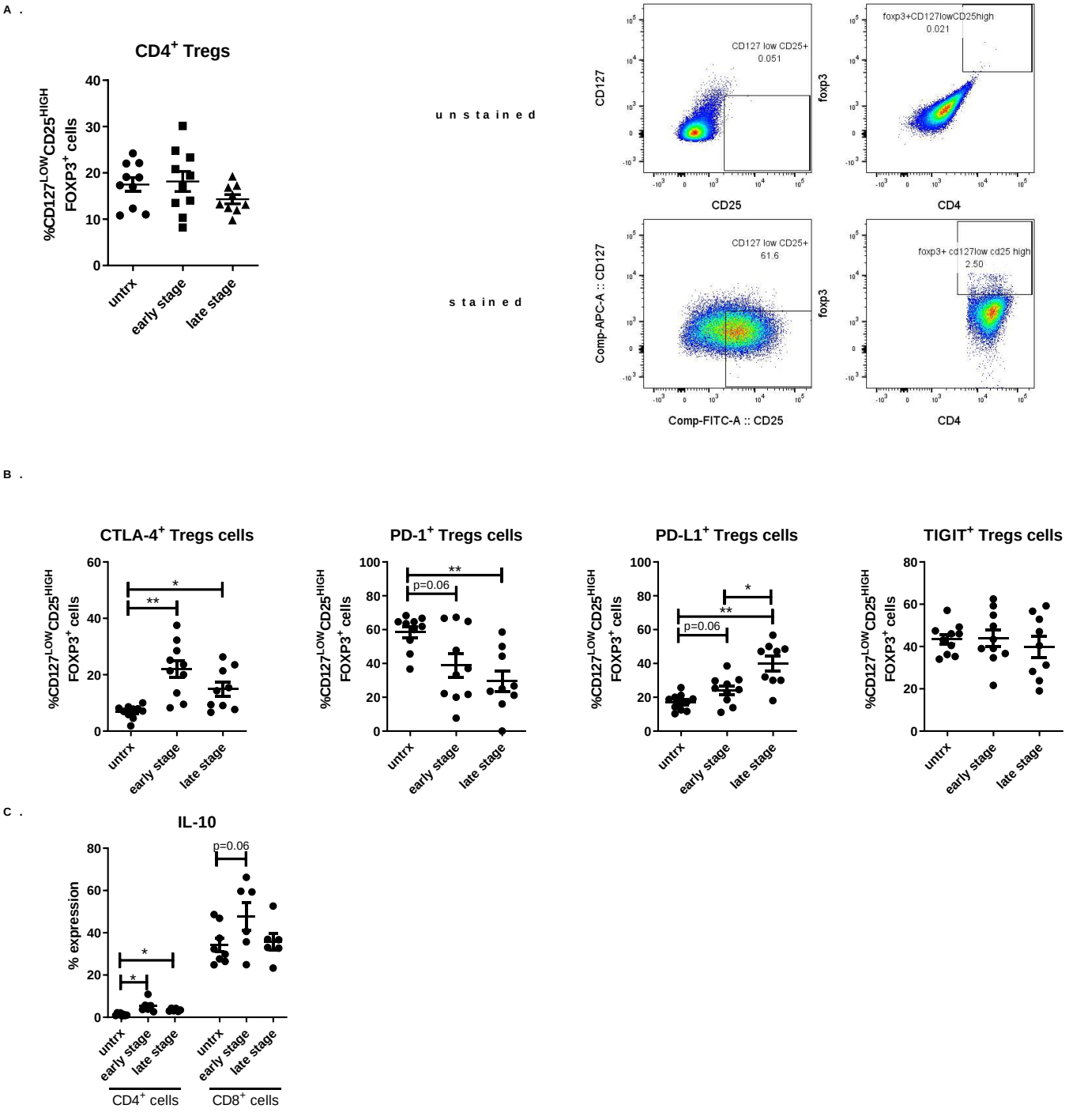
A .
CD4+ Tregs
%CD127LOWCD25HIGH FOXP3+ cells
untrx
early stage
late stage
unstained
stained
CD127 low CD25+
0.051
foxp3+CD127lowCD25high
0.021
CD127
foxp3
CD25
CD4
CD127 low CD25+
61.6
foxp3+ cd127low cd25 high
2.50
Comp-APC-A :: CD127
Comp-FITC-A :: CD25
B .
CTLA-4+ Tregs cells
PD-1+ Tregs cells
PD-L1+ Tregs cells
TIGIT+ Tregs cells
p=0.06
C .
IL-10
% expression
CD4+ cells
CD8+ cells
D .
IL-10
% CD4+ cells
% CD8+ cells
untrx
niv
atez
ipi
niv+atez
niv+ipi
early stage
late stage
(-) ACM
(+)early stage ACM
(+)late stage ACM

Figure 4.6: ACM derived from OGJ patients increases IL-10 production by T cells, an effect which is attenuated by ICB. (A) The effect of early stage ACM (n=6) and late stage ACM (n=6) on the frequency of $CD4^+$ Treg cells was assessed by flow cytometry. (B) The effect of early stage ACM (n=6) and late stage ACM (n=6) on the expression of TIGIT, CTLA-4, PD-1 and PD-L1 was assessed on the surface of $CD4^+$ Treg cells by flow cytometry. (C) The effect of ACM on the secretion of anti-inflammatory regulatory cytokine IL-10 was also assessed in $CD3^+CD4^+$ and $CD3^+CD8^+$ cells by flow cytometry. (D) The effect of single agent nivolumab, single agent atezolizumab, single agent ipilimumab, dual nivolumab-atezolizumab or dual nivolumab-ipilimumab in the absence or presence of early stage ACM (n=6) and late stage ACM (n=6) on the secretion of anti-inflammatory regulatory cytokine IL-10 was also assessed in $CD3^+$, $CD3^+CD4^+$ and $CD3^+CD8^+$ cells by flow cytometry. $CD4^+$ Treg cells were characterised as the frequency of $CD4^+CD127^{LOW}CD25^{HIGH}$ that were $FOXP3^+$. Representative dot plots displayed in (A) showing gating strategy for Treg cells: after gating on $CD4^+$ T cells, these cells within the $CD4^+$ gate were gated on $CD127^{LOW}CD25^{HIGH}CD4^+$ T cells, followed by an additional gate drawn around $FOXP3^+$ cells that were $CD4^+CD127^{LOW}CD25^{HIGH}$ cells. Paired, non-parametric t test and data presented as percentages ± SEM. *$p<0.05$ and **$p<0.01$.

4.2.6 ACM derived from early stage OGJ patients was more inflammatory than ACM derived from late stage OGJ patients and increased the proliferation rate of OE33 cells

We next profiled the ACM from OGJ patients with early versus late stage tumours to determine if there was a significant difference in the pro-inflammatory profile of the visceral fat secretome. ACM derived from OGJ patients with early stage tumours had significantly increased levels of pro-inflammatory TNF-α cytokine compared with ACM derived from OGJ patients with late stage tumours (early stage: 2,730 ± 1,412 vs. late stage: 806.1 ± 131.8 pg/gram p=0.05) (**Figure 4.7A**). Similarly, ACM derived from OGJ patients with early stage tumours had increased levels of other pro-inflammatory cytokines: IL-1RA, IL5 and IL-17A cytokines compared with ACM derived from OGJ patients with late stage tumours (IL-1RA- early stage: 29,939 ± 13,234 vs. late stage: 7,312 ± 1,452 pg/gram p=0.08, IL-5- early stage: 3.68 ± 13.98 vs. late stage: 7.20 ± 2.5 pg/gram p=0.06, IL-17A- early stage: 62.00 ± 10.81 vs. late stage: 40.61 ± 8.5 pg/gram p=0.08) (**Figure 4.7B-D).** There was no significant difference in the levels of the remaining 49 mediators in ACM derived from early versus late stage OGJ

patients which included immunomodulatory, pro-inflammatory and pro-angiogenic mediators shown in **Figure 4.8**.

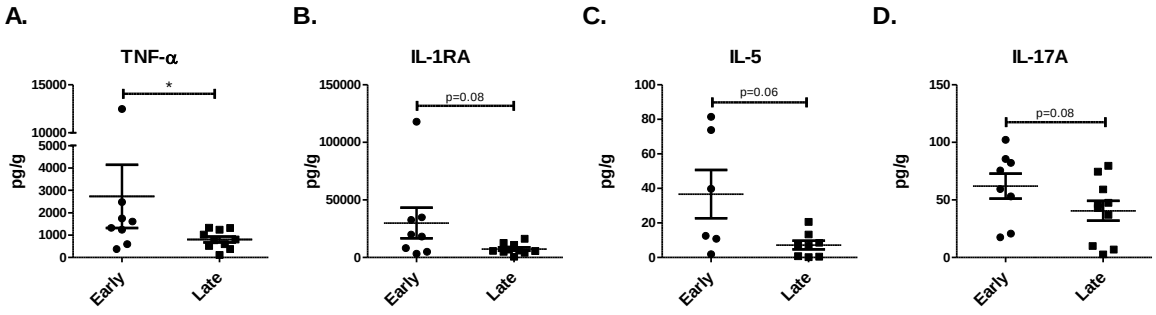

Figured 4.7: TNF-α was significantly decreased in ACM derived from late stage OGJ patients compared with early stage OGJ patients. ACM from OGJ patients with early stage tumours (pathological staging 0-II, n=8) versus late stage tumours (pathological staging III-IV, n=10) was screened for a panel of pro-inflammatory mediators, pro-angiogenic mediators and immunomodulatory cytokines using multi-plex ELISA. Mann-Whitney test, *p≤0.05. Only mediators shown that were significantly different (or bordering significance) between OGJ patients with early vs. late stage ACM are shown. Data was normalised to pg/g.

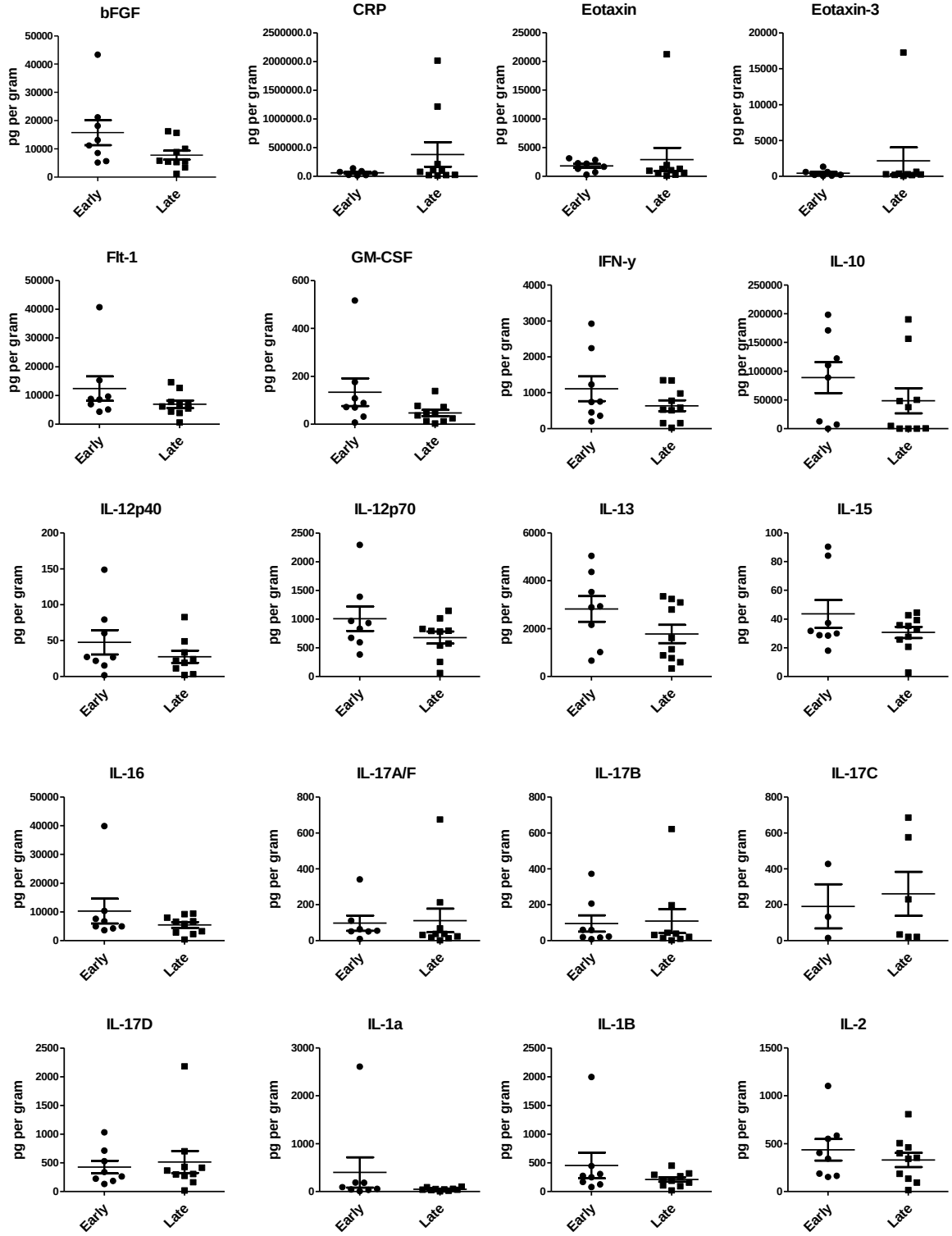
bFGF
CRP
Eotaxin
Eotaxin-3
Flt-1
GM-CSF
IFN-y
IL-10
IL-12p40
IL-12p70
IL-13
IL-15
IL-16
IL-17A/F
IL-17B
IL-17C
IL-17D
IL-1a
IL-1B
IL-2
pg per gram
Early
Late

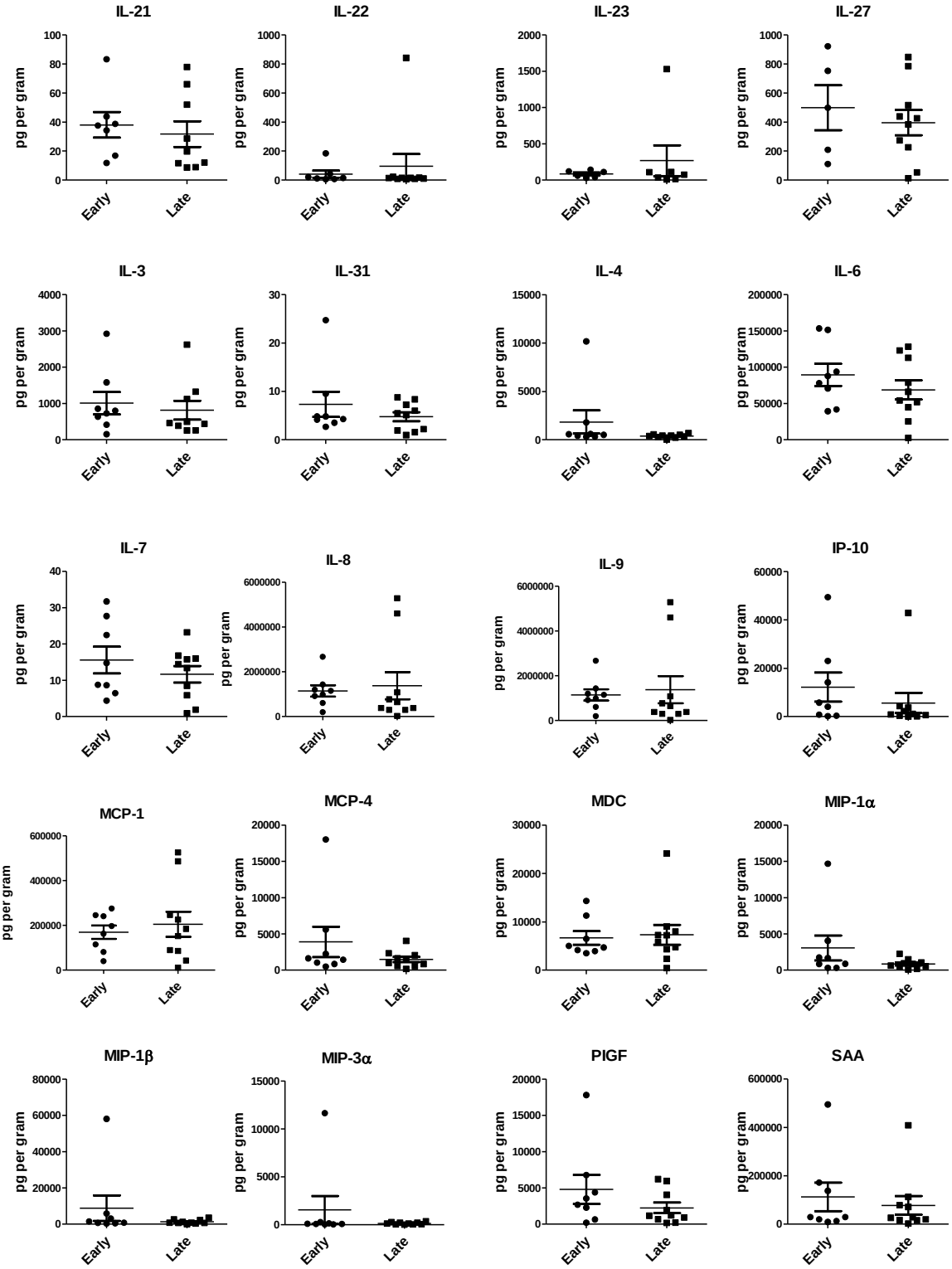
IL-21
IL-22
IL-23
IL-27
IL-3
IL-31
IL-4
IL-6
IL-7
IL-8
IL-9
IP-10
MCP-1
MCP-4
MDC
MIP-1α
MIP-1β
MIP-3α
PIGF
SAA
pg per gram
Early
Late

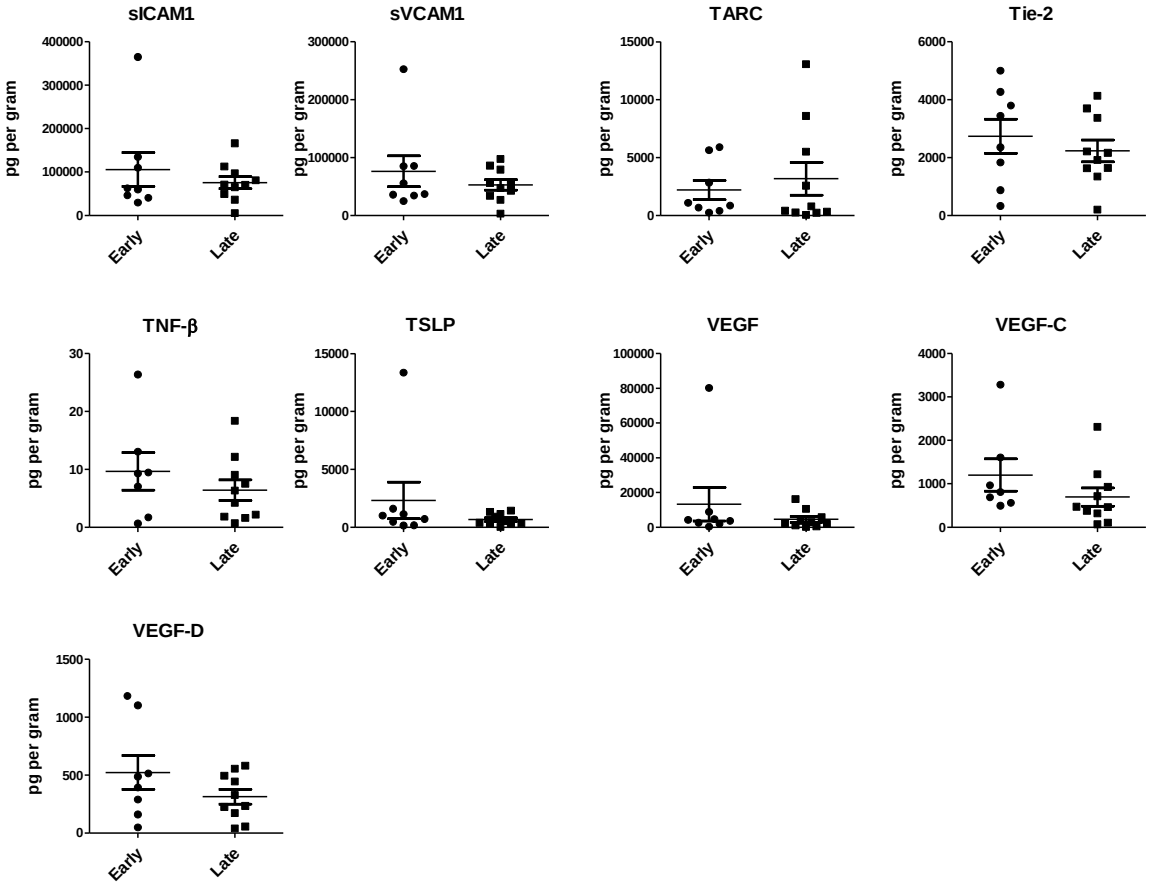

Figure 4.8: There was no significant difference in the levels of a range of pro-inflammatory mediators, pro-angiogenic mediators and immunomodulatory cytokines in the ACM from OGJ patients with early versus late stage tumours. ACM from OGJ patients with early stage tumours (pathological staging 0-II, n=8) versus late stage tumours (pathological staging III-IV, n=10) was screened for a panel of pro-inflammatory mediators, pro-angiogenic mediators and immunomodulatory cytokines using multi-plex ELISA. Mann-Whitney test. Only mediators shown that were not significantly between OGJ patients with early vs. late stage ACM. Mann-Whitney test, data was normalised to pg/g.

Given that early stage ACM exhibited a more pro-inflammatory profile than late stage ACM displaying increased levels of pro-inflammatory and tumour-promoting cytokines TNF-α, IL-1RA, IL5 and IL-17A which play important roles in promoting metastasis, tumour cell survival and growth and driving pro-tumourigenic phenotypes which support the hallmarks of caner this study sought to investigate if ACM derived from early and late stage OGJ patients enhanced tumour cell proliferation and if the ACM might counteract the anti-proliferative effect of the first-line FLOT chemotherapy regimen.

Early stage ACM significantly increased and late stage ACM increased the proliferation of OE33 cells compared with untreated cells (untrx: 110.7 ± 2.9 vs. early ACM: 131.6 ± 7.1, p=0.04 and late ACM: 133.3 ± 9.5, p=0.06) (**Figure 4.9A**). However, early stage and late stage ACM treatment in combination with the FLOT regimen did not significantly increase the proliferation of OE33 cells compared with FLOT treatment alone (**Figure 4.9B**). Interestingly, there was a subcohort of ACM derived from OGJ patients that decreased the proliferation of OE33 cells in combination with FLOT compared with FLOT treatment alone (FLOT: 91.74 ± 2.2 vs. FLOT+ACM: 74.93 ± 4.9, p=0.06) (**Figure 4.9C**). Furthermore, there was a subcohort of ACM derived from OGJ patients that increased the proliferation of OE33 cells in combination with FLOT compared with FLOT treatment alone (FLOT: 79.92 ± 1.2 vs. FLOT+ACM: 111.5 ± 6.5, p=0.01) (**Figure 4.9D**). There was no discernible clinical features that could categorise these patients two subcohorts of patients (**Figure 4.9C-D**).

Overall, ACM from both early and late stage OGJ patients increased the proliferation of OE33 cells compared with untreated cells. However, ACM categorised based on early vs. late stage tumours did not significantly abrogate the anti-proliferative effects of the first-line FLOT chemotherapy regimen. Interestingly, there were 2 subcohorts of ACM derived from OGJ patients that enhanced the anti-proliferative effects of FLOT and conversely abrogated the anti-proliferative effects of FLOT. These 2 subcohorts could not be categorised based on any clinical features so therefore, the molecular composition of the ACM is likely the discernible features.

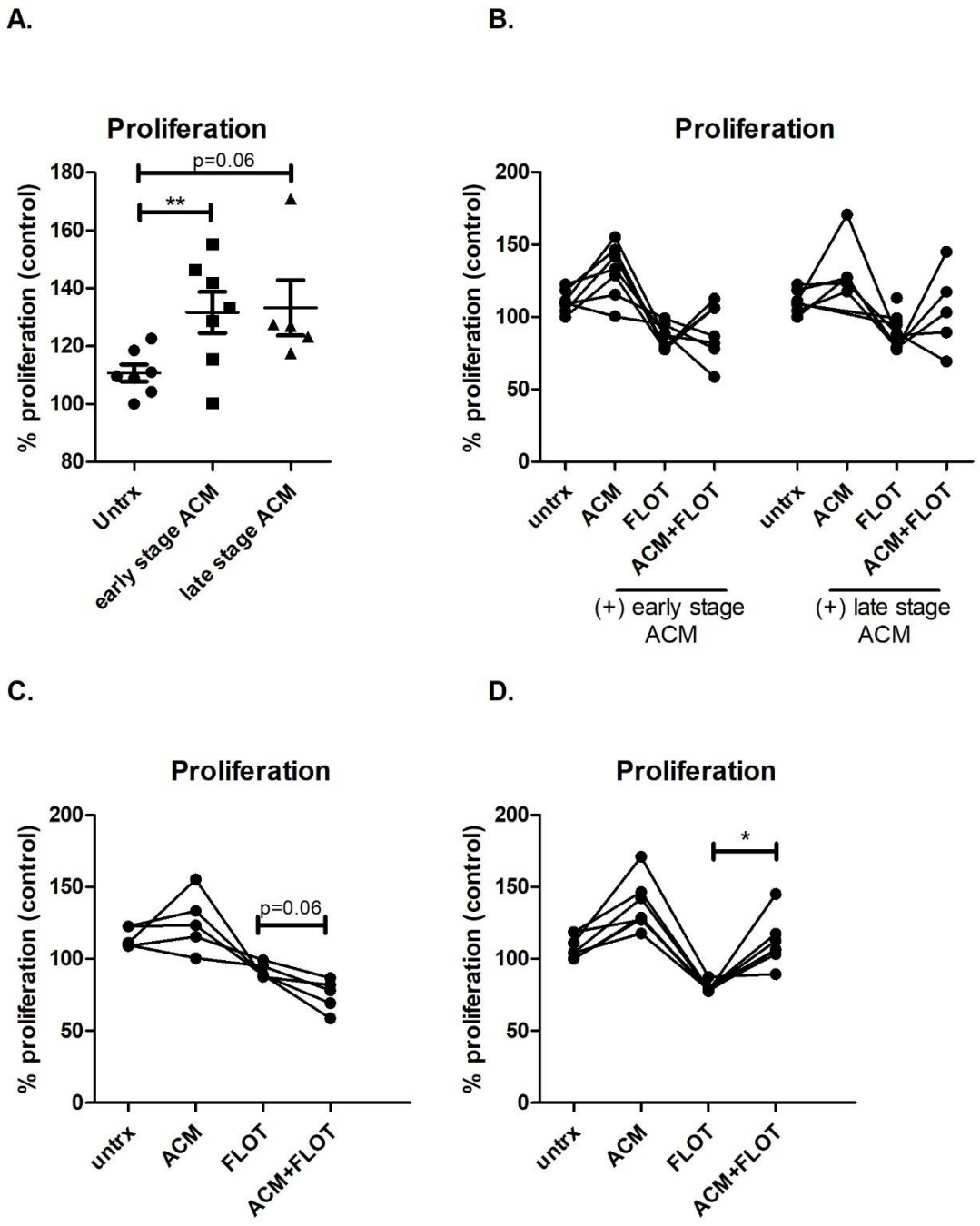

Figure 4.9: ACM derived from early stage OGJ patients significantly increased the proliferation rate of OE33 cells. OE33 cells were cultured in the absence (n=7) and presence of early stage ACM (n=7) and late stage ACM (n=5) using a 1 in 2 dilution and the proliferation rate was determined using a BrdU assay (A). OE33 cells were cultured in the absence (n=7) and presence of early stage ACM (n=7) and late stage ACM (n=5) using a 1 in 2 dilution (+) or (-) FLOT combination chemotherapy regimen and the proliferation rate was determined using a BrdU assay (B). A subcohort of ACM derived from OGJ patients (not categorised based on any clinical feature) increased the cytotoxicity of FLOT chemotherapy regimen (C) and

decreased the cytotoxicity of the FLOT chemotherapy regimen (D) demonstrated using a BrdU assay. Paired non-parametric t-test, *p<0.05.

4.3 Discussion

Several studies have highlighted how the negative effect of obesity and how obesity creates a vulnerability that can be harnessed for cancer treatment with the use of PD-1 ICB[100]. These findings collectively demonstrate that PD-1 is upregulated on T cells in obese murine cancer models and patients, which also harbour an increased dysfunctional T cell phenotype compared with their non-obese counterparts[100]. In addition, leptin a key satiety hormone, is increased in obese fat compared with non-obese fat and has been shown to directly increase PD-1 expression on the surface of T cells[100]. However, obesity was associated with increased efficacy of PD-1/PD-L1 ICB in both tumour-bearing mice and human cancer patients[100]. Administering PD-L1 ICB was more effective in obese cancer patients demonstrated by an increase in progression-free survival and overall survival compared with non-obese melanoma patients[100]. Therefore, this study aimed to investigate the effect of the visceral adipose tissue secretome (compartment where fat is deposited) from OGJ patients, on T cell phenotypes and whether addition of PD-1, PD-L1 or CTLA-4 ICB might enhance an anti-tumour T cell phenotypes. OGJ is an obesity-associated cancer however, given that the majority of OGJ patients have lost a significant proportion of weight by the time of diagnosis due to difficulty swallowing food as a result of tumour obstruction in the oesophagus, patients are no longer categorised as obese however are often still overweight. Additionally, at the time of surgery which is post-chemo(radio)therapy treatment patients have continued to lose weight and are often sarcopenic and cachectic at the time the visceral adipose fat is sampled. Therefore, for the purpose of this study we focussed on the effect of the visceral adipose tissue secretome based on early versus late stage tumours, on T cell phenotype and investigated whether addition of ICB might enhance the anti-tumour T cell response.

ACM from both early and late stage cancer patients significantly increased a range of inhibitory ICs including TIGIT, A2aR, PD-L2 and CD160 on the surface of T cells, however, there was no significant difference between early stage or late stage ACM. TIGIT, A2aR, PD-L2 and CD160 signalling dampens Th1 anti-tumour immunity and promotes a Treg phenotype promoting cancer progression[302]. Therefore, the ACM secretome may be creating a therapeutic niche for the use of ICB to harness anti-tumour immunity through blocking inhibitory signalling of TIGIT A2aR, PD-L2 and CD160 on the surface of T cells. Interestingly, ACM

derived from both early and late stage OGJ patients significantly decreased other ICs such as LAG-3, CTLA-4 and PD-1 on the surface of T cells. This dichotomous effect of ACM on the expression profile of ICs on T cells suggests that careful selection of ICs, such as TIGIT, A2aR, PD-L2 and CD160 may be more appropriate to target in OGJ patients. Furthermore, ACM from both early and late stage OGJ patients significantly increased the expression of co-stimulatory marker CD27 on the surface of T cells highlighting the immunostimulatory effect of both early and late stage ACM. CD27 has been identified as both a marker and mediator of T cell activation promoting T cell signalling[303]. This may also indicate that the immunostimulatory effects of early and late stage ACM may also promote increased acquisition of a dysfunctional and exhausted T cell phenotype longitudinally perhaps through concomitant upregulation of ICs (TIGIT, A2aR, PD-L2 and CD160), which could be exploited in OGJ patients through the use of ICB targeting TIGIT, A2aR, PD-L2 or CD160 to harness anti-cancer immunity and reinvigorate exhausted T cells in this setting.

As there was no significant difference in the effect of ACM derived from early or late stage OGJ tumours on IC expression profiles of the $CD4^+$ or $CD8^+$ T cell compartments, this would suggest that tumour stage would not affect the expression of the targets of these ICBs so in this instance tumour stage may not be a useful factor in clinical decision making for selecting ICB.

An important focus of this study was to investigate the effect of ACM on IC expression profiles of specific T cell subsets to garner a greater understanding of what ICs are expressed on anti-tumour and tumour-promoting T cells. Interestingly, we observed that ACM differentially affected the expression of ICs on Th1-like, Th1/17-like, Th17-like and Treg-like cells. Although ACM decreased CTLA-4 expression on the surface of the entire T cell population a dichotomous effect was observed on specific T cell subsets. ACM significantly increased CTLA-4 expression on the surface of Th1-like cells and Treg-like cells however downregulated CTLA-4 expression on the surface of Th1/17-like cells and Th17-like cells. This highlights the importance of investigating the IC expression profile on specific T cell subsets to help guide selection of appropriate ICs to target in clinical trials. CTLA-4 plays an important role in promoting conversion of Th1 cell types into Treg cell types and enhancing Treg function[304]. Perhaps in this setting ACM may be driving the conversion of Th1-like cells to Treg cells via upregulation of CTLA-4. CTLA-4 also plays an integral role in maintain a Treg phenotype[304,305] Therefore, CTLA-4 blockade may be a more appropriate IC to target for boosting Th1-like immunity in OGJ patients. In addition, ACM derived from both early and late stage tumours significantly increases PD-L1 expression on the surface of Treg cells,

however, late stage ACM increases PD-L1 more substantially on the surface of Treg cells. In contrast, ACM from both early and late stage OGJ patients decreases PD-1 expression on the surface of Treg cells. Amarnath *et al*., have indicated that PD-L1 back-signalling in T cells induces the conversion of Th1 cells into a regulatory T cell phenotype[306]. These findings collectively highlight that targeting PD-L1 and not just PD-1 alone may be more beneficial in harnessing anti-tumour immunity in particular in the OGJ setting.

ACM derived from OGJ patients with early stage tumours significantly increased the production of IFN-γ by T cells compared with untreated cells however, this trend was not observed by ACM derived from OGJ patients with late stage tumours. This highlights the immunomodulatory potential of the ACM derived from patients with early stage tumours which perhaps may have anti-cancer properties. This IFN-γ-promoting effect is not observed by late stage ACM and highlights the immunosuppressive ability of more advanced stage tumours in co-opting distal organs to dampen their innate anti-cancer mechanisms and perhaps sculpt the visceral adipose tissue into an immunosuppressive tumour permissive niche amenable to metastatic deposition and colonisation. This phenomenon has been documented in several cancer types where the primary tumour primes distal organs into immunosuppressive pre-metastatic niches[307]. Pre-metastatic niches are microenvironments created by the distal primary tumour in distant organs whereby the primary tumour secretes soluble factors and tumour-derived extracellular vesicles which home to distant sites creating conducive environment for survival and outgrowth of tumour cells before their arrival at these sites[307].

To further support this hypothesis that ACM derived from early stage OGJ patients exhibits potential anti-cancer properties, ACM derived from OGJ patients with early stage tumours possessed higher levels of IL-5 which possess immunostimulatory properties in promoting Th1 anti-tumour immunity and mice deficient in IL-5 exhibited reduced anti-tumour immunity[308]. IL-5 is critical for differentiation of bone marrow progenitors into eosinophils, mature eosinophils fail to develop in IL-$5^{-/-}$ mice. Furthermore, the loss of systemic antitumor immunity was associated with the absence of eosinophils at the tumour challenge sites in IL-$5^{-/-}$ mice[308].

In stark contrast, although ACM derived from early stage OGJ patients increased IFN-γ production by T cells during a short term 48h culture, this study also identified that ACM derived from OGJ patients with early stage tumours exhibited a more pro-inflammatory and tumour-promoting secretome than ACM derived from OGJ patients with late stage tumours, demonstrated by higher levels of pro-inflammatory TNF-α and IL-1RA. IL-1RA has been

implicated in promoting tumour-associated macrophage-mediated metastasis in breast cancer[309]. Additional studies have reported similar roles for IL-1RA in promoting tumour invasiveness and metastasis in other cancer types[310]. TNF-α has been implicated in several cancer types in promoting tumour cell migration invasion and metastasis[311] as well as promoting pro-tumourigenic immune cell phenotypes such as neutrophils[312] and tumour-associated macrophages[313] and promoting resistance to current standard of care regimens via enhancing an apoptotic tumour cell resistant phenotype[90]. Collectively, this highlights that factors withing the visceral adipose tissue of OGJ patients with early stage tumours may possess a greater potential to promote tumour progression and metastasis and may also play a role in promoting progression of early stage tumours to more advanced stage tumours. ACM derived from late stage OGJ patients had lower levels of TNF-α and IL-1RA this may be a reflection of a switch in dependence of soluble factors by the tumour to promote tumour progression and perhaps metastatic colonisation within the adipose tissue of late stage OGJ patients. At this advanced stage OGJ patients may already harbour micrometastatic deposits in distal organs including the visceral adipose tissue so perhaps these pro-metastatic factors are less essential at this stage and there may be other factors that are promoting outgrowth of the tumour that may increase instead which were not included in this screen. Overall, further studies are required to investigate if TNF-α or IL-1RA may be playing a role in creating a pre-metastatic niche in the visceral adipose tissue of early stage OGJ patients and whether targeting these soluble factors might prevent metastatic dissemination to the visceral adipose compartment in OGJ patients or prevent tumour progression to more advanced stages. However, ICB only attenuated TNF-α production by T cells in the presence of late stage ACM and not early stage ACM highlighting that the pro-inflammatory effect of ACM from early stage OGJ patients may not be amenable to abrogation by these ICBs. Although ICB-mediated downregulation of TNF-α in the presence of late stage ACM would be a beneficial effect to dampen tumour-promoting inflammatory responses which drive resistance to current standards of neodjuvant care particularly in late stage OGJ tumours which are more resistant to chemo(radio)therapy regimens[314]. These findings highlight that ICB may be useful in attenuating tumour-promoting inflammation in more advanced stage OGJ tumours.

Complementary findings also highlighted that ACM-derived from early stage OGJ patients and not late stage OGJ patients significantly increased the production of IL-17 by T cells. The role of IL-17 in either promoting or dampening anti-tumour immunity has been controversial with opposing studies reporting conflicting effects of IL-17 in either promoting or inhibiting anti-

tumour immunity in different solid tumour types[315]. To further support this hypothesis that ACM derived from OGJ patients with early stage tumours is promoting IL-17 immunity higher levels of IL-17 were found in the secretome from early stage ACM compared with late stage ACM of OGJ patients. Lu et al identified an anti-tumour role for IL-17 in enhancing anti-tumour immunity by promoting the migration of NK cells, T cells and dendritic cells in oesophageal squamous cell carcinoma patients and in enhancing the killing capability of B cells through enhanced expression of Granzyme B and FasL[316]. In contrast, IL-17 promoted breast tumour progression via recruiting pro-tumorigenic neutrophils to the tumour site[317]. ICB attenuated IL-17 production by T cells in the presence of ACM which may be a beneficial effect to dampen tumour-promoting inflammatory responses in the OGJ setting given its incidence is strongly-associated with obesity-driven inflammation[314].

This study highlights the immunostimulatory role of the visceral adipose tissue secretome from both early and late stage OGJ patients however, these immunostimulatory propagating effects appear to be diminished in the ACM from more advanced stage patients which perhaps may be a reflection of formation of an immunosuppressive pre-metastatic niche in the visceral adipose tissue of late stage OGJ patients. However, in stark contrast increased levels of pro-metastatic IL-1RA and TNF-α soluble factors were upregulated in early stage ACM compared with late stage ACM. It is unclear if these factors may be playing a role in promoting the progression of early stage tumours to late stage tumours in OGJ however, these soluble factors have been identified as potential mediators for priming of pre-metastatic niches in other cancer types. Therefore, IL-1RA and TNF-α soluble factors warrant further investigation regarding their potential role in driving tumour progression in OGJ and also as potential therapeutic targets to prevent metastasis to the visceral adipose tissue compartment (omentum).

Importantly, this study demonstrated that ACM derived from both early and late stage OGJ patients upregulates inhibitory ICs TIGIT, A2aR, PD-L2 and CD160 on the surface of T cells and specifically upregulates CTLA-4 on the surface of Th1-like cells and Treg cells thus, creating a therapeutic vulnerability that may be exploited by ICB to harness anti-tumour immunity. Furthermore, early and late stage ACM upregulated PD-L1 on the surface of Treg cells. Of particular note late stage ACM had a more substantial effect in upregulating PD-L1 on the surface of Treg cells compared with early stage ACM perhaps suggesting that ACM from late stage OGJ patients possess more immunoinhibitory effects compared with early stage ACM. These findings highlight that blockade of PD-L1 and CTLA-4 may be a more rational

therapeutic strategy that combining CTLA-4 blockade with PD-L1 blockade, particularly when ACM downregulated PD-1 on the surface of T cells and specific Th1-like and Treg subsets. Collectively, these findings highlight that the visceral adipose tissue of OGJ patients possesses both immunostimulatory and immunoinhibitory effects and upregulated a range of inhibitory ICs on T cell surfaces in particular CTLA-4 on the surface of Th1-like cells. Thus a rationale is identified for the use of ICB to exploit these immunomodulatory effects of the visceral adipose tissue secretome in OGJ patients to promote anti-cancer responses.

Chapter 5 – ICB synergises with first-line chemotherapy regimens to boost efficacy of chemotherapy via immune-independent mechanisms

Hypothesis

First-line chemotherapy regimens signficantly alter IC expression profiles of OGJ cells. Tumour-expressed immune checkpoint ligands and receptors provide OGJ cells with a survivial advantage and blockade of immune checkpoints enhances chemotherapy toxicity.

5.1.1 Highlights

- OGJ cells express several inhibitory IC ligands and receptors.
- Chemotherapy upregulates ICs on the surface of OGJ cells which is sustained for up to 3 weeks post-treatment, returning to baseline upon complete tumour cell recovery.
- Pro-survival MEK signalling mediated FLOT-induced upregulation of PD-L1, TIM-3, LAG-3 and A2aR on OGJ cells promoting a more immune-resistant phenotype.
- Single agent PD-1, PD-L1 and A2aR blockade decreased OGJ cell viability, proliferation and mediated apoptosis.
- ICs are enriched on stem-like and senescent OGJ cells following chemotherapy.
- Mechanistic insights demonstrated that blockade of the PD-1 axis decreased stem-like marker ALDH and expression of DNA repair genes.
- Importantly, combining single agent PD-1, PD-L1 and A2aR blockade with FLOT synergistically enhanced cytotoxicity in OGJ cells.
- These findings reveal novel mechanistic insights into the immune-independent functions of IC-intrinsic signalling in OGJ cells with important clinical implications for boosting the efficacy of the first-line FLOT chemotherapy regimen in OGJ in combination with ICB to not only boost anti-tumour immunity but also to suppress IC-mediated promotion of key hallmarks of cancer that drive tumour progression.

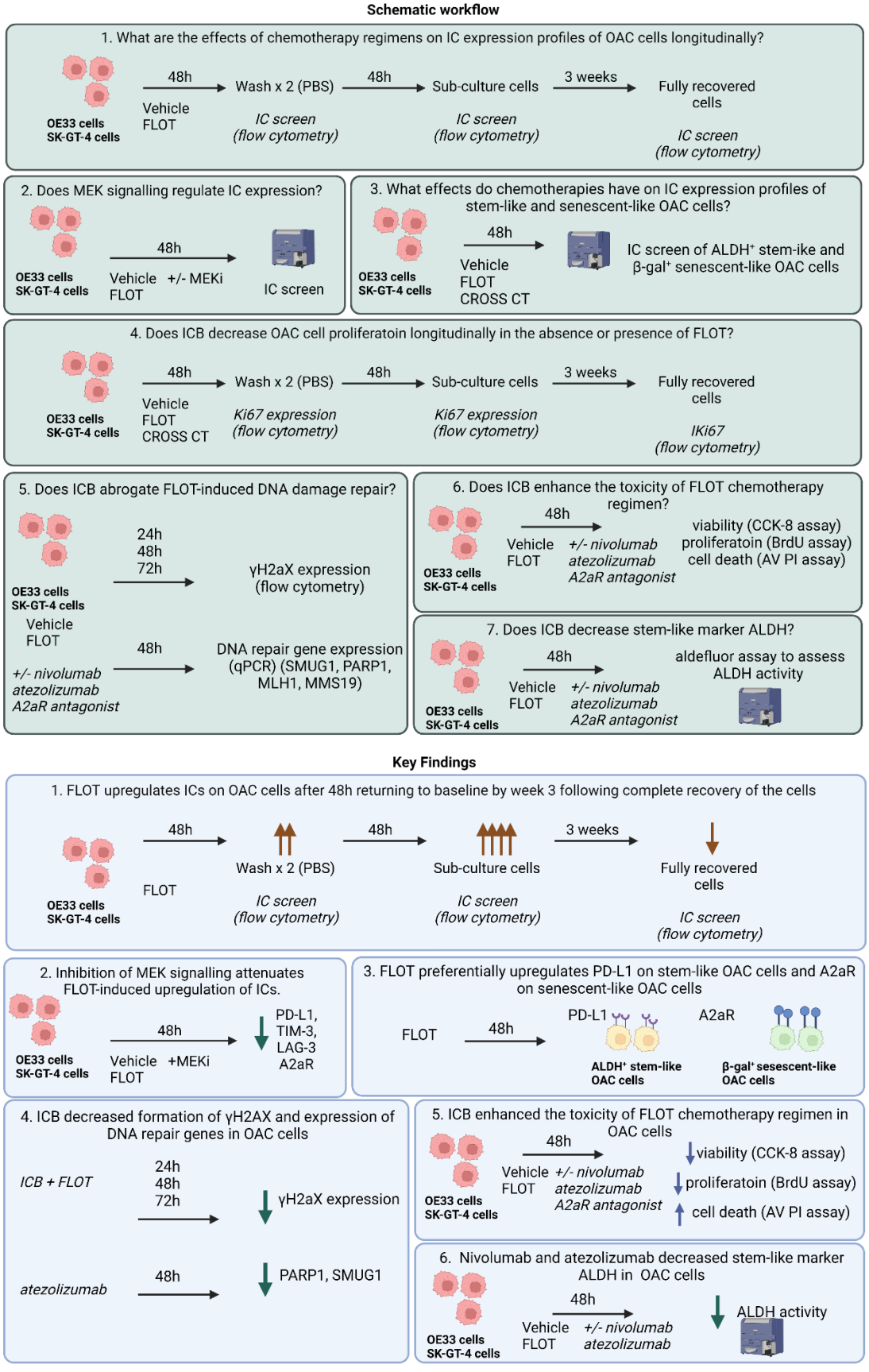

Graphical abstract: Schematic workflow – 1. OAC cells were treated for 48h with FLOT

chemotherapy regimen and screened for IC expression longitudinally. 2. OAC cells were treated with FLOT +/- meki and IC expression was assessed. 3. The effect of FLOT and CROSS CT on IC expression profiles was assessed on $ALDH^+$ stem-like OAC cells and $\beta\text{-gal}^+$ senescent-like OAC cells. 4. Longitudinal effects of ICB on the proliferative index of OAC cells was investigated by Ki67 analysis. 5. The effects of ICB in the absence and presence of FLOT on DNA repair gene expression was assessed by qPCR. 6. The ability of ICB to enhance the toxicity of FLOT was also assessed by a CCK-8, BrdU and AV PI assay. 7. The ability of ICB to decrease stem-like marker ALDH was also investigated using an aldefluor assay. Key findings – 1. OAC cells were treated for 48h with FLOT chemotherapy regimen and screened for IC expression longitudinally. 2. OAC cells were treated with FLOT +/- meki and IC expression was assessed. 3. The effect of FLOT and CROSS CT on IC expression profiles was assessed on $ALDH^+$ stem-like OAC cells and $\beta\text{-gal}^+$ senescent-like OAC cells. 4. Longitudinal effects of ICB on the proliferative index of OAC cells was investigated by Ki67 analysis. 5. The effects of ICB in the absence and presence of FLOT on DNA repair gene expression was assessed by qPCR. 6. The ability of ICB to enhance the toxicity of FLOT was also assessed by a CCK-8, BrdU and AV PI assay. 7. The ability of ICB to decrease stem-like marker ALDH was also investigated using an aldefluor assay.

5.1.2 Introduction

Treatment options for OGJ patients include the FLOT or MAGIC combination chemotherapy regimens before surgery (neoadjuvant) and after surgery (adjuvant)[318]. The FLOT chemotherapy regimen includes 3 different classes of drugs with distinct mechanisms of action, the anti-metabolite 5-fluorouracil (5-FU), a platinum-based DNA intercalator oxaliplatin and a taxane anti-microtubule docetaxel[318]. Leucovorin is a reduced form of folinic acid and is given as part of the FLOT regimen[319]. Leucovorin increases the toxicity of 5-FU by stabilising the binding of 5-FU to its drug target thymidylate synthetase prolonging the stability of 5-FU *in vivo*[320]. The MAGIC chemotherapy regimen includes a topoisomerase inhibitor epirubicin, a platinum-based DNA intercalator cisplatin and an anti-metabolite 5-FU (ECF) or capecitabine (a pro-drug of 5-FU) (ECX)[321]. Patients may also receive neoadjuvant chemotherapy with concurrent localised radiation, the CROSS regimen, which includes an anti-microtubule taxane paclitaxel and a platinum-based chemotherapy carboplatin in combination with daily 1.8 Gy doses of X-Ray radiation across 23 fractions with a cumulative dose of 41.4 Gy[322]. Response rates to the standard of care chemotherapy regimens remain low with a complete pathologic response rate of 16.6%[323] and subsequent clinical outcomes are dismal with a median overall

survival rate of 50 months[323] and 5-year overall survival rates as low as 15-40% depending on tumour stage at clinical presentation in OGJ[96].

Improvements in the efficacy of first-line chemotherapy regimens were achieved through combining immune checkpoint blockade (ICB) with chemotherapy as depicted in the recent findings from the phase III Checkmate 649 trial, which demonstrated the synergy between nivolumab and first-line chemotherapy (FOLFOX and XELOX) in previously untreated OGJ patients (n=1,581), in which a significant improvement in overall survival in patients with a PD-L1 combined positive score of 5 or greater was observed (14.4 months (nivolumab + chemotherapy arm) vs. 11.1 months (chemotherapy arm))[136]. Furthermore, the nivolumab + chemotherapy arm also reduced the risk of death by 29% (HR, 0.71; 98.4% CI, 0.59-0.86; $p<0.0001$)[136]. The findings from this trial highlight the potential synergy that can be exploited between chemotherapy and ICB in the first-line setting. Rational explanations for the improvement in overall survival are likely attributed to the ICB-mediated reinvigoration of anti-tumour immune responses. Moreover, mounting evidence in the literature suggest that the FOLFOX/XELOX chemotherapy regimens may possess immunostimulatory properties with the potential ability to convert a 'cold non-inflamed' tumour microenvironment into a 'hot inflamed' tumour microenvironment. 5-fluorouracil and oxaliplatin chemotherapies which comprise the FLOT regimen, have been shown to induce immunogenic tumour cell death in several cancer types. Therefore, addition of ICB to the FOFLOX/XELOX regimen likely reinvigorated exhausted anti-tumour immunity and prevented exhaustion of chemotherapy-induced anti-tumour immune responses, producing synergistic amplification of anti-tumour immunity which translated into durable clinical responses in gastroesophageal cancer patients. Oxaliplatin induced immunogenic cell death in colorectal cancer[141], lung carcinoma[150,151] and 5-FU induced immunogenic cell death in colon carcinoma[155] and gastric cancer[140]. Immunogenic cell death is a particular modality of cell death that can be triggered by selected anticancer chemotherapeutics[324]. Tumour cells undergoing immunogenic cell death which is characterised by the release or exposure of danger associated molecular patterns by tumour cells that stimulate the attraction, activation and maturation of dendritic cells and eventually the antigen-specific priming of cytotoxic T lymphocytes[325]. This can induce an adaptive anticancer immune response that targets residual cancer cells with the same antigenic profile[326]. However, aside from ICB-mediated inhibition of immune evasion, another explanation may be attributed to the effect of ICB on immune-independent hallmarks of cancer. Several studies have now shown that IC receptors such as PD-1, TIM-3, VISTA, A2aR and TIGIT are

expressed on the surface of a subpopulation of cancer cells in a range of malignancies including OGJ[327], melanoma[192], pancreatic[185], gastric[188,194] cervical[233], lung[186,190], ovarian[189], endometrial[189] and colorectal cancer[191]. Although inhibitory ICs are only found on a subpopulation of cancer cells, the clinical relevance should not be underestimated and it is important to investigate the phenotype of cancer cells expressing inhibitory ICs. Emerging studies have shown that melanoma and breast cancer stem-like cells were enriched for the expression of PD-1 and PD-L1[328], respectively. However, the phenotype and expression profile of inhibitory IC receptors and ligands by OGJ cells is unknown.

Recent studies have demonstrated that activation of both inhibitory IC ligands and receptors including PD-L1, PD-L2, TIM-3 and PD-1 on the surface of cancer cells promoted various immune-independent hallmarks of cancer such as metabolism, proliferation, invasion and metastasis, DNA repair and chemoresistance[182,184–186,188,194,232,329]. Blocking inhibitory IC ligands and receptors on cancer cell surfaces suppresses various hallmarks of cancer including invasion, chemoresistance, proliferation, glycolysis and DNA repair[182,184–186,188,194,232,329]. No studies exist demonstrating novel immune-independent functions of inhibitory IC ligands or receptors in OGJ, however there are several studies demonstrating these novel immune-independent functions in gastric cancer[188,194], which is molecularly very similar to OGJ. Moreover, the PD-1 axis has been implicated in conferring chemo(radio)-resistance through promotion of stem-like characteristic in lung cancer[330] and enhancement of radiation-induced DNA repair in osteosarcoma[331].

This study profiles the expression of a wide range of inhibitory IC ligands and receptors on the surface of OGJ cells *in vitro* and in *ex vivo* biopsies to identify potential therapeutic targets. The effect of clinically relevant combination chemotherapies (FLOT, CROSS chemotherapy (CROSS CT) and MAGIC) on the expression of ICs on OGJ was assessed *in vitro*. This study particularly focuses on the first-line FLOT chemotherapy regimen and explores FLOT chemotherapy regimen alters IC expression profiles of OGJ cells longitudinally. The phenotype of OGJ cells expressing ICs, specifically the stem-like and senescent-like properties of OGJ cells expressing IC ligands and receptors is assessed. The effect of single agent ICB on the viability of OGJ cells is also assessed including the ability of ICB to enhance FLOT chemotherapy cytotoxicity in OGJ cells. Mechanistic insights are also provided surrounding the regulation of FLOT-induced upregulation of ICs on OGJ cells and the effect of IC signalling on OGJ cell proliferation, DNA repair and expression of cancer stem-like markers with and without FLOT treatment. Collectively, the findings of this study will enhance our

understanding of the immune-independent mechanisms of action of ICBs in OGJ, which will offer important translational clinical insights for the design of synergistic ICB-chemotherapy combinations for OGJ patients.

5.1.3 Specific Aims

1. Profile the expression of inhibitory IC ligands and receptors on the surface of OGJ cells *in vitro* and in *ex vivo* biopsies.
2. Assess the effect of clinically relevant combination chemotherapies (FLOT, CROSS chemotherapy (CROSS CT) and MAGIC) on the expression of ICs on OGJ.
3. Longitudinally profile the effect of FLOT on the dynamic IC expression profiles of OGJ cells.
4. Determine if pro-survival MEK signalling in OGJ cells regulates IC expression.
5. Assess the phenotype of OGJ cells expressing ICs, specifically the stem-like and senescent-like cells.
6. Investigate if single agent ICB affects the survival of OGJ cells and alters the expression of DNA repair genes or expression of the stem-like marker ALDH.

5.2 Results

5.2.1 A subpopulation of normal oesophageal epithelial cells and OGJ cells express inhibitory IC ligands and inhibitory IC receptors

Emerging studies have shown that cancer cells not only express inhibitory IC ligands but also inhibitory IC receptors including PD-1, TIGIT and TIM-3 in OGJ[327], melanoma[192], pancreatic[185], gastric[188,194] cervical[233], lung[186,190], ovarian[189], endometrial[189] and colorectal cancer[191]. In addition, IC receptor TIM-3 has also been identified on normal gastric epithelial cells[188] as well as normal cervical epithelial cells[187]. Therefore, we screened normal oesophageal epithelial (Het1α cells) and OGJ cells for the expression of both inhibitory IC ligands and receptors. OE33 and SK-GT-4 OGJ cell lines were employed in this study and were established from tumours that had progressed from the pre-malignant Barret's oesophagus condition to OGJ. While the OE33 cells are poorly differentiated, the SK-GT-4 cells are well differentiated which helps to encapsulate the heterogeneous nature of OGJ.

Het1α cells and both OGJ cell lines expressed low levels of PD-L1 (Het1α 0.38 ± 0.1%, OE33 1.16 ± 0.2% and SK-GT-4 cells 1.29 ± 0.2%), PD-L2 (Het1α 0.29 ± 0.2%, OE33 2.11 ± 0.7% and SK-GT-4 cells 1.06 ± 0.2%) and CD160 (Het1α 0.67 ± 0.3%, OE33 1.63 ± 0.2% and SK-

GT-4 cells 1.18 ± 0.3%) (**Figure 5.1**). PD-1 is also expressed by Het1α cells and both OGJ cell lines (Het1α 27.80 ± 5.6%, OE33 22.64 ± 9.6% and SK-GT-4 cells 7.88 ± 2.8%), as are TIGIT (Het1α 30.00 ± 5.1%, OE33 12.76 ± 5.2% and SK-GT-4 cells 6.77 ± 2.1%), TIM-3 (Het1α 0.48 ± 0.2%, OE33 0.80 ± 0.2% and SK-GT-4 cells 1.28 ± 0.4%), LAG-3 (Het1α 0.64 ± 0.2%, OE33 0.6500 ± 0.1% and SK-GT-4 0.64 ± 0.2%) and A2aR (Het1α 0.37 ± 0.1%, OE33 0.82 ± 0.1% and SK-GT-4 cells 1.13 ± 0.2%) (**Figure 5.1**). Furthermore, the expression profile of ICs was significantly different between the Het1α cells and the two OGJ cell lines. A significantly higher percentage of SK-GT-4 cells expressed PD-L1 and LAG-3 compared with Het1α cells (**Figure 5..**). In addition, there was a significantly higher percentage of OE33 cells positive for CD160 and A2aR compared with Het1α cells (**Figure 5.1**). Interestingly, PD-1 and TIGIT were expressed on a significantly higher percentage of Het1α cells compared with the SK-GT-4 cell line (**Figure 5.1**). A higher percentage of SK-GT-4 cells expressed LAG-3 compared with the OE33 cells (**Figure 5.1**). There was no other significant differences in IC expression levels for the other inhibitory IC proteins between the cell lines.

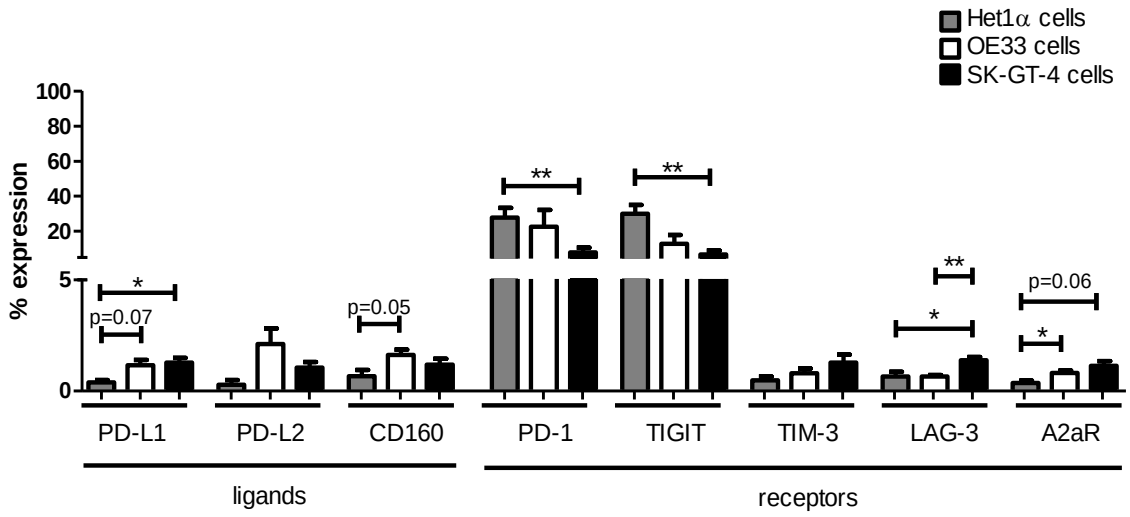

Figure 5.1: Normal oesophageal epithelial cells and OGJ cells basally express both inhibitory IC ligands and receptors *in vitro*. Basally Het1α cells, OE33 cells and SK-GT-4 cells were screened for the percentage expression of inhibitory IC ligands PD-L1, PD-L2, CD160 (n=3) and inhibitory IC receptors PD-1, TIGIT, TIM-3, LAG-3 and A2aR (n=3) *in vitro* by flow cytometry. Mann Whitney test *p<0.05 and **p<0.001. Gating strategy and representative dot plots for assessing IC expression is shown in Appendix **Figure A5.1**.

5.2.2 Chemotherapy promotes a more immune-resistant phenotype through upregulation of inhibitory IC ligands on OGJ cells *in vitro*

Previous studies have shown that single agent cisplatin and 5-FU increase PD-L1 on the surface of lung cancer[332] and OGJ cells[333] *in vitro* respectively, which may drive immune evasion and resistance to chemotherapy. Therefore, we sought to investigate the effect of clinically-relevant single agent chemotherapies on the expression of a range of inhibitory IC ligands (PD-L1, PD-L2 and CD160) on the surface of OE33 cells by flow cytometry (**Figure 5.4**) using IC_{50} doses pre-optimised using a CCK-8 assay (**Figure 5.2**). Importantly, we also assessed the effect of the combination chemotherapy regimens FLOT, CROSS CT and MAGIC on the expression of a range of inhibitory IC ligands on the surface of OE33 and SK-GT-4 cells by flow cytometry (**Figure 5.4**) using IC_{50} doses pre-optimised using a CCK-8 assay (**Figure 5.3**).

For single agent chemotherapies an IC_{50} dose was used. To obtain IC_{50} doses for combination FLOT, CROSS CT and MAGIC regimens; OE33 and SK-GT-4 cells were treated with increasing doses of single agent chemotherapies that comprise the FLOT, CROSS CT and MAGIC regimens to identify IC_{10}, IC_{25} and IC_{50} doses for each chemotherapy at a 48h time point (**Figure 5.2**). Subsequently, OE33 and SK-GT-4 cells were then treated with the combination regimens for 48h using an IC_{10}, IC_{25} or IC_{50} dose of each drug to obtain an inhibitory concentration of combination doses which killed 50% of the cells (**Figure 5.2**). The combination doses that reduced the viability of OE33 and SK-GT-4 cells by 50% were used for all the experiments in this study. Single agent 5-FU, oxaliplatin and docetaxel significantly increased the percentage of OE33 cells expressing PD-L1 (untreated 1.31 ± 0.5%, 5-FU 26.35 ± 6.4% (p=0.01), oxaliplatin: 13.59 ± 2.1% (p=0.0007) and docetaxel: 3.40 ± 2.1% (p=0.02)), (**Figure 5.4A**). The combination FLOT regimen also significantly increased PD-L1 expression on OE33 cells (1.16 ± 0.2% vs. 14.08 ± 3.5%, (p=0.01)) and SK-GT-4 cells (1.62 ± 0.3% vs. 43.0 ± 3.6%, (p=0.01)), (**Figure 5.4B**). Similarly, single agent 5-FU, oxaliplatin and docetaxel as well as the combined FLOT regimen significantly increased the percentage of OE33 and SK-GT-4 cells expressing PD-L2 (**Figure 5.4A** and **Figure 5.4B**). Single agent carboplatin (but not paclitaxel or CROSS CT) significantly increased PD-L1 (and PD-L2 expression on the surface of OE33 cells. However, CROSS CT significantly increased PD-L1 and PD-L2 on the surface of SK-GT-4 cells (**Figure 5.4A**). However, only single agent carboplatin significantly increased CD160 on the surface of OE33 cells, as did FLOT and CROSS CT regimens. There was no significant changes observed for CD160 expression on the SK-GT-4 cell line (**Figure 5.4A**). Single agent cisplatin and 5-FU but not epirubicin significantly

increased PD-L1 expression on OE33 cells (untreated 1.44 ± 0.6% vs. cisplatin 12.65 ± 4.6% (p=0.04) and 5-FU 26.35 ± 6.4% (p=0.01)), (**Figure 5.4A**). Similar results were observed for PD-L2 on OE33 cells (**Figure 5.4A.**. The combination MAGIC regimen had no effect on IC ligand expression on OE33 cells, however PD-L1 was significantly increased post-MAGIC treatment on the surface of SK-GT-4 cells (untreated 1.62 ± 0.3% vs. MAGIC 21.13 ± 3.3%, (p=0.03)), (**Figure 5.4B**).

Overall, 5-FU and the combination FLOT regimen had the greatest effect at upregulating inhibitory IC ligands, in particular PD-L1, on the surface of OGJ cells *in vitro*.

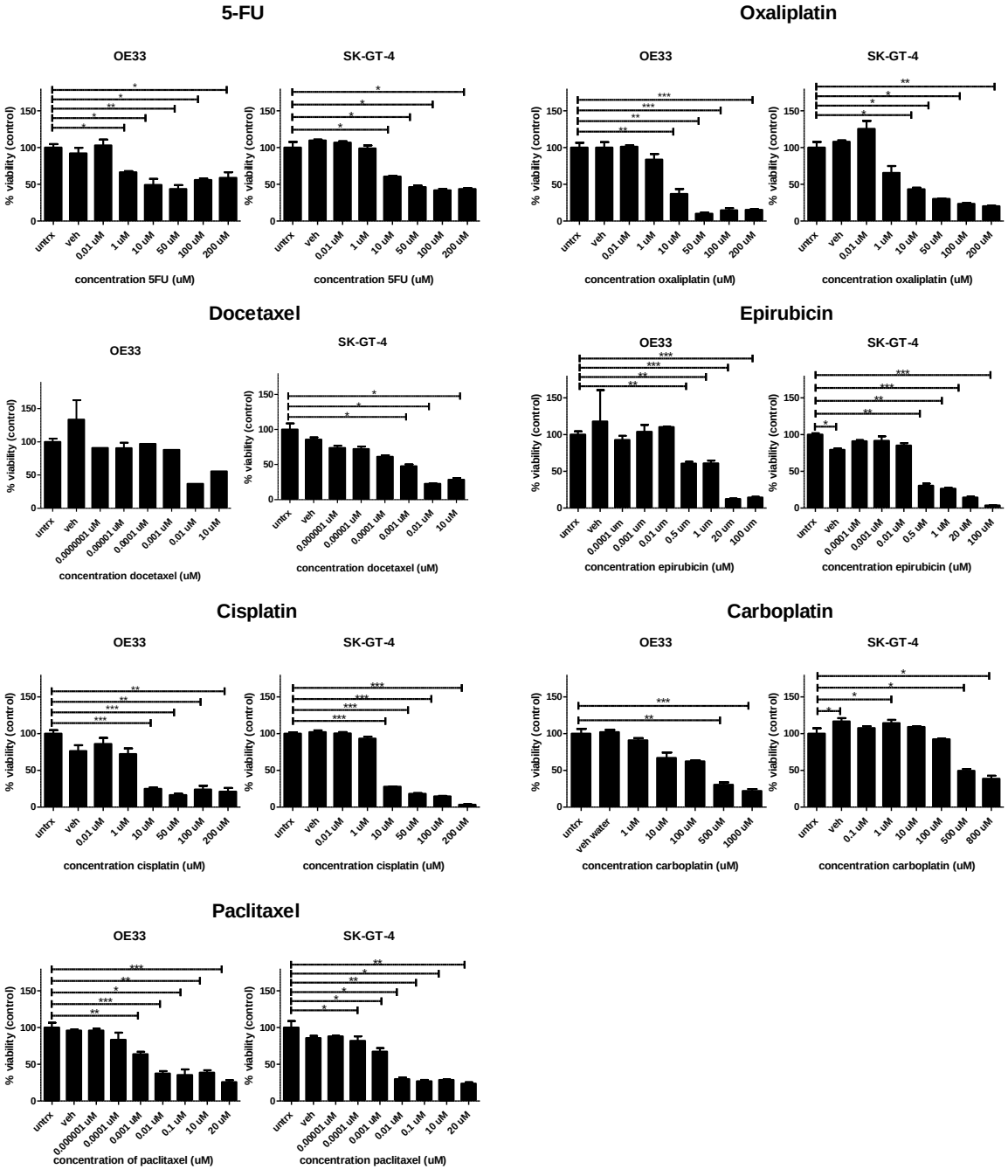

Figure 5.2: Clinically-relevant single agent chemotherapies display increasing cytotoxicity in a dose-dependent manner against OGJ cells *in vitro* following 48h. OE33 cells and SK-GT-4 cells were treated with a range of increasing concentrations of single agent 5-FU, oxaliplatin, docetaxel, epirubicin, cisplatin, carboplatin and paclitaxel for 48h. Cell viability was determined by CCK-8 assay (n=3). Paired parametric t test, *p<0.05, **p<0.001, ***p<0.0001.

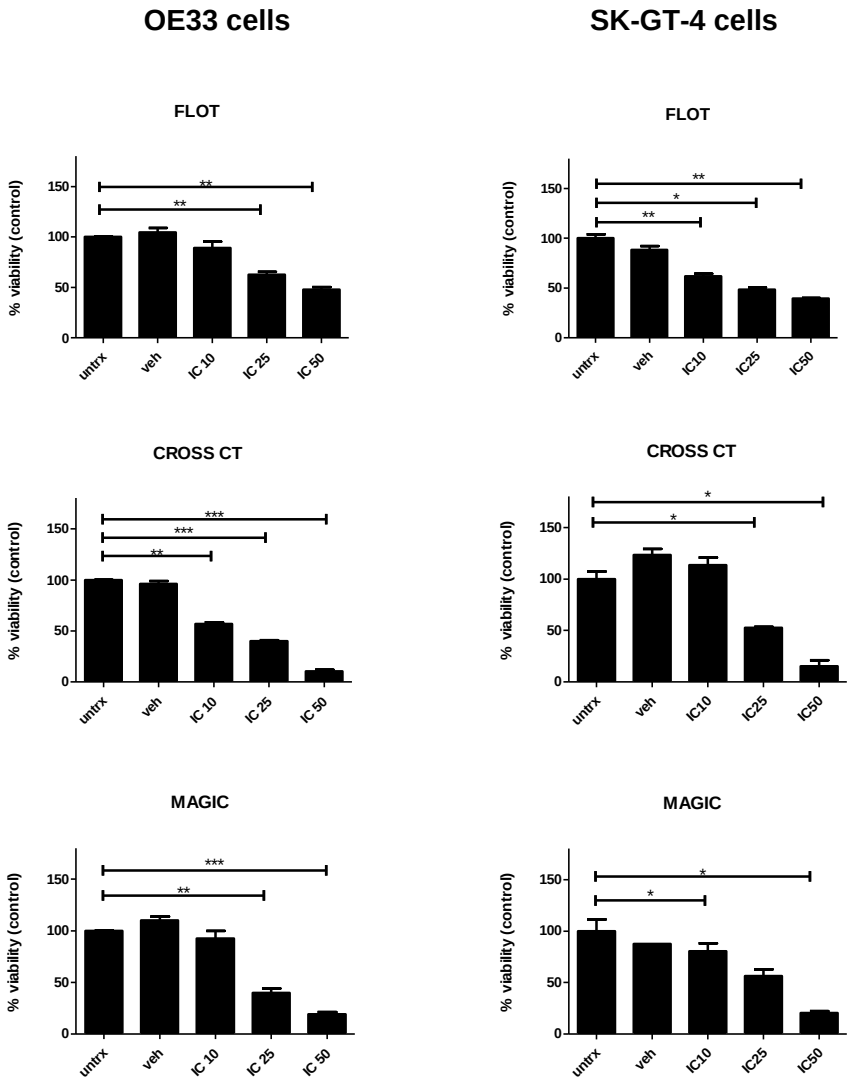

Figure 5.3: Clinically-relevant combination chemotherapy regimens FLOT, CROSS CT and MAGIC display increasing cytotoxicity in a dose-dependent manner against OGJ cells *in vitro* following 48h. OE33 cells and SK-GT-4 cells were treated with clinically-relevant chemotherapy combination regimens: FLOT (5-fluorouracil, oxaliplatin and docetaxel), CROSS CT (carboplatin and paclitaxel) and MAGIC (epirubicin, cisplatin and 5-fluorouracil) chemotherapy regimens for 48h. Cell viability was determined by CCK-8 assay (n=3). Paired parametric t test, *p<0.05, **p<0.001, ***p<0.0001.

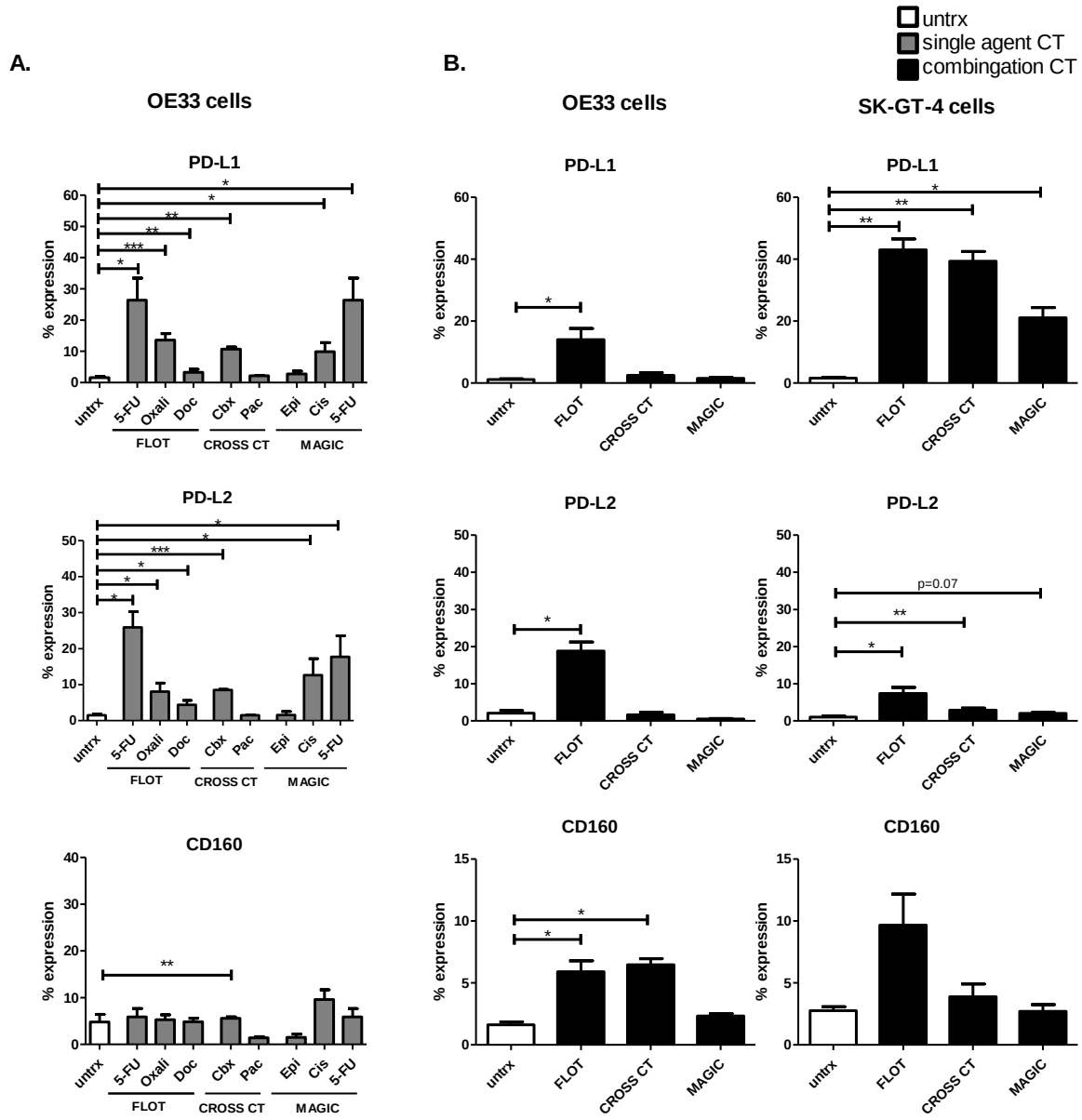

Figure 5.4: Chemotherapy regimens significantly alter the surface expression of a range of inhibitory IC ligands on the surface of viable OGJ cells. OE33 cells and SK-GT-4 cells were treated with clinically-relevant single agent chemotherapies (A) and combination chemotherapy regimens FLOT, CROSS CT and MAGIC (B) for 48h *in vitro* and the percentage of viable OE33 and SK-GT-4 cells expressing inhibitory IC ligands was determined by flow cytometry. Single agent chemotherapies included 5-FU, oxaliplatin (oxali) and docetaxel (doc) (comprise the FLOT regimen), carboplatin (cbx) and paclitaxel (pac) (comprise the CROSS CT regimen) and epirubicin (epi), cisplatin (cis) and 5-FU (comprise the MAGIC regimen). IC ligands assessed include PD-L1, PD-L2 and CD160 (n=3). Paired parametric t-test, *p<0.05, **p<0.001 and ***p<0.0001.

5.2.3 Chemotherapy promotes a more immune-resistant phenotype through upregulation of inhibitory IC receptors on OGJ cells *in vitro*

As we demonstrated that single agent chemotherapy and combination chemotherapy regimens significantly altered the expression profile of inhibitory IC ligands on the surface of OGJ cells, we also assessed the effect of these chemotherapies on the expression profile of a panel of inhibitory IC receptors on OGJ cells (**Figure 5.5**). Treatment with single agent chemotherapies or combination chemotherapy regimens did not significantly affect the percentage of OE33 cells expressing PD-1 or TIGIT (**Figure 5.5A**). However, FLOT and CROSS CT regimens significantly increased PD-1 expression on SK-GT-4 cells (untreated: 7.88 ± 2.7% vs. FLOT: 10.85 ± 3.2%, (p=0.002) and CROSS CT: 10.30 ± 3.2%, (p=0.01)), and MAGIC significantly increased the expression of TIGIT on the surface of SK-GT-4 cells (untreated: 6.77 ± 2.1% vs. MAGIC: 12.11 ± 1.9%, (p=0.02)), (**Figure 5.5A**). Single agent 5-FU (but not oxaliplatin or docetaxel) and the combined FLOT regimen significantly increased the percentage of OE33 cells expressing TIM-3 (untreated: 2.6 ± 0.6% vs. 5-FU: 11.81 ± 2.9%, (p=0.04)), and untreated: 0.80 ± 0.2% vs. FLOT: 8.10 ± 0.9% (p=0.0003)) (**Figure 5.5A** and **Figure 5.5B**). Similarly, FLOT significantly increased the percentage of SK-GT-4 cells expressing TIM-3 (**Figure 5.5A** and **Figure 5.5B**). Single agent carboplatin (but not paclitaxel or CROSS CT) significantly increased the percentage of OE33 cells expressing TIM-3 (**Figure 5.5A** and **Figure 5.5B**). Similarly, CROSS CT significantly increased the percentage of SK-GT-4 cells expressing TIM-3 (**Figure 5.5A** and **Figure 5.5B**). The MAGIC regimen did not significantly affect the percentage of OE33 or SK-GT-4 cells expressing TIM-3, however, single agent cisplatin and 5-FU (but not epirubicin) significantly increased the percentage of OE33 cells expressing TIM-3 (**Figure 5.5A** and **Figure 5.5B)**. The percentage of OE33 cells expressing LAG-3 was significantly increased following single agent 5-FU and docetaxel treatment (but not oxaliplatin) as well as combination FLOT treatment (**Figure 5.5A** and **Figure 5.5B**). Furthermore, carboplatin (but not paclitaxel) significantly increased Lag-3 expression in OE33 cells, as did the CROSS CT regimen. Additionally, FLOT and CROSS significantly increased LAG-3 expression in the SK-GT-4 cells (**Figure 5.5A** and **Figure 5.5B**). MAGIC had no effect on the percentage of OE33 and SK-GT-4 cells expressing LAG-3, however, single agent cisplatin and 5-FU (but not epirubicin) significantly increased LAG-3 expression in OE33 cells (**Figure 5.5A** and **Figure 5.5B**). 5-FU and docetaxel (but not oxaliplatin) significantly increased the percentage of OE33 cells expressing A2aR, as did the combined FLOT regimen. Furthermore, single agent carboplatin (but not paclitaxel) significantly increased the

percentage of OE33 cells expressing A2aR, as the CROSS CT regimen (**Figure 5.5A** and **Figure 5.5B**). While epirubicin significantly decreased the percentage of OE33 cells expressing A2aR and 5-FU significantly increased the expression of A2aR on OE33 cells, (single agent cisplatin or the combination MAGIC regimen had no significant effect on A2aR expression). Only the FLOT regimen significantly increased the percentage of SK-GT-4 cells expressing A2aR (**Figure 5.5A** and **Figure 5.5B**).

Similarly, in addition to single agent 5-FU and combination FLOT chemotherapy regimen having the greatest effect in upregulating IC ligand expression on OGJ cells, 5-FU and FLOT also had the greatest effect in upregulating inhibitory IC receptors in particular LAG-3, TIM-3 and A2aR on the surface of OGJ cells *in vitro*.

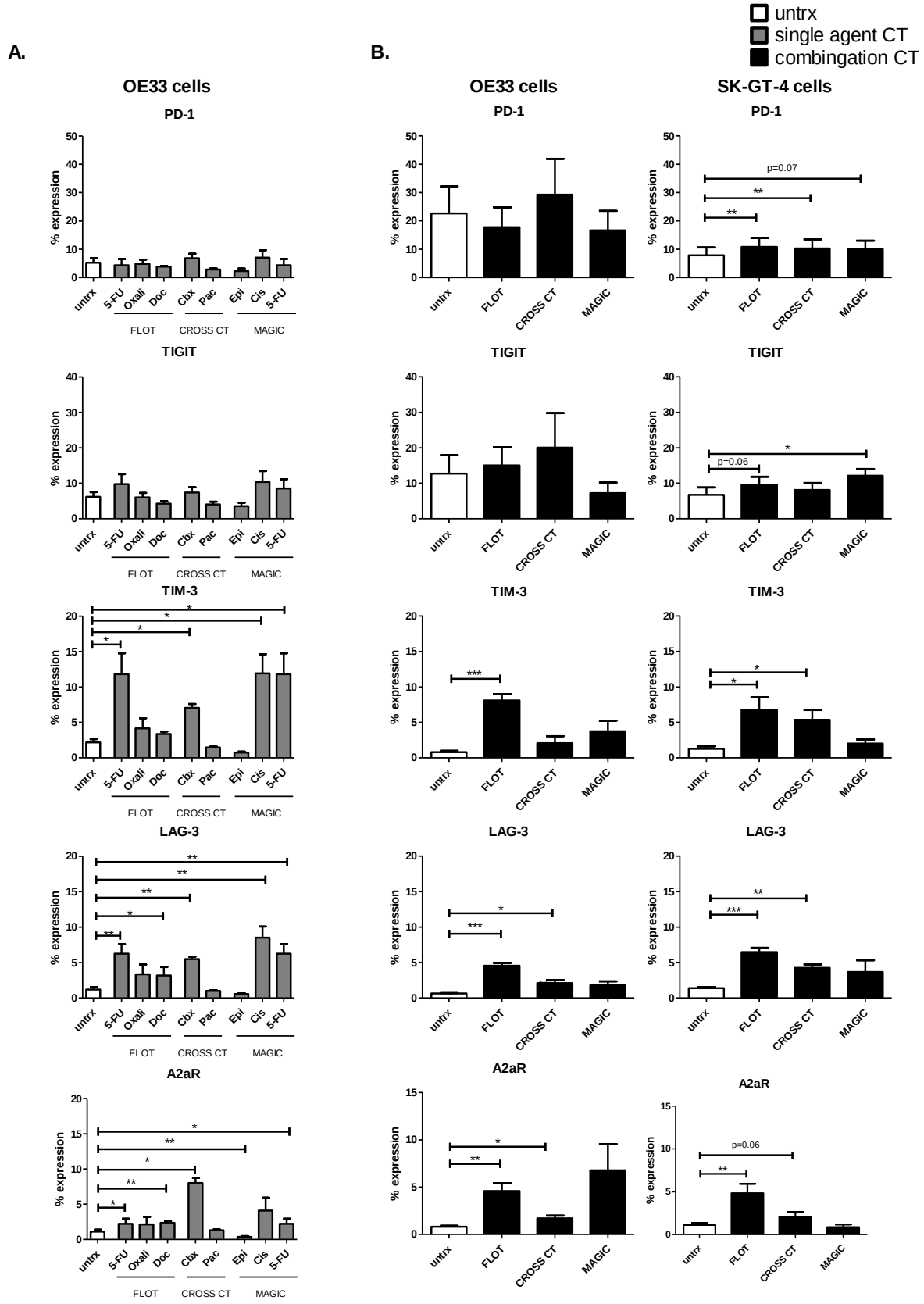

Figure 5.5: Chemotherapy regimens significantly increase a range of inhibitory IC receptors on the surface of viable OGJ cells. OE33 cells and SK-GT-4 cells were treated with clinically-relevant

single agent chemotherapies (A) and combination chemotherapy regimens FLOT, CROSS CT and MAGIC (B) for 48h *in vitro* and the percentage of viable OE33 and SK-GT-4 cells expressing inhibitory IC receptors was determined by flow cytometry including PD-1, TIGIT, TIM-3, LAG-3 and A2aR (n=4). Single agent chemotherapies included 5-FU, oxaliplatin (oxali) and docetaxel (doc) (comprise the FLOT regimen), carboplatin (cbx) and paclitaxel (pac) (comprise the CROSS CT regimen) and epirubicin (epi), cisplatin (cis) and 5-FU (comprise the MAGIC regimen). Paired t-test, *p<0.05, **p<0.001 and ***p<0.0001. Gating strategy and representative dot plots for assessing IC expression is shown in Appendix **Figure A5.1**.

5.2.4 Chemotherapy-induced upregulation of ICs on the surface of OGJ cells is maintained up to 3 weeks post-treatment

We have previously demonstrated that first-line chemotherapy combinations FLOT and CROSS upregulated ICs on the surface of OGJ cells following 48h treatment *in vitro*[229]. Therefore, we sought to investigate how long this chemotherapy-induced upregulation of ICs on the surface of OGJ cells is maintained by longitudinally profiling IC expression on the surface of OE33 cells following 48h treatment with vehicle control or FLOT chemotherapy regimen (**Figure 5.6A**).

48h treatment with FLOT significantly increased PD-L1 expression on the surface of OE33 cells compared with the vehicle control at 48h (50.85 ± 1.2 vs. 2.65 ± 0.3%, p<0.0001, **Figure 5.6B**). Interestingly, FLOT-induced PD-L1 upregulation on the surface of OE33 cells remained upregulated at 4 days (45.35 ± 1.5 vs. 1.63 ± 0.5%, p<0.0001) and 21 days (8.88 ± 0.3 vs. 0.97 ± 0.1%, p<0.0001, **Figure 5.6B**) post-treatment compared with the vehicle control (**Figure 5.6B**). Following subculture of recovered FLOT-treated OE33 cells PD-L1 was significantly upregulated compared with the vehicle control (3.15 ± 0.2 vs. 1.15 ± 0.1, p=0.007, **Figure 5.6B**).

Similarly, 48h treatment with FLOT significantly increased PD-L2 expression on the surface of OE33 cells compared with the vehicle control at 48h (38.45 ± 0.7 vs. 2.28 ± 0.2%, p<0.0001, **Figure 5.6B**). FLOT-induced PD-L2 upregulation on the surface of OE33 cells remained upregulated at 4 days (36.33 ± 6.8 vs. 2.5 ± 0.9, p=0.01) and 21 days (3.7 ± 0.1 vs. 2.58 ± 0.2, p=0.001, **Figure 5.6B**) post-treatment compared with the vehicle control (**Figure 5.6B**). In contrast to PD-L1, following subculture of recovered FLOT-treated OE33 cells PD-L2 expression had returned to baseline with no significant difference when compared with the vehicle control (**Figure 5.6B**).

Although 48h treatment with FLOT did not significantly alter CD160 expression on the surface of OE33 cells compared with the vehicle control at 48h, CD160 was significantly upregulated 4 days post-FLOT treatment compared with the vehicle control (73.53 ± 5.6 vs. 3.75 ± 0.7, p=0.0008, **Figure 5.6B**). However, CD160 expression had returned to baseline 21 days post-FLOT treatment and following subculture of recovered FLOT-treated OE33 cells with no significant difference when compared with the vehicle control (**Figure 5.6B**).

Following 48h treatment with FLOT, PD-1 expression increased on the surface of OE33 cells on day 2 (46.18 ± 4.3 vs. 22.60 ± 4.4, p=0.06) and on day 4 compared with the vehicle control (28.95 ± 7.5 vs. 12.02 ± 5.5%, p=0.06, **Figure 5.6C**). Furthermore, following subculture of recovered FLOT-treated OE33 cells there was a reduction in PD-1 expression compared with the vehicle control (10.92 ± 0.8 vs. 17.63 ± 0.8, p=0.06, **Figure 5.6C**).

TIGIT expression increased on the surface of OE33 cells compared with the vehicle control at 48h (68.58 ± 3.0 vs. 57.0 ± 2.0%, p=0.06, **Figure 5.6C**) and remained upregulated at 4 days (67.28 ± 6.8 vs. 43.65 ± 3.1, p=0.01). However, 21 days post-FLOT treatment TIGIT expression returned to baseline and was comparable with the vehicle control (**Figure 5.6C**). Interestingly, following subculture of recovered FLOT-treated OE33 cells, TIGIT was significantly decreased compared with the vehicle control (9.17 ± 0.8 vs. 13.80 ± 0.9%, p=0.004, **Figure 5.6C**).

Similar to TIGIT, following 48h treatment with FLOT, TIM-3 expression increased on the surface of OE33 cells compared with the vehicle control at 48h (6.65 ± 0.9 vs. 1.8 ± 0.1, p=0.09, **Figure 5.6C**) and remained upregulated at 4 days (12.53 ± 1.3 vs. 1.51 ± 0.1%, p=0.003) (**Figure 5.6C**). Similarly, to TIGIT, following subculture of recovered FLOT-treated OE33 cells was a significant reduction in TIM-3 expression compared with the vehicle control (0.41 ± 0.1 vs. 1.95 ± 0.4%, p=0.05, **Figure 5.6C**).

Following 48h treatment with FLOT, LAG-3 was significantly increased on the surface of OE33 cells compared with the vehicle control at 48h (4.19 ± 0.1 vs. 1.90 ± 0.4%, p=0.03, **Figure 5.6C**) and remained upregulated at 21 days (19.50 ± 0.1 vs. 4.43 ± 0.3%, p=0.009, **Figure 5.6C**). Similar, to findings observed for TIGIT and TIM-3, following subculture of recovered FLOT-treated OE33 cells, LAG-3 expression decreased compared with the vehicle control (0.76 ± 0.2 vs. 1.71 ± 0.4%, p=0.06, **Figure 5.6C**).

Although 48h treatment with FLOT did not significantly alter A2aR expression on the surface of OE33 cells compared with the vehicle control at 48h, A2aR was significantly upregulated 4 days post-FLOT treatment (5.41 ± 0.6 vs. 1.41 ± 0.2%, p=0.004) and 21 days (1.78 ± 0.1 vs.

1.12 ± 0.2%, p=0.02, **Figure 5.6C**). Similarly, following subculture of recovered FLOT-treated OE33 cells, A2aR expression was decreased compared with the vehicle control (0.90 ± 0.1 vs. 2.16 ± 0.4%, p=0.06, **Figure 5.6C**).

Overall, several ICs were significantly upregulated on the surface of OE33 cells longitudinally including PD-L1, PD-L2, CD160, TIGIT, TIM-3, LAG-3 and A2aR. Interestingly, PD-L1 remained increased compared with the vehicle control following subculture of FLOT-recovered OE33 cells at 24 days, whilst PD-L2 and CD160 returned to baseline expression levels. Interestingly, PD-1, TIGIT, TIM-3, LAG-3 and A2aR expression were decreased compared with the vehicle control following subculture of FLOT-recovered OE33 cells at 24 days.

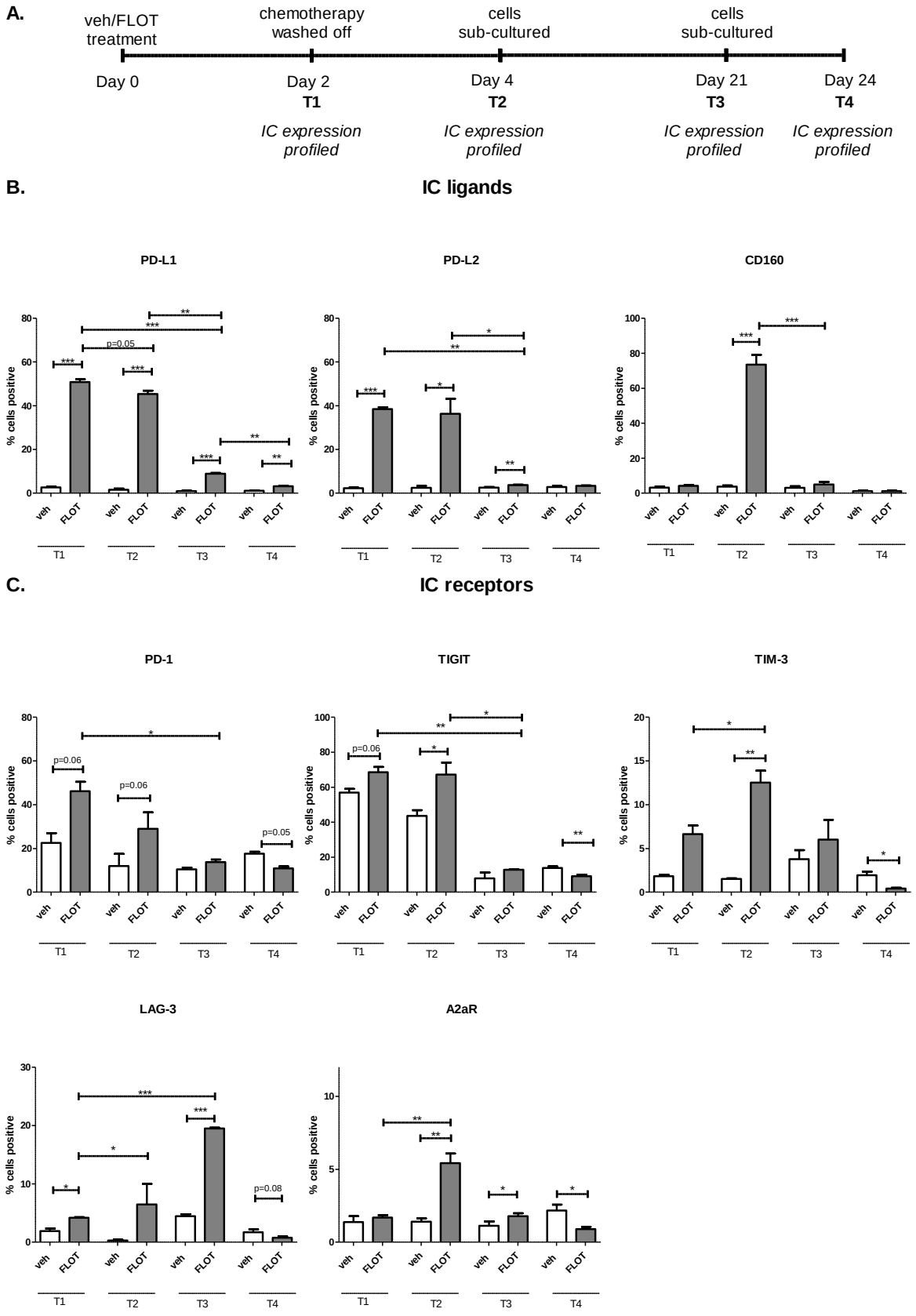

Figure 5.6: FLOT upregulates ICs on the surface of OGJ cells *in vitro*, an effect which is maintained 3 weeks post-treatment. OE33 cells were treated with vehicle control (veh) or FLOT for

48h (T1), washed twice and allowed to grow for an additional 48h (T2) after which the cells were sub-cultured in new flasks and left to recover for 3 weeks (T3). Following complete recovery, the cells were sub-cultured 1 in 2 and screened for IC expression 3 days later (T4). IC ligand and receptor expression was profiled on the surface of OE33 cells longitudinally by flow cytometry at T1, T2, T3 and T4 (n=3). A) represents a schematic of experimental setup. B) IC ligands expression profiles for PD-L1, PD-L2 and CD160. C) IC receptor profiles for PD-1, TIGIT, TIM-3, LAG-3 and A2aR. Paired parametric t-test, *p<0.05, **p<0.01 and ***p<0.001. Gating strategy and representative dot plots for assessing IC expression is shown in **Figure A5.1**.

5.2.5 Pro-survival MEK signalling upregulates ICs on the surface of OGJ cells following chemotherapy treatment

Chemotherapy-induced upregulation of ICs on the surface of OGJ cells suggests these tumour cells may be employing ICs as an adaptive survival mechanism to overcome genotoxic stress. However, the signalling pathways mediating FLOT-induced IC upregulation remain unknown. Therefore, we sought to investigate if the pro-survival signalling pathway MEK may be regulating the chemotherapy-induced upregulation of ICs.

Inhibition of MEK signalling significantly reduced the basal expression of PD-L1 on the surface of SK-GT-4 cells compared with the vehicle control (0.82 ± 0.3 vs. 2.13 ± 0.1%, p=0.02) (**Figure 5.7A**). Moreover, inhibition of MEK signalling significantly decreased FLOT-induced PD-L1 upregulation on the surface of OE33 cells (28.24 ± 6.8 vs. 31.63 ± 7.1%, p=0.03) and SKGT-4 cells (8.75 ± 1.6 vs. 31.38 ± 6.5%, p=0.008) compared with FLOT treatment alone (**Figure 5.7A**).

Inhibition of MEK signalling significantly increased the expression of PD-L2 on the surface of OE33 cells (3.51 ± 0.7 vs. 1.72 ± 0.1%, p=0.02) and SK-GT-4 cells (5.79 ± 0.9 vs. 2.93 ± 0.4%, p=0.001) compared with the vehicle control (**Figure 5.7A**). However, inhibition of MEK signalling did not alter the expression of FLOT-induced PD-L2 expression compared with FLOT treatment alone in either cell line.

Similarly, inhibition of MEK signalling significantly increased the expression of CD160 on the surface of OE33 cells (2.69 ± 0.1 vs. 1.4 ± 0.1%, p=0.002) and SK-GT-4 cells (1.32 ± 0.1 vs. 0.60 ± 0.1%, p=0.04) compared with the vehicle control (**Figure 5.7A**). Moreover, inhibition of MEK signalling in combination with FLOT treatment significantly increased the expression of CD160 on the surface of OE33 cells compared with FLOT treatment alone (3.90 ± 0.8 vs. 2.84 ± 0.6%, p=0.03) compared with the vehicle control (**Figure 5.7A**).

Inhibition of MEK signalling significantly increased the expression of PD-1 on the surface of OE33 cells (11.15 ± 2.5 vs. 6.97 ± 1.3%, p=0.01) compared with the vehicle control (**Figure 1B**). In contrast, inhibition of MEK signalling significantly decreased the expression of PD-1 on the surface of SK-GT-4 cells (15.39 ± 4.3 vs. 20.20 ± 2.8%, p=0.001) compared with the vehicle control (**Figure 5.7B**). Inhibition of MEK signalling did not significantly alter the expression of TIGIT on the surface of OE33 or SK-GT-4 cells basally or in combination with FLOT treatment (**Figure 5.7B**).

Moreover, inhibition of MEK signalling significantly reduced the expression of basal levels of TIM-3 on the surface of SK-GT-4 cells compared with the vehicle control (1.36 ± 0.3 vs. 2.26 ± 0.2%, p=0.05) (**Figure 5.7A**). Moreover, inhibition of MEK signalling significantly decreased FLOT-induced TIM-3 upregulation on the surface of OE33 cells (3.92 ± 0.2 vs. 24.53 ± 3.8%, p=0.03) and SKGT-4 cells (3.35 ± 0.3 vs. 9.09 ± 0.5%, p=0.001) compared with FLOT treatment alone (**Figure 5.7A**).

MEK inhibition significantly increased the expression of basal levels of LAG-3 on the surface of OE33 cells compared with the vehicle control (1.77 ± 0.1 vs. 0.96 ± 0.1%, p=0.02) (**Figure 5.7A**). In contrast, inhibition of MEK signalling significantly decreased FLOT-induced LAG-3 upregulation on the surface of SKGT-4 cells (5.80 ± 0.8 vs. 9.03 ± 0.8%, p=0.002) compared with FLOT treatment alone (**Figure 5.7A**).

Additionally, inhibition of MEK signalling significantly decreased the expression of basal levels of A2aR on the surface of SK-GT-4 cells compared with the vehicle control (2.08 ± 0.3 vs. 2.60 ± 0.3, p=0.04) (**Figure 5.7A**). Similarly, inhibition of MEK signalling significantly decreased FLOT-induced A2aR upregulation on the surface of SKGT-4 cells (4.47 ± 0.9 vs. 8.80 ± 1.6, p=0.002) compared with FLOT treatment alone (**Figure 5.7A**). In addition, there were a reduction in FLOT-induced A2aR upregulation on the surface of OE33 cells compared with FLOT treatment alone (8.74 ± 0.9 vs. 16.83 ± 2.7, p=0.06, **Figure 5.7A**).

Overall, MEK signalling regulated FLOT-induced upregulation of PD-L1, TIM-3, LAG-3 and A2aR on the surface of OGJ cells.

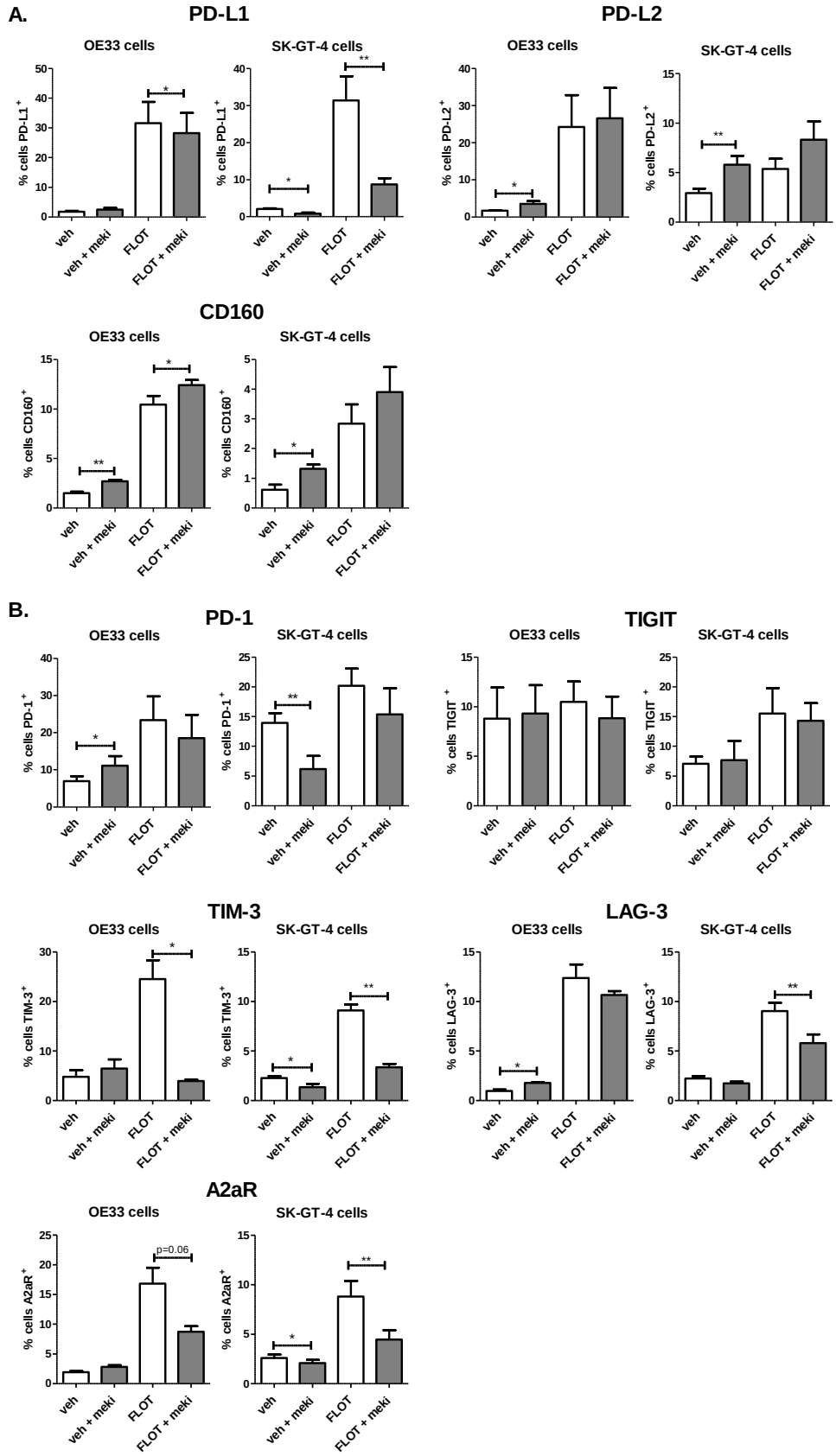

Figure 5.7: Inhibition of MEK signalling attenuates chemotherapy-induced upregulation of PD-L1, TIM-3, LAG-3 and A2aR on the surface of OGJ cells *in vitro*. OE33 cells and SK-GT-4 cells

were treated with and without FLOT chemotherapy regimen in the absence and presence of a MEK inhibitor (meki) for 48h and the expression of IC ligands (PD-L1, PD-L2 and CD160) and IC receptors (PD-1, TIGIT, TIM-3, LAG-3 and A2aR) on the surface of OGJ cells was determined by flow cytometry. *p<0.05 and **p<0.01, experiments repeated n=3 times, paired parametric t-test. Gating strategy and representative dot plots for assessing IC expression is shown in Appendix **Figure A5.1**.

5.2.6 The FLOT chemotherapy regimen enhances a stem-like phenotype and preferentailly upregulates PD-L1 and TIM-3 on the surface of stem-like OGJ cells *in vitro*

Our data suggests that chemotherapy regimens enhance a more immune resistant phenotype in OGJ cells, demonstrated by the upregulation of inhibitiory IC ligands and receptors on OGJ cells following FLOT and CROSS CT treatment. Therefore, we sought to investigate if chemotherapy regimens could enhance a more stem-like phentoype in OGJ cells, which are thought to be responsible for tumour recurrence and treatment resistance[334,335]. OE33 and SK-GT-4 cells were treated with FLOT, CROSS CT and MAGIC regimens for 48h and the level of ALDH activity was measured, which is an established marker of stemness in OGJ[336] (**Figure 5.8A**). Following FLOT treatment, ALDH activity in OE33 cells was significantly increased (untreated: 15.59 ± 3.4% vs. FLOT: 33.97 ± 4.6%, (p=0.01) (**Figure 5.8A**). However, following CROSS CT the level of ALDH activity was significantly decreased in OE33 cells (untreated: 15.59 ± 3.4% vs. 7.42 ± 1.8%, (p=0.02)) (**Figure 5.8A**). MAGIC did not significantly alter ALDH activity in OE33 cells (**Figure 5.8A**). Following FLOT treatment of SK-GT-4 cells, ALDH activity was significantly increased (untreated: 29.40 ± 9.9% vs. FLOT: 55.17 ± 4.9%, (p=0.02)) (**Figure 5.8A**). However, CROSS and MAGIC did not significantly alter ALDH activity in SK-GT-4 cells (**Figure 5.8A**).

Given that chemotherapy regimens upregulated inhibitory IC ligands and receptors on a subpopulation of OGJ cells and that FLOT chemotherapy regimen enhanced a more stem-like phenotype in OGJ cells, we examined if these OGJ cells exhibiting a stem-like phenotype had an altered expression of inhibitory IC ligands and receptors basally and following chemotherapy treatment. We found that inhibitory IC ligands and receptors are expressed on stem-like and non-stem-like OGJ cells basally and following chemotherapy treatment (**Figure 5.8B).** Basally, there was no significant difference in the percentage of OE33 or SK-GT-4 cells expressing PD-L1 and PD-L2 between the stem-like and non-stem-like compartment in OGJ cells (**Figure 5.8B**). Following FLOT chemotherapy treatment, PD-L1 was significantly increased on the surface of $ALDH^+$ stem-like SK-GT-4 cells (untreated $ALDH^+$: 1.73 ± 0.4%

vs. FLOT ALDH$^+$: 8.86 ± 0.7%, (p=0.01)), (**Figure 5.8B**). Basally, there was a significantly higher percentage of ALDH$^-$ non-stem-like OE33 cells expressing PD-1, TIGIT and TIM-3 compared to the ALDH$^+$ stem-like OE33 cells (PD-1: 45.07 ± 3.3% vs. 0.25 ± 0.1%, respectively (p=0.005), TIGIT: 28.00 ± 3.2% vs. 0.32 ± 0.1%, respectively (p=0.01) and TIM-3: 0.55 ± 0.1% vs. 0.13 ± 0.04%, respectively (p=0.05)) (**Figure 5.8C**). Similarly, there was a significantly higher percentage of ALDH$^-$ non-stem-like SK-GT-4 cells expressing TIGIT compared to the ALDH$^+$ stem-like SK-GT-4 cells (11.42 ± 1.3% vs. 0.34 ± 0.1%, respectively (p=0.01)) (**Figure 5.8C**). Following FLOT, CROSS CT and MAGIC chemotherapy treatment the percentage of OE33 cells expressing PD-1 and TIGIT was significantly higher in the ALDH$^-$ non-stem-like compartment compared to the ALDH$^+$ stem-like compartment basally (**Figure 5.8C**). Similar findings were observed for TIGIT in the SK-GT-4 cell line (**Figure 5.8C**). However, the percentage of cells expressing PD-1 was significantly increased in the ALDH$^-$ non-stem-like compartment of SK-GT-4 cells following FLOT and CROSS CT treatment (untreated ALDH$^-$: 12.91 ± 4.5%, FLOT ALDH$^-$: 16.25 ± 5.2% (p=0.03) and CROSS CT ALDH$^-$: 16.19 ± 4.9% (p=0.01)). TIM-3 was significantly increased on ALDH$^+$ stem-like SK-GT-4 cells following FLOT (untreated ALDH$^+$: 1.15 ± 0.3% and FLOT ALDH$^+$: 6.47 ± 1.2%, (p=0.03)) (**Figure 5.8C**).

Overall, the FLOT regimen enhanced a stem-like phenotype in both OE33 and SK-GT-4 cells demonstrated by an increase in ALDH activity. Inhibitory ICs PD-L1 and TIM-3 were enriched in the stem-like compartment of OGJ cells following chemotherapy treatment. However, PD-1 and TIGIT were preferentialy expressed on non-stem-like OGJ cells basally and following chemotherapy treatment.

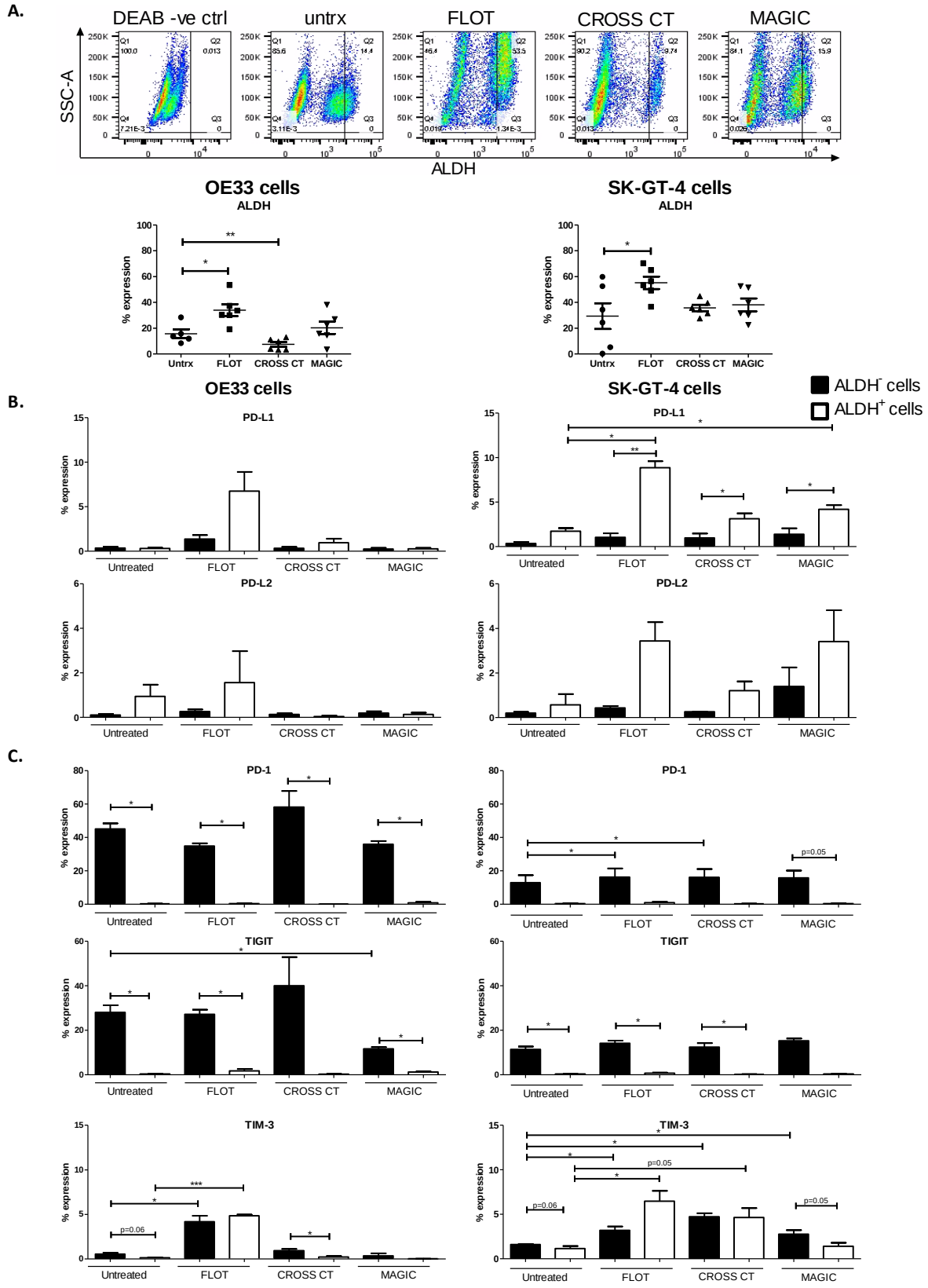

Figure 5.8: The FLOT chemotherapy regimen significantly increases ALDH activity and preferentially upregulates PD-L1 and TIM-3 on the surface of stem-like OGJ cells *in vitro*. OE33 cells and SK-GT-4 cells were treated with FLOT, CROSS CT and MAGIC chemotherapy regimens for

48h *in vitro.* (A) The level of ALDH activity was determined in viable OGJ cells by flow cytometry (n=6). The percentage of viable non-stem-like and stem-like OE33 and SK-GT-4 cells expressing inhibitory IC ligands (B) and inhibitory IC receptors (C) was determined by flow cytometry. Inhibitory IC ligand expression (PD-L1, PD-L2 and CEACAM-1) and inhibitory IC receptor expression (PD-1, TIGIT and TIM-3) was assessed on $ALDH^-$ non-stem-like and $ALDH^+$ stem-like OGJ cells (n=3). Representative dot plots showing level of ALDH activity in ALDH negative DEAB control (DEAB -ve ctrl), basally (untrx) and following FLOT, CROSS CT and MAGIC chemotherapy treatment in OE33 cells (A). Paired parametric t-test, *p<0.05, **p<0.001 and ***p<0.0001.

5.2.7 The FLOT chemotherapy regimen enhances a senescent-like phenotype and upregulates A2aR on the surface of senescent-like OGJ cells *in vitro*

Senescent cancer cells play an important role in conferring treatment resistance and in orchestrating a tumour-promoting milieu of immuosuppressive cells within the tumour microenvirnoment via the secretion of a range of pro-inflammatory markers known as the senescence-associated secretory phentoype (SASP). Characterisation of senescent cells can be performed by assessing multiple markers such as an enlarged morphology, activation of p53-p21 and/or p16-Rb tumour suppressor pathways, induction of $p16^{INK4a}$, the presence of persistent DNA damage response, an increase in β-galactosidae ($\beta\text{-gal}^+$) expression, and the appearance of senescent-associated distension of satellites and telomere-associated DNA damage foci[337,338]. We aimed to determine the effect of OGJ chemotherapy regimens on the induction of a senescent-like phenotype in OGJs using the well-established marker $\beta\text{-gal}^+$ as a marker of senescent-like cells (**Figure 5.9A**).

Following FLOT, CROSS CT and MAGIC treatment the percentage of OE33 cells expressing the senescent marker $\beta\text{-gal}^+$ was significantly increased (untreated: 2.55 ± 0.3% vs. FLOT: 28.59 ± 5.5%, (p=0.005), CROSS CT: 9.28 ± 1.3% (p=0.004) and MAGIC: 14.33 ± 2.3%, (p=0.002)), (**Figure 5.9A**). Following FLOT and MAGIC treatment the percentage of SK-GT-4 cells expressing $\beta\text{-gal}^+$ was also significantly increased (untreated: 2.80 ± 0.4% vs. FLOT: 12.55 ± 2.9%, (p=0.03) and MAGIC: 9.34 ± 1.4% (p=0.01)). However, CROSS CT treatment did not sigificantly alter the percentage of SK-GT-4 cells expressing $\beta\text{-gal}^+$ (**Figure 5.9A**).

Given that FLOT, CROSS CT and MAGIC regimens induced the expression of the senescene marker β-galactosidase in OGJ cells *in vitro* we sought to investigate if ICs are expressed on these OGJ cells and whether chemotherapy upregulates them further (**Figure 5.9B**). As ICs play an important role in immune evasion, the expression of ICs on senescent OGJ cells may represent a drug targetable mechanism of immune evasion. Following FLOT treatment the

percentage of senescent OE33 cells expressing TIM-3 was significantly increased (untreated: 0.54 ± 0.1% vs. FLOT: 14.40 ± 1.9% (p=0.02)) (**Figure 5.9C**). Similarly, following FLOT treatment the percentage of OE33 cells expressing A2aR was significantly increased (untreated: 0.85 ± 0.1% vs. FLOT: 22.10 ± 3.0% (p=0.02)) (**Figure 5.9C**). There was no significant differences observed in the SK-GT-4 cell line (**Figure 5.9C**). We also found that TIGIT was expressed at significantly higher levels on the surface of β-gal^{+} SK-GT-4 compared with β-gal^{-} SK-GT-4 cells, basally and following FLOT, CROSS CT and MAGIC treatment (but not OE33 cells). Overall, FLOT had the greatest effect at inducing the senescence marker β-galactosidase in OGJ cells and enriched β-gal^{+} OE33 cells for TIM-3 and A2aR expression.

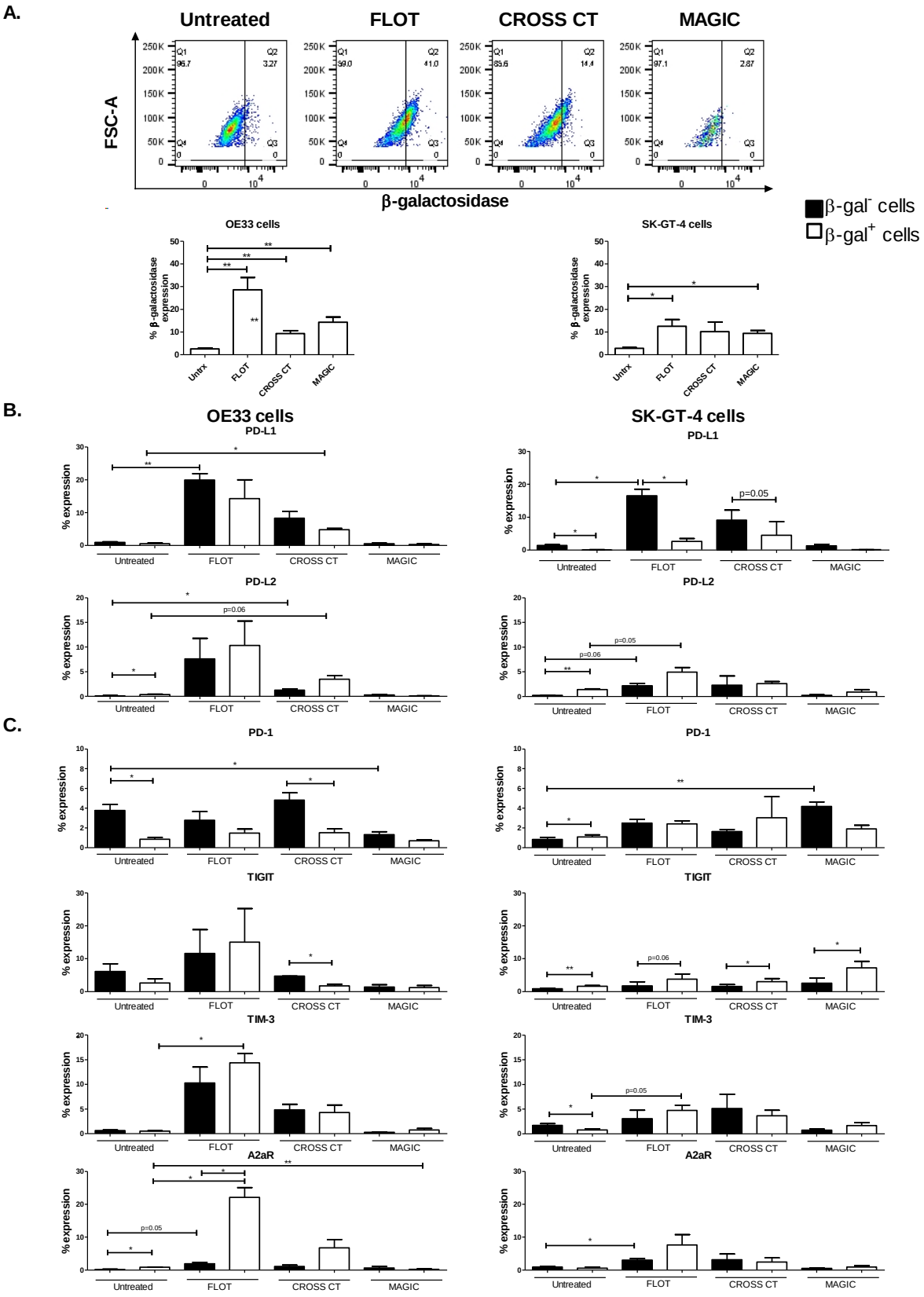

Figure 5.9: The FLOT chemotherapy regimen enhances a senescent-like phenotype and preferentially upregulates A2aR on the surface of senescent-like OGJ cells *in vitro*. OE33 and SK-GT-4 cells were treated with FLOT, CROSS CT and MAGIC chemotherapy regimens for 48h *in vitro.*

The percentage of viable senescent-like (β-galactosidase positive) OGJ cells was determined by flow cytometry (n=3) (A). The percentage of viable senescent (β-gal$^+$) and non-senescent (β-gal$^-$) OGJ cells expressing inhibitory IC ligands (PD-L1 and PD-L2) (B) and inhibitory IC receptors (PD-1, TIGIT, TIM-3 and A2aR) (C) was determined by flow cytometry (n=3). Representative dot plots showing the percentage of viable cells positive for β-galactosidase expression basally (untrx) and following FLOT, CROSS CT and MAGIC chemotherapy regimens in OE33 cells (A). Paired parametric t test, *p<0.05 and **p<0.001.

5.2.8 A subpopulation of OGJ cells expressing inhibitory IC ligands and inhibitory IC receptors were identified in OGJ tumour tissue biopsies *ex vivo*

Following our *in vitro* studies demonstrating that OGJ cells express a range of inhibitory IC ligands and receptors, which are upregulated following chemotherapy treatment on stem-like and senescent-like OGJ cells, we screened treatment-naïve (n=10), post-FLOT chemotherapy (n=5) and post-CROSS chemoradiotherapy (n=5) OGJ tumour biopsies for the expression of a range of inhibitory IC ligands and receptors *ex vivo*. OGJ cells were characterised as CD45$^-$ CD31$^-$ as previously reported[339]. CD45 cells comprise the immune cell compartment and CD31 cells are expressed on endothelial cells and immune cells. Therefore gating on CD31 negative and CD45 negative cells allowed us to examine the IC expression profiled on cancer cells as previously described in[339].

A subpopulation of OGJ cells expressing inhibitory IC ligands and receptors were identified in the treatment-naïve, post-FLOT and post-CROSS setting *ex vivo* (**Figure 5.10**). The percentage of OGJ cells expressing PD-L1 in treatment-naïve, post-FLOT and post-CROSS OGJ tumour biopsy tissue was: 0.49 ± 0.22%, 0.4 ± 0.2% and 0.37 ± 0.1%, respectively. The percentage of OGJ cells expressing PD-L2 in treatment-naïve, post-FLOT and post-CROSS OGJ tumour biopsy tissue was: 0.28 ± 0.1%, 0.08 ± 0.03% and 0.20 ± 0.1%, respectively. CD160 was identified on 0.86 ± 0.2%, 0.59 ± 0.2% and 0.82 ± 0.5% of OGJ cells in treatment-naïve, post-FLOT and post-CROSS OGJ tumour biopsy tissue, respectively (**Figure 5.10**). PD-1 was identified on 5.13 ± 1.0%, 6.30 ± 2.3% and 3.72 ± 1.5% of OGJ cells in treatment-naïve, post-FLOT and post-CROSS tumour biopsy tissue. The percentage of treatment-naïve, post-FLOT and post-CROSS OGJ cells expressing TIGIT was 3.40 ± 0.6%, 1.60 ± 0.4% and 3.15 ± 1.6%, respectively (**Figure 5.10**). TIM-3 was identified on 3.83 ± 1.2%, 0.88 ± 0.2% and 1.35 ± 0.5% of OGJ cells in treatment-naïve, post-FLOT and post-CROSS tumour biopsy tissue, respectively. The percentage of OGJ cells expressing LAG-3 in treatment-naïve, post-FLOT

and post-CROSS tumour biopsy tissue was: 2.42 ± 0.4, 0.89 ± 0.3% and 3.29 ± 1.2%, respectively (**Figure 5.10.**). A2aR was identified on 3.6 ± 0.8%, 3.62 ± 0.8% and 4.0 ± 1.6% in treatment-naïve, post-FLOT and post-CROSS tumour biopsy tissue, respectively (**Figure 5.10)**. Post-FLOT chemotherapy treatment the percentage of OGJ cells expressing TIM-3, LAG-3 and A2aR were significantly lower (p=0.0235, p=0.0077 and p=0.0414, respectively). There was no significant difference between IC expression in the treatment-naïve cohort compared to the post-treatment cohort for the other IC ligands and receptors.

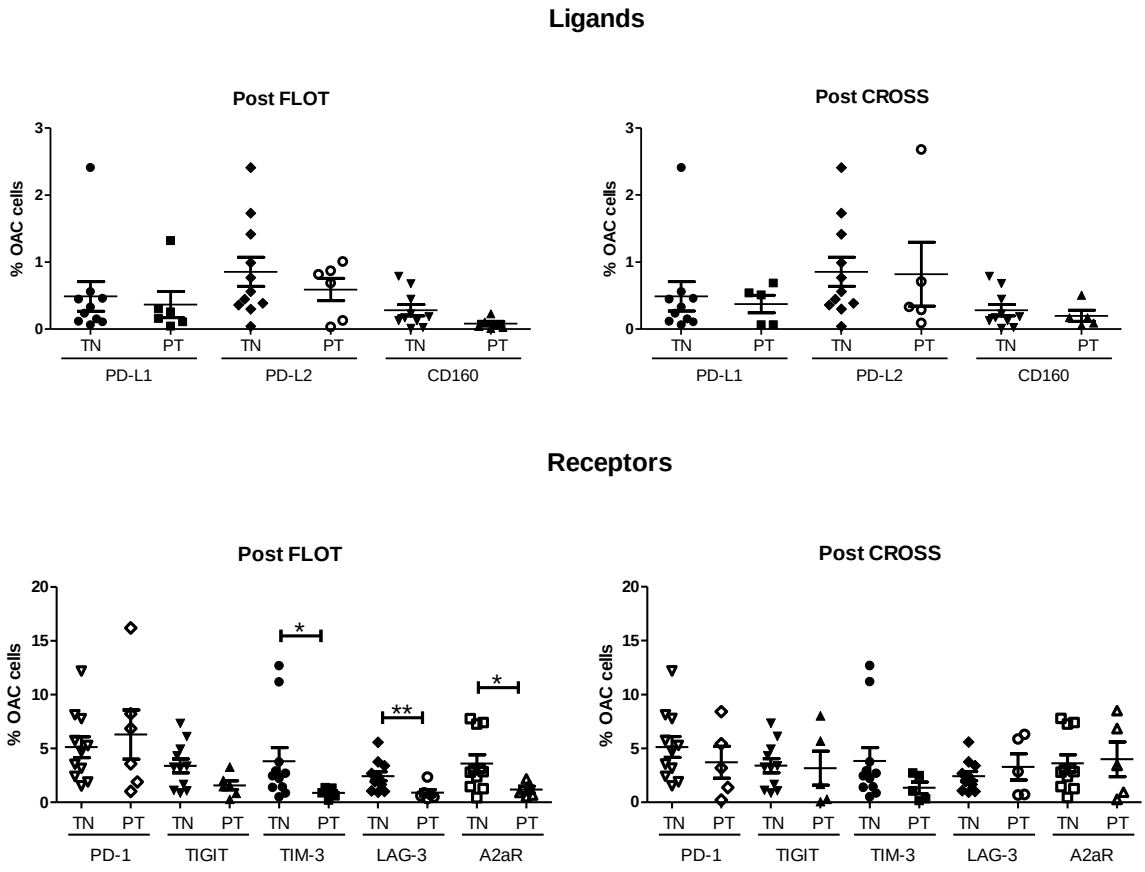

Figure 5.10: TIM-3, LAG-3 and A2aR IC receptors are expressed at significantly lower levels on viable OGJ cells in post-FLOT but not post-CROSS treatment tumour tissue biopsies. OGJ cells characterised as $CD45^{-}CD31^{-}$ were screened for the surface expression of a panel of inhibitory IC ligands (PD-L1, PD-L2 and CD160) and receptors (PD-1, TIGIT, TIM-3, LAG-3 and A2aR) in OGJ tumour tissue biopsies at the treatment-naïve (TN) setting at time of diagnosis (n=10) and post-neoadjuvant treatment (PT) at surgical resection (n=10) *ex vivo* using flow cytometry. Post-treatment:

FLOT (n=5) and CROSS (n=5). Mann Whitney test *p<0.05 and **p<0.001. Gating strategy and representative dot plots for assessing IC expression is shown in Appendix **Figure A5.1.**

Following identification of a subpopulation of OGJ cells expressing inhibitory IC ligands and receptors *in vitro* and *ex vivo*, we investigated the correlative relationship between IC expression on OGJ cells and clinical patient characteristics and tumour features (**Table 5.1**). We observed a strong correlation between IC expression on OGJ cells with the expression of other ICs in the treatment-naïve and post-treatment setting of OGJ patients. There was a strong and significant positive correlation (r=0.81) between the percentage of OGJ cells expressing LAG-3 and treatment response (p=0.03) in the treatment-naïve setting (**Table 5.1.**). In the post-treatment setting there was a strong negative correlation between the percentage of OGJ cells expressing PD-L2 (r=-0.83), Lag-3 (r=-0.70) and A2aR (r=-0.72) with treatment response, clinical T stage and serosal invasion, respectively (p=0.002, 0.03 and 0.02, respectively) (**Table 5.1.**).

Table 5.1. Correlation of IC expression with IC expression on OGJ cells and clinical characteristics and features in the treatment-naïve and post-treatment setting.

Treatment-naïve cohort			
IC protein	**correlated variable**	**Spearman r**	**P value (two-tailed)**
PD-L1	PD-L2	0.67	0.03000
CD160	PD-L2	0.69	0.03000
CD160	LAG-3	0.71	0.02000
CD160	PD-1	0.68	0.03000
PD-L2	CD160	0.69	0.03000
PD-L2	LAG-3	0.70	0.03000
TIGIT	PD-1	0.65	0.04000
LAG-3	CD160	0.71	0.02000
LAG-3	PD-L2	0.70	0.03000
LAG-3	PD-1	0.66	0.04000
A2aR	PD-1	0.66	0.04000
PD-1	CD160	0.68	0.03000
PD-1	TIGIT	0.65	0.04000
PD-1	LAG-3	0.66	0.04000
PD-1	A2aR	0.66	0.04000

CD160	weight	-0.75	0.01000
PD-L2	weight	-0.71	0.02000
PD-1	weight	-0.73	0.04000
LAG-3	treatment response	0.81	0.03000
PD-1	weight	-0.73	0.02000
Post-treatment cohort			
IC protein	**correlated variable**	**Spearman r**	**P value (two-tailed)**
PD-L1	TIM-3	0.63	0.03885
PD-L1	LAG-3	0.69	0.01857
TIM-3	PD-L1	0.63	0.03885
TIM-3	A2aR	0.87	0.00045
LAG-3	PD-L1	0.69	0.01857
A2aR	TIM-3	0.87	0.00045
PD-L2	treatment response	-0.83	0.00172
LAG-3	clinical T stage	-0.70	0.02529
A2aR	serosal invasion	-0.72	0.01844

Only significant correlations shown. Spearman correlation. Spearman r 0.4-0.59 moderate, 0.6-0.79 strong and 0.8-1 very strong. *p<0.05.

5.2.9 Blockade of PD-L1, PD-1 and A2aR intrinsic signalling in OGJ cells enhances the toxicity of the FLOT regimen

Given the observation that the pro-survival MEK signalling pathway regulated FLOT-induced PD-L1 and A2aR upregulation on the surface of OGJ cells, we investigated if blockade of PD-1 (nivolumab), PD-L1 (atezolizumab) or A2aR signalling axes in OGJ cells might enhance the toxicity of FLOT chemotherapy regimen (**Figure 5.11**).

Single agent nivolumab and single agent A2aR antagonist significantly decreased the viability of OE33 cells compared with untreated cells (72.48 ± 5.9 vs. 102.4 ± 1.8%, p=0.03 and 74.76 ± 2.4 vs. 102.4 ± 1.8%, p=0.0003, respectively **Figure 5.11A**).

Similar results were observed in the SK-GT-4 cell line; single agent nivolumab and single agent A2aR antagonist significantly decreased the viability of SK-GT-4 cells compared with untreated cells (86.93 ± 2.6 vs. 100.0 ± 1.3%, p=0.004 and 90.61 ± 3.6 vs. 100.0 ± 1.3%, p=0.02, respectively **Figure 5.11A**). Combining A2aR antagonist with FLOT significantly decreased the viability of OE33 cells compared with FLOT treatment alone (64.84 ± 2.5 vs. 67.29 ± 10.78%, p=0.002, **Figure 5.11A**). Combining nivolumab with FLOT significantly

decreased the viability of SK-GT-4 cells compared with FLOT treatment alone (25.67 ± 2.3 vs. 33.72 ± 2.2%, p=0.02, **Figure 5.11A**).

Combining FLOT with nivolumab decreased the viability of OE33 cells (10.77 ± 2.3 vs. 72.48 ± 5.9%, p=0.06), and significantly decreased the viability in SK-GT-4 cells (25.67 ± 2.3 vs. 86.93 ± 2.6%, p<0.0001), compared with nivolumab treatment alone (**Figure 5.11A)**. Combining FLOT with atezolizumab significantly decreased the viability of SK-GT-4 cells (28.76 ± 2.2 vs. 91.93 ± 4.6%, p=0.0001), compared with atezolizumab treatment alone (**Figure 5.11A)**. Combining FLOT with A2aR antagonism significantly decreased the viability of OE33 cells (64.84 ± 2.5 vs. 74.76 ± 2.4%, p=0.03), and SK-GT-4 cells (32.58 ± 1.2 vs. 91.93 ± 4.6%, p<0.0001), compared with A2aR antagonism alone (**Figure 5.11A)**.

Overall, single agent nivolumab and A2aR antagonism significantly decreased the viability of OGJ cells alone. Interestingly, combining nivolumab or A2aR antagonist with the FLOT regimen significantly enhanced the reduction in viability of OGJ cells compared with FLOT treatment alone. In addition, combining FLOT chemotherapy with single agent nivolumab, atezolizumab or A2aR antagonism significantly enhanced the reduction in viability of OGJ cells compared with ICB treatment alone.

Given these findings we sought to investigate how blockade of the PD-1, PD-L1 or A2aR signalling axes alone and in combination with FLOT might affect the proliferation of OE33 cells longitudinally (**Figure 5.11B**). Single agent nivolumab significantly decreased Ki67 expression in OE33 cells at days 4 days (72.68 ± 0.2 vs. 100.0 ± 0.4%, p<0.0001) and 21 days (71.07 ± 0.2 vs. 100.0 ± 3.0%, p=0.01) compared with vehicle treated cells (**Figure 5.11C**). Similarly, single agent atezolizumab significantly decreased Ki67 expression in OE33 cells 4 days (61.34 ± 0.4 vs. 100.0 ± 3.0%, p<0.0001) and 21 days (61.34 ± 0.4 vs. 100.0 ± 3.0%, p=0.005) compared with vehicle treated cells (**Figure 5.11C**). Single agent A2aR antagonist significantly increased Ki67 expression in OE33 cells at 4 days (139.9 ± 0.3 vs. 100.0 ± 3.0%, p<0.0001) and decreased Ki67 expression at 21 days (63.68 ± 0.2 vs. 100.0 ± 3.0%, p=0.007) compared with vehicle treated cells (**Figure 5.11C**).

Interestingly, 48h FLOT treatment significantly increased Ki67 expression in OE33 cells compared with the vehicle control 2 days (224.4 ± 12.4 vs. 100.0 ± 4.0%, p=0.0008), 4 days (183.3 ± 1.8 vs. 100.0 ± 0.4%, p<0.001) and 21 days (145.95 ± 5.2 vs. 100.0 ± 3.0%, p=0.002) post-treatment (**Figure 5.11C**). However, Ki67 expression was significantly decreased in the FLOT treated cells 21 days post-treatment compared with FLOT treated cells 4 days post-

treatment (145.95 ± 5.2 vs. 183.3 ± 1.8 vs. 100.0 ± 0.4%, p=0.01) and compared with FLOT-treated cells 2 days post-treatment (145.95 ± 5.2 vs. 224.4 ± 12.4%, p=0.03) (**Figure 5.11C**). Interestingly, single agent nivolumab in combination with FLOT treatment significantly decreased Ki67 expression in OE33 cells compared with FLOT treatment alone 2 days post-treatment (159.8 ± 6.1 vs. 224.4 ± 12.36%, p=0.005) and 4 days post-treatment (170.3 ± 0.4 vs. 183.3 ± 1.8%, p=0.003) (**Figure 5.11C**). Similarly, single agent atezolizumab in combination with FLOT treatment significantly decreased Ki67 expression in OE33 cells compared with FLOT treatment alone 2 days post-treatment (151.9 ± 3.7 vs. 224.4 ± 12.36%, p=0.02) and 21 days post-treatment (112.2 ± 4.6 vs. 145.9 ± 5.2%, p=0.02) (**Figure 5.11C**). Additionally, single agent A2aR antagonist in combination with FLOT treatment significantly decreased Ki67 expression in OE33 cells compared with FLOT treatment alone 2 days post-treatment (155.8 ± 5.8 vs. 224.4 ± 12.36%, p=0.02), 4 days post-treatment (152.7 ± 2.5 vs. 183.3 ± 1.8%, p=0.0001) and 21 days post-treatment (80.49 ± 4.6 vs. 145.9 ± 5.2%, p=0.0007) (**Figure 5.11C**).

Overall, single agent nivolumab, atezolizumab and A2aR antagonism significantly decreased the proliferation of OGJ cells alone. Interestingly, combining single agent nivolumab, atezolizumab and A2aR antagonism with the FLOT regimen significantly decreased the proliferation of OGJ cells compared with FLOT treatment alone. Taken together these findings suggest that inhibition of the PD-1 axis or A2aR axis decreases the survival of OGJ cells and when combined with the FLOT regimen synergistically enhance the toxicity of FLOT against OGJ cells *in vitro*.

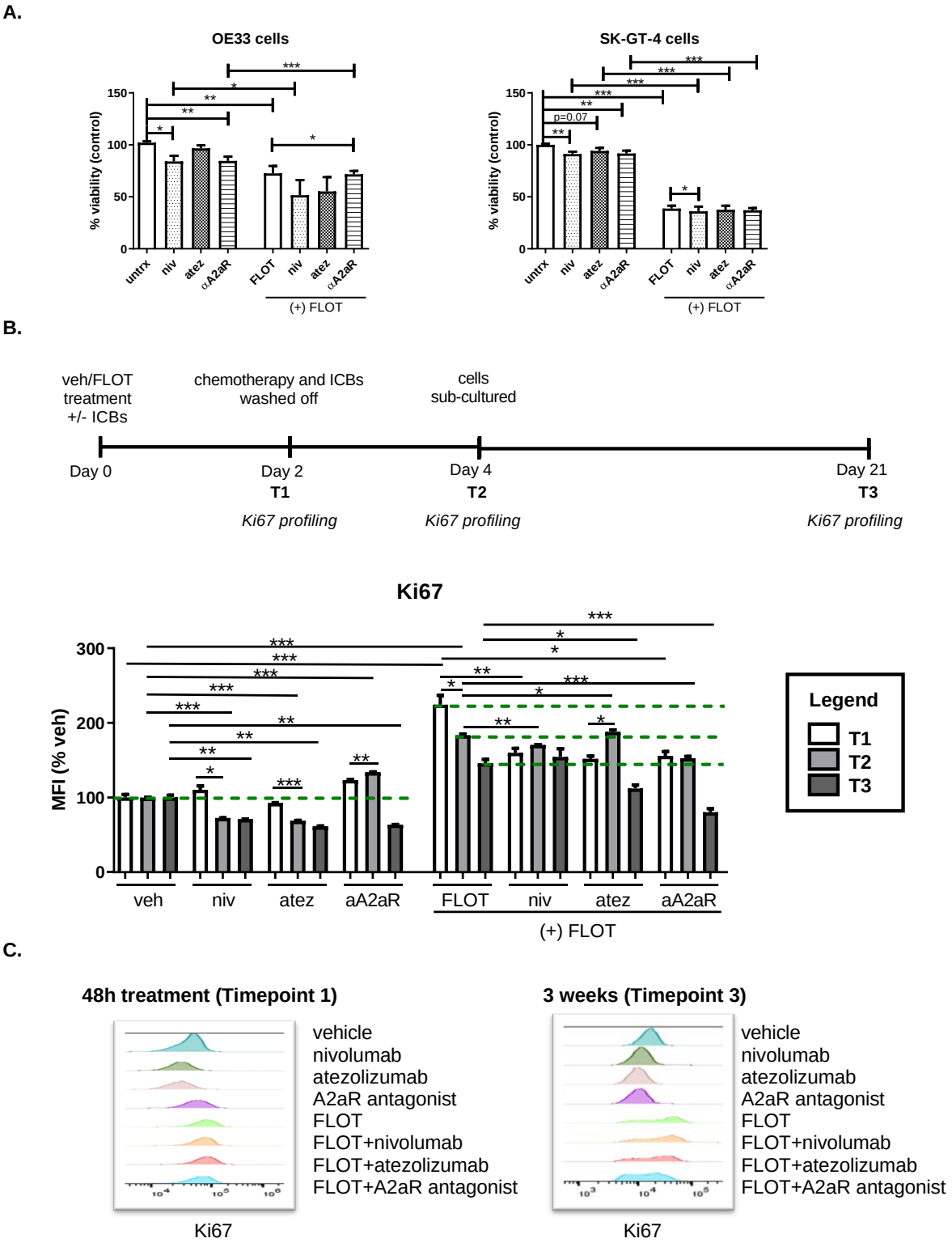

Figure 5.11: Atezolizumab enhances the toxicity of FLOT chemotherapy regimen in OGJ cells demonstrated by a significant decrease in viability and proliferation. (A) OE33 cells and SK-GT-4 cells were treated with nivolumab (10 μg/ml), atezolizumab (10 μg/ml) or A2aR antagonist (3 μM) in the absence or presence of FLOT regimen for 48h and a CCK-8 assay was performed. Experiments were carried out for an n=4 independent experimental repeats using duplicate technical replicates. (B-

C) OE33 cells were treated with nivolumab (10 μg/ml), atezolizumab (10 μg/ml) or A2aR antagonist (3 μM) in the absence or presence of FLOT regimen for 48h (timepoint 1: T1), washed twice and allowed to grow for an additional 48h (T2) after which the cells were sub-cultured in new flasks and left to recover for 3 weeks (T3). Schematic representation of experimental setup depicted in (B). (C) Ki67 mean fluorescence intensity (MFI) was assessed by intracellular flow cytometry in viable OE33 cells and these experiments were carried out for an n=4 independent experimental replicates using singlet technical replicates. MFI is expressed as a percentage of vehicle control ± SEM. (C) Representative histograms displayed for each treatment at T1 and T3 showing effect of each treatment on Ki67 expression in OE33 cell line. Kruskal-Wallis was used for part (A) and a Two-way Anova using Benjamini and Hochberg to correct for false discovery rate was used for part (C), *p<0.05, **p<0.01 and ***p<0.001.

Given these findings we next aimed to investigate how blockade of PD-1, PD-L1 or A2aR signalling axes alone and in combination with FLOT might affect OGJ cell apoptosis and induce cell death (**Figure 5.12**).

Single agent nivolumab significantly induced cell death in OE33 cells compared with the vehicle control (9.71 ± 0.1 vs. 9.19 ± 0.04%, p=0.02), demonstrated by a significant increase in late stage apoptotic cells (**Figure 5.12**). Similarly, single agent A2aR antagonist significantly induced cell death in OE33 cells (19.25 ± 0.2 vs. 9.19 ± 0.04%, p<0.0001) and in SK-GT-4 cells (6.88 ± 0.1 vs. 5.21 ± 0.1%, p=0.001) compared with the vehicle control, demonstrated by a significant increase in late stage apoptotic cells (**Figure 5.12**). In addition, single agent nivolumab (9.13 ± 0.3 vs. 5.8 ± 0.4%, p=0.005) and A2aR antagonist (12.10 ± 0.6 vs. 5.8 ± 0.4%, p=0.0004) significantly increased the percentage of early stage apoptotic SK-GT-4 cells compared with untreated cells (**Figure 5.12**).

Combining single agent nivolumab (23.78 ± 2.4 vs. 18.33 ± 2.2%, p=0.04), atezolizumab (27.23 ± 4.1 vs. 18.33 ± 2.2%, p=0.04) or A2aR antagonist (28.45 ± 0.8 vs. 18.33 ± 2.2%, p=0.04) with FLOT significantly induced cell death in OE33 cells compared with FLOT treated cells, demonstrated by a significant increase in late stage apoptotic cells/dead cells (**Figure 5.12**). Similarly, combining single agent atezolizumab (10.28 ± 0.4 vs. 8.44 ± 0.3%, p=0.04) or A2aR antagonist (12.00 ± 0.7 vs. 8.44 ± 0.3%, p=0.04) with FLOT significantly induced cell death in SK-GT-4 cells compared with FLOT treated cells, demonstrated by a significant increase in late stage apoptotic cells (**Figure 5.12**).

Although, combining single agent nivolumab with FLOT did not significantly enhance SK-GT-4 cell death, a significant increase in early stage apoptotic SK-GT-4 cells was observed using combination nivolumab with FLOT compared with FLOT alone (27.15 ± 1.7 vs. 13.73 ± 1.6%, p=0.0002) (**Figure 5.12**). Similarly, combining single agent atezolizumab (27.15 ± 1.7 vs. 13.73 ± 1.6%, p=0.001) or A2aR

antagonist (24.90 ± 1.9 vs. 13.73 ± 1.6%, p=0.0003) with FLOT significantly induced increased the percentage of early stage apoptotic SK-GT-4 cells compared with FLOT treated cells (**Figure 5.12**).

Given the stark differences in ICB toxicity between both cell lines we also compared the frequency and MFI of IC expression between the two cell lines (**Figure 5.12E-F**). Of note the SK-GT-4 cell line expressed significantly higher frequencies (13.97 ± 1.6 vs. 6.97 ± 1.3%, p=0.0001) and MFI levels (5184 ± 61.4 vs. 3867 ± 50.0%, p=0.0001) for PD-1 compared with the OE33 cell line, which may explain the enhanced toxicity of nivolumab treatment against the SK-GT-4 cell line (**Figure 5.12E-F**). Although the frequency of PD-L1 expression was comparable between the OE33 cell line and the SK-GT-4 cell line, the OE33 cells did have significantly higher MFI levels for PD-L1 compared with the SK-GT-4 cell line basally (3142 ± 8.9 vs. 1924 ± 27.6%, p=0.005) (**Figure 5.12E-F**). In this context, single agent atezolizumab significantly induced cell death/late stage apoptosis in OE33 cells only and not in the SK-GT-4 cell line. Therefore, differences in the basal expression MFI levels of PD-1 and PD-L1 between the OE33 and SK-GT-4 cell lines may explain the observed differences in toxicity for single agent nivolumab and atezolizumab. A2aR frequency and MFI levels were comparable between both cell lines (**Figure 5.12E-F**), and as such the expression levels of A2aR does not offer a potential explanation in the observed differences in sensitivity to A2aR antagonism between the two cell lines. Overall, these findings highlight that single agent PD-1, PD-L1 and A2aR IC blockade induced apoptosis and OGJ cell death. Furthermore, combining ICB with the FLOT chemotherapy regimen enhanced induction of apoptosis in OGJ cells and OGJ cell death.

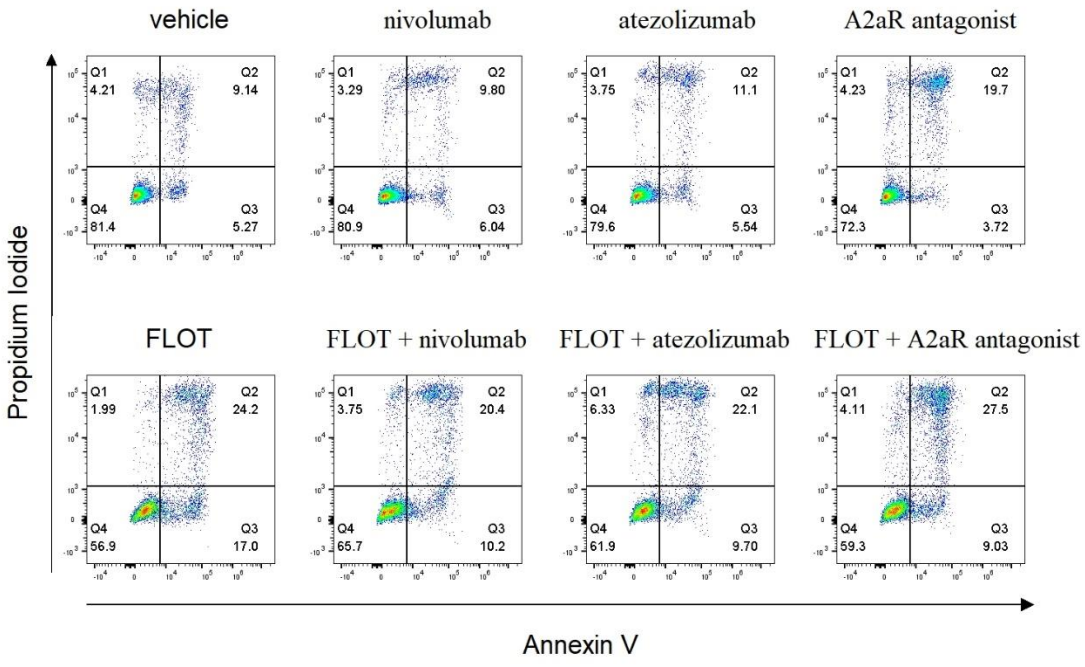

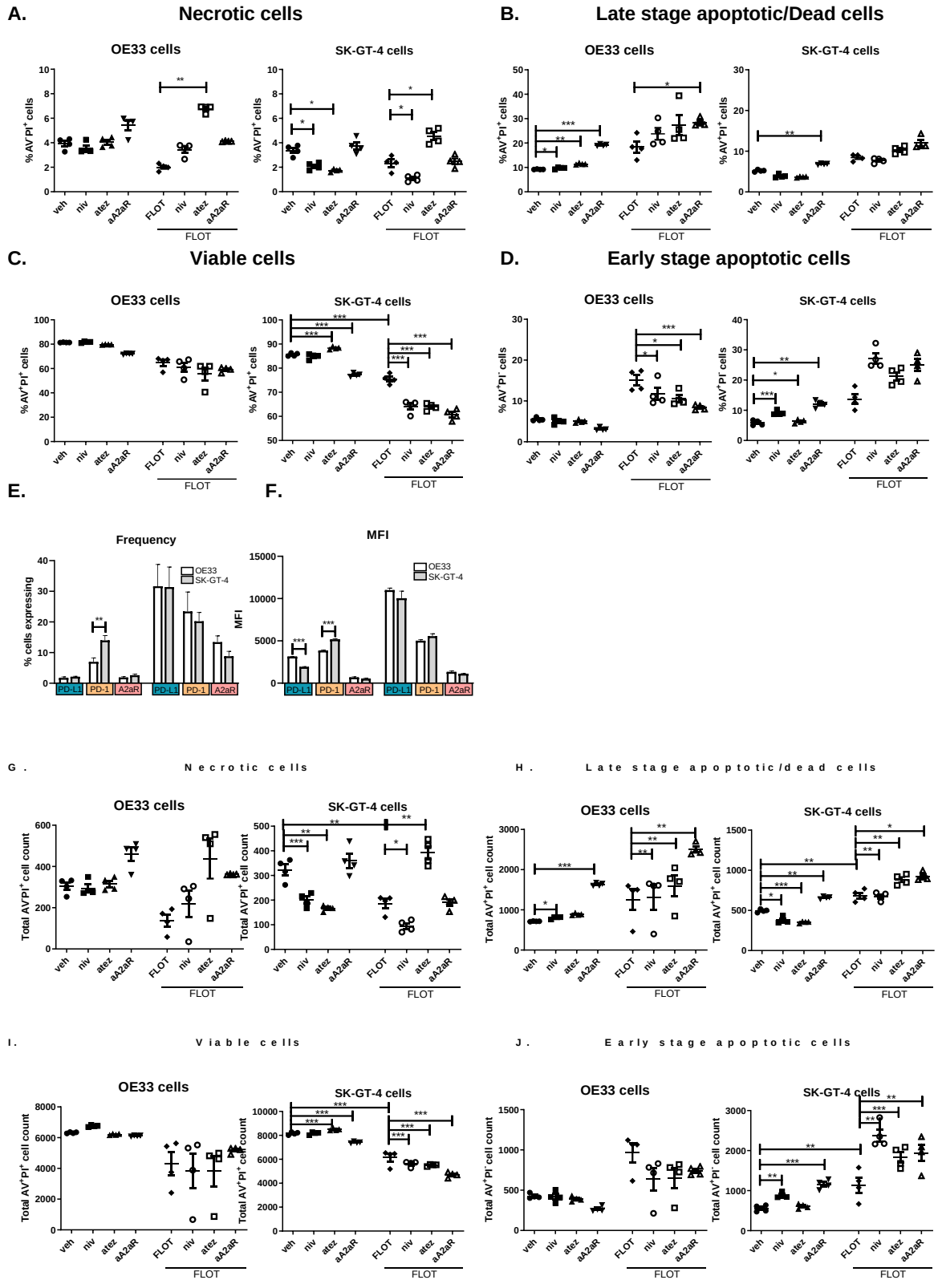

Figure 5.12: PD-1, PD-L1 and A2aR blockade enhances the toxicity of FLOT chemotherapy regimen demonstrated by a significant reduction in the percentage of viable cells and increase in late stage apoptotic cells. OE33 cells and SK-GT-4 cells were treated with nivolumab (10 μg/ml),

atezolizumab (10 μg/ml) or A2aR antagonist (3 μM) in the absence or presence of FLOT regimen for 48h. Viability was determined by flow cytometry using annexin V propidium iodide assay. Necrotic cells ((A) AV^-PI^+), late stage apoptotic/dead cells ((B) AV^+PI^+), viable cells ((C) AV^-PI^-) and early stage apoptotic cells ((D) AV^+PI^-), dead were characterised. Representative dot plots shown for each treatment in OE33 cell line. Experiments repeated for n=4 independent experimental repeats using singlet technical replicates. Kruskal-Wallis used for part (A-D) and Mann-Whitney test used for part (E-F), *p<0.05, **p<0.01 and ***p<0.001. (G-J) depict the total cell counts of necrotic cells ((A) AV^-PI^+), late stage apoptotic/dead cells ((B) AV^+PI^+), viable cells ((C) AV^-PI^-) and early stage apoptotic cells ((D) AV^+PI^-) was determined by flow cytometry using annexin V propidium iodide assay.

5.2.10 Blockade of IC signalling in OGJ cells decreases the formation of γH2AX and expression of DNA repair genes

We have shown that PD-1, PD-L1 and A2aR signalling confers OGJ cells with a survival advantage as their blockade alone reduces OGJ cell viability and can enhance FLOT chemotherapy toxicity. Interestingly, studies have implicated a role for PD-L1 intrinsic signalling in mediating DNA repair in colon cancer[340]. Therefore, to achieve a greater understanding of the mechanisms of action behind enhanced FLOT cytotoxicity in combination with ICB, this study assessed if blockade of these IC pathways might alter the formation of γH2AX alone and in combination with FLOT chemotherapy (**Figure 5.13**). Tumour cells rapidly proliferate and typically acquire DNA damage during replication generating genotoxic stress, which ultimately leads to tumour cell death if left unrepaired. Formation of γH2AX foci is an important step in the initiation of DNA repair.

Single agent nivolumab, atezolizumab and A2aR antagonist significantly decreased the levels of γH2AX expression in OE33 cells following 24h treatment compared with the vehicle control (nivolumab: 1352 ± 15.09 vs. 1507 ± 8.51%, p=0.005, atezolizumab: 1383 ± 6.8 vs. 1507 ± 8.51%, p=0.002 and A2aR antagonist: 1416 ± 13.6 vs. 1507 ± 8.51%, p=0.02) (**Figure 5.13A**). Similar findings were observed in the SK-GT-4 cell line where single agent nivolumab, atezolizumab and A2aR antagonist significantly decreased the levels of γH2AX expression in OE33 cells following 24h compared with the vehicle control (nivolumab: 4167 ± 50.85 vs. 4491 ± 32.9%, p=0.001, atezolizumab: 4129 ± 33.1 vs. 4491 ± 32.9%, p=0.002 and A2aR antagonist: 2791 ± 38.6 vs. 4491 ± 32.9%, p<0.0001) (**Figure 5.13A**).

Following 24h treatment with FLOT the levels of γH2AX expression in OE33 cells was significantly increased compared with the vehicle control (2756 ± 29.05 vs. 1507 ± 8.5%, p<0.0001). Interestingly, combining single agent nivolumab, atezolizumab and A2aR

antagonist with the FLOT regimen significantly decreased the levels of γH2AX expression in OE33 cells following 24h compared with FLOT treated cells (nivolumab: 1937 ± 9.9 vs. 2756 ± 29.0%, p=0.0001, atezolizumab: 1836 ± 12.1 vs. 2756 ± 29.0%, p=0.0001 and A2aR antagonist: 2232 ± 11.8 vs. 2756 ± 29.0%, p=0.0002) (**Figure 5.13A**).

Similar findings were observed in the SK-GT-4 cell line (**Figure 5.13A**). Following 24h treatment with FLOT the levels of γH2AX expression in SK-GT-4 cells was significantly increased compared with the vehicle control (5694 ± 49.6 vs. 4491 ± 32.9%, p=0.0001). Similarly, combining single agent nivolumab with the FLOT regimen significantly decreased the levels of γH2AX expression in SK-GT-4 cells following 24h compared with FLOT treated cells (4414 ± 13.1 vs. 5694 ± 49.6%, p<0.0001) (**Figure 5.13A**). However, in contrast combining single agent nivolumab with the FLOT regimen significantly increased the levels of γH2AX expression in SK-GT-4 cells following 24h compared with FLOT treated cells (nivolumab: 4.44 ± 4.1 vs. 4.44 ± 4.1%, p<0.0001) (**Figure 5.13A**). Overall, similar trends were observed at 48h and72h in which single agent nivolumab, atezolizumab and A2aR antagonism decreased γH2AX expression in OE33 and SK-GT-4 cells compared with the vehicle control (**Figure 5.13A**). Similarly, at 48h and 72h timepoints, combining single agent nivolumab, atezolizumab and A2aR antagonist with the FLOT regimen significantly decreased the levels of γH2AX expression in OGJ cells compared with FLOT treated cells (**Figure 5.13A**).

Tu et *al.*,[341] demonstrated that intracellular PD-L1 acts as an RNA binding protein enhancing the mRNA stability of NBS1 and BRCA1, thus upregulating the expression of DNA repair proteins NBS1 and BRCA1. Therefore, this study assessed if ICB might alter the expression of DNA repair genes PARP1, SMUG1, MLH1 and MMS19 alone and in combination with FLOT chemotherapy (**Figure 5.13**). These particular set of DNA repair genes were upregulated in OGJ tumours that were resistant to first-line chemo(radio)therapy regimens[342]. Single agent atezolizumab significantly reduced the mRNA expression levels of PARP1 and SMUG1 compared with the vehicle control (PARP1: 0.41 ± 0.1 vs. 0.78 ± 0.2%, p=0.005 and SMUG1: 0.45 ± 0.1 vs. 0.83 ± 0.1%, p=0.008) (**Figure 5.13B**). Interestingly, combining A2aR antagonist with the FLOT regimen significantly increased the mRNA expression levels of MMS19 compared with FLOT treated cells (1.12 ± 0.1 vs. 0.13 ± 0.06%, p=0.03) (**Figure 5.13B**).

Overall, single agent nivolumab, atezolizumab and A2aR antagonist decreased γH2AX expression in OGJ cells and decreased the gene expression of DNA repair genes. Similarly, combining single agent nivolumab, atezolizumab with FLOT chemotherapy decreased γH2AX

expression in OGJ cells and expression of DNA repair genes. Interestingly, although single agent A2aR antagonist decreased γH2AX expression in OGJ cells, an increase in expression of DNA repair genes was observed.

A.

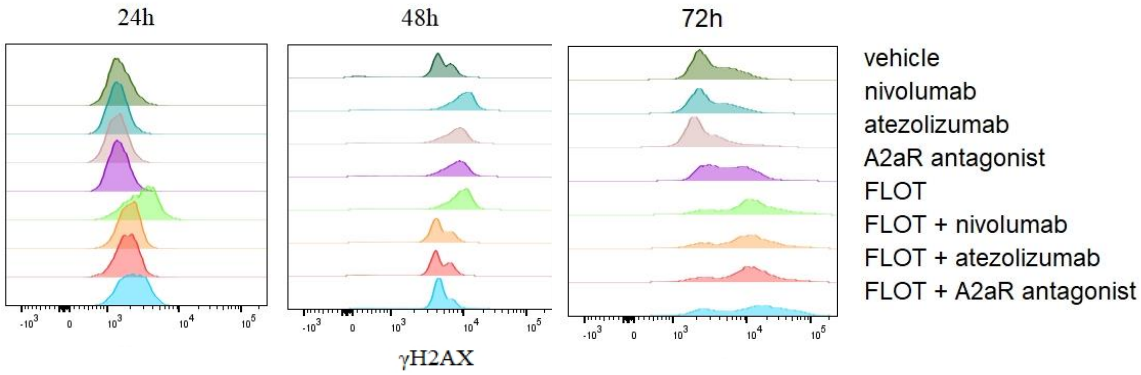

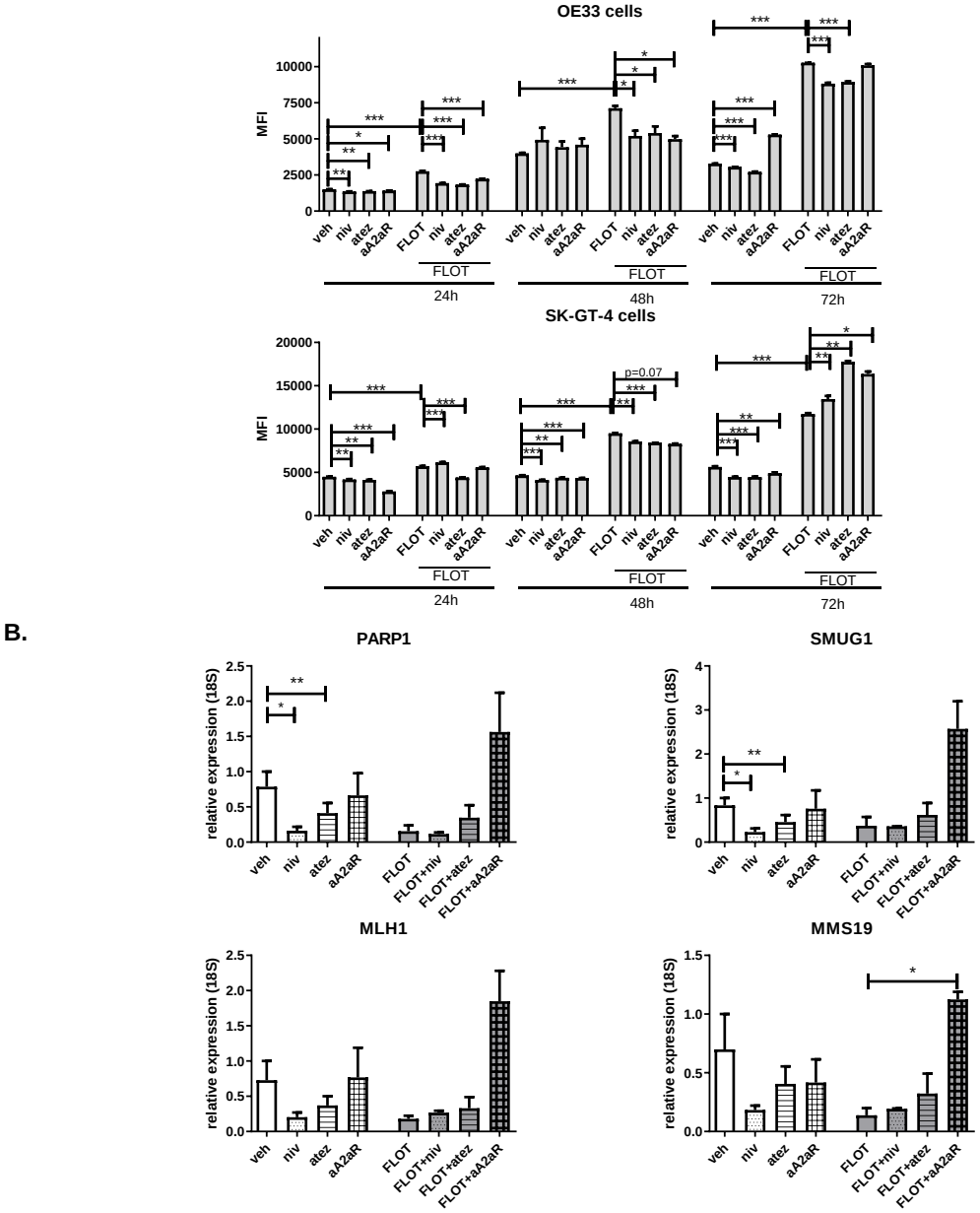

Figure 5.13: Single agent nivolumab and atezolizumab decreased the levels of γH2AX and the levels of DNA repair genes *in vitro.* (A) OE33 cells and SK-GT-4 cells were treated with nivolumab (10 μg/ml), atezolizumab (10 μg/ml) or A2aR antagonist (3 μM) in the absence or presence of FLOT regimen for 24h, 48h and 72h. Expression of γH2aX was determined by intracellular flow cytometry. γH2ax expression is presented as MFI. Representative histograms showing the levels of γH2AX in OE33 cells for each treatment at 24h, 48h and 72h. Experiments repeated for an n=4 independent experimental repeats using singlet technical replicates. (B) SK-GT-4 cells were treated with nivolumab (10 μg/ml), atezolizumab (10 μg/ml) or A2aR antagonist (3 μM) in the absence or presence of FLOT regimen for 48h. mRNA expression levels of PARP1, SMUG1, MMS19 and MLH1 were determined by qPCR. qPCR experiments were conducted for an n=3 independent experimental replicates in

triplicate technical replicates. Expression presented as relative quantity of 18S housekeeping gene. Two-way Anova using Benjamini and Hochberg to correct for false discovery rate in part (A) and Kruskal-Wallis used in part (B) *p<0.05 and **p<0.01, ***p<0.001.

5.2.11 Blockade of PD-1 axis signalling in OGJ cells decreases ALDH stem-like marker

Cancer stem-like cells exist as part of a subpopulation within tumours and are thought to be a primary reason for tumour recurrence. Moreover, our findings demonstrate that ICB decreases OGJ cell proliferation and viability and induced OGJ cell apoptosis and cell death in a subpopulation of OGJ cells. In section 5.3.6 these findings demonstrated that FLOT chemotherapy regimen significantly increased ALDH stem-like marker expression in OGJ cells. Therefore, this study assessed if ICB might be targeting the stem-like compartment within a population of OGJ cells so this study investigated the effect of ICB on the levels of ALDH stem-like marker in OGJ cells alone and in combination with FLOT (**Figure 5.14**).

We found that single agent atezolizumab significantly decreased ALDH activity in OE33 cells compared with the vehicle control (28.44 ± 2.5 vs. 34.67 ± 2.1%, p=0.004) (**Figure 5.14**). However, FLOT chemotherapy treatment significantly increased ALDH activity in OE33 cells compared with the vehicle control in OE33 cells (48.12 ± 3.7 vs. 28.44 ± 2.5 %, p=0.01) (**Figure 5.14**). Interestingly, nivolumab significantly attenuated the FLOT-induced increase in ALDH activity in OE33 cells compared with FLOT treated cells (38.13 ± 4.0 vs. 48.12 ± 3.7%, p=0.02) (**Figure 5.14**).

Similarly, there were trends toward a significant decrease in ALDH activity following single agent atezolizumab treatment compared with the vehicle control in SK-GT-4 cells (3.39 ± 1.3 vs. 12.11 ± 4.8%, p=0.08) (**Figure 5.14**).

Overall, PD-L1 blockade decreased the expression of ALDH stem-like marker in OGJ cells and PD-1 blockade attenuated the FLOT-induced increase in ALDH activity in OGJ cells.

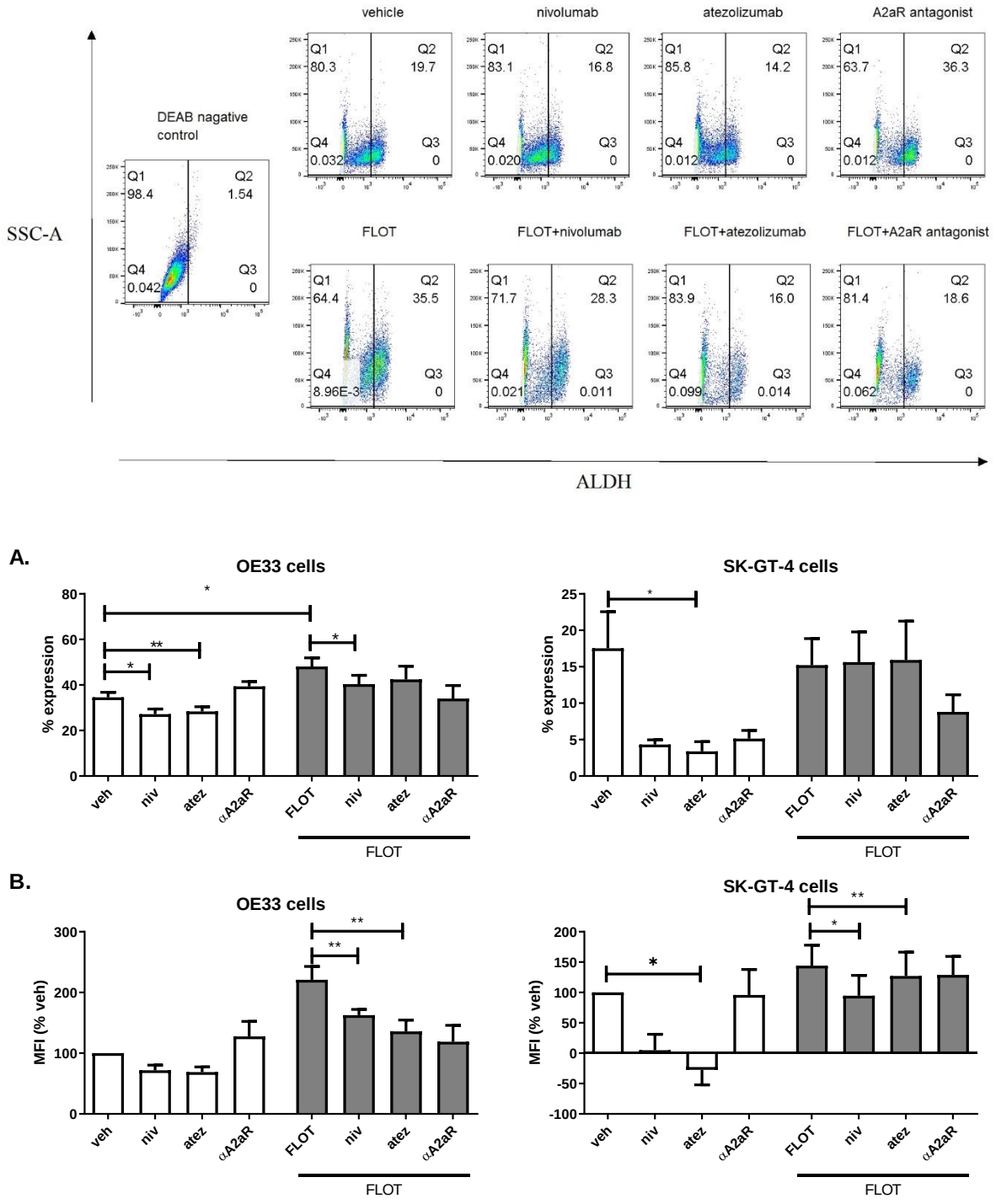

Figure 5.14: Nivolumab and atezolizumab treatment decrease the percentage of ALDH$^+$ stem-like OGJ cells *in vitro*. OE33 cells and SK-GT-4 cells were treated with nivolumab (10 μg/ml), atezolizumab (10 μg/ml) or A2aR antagonist (3 μM) in the absence or presence of the FLOT regimen for 48h. ALDH activity was determined using an aldefluor assay by flow cytometry. Representative dot plots shown for each treatment and for the DEAB negative control which was used to assess baseline fluorescence to allow accurate gating for ALDH activity. **A** depicts the frequency of ALDH+ OAC cells and **B** depicts the median fluorescence intensity of ALDH as a percentage of the vehicle control.

Experiments repeated for an n=4 independent experimental repeats using singlet technical replicates. *p<0.05 and **p<0.01, Kruskal-Wallis statistical test.

5.3 Discussion

It has previously been shown that tumour cells express an array of both IC ligands and IC receptors[229]. Furthermore, tumour cell-expressed ICs have also been implicated as a potential mechanism of chemo(radio)-resistance in a range of cancer types[175,176,202,203]. Firstly, by immune-dependent pathways via binding of ICs expressed on tumour cells with their cognate receptors or ligands on tumour-infiltrating immune cells negatively regulating anti-tumour function of these infiltrating immune cells[171]. Chemotherapy-induced PD-L1 upregulation on the surface of breast cancer cells results in immune evasion via ligation of PD-L1 to PD-1 on T cells, thereby inducing T cell apoptosis[171]. Alternatively, immune-independent mechanisms mediated by ICs have recently been recognised as potential mechanisms of resistance employed by tumour cells to attenuate the efficacy of chemo(radio)therapy efficacy. Such mechanisms include promotion of key hallmarks of cancer via IC-intrinsic signalling in tumour cells including tumour cell metastasis[194], enhanced DNA repair[331], tumour cell proliferation[343], cancer stem-like activity[330] and glycolysis[236] in tumour cells. Two cell lines were used in those study to help encapsulate the heterogeneity observed between tumours from different patients. The OE33 cell line was established from a poorly differentiated stage IIA adenocarcinoma which had progressed from Barrett's metaplasia in a 73-year old female patient. Whereas, the SK-GT-4 cell line was established from a well differentiated oesophageal adenocarcinoma which had also progressed from Barrett's metaplasia but from an 89-year-old male.

We demonstrated that the FLOT chemotherapy regimen enhanced a more stem-like and senescent-like phenotype in OGJ cells and perhaps may be selecting for a more therapeutically resistant phenotype. Interestingly, the CROSS CT regimen significantly reduced ALDH activity in OE33 cells. This may suggest that the chemotherapies comprising the CROSS CT regimen may be attenuating a stem-like phentoype in certain OGJs. Our study demonstrates that FLOT, CROSS CT and MAGIC chemotherapy regimens all enhance a senescent-like phenotype in OGJ cells *in vitro,* whereby again we saw that FLOT substantially enhanced a senescent-like phenotype. Chemotherapy regimens are cytotoxic to tumour cells and often promote immunogenic cell death, this study highlights the double-edged sword of

chemotherapy, where we observed that the FLOT regimen in particular may also elicit tumour promoting effects through selecting for a more aggressive cancer cell phenotypes[163].

Furthermore, elements of the PD-1 signalling axis namely the PD-1 receptor and its cognate ligand PD-L1 have been identified on the surface of stem-like tumour cells in melanoma[261] and lung cancer[330]. We have previously shown that FLOT upregulates PD-L1 preferentially on the surface of stem-like OGJ cells[229]. In addition, PD-1 and PD-L1 tumour cell intrinsic signalling has been shown to promote stem-like characteristics in both melanoma and lung cancer cells [261,330]. Similarly, the findings of this study demonstrated that blockade of the PD-1 signalling axis decreased ALDH stem-like marker in OGJ cells. Collectively, these findings highlight an immune-independent role for the PD-1 axis signalling cascade in driving a treatment resistant phenotype, as cancer stem-like cells are thought to play a pivotal role in resistance to first-line chemotherapy regimens and subsequent tumour recurrence[334,335].

However, emerging studies have shown that inhibitory IC receptors PD-1[182,184–186], TIM-3[232,188], TIGIT[329] and A2aR[194] are also expressed on lung, melanoma, colorectal[329], cervical[232] and gastric[188,194] cancer cells. Our study identified a subpopulation of OGJ cells expressing inhibitory IC receptors PD-1, TIGIT, TIM-3, LAG-3, A2aR and inhibitory IC ligands PD-L1, PD-L2 *in vitro* and *ex vivo*. A complementary study by Kollmann D. *et al*., showed that PD-1 was expressed on 77% of OGJ patient tumour cells (n=168) at levels greater than 5%, determined by immunohistochemical analysis and was associated with significantly decreased 5-year overall survival compared to those who lacked PD-1-expressing OGJ cells in their tumours (43.5% versus 68.8%, respectively)[344].

This study also profiled the dynamic alterations in the IC expression profiles of OGJ cells post-FLOT treatment until complete recovery of OGJ cells. Interestingly, IC expression was significantly upregulated in the immediate days post-FLOT treatment and was sustained longitudinally for up to 3 weeks on the surface of tumour cells. Upon complete recovery and subculture of tumour cells we found that although PD-L1 had substantially reduced, expression of PD-L1 remained significantly higher on the surface of post-FLOT tumour cells compared with untreated cells. Chemotherapy has been shown to select for a more treatment resistant tumour cell phenotype. Interestingly an isogenic model of cisplatin resistant lung cancer cells displayed significantly higher levels of PD-L1 expression compared with matched cisplatin sensitive cells[201]. Therefore, considering the findings of this study in context with the wider literature, the increased expression of PD-L1 on the surface of recovered OGJ cells may suggest that PD-L1 expression may identify but also confer a more treatment resistant phenotype.

The percentage of cells expressing LAG-3, A2aR and TIM-3 were significantly lower post-FLOT treatment compared with the treatment-naïve setting ex vivo and similar findings were observed *in vitro* (3 weeks post-treatment). However, treatment of OE33 and SK-GT-4 cells with FLOT for 48h *in vitro* significantly increased IC expression on the surface of OGJ cells including LAG-3, A2aR and TIM-3. The *in vitro* experiments recapitulate the direct effects of chemotherapy on IC expression on OGJ cells using an *in vitro* culture system. In contrast, the analysis of IC expression in tumour biopsy tissue encapsulates the effect of the entire tumour microenvironment on IC expression in the treatment-naïve setting as well as the combined direct and indirect effects of FLOT and CROSS CRT 6 weeks post-treatment. It is also important to highlight that the post-treatment tumour biopsies are sampled 6 weeks post treatment at the time of surgical resection of the tumour specimen and not at the time of chemotherapy treatment. IC expression likely changes dynamically and longitudinally in parallel with the ever-evolving tumour mass.

5-FU had the most substantial effect in upregulating ICs on the surface of OGJ cells. Additionally, the FLOT regimen consistently upregulated both inhibitory IC ligands and receptors on OGJ cells *in vitro* to a greater extent than the CROSS CT and MAGIC chemotherapy regimens. ICs play an integral role in maintaining immunotolerance and are key players in mediating tumour immune evasion, therefore this suggests that FLOT may be promoting immunogenic cell death in OE33 and SK-GT-4 cells as an increase in ICs are observed which have an integral role in controlling the magnitude and duration of immune activation. Studies have shown that oxaliplatin and 5-FU, which comprise the FLOT regimen have immunostimulatory properties and induce immunogenic cell death in lung and colon cancer cells[345,346]. Complementary studies have also shown that 5-FU increases PD-L1 on the surface of OE33 and HCT-116 cells[333] and similarly, cisplatin increases PD-L1 on the surface of lung cancer cells[332].

The findings from this study demonstrated that signalling through RAS/RAF/MEK/ERK (MAPK) signalling cascade upregulated several IC proteins including PD-L1, TIM-3, LAG-3 and A2aR on the surface of OGJ cells following FLOT treatment. A complementary study demonstrated that MAPK signalling regulated epidermal growth factor- and interferon-gamma-induced PD-L1 expression in lung adenocarcinoma cells and that inhibition of MEK1/2 attenuated PD-L1 upregulation[347]. MEK signalling has pleiotropic effects in enhancing fundamental pro-tumourigenic processes, including tumour cell growth, survival and differentiation[348]. Collectively, these findings support a rationale for combination MAPK

signalling and PD-L1 blockade to boost anti-tumour immunity as MAPK-induced upregulation of novel ICs such as TIM-3, LAG-3 and A2aR might represent mechanisms of immune escape or acquired resistance to PD-L1 ICB. A study in murine models further supports this rationale as MAPK inhibition in combination with anti-PD-L1 ICB resulted in synergistic and durable tumour regression even where either agent alone was only modestly effective[349]. The combination promoted T cell anti-tumour activity in combination with PD-L1 ICB[349]. Although MEK inhibition did profoundly block naive $CD8^+$ T cell priming, an increased number of tumour-infiltrating, effector-phenotype, antigen-specific $CD8^+$ T cells was observed[349]. Furthermore, MEK inhibition protected tumour-infiltrating $CD8^+$ T cells from chronic TCR stimulation-induced cell death while sparing cytotoxic activity[349]. MEK inhibition mediated downregulation of ICs on tumour cells may have also contributed to these synergistic effects.

The upregulation of ICs on the surface of OGJ cells suggests these ICs may offer some level of protection against chemotherapy or perhaps they may be upregulated in an attempt to repair the chemotherapy-induced damage to the cell. Emerging studies have shown that IC receptors and ligands directly enhance glycolysis[180], proliferation[182], invasion, migration[233,183] and DNA repair[181] via cancer cell-intrinsic signalling. Several studies have demonstrated that DNA damage signalling upregulates PD-L1 expression on the surface of cancer cells[175,176,203] and PD-L1 cancer cell-intrinsic signalling mediates DNA repair[176,203]. Blockade of PD-L1 on the surface of OGJ cells could potentially prevent repair of the chemotherapy-induced DNA damage thereby, enhancing chemotherapy toxicity. It is unclear whether the viable OGJ cells that survived chemotherapy treatment had upregulated inhibitory ICs on their cell surface or if the chemotherapy treatment selectively killed OGJ cells that lacked inhibitory IC expression enriching for OGJ cells that express inhibitory ICs. The former may suggest that OGJ cells upregulate inhibitory ICs perhaps as a survival advantage to facilitate immune evasion or perhaps IC-intrinsic signalling is promoting immune-independent mechanisms of resistance to chemotherapy-induced cell death. The latter suggests that ICs are expressed on the surface of OGJ cells that are more resistant to chemotherapy-induced cell death and persist following treatment. Our results demonstrate that chemotherapy preferentially upregulates PD-L1 and TIM-3 ICs on a more stem-like OGJ cell phenotype *in vitro*. Additionally, FLOT chemotherapy significantly upregulated TIM-3 and A2aR on a subpopulation of senescent-like OGJ cells. Other studies have shown that PD-L1 is enriched on cancer stem cells and provides a mechanism of immune escape[328]. TIM-3 has also been identified on cervical and gastric cancer

cells and induced invasion and migration of HeLa cells *in vitro*[232]. High levels of TIM-3 expression on gastric cancer cells correlated with metastasis in gastric cancer patients[188]. Shi Z. *et al*., demonstrated that A2aR signalling via PI3K-AKT-mTOR upregulated stemness-associated and EMT-like proteins in gastric cancer cells *in vitro* and that A2aR knockout murine models resulted in a decrease in the number and size of micrometastatic lesions in the lungs of mice[194]. Ultimately, the expression of inhibitory IC ligands and receptors on OGJ cells may function in tandem to offer OGJ cells a survival advantage via promoting a range of cancer hallmarks.

PD-L1 upregulation is associated with activation of the DNA double-strand break repair pathway in patients with colon cancer[340]. Furthermore, several studies have shown that accumulation of damaged DNA and subsequent DNA damage signalling mediates upregulation of PD-L1 on the surface of tumour cells[181,350,351]. In turn, studies have identified a role of PD-L1 tumour cell intrinsic signalling in enhancing the DNA damage response[352]. Tu et *al*.,[341] discovered that intracellular PD-L1 acts as an RNA binding protein that regulates the mRNA stability of NBS1 and BRCA1, thus enhancing repair of damaged DNA. In light of the mounting evidence that PD-L1 has a positive feedback regulatory role in the DNA damage response in cancer, our findings further consolidate this novel immune-independent role in OGJ. We demonstrated that inhibition of the PD-1 signalling axis in OGJ cells decreased expression of γH2AX,a surrogate marker of DNA damage and possess an important role in the DNA damage signalling response and subsequent repair of damaged DNA[353], and inhibited expression of DNA repair genes PARP1 and SMUG1 alone and in combination with FLOT.

FLOT comprises of a unique cocktail of chemotherapies including 5-FU (an anti-metabolite), oxaliplatin (DNA intercalator) and docetaxel (taxane) with specific mechanisms of action that target distinct phases of the cell cycle. 5-FU exerts its anticancer effects through inhibition of thymidylate synthase and incorporation of its metabolites into RNA and DNA resulting in damage to these RNAs and DNAs generating considerable amounts of cellular genotoxic stress and hindering the normal functioning and homeostasis of cellular processes that require these RNAs and DNAs[13]. Oxaliplatin, a platinum-based chemotherapy intercalates with cellular DNA forming platinum-DNA adducts, which induce DNA damage and block DNA replication[354]. Docetaxel inhibits microtubular depolymerization, and attenuates the effects of bcl-2 and bcl-xL gene expression which ultimately culminates in G2/M phase cell cycle arrest apoptotic cell death[355]. Although FLOT induced apoptosis within 48h and decreased viability, we also observed that FLOT increased the proliferation of OGJ cells, however, the observed

FLOT-induced proliferation of OGJ cells was diminished longitudinally. Although this initial increase in proliferation was surprising the FLOT regimen may collectively hinder DNA damage signalling or DNA repair and subsequent cell cycle arrest initially or may prevent delays through the cell cycle. This may subsequently cause the cells to undergo cell cycling at a faster rate increasing their proliferation at first which then deceases longitudinally as the FLOT-treated cells die off in culture.

There are a number of studies in the literature highlighting that PD-1, PD-L1 and A2aR intrinsic signalling in tumour cells also promote tumour cell proliferation in a range of cancer types including hepatocellular carcinoma[356], lung, melanoma[343], ovarian[343], pancreatic[185], gastric[187,188,194] and cervical cancer[187]. The findings of this study further substantiate the immune-independent role of PD-1, PD-L1 and A2aR tumour cell-intrinsic signalling in promoting proliferation of tumour cells in the context of OGJ. Similarly, Liu, N. *et al*., demonstrated that PD-1 blockade enhanced chemosensitivity to 5-FU in a 5-FU resistant gastric cancer cell line[202]. These important clinically-relevant findings suggest that ICBs might synergise with combination chemotherapy regimens in patients to enhance chemotherapy-induced OGJ cell death in an immune-independent manner and highlights the need for further studies to answer this question. In addition, these findings may be reflective of the limited benefit observed from clinical trials testing combination ICI-chemotherapy regimens, but this may translate to a measurable improvement in clinical outcomes. We also demonstrated that PD-L1 is upregulated on stem-like OGJ cells *in vitro* and therefore, blockade of the PD-1 signalling axis may be reducing the survival of stem-like OGJ cells and subsequently enhancing the efficacy of chemotherapy, which could translate to a clinically meaningful improvement in outcomes for patients. This may account for the limited effect observed in the decrease in viability when ICB is added to FLOT as stem-like cells only comprise a subpopulation of a tumour cell population. However, from a clinical perspective this minimal but significant reduction in viability if it were in the stem-like compartment would be a very desirable effect and highlight a strong rationale for combining PD-1 ICBs with first-line chemotherapy regimens.

In summary, the findings from this study highlight the novel immune-independent functions of IC tumour cell-intrinsic signalling in OGJ cells, promoting a range of hallmarks of cancer including enhancing tumour cell growth and proliferation, upregulating ALDH activity in stem-like cancer cells and enhancement of DNA repair. Importantly, blockade of the PD-1 signalling axis suppressed tumour cell growth, decreased cancer stem-like marker ALDH and

expression of DNA repair genes alone and in combination with the FLOT chemotherapy regimen. Combining PD-L1, PD-1 or A2aR ICB with the FLOT regimen synergistically enhanced chemotherapy cytotoxicity in OGJ cells. Overall, this highlights a strong clinical rational for combining ICB with the first-line chemotherapy regimens to not only reinvigorate anti-tumour immunity and prevent immune exhaustion but to directly enhance the cytotoxicity of FLOT via inhibition of immune-independent hallmarks of cancer mediated by IC-intrinsic signalling in OGJ cells.

Chapter 6 – Cooperation between chemotherapy and immune checkpoint blockade to boost anti-tumour T cell-mediated immunity in OGJ

Hypothesis

First-line chemotherapy regimens significantly alter T cell phenotypes and immune checkpoint expression profiles and combining immune checkpoint blockade with first-line chemotherapy regimens will achieve synergistic responses

6.1.1 Highlights

- FLOT and CROSS chemotherapy regimens induce immunogenic cell death (ICD) in OGJ. In contrast, the MAGIC regimen appears to decrease ICD.
- The FLOT and CROSS chemotherapy-treated oesophagogastric adenocarcinoma tumour microenvironment increases $CD69^+$ T cells yet decreases $CD27^+$ T cells *in vitro* and *ex vivo.*
- The secretome of FLOT and CROSS chemotherapy-treated OGJ cells (OE33) enhances OGJ patient-derived lymphocyte cytotoxicity.
- Expression of ICs on T cells positively correlated with a subsequent poor response to neoadjuvant treatment and more advanced tumours.
- First-line chemotherapy regimens substantially altered IC expression profiles of T cells increasing PD-1, A2aR, KLRG-1, PD-L1, PD-L2 and CD160 and decreasing TIM-3 and LAG-3 on OGJ donor T cells *ex vivo.*
- In addition, pro-inflammatory T cell cytokine profiles were enhanced by first-line chemotherapy regimens *ex vivo*.
- T cell activation status was significantly altered by FLOT and CROSS chemotherapy regimens; both chemotherapy regimens upregulated co-stimulatory markers ICOS and CD69 yet downregulated co-stimulatory marker CD27.
- However, ICB attenuated chemotherapy-induced downregulation of CD27 on T cells and promoted differentiation of effector memory T cells into a terminally differentiated state *ex vivo*.
- Importantly, dual nivolumab-ipilimumab treatment enhanced OGJ lymphocyte-mediated cytolysis of OE33 OGJ cells.
- These findings highlight a link between chemotherapy and the development of immune-resistance, reaffirming the rationale to administer ICBs concurrently with first-line chemotherapies to prevent potential IC-mediated suppression of chemotherapy-induced anti-tumour immunity. The synergy between ICB and first-line chemotherapies to boost anti-tumour immunity is also highlighted.

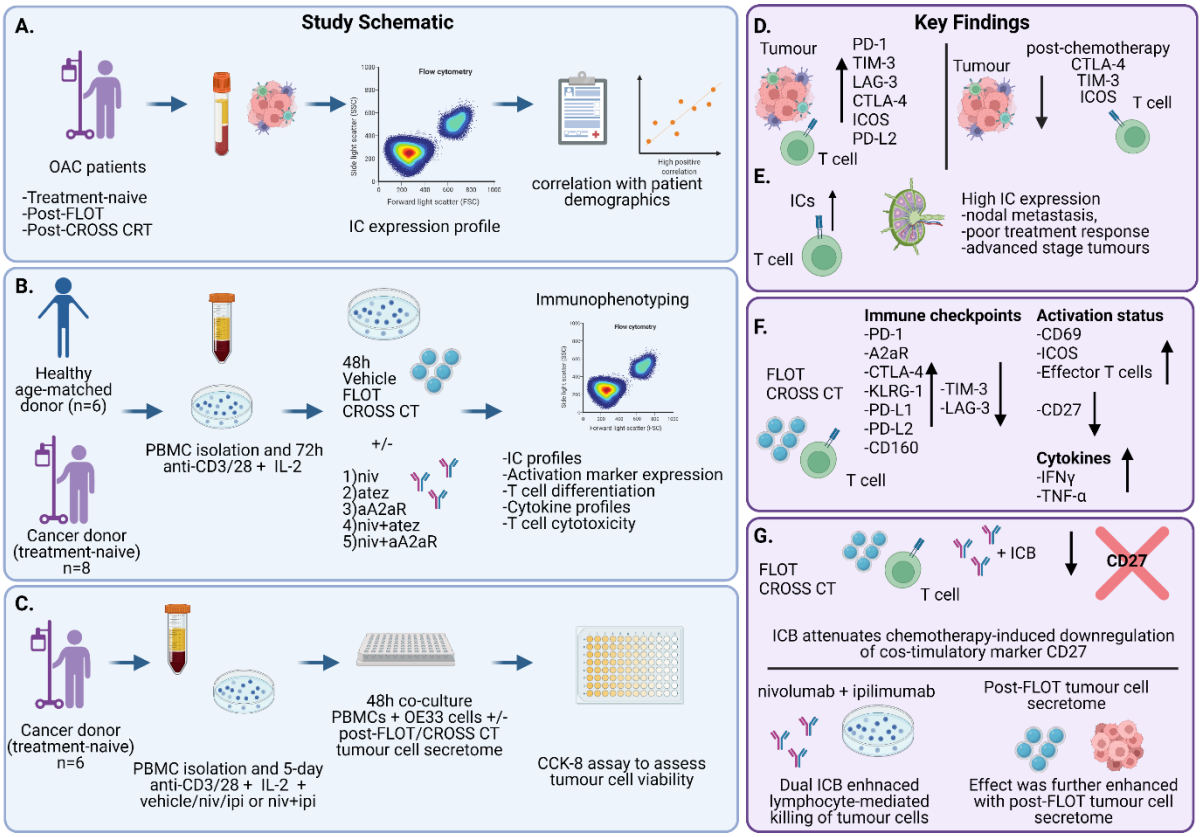

Graphical abstract: Study schematic - (A) Immune checkpoint (IC) expression profiles of T cells in tumour biopsies and whole blood from OAC patients was assessed by flow cytometry and correlated with clinical demographics. (B) The effect of first-line chemotherapy regimens on anti-tumour T cell phenotypes was next assessed using flow cytometry. PBMCs were isolated from age-matched healthy donor and OAC donor blood and expanded *ex vivo* for 72h using anti-CD3/28 + IL-2 T cell activation protocol followed by an additional 48h treatment with vehicle, FLOT or CROSS chemotherapy (CT) regimens in the absence and presence of immune checkpoint blockade (ICB). (C) The ability of ICB to boost the cytolytic effector function of OAC donor lymphocytes was next assessed in the absence and presence of post-vehicle/FLOT/CROSS CT tumour cell secretome to determine if the chemotherapy altered tumour microenvironment enhanced lymphocyte-mediated killing of tumour cells. Collection of post-chemotherapy tumour cell secretome: OE33 cells were treated for 48h with vehicle/FLOT/CROSS CT and washed twice with PBS. Tumour cell secretome was then harvested an additional 48h later. Key Findings – (D) ICs were upregulated on tumour-infiltrating T cells. CTLA-4, TIM-3 and ICOS were decreased 6 weeks post-FLOT or CROSS chemoradiotherapy treatment on tumour-infiltrating T cells. (E) IC expression correlated with more advanced staged tumours, nodal metastasis and poor response to treatment. (F) The direct 48h effects of FLOT and CROSS CT treatment revealed that these regimens upregulated a range of ICs and downregulated TIM-3 and LAG-3 on T cells *ex vivo*. Co-stimulatory markers were differentially affected, ICOS and CD69 were upregulated however CD27

was downregulated on T cells. Anti-tumour T cell cytokine profiles were also enhanced. (G) ICB attenuated the chemotherapy-mediated downregulation of CD27. Dual nivolumab and ipilimumab treatment increased lymphocyte-mediated killing of tumour cells which was further enhanced in the presence of post-FLOT tumour cell secretome suggesting the potential of immunostimulatory synergism between first-line OAC chemotherapy regimens and ICB.

6.1.2 Introduction

Targeting inhibitory immune checkpoints (ICs) is an attractive therapeutic strategy to reinvigorate exhausted anti-tumour immunity in oeosphageal adenocarcinoma (OGJ)[163]. The current standard of care for resectable OGJ includes the peri-operative FLOT chemotherapy-based regimen[9]. The FLOT regimen includes 5-fluorouracil (5-FU), leucovorin, oxaliplatin and a taxane (such as the anti-microtubule agent docetaxel) before (neoadjuvant) and after surgery (adjuvant). The perioperative MAGIC chemotherapy regimen was commonly used as part of the standard of care up until recent years as findings from the FLOT4 trial demonstrated that FLOT was superior than MAGIC (median overall survival: 50 months vs. 35 months)[357]. Therefore, the MAGIC chemotherapy regimen is no longer used as part of the standard of care for OGJ patients [9]. The MAGIC chemotherapy regimen includes a topoisomerase inhibitor epirubicin, a platinum-based DNA intercalator cisplatin and an anti-metabolite 5-FU (ECF) or capecitabine (a pro-drug of 5-FU) (ECX)[321]. Multimodal chemoradiotherapy is also an option for OGJ patients and includes the CROSS regimen (paclitaxel and carboplatin with a cumulative radiation dose of 41.4 Gy over 23 fractions) followed by surgery[12]. However, a significant proportion of OGJ patients fail to derive a curative response from current standards of care, with only approximately 30% of patients achieving a complete pathological response[20]. Immune checkpoint blockers (ICBs) are an immunotherapeutic option for OGJ patients and have already exhibited clinical efficacy in a wide range of cancer types. Immunotherapy is now considered by many as the fifth pillar of cancer therapy along with surgery, chemotherapy, radiotherapy and molecular targeted therapies[21].

This timely study investigates the immunostimulatory and immunosuppressive properties of single agent chemotherapies and combination chemotherapy regimens used in the treatment of OGJ patients on T cell activation status and cytotoxicity. Combining immunostimulatory chemotherapies which are capable of inducing immunogenic cell death (ICD) with ICIs to synergistically enhance anti-tumour immunity is emerging as an attractive therapeutic tool[130,358]. However, there is a wide range of chemotherapies that comprise the standard of care

for OGJ patients and little is known regarding their ability to induce ICD, which is necessary to break peripheral tolerance. The potential of FLOT, CROSS or MAGIC chemotherapies to elicit ICD in OGJ cells or decrease surrogate markers of immunogenicity remains largely unknown. Furthermore, the OGJ tumour microenvironment (TME) consists of immunosuppressive cellular factors and soluble mediators, which will be profoundly altered by chemoradiotherapy (CRT) treatment[98,359], particularly within the treatment-resistant tumours which remain post-FLOT chemotherapy and post-CROSS CRT. Therefore, we also assessed T cell activation status in the treatment-naïve setting and post-FLOT and post-CROSS CRT setting by profiling OGJ patient-derived circulating T cells and tumour-infiltrating T cells. The effect of the tumour conditioned media collected from *ex vivo* tumour explants post-FLOT and post-CROSS CRT on T cell activation and lymphocyte-mediated killing of OE33 cells were also investigated. This data will help guide the rational combination of immunostimulatory combination chemotherapy regimens with ICIs for treating OGJ.

Immune checkpoint (IC) pathways control the magnitude and duration of the immune response, preventing overactivation of the immune system, which could lead to the development of autoimmunity[58]. ICBs block IC pathways, reinvigorating anti-tumour immunity[21]. Single agent pembrolizumab (Keytruda), an anti-PD-1 monoclonal antibody, was FDA-approved for the treatment of advanced or recurrent oesophagogastric cancers in the third-line setting for tumours expressing PD-L1 (combined positive score (CPS) ≥1)[63]. In 2021, nivolumab (Opdivo) was FDA approved for patients with completely resected esophageal or gastroesophageal junction cancer with residual pathologic disease who have received neoadjuvant chemoradiotherapy based on findings from the CHECKMATE-577 trial (NCT02743494).

To date the majority of clinical trials in all cancers including OGJ have largely focussed on testing the efficacy of blocking PD-1 and CTLA-4 IC pathways, despite the vast array of potentially targetable ICs expressed on the surfaces of T cells[59–62].

Novel ICs which represent targetable therapeutic options for OGJ patients, to be given alone or in combination with PD-1 or CTLA-4 ICB, include lymphocyte activation gene-3 (LAG-3), T cell immunoglobulin-mucin domain-3 (TIM-3), T cell immunoglobulin and ITIM domain (TIGIT), adenosine A2a receptor (A2aR)[21] and CD160 (ligand for herpes virus entry mediator)[21]. Despite belonging to the same class of receptors as PD-1 and CTLA-4, the ICs TIM-3, TIGIT and LAG-3 exhibit unique functions, especially at tissue sites where they regulate distinct aspects of immunity[289].

Interestingly, recent studies have demonstrated that combining immune checkpoint blockers (ICB) with the standard of care chemotherapy regimens in OGJ patients can boost clinical outcomes[136]. ICBs are thought to be largely ineffective in non-immunogenic 'cold' tumours, where there is an absence of pre-existing anti-tumour immunity and therefore no immune response to reinvigorate[67]. However, chemotherapies are emerging as a valuable tool to convert 'cold' tumours to 'hot' tumours through different mechanisms. For example, chemotherapy-induced DNA damage in cancer cells can generate neoantigens, which then activate anti-tumour specific T cell responses. This is an attractive strategy to sensitise TMB-low tumours to ICBs[129]. In addition, immunostimulatory chemotherapies induce immunogenic cell death via the release of damage-associated molecular patterns into the extracellular tumour microenvironment[146]. Damage-associated molecular patterns induce maturation and activation of dendritic cells and subsequent activation and mobilisation of anti-tumour T cells to the tumour site[147].

To support the synergy between chemotherapy and ICB combinations in OGJ the phase III CheckMate 649 trial demonstrated that combining nivolumab with first-line chemotherapy (FOLFOX and XELOX) in previously untreated OGJ patients (n=1,581), significantly improved overall survival in patients with a PD-L1 combined positive score of 5 or greater (14.4 months (nivolumab + chemotherapy arm) vs. 11.1 months (chemotherapy arm))[136]. Furthermore, the nivolumab + chemotherapy arm also reduced the risk of death by 29% (HR, 0.71; 98.4% CI, 0.59-0.86; $p<0.0001$)[136]. The findings from this trial highlight the potential therapeutic synergy that can be exploited between chemotherapy and ICB.

However, the effects of chemotherapy on IC expression profiles in the context of OGJ remain unknown, as are the direct and indirect effects of first-line chemotherapy regimens on anti-tumour T cell responses in OGJ. This study aims to address these important gaps in research knowledge by profiling IC expression in OGJ patients in the neoadjuvant and adjuvant setting. The direct effects of first-line chemotherapy regimens FLOT and CROSS on T cell cytokine profiles and anti-tumour T cell responses are also investigated. These findings may help inform the selection of appropriate ICs to target in OGJ and the sequenced timing of ICB with current standards of care.

6.1.3 Specific aims

1. Investigate the ability of first-line chemotherapy regimens to induce immunogenic cell death in OGJ cell lines *in vitro*.

2. Assess the direct and indirect effects of first-line chemotherapy regimens on T cell activation status and cytokine profiles using *in vitro* and *ex vivo* culture systems to simulate the tumour microenvironment.
3. Determine if the chemotherapy-altered tumour cell secretome hinders or potentiates lymphocyte-mediated cytolysis of OGJ cells *in vitro*.
4. Investigate the IC expression profile of circulating and tumour-infiltrating T cells in the treatment naïve and post-neoadjuvant treatment setting of OGJ patients.
5. Assess the direct effects of first-line chemotherapies on IC expression profiles of healthy donor and OGJ patient-derived T cells *ex vivo*.
6. Determine if ICB alters IC expression profiles of OGJ patient-derived T cells *ex vivo* which could mediate acquired resistance to ICB.
7. Investigate if ICB might enhance OGJ patient-derived T cell activation status in the absence or presence of first-line chemotherapies *ex vivo*.
7. Determine if ICB might potentiate OGJ patient-derived lymphocyte mediated cytolysis of OGJ cells *in vitro* in the absence or presence of post-FLOT or post-CROSS CT tumour cell secretome.

6.2 Results

6.2.1 FLOT and CROSS chemotherapy regimens upregulate surrogate markers of immunogenicity on OGJ cell lines

As the immunogenicity of tumours vary significantly across patients, we investigated the basal immunogenicity of two OGJ cell lines (OE33 and SK-GT-4 cells). Both cell lines were screened by flow cytometry for the surface expression of damage-associated molecular patterns (DAMPs), which included high-mobility group box-1 protein (HMGB1), calreticulin, MIC-A/B, human leukocyte antigen complex–DR isotype (HLA-DR) and MHC class I-related chain-related gene A/B (MIC A/B)[360]. SK-GT-4 cells had a significantly higher percentage expression of HMGB1 compared to OE33 cells (7.51±0.9 vs. 1.95±0.5%, p=0.005) (**Figure 6.1A**). Similarly, there was also a significantly higher percentage of SK-GT-4 cells expressing calreticulin basally compared to OE33 cells (10.69 ± 0.7 vs. 1.86 ± 0.2%, p=0.0003) (**Figure 6.1A**). There was no significant difference in the expression of MIC-A/B between OE33 cells and SK-GT-4 cells (**Figure 6.1A**). There was no statistically significant difference between the percentage of OE33 cells and SK-GT-4 cells expressing HLA-DR (p=0.06) (**Figure 6.1A**).

An important therapeutic rationale for combining chemotherapy with ICIs is the chemotherapy-induction of ICD in tumour cells, thus generating an anti-tumour immune response whereby the addition of ICIs prevents or overrides exhaustion of the chemotherapy-induced anti-tumour immune response[163]. Therefore, we sought to investigate if the single agent chemotherapies used to treat OGJ and their combination as part of the FLOT, CROSS CT and MAGIC chemotherapy regimens upregulate markers of ICD in these two OGJ cells lines: the OE33 cell line which basally expresses lower levels of DAMPs than the SK-GT-4 cell line (**Figure 6.1A**). OE33 and SK-GT-4 cells were treated with an IC_{50} dose of single agent chemotherapies or an IC_{50} dose of a combination chemotherapy regimen FLOT, CROSS CT or MAGIC for 48h. The IC_{50} dose for each combination chemotherapy regimen comprised of lower doses of each single agent chemotherapy but resulted in an overall 50% reduction in viability.

FLOT treatment significantly increased the percentage of OE33 and SK-GT-4 cells expressing HMGB1 (OE33: untrx 2.36 ± 0.5 vs 11.23 ± 1.8%, p=0.0007 and SK-GT-4: 5.63 ± 1.2 vs 13.17 ± 2.0%, p=0.004), (**Figure 6.1B**). Conversely, MAGIC treatment significantly decreased the percentage of OE33 cells expressing HMGB1 (2.36 ± 0.5 vs 0.50 ± 0.1%, p=0.03) and specifically epirubicin, a component of the MAGIC regimen, significantly decreased the percentage of SK-GT-4 cells expressing HMGB1 (5.63 ± 1.2 vs. 1.09 ± 0.5%, p=0.02), (**Figure 6.1B**) Treatment with the remaining single agent chemotherapies or CROSS CT regimen did not significantly affect the expression levels of HMGB1.

Following FLOT, CROSS CT and MAGIC chemotherapy treatment, the percentage of OE33 cells and SK-GT-4 cells expressing calreticulin did not significantly change (**Figure 6.1B**). However, single agent treatment with carboplatin and cisplatin, which comprise the CROSS regimen and MAGIC regimen respectively, significantly increased the percentage of OE33 cells expressing calreticulin (untrx: 5.59 ± 1.6% vs. carboplatin: 33.57 ± 1.8% p=0.01, and cisplatin: 27.57 ± 1.7%, p=0.03) (**Figure 6.1B**). Additionally, following single agent 5-FU and docetaxel treatment there was an increase in the percentage of OE33 cells expressing calreticulin (untrx: 5.59 ± 1.6% vs. 5-FU: 24.03 ± 1.6% p=0.06, and docetaxel: 30.07 ± 3.3%, p=0.06) (**Figure 6.1B**).

Single agent 5-FU and oxaliplatin (comprise the FLOT regimen) significantly increased the percentage of OE33 cells expressing MIC-A/B (untrx: 31.54 ± 11.7 vs. 5-FU: 62.75 ± 5.6%, p=0.007 and oxaliplatin: 65.73 ± 5.8%, p=0.004) (**Figure 6.1B**). Similar findings were found in the SK-GT-4 cells using 5-FU and docetaxel and the FLOT combination regimen (untrx: 7.84 ± 1.7 vs. 5-FU: 17.06 ± 1.3% p= 0.02, docetaxel: 21.82 ± 3.0% p= 0.02 and FLOT: 20.8

± 3.5% p=0.02) (**Figure 6.1B**). Single agent carboplatin or paclitaxel and the combination CROSS CT regimen did not significantly affect the percentage of OE33 cells expressing MIC-A/B, whereas single agent carboplatin, paclitaxel and CROSS CT regimen significantly increased the percentage of SK-GT-4 cells expressing MIC-A/B (untrx: 7.84 ± 1.7% vs. carboplatin: 25.7 ± 5.1% p=0.04, paclitaxel: 29.96 ± 4.0% p=0.007 and CROSS CT: 31.43 ± 2.8%, p=0.0005) (**Figure 6.1B**). Furthermore, single agent epirubicin significantly decreased the percentage of OE33 and SK-GT-4 cells expressing MIC-A/B (untrx: 7.84 ± 1.7% vs. epirubicin: 4.31 ± 0.9% p=0.001) (**Figure 6.2B**). Whereas, cisplatin significantly increased MIC-A/B expression levels in the OE33 cells and SK-GT-4 cells (untrx: 7.84 ± 1.7% vs. cisplatin: 27.8 ± 1.0% p=0.007). MAGIC regimen only significantly increased the percentage of MIC-A/B positive cells in the OE33 cell line (untrx: 7.84 ± 1.7% vs. MAGIC: 29.82 ± 10.2% p=0.007) but not the SK-GT-4 cell line (**Figure 6.1B**).

Treatment with single agent chemotherapies comprising the FLOT regimen as well as the combination FLOT regimen significantly increased the percentage of OE33 cells expressing HLA-DR (untrx: 1.06 ± 0.1% vs. 5-FU: 3.27 ± 0.2%, p=0.0002, docetaxel: 2.60 ± 0.5%, p=0.04 and FLOT: 8.7 ± 1.5%, p=0.002) (**Figure 6.1B**). Similar findings were observed in the SK-GT-4 cell line (untrx: 0.89 ± 0.1% vs. 5-FU: 3.35 ± 0.7%, p=0.01, oxaliplatin: 3.6 ± 0.6%, p=0.003, docetaxel: 4.17 ± 0.9%, p=0.01 and FLOT: 5.0 ± 0.3% p<0.0001) (**Figure 6.1B**). Single agent treatment with carboplatin or paclitaxel did not significantly affect the percentage of OE33 cells expressing HLA-DR, however, CROSS CT treatment significantly increased the percentage of HLA-DR$^+$ OE33 cells (untrx: 1.06 ± 0.1% vs. CROSS CT: 3.46 ± 0.6% p=0.006). Similar findings were observed in the SK-GT-4 cell line where single agent carboplatin and paclitaxel as well as the combination of both (CROSS CT), significantly increased the percentage of HLA-DR$^+$ SK-GT-4 cells (untrx: 0.89 ± 0.1% vs. carboplatin: 3.34 ± 1.0% p=0.04, paclitaxel: 5.80 ± 1.0%, p=0.002 and CROSS CT: 4.11± 0.7%, p=0.003) (**Figure 6.1B**). Cisplatin significantly increased the percentage of OE33 and SK-GT-4 cells expressing HLA-DR whereas, epirubicin significantly increased HLA-DR expression on OE33 cells yet paradoxically decreased the percentage of SK-GT-4 cells expressing HLA-DR (OE33 untrx: 1.06 ± 0.1% vs. cisplatin: 4.43 ± 0.9%, p=0.02 and epirubicin: 5.0 ± 1.07%, p=0.006 and SK-GT-4: untrx: 0.89 ± 0.1% vs. cisplatin: 8.03 ± 1.7%, p=0.004 and epirubicin: 0.18 ± 0.04%, p=0.0008) Additionally, there was a decrease in HLA-DR expression on OE33 cells following MAGIC treatment (1.06 ± 0.1% vs. 0.64 ± 0.1% p=0.05, respectively).

Overall, the FLOT and CROSS CT regimens demonstrated the greatest immunogenic potential via upregulation of surrogate markers of ICD upon treatment with single agent chemotherapies comprising these regimens or the combination of these chemotherapies. MAGIC demonstrated the least immunogenic potential and in particular single agent epirubicin decreased surrogate markers of ICD and may be a key contributor to the reduced ICD potential of MAGIC compared with FLOT and CROSS CT regimens.

A.


OE33 cells
SK-GT-4 cells
% cells expressing
30
20
10
0
**
***
P = 0.06
HMGB1
calreticulin
MIC-A/B
HLA-DR

B.

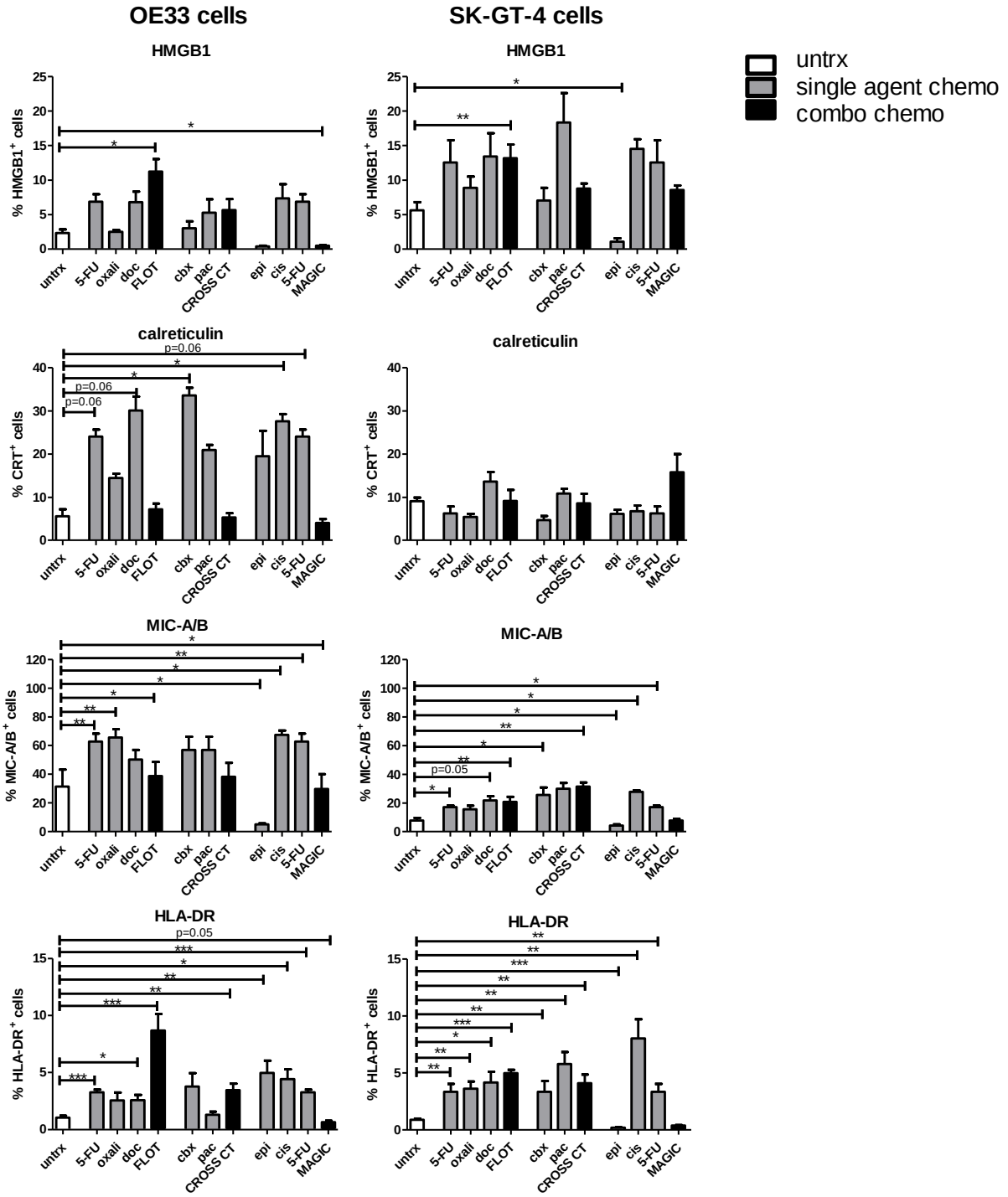
OE33 cells
SK-GT-4 cells
untrx
single agent chemo
combo chemo
HMGB1
% HMGB1+ cells
calreticulin
% CRT+ cells
p=0.06
MIC-A/B
% MIC-A/B+ cells
p=0.05
HLA-DR
% HLA-DR+ cells
untrx
5-FU
oxali
doc
FLOT
cbx
pac
CROSS CT
epi
cis
5-FU
MAGIC

Figure 6.1: FLOT and CROSS chemotherapy regimens significantly upregulate DAMPs on the surface of viable OE33 and SK-GT-4 cells *in vitro*. (A) OE33 and SK-GT-4 cells were screened for the basal expression of HMGB1, calreticulin, MIC-A/B and HLA-DR by flow cytometry, n=3, unpaired parametric t-test. (B) OE33 cells and SK-GT-4 cells were treated with clinically relevant single agent chemotherapies (single agent chemo) or combination chemotherapy regimens (combo chemo) FLOT, CROSS CT and MAGIC for 48h. Surface expression of HMGB1, CRT, MIC-A/B and HLA-DR on viable OGJ cells was determined by flow cytometric analysis. Zombie viability dye was used to exclude dead cells. Paired parametric t-test compared to untreated (untrx) controls, n=3 *p<0.05, **p<0.01, ***p<0.001. Gating strategy and representative dot plots for DAMP expression on the surface of OGJ cells are shown in Appendix **Figure A6.1**.

6.2.2 Clinically-relevant single agent chemotherapies directly upregulate markers of T cell activation on viable Jurkat cells

To successfully identify immunostimulatory chemotherapies as complementary synergistic partners to combine with immunotherapies for OGJ patients it is important to determine the effect of individual chemotherapies on T cell activation state. Existing research demonstrates that chemotherapies have profound systemic immunomodulatory properties through depletion of Tregs and MDSCs in lung cancer. Depending on the agent, chemotherapies can enhance or suppress anti-tumour immunity. A significant proportion of this research has focused on a limited number of chemotherapies in particular cyclophosphamide. However, eight different chemotherapies are used in several combination regimens as part of the standard of care for treating OGJ patients and their effect of T cell activation status is unknown and remains largely under-investigated.

Therefore, we sought to investigate the effect of single agent clinically-relevant chemotherapies on the activation status of activated T cells (**Figure 6.3**). Jurkat cells were activated in the presence of an IC_{50} dose of single agent 5-FU, capecitabine, cisplatin, oxaliplatin, epirubicin, docetaxel, carboplatin and paclitaxel and the expression of markers reflective of T cell activation status were assessed including: CD62L, CD45RA, CD45RO, CD27 and CD69 (**Figure 6.3**). 48h IC_{50} doses for Jurkat cells are in (**Figure 6.2**). Upon T cell activation CD62L and CD45RA downregulate and CD27 and CD69 upregulate and are characteristic features of T cell activation.

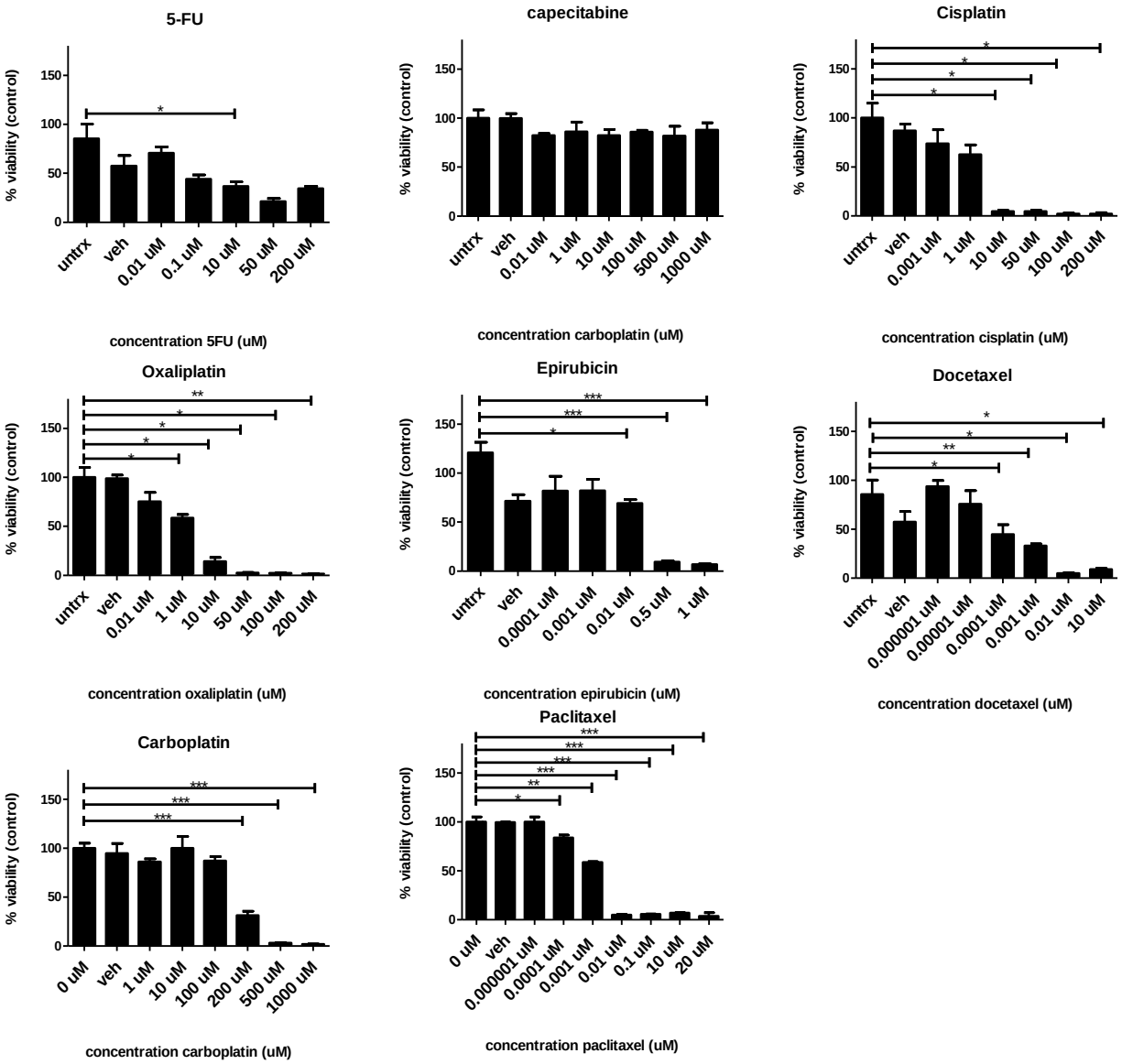

Figure 6.2 Clinically relevant single agent chemotherapies display increasing cytotoxicity in a dose-dependent manner against Jurkat cells following 48h. Jurkat cells were treated with a range of increasing concentrations of single agent 5-fluorouracil, capecitabine, cisplatin, oxaliplatin, epirubicin, docetaxel, carboplatin and paclitaxel for 48h. Cell viability was assessed by a CCK-8 assay. (n=3) Expression presented as a percentage ±SEM of the untreated control. Paired parametric t-test, *p<0.05, **p<0.01 and ***p<0.001.

Capecitabine, oxaliplatin and epirubicin significantly decreased the percentage of Jurkat cells expressing CD62L (untreated activated: 35.17 ± 5.0 vs. capecitabine: 15.1 ± 4.7, oxaliplatin: 17.93 ± 2.7 and epirubicin: 1.85 ± 0.3% respectively, p=0.0161, p=0.0203 and p=0.0195,

respectively), (**Figure 6.3A**). 5-FU, cisplatin, docetaxel, carboplatin and paclitaxel did not significantly affect the percentage of Jurkat cells expressing CD62L.

Following epirubicin and docetaxel treatment the percentage of Jurkat cells expressing CD45RA was significantly decreased (untreated activated: 96.10 ± 0.7 vs. epirubicin: 75.30 ± 2.9 and docetaxel: 90.37 ± 0.8% respectively, p=0.0130 and p=0.0198, respectively), (**Figure 6.3A**). 5-FU, capecitabine, cisplatin, oxaliplatin, carboplatin and paclitaxel did not significantly affect the percentage of cells expressing CD45RA, (**Figure 6.3A**).

Following cisplatin, oxaliplatin and docetaxel treatment the percentage of Jurkat cells expressing CD45RO had significantly increased (untreated activated: 21.30 ± 2.2 vs. cisplatin: 34.57 ± 2.2, oxaliplatin: 35.67 ± 5.2 and docetaxel: 32.33 ± 3.59%, respectively, p=0.0087, p=0.0423 and p=0.0180, respectively), (**Figure 6.3A**). Epirubicin significantly decreased the percentage of Jurkat cells expressing CD45RO (untreated activated: 21.30 ± 2.2 vs. epirubicin: 6.81 ± 1.2%, p=0.0055), (**Figure 6.3A**). 5-FU, capecitabine, carboplatin and paclitaxel did not significantly affect the percentage of Jurkat cells expressing CD45RO, (**Figure 6.3A**).

Cisplatin, oxaliplatin and docetaxel significantly increased the percentage of Jurkat cells expressing CD27 (untreated activated: 8.02 ± 1.6 vs. cisplatin: 22.17 ± 0.9, oxaliplatin: 17.17 ± 2.1 and. docetaxel: 26.17 ± 1.0%, respectively, p=0.0188, p=0.0216 and p=0.0025, respectively), (**Figure 6.3A**). 5-FU, capecitabine and epirubicin did not significantly affect the percentage of Jurkat cells expressing CD27, (**Figure 6.3A**). Epirubicin significantly decreased the percentage of Jurkat cells positive for CD69 expression (untreated activated: 28.50 ± 4.5 vs. 1.85 ± 0.3%, respectively p=0.0304), (**Figure 6.3A**). 5-FU, capecitabine, cisplatin, oxaliplatin, docetaxel, carboplatin and paclitaxel did not significantly affect the percentage of Jurkat cells positive for CD69 expression, (**Figure 6.3A**).

Capecitabine, oxaliplatin, epirubicin and docetaxel significantly decreased the frequency of naïve Jurkat cells (untreated activated: 37.6 ± 3.1 vs. capecitabine: 14.76 ± 3.5, oxaliplatin: 16.2 ± 0.5, epirubicin: 2.43 ± 0.3 and docetaxel: 21.7 ± 0.1%, respectively p=0.0109, p=0.0176, p=0.0086 and p=0.0355, respectively), (**Figure 6.3B**). 5-FU, carboplatin and paclitaxel did not significantly affect the frequency of naïve Jurkat cells, (**Figure 6.3B**).

Only epirubicin significantly increased the percentage of central memory Jurkat cells (untreated activated: 9.030 ± 2.1 vs. epirubicin: 50 ± 4.5%, respectively p=0.0152), (**Figure 6.3B**). Capecitabine, cisplatin, oxaliplatin and epirubicin significantly increased the percentage of pre-terminally differentiated effector memory Jurkat cells (untreated activated: 15.43 ± 0.8 vs. capecitabine: 29.17 ± 3.7, cisplatin: 22.63 ± 1.4, oxaliplatin: 27.3 ± 3.2 and epirubicin: 50

± 4.5%, respectively p=0.0416, p=0.0379, p=0.0485 and p=0.0213, respectively), (**Figure 6.3B**). 5-FU, docetaxel, carboplatin and paclitaxel did not significantly affect the percentage of pre-terminally differentiated effector memory Jurkat cells, (**Figure 6.3B**).

Capecitabine, oxaliplatin and docetaxel significantly increased the percentage of effector memory Jurkat cells (untreated activated: 37.97 ± 5.5, capecitabine: 49.2 ± 5.1, oxaliplatin: 46.1 ± 6.1 and docetaxel: 45.8 ± 4.2%, respectively, p=0.0226, p=0.0014 and p=0.0261, respectively), (**Figure 6.3B**). 5-FU, cisplatin, epirubicin, carboplatin and paclitaxel did not significantly affect the frequency of effector memory Jurkat cells, (**Figure 6.3B**).

Overall, cisplatin, oxaliplatin and docetaxel appeared to have the greatest effect at enhancing T cell activation demonstrated by upregulation of markers of T cell activation (CD27 and CD45RO), whereas epirubicin decreased CD45RO and CD69 T cell activation markers.

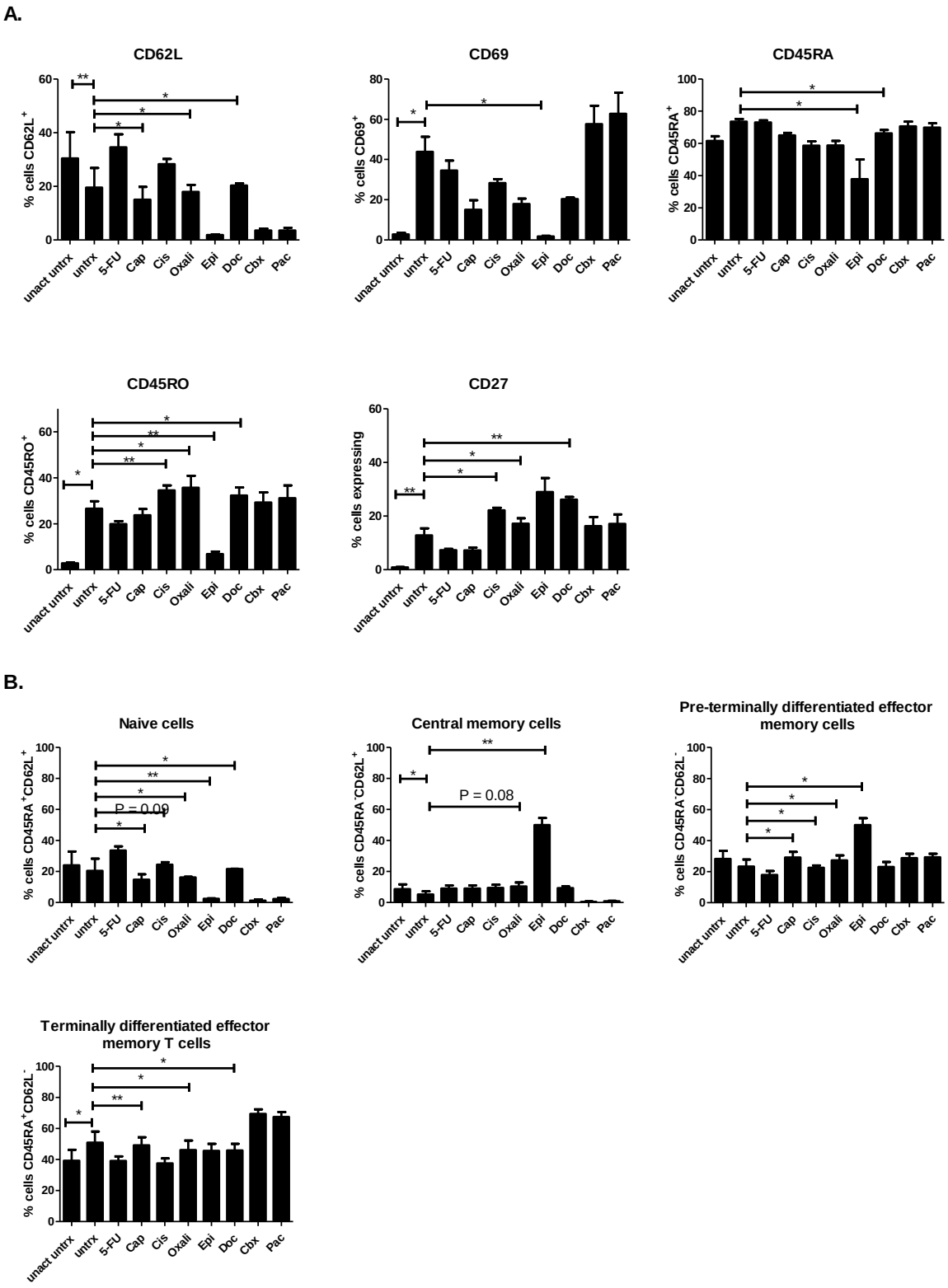

Figure 6.3: Single agent cisplatin, oxaliplatin and docetaxel significantly increase the percentage of viable Jurkat cells expressing CD27 and CD45RO *in vitro*. Jurkat cells were activated with plate bound anti-CD3 and anti-CD28 for 48h in the presence or absence of single agent 5-fluorouracil (5-FU), capecitabine (cap), cisplatin (cis), oxaliplatin (oxali), epirubicin (epi), docetaxel (doc), carboplatin

(cbx) or paclitaxel (pac) using a pre-optimised 48h IC_{50} dose. The expression of markers reflective of T cell activation state were assessed on viable Jurkat cells using a zombie viability dye to exclude dead cells by flow cytometry. Marker assessed included: CD62L, CD69, CD45RA, CD45RO, and CD27 (A). The percentage of viable naïve ($CD45RA^+CD62L^+$), central memory ($CD45RA^-CD62L^+$), pre-terminally differentiated effector memory ($CD45RA^-CD62L^-$) and effector memory ($CD45RA^+CD62L^-$) Jurkat cells were also determined by flow cytometry (B). Experiments repeated n=3 times, paired parametric t-test, *p<0.05, **p<0.01 and ***p<0.001.

6.2.3 FLOT and CROSS CT regimens directly alter the expression of co-stimulatory molecules on the surface of OGJ patient-derived T cells and increase the percentage of effector memory T cells

Expression of T cell activation markers including ICOS play important roles in promoting effector T cell function in anti-tumour immune responses[361]. Therefore, to further interrogate the direct effects of first-line chemotherapy regimens on T cell activation status, healthy donor (HD) and OGJ patient-derived (CD) PBMCs were treated *ex vivo* with either a vehicle or first-line combination chemotherapy regimens FLOT or CROSS CT and the expression of T cell activation markers and differentiation state were subsequently profiled (**Figure 6.4**).

Interestingly, ICOS was expressed at significantly lower levels on the surface of T cells from CDs compared with HDs within the $CD4^+$ T cell compartment (33.77 ± 5.7 vs. 77.80 ± 3.3% p=0.002) and $CD8^+$ T cell compartment (40.47 ± 5.8 vs. 67.20 ± 3.9% p=0.008), (**Figure 6.4A**). There was also a significantly higher frequency of central memory $CD4^+$ T cells from CDs compared with HDs (20.08 ± 5.2 vs. 4.6 ± 1.2% p=0.02). CD62L was expressed at significantly higher levels on the surface of $CD4^+$ T cells from CDs compared with $CD4^+$ T cells from HDs (68.78 ± 2.8 vs. 30.33 ± 5.7% p=0.002) (**Figure 6.4A**). Additionally, there was significantly lower frequencies of terminally differentiated effector memory $CD4^+$ T cells from CDs compared with HDs (6.12 ± 3.8 vs. 25.28 ± 6.6%, p=0.03 and p=0.02) (**Figure 6.4A**).

FLOT and CROSS CT significantly altered the expression of T cell activation markers in HDs and CDs. Interestingly, FLOT and CROSS CT significantly increased ICOS expression on the surface of CD $CD4^+$ T cells (51.47 ± 5.7, vs. 50.75 ± 6.3 and 33.77 ± 5.7%, p=0.03 and p=0.03) and $CD8^+$ T cells (53.32 ± 4.8 vs. 55.20 ± 4.6 and 40.47 ± 5.8%, p=0.03 and p=0.03) compared with the vehicle control from CDs (**Figure 6.4A**). However, FLOT and CROSS CT had no significant effect on ICOS expression on the surface of T cells from HDs (**Figure 6.4A**). FLOT and CROSS CT significantly decreased CD62L expression on the surface of $CD4^+$ T cells compared with the vehicle control in both HDs (23.77 ± 4.7, vs. 19.51 ± 4.8 and 30.33 ± 5.7%,

p=0.03 and p=0.03) and CDs (47.55 ± 2.3, vs. 45.82 ± 4.9 and 68.78 ± 2.8%, p=0.03 and p=0.03), (**Figure 6.4A**). Similarly, FLOT and CROSS CT also significantly decreased CD62L expression on the surface of $CD8^+$ T cells compared with the vehicle control in both HDs (22.40 ± 3.5, vs. 14.44 ± 3.2 and 32.10 ± 5.1%, p=0.03 and p=0.03) and CDs (30.67 ± 3.7 vs. 27.15 ± 4.0 and 47.72 ± 6.8%, p=0.03 and p=0.03) (**Figure 6.4A**). FLOT and CROSS CT significantly increased CD69 expression on the surface of $CD4^+$ T cells (15.86 ± 4.3 vs. 15.57 ± 4.1 and 8.73 ± 4.2%, p=0.03 and p=0.03) and $CD8^+$ T cells compared with the vehicle control from CDs (15.01 ± 1.7 vs. 17.02 ± 2.4 and 7.33 ± 2.1%, p=0.03 and p=0.03) but not HDs (**Figure 6.4A**). In contrast, FLOT and CROSS CT significantly decreased CD27 expression on the surface of $CD4^+$ T cells compared with the vehicle control in both HDs (20.79 ± 5.8 vs. 26.51 ± 7.7 and 31.27 ± 7.4%, p=0.03 and p=0.03) and CDs (10.39 ± 1.9 vs. 11.25 ± 2.4 and 27.97 ± 4.9%, p=0.03 and p=0.03) (**Figure 6.4A**). Similarly, FLOT and CROSS CT significantly decreased CD27 expression on the surface of $CD8^+$ T cells compared with the vehicle control in both HDs (15.27 ± 4.8 vs. 20.63 ± 6.7 and 26.67 ± 7.3%, p=0.03 and p=0.03) and CDs (5.03 ± 1.5 vs. 5.73 ± 1.4 and 16.98 ± 2.7%, p=0.03 and p=0.03) (**Figure 6.4A**). Chemotherapy treatment had no significant effects on CD45RA expression on the surface of T cells in both HDs and CDs (**Figure 6.4A**).

FLOT significantly decreased the percentage of naïve $CD4^+$ T cells compared with the vehicle control in CDs (1.53 ± 0.6 vs. 3.49 ± 1.8, p=0.03) but not HDs (**Figure 6.4B**). However, FLOT significantly decreased the percentage of naïve $CD8^+$ T cells compared with the vehicle control in both CDs (3.98 ± 1.2 vs. 8.95 ± 3.1, p=0.03) and HDs (1.72 ± 0.7 vs. 5.30 ± 1.8, p=0.03) **Figure 6.4B**). The percentage of central memory $CD4^+$ T cells was significantly decreased post-CROSS CT treatment compared with the vehicle control in CDs (7.41 ± 2.0 vs. 20.08 ± 5.2, p=0.03) but not HDs (**Figure 6.4B**). Similar trends were observed whereby CROSS CT significantly decreased the frequency of central memory $CD8^+$ T cells compared with the vehicle control in CDs (4.87 ± 1.2 vs. 14.57 ± 3.1, p=0.03) only but not HDs (**Figure 6.4B**). Interestingly, FLOT and CROSS CT significantly increased the frequency of effector memory $CD4^+$ T cells compared with the vehicle control in CDs (82.40 ± 3.3 vs. 80.72 ± 2.6 and 64.13 ± 4.0, p=0.03 and p=0.03) and HDs (71.35 ± 6.5 vs. 65.50 ± 7.6 and 59.95 ± 7.4, p=0.03 and p=0.03) (**Figure 6.4B**). Similarly, FLOT and CROSS CT significantly increased the frequency of effector memory $CD8^+$ T cells compared with the vehicle control in CDs (84.08 ± 5.5 vs. 84.02 ± 2.5 and 69.53 ± 6.5, p=0.03 and p=0.03) and HDs (74.13 ± 5.3 vs. 66.42 ± 6.6 and 60.07 ± 7.2, p=0.03 and p=0.03) (**Figure 6.4B**). FLOT and CROSS CT significantly decreased

the percentage of terminally differentiated effector memory $CD8^+$ T cells compared with the vehicle control in HDs (15.56 ± 5.2, 19.47 ± 6.6 vs. 24.83 ± 6.8%, p=0.03 and p=0.03) but not from CDs (**Figure 6.4B**).

In summary, CD T cells expressed significantly lower levels of co-stimulatory IC ICOS on their surface compared with HDs. Furthermore, first-line combination chemotherapy regimens substantially altered the expression of co-stimulatory ICs on the surface of T cells from CDs and HDs, as well as T cell differentiation status. Both FLOT and CROSS CT significantly reduced the expression of co-stimulatory IC CD27 on the surface T cells from both CDs and HDs, whereas FLOT and CROSS significantly upregulated co-stimulatory IC CD69 on the surface of CD T cells but not HD T cells. In addition, FLOT and CROSS CT significantly increased the frequency of effector memory T cells in both CD- and HD-derived PBMCs.

A.

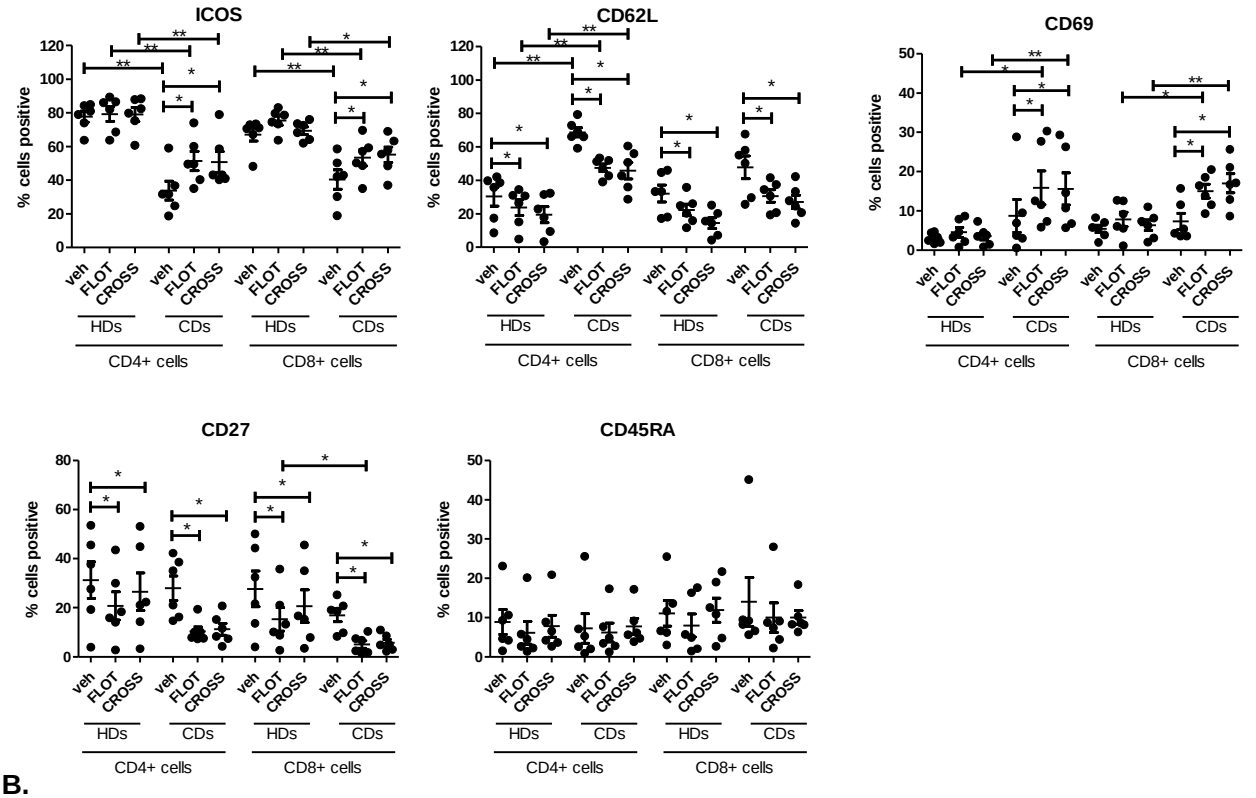
ICOS
CD62L
CD69
CD27
CD45RA
% cells positive
veh
FLOT
CROSS
HDs
CDs
CD4+ cells
CD8+ cells

B.

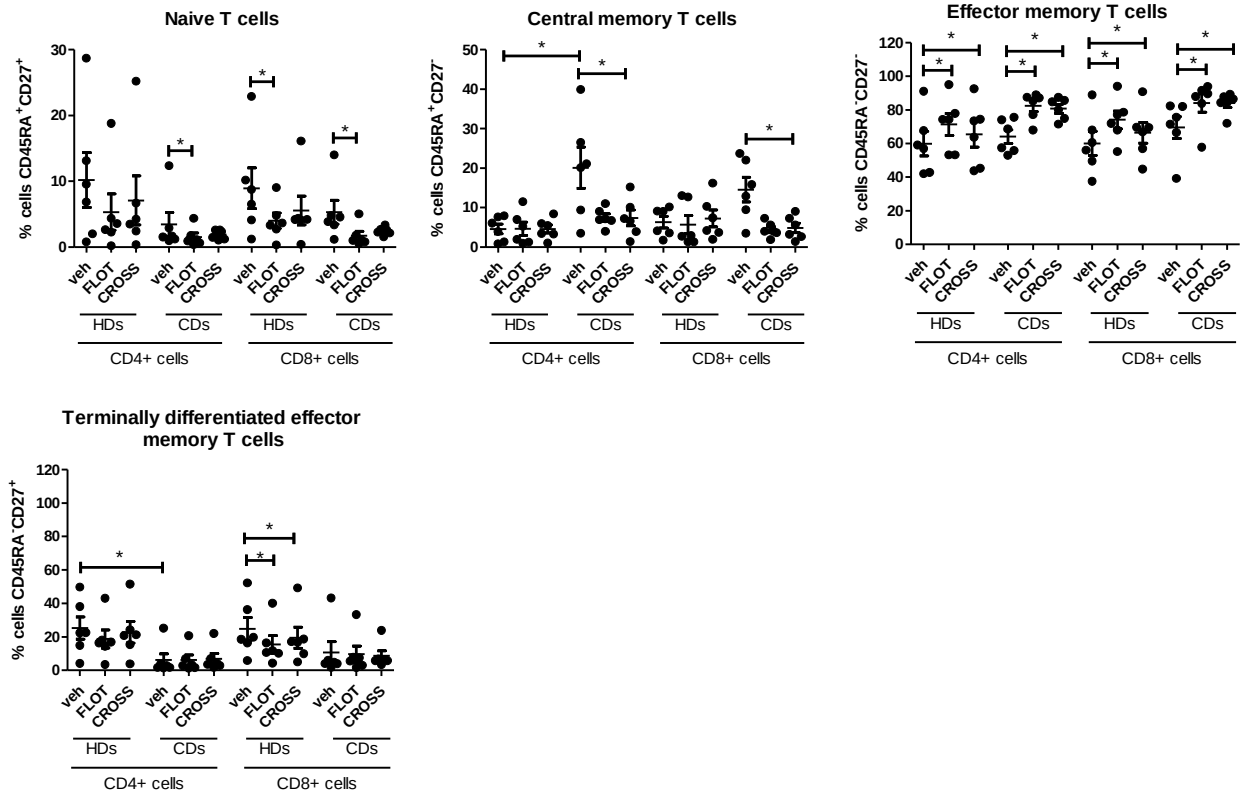
Naive T cells
Central memory T cells
Effector memory T cells
Terminally differentiated effector memory T cells
% cells CD45RA+CD27+
% cells CD45RA+CD27-
% cells CD45RA-CD27+
% cells CD45RA-CD27-
veh
FLOT
CROSS
HDs
CDs
CD4+ cells
CD8+ cells

Figure 6.4: FLOT and CROSS CT regimens upregulate co-stimulatory markers ICOS and CD69 and downregulate co-stimulatory marker CD27 on the surface of OGJ T cells. PBMCs were activated with plate bound anti-CD3 and anti-CD28 for 72h followed by 48h treatment with FLOT and CROSS CT regimens. Expression of a range of markers reflective of T cell activation status (ICOS, CD27, CD69, CD62L and CD45RA) was assessed on viable $CD3^+CD4^+$ and $CD3^+CD8^+$ by flow cytometry on the surface of age-matched healthy donor (HDs) PBMCS (n=6) and treatment-naïve OGJ T cells (CDs) (n=8) (A). The percentage of viable naïve ($CD27^+CD45RA^+$), central memory ($CD27^+CD45RA^-$), effector memory ($CD27^-CD45RA^-$) and terminally differentiated effector memory ($CD27^-CD45RA^+$) $CD3^+CD4^+$ and $CD3^+CD8^+$ cells was also determined by flow cytometry (B). *p<0.05, **p<0.01 and ***p<0.001 paired non-parametric t-test to compare effect of treatments within HDs and CDs respectively and unpaired non-parametric to compare the effect of treatments between HDs vs. CDs. Gating strategy and representative dot plots showing the direct effect of FLOT and CROSS CT on activation marker expression on the surface of T cells and T cell differentiation status are shown in Appendix **Figure A6.2**.

6.2.4 Conditioned media from FLOT and CROSS CT chemotherapy-treated OGJ cells alters the activation phenotype of T cells

To successfully identify immunostimulatory chemotherapies as synergistic partners to combine with immunotherapies for OGJ patients, it is important to elucidate how the chemotherapy regimens may alter the secretome from OGJ cells which may subsequently affect T cell activity. To address this, we examined the effect of *in vitro* conditioned media from FLOT, CROSS CT and MAGIC chemotherapy-treated OGJ cells (OE33 and SK-GT-4) on T cell activation. The markers used to assess $CD3^+$, $CD3^+CD4^+$ and $CD3^+CD8^+$ T cell activation included: CCR7, CD45RO, CD27, CD69, CD45RA and CD62L, determined by flow cytometry (**Figure 6.5**). The percentages of viable naïve ($CD45RA^+CD62L^+$), central memory ($CD45RA^-CD62L^+$), effector memory ($CD45RA^-CD62L^-$) and terminally differentiated effector memory ($CD45RA^+CD62L^-$) $CD3^+CD4^+$ and $CD3^+CD8^+$ cells were also determined[362] (**Figure 6.5**).

FLOT and MAGIC OE33 conditioned media significantly increased the percentage of CCR7-expressing $CD3^+CD4^+$ T cells (untreated OE33: 4.08 ± 1.7 vs. FLOT OE33: 31 ± 2.7 and MAGIC OE33: 21.83 ± 1.7%, respectively p=0.01 and p=0.03, respectively), (**Figure 6.5A**). CROSS CT and MAGIC OE33 conditioned media significantly decreased the percentage of $CD3^+CD4^+$ T cells expressing CD45RO marker of T cell memory (OE33 untreated: 53.70 ± 2.0 vs. CROSS CT OE33: 31 ± 1.0 and MAGIC OE33: 36.57 ± 2.0%, respectively p=0.01 and

p=0.04, respectively), (**Figure 6.5A**). FLOT and MAGIC OE33 conditioned media significantly increased the percentage of CD69-expressing $CD3^+CD4^+$ T cells (untreated: 16.14 ± 5.2 vs. FLOT OE33: 28.5 ± 4.3 and MAGIC OE33: 27.27 ± 7.0%, respectively p=0.008 and p=0.04, respectively), (**Figure 6.5A**). CROSS CT OE33 conditioned media significantly increased the percentage of CD69-expressing $CD3^+CD4^+$ T cells (untreated: 16.14 ± 5.2 vs. CROSS CT OE33: 30.19 ± 1.9%, respectively p=0.05), (**Figure 6.5A**). Similarly, FLOT and CROSS CT SK-GT-4 conditioned media significantly increased the percentage of CD69-expressing $CD3^+CD4^+$ cells (untreated: 16.14 ± 5.2, FLOT SK-GT-4: 27.77 ± 4.3 and CROSS CT SK-GT-4: 24.03 ± 6.2%, respectively, p=0.01 and p=0.02, respectively), (**Figure 6.5A**). FLOT and MAGIC OE33 conditioned media decreased the percentage of CD27-expressing $CD3^+CD4^+$ T cells (untreated: 74.83 ± 3.1 vs. FLOT OE33: 68.83 ± 3.32 and MAGIC OE33: 52.17 ± 4.3%, respectively, p=0.03 and p=0.04, respectively), (**Figure 6.5A**). CROSS CT significantly decreased the percentage of CD27-expressing $CD3^+CD4^+$ T cells (untreated: 74.83 ± 3.1 vs. CROSS CT OE33: 67.23 ± 3.5%, respectively p=0.0536), (**Figure 6.5A**). CROSS CT OE33 conditioned media decreased the percentage of $CD45RO^+$ $CD3^+CD8^+$ T cells (untreated OE33: 50.63 ± 2.3 vs. CROSS CT OE33: 33.27 ± 3.4%, respectively p=0.03), (**Figure 6.5B**). In contrast, FLOT, CROSS CT and MAGIC SK-GT-4 conditioned media significantly increased the percentage of $CD45RO^+$ $CD3^+CD8^+$ cells (untreated: 39.17 ± 3.9 vs. FLOT SK-GT-4: 53.9 ± 4.0, CROSS CT SK-GT-4: 52.47 ± 2.4 and MAGIC SK-GT-4: 58.6 ± 4.6%, respectively, p=0.04 p=0.01 and p=0.01, respectively), (**Figure 6.5B**).

In addition, FLOT OE33 conditioned media significantly decreased the percentage of central memory $CD3^+CD4^+$ cells (OE33 untreated: 21.73 ± 4.9 vs. FLOT OE33: 19.9 ± 5.2%, respectively p=0.02), (**Figure 6.5A**). Similarly, CROSS CT SK-GT-4 cells significantly decreased the percentage of $CD3^+CD8^+$ central memory cells (untreated: 11.11 ± 4.34 vs. CROSS CT OE33: 10.22 ± 4.4% respectively, p=0.04), (**Figure 6.5B**). Interestingly, FLOT OE33 conditioned media significantly increased the percentage of effector memory $CD3^+CD4^+$ cells (untreated: 9.17 ± 3.2 vs. FLOT OE33: 12.09 ± 3.3%, respectively p=0.03), (**Figure 6.5A**). Similarly, FLOT SK-GT-4 conditioned media significantly increased the percentage of effector memory $CD3^+CD8^+$ cells (SK-GT-4 untreated: 9.49 ± 3.9 vs. FLOT SK-GT-4: 13.82 ± 3.3%, respectively p=0.04), (**Figure 6.5B**). Furthermore, CROSS CT-treated OE33 conditioned media significantly increased the percentage of terminally differentiated effector memory $CD3^+CD8^+$ cells (OE33 untreated: 25.33 ± 2.5 vs. CROSS CT OE33: 58.87 ± 7.2%, respectively p=0.02), (**Figure 6.5B**).

Overall, the conditioned media from OGJ cells treated with combination chemotherapy regimens significantly altered the activation status of T cells. Specifically, FLOT and MAGIC regimens significantly enhanced frequencies of CCR7-expressing T cells, whereas FLOT and CROSS CT treatment increased frequencies of CD69-expressing T cells yet decreased frequencies of their CD27-expressing counterparts. In addition, FLOT and CROSS CT chemotherapy regimens significantly decreased the frequencies of central memory T cells, whilst increasing the percentages of effector memory T cells.

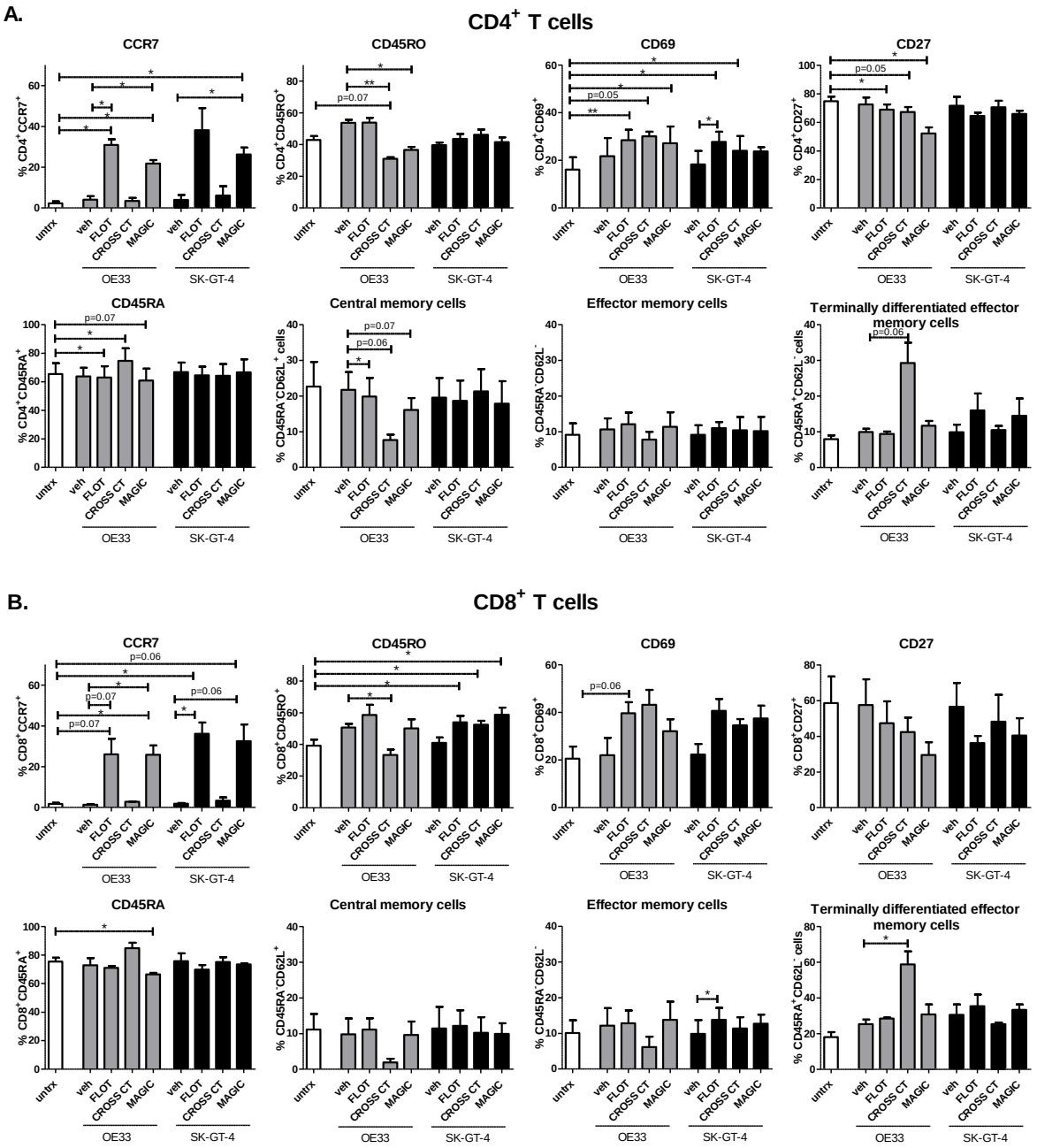

Figure 6.5: Conditioned media from FLOT and CROSS chemotherapy-treated OGJ cells increases the percentage of viable T cells expressing CD69, whereas FLOT and MAGIC decrease CD27 expression. PBMCs were activated with plate bound anti-CD3 and anti-CD28 and untreated (untrx) or concurrently treated with supernatant harvested from OE33 and SK-GT-4 cells vehicle control treated (veh) or treatment with FLOT, CROSS CT or MAGIC chemotherapy regimens for 48h (IC_{50} dose). The effect of the supernatant on viable $CD3^+CD4^+$ (A) and $CD3^+CD8^+$ (B) T cell activation status was determined by CCR7, CD45RO, CD62L, CD45RA, CD27 and CD69 expression by flow cytometry. The percentage of viable naïve ($CD45RA^+CD62L^+$), central memory ($CD45RA^-CD62L^+$), pre-terminally differentiated effector memory ($CD45RA^-CD62L^-$) and effector memory

($CD45RA^+CD62L^-$) $CD3^+CD4^+$ (A) and $CD3^+CD8^+$ (B) cells was also determined by flow cytometry. A zombie viability dye was used to exclude dead cells from the analysis. n=3 supernatants from each cell line was used to treat one healthy donor. Paired parametric t-test, *p<0.05 and **p<0.01. Gating strategy and representative dot plots showing the effect of the post-FLOT and post-CROSS CT tumour cell conditioned media on activation marker expression on the surface of T cells and T cell differentiation status are shown in Appendix **Figure A6.3**.

6.2.5 Tumour conditioned media (TCM) from OGJ tumour biopsies post-FLOT and post-CROSS CRT treatment significantly alters the activation profile of T cells *ex vivo*

In light of the *in vitro* results using conditioned media from OGJ cell lines treated with FLOT or CROSS CT regimens, which reflected the secreted factors from just epithelial cells, we next assessed tumour conditioned media (TCM) from post-FLOT and post-CROSS CRT patients, which facilitated simulation of the entire tumour microenvironment. Healthy donor PBMCs were activated in the presence or absence of post-FLOT or post-CROSS CRT TCM. The *ex vivo* findings validated the results of the *in vitro* experiments demonstrating that post-FLOT and post-CROSS CRT conditioned media significantly decreased the percentage of $CD3^+CD27^+$ cells (72.23 ± 5.5 vs. 21.72 ± 9.6 and 32.28 ± 6.4%, p=0.003 and p=0.02, respectively), (**Figure 6.6A**). Similar findings were found within the $CD4^+$ and $CD8^+$ T cell compartments. In addition, the post-FLOT and post-CROSS CRT conditioned media significantly increased the percentage of $CD3^+CD8^+CD69^+$ cells compared with untreated cells (27.62 ± 4.2 vs. 43.55 ± 5.4% and 45.76 ± 1.1%, p=0.04 and p=0.01, respectively), (**Figure 6.6A**). Similar findings were observed using the post-FLOT conditioned media only within the $CD4^+$ T cell compartment. The percentage of CD62L expressing $CD3^+$ cells were significantly decreased in the post-FLOT and post-CROSS conditioned media compared with untreated cells (81.52 ± 2.0 vs. 43.52 ± 9.2% and 64.67 ± 3.6%, p=0.02 and p=0.01, respectively), (**Figure 6.6A**). Similar findings were observed in the CD4 and CD8 cell compartment (**Figure 6.6A**). Frequencies of $CD45RA^+$ T cells were significantly decreased within the $CD3^+$ population and within the $CD4^+$ and $CD8^+$ subsets following treatment with either post-FLOT and post-CROSS CRT TCM compared with untreated cells (83.97 ± 2.9 vs. 70.82 ± 1.8% and 68.78 ± 0.6%, p=0.03 and p=0.003, respectively), (**Figure 6.6A**). Similar trends were observed in the CD4 and CD8 T cell compartments. Furthermore, the percentage of $CD3^+CD45RO^+$ T cells were significantly decreased following treatment with the post-CROSS CRT TCM compared with untreated cells (39.05 ± 2.1 vs. 29.6 ± 2.1%, p=0.02), (**Figure 6.6A**). No significant changes were observed for changes in the percentages of $CD4^+$ or $CD8^+$ T cells expressing

CD45RO following treatment with either the post-FLOT or post-CROSS CRT TCM compared with untreated cells.

Following treatment with either the post-FLOT or post-CROSS CRT TCM the percentages of naïve $CD3^+$, CD3+CD4+ and $CD3^+CD8^+$ T cells were significantly decreased, characterised by CD45RA and CD62L co-expression. Additionally, treatment with post-CROSS CRT TCM significantly increased the percentage of central memory T cells within the $CD3^+$, CD3+CD4+ and $CD3^+CD8^+$ T cell compartment (**Figure 6.6B**). Effector memory $CD3^+$ cells were increased by post-FLOT and post-CROSS CRT TCM, characterised by $CD45RA^-CD62L^-$ (6.9 ± 0.8 vs. 17.42 ± 1.7% and 13.22 ± 0.6%, p=0.01 and p=0.001), (**Figure 6.6B**). Similar increases in effector memory T cells were specifically observed in the $CD3^+CD4^+$ and $CD3^+CD8^+$ compartment by post-FLOT and post-CROSS CRT TCM treatment, characterised by $CD45RA^-CD62L^-$. Finally, the percentage of terminally differentiated effector memory $CD3^+$, $CD3^+CD4^+$ and $CD3^+CD8^+$ T cells were significantly increased following treatment with post-FLOT and post-CROSS CRT TCM, characterised by $CD45RA^+CD62L^-$.

Overall, we observed that PBMCs activated in the presence of conditioned media generated from OGJ patient-derived tumour biopsies at time-points post-FLOT and post-CROSS CRT treatment decreased CD27 and increased CD69 expression. Additionally, significant decreases in the frequencies of naïve T cells and subsequent increases in the frequencies of T cells displaying phenotypes representative of central memory, effector memory and terminally differentiated effector memory T cells were observed.

A.

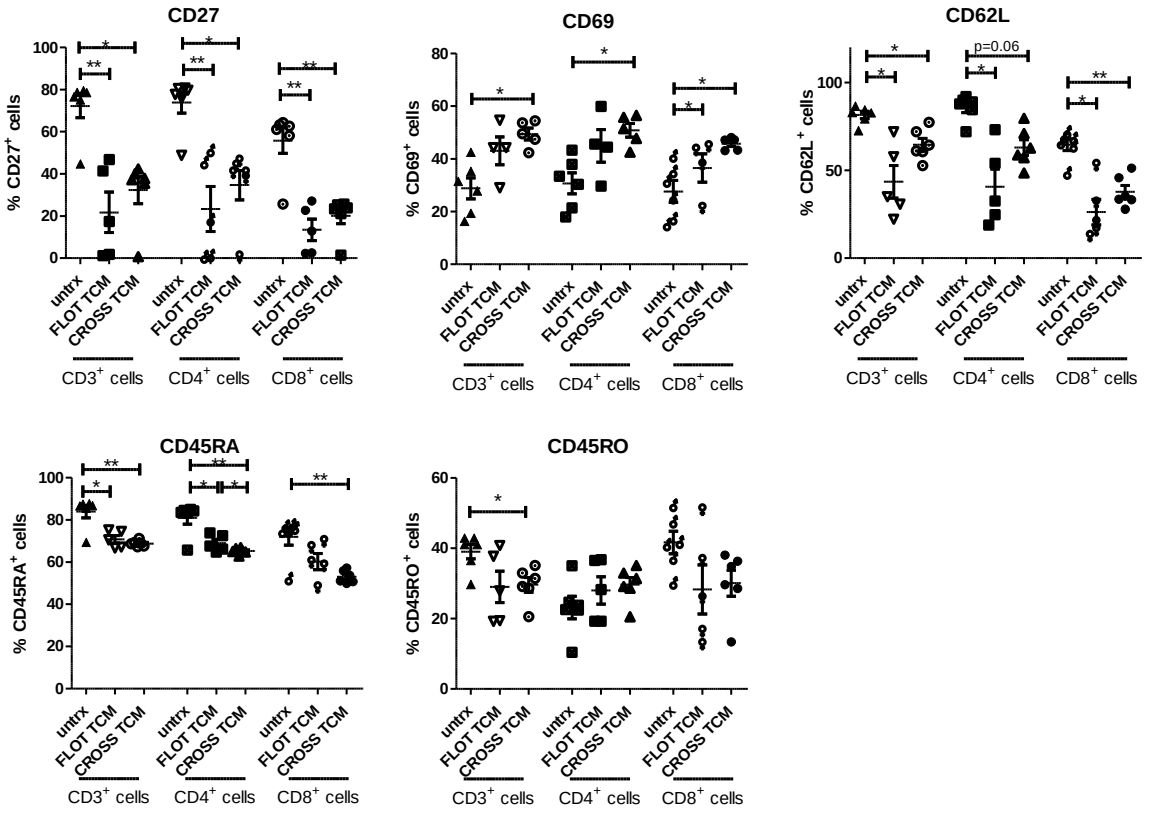
CD27
% CD27+ cells
CD69
% CD69+ cells
CD62L
% CD62L+ cells
p=0.06
CD45RA
% CD45RA+ cells
CD45RO
% CD45RO+ cells
untrx
FLOT TCM
CROSS TCM
CD3+ cells
CD4+ cells
CD8+ cells

B.

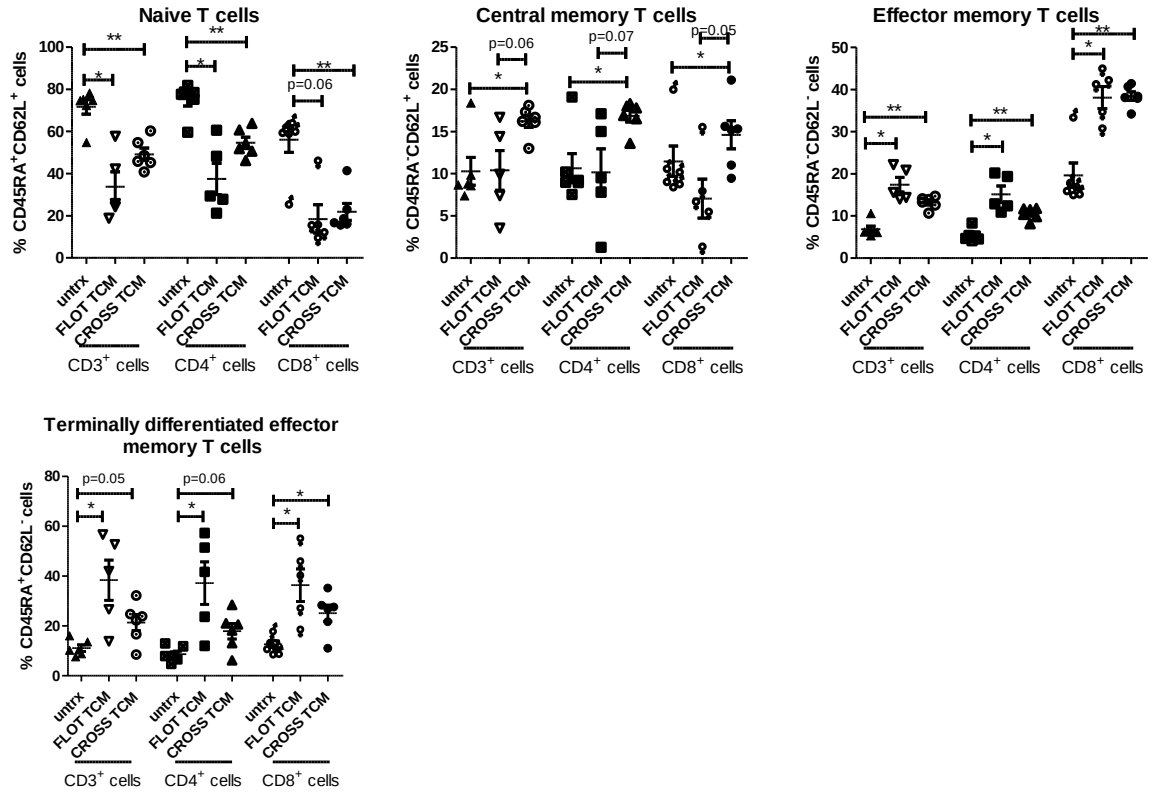
Naive T cells
% CD45RA+CD62L+ cells
Central memory T cells
% CD45RA-CD62L+ cells
p=0.06
p=0.07
p=0.05
Effector memory T cells
% CD45RA-CD62L- cells
untrx
FLOT TCM
CROSS TCM
CD3+ cells
CD4+ cells
CD8+ cells

Terminally differentiated effector memory T cells
% CD45RA+CD62L- cells
p=0.05
p=0.06
untrx
FLOT TCM
CROSS TCM
CD3+ cells
CD4+ cells
CD8+ cells

Figure 6.6: Conditioned media generated from OGJ patient-derived tumour at time points post-FLOT and post-CROSS treatment significantly increases the frequencies of CD69$^+$, central memory and effector memory T cells, yet decreases the percentage of CD27-expressing T cells *ex vivo.* Healthy donor PBMCs were activated with plate bound anti-CD3 and anti-CD28 in the absence or presence of post-FLOT (n=5) and post-CROSS (n=6) conditioned media for 48h. CD3$^+$, CD3$^+$CD4$^+$ and CD3$^+$CD8$^+$ cells were assessed for CD27, CD69, CD62L and CD45RA expression by flow cytometry (A). The percentages of naïve (CD45RA$^+$CD62L$^+$), central memory (CD45RA$^-$CD62L$^+$), pre-terminally differentiated effector memory (CD45RA$^-$CD62L$^-$) and effector memory (CD45RA$^+$CD62L$^-$) cells were determined by flow cytometry (B). Paired non-parametric t-test, *p<0.05 and **p<0.01.

6.2.6 Significantly lower frequencies of CD27-expressing tumour-infiltrating T cells were detected post-FLOT chemotherapy and post-CROSS chemoradiotherapy regimens

To provide further validation of our *in vitro* and *ex vivo* data showing that the secretome of FLOT and CROSS CT treatment of OGJ tumours can significantly alter the CD27 and CD69 expression and the differentiation status of T cells, we directly profiled the activation status of T cells in the peripheral blood and tumour of a cohort of OGJ patients in the treatment-naïve, post-FLOT and post-CROSS CRT clinical setting (**Figure 6.7**).

Indeed, we found that the percentages of CD3$^+$CD27$^+$ cells in peripheral circulation were significantly lower post-FLOT chemotherapy compared to the treatment-naïve setting (38.38 ± 5.1 vs. 16.62 ± 5.4%, p=0.02), (**Figure 6.7**). Similarly, the percentages of tumour-infiltrating CD3$^+$CD27$^+$ cells were significantly lower post-FLOT chemotherapy compared to the treatment-naïve setting (16.1 ±2.7 vs. 5.41 ± 2.6%, p=0.01), (**Figure 6.7**). This was also observed in the CD4$^+$ T cell compartment, with a decrease in the percentage of tumour-infiltrating CD3$^+$CD4$^+$CD27$^+$ post-FLOT chemotherapy compared with the treatment-naïve tissue (16.22 ± 3.6 vs. 4.64 ± 1.8%, p=0.03), (**Figure 6.7**). Similarly, the frequency of tumour-infiltrating CD3$^+$CD8$^+$CD27$^+$ T cells were significantly lower post-CROSS chemoradiation compared with the treatment-naïve setting (16.8 ± 3.1 vs. 4.64 ± 1.9%, p=0.03), (**Figure 6.7**).

In line with our in vitro and ex vivo data, the percentages of circulating CD3$^+$CD8$^+$CD69$^+$ cells were significantly higher post-CROSS CRT treatment compared with treatment-naïve (9.34 ± 2.6 vs. 40.25 ± 12.8%, p=0.01), (**Figure 6.7**). Similar findings were observed in the tumour tissue, wherein post-CROSS CRT the percentages of tumour-infiltrating CD3$^+$CD8$^+$CD69$^+$ T cells were significantly higher compared with treatment-naïve tumour tissue (63.3 ± 10.0 vs. 90.08 ± 3.0%, p=0.04), (**Figure 6.7**). The frequencies of circulating peripheral blood

$CD3^+CD62L^+$ T cells were significantly lower post-FLOT chemotherapy compared with treatment-naive (36.62 ± 4.7 vs. 15.34 ± 4.1%, p=0.01), (**Figure 6.7**). Additionally, there was lower frequencies of peripheral blood circulating central memory $CD3^+CD8^+$ T cells post-FLOT compared with treatment-naïve (11.55 ± 1.7 vs. 5.22 ± 2.4%, p=0.05), (**Figure 6.7**). A similar decrease was also observed in tumour-infiltrating central memory $CD3^+CD8^+$ T cells post-FLOT compared with treatment-naive (3.23 ± 0.9 vs. 1.33 ± 0.6%, p=0.06), (**Figure 6.7**).

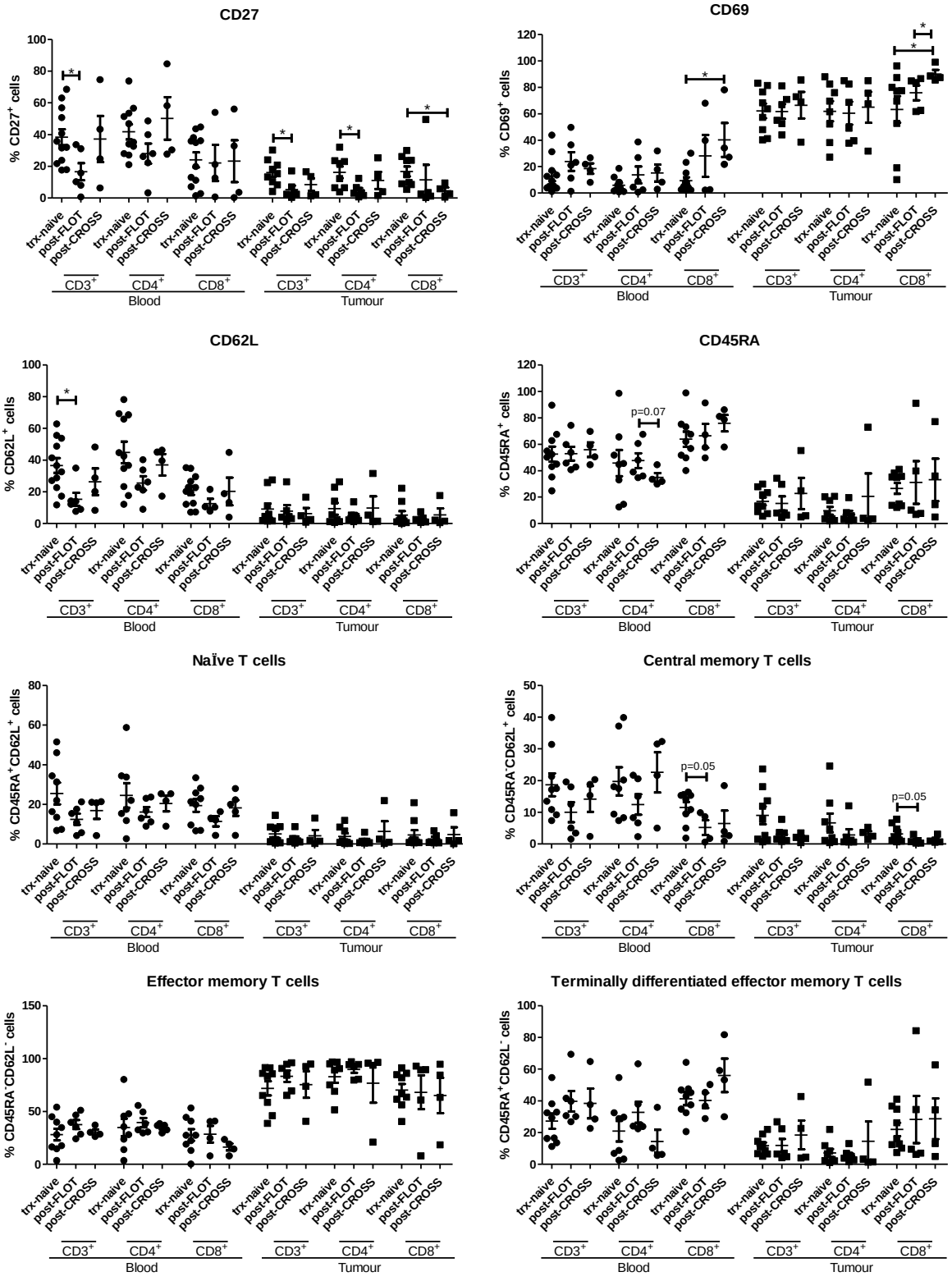

Figure 6.7: Post-FLOT chemotherapy and post-CROSS chemoradiotherapy the percentage of tumour-infiltrating T cells expressing CD27 is significantly lower whereas the percentage of tumour-infiltrating T cells expressing CD69 is significantly higher post-CROSS in OGJ patients. $CD3^+$, $CD3^+CD4^+$ and $CD3^+CD8^+$ cells in circulating peripheral blood and infiltrating tumour tissue of

OGJ patients in the treatment-naïve setting and post-treatment setting at surgical resection was assessed for CD27, CD69, CD62L and CD45RA expression (A). The percentage of naïve ($CD45RA^{+}CD62L^{+}$), central memory ($CD45RA^{-}CD62L^{+}$), effector memory ($CD45RA^{-}CD62L^{-}$) and terminally differentiated effector memory ($CD45RA^{+}CD62L^{-}$) cells was also determined by flow cytometry. (Blood: treatment-naïve: n=12, post-FLOT: n=5 and post-CROSS CRT: n=5. Tumour: treatment-naïve: n=10, post-FLOT: n=5 and post-CROSS CRT: n=5). Mann-Whitney test, *p<0.05.

6.2.7 Frequencies of $CD69^{+}$ T cells following culture with post-FLOT/CROSS CRT conditioned media negatively correlated with levels of soluble pro-angiogenic and immunosuppressive factors

Given the high prevalence of treatment failure and lack of clinical biomarkers to predict response to neo-adjuvant CT and CRT, we sought to investigate if the frequency of activated T cells in peripheral blood circulation or infiltrating tumour tissue biopsies correlated with a better prognosis or subsequent treatment response in the treatment-naïve cohort of this study (**Table 6.1**) and the post-treatment cohort of patients (**Table 6.2**). The frequencies of circulating peripheral blood naïve $CD3^{+}$ cells (r=0.97) and $CD4^{+}$ T cells (r=0.97) very strongly correlated with a subsequent better treatment response (p=0.005 and p=0.005, respectively), (**Table 6.1**). Additionally, the frequencies of circulating peripheral blood $CD3^{+}CD8^{+}CD27^{+}$ (r=0.84) very strongly positively correlated with a subsequent better treatment response (p=0.02) (**Table 6.1**). The frequency of circulating peripheral blood terminally differentiated effector memory $CD8^{+}$ cells (r=-0.86, p=0.01) and $CD4^{+}$ cells (r=-0.85, p=0.03) negatively correlated with lymph node metastasis in the treatment-naïve setting (**Table 6.1**).

The frequency of peripheral blood circulating $CD3^{+}CD27^{+}$ T cells strongly correlated (r=0.69) with a better treatment response in the post-treatment setting (p=0.04), (**Table 6.2**). There was a very strong positive correlation (r=0.80) with the frequency of peripheral blood circulating central memory $CD8^{+}$ cells with a better treatment response in the post-treatment setting (**Table 6.2**).

In addition, T cell activation status following 48h treatment with post-FLOT or post-CROSS CRT conditioned media was also correlated with the levels of soluble pro-inflammatory and pro-angiogenic analytes that were present in the TCM. The percentage of $CD4^{+}CD69^{+}$ T cells and effector memory $CD8^{+}$ T cells negatively correlated with the levels of pro-angiogenic factors PIGF and VEGFA present in the conditioned media ($CD4^{+}CD69^{+}$ T cells: r= -0.76 (p=0.01) and -0.89 (p=0.0005), respectively and effector memory $CD8^{+}$ T cells: r= -0.72 (p=0.01) and -0.77 (p=0.009), respectively) (**Figure 6.8.**). Overall, T cell activation status of

circulating and tumour-infiltrating T cells correlated with response to treatment and adverse tumour biology as well as levels of immunosuppressive and pro-angiogenic PIGF and VEGFA present within the TME.

Table 6.1. Correlation of peripheral blood and tumour-infiltrating T cell activation status with clinical characteristics in the treatment-naïve tissue. Only significant correlations shown. Spearman r 0.4-0.59 moderate, 0.6-0.79 strong and 0.8-1 very strong. CROSS CRT=0, FLOT=1, OGJ=0, OGJ=1, female=0, male=1. *p<0.05, **p<0.01.

T cell population	Correlated variable	Spearman r	p value
Peripheral blood			
$CD3^+CD45RA^+$	Increased age	0.8333	0.0053
$CD3^+CD4^+CD45RA^+$	Increased age	0.7857	0.0208
$CD3^+CD8^+CD27^+$	Increased age	0.6795	0.0151
$CD3^+CD8^+CD45RA^+$	Increased age	0.9167	0.0005
Effector memory $CD8^+$	Increased age	-0.8368	0.0049
Terminally differentiated effector memory $CD3^+$	Increased age	0.8000	0.0096
Naïve $CD3^+$	Improved trx response[a]	0.9747	0.0048
Naïve $CD4^+$	Improved trx response[a]	0.9747	0.0048
$CD3^+CD8^+CD27^+$	Improved trx response[a]	0.8444	0.0168
$CD3^+CD45RA^+$	Nodal metastasis[a]	-0.8233	0.0229
Terminally differentiated effector memory $CD4^+$	Nodal metastasis[a]	-0.8533	0.0307
$CD3^+CD8^+CD45RA^+$	Nodal metastasis[a]	-0.8233	0.0229
Terminally differentiated effector memory $CD8^+$	Nodal metastasis[a]	-0.8608	0.0129
Tumour			
$CD3^+CD27^+$	Increased BMI	-0.6667	0.0499
$CD3^+CD4^+CD27^+$	Increased BMI	-0.6696	0.0208
$CD3^+CD8^+CD69^+$	Increased BMI	-0.7167	0.0298

[a]determined by PET/CT. *Abbreviations: trx; treatment.*

Table 6.2. Correlation of peripheral blood and tumour-infiltrating T cell activation status with clinical characteristics in the post-treatment tissue. Only significant correlations shown. Spearman r 0.4-0.59 moderate, 0.6-0.79 strong and 0.8-1 very strong. CROSS CRT=0, FLOT=1, OGJ=0, OGJ=1, female=0, male=1. *p<0.05, **p<0.01.

T cell population	Correlated variable	Spearman r	P value
Peripheral blood			
$CD3^+CD8^+CD45RA^+$	Increased age	-0.93	0.0007
Effector memory $CD8^+$	Increased age	0.92	0.0011
$CD3^+CD8^+CD45RA^+$	Diagnosis	-0.76	0.03
Effector memory $CD8^+$	Diagnosis	0.76	0.03
$CD3^+CD4^+CD45RA^+$	Neo-adjuvant trx	0.64	0.0464
$CD3^+CD27^+$	Improved trx response[a]	0.69	0.0399
$CD3^+CD62L^+$	Improved trx response[a]	0.75	0.0202
Terminally differentiated effector memory $CD3^+$	Improved trx response[a]	-0.75	0.0202
$CD3^+CD4^+CD62L^+$	Improved trx response[a]	0.83	0.0061
Central memory $CD8^+$ cells	Improved trx response[a]	0.8	0.0291
Terminally differentiated effector memory $CD8^+$	Advanced tumour stage[a]	-0.76	0.03
$CD3^+CD4^+CD45RA^+$	Advanced tumour stage[b]	0.82	0.0067
Terminally differentiated effector memory $CD4^+$	Advanced tumour stage[b]	0.69	0.0387
$CD3^+CD4^+CD45RA^+$	Nodal metastasis[b]	0.67	0.0479
Effector memory $CD4^+$	Nodal metastasis[b]	-0.73	0.0266
Tumour			
Central memory $CD4^+$ cells	Increased age	0.68	0.0305
$CD3^+CD8^+CD69^+$	Neo-adjuvant trx	-0.78	0.0133
$CD3^+CD8^+CD27^+$	Improved trx response[a]	-0.72	0.0276
$CD3^+CD8^+CD45RA^+$	Improved trx response[a]	-0.68	0.0434
Terminally differentiated effector memory $CD8^+$	Improved trx response[a]	-0.68	0.0434
Terminally differentiated effector memory $CD3^+$	Nodal metastasis[b]	-0.75	0.0204

$CD3^+CD62L^+$	Advanced tumour stage[b]	0.74	0.0213
$CD3^+CD4^+CD62L^+$	Advanced tumour stage[b]	0.7	0.0345
$CD3^+CD4^+CD45RA^+$	Advanced tumour stage[b]	0.71	0.0313
Effector memory $CD4^+$	Advanced tumour stage[b]	-0.8	0.0099
Terminally differentiated effector memory $CD4^+$	Advanced tumour stage[b]	0.85	0.0036
Central memory $CD4^+$ cells	Increased BMI	-0.71	0.0227

[a]determined by PET/CT; [b] determined pathologically. *Abbreviations: trx; treatment.*

Figure 6.8: Corogram demonstrating the correlation values between T cell activation status following 24h treatment with post-FLOT or post-CROSS CRT conditioned media with the levels of pro-inflammatory and pro-angiogenic analytes in the TCM. Only significant correlations shown. Spearman r 0.4-0.59 moderate, 0.6-0.79 strong and 0.8-1 very strong. Blue and red refer to positive and negative correlations, respectively. *p<0.05, **p<0.01.

6.2.8 FLOT and CROSS CT regimens enhance the production of pro-inflammatory cytokines IFN-γ and TNF-αand decrease IL-2 production in OGJ patient-derived T cells *ex vivo*

To acquire a deeper understanding of the direct immunostimulatory or immunoinhibitory effects of first-line chemotherapy regimens on T cells, activated HD- and CD-derived PBMCs were treated *ex vivo* with either a vehicle, FLOT or CROSS CT regimens and production of anti-tumour cytokines and the cytotoxic potential of T cells was assessed (**Figure 6.9**).

Interestingly, circulating $CD4^+$ T cells from CDs produced significantly higher amounts of IFN-γ compared with $CD4^+$ T cells from HDs (12.82 ± 2.5% vs. 4.9 ± 0.8%, p=0.03) *ex vivo* (**Figure 6.9C**). In addition, FLOT significantly increased IFN-γ production compared with the vehicle control in $CD4^+$ T cells from both CDs and HDs (CDs: 30.96 ± 4.1% vs. 12.82 ± 2.5%, p=0.008 and HDs: 13.78 ± 2.8% vs. 4.9 ± 0.8%, p=0.03) (**Figure 6.9C**) Similarly, FLOT significantly increased IFN-γ production compared with the vehicle control in $CD8^+$ T cells from both CDs and HDs (CDs: 19.96 ± 2.3% vs. 12.49 ± 2.1%, p=0.03 and HDs: 25.02 ± 4.5% vs. 6.0 ± 1.0%, p=0.01) (**Figure 6.9C**)

Furthermore, $CD4^+$ T cells from CDs produced significantly higher amounts of TNF-α compared with $CD4^+$ T cells from HDs (20.17 ± 3.2% vs. 9.50 ± 4.2%, p=0.04) (**Figure 6.9C**). Similar trends were found within the $CD8^+$ T cell compartment, where $CD8^+$ T cells from CDs produced significantly higher amounts of TNF-α compared with $CD8^+$ T cells from HDs (16.63 ± 2.4% vs. 7.19 ± 2.9%, p=0.02) (**Figure 6.9C**). Interestingly, FLOT significantly increased the production of TNF-α by $CD4^+$ T cells and $CD8^+$ T cells compared with the vehicle control from CDs but not from HDs ($CD4^+$ T cells: 34.68 ± 4.9% vs. 20.17 ± 3.2%, p=0.003 and $CD8^+$ T cells: 27.95 ± 4.2% vs. 16.63 ± 2.4%, p=0.002), (**Figure 6.9C**). Similarly, CROSS CT significantly increased the production of TNF-α by $CD8^+$ T cells compared with the vehicle control from CDs but not from HDs ($CD8^+$ T cells: 24.38 ± 2.9% vs. 16.63 ± 2.4%, p=0.02), (**Figure 6.9C**).

$CD4^+$ T cells from CDs produced significantly higher amounts of IL-2 compared with $CD4^+$ T cells from HDs (30.62 ± 10.03% vs. 8.01 ± 1.9%, p=0.04) (**Figure 6.9C.**). In addition, FLOT and CROSS CT significantly decreased the production of IL-2 by $CD4^+$ T cells compared with the vehicle control in CDs (21.52 ± 7.0% vs. 18.37 ± 9.4% and 30.62 ± 10.03%, respectively p=0.03 and p=0.03), but did not significantly affect IL-2 production by T cells from HDs (**Figure 6.9C**). In addition, there was an increase in CD107a degranulation post-FLOT compared with the vehicle control in HDs but no significant effects were observed post-chemotherapy treatment in the CDs (p=0.06) (**Figure 6.9D**).

Overall, chemotherapy treatment had a more substantial effect in altering T cell cytokine profiles from CDs compared with HDs. Chemotherapy treatment significantly increased the production of pro-inflammatory IFN-γ and TNF-α cytokines and significantly decreased IL-2 production in T cells from CDs.

A.

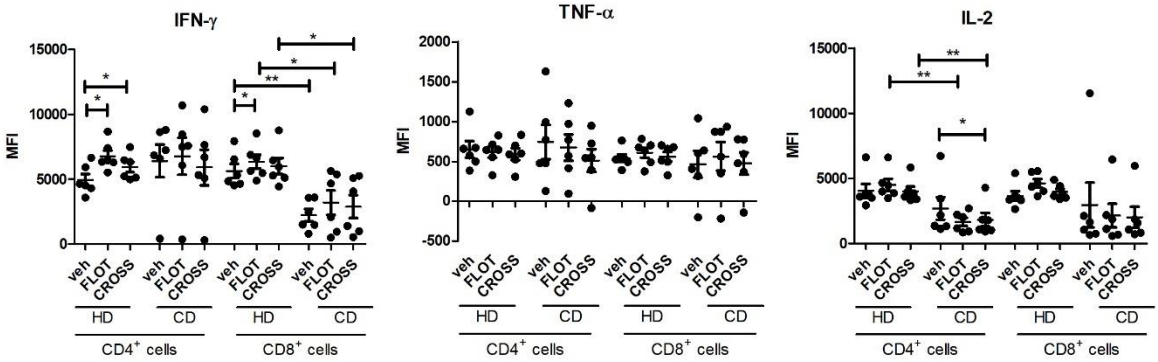
IFN-γ
TNF-α
IL-2
MFI
15000
10000
5000
0
2000
1500
1000
500
-500
*
**
veh
FLOT
CROSS
HD
CD
CD4+ cells
CD8+ cells

B.

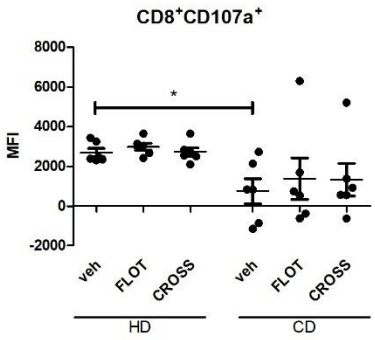
CD8+CD107a+
MFI
8000
6000
4000
2000
0
-2000
*
veh
FLOT
CROSS
HD
CD

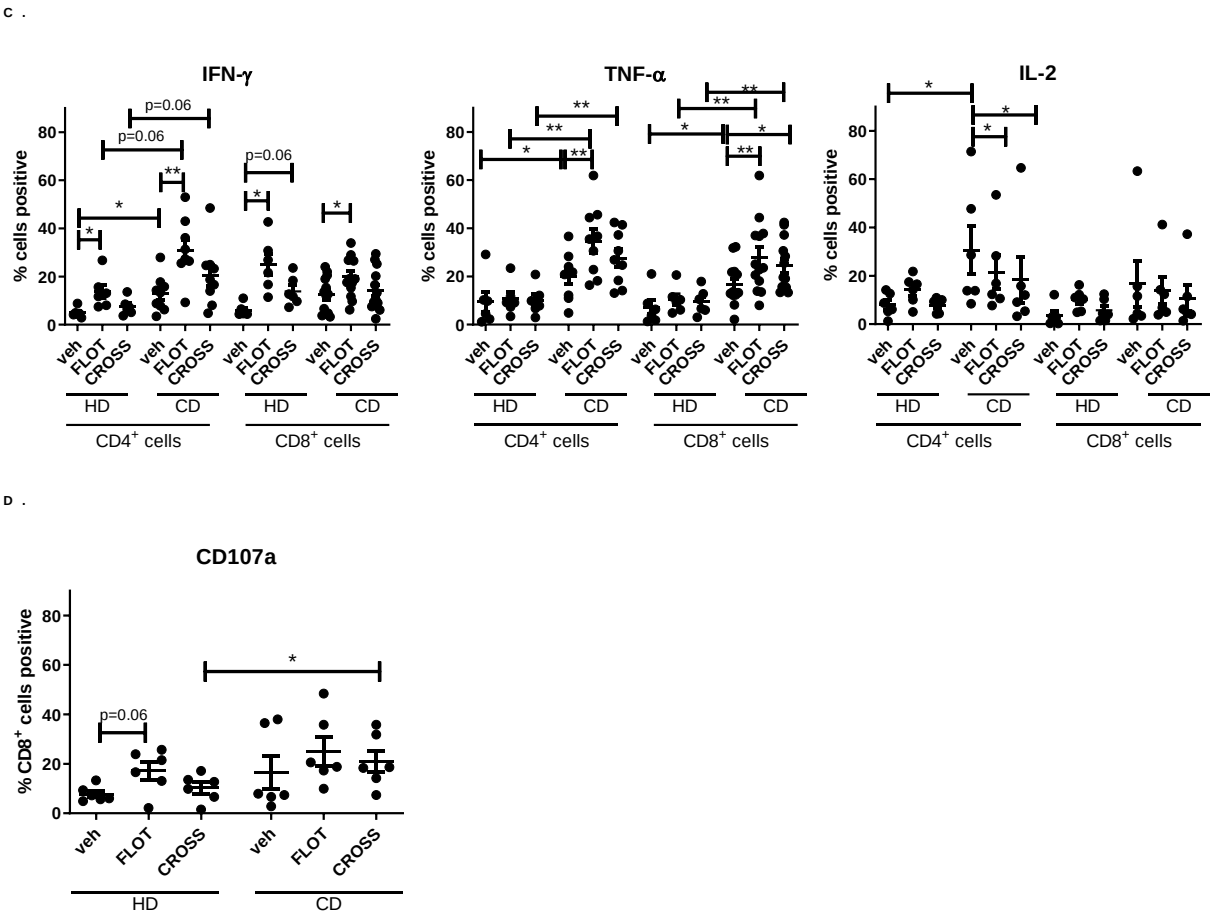

Figure 6.9: FLOT and CROSS CT regimens increase the percentage of TNF-α and IFN-γ producing OGJ patient-derived T cells and decrease the percentage of IL-2 producing OGJ patient-derived T cells *ex vivo.* Age-matched healthy donor (HDs) (n=6) and OGJ donor (CDs) (n=6) PBMCs were activated with plate bound anti-CD3 and anti-CD28 for 72h followed by 48h treatment with FLOT and CROSS CT regimens or vehicle control (veh). The percentage of $CD3^+CD4^+$ and $CD3^+CD8^+$ cells producing IFN-γ, TNF-α and IL-2 were assessed by intracellular flow cytometry (A depicts MFI and D depicts frequency). The percentage of degranulating $CD8^+$ T cells was also determined using a CD107a degranulation by flow cytometry (B depicts MFI and D depicts frequency). *p<0.05, **p<0.01 paired non-parametric t-test to compare effect of treatments within age-matched HDs and CDs, respectively and unpaired non-parametric to compare the effect of treatments between HDs vs. CDs. Gating strategy and representative dot plots showing the direct effect of FLOT and CROSS CT on T cell cytokine production is shown in **Figure A6.4**.

The immune contexture of solid tumours is shaped by the cell types, profiles, polarisation and modulation of immune cells within the TME and ultimately influences the resulting anti-tumour response and ICI efficacy. T cells play a pivotal role in OGJ development and

progression, depending on the cytokine profile, and may suppress or enhance anti-tumour immunity through Th2-like responses or Th1-like responses, respectively[363]. Herein, we examined the effects of soluble factors secreted by OGJ cells following FLOT, CROSS CT and MAGIC treatment on T cell cytokine profiles and $CD8^+$ T cell degranulation to elucidate the effects of pre-treated TME on T cell function. The secretion of Th1-like cytokines including IFN-γ and TNF-α, Th2-like cytokines including IL-4 and IL-10 and the Th17-like cytokine IL-17A were assessed by intracellular flow cytometry in $CD3^+$, $CD3^+CD4^+$ and $CD3^+CD8^+$ cells (**Figure 6.10**). CROSS CT and MAGIC OE33 conditioned media appeared to enhance a Th1-like phenotype in T cells, (**Figure 6.10**). CROSS CT OE33 conditioned media enhanced a more Th2-like/regulatory-like phenotype in T cells demonstrated by a decrease in IFN-γ-producing $CD3^+CD4^+$ T cells (untreated: 2.78 ± 0.5 vs. CROSS CT OE33: 1.83 ± 0.6%, respectively p=0.03), (**Figure 6.10A**) and an increase in IL-10-producing $CD3^+CD8^+$ T cells (untreated: 3.07 ± 1.6 vs. CROSS CT OE33: 4.24 ± 1.6%, respectively p=0.01), (**Figure 6.10B**). Similarly, MAGIC OE33 conditioned media enhanced a T_{H2}-like phenotype in T cells demonstrated by an increase in IL-4-producing $CD3^+CD8^+$ T cells (untreated OE33: 0.60 ± 0.2 vs. MAGIC OE33: 1.45 ± 0.2%, respectively p=0.02) and IL-10-producing $CD3^+CD8^+$ T cells (untreated: 3.07 ± 1.6 vs. MAGIC OE33: 4.13 ± 1.5%, respectively p=0.007), (**Figure 6.10B**). In contrast, FLOT SK-GT-4 conditioned media promoted a more T_{H1}-like phenotype in T cells demonstrated by a significant increase in TNF-α-producing $CD3^+CD8^+$ T cells (untreated SK-GT-4: 2.25 ± 0.8 vs. FLOT SK-GT-4: 4.75 ± 1.1% respectively, p=0.02), (**Figure 6.10B**). Additionally, we also examined the effect of FLOT, CROSS CT and MAGIC OGJ cell conditioned media on $CD8^+$ T cell cytotoxic potential by CD107a expression (**Figure 6.10C**)**.** The FLOT and CROSS CT OE33 conditioned media significantly increased the percentage of $CD107a^+CD3^+CD8^+$ T cells (OE33 untreated: 4.47 ± 2.5 vs. OE33 FLOT: 8.58 ± 2.3% and OE33 CROSS CT: 12.74 ± 2.2%, respectively, p=0.004 and p=0.01, respectively), (**Figure 6.10C**)**.** Similarly, the CROSS CT SK-GT-4 conditioned media significantly increased the percentage of viable $CD107a^+CD3^+CD8^+$ T cells (SK-GT-4 untreated: 4.2 ± 1.5 vs. SK-GT-4 CROSS CT: 10.87 ± 0.8%, respectively p=0.04), (**Figure 6.10C**)

Overall, FLOT and CROSS CT conditioned media from OE33 cells enhanced T_{H2}-like phenotype. In contrast, FLOT conditioned media from SK-GT-4 cells enhanced a T_{H1}-like phenotype. CROSS CT conditioned media from both OE33 and SK-GT-4 cells enhanced the cytotoxic potential of T cells, whereas only the FLOT conditioned media from OE33 cells enhanced CD107a expression.

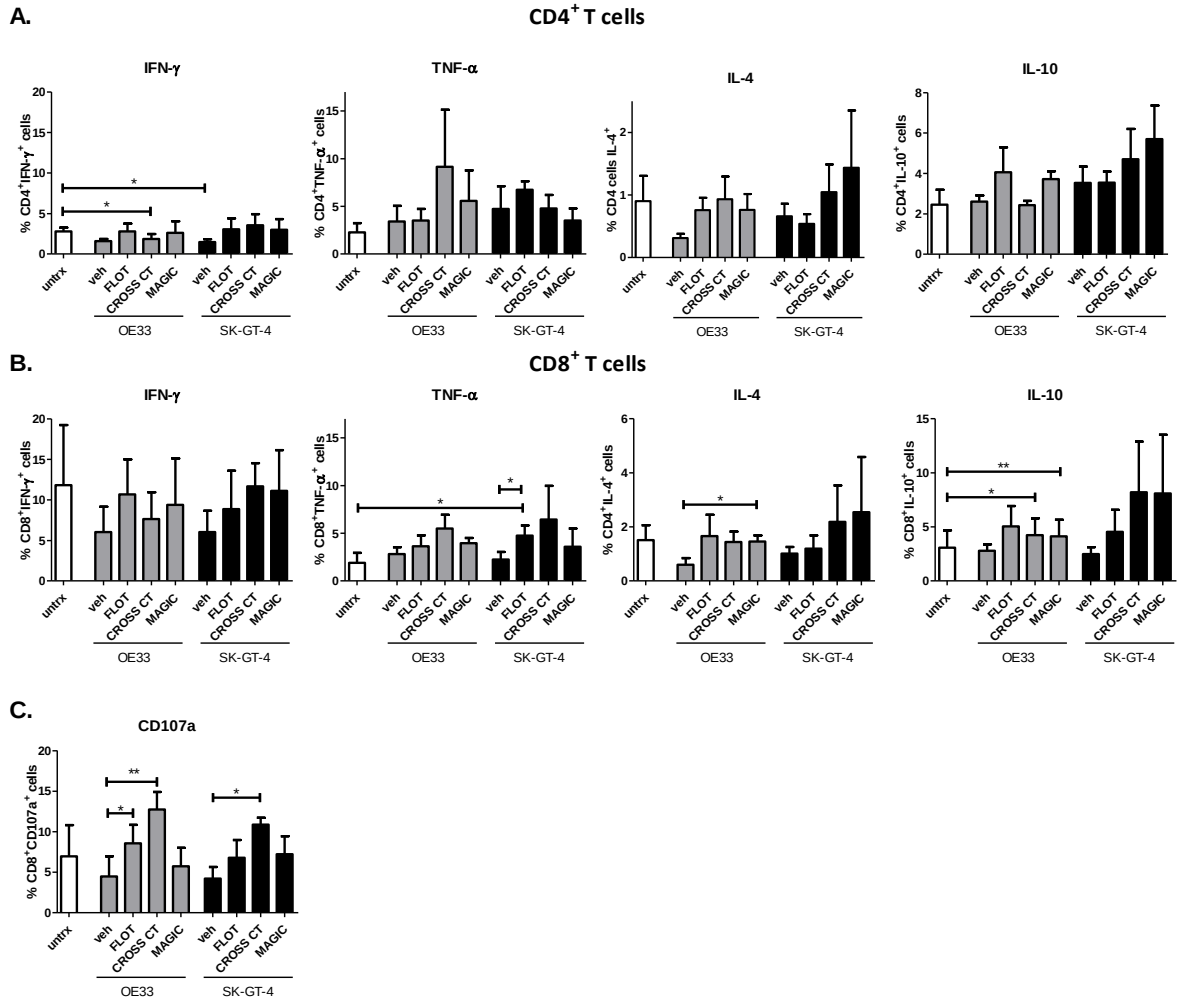

Figure 6.10: Conditioned media from FLOT and CROSS chemotherapy-treated OGJ cells increases the cytotoxic potential of CD8$^+$ T cells *in vitro*. Activated PBMCs were untreated or concurrently treated with supernatant harvested from vehicle control treated (veh) OE33 and SK-GT-4 cells or following 48h treatment with FLOT, CROSS CT or MAGIC chemotherapy regimens (IC_{50} dose). The effect of the supernatant on viable $CD3^+CD4^+$ (A) and $CD3^+CD8^+$ (B) T cell cytokine production was determined by assessing the expression of IFN-γ, TNF-α, IL-10, IL-4 and IL-17A by intracellular flow cytometry. (C) The effect of the supernatant on viable $CD3^+CD8^+$ T cell cytotoxicity was determined by assessing the expression of CD107a expression by flow cytometry. A zombie viability dye was used to exclude dead cells from the analysis and n=3 biological replicates of supernatants from each cell line was used to treat one healthy donor. Paired parametric t-test, *$p<0.05$ and **$p<0.01$. Gating strategy and representative dot plots showing the effect of the post-FLOT and post-CROSS CT tumour cell conditioned media T cell cytokine production is shown in Appendix **Figure A6.4**.

6.2.9 The chemotherapy-treated OE33 tumour cell secretome enhances lymphocyte-mediated killing of OE33 cells

Overall, our *in vitro* and *ex vivo* findings suggest that chemotherapy regimens may enhance the immunogenicity of OGJ cells and enhance T cell activation to ultimately improve anti-tumour immunity and elimination of the tumour. Therefore, as a proof-of-principle experiment to test this hypothesis we carried out a cytolysis assay to determine if the post-FLOT and post-CROSS CT altered OE33 tumour cell secretome might alter the killing capacity of lymphocytes isolated from treatment-naïve OGJ patient blood. OE33 cells were treated for 48h with chemotherapy regimens, washed twice to ensure the removal of the chemotherapy drugs and the OE33 conditioned media was collected 48h later. OGJ treatment-naïve PBMCs were activated with anti-CD3/28 and IL-2 *ex vivo* and co-cultured with OE33 cells (5:1 or 10:1 E:T ratios) in the presence of untreated OE33 conditioned media or post-FLOT- and post-CROSS CT-treated OE33 tumour cell conditioned media to determine if the lymphocyte mediated-killing of OE33 cells would be enhanced by the secretome of OE33 (**Figure 6.11**).

The post-FLOT OE33 tumour cell secretome significantly enhanced OGJ lymphocyte-mediated killing of OE33 cells *ex vivo* compared with the post-vehicle OE33 tumour cell secretome (5:1 E:T: 72.98 ± 11.5 vs 83.74 ± 11.5%%, p=0.03) (**Figure 6.11**). Similarly, the post-CROSS CT OE33 tumour cell secretome significantly enhanced OGJ lymphocyte-mediated killing of OE33 cells *ex vivo* compared with the post-veh OE33 tumour cell secretome (5:1 E:T: 74.9 ± 9.7 vs. 83.74 ± 11.5%, p=0.03) (**Figure 6.11**). There was no significant effect using an E:T ratio of 10:1 (**Figure 6.11**).

Overall, these findings suggest that the FLOT and CROSS CT regimens alter the OE33 tumour cell secretome which directly enhances OGJ effector lymphocyte mediated killing of OE33 cells *ex vivo*.

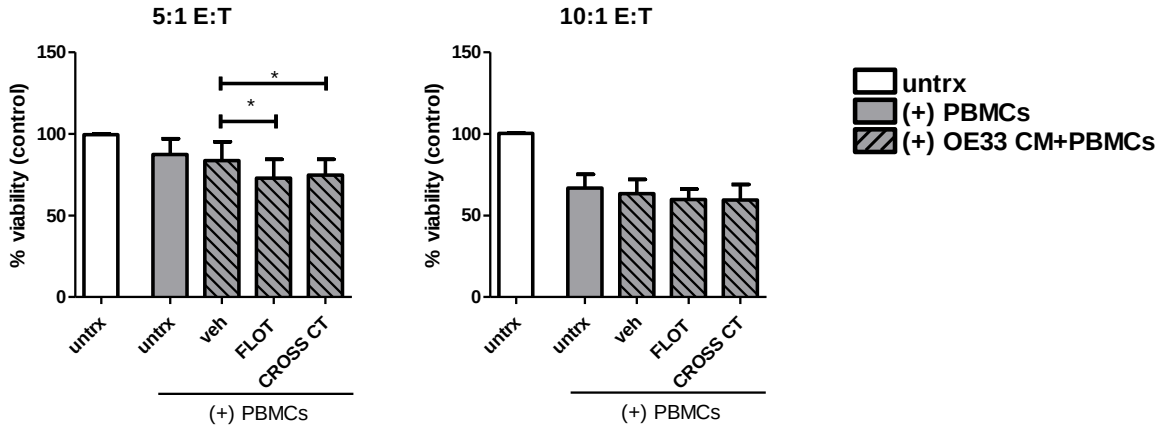

Figure 6.11: Post-FLOT- and post-CROSS CT-treated OE33 conditioned media enhances OGJ lymphocyte-mediated killing of OE33 cells. OE33 cells were untreated (untrx) or treated with vehicle control (veh)-, FLOT- or CROSS CT-treated OE33 conditioned media (CM) for 48h. OGJ PBMCs were also co-cultured with OE33s in an effector:target (E:T) ratio of 5:1 and 10:1 (50,000:10,000, 100,000:10,000) for 48h. PBMCs were isolated from treatment-naïve OGJ patients (n=6) and were activated for 5 days prior to the co-culture with OGJ cells using anti-CD3/28 and IL-2. A CCK8 assay was used to determine the viability of OE33 cells (n=6). Mann Whitney t-test, technical duplicates were used, *$p<0.05$.

6.2.10 Immune checkpoint proteins are significantly upregulated on tumour-infiltrating T cells compared with peripheral circulating T cells in OGJ patients

ICB to reinvigorate anti-tumour immunity has been the most successful immunotherapy in solid malignancies[98]. Blockade of the PD-1 or CTLA-4 axes in OGJ and other cancer types has been the most investigated[299]. However, there exists a wide range of novel ICs that might also present viable therapeutic targets to stimulate anti-tumour immunity in these patients[364]. Therefore, this study profiles the expression of a wide range of ICs including PD-1, its ligands PD-L1 and PD-L2, CTLA-4 and novel ICs including TIGIT, TIM-3, LAG-3 A2aR and ICOS and CD160 on circulating and tumour-infiltrating T cells in treatment-naïve, post-FLOT chemotherapy and post-CROSS CRT OGJ patients to help ascertain how these first-line chemotherapy regimens affect IC expression.

PD-1 was significantly upregulated on the surface of tumour-infiltrating $CD4^+$ T cells compared with those in peripheral circulation in the treatment-naïve setting (53.99 ± 7.0 vs. 24.05 ± 3.5%, p=0.003), (**Figure 6.12C**). Similar trends were found in the $CD8^+$ T cell compartment where tumour-infiltrating $CD8^+$ T cells expressed significantly higher levels of

PD-1 compared with those in peripheral circulation in the treatment-naïve setting (55.53 ± 6.0 vs. 31.48 ± 4.6%, p=0.007), (**Figure 6.12C**).

There was an increase in TIM-3 expression on tumour-infiltrating $CD4^+$ T cells compared with circulating $CD4^+$ T cells in the treatment-naïve setting (24.98 ± 6.5 vs. 10.433 ± 2.8%, p=0.06) (**Figure 6.12E**). Similar effects were found post-FLOT chemotherapy treatment, where TIM-3 was significantly upregulated on the surface of tumour-infiltrating T cells compared with circulating $CD4^+$ T cells (17.69 ± 4.7 vs. 2.86 ± 0.9%, p=0.007), (**Figure 6.12E**). TIM-3 was also significantly upregulated on the surface of tumour-infiltrating $CD8^+$ T cells compared with those in peripheral circulation in the treatment-naïve setting (22.86 ± 6.1 vs. 3.19 ± 0.9%, p=0.009) and the post-FLOT setting (23.24 ± 6.6 vs. 2.13 ± 0.8%, p=0.004), (**Figure 6.12E**). There was a decrease in TIM-3 expression on the surface of tumour-infiltrating $CD4^+$ T cells post-FLOT chemotherapy (17.69 ± 4.7 vs. 24.98 ± 6.5%, p=0.08) and post-CROSS chemoradiotherapy compared with the treatment-naïve setting (5.10 ± 2.5 vs. 24.98 ± 6.5%, p=0.07) (**Figure 6.12E**). In contrast, there was an increase in TIM-3 expression on the surface of circulating $CD8^+$ T cells post-CROSS chemoradiotherapy compared with the treatment-naïve setting (4.33 ± 0.7 vs. 3.20 ± 0.9%, p=0.07) (**Figure 6.12E**).

Additionally, LAG-3 was significantly upregulated on the surface of tumour infiltrating $CD4^+$ T cells compared with those in circulation in the treatment-naïve setting (31.88 ± 6.2 vs. 14.05 ± 5.1%, p=0.01), (**Figure 6.12F**). Similarly, LAG-3 was significantly upregulated on the surface of tumour infiltrating $CD4^+$ T cells compared with those in circulation in the post-FLOT setting (16.58 ± 2.5 vs. 6.66 ± 2.1%, p=0.007), (**Figure 6.12F**).

CTLA-4 was significantly increased on the surface of tumour-infiltrating $CD4^+$ T cells compared with those in circulation in the treatment-naïve setting (27.81 ± 7.5 vs. 7.57 ± 2.9%, p=0.03), (**Figure 6.12H**). Interestingly, there was a decrease in the expression levels of CTLA-4 on the surface of tumour-infiltrating $CD4^+$ T cells post-FLOT compared with the treatment-naïve setting (8.79 ± 2.5 vs. 27.81 ± 7.5%, p=0.07), (**Figure 6.12H**).

Stimulatory IC ICOS was also significantly upregulated on the surface of tumour-infiltrating $CD8^+$ T cells compared with those in circulation in the treatment-naïve setting (24.19 ± 5.2 vs. 11.88 ± 4.1%, p=0.01), (**Figure 6.12I**). Interestingly, there was a significant decrease in the expression of ICOS on the surface of tumour-infiltrating CD4+ T cells post-FLOT compared with the treatment-naïve setting (5.12 ± 1.6 vs. 24.19 ± 5.2%, p=0.01), (**Figure 6.12I**).

PD-L2 was also significantly upregulated on the surface of tumour-infiltrating $CD4^+$ T cells compared with those in circulation in the treatment-naïve setting and the post-FLOT setting

(7.38 ± 1.7 vs. 2.39 ± 0.6%, p=0.001), (**Figure 6.12K**). Similarly, PD-L2 was also significantly upregulated on the surface of tumour-infiltrating $CD4^+$ T cells compared with those in circulation in the post-FLOT setting (5.19 ± 1.2 vs. 1.95 ± 0.2%, p=0.01), (**Figure 6.12K**). In addition, PD-L2 was significantly upregulated on the surface of tumour-infiltrating $CD8^+$ T cells compared with those in circulation in the treatment-naïve setting (9.99 ± 3.0 vs. 1.77 ± 0.6%, p=0.001), (**Figure 6.12K**). There were no other significant changes.

Overall, inhibitory ICs TIM-3, LAG-3, CTLA-4 and PD-L2 and stimulatory IC ICOS were significantly upregulated on tumour-infiltrating T cells compared with peripheral circulating T cells in OGJ patients. ICOS was significantly deceased on tumour-infiltrating $CD8^+$ T cells post-FLOT treatment.

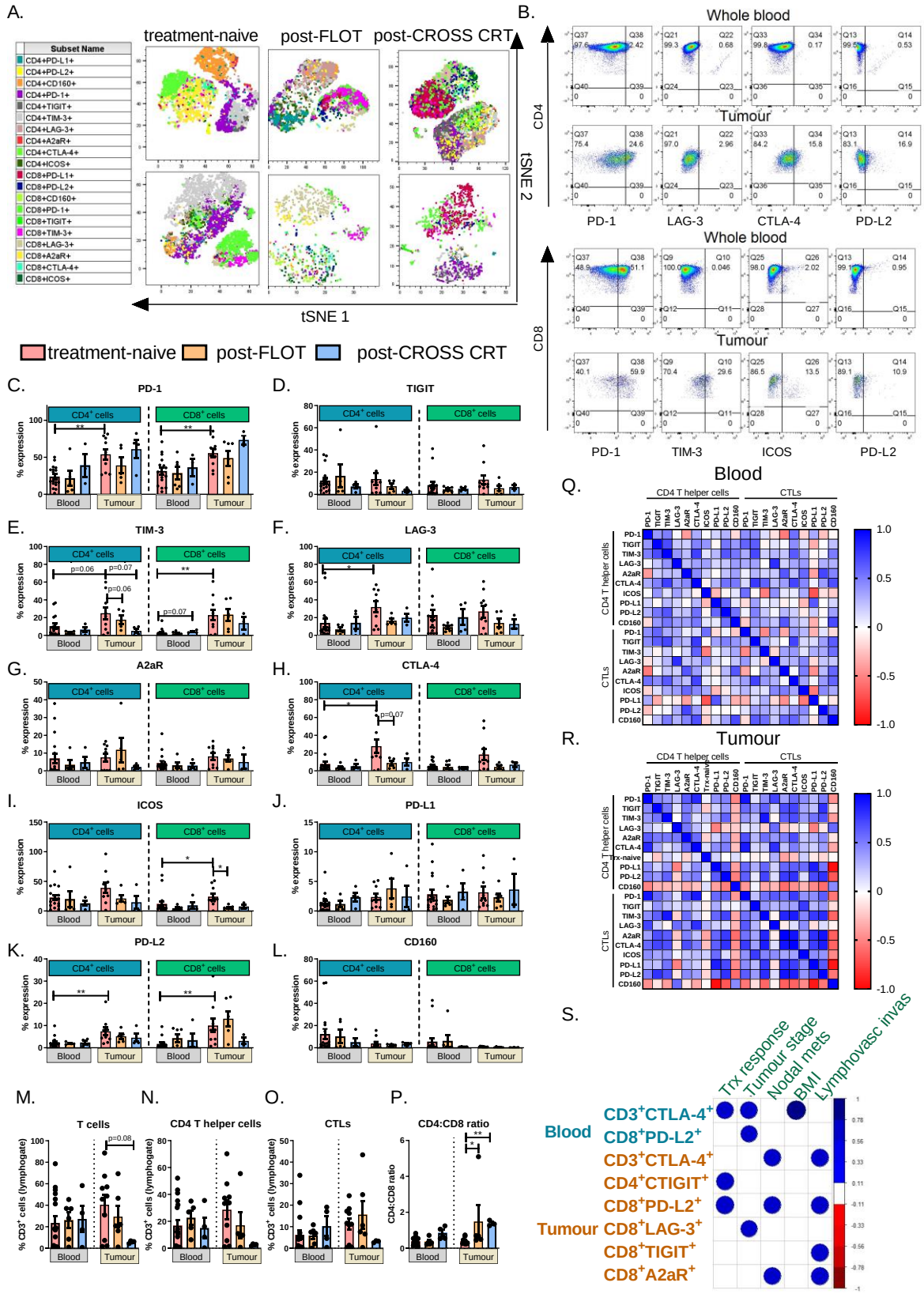

Figure 6.12: Expression of IC receptors and ligands on the surface of circulating T cells and tumour-infiltrating T cells in treatment-naïve, post-FLOT and post-CROSS CRT OGJ patients. (A) tSNE plots displaying spatial distribution of $CD4^+$ and $CD8^+$ cells expressing ICs in peripheral blood

and infiltrating tumour tissue in a treatment-naïve, post-FLOT and post-CROSS CRT patient. (B) Representative dot plots depicting the ICs that were significantly upregulated on tumour-infiltrating $CD4^+$ and $CD8^+$ T cells compared with peripheral blood from a treatment-naïve patients. (C-L). Graphs displaying the frequency of $CD4^+$ and $CD8^+$ T cells expressing ICs in circulation and infiltrating tumour tissue in the treatment-naïve versus post-FLOT and post-CROSS CRT setting. Frequency of T cells (M), CD4 T helper cells (N) and CTLs (O) and the CD4:CD8 ratio assessed in whole blood and infiltrating tumour tissue in treatment-naïve versus post-FLOT and post-CROSS CRT patients. Correlation matrix for IC expression on T cells in whole blood (Q) and tumour tissue (R) in treatment-naïve setting. Corrogram displaying significant correlations between ICs and clinical data from treatment-naïve patients (S). Patient cohort includes treatment-naïve OAC patients (blood: n=17 and tumour: n=10), post-FLOT (blood: n=6 and tumour: n=6) and post-CROSS CRT (blood: n=4 and tumour: n=4). Mann Whitney test to compare between 2 groups and Spearman correlation used for correlative analysis *$p<0.05$, **$p<0.01$.

6.2.11 Single agent chemotherapies directly upregulate inhibitory IC ligands and receptors on the surface of Jurkat cells

Given the vast amount of ongoing research combining ICIs with conventional chemotherapy regimens for treating OGJ it is important to elucidate the effect of chemotherapy on the expression of inhibitory IC proteins. Therefore, we sought to investigate the effect of single agent chemotherapies on the expression of inhibitory IC ligands on the surface of viable T cells and OGJ cells. This will help inform the development of rational combination of specific ICIs with specific chemotherapies in OGJ which is also translatable to other cancer types.

Jurkat cells were activated with plate bound anti-CD3 and anti-CD28 in the presence or absence of an IC_{50} dose of single agent chemotherapies and the expression of inhibitory IC ligands PD-L1, PD-L2 and CD160 were assessed by flow cytometry (Figure 6.13**.**). Similarly, OE33 cells were treated with an IC_{50} dose of clinically relevant single agent chemotherapies for 48h and the expression of inhibitory IC ligands PD-L1, PD-L2 and CD160 were assessed by flow cytometry. The chemotherapies investigated include: 5-FU, capecitabine, cisplatin, oxaliplatin, epirubicin, docetaxel, carboplatin and paclitaxel.

Following 5-FU and capecitabine treatment the percentage of OE33 cells expressing PD-L1 was significantly increased (untreated: 1.31 ± 0.5 vs 5-FU: 26.35 ± 26.4 and capecitabine: 25.30 ± 4.8%, respectively, p=0.0132, p=0.0030, respectively), (**Figure 6.13**). However, 5-FU and capecitabine did not significantly affect the percentage of Jurkat cells expressing PD-L1, (**Figure 6.13**).

Similarly, following 5-FU and capecitabine treatment the percentage of OE33 cells expressing PD-L2 was significantly increased (untreated: 1.44 ± 0.6 vs. 5-FU: 25.95 ± 4.3 and capecitabine: 25.47 ± 6.0%, respectively p=0.0111 and p=0.0114, respectively), (**Figure 6.13**). However, 5-FU and capecitabine did not significantly affect the percentage of Jurkat cells expressing PD-L2, (**Figure 6.13**). 5-FU and capecitabine did not significantly affect the percentage of OE33 cells or Jurkat cells expressing CD160, (**Figure 6.13**).

Cisplatin significantly increased the percentage of OE33 cells (untreated: 1.31 ± 0.5 vs. cisplatin: 9.90 ± 9.9%, respectively p=0.0192) and Jurkat cells expressing PD-L1 (untreated: 0.31 ± 0.1 vs. cisplatin: 8.10 ± 0.9%, respectively, p=0.0124), (**Figure 6.13**). Oxaliplatin significantly increased the percentage of OE33 cells expressing PD-L1 (untreated: 1.31 ± 0.5 vs. oxaliplatin: 13.59 ± 2.1%, respectively p=0.0007), (**Figure 6.13**). Following oxaliplatin treatment the percentage of Jurkat cells expressing PD-L1 was not significantly affected, (**Figure 6.13**).

Cisplatin and oxaliplatin significantly increased the percentage of OE33 cells expressing PD-L2 (untreated: 1.44 ± 0.6 vs. cisplatin: 12.65 ± 4.6 and oxaliplatin: 8.06 ± 2.4%, respectively p=0.0493 and p=0.0214, respectively), (**Figure 6.13**). Cisplatin did not significantly affect the percentage of OE33 cells expressing PD-L2 however, oxaliplatin significantly increased the percentage of Jurkat cells expressing PD-L2 (untreated: 1.78 ± 0.3 vs. cisplatin: 11.57 ± 0.3 and oxaliplatin: 4.80 ± 0.5%, respectively p=0.0625 and p=0.0320), (**Figure 6.13**).

Cisplatin and oxaliplatin did not significantly affect the percentage of OE33 cells expressing CD160, (**Figure 6.13**). However, cisplatin and oxaliplatin significantly increased the percentage of Jurkat cells expressing CD160 (untreated: 1.41 ± 0.3 vs. cisplatin: 8.72 ± 0.2 and oxaliplatin: 4.14 ± 0.4%, respectively p=0.0026 and p=0.0209), (**Figure 6.13**).

Epirubicin did not significantly affect the percentage of OE33 cells expressing PD-L1, PD-L2 and CD160 or Jurkat cells expressing PD-L2 and CD160, (**Figure 6.13**).

Docetaxel significantly increased the percentage of Jurkat and OE33 cells expressing PD-L1 (Jurkat cells untreated: 0.31 ± 0.6 vs. docetaxel: 3.66 ± 0.7%, respectively p=0.0338 and OE33 cells untreated: 1.31 ± 0.5 vs. docetaxel: 3.40 ± 2.1%, respectively p=0.0230), (**Figure 6.13**). Docetaxel significantly increased the percentage of Jurkat cells expressing PD-L2 (untreated: 1.78 ± 0.3 vs docetaxel: 10.11 ± 1.1%, respectively p=0.0243), (**Figure 6.13**). However, docetaxel did not significantly affect the percentage of OE33 cells expressing PD-L2, (**Figure 6.13**). Docetaxel significantly increased the percentage of Jurkat cells positive for CD160 expression (untreated: 1.41 ± 0.31 vs. docetaxel: 10.55 ± 1.5%, respectively p=0.0168),

(**Figure 6.13.**). However, docetaxel did not significantly affect the percentage of OE33 cells expressing CD160, (**Figure 6.13**).

Overall, 5-FU and capecitabine had the greatest effect at upregulating inhibitory IC ligands on the surface of OGJ cells, however, did not upregulate IC ligands on the surface of Jurkat cells. Additionally, inhibitory IC ligands were upregulated to a greater extent on OGJ cells compared to Jurkat cells.

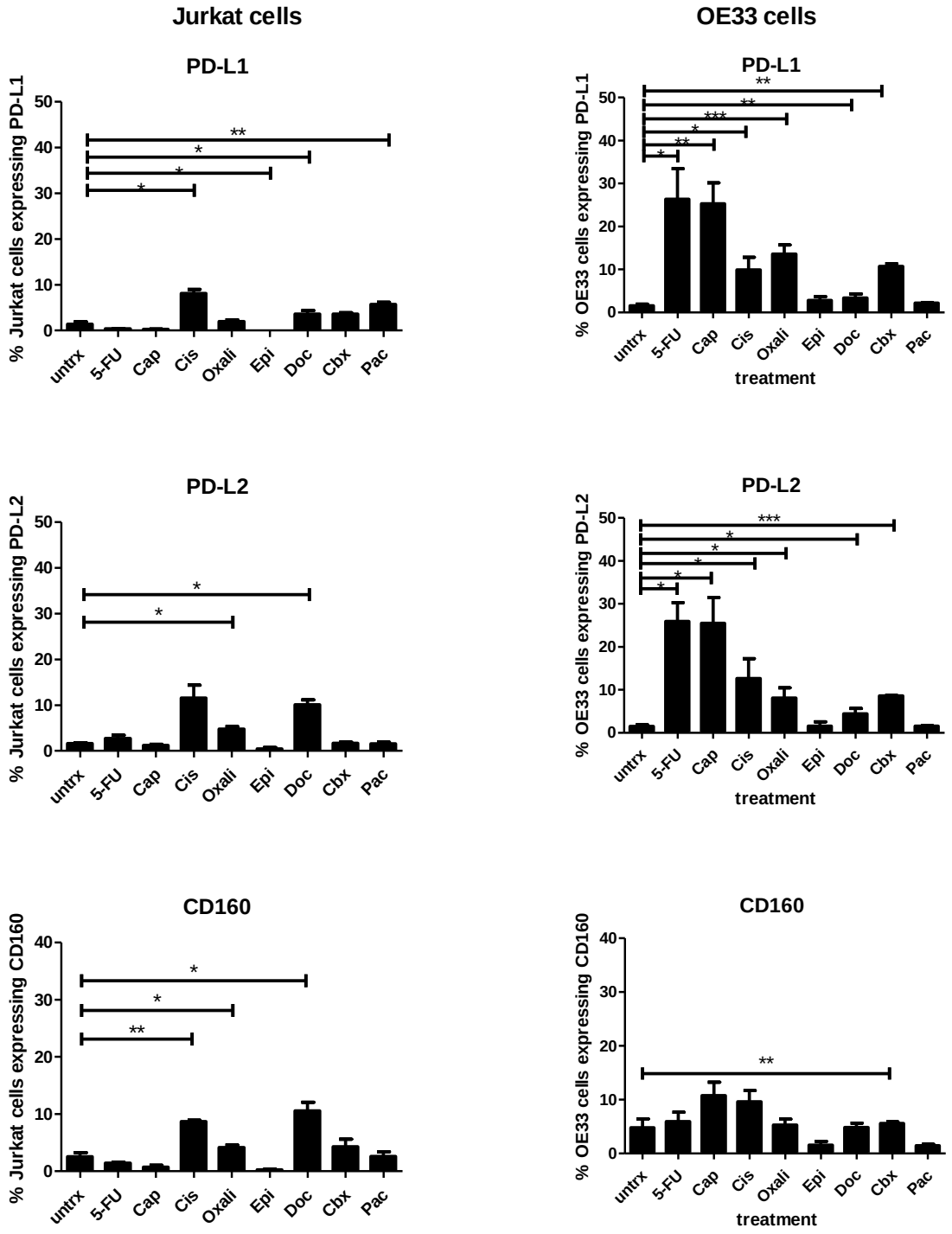

Figure 6.13: Clinically-relevant single agent chemotherapies significantly increase the surface expression of inhibitory IC ligands on the surface of viable activated Jurkat cells following 48h treatment *in vitro*. Jurkat cells were activated with plate bound anti-CD3 and anti-CD28 for 48h in the presence or absence of single agent 5-fluorouracil (5-FU), capecitabine (cap), cisplatin (cis), oxaliplatin (oxali), epirubicin (epi) and docetaxel (doc), carboplatin (cbx) and paclitaxel (pac) using a pre-optimised 48h IC_{50} dose. The expression of inhibitory IC ligands PD-L1, PD-L2 and CD160 was

assessed by flow cytometry on the surface of viable Jurkat cells and OE33 cells. Experiments repeated n=3 times, paired parametric t-test. *p<0.05, **p<0.01, ***p<0.001.

Similarly, we sought to investigate the effect of single agent chemotherapies on the expression of inhibitory IC receptors on the surface of viable T cells and OGJ cells to help guide the rational incorporation of ICIs with current standards of neoadjuvant chemotherapy care in OGJ. Jurkat cells were activated with plate bound anti-CD3 and anti-CD28 in the presence or absence of an IC_{50} dose of single agent chemotherapies and the expression of inhibitory IC receptors PD-1, TIGIT, TIM-3, LAG-3 and VISTA were assessed by flow cytometry (**Figure 6.14**). Similarly, OE33 cells were treated with an IC_{50} dose of clinically relevant single agent chemotherapies for 48h and the expression of inhibitory IC receptors PD-1, TIGIT, TIM-3, LAG-3 and VISTA were assessed by flow cytometry. The chemotherapies investigated include: 5-FU, capecitabine, cisplatin, oxaliplatin, epirubicin, docetaxel, carboplatin and paclitaxel.

Treatment with single agent chemotherapies did not significantly affect the percentage of OE33 cells expressing PD-1 (**Figure 6.14**). Similarly, 5-FU, capecitabine, cisplatin, oxaliplatin and epirubicin did not significantly affect the percentage of Jurkat cells expressing PD-1 (**Figure 6.14**). However, docetaxel increased the percentage of Jurkat cells expressing PD-1 whereas, carboplatin and paclitaxel decreased the percentage of Jurkat cells expressing PD-1 (untreated: 67.63 ± 9.5 vs. docetaxel: 55.50 ± 3.5, carboplatin: 91.3 ± 2.0 and paclitaxel: 76.43 ± 2.8%, paclitaxel, respectively p=0.0233, 0.0219 and 0.0052, respectively), (**Figure 6.14**).

5-FU and capecitabine did not significantly affect the percentage of Jurkat cells or OE33 cells expressing TIGIT. Cisplatin did not significantly affect the percentage of OE33 cells expressing TIGIT, however, cisplatin significantly increased the percentage of Jurkat cells expressing TIGIT (untreated: 2.07 ±0.8 vs. cisplatin: 14.7 ± 3.3%, respectively p = 0.0436). Oxaliplatin, carboplatin and paclitaxel did not significantly affect the percentage of Jurkat cells and OE33 cells expressing TIGIT. Epirubicin significantly increased the percentage of Jurkat cells expressing TIGIT (untreated: 2.07 ± 0.8 vs. epirubicin: 17.93 ± 0.7, respectively p=0.0076). However, epirubicin did not significantly affect the percentage of OE33 cells expressing TIGIT. Docetaxel significantly increased the percentage of Jurkat cells expressing TIGIT (untreated: 2.07 ± 0.8 vs. docetaxel: 18.17 ± 1.6%, respectively p=0.0201). However, the percentage of OE33 cells expressing TIGIT was not significantly affected by docetaxel.

Treatment with single agent chemotherapies did not affect the percentage of Jurkat cells expressing TIM-3, however, single agent 5-FU, capecitabine, cisplatin and carboplatin significantly increased the percentage of OE33 cells expressing TIM-3 (untreated: 2.6 ± 0.6 vs. 5-FU: 11.81 ± 2.9, capecitabine: 10.31 ± 1.4, cisplatin: 11.9 ± 2.7 and carboplatin: 7.06 ± 0.5%, respectively p=0.0426, p=0.0011, 0.0327 and 0.0105 respectively). The remaining chemotherapies oxaliplatin, epirubicin, docetaxel and paclitaxel did not significantly affect the percentage of OE33 cells expressing TIM-3.

5-FU and capecitabine did not significantly affect the percentage cells expressing LAG-3 in Jurkat cells, however, 5-FU and capecitabine significantly increased the percentage of OE33 cells expressing LAG-3 (untreated: 1.19 ± 0.5 vs. 5-FU: 6.3 ± 1.3 and capecitabine: 6.51 ± 1.1%, respectively p=0.0024 and p=0.0073). Cisplatin significantly increased the percentage of Jurkat cells expressing LAG-3 (untreated: 1.50 ± 0.4 vs. cisplatin: 27.53 ± 1.2%, respectively p=0.0014). Similarly, cisplatin significantly increased the percentage of OE33 cells expressing LAG-3 (untreated: 1.19 ± 0.53 vs. 8.51 ± 1.6%, respectively p=0.0036). Oxaliplatin significantly increased the percentage of Jurkat cells expressing LAG-3 (untreated: 1.50 ± 0.4 vs. 9.80 ± 0.5%, respectively p=0.0091)). However, oxaliplatin did not significantly affect the percentage of OE33 cells expressing LAG-3 (untreated: 1.19 ± 0.5 vs. oxaliplatin: 3.33 ± 1.4%, respectively p=0.0692). Epirubicin did not significantly affect the percentage of Jurkat cells or OE33 cells expressing LAG-3. Docetaxel significantly increased the percentage of Jurkat cells expressing LAG-3 (untreated: 1.50 ± 0.4 vs. docetaxel: 20.47 ± 1.0%, respectively p=0.0044). However, docetaxel did not significantly affect the percentage of OE33 cells expressing LAG-3. Carboplatin significantly increased the percentage of LAG-3 expressing cells in the OE33 cells (1.21 0.3 vs 5.49 0.4%, respectively p=0.0056) but not the Jurkat cells. Additionally, paclitaxel significantly increased the percentage of Jurkat cell expressing LAG-3 (1.46 0.2 vs 5.54 0.9%, respectively p=0.0499), but not the OE33 cells.

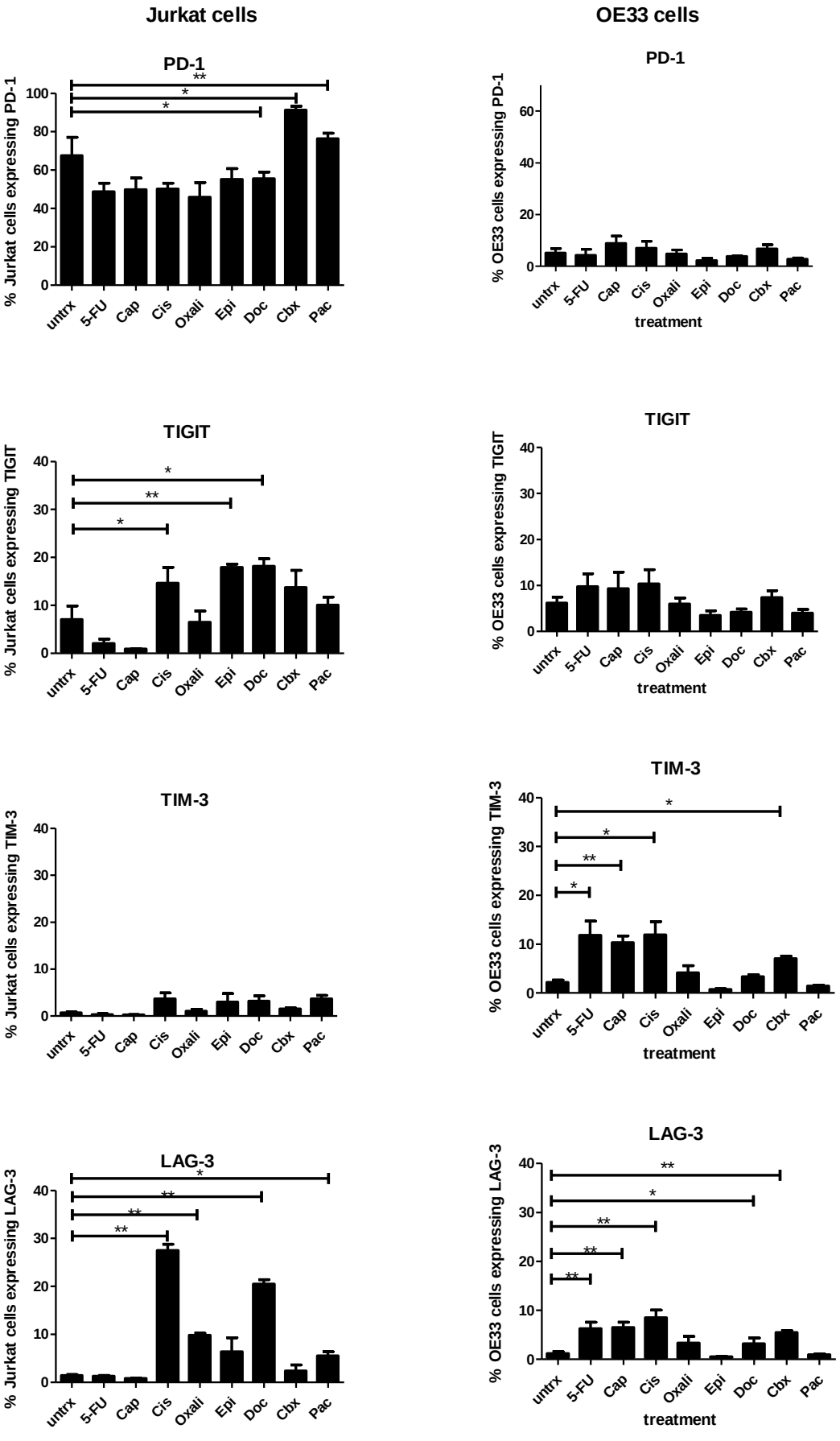
Jurkat cells
OE33 cells
PD-1
% Jurkat cells expressing PD-1
% OE33 cells expressing PD-1
TIGIT
% Jurkat cells expressing TIGIT
% OE33 cells expressing TIGIT
TIM-3
% Jurkat cells expressing TIM-3
% OE33 cells expressing TIM-3
LAG-3
% Jurkat cells expressing LAG-3
% OE33 cells expressing LAG-3
untrx
5-FU
Cap
Cis
Oxali
Epi
Doc
Cbx
Pac
treatment

Figure 6.14: Clinically relevant single agent chemotherapies significantly increase the surface expression of inhibitory IC receptors on the surface of viable activated Jurkat cells and OE33 cells following 48h treatment *in vitro*. Jurkat cells were activated with plate bound anti-CD3 and anti-CD28 for 48h in the presence or absence of single agent 5-fluorouracil (5-FU), capecitabine (cap), cisplatin (cis), oxaliplatin (oxali), epirubicin (epi), docetaxel (doc), carboplatin (cbx) and paclitaxel (pac) using a pre-optimised 48h IC_{50} dose. OE33 cells were treated for 48h in the presence or absence of single agent 5-fluorouracil (5-FU), capecitabine (cap), cisplatin (cis), oxaliplatin (oxali), epirubicin (epi), docetaxel (doc), carboplatin (cbx) and paclitaxel (pac) using a pre-optimised 48h IC_{50}. The expression of inhibitory IC receptors PD-1, TIGIT, TIM-3 and LAG-3 was assessed by flow cytometric analysis on viable Jurkat cells. Experiments repeated n=3 times, paired parametric t-test. *$p<0.05$ and **$p<0.01$.

6.2.12 Combination FLOT and CROSS CT treatment differentially altered IC expression on T cells from OGJ patients compared to healthy donors

As clinically-relevant single agent chemotherapies significantly altered the expression profile of ICs on the surface of Jurkat cells. We next investigated the direct effects of FLOT and CROSS CT on IC expression profiles on T cells from OGJ patients remains unknown. Therefore, to help guide the selection of the most appropriate ICs to target in combination with first-line chemotherapies in OGJ, non-cancer age-matched healthy donor (HD) PBMCs and OGJ cancer donor (CD) PBMCs were treated *ex vivo* with FLOT or CROSS CT and IC expression was profiled following 48h treatment (**Figure 6.15**).

There were significant differences in IC expression profiles of T cells from HDs versus CDs. PD-1 was expressed at significantly lower levels on the surface of $CD4^+$ T cells from CDs compared with HDs basally (52.12 ± 8.7 vs. 76.40 ± 2.0%, p=0.02), (**Figure 6.15B**). Similar trends were found within the $CD8^+$ T cell compartment, where PD-1 was expressed at significantly lower levels on the surface of $CD8^+$ T cells from CDs compared with HDs (39.95 ± 7.9 vs. 69.07 ± 2.8%, p=0.002), (**Figure 6.15B**). TIM-3 was expressed at significantly higher levels on the surface of $CD4^+$ T cells from CDs compared with HDs (33.87 ± 7.7 vs. 3.26 ± 0.9%, p=0.0007), (**Figure 6.15D**). Similarly, TIM-3 was also expressed at significantly higher levels on the surface of $CD8^+$ T cells from CDs compared with HDs (36.63 ± 4.2 vs. 2.01 ± 0.2%, p=0.0007). LAG-3 and A2aR were expressed at significantly higher levels on the surface of $CD8^+$ T cells from CDs compared with HDs (39.94 ± 7.8 vs. 9.02 ± 2.1%, p=0.004 and 5.11 ± 2.1 vs. 1.31 ± 0.3%, p=0.05, respectively) (**Figure 6.15E and F**).

FLOT and CROSS CTs significantly altered IC expression on the surface of T cells from both CDs and HDs (**Figure 6.15**). FLOT upregulated PD-1 on the surface of $CD8^+$ T cells from CDs *ex vivo* (59.14 ± 6.7 vs. 39.95 ± 7.9%, p=0.03), (**Figure 6.15B**). In contrast, CROSS CT significantly decreased TIM-3 expression on the surface of $CD8^+$ T cells from CDs compared with the vehicle control (26.59 ± 2.7 vs. 36.63 ± 4.2%, p=0.01), (**Figure 6.15E**). Interestingly, FLOT significantly upregulated LAG-3 on the surface of $CD4^+$ T cells from HDs and from CDs (8.96 ± 1.4 vs. 5.21 ± 0.7%, p=0.03 and 23.17 ± 5.5 vs. 18.44 ± 5.6%, p=0.01, respectively), (**Figure 6.15E**). In contrast, CROSS CT significantly downregulated LAG-3 on the surface of $CD4^+$ T cells from (3.27 ± 0.8 vs. 5.21 ± 0.7%, p=0.03), (**Figure 6.15E**). However, CROSS CT significantly decreased LAG-3 expression on the surface of $CD8^+$ T cells from CDs compared with the vehicle control (39.94 ± 7.8 vs. 27.14 ± 8.6%, p=0.04), (**Figure 6.15E**). Additionally, FLOT and CROSS CT significantly upregulated A2aR on the surface of $CD4^+$ T cells compared with the vehicle control from CDs (5.77 ± 1.1 vs. 7.36 ± 1.4, 2.58 ± 1.0%, p=0.02 and p=0.01), (**Figure 6.15F**). Similarly, FLOT significantly upregulated A2aR on the surface of $CD8^+$ T cells compared with the vehicle control from CDs (10.36 ± 2.4 vs. 5.11 ± 5.1% p=0.03), (**Figure 6.15F**). Interestingly, FLOT significantly increased the expression of CTLA-4 on the surface of $CD8^+$ T cells compared with the vehicle from HDs (9.42 ± 1.7 vs. 4.07 ± 0.6% p=0.03), (**Figure 6.15G**). FLOT and CROSS CT significantly upregulated KLRG-1 on the surface of $CD4^+$ T cells compared with the vehicle control in both HDs (5.84 ± 1.2 vs. 3.83 ± 1.1 and 2.03 ± 0.6% p=0.03 and p=0.03) and CDs (6.07 ± 1.5 vs. 7.28 ± 2.4 and 1.67 ± 0.5% p=0.007 and p=0.007), (**Figure 6.15H**). Similarly, FLOT and CROSS CT significantly upregulated KLRG-1 on the surface of $CD8^+$ T cells compared with the vehicle control in both HDs (14.45 ± 4.7 vs. 11.58 ± 5.1 and 5.7 ± 3.1% p=0.03 and p=0.03) and CDs (9.57 ± 1.2% vs. 11.23 ± 1.6% and 3.71 ± 0.5% p=0.01 and p=0.01), (**Figure 6.15H**). FLOT significantly upregulated PD-L1 on the surface of $CD4^+$ compared with the vehicle control from HDs (6.69 ± 2.3 vs. 1.27 ± 0.3%, p=0.03), and from CDs (15.41 ± 4.3 vs. 7.18 ± 2.3%, p=0.02), *ex vivo* (**Figure 6.15I**). Similarly, FLOT significantly upregulated PD-L1 on the surface of $CD8^+$ compared with the vehicle control from HDs (7.64 ± 2.4 vs. 1.48 ± 0.5%, p=0.03), and from CDs (13.32 ± 4.5 vs. 3.44 ± 1.14%, p=0.03), *ex vivo* (**Figure 6.15I**). In addition, CROSS CT significantly upregulated PD-L1 on the surface of $CD8^+$ compared with the vehicle control from CDs (16.99 ± 7.4 vs. 3.44 ± 1.14%, p=0.03), *ex vivo* (**Figure 6.15I**). CROSS CT significantly upregulated PD-L2 on the surface of $CD8^+$ T cells compared with the vehicle control from CDs (17.05 ± 6.1 vs. 5.78 ± 2.5%, p=0.05), (**Figure 6.15J**). In addition,

FLOT significantly upregulated CD160 on the surface of $CD4^+$ T cells compared with the vehicle control from CDs (5.13 ± 0.8 vs. 2.5 ± 1.0%, p=0.05), (**Figure 6.15K**). FLOT and CROSS CT significantly upregulated CD160 on the surface of $CD8^+$ T cells compared with the vehicle control from CDs (15.00 ± 4.7% vs. 16.52 ± 5.0% and 7.49 ± 3.2% p=0.01 and p=0.05), (**Figure 6.15K**).

Overall, PD-1 was expressed at significantly lower levels on T cells from CDs compared with HDs. However, TIM-3, LAG-3 and A2aR were expressed at significantly higher levels on the surface of T cells from CDs compared with HDs. A range of ICs were directly upregulated following FLOT and CROSS CT treatment *ex vivo* which included: PD-1, A2aR, CTLA-4, KLRG-1, PD-L1, PD-L2 and CD160. Interestingly, CROSS CT significantly decreases TIM-3 and LAG-3 on the surface of $CD8^+$ T cells ex vivo from CDs. FLOT and CROSS CT had a more substantial effect in altering IC expression on T cells from CDs than HDs.

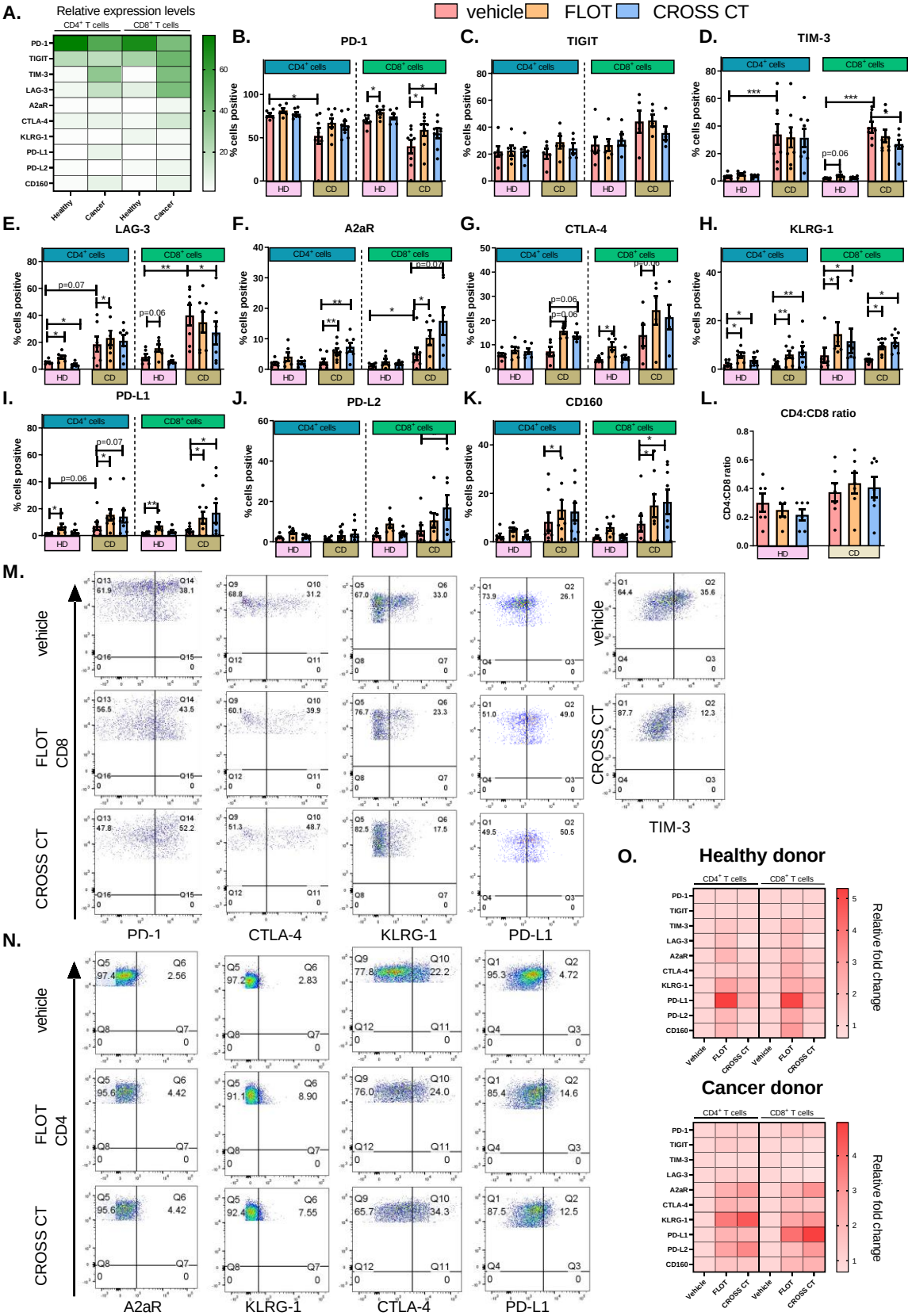
A.
Relative expression levels
CD4+ T cells
CD8+ T cells
PD-1
TIGIT
TIM-3
LAG-3
A2aR
CTLA-4
KLRG-1
PD-L1
PD-L2
CD160
Healthy
Cancer
Healthy
Cancer
vehicle
FLOT
CROSS CT
B. PD-1
C. TIGIT
D. TIM-3
E. LAG-3
F. A2aR
G. CTLA-4
H. KLRG-1
I. PD-L1
J. PD-L2
K. CD160
L. CD4:CD8 ratio
% cells positive
CD4:CD8 ratio
HD
CD
M.
vehicle
FLOT
CROSS CT
CD8
CD4
TIM-3
PD-1
CTLA-4
KLRG-1
PD-L1
N.
A2aR
KLRG-1
CTLA-4
PD-L1
O.
Healthy donor
Cancer donor
Relative fold change
Vehicle
FLOT
CROSS CT

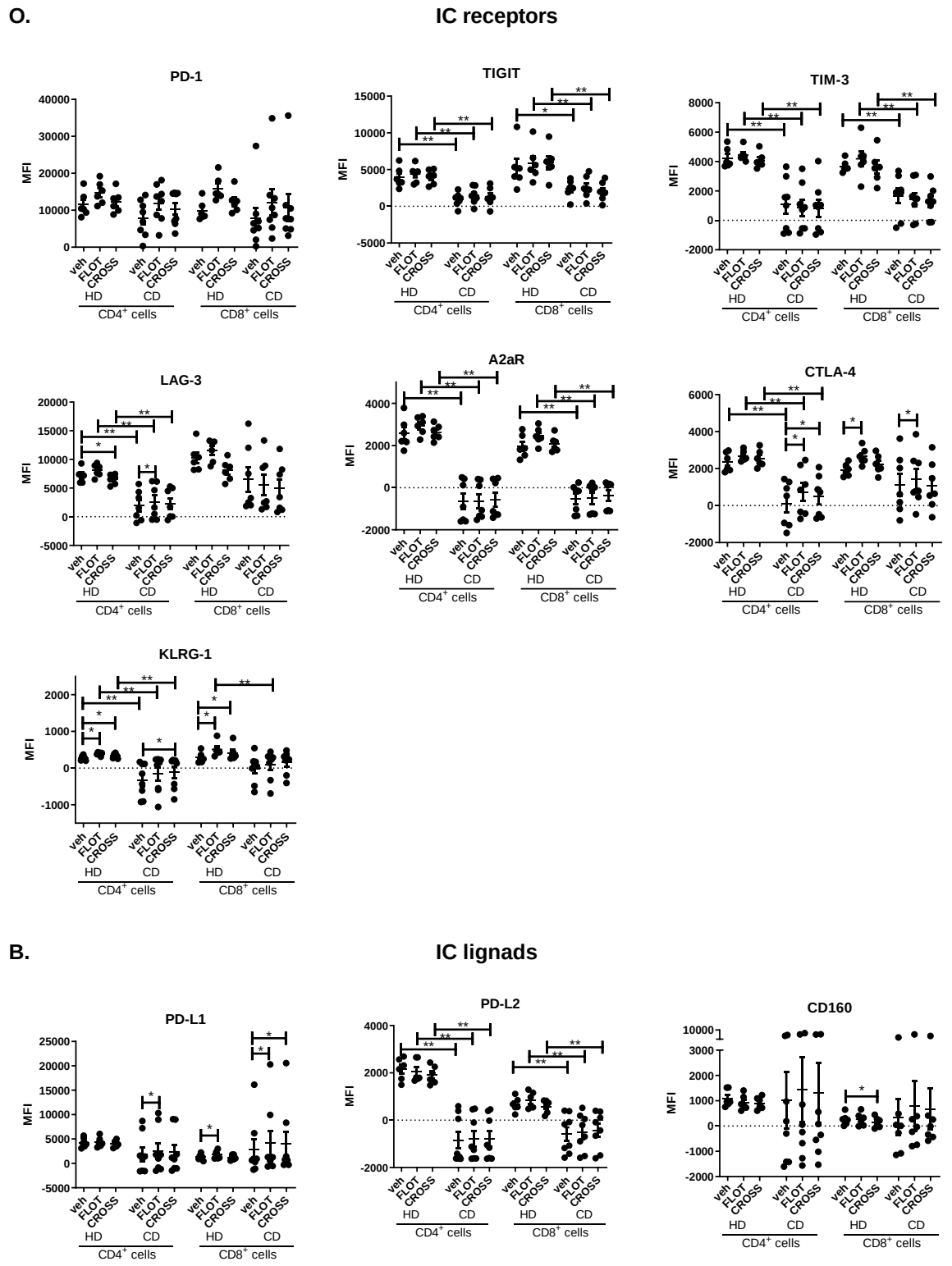

Figure 6.15: FLOT and CROSS CT treatment significantly increases the percentage of T cells expressing PD-1, A2aR, KLRG-1 and PD-L1, while decreasing the percentage of T cells expressing TIM-3 and LAG-3. Donor PBMCs were activated with plate bound anti-CD3, anti-CD28 and IL-2 for 72h followed by 48h treatment with FLOT and CROSS CT regimens. The percentage of viable $CD4^+$ and $CD8^+$ cells expressing IC proteins were assessed by flow cytometry. (A) Heat map

summarising the expression levels of ICs on CD4 and CD8 cells from healthy donors (HDs) versus cancer donors (CDs). Graphs showing effect of vehicle, FLOT and CROSS CT on PD-1 (B), TIGIT (C), TIM-3 (D), LAG-3 (E), A2aR (F), CTLA-4 (G) and KLRG-1 (H), PD-L1 (I), PD-L2 (J) and CD160 (K) IC proteins. (L) Presents the CD4:CD8 ratio. (M) and (N) detail representative dot plots of IC expression on CD4 and CD8 cells post-vehicle, FLOT or CROSS CT from CDs. (O) Heatmaps summarising the effect of FLOT and CROSS CT on IC expression profiles of CD4 and CD8 cells as a fold change relative to the vehicle control. Healthy age-matched donors (HD) (n=6) and OAC cancer donors (CD) (n=8). *p<0.05, **p<0.01 and ***p<0.001 Wilcoxon test to compare effect of treatments within HDs and CDs, and Mann Whitney to compare between HDs vs. CDs. (O) and (P) depict the effects of chemotherapy on the MFI expression of IC ligands and receptors. Gating strategy and representative dot plots showing the effect of FLOT and CROSS CT on IC expression profiles of T cells is shown in Appendix **Figure A6.6**.

6.2.13 Blockade of the PD-1 signalling axis decreases LAG-3, CTLA-4 and PD-L1 and increases PD-L2 on the surface of OGJ-derived T cells

Koyama et al., demonstrated that TIM-3 upregulation following PD-1 blockade was a mechanism of acquired resistance to nivolumab in non-small cell lung cancer patients[365]. This study investigated if nivolumab, atezolizumab, A2aR antagonism, dual nivolumab-atezolizumab or dual nivolumab-A2aR antagonism affected the expression of ICs on the surface of OGJ-derived T cells in the context of OGJ, which might contribute to the development of ICB resistance in OGJ patients.

A2aR antagonism and dual nivolumab-A2aR antagonism significantly upregulated TIGIT on the surface of $CD4^+$ T cells compared with untreated cells (23.78 ± 3.6% vs. 25.48 ± 3.7%, 20.47 ± 3.9%, p=0.03 and p=0.02), (**Figure 6.16A**). In contrast nivolumab significantly decreased the expression of TIGIT on the surface of $CD8^+$ T cells compared with untreated cells (38.54 ± 7.8% vs. 44.24 ± 8.3%, p=0.009), (**Figure 6.16A**).

Atezolizumab and dual nivolumab-atezolizumab significantly decreased LAG-3 expression on the surface of $CD4^+$ T cells compared with untreated cells (12.67 ± 4.0% vs. 12.98 ± 4.0%, 18.44 ± 5.5%, p=0.03 and p=0.03, respectively) (**Figure 6.16A**). Similarly, atezolizumab, A2aR antagonism, dual nivolumab-atezolizumab and dual nivolumab-A2aR antagonism significantly decreased LAG-3 expression on the surface of $CD8^+$ T cells compared with untreated cells (26.93 ± 4.9%, 25.28 ± 6.8%, 28.57 ± 5.7%, 24.93 ± 5.9% vs 39.94 ± 7.8%: p=0.01, p=0.03 p=0.007 and p=0.01, respectively), (**Figure 6.16A**).

Nivolumab, atezolizumab and dual nivolumab-atezolizumab significantly decreased CTLA-4 expression on the surface of $CD4^+$ T cells compared with untreated cells (4.55 ± 1.85% vs. 4.01 ± 1.7%, 4.36 ± 1.7% and 7.24 1.9%, p=0.03, p=0.01 and p=0.02) (**Figure 6.16A**). Similarly, nivolumab significantly decreased CTLA-4 expression on the surface of $CD8^+$ T cells compared with untreated cells (7.61 ± 2.7% vs. 14.01 ± 4.4%, p=0.04), (**Figure 6.16A**). ICB did not significantly affect the expression of TIM-3, A2aR (**Figure 6.16A**). Nivolumab significantly decreased PD-1 expression on the surface of T cells demonstrating that nivolumab was blocking the binding site of the anti-PD-1 fluorochrome-conjugated antibody (**Figure 6.16A**).

Furthermore, nivolumab and dual nivolumab-A2aR antagonism significantly decreased PD-L1 expression on the surface of $CD8^+$ T cells compared with untreated cells (1.16 ± 0.7% vs. 2.45 ± 1.6% and 3.44 ± 1.1%, p=0.01 and p=0.01), (**Figure 6.16B**). Interestingly, dual nivolumab-A2aR antagonism significantly increased the expression of PD-L2 on the surface of $CD8^+$ T cells compared with untreated cells (4.89 ± 1.4% vs. 3.52 ± 1.2%, p=0.02), (**Figure 6.16B**). ICB did not significantly affect the expression of CD160 (**Figure 6.16B**).

Overall, ICB significantly altered IC expression on the surface of OGJ T cells increasing T cell expression of TIGIT and PD-L2, and decreasing T cell expression of LAG-3, CTLA-4 and PD-L1.

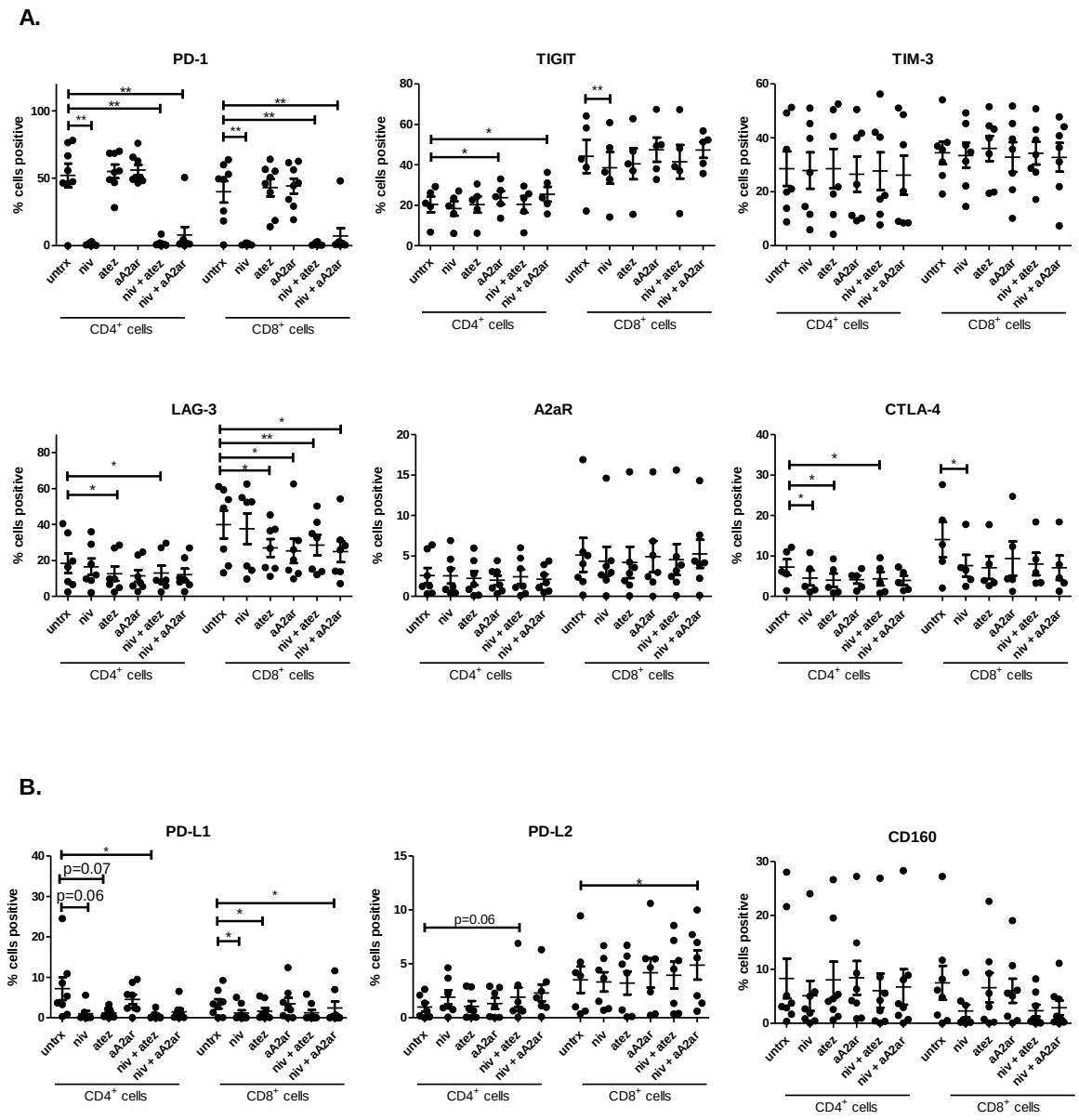

Figure 6.16: Blockade of the PD-1 signalling axis decreases the percentage of LAG-3$^+$, CTLA-4$^+$ and PD-L1$^+$ T cells, whereas dual nivolumab-atezolizumab treatment increases the percentage of PD-L2$^+$ T cells *ex vivo*. OGJ donor PBMCs were activated with plate bound anti-CD3 and anti-CD28 and IL-2 for 72h followed by 48h treatment single agent nivolumab, atezolizumab, A2aR antagonist, dual nivolumab-atezolizumab and dual nivolumab-A2aR antagonist. The percentage of viable CD3$^+$CD4$^+$ and CD3$^+$CD8$^+$ cells expressing IC receptors (A) (PD-1, TIGIT, TIM-3, LAG-3, A2aR, CTLA-4 and KLRG1) and IC ligands (B) (PD-L1, PD-L2 and CD160) was assessed by flow cytometry (n=8). *p<0.05, **p<0.01, paired non-parametric t-test.

6.2.14 Single and combination blockade of the PD-1, PD-L1 and A2aR pathways attenuates the FLOT- and CROSS CT-induced CD27 downregulation on the surface of OGJ T cells and promotes differentiation of effector memory T cells toward a terminally differentiated state

To further understand if ICB might synergise with chemotherapy treatment in OGJ we investigated what effect combining ICB with FLOT or CROSS CT regimens has the activation status of OGJ patient-derived T cells.

Single agent nivolumab and atezolizumab or dual nivolumab-A2aR antagonism significantly increased CD27 expression on the surface of $CD4^+$ T cells compared with the vehicle control (nivolumab:39.83 ± 5.6% vs. atezolizumab:45.07 ± 4.4%, dual nivolumab-A2aR antagonism:51.83 ± 6.9%, vehicle control:27.97 ± 4.9%, p=0.03, p=0.03, p=0.03 respectively) (**Figure 6.17A**). Similarly, there were trends toward an increase in CD27 expression on the surface of $CD4^+$ T cells following single agent A2aR antagonism compared with the vehicle control (p=0.06), (**Figure 6.17A**).

Although FLOT significantly decreased CD27 expression on the surface of $CD4^+$ T cells compared with the vehicle control (10.39 ± 1.9%, vs. 27.97 ± 4.9%, p=0.03), the addition of ICB with concomitant FLOT treatment attenuated FLOT-induced downregulation of CD27 on the surface of $CD4^+$ T cells *ex vivo* (**Figure 6.17A**). Single agent nivolumab, atezolizumab, A2aR antagonism, dual nivolumab-atezolizumab dual and nivolumab-A2aR antagonism significantly increased CD27 on the surface of $CD4^+$ T cells in combination with FLOT compared with FLOT treated cells (nivolumab:16.18 ± 2.6%, atezolizumab:20.02 ± 3.7%, A2aR antagonism:31.10 ± 3.9%, dual nivolumab-atezolizumab:22.03 ± 2.9%, dual nivolumab-A2aR antagonism:31.55 ± 4.7% vs. FLOT:10.39 ± 1.9%, p=0.03, p=0.03, p=0.03, p=0.03, p=0.03, p=0.03 respectively), (**Figure 6.17A**). Similar trends were found within the $CD8^+$ T cell compartment.

CROSS CT also significantly decreased CD27 expression on the surface of $CD4^+$ T cells compared with untreated cells (11.25 ± 2.4 vs. 27.97 ± 4.9%, p=0.03) however, the addition of ICB with concomitant CROSS CT treatment attenuated CROSS CT-induced downregulation of CD27 on the surface of $CD4^+$ T cells *ex vivo* (**Figure 6.17A**). Single agent nivolumab, atezolizumab, A2aR antagonism, dual nivolumab-atezolizumab dual and nivolumab-A2aR antagonism significantly increased CD27 on the surface of $CD4^+$ T cells in combination with CROSS CT compared with CROSS CT only treated cells (nivolumab:17.63 ± 2.6%, atezolizumab:21.24 ± 4.0%, A2aR antagonism:28.4 ± 4.5%, dual nivolumab-

atezolizumab:22.49 ± 4.1%, dual nivolumab-A2aR antagonism:29.95 ± 6.0% vs. CROSS CT:11.25 ± 2.4% p=0.03, p=0.03, p=0.03, p=0.03, p=0.03, p=0.03 respectively), (**Figure 6.17A**). Similar trends were found within the $CD8^+$ T cell compartment.

Single agent nivolumab, atezolizumab and dual nivolumab-atezolizumab significantly decreased the frequency of effector memory $CD4^+$ T cells *ex vivo* compared with the vehicle control (nivolumab:56.08 ± 4.05%, atezolizumab:50.47 ± 3.7%, dual nivolumab-atezolizumab:45.47 ± 3.4% and vehicle control:64.13 ± 4.0%, p=0.03, p=0.03, p=0.03, respectively), (**Figure 6.17B)**.Single agent nivolumab, atezolizumab, A2aR antagonism or dual nivolumab-atezolizumab significantly increased the frequency of terminally differentiated effector memory $CD4^+$ T cells *ex vivo* compared with the vehicle control (nivolumab:30.52 ± 6.1%, atezolizumab:34.25 ± 6.8%, A2aR antagonism:37.84 ± 10.62%, dual nivolumab-atezolizumab:40.08 ± 8.2% and vehicle control:20.08 ± 5.2% p=0.03, p=0.03, p=0.03, p=0.03 respectively), (**Figure 6.17B**).

Although FLOT significantly increased the frequency of effector memory $CD4^+$ T cells compared with the vehicle control (82.4 ± 3.3% vs. 64.13 ± 4.1%, p=0.03) and subsequently decreased the frequency of terminally differentiated effector memory $CD4^+$ T cells compared (7.46 ± 0.1% vs. 20.08 ± 5.2%, p=0.06), the addition of ICB attenuated these effects (**Figure 6.17B**). ICB decreased the frequency of effector memory $CD4^+$ T cells and subsequently increased the frequency of terminally differentiated $CD4^+$ memory T cells with concomitant FLOT treatment *ex vivo* (**Figure 6.17B**).

Single agent nivolumab, atezolizumab, A2aR antagonism, dual nivolumab-atezolizumab and dual nivolumab-A2aR antagonism significantly decreased the frequency of effector memory $CD4^+$ T cells in combination with FLOT *ex vivo* compared with FLOT treated cells (nivolumab:77.50 ± 3.7%, atezolizumab:74.92 ± 3.7%, A2aR antagonism:65.75 ± 2.2%, dual nivolumab-atezolizumab:73.65 ± 2.9% and dual nivolumab-A2aR antagonism:65.65 ± 1.6% and FLOT:82.40 ± 3.3%, p=0.03, p=0.03, p=0.03, p=0.03 and p=0.03 respectively) (**Figure 6.17B**). Single agent nivolumab, atezolizumab, A2aR antagonism or dual nivolumab-atezolizumab in combination with FLOT significantly increased the frequency of terminally differentiated effector memory $CD4^+$ T cells *ex vivo* compared with FLOT treated cells (nivolumab:11.93 ± 2.5%, atezolizumab:13.83 ± 2.5%, A2aR antagonism:22.75 ± 4.9%, dual nivolumab-atezolizumab:15.59 ± 2.9% and FLOT:7.47 ± 0.1%, p=0.03, p=0.03, p=0.03, p=0.03 and p=0.03 respectively), (**Figure 6.17B**). Similar effects were observed within the $CD8^+$ T cell compartment.

Similarly, although CROSS CT significantly increased the frequency of effector memory $CD4^+$ T cells compared with the vehicle control (80.72 ± 2.6% vs. 64.13 ± 4.1%, p=0.03) and subsequently decreased the frequency of terminally differentiated effector memory $CD4^+$ T cells (7.40 ± 1.9% vs. 20.08 ± 5.2%, p=0.03), the addition of ICB attenuated these effects (**Figure 6.17B**). ICB decreased the frequency of effector memory $CD4^+$ T cells and subsequently increased the frequency of terminally differentiated $CD4^+$ memory T cells with concomitant CROSS CT treatment *ex vivo* (**Figure 6.17B**).

Single agent nivolumab, A2aR antagonism and dual nivolumab-A2aR antagonism significantly decreased the frequency of effector memory $CD4^+$ T cells in combination with CROSS CT *ex vivo* compared with CROSS CT treated cells (nivolumab:76.18 ± 2.4%, A2aR antagonism:68.28 ± 3.3%, dual nivolumab-A2aR antagonism:66.27 ± 3.6% and CROSS CT:80.72 ± 2.6%, p=0.03, p=0.03, p=0.03, p=0.03 respectively), (**Figure 6.17B**). Subsequently, single agent nivolumab, atezolizumab, A2aR antagonism, dual nivolumab-atezolizumab, or dual nivolumab-A2aR antagonism in combination with CROSS CT significantly increased the frequency of terminally differentiated effector memory $CD4^+$ T cells *ex vivo* compared with CROSS CT treated cells (nivolumab:12.91 ± 3.2%, atezolizumab:15.30 ± 4.4%, A2aR antagonism:22.15 ± 5.2%, dual nivolumab-atezolizumab:16.03 ± 4.6%, dual nivolumab-A2aR antagonism:21.96 ± 6.9% and CROSS CT:7.40 ± 2.0%, p=0.03, p=0.03, p=0.03, p=0.03 respectively), (**Figure 6.17B**). Similar trends were observed within the $CD8^+$ T cell compartment (**Figure 6.17B**).

Overall, FLOT and CROSS CT significantly decreased CD27 expression on the surface of T cells however, the addition of ICB with concomitant FLOT or CROSS CT treatment attenuated the chemotherapy-induced downregulation of CD27 on the surface of T cells *ex vivo.* Interestingly, FLOT and CROSS CT significantly increased the frequency of effector memory T cells and decreased the frequency of terminally differentiated effector memory T cells, however, addition of ICB significantly decreased the frequency of effector memory T cells and subsequently increased the frequency of terminally differentiated effector memory T cells *ex vivo*.

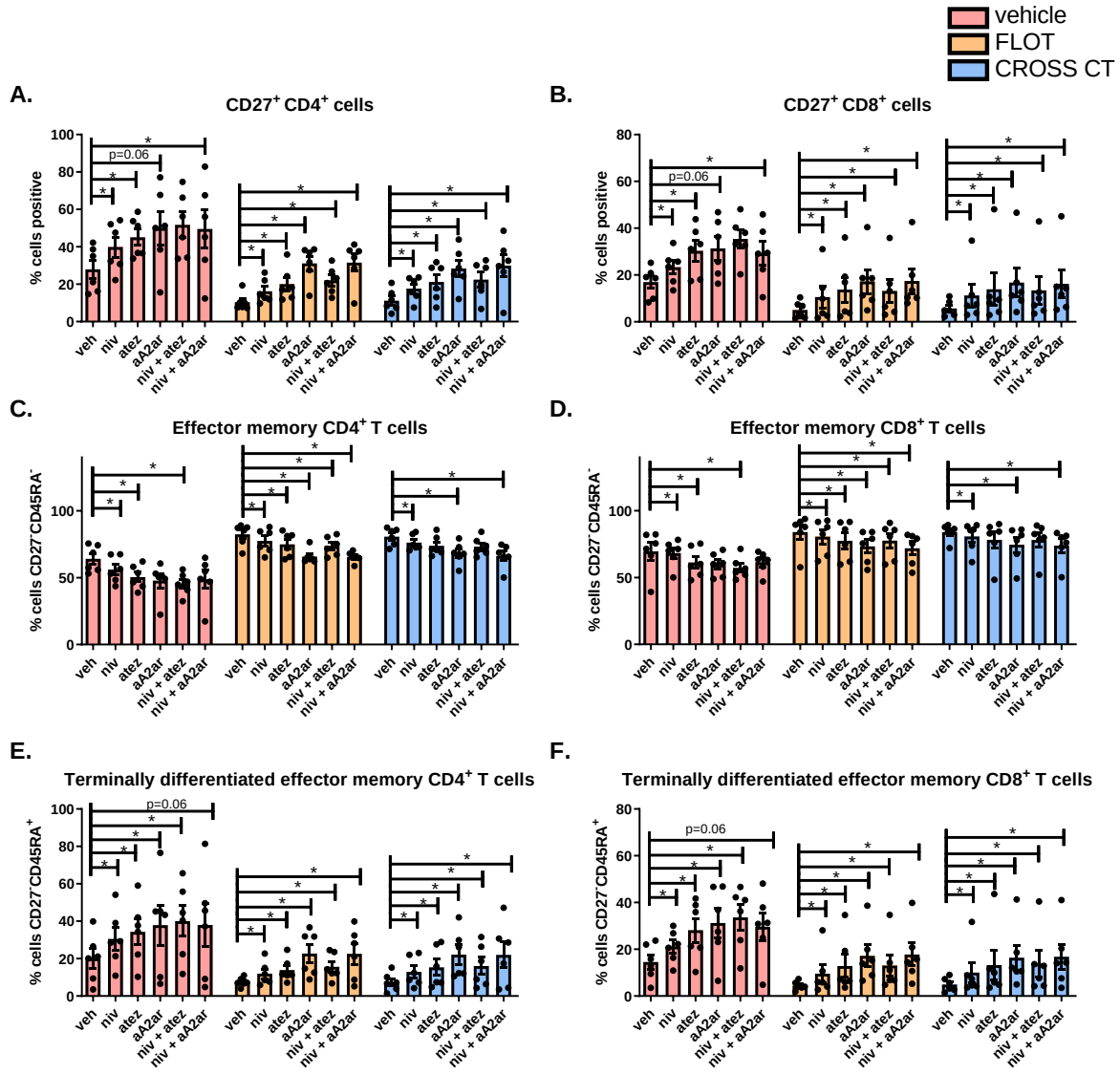

Figure 6.17: Single agent nivolumab, atezolizumab, A2aR antagonism and dual immune checkpoint blockade attenuates chemotherapy-induced downregulation of CD27 on the surface of T cells and promotes differentiation of effector memory cells into a terminally differentiated state *ex vivo*. OGJ donor PBMCs (n=8) were activated with plate bound anti-CD3 and anti-CD28 for 72h followed by 48h treatment with FLOT and CROSS CT regimens in the absence or presence of single agent nivolumab, atezolizumab, A2aR antagonist, dual nivolumab-atezolizumab, dual nivolumab-A2aR antagonist or vehicle control (veh). Expression of a range of markers reflective of T cell activation status (ICOS, CD27, CD69, CD62L and CD45RA) was assessed on viable $CD3^+CD4^+$ and $CD3^+CD8^+$ cells by flow cytometry (A). Only effect on CD27 expression shown. The effect on T cell differentiation states was assessed (B) including percentage of viable naïve ($CD27^+CD45RA^+$), central memory ($CD27^+CD45RA^-$), effector memory ($CD27^-CD45RA^-$) and terminally differentiated effector memory ($CD27^-CD45RA^+$) $CD3^+CD4^+$ and $CD3^+CD8^+$ cells by flow cytometry. Only effect

on effector memory and terminally differentiated effector memory cells is shown. *p<0.05, paired non-parametric t-test.

6.2.15 IC expression correlates with subsequent poor response to treatment and more advanced staged tumours; ICB enhances lymphocyte-mediated cytolysis of OE33 cells in the presence of post-FLOT and post-CROSS CT tumour cell secretome

Humphries *et al.*, demonstrated that the levels of CD3, CD4, CD8, ICOS and PD-1 were individually predictive of better overall survival in OGJ by immunohistochemistry[366]. In this study we correlated the frequency of circulating and tumour-infiltrating T cells expressing ICs with clinical characteristics within our patient cohort. Interestingly, the frequency of circulating $CD3^+ICOS^+$ cells positively correlated with nodal metastasis (r=0.7 and p=0.02) (**Figure 6.18** and **Table 6.3**). In addition, the frequency of circulating $CD3^+CTLA\text{-}4^+$ cells positively correlated with a poor pathologic response to neoadjuvant treatment determined by tumour regression grade using the Mandard scoring system (r=0.68 and p=0.04) (**Figure 6.18** and **Table 2**). Moreover, the frequency of $CD3^+CTLA\text{-}4^+$ cells and $CD8^+PD\text{-}L2^+$ cells positively correlated with more advanced stage tumours (r=0.71 and p=0.02, and r=0.65 and p=0.04, respectively) (**Figure 6.18** and **Table 6.3**).

The frequency of tumour-infiltrating $CD3^+CTLA\text{-}4^+$ cells, $CD8^+PD\text{-}L2^+$ cells and $CD8^+A2aR^+$ cells positively correlated with nodal metastasis (r=0.68 and p=0.03, r=0.68 and p=0.03 and r=0.68 and p=0.03) (**Figure 6.18** and **Table 6.3**). The frequency of tumour-infiltrating $CD3^+CTLA\text{-}4^+$, $CD8^+PD\text{-}L2^+$, $CD8^+TIGIT^+$, $CD8^+A2aR^+$ cells positively correlated with lymphovascular invasion (r=0.72 and p=0.03, r=0.72 and p=0.03 and r=0.72 and p=0.03) (**Figure 6.18** and **Table 6.3**). The frequency of tumour-infiltrating $CD4^+TIGIT^+$ cells and $CD8^+PD\text{-}L2^+$ cells positively correlated with a poor response to subsequent neoadjuvant treatment determined by tumour regression grade (r=0.72 and p=0.04, r=0.75 and p=0.03) (**Figure 6.18** and **Table 6.3**). In addition, the frequency of tumour-infiltrating $CD8^+LAG\text{-}3^+$ cells positively correlated with more advanced stage tumours (r=0.65 and p=0.04) (**Figure 6.18** and **Table 6.3**).

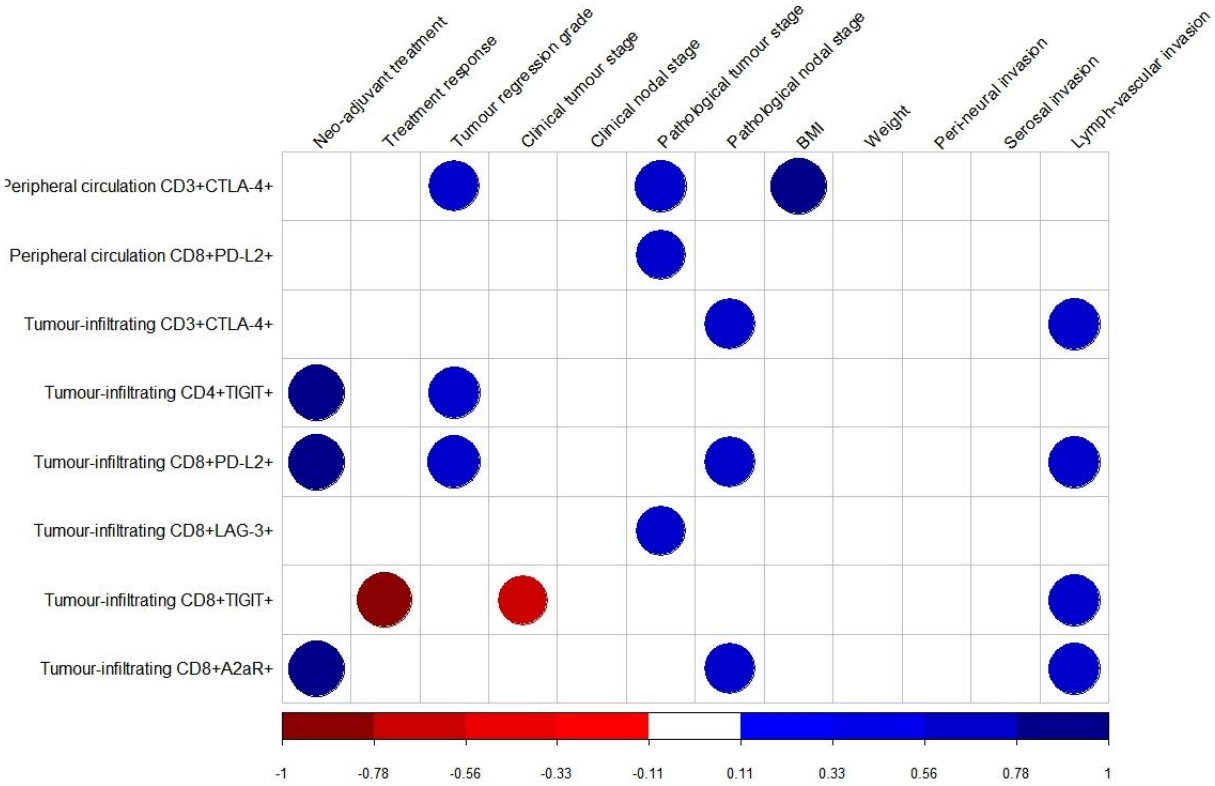

Figure 6.18: IC expression correlates with more advanced stage tumours. (A). Corrplot showing the correlations between the frequency of circulating (n=17) and tumour-infiltrating (n=10) T cells expressing ICs from treatment-naïve OGJ patients with clinical demographics. Only significant data shown. *p<0.05. Blue circle indicates a positive correlation and a red circle indicates a negative correlation.

Table 6.3. The frequency of $CD3^+CTLA\text{-}4^+$ circulating peripheral blood T cells positively correlates with a subsequent poor pathologic treatment response in the neoadjuvant setting in OGJ patients.

Peripheral circulation			
ICs	Clinical characteristics	R value	P value
$CD3^+CTLA\text{-}4^+$	Tumour regression grade	0.68	0.04
$CD3^+CTLA\text{-}4^+$	Pathological tumour stage	0.71	0.02
$CD8^+PD\text{-}L2^+$	Pathological tumour stage	0.65	0.04
Tumour-infiltrating			
ICs	Clinical characteristics	R value	P value
$CD3^+CTLA\text{-}4^+$	Pathological nodal stage	0.68	0.03
$CD3^+CTLA\text{-}4^+$	Lympho-vascular invasion	0.72	0.03

$CD4^+TIGIT^+$	Tumour regression grade	0.72	0.04
$CD8^+PD\text{-}L2^+$	Tumour regression grade	0.75	0.03
$CD8^+PD\text{-}L2^+$	Pathological nodal stage	0.68	0.03
$CD8^+PD\text{-}L2^+$	Lympho-vascular invasion	0.72	0.03
$CD8^+LAG\text{-}3^+$	Pathological tumour stage	0.65	0.04
$CD8^+TIGIT^+$	Lympho-vascular invasion	0.72	0.03
$CD8^+A2aR^+$	Pathological nodal stage	0.68	0.03
$CD8^+A2aR^+$	Lympho-vascular invasion	0.72	0.03

The percentage of $CD3^+$, $CD3^+CD4^+$ and $CD3^+CD8^+$ cells expressing inhibitory ICs including PD-L1, CD160, TIM-3, PD-L2, TIGIT, LAG-3, ICOS, A2aR, CTLA-4 and PD-1 OGJ tumour tissue in the treatment-naïve setting was correlated with patient demographics and clinical features of the tumour (n=10). Patient demographics and clinical features included gender, age, tumour type (OGJ=0 and OGJ=1), neo-adjuvant treatment received (CROSS=0 and FLOT=1), treatment response (determined by radiographic features using PET/CT), tumour regression grade (TRG), clinical tumour stage and nodal involvement, pathological tumour stage and nodal involvement, body mass index (BMI kg/m^2), peri-neural invasion, serosal invasion and lymph-vascular invasion. BMI and weight measurement was recorded post-treatment. Spearman correlation. Only significant data shown.

Overall, the frequency of tumour-infiltrating T cells expressing ICs correlated with more advanced stage tumours and subsequent poor response to neoadjuvant treatment. In light of these findings, we sought to investigate if ICB might enhance lymphocyte-mediated cytolysis of OE33 OGJ cells using treatment-naïve OGJ PBMCs that were pre-activated in the presence or absence of nivolumab, ipilimumab or dual nivolumab-ipilimumab (**Figure 6.19**).

Dual nivolumab-ipilimumab treatment significantly enhanced lymphocyte-mediated killing of OE33 cells compared with untreated lymphocytes, (65.56 ± 6.3% vs. 88.52 ± 11.31%, p=0.01). In addition, given that CHECKMATE 649 demonstrated that the addition of nivolumab to first-line chemotherapy regimens (FLOT/XELOX) increased the OS of oesophagogastric patients[136], we also investigated if ICB might synergise with chemotherapy treatment to enhance lymphocyte-mediated killing of OGJ cells. Therefore, untreated lymphocytes and ICB-treated lymphocytes were co-cultured with OE33 cells in the absence or presence of vehicle control, FLOT- or CROSS CT-treated OE33 tumour cell secretome (**Figure 6.19**). This experimental setup was designed to mimic the clinical scheduling of ICB with chemotherapy, as ICB is typically administered following chemotherapy (days to weeks) at a timepoint in which the tumour has been exposed and altered by the chemotherapy, but the chemotherapy has been excreted by the body (**Figure 6.19A**). In the presence of post-FLOT tumour cell secretome dual nivolumab-ipilimumab treatment significantly enhanced lymphocyte-mediated

killing of OE33 cells compared with untreated lymphocytes (45.51 ± 10.20% vs. 73.94 ± 13.54%, p=0.01) (**Figure 6.19B**). Similarly, in the presence of post-CROSS CT tumour cell secretome, dual nivolumab-ipilimumab treatment significantly enhanced lymphocyte-mediated killing of OE33 cells compared untreated lymphocytes (47.64 ± 10.09% vs. 75.53 ± 11.51%, p=0.02) (**Figure 6.19B**).

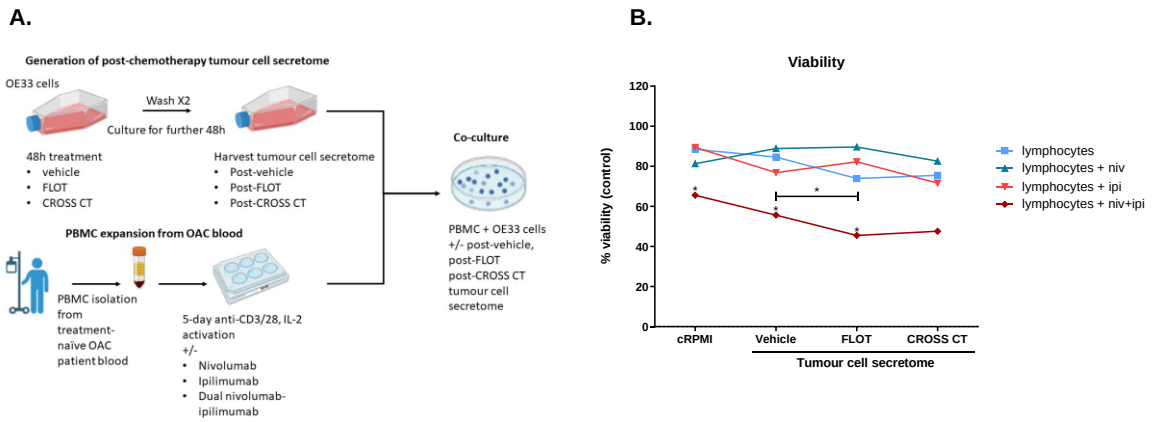

Figure 6.19: Dual nivolumab-ipilimumab synergises with chemotherapy enhancing OGJ lymphocyte-mediated killing of OE33 cells. (A) Schematic representation of co-culture experiment. (B) OE33 cells were untreated (untrx) or treated with vehicle (veh)-, FLOT- or CROSS-treated OE33 conditioned media for 48h. Activated treatment-naïve OAC patient-derived PBMCs were also co-cultured with OE33s in an effector:target (E:T) ratio of 5:1 (50,000:10,000) for 48h. PBMCs pre-activated for 5 days using anti-CD3/28 in the absence or presence of nivolumab (10 µg/ml), ipilimumab (10 µg/ml) or dual nivolumab-ipilimumab (10 µg/ml and 10 µg/ml). A CCK8 assay was used to determine the viability of OE33 cells (experiments carried out n=6 independent experimental repeats with duplicate technical replicates). Wilcoxon t test. *p<0.05 denotes a significant difference in tumour cell viability between untreated lymphocytes (blue line) versus lymphocytes treated with nivolumab (turquoise line), ipilimumab (orange line) or dual niv+ipi (red line).

6.3 Discussion

Chemotherapy is garnering a lot of attention as a complementary partner to combine with ICB therapy to expand the efficacy of ICB for a greater spectrum of patients[163] and is well-established for the treatment of lung cancer and melanoma, whereby combining ICB with chemotherapy substantially enhanced the efficacy of chemotherapy compared with either

modality alone, achieving durable clinical responses[204]. Until now PD-1 ICB was mainly assessed in the adjuvant setting for OGJ patients as second- or third-line agents and mainly administered as a single agent[65]. An improvement in some but not all survival endpoints were observed when anti-PD1, anti-PD-L1 and anti-CTLA-4 ICBs were administered to patients with advanced gastroesophageal cancers in the second- and third-line setting[65]. The objective response rates were 9.9%, 12.0% and 2.1%, respectively and the disease control ratios were 33.3%, 34.7% and 30.1%, respectively[65]. The median progression-free survival was 1.6, 1.6 and 2.9 months, respectively and the median overall survival of the three groups was 6.0, 5.4 and 7.7 months, respectively[65]. However, patients receiving further adjuvant treatment often harbour more advanced stage and resistant tumours compared with treatment-naïve tumours which have yet to be exposed to conventional chemoradiotherapy regimens[367]. Current standard of care regimens can promote the generation of a more stem-like and treatment refractory neoplastic phenotype therefore, administering ICB sooner to patients in the first-line treatment-naïve setting might result in a greater proportion of patients benefiting from these agents[229,368]. Theoretically administering ICB in the neoadjuvant setting when there is an intact and larger tumour (greater amount of tumour antigens) may have a greater probability of achieving long-term immunologic memory and tumour control as opposed to treatment in the adjuvant setting, which typically comprises of patients with micrometastatic disease and a more treatment resistant tumour[368]. In support of this rationale, recent findings from the CheckMate 649 trial demonstrated that the combination of nivolumab with first-line chemotherapy regimens improved overall survival of patients more significantly than either modality alone[136]. This observed synergy is thought to be mediated by immunostimulatory chemotherapies which synergise with ICB in 'cold' non-inflamed tumours by inducing immunogenic tumour cell death, which subsequently results in recruitment of tumour-specific T cells to the tumour and is often characterised by an inflamed signature[130]. However, not all chemotherapies are immunostimulatory and this will depend on the dose of the chemotherapy and type of agent used[163]. This study highlighted the synergism between first-line chemotherapies used in OGJ and ICB, whereby ICB was more effective in enhancing lymphocyte-mediated killing of OGJ cells in the presence of post-FLOT and post-CROSS chemotherapy tumour cell secretome. In addition, FLOT and CROSS CT OGJ cell line conditioned media increased the cytotoxic potential of T cells *in vitro*. Collectively, these results may suggest that FLOT- and CROSS CT-induced alterations in the TME potentiate T cell activation. The observed synergism may be due to the release of tumour antigens and DAMPs from tumour cells exposed to FLOT or

CROSS chemotherapies, which could be enhancing lymphocyte activation via upregulation of co-stimulatory molecules and subsequent killing. Overall, the FLOT and CROSS CT regimens upregulated immunogenic markers on viable OGJ cells whereas, MAGIC decreased immunogenic markers on viable OGJ cells *in vitro* suggesting that FLOT and CROSS CT regimens induce ICD to a greater extent that the MAGIC regimen, highlighting FLOT and CROSS CT regimens as more appropriate synergistic partners to combine with ICIs in OGJ. Similar results were observed with single agent chemotherapies on ICD, demonstrating that each chemotherapy that forms the FLOT or CROSS CT regimen enhanced the immunogenicity of OGJ cells via increased expression of at least one surrogate marker of ICD on viable and dead OGJ cells. However, we observed that epirubicin, which comprises the MAGIC regimen, decreased HMGB1, MIC-A/B and HLA-DR on OGJ cells, whereas, 5-FU and cisplatin (the other chemotherapies that comprise the MAGIC regimen) increased these markers of ICD. The key difference between the MAGIC regimen and the FLOT and CROSS regimens is the substitution of a taxane for the anthracycline epirubicin. Epirubicin may induce a type of genotoxic stress within the cancer cell that results in immunogenically silent cell death. HMGB1 binds toll-like receptor (TLR)-4 on the surface of antigen presenting cells, stimulating their activation and maturation[153]. It has been reported that docetaxel (lung adenocarcinoma[154]), oxaliplatin (colorectal cancer[141] and lung carcinoma[151]) and 5-FU (colon carcinoma cells[155]) all induce tumour cell secretion of HMGB1. Paclitaxel, but not carboplatin, was found to induce ICD through the release of HMGB1 and activation of TLR-4-dependent and -independent pathways in ovarian cancer[156]. Single agent chemotherapy treatment did not significantly upregulate HMGB1 on OGJ cells, however their combination as part of the FLOT and CROSS CT regimen did, further supporting a rationale for combining different chemotherapies with distinct mechanisms of action to not only reduce the development of chemoresistance via cancer cell intrinsic genetic mutations but also due to their ability to increase immunogenic cell death in combination.

Calreticulin is a pre-apoptotic marker which translocates from the endoplasmic reticulum to the cell surface as a result of endoplasmic reticulum stress[148]. Membrane exposure of calreticulin acts as a phagocytic signal and attracts antigen presenting cells to the tumour site and promotes their subsequent activation and maturation[148]. In our study, 5-FU, docetaxel and cisplatin increased calreticulin expression on the surface of viable OE33 cells, however the combination chemotherapy regimens FLOT, CROSS CT or MAGIC did not significantly increase calreticulin. In contrast, oxaliplatin induced cell surface calreticulin expression in

colorectal cancer[141] and murine lung carcinoma cell lines[150], while docetaxel induced calreticulin cell surface expression in breast, prostate and colorectal cancer cell lines *in vitro.* Collectively, our study and previous studies highlight that the ability of chemotherapies to induce ICD depends on the specific combination of drugs used which likely alters the type and level of genotoxic stress within the cell and ultimately dictates whether the cell will die in an immunogenic manner or an immunologically silent manner. In addition, the specific organ of origin and genetic landscape of the cancer cell lines likely plays an important role in whether a chemotherapy agent or regimen will induce ICD[151].

It is well established that tumour cells and stromal cells within the OGJ TME secrete an array of immunosuppressive soluble factors[369]. Chemotherapy and radiotherapy have a substantial effect on the TME contexture and may propagate, dampen, or skew an immunosuppressive milieu toward an immune competent TME[163,299]. This study aimed to encapsulate the effect of these chemotherapy regimens on the OGJ cell line secretome, reflective of epithelial cells only, and the whole TME using tumour explants and their subsequent effects on T cell activation. Both the *in vitro* and *ex vivo* culture systems resulted in a significant reduction in the percentage of $CD27^+$ T cells following treatment with FLOT, CROSS CT and MAGIC OGJ cell conditioned media as well as treatment with post-FLOT and post-CROSS CRT TCM. These findings were further supported through immunophenotyping of T cells in OGJ patient-derived peripheral blood and tumour tissue, which also demonstrated that the frequencies of $CD27^+$ T cells were significantly lower post-FLOT and post-CROSS CRT in tumour tissue. The implications of these findings on anti-tumour immunity in OGJ patients are not clear as the role of CD27 signalling in cancer remains conflicting. CD27 signalling either leads to improved T cell function or to T cell dysfunction, likely dependent upon the amount, duration, and timing of the expression of the CD27 ligand (CD70)[370,371], offering a likely explanation to the conflicting evidence for CD27–CD70 interaction in promoting or inhibiting anti-cancer immunity. CD27, is a co-stimulatory immune checkpoint receptor and a member of the tumour necrosis factor receptor superfamily and functions in eliciting T cell responses[372]. CD27 signalling promotes cell T cell survival, enhances antigen receptor–mediated proliferative signals, and increases effector function[372]. In addition, CD27 signalling increases the production of the T-cell growth/survival factor IL-2, which is also a key survival factor for regulatory T cells[373]. Claus *et al*., demonstrated using fibrosarcoma, colon adenocarcinoma and melanoma tumour-bearing wild-type mice, that the CD27–CD70 interaction increased the frequency of regulatory T cells, reduced tumour-specific T-cell responses, increased

angiogenesis, and promoted tumour growth[374]. Moreover, this study reported that CD27 signalling reduced apoptosis of regulatory T cells *in vivo* and induced $CD4^+$ effector T cells to produce interleukin-2, a key survival factor for all effector T cells including regulatory T cells[374]. Consequently, the frequency of regulatory T cells and growth of solid tumours were reduced in *Cd27*deficient mice and in wild-type mice treated with monoclonal antibody to block CD27 signalling[374,375]. Constitutive expression of CD70 on tumour cells has been documented in cancer in contrast with its limited expression in normal healthy individuals[376,377]. In contrast, injection of CD27-activating antibody improved tumour rejection[375,378] and *cd70* transgenic mice were protected against poorly immunogenic tumour cells[379,380]. Given the reported conflicting roles of CD27 in both promoting and/or hindering anti-tumour immunity in the literature, the downregulation of CD27 on T cells following neoadjuvant treatment in OGJ patients in this study may be detrimental or beneficial in promoting anti-tumour immunity and may likely be dependent on the tumour immune contexture within patients. Further studies are warranted to determine its biological significance and therapeutic potential in OGJ.

Interestingly, both FLOT and CROSS CT directly and indirectly increased the percentage of $CD69^+$ T cells. Furthermore, both FLOT and CROSS CT regimens significantly upregulated co-stimulatory markers ICOS on the surface of T cells *ex vivo* suggesting that these first-line chemotherapy regimens are immunostimulatory. Co-stimulatory CD69 regulates inflammation through T cell migration, retention in tissues, and plays an important role sustaining T cell activation, proliferation, cytolytic activity[381]. ICOS regulates T cell proliferation and survival, as well as secretion of IL-4, IL-10, and IFN-γ[382,383]. In addition, ICOS is emerging as an important biomarker of responses to immunotherapy. Tang *et al.*, demonstrated that an increased frequency of $ICOS^+$CD4 T cells is a pharmacodynamic biomarker of response to anti-CTLA-4 ICB[384]. A similar study highlighted the predictive value of ICOS, in which ICOS expression was shown to be an indicator of T cell-mediated immune responses following treatment with a STING agonist in Lewis lung carcinoma murine models[385]. Our data demonstrate that both FLOT and CROSS chemotherapy regimens increase the production of pro-inflammatory IFN-γ and TNF-α cytokines, supporting a rationale that FLOT and CROSS chemotherapy regimens are immunostimulatory and may synergise with ICB to boost anti-tumour immunity. These findings suggest that first-line chemotherapies might play an important role in ‘warming up’ a ‘cold’ non-inflamed tumour microenvironment, which are typically unresponsive to ICBs[386].

Tumours co-opt certain immune checkpoint pathways as a major mechanism of immune resistance[387]. In this study PD-1, TIM-3, LAG-3, CTLA-4 and PD-L2 were significantly upregulated on tumour-infiltrating T cells compared with peripheral circulating T cells in OGJ patients, which might reflect a more exhausted T cell phenotype mediated by IC-intrinsic signalling in the tumour microenvironment and supporting the therapeutic targeting of multiple ICs to reinvigorate anti-tumour immunity in OGJ.Several studies have shown that chemotherapies upregulate PD-L1 on the surface of tumour cells in colorectal, gastric[202], breast[171], head and neck[173] and lung cancer[186,200]. In this study, FLOT and CROSS chemotherapies induced upregulation of ICs on T cells. This data underlines the double-edged sword of immune stimulation whereby immune activation is always balanced with a parallel induction of homeostatic immune inhibition[387]. Additionally, the hypothesis that FLOT and CROSS chemotherapy regimens might be stimulating anti-tumour immune responses is further supported highlighting a link between chemotherapy and promotion of immune resistance mediated by ICs. A rationale is supported for combining ICBs with concomitant chemotherapy that specifically block the ICs that are upregulated by chemotherapies which include: PD-1, A2aR, CTLA-4, KLRG-1, PD-L1, PD-L2 and CD160. The chemotherapy-induced upregulation of this wide array of ICs on the surface of T cells might be detrimental to the development and progression of an anti-tumour immune response and may also inhibit chemotherapy-induced immune stimulation.

Interestingly, the findings from this study demonstrated that expression of ICs on circulating and tumour-infiltrating T cells correlated with more advanced stage tumours and subsequent poor response to neoadjuvant FLOT chemotherapy and CROSS chemoradiotherapy treatment, supporting a role for ICs in promoting disease progression. Similarly, studies by Okadome *et al*., demonstrated that PD-L1 and PD-L2 are unfavourable biomarkers in oesophagogastric cancers[388]. Moreover, PD-1 was identified as a biomarker of decreased progression free survival and more advanced stage OGJ tumours[184]. Collectively, the findings of this study taken into consideration with the existing literature further substantiates that ICs might play an important role in disease progression in OGJ and perhaps also resistance to first-line chemotherapies supporting a rationale for the use of ICB to potentially enhance clinical outcomes in these patients.

Furthermore, in the clinic, dual blockade of CTLA-4 and PD-1 can achieve a more effective anti-tumour immune response in melanoma as both the CTLA-4 and PD-1 axes inhibit T cell activation and function using non-redundant mechanisms[209]. Combined use of nivolumab and

ipilimumab has been FDA-approved in melanoma, MSI-H and DNA mismatch repair-deficient metastatic colorectal cancer and kidney cancer[217] but not in OGJ patients. This study affirms the therapeutic potential for dual ICB whereby the highest levels of lymphocyte-mediated cytolysis of OGJ cells was observed with dual nivolumab-ipilimumab treatment compared with either treatment alone.

Interestingly, CROSS chemotherapies significantly decreases TIM-3 and LAG-3 on the surface of $CD8^+$ T cells *ex vivo*. Anderson *et al*., have extensively reviewed the literature and reported that TIM-3 and LAG-3 have unique functions in anti-cancer immune responses[289]. Similarly, there were trends toward a significant reduction in TIM-3 and LAG-3 expression on the surface of tumour-infiltrating $CD4^+$ T cells post-FLOT and post-CROSS chemoradiotherapy. TIM-3 and LAG-3 are transiently upregulated on the surface of activated $CD4^+$ and $CD8^+$ T cells and are expressed on a small fraction of $CD4^+FOXP3^+$ T cells in circulation, however, they are highly expressed on Tregs at sites of tissue inflammation[289]. Therefore, the findings from this study might suggest that the chemotherapy-induced downregulation of TIM-3 and LAG-3 may reflect a reduction in the frequency of regulatory type T cells in the *ex vivo* culture system and in OGJ patients post-chemo(radio)therapy treatment. Furthermore, FLOT and CROSS chemotherapies significantly decreased the production of IL-2 by T cells *ex vivo* in this study. IL-2 promotes the expansion of effector T cells including regulatory T cells[389], therefore, the FLOT and CROSS chemotherapy-induced decrease in IL-2 production by T cells may in turn decrease regulatory T cell expansion and support development of anti-tumour immunity. Studies have demonstrated that taxanes including docetaxel, which forms part of the FLOT regimen and paclitaxel which forms part of the CROSS regimen, depletes Treg cells in non-small cell lung cancer patients[390,391]. Further studies will be required to determine how first-line FLOT and CROSS CT/CRT regimens alter Treg phenotype, function and viability in particular do these chemotherapy regimens selectively kill Treg cells or can they promote differentiation of Treg cells into an anti-tumour phenotype.

In conclusion, this study suggests that FLOT and CROSS chemotherapy regimens may enhance the immunogenicity of OGJ tumours and subsequently enhance lymphocyte-mediated killing of OGJ cells. TIM-3 and LAG-3 were upregulated on tumour-infiltrating T cells and may represent novel therapeutic targets to target in combination with PD-1 and/or CTLA-4 ICBs. Additionally, the potential synergy between ICB and first-line chemotherapy regimens in OGJ are also highlighted. Importantly, this study also demonstrates that first-line chemotherapy regimens upregulate ICs on T cell surfaces reaffirming the rationale to administer ICBs

concurrently with first-line chemotherapies in OGJ to prevent potential IC-mediated suppression of chemotherapy-induced anti-tumour immunity.

Chapter 7 – Discussion

7.1 Discussion

OGJ is an aggressive malignancy with a high propensity to metastasise due to late stage presentation in the clinic, attributed to it's indolent nature and lack of clinical indicators in early stages of the disease[392]. Not surprisingly the heterogeneous nature of the tumour, often accompanied with advanced stage tumours, gives rise to poor response rates to the current standards of care with a high risk of tumour recurrence for OGJ patients[393]. Therefore, urgent new treatment options are needed for these patients. ICBs have garnered a significant amount of attention for their tremendous efficacy in advanced stage disease, inducing durable regression for some patients and giving patients with otherwise no treatment options new hope[98]. Unfortunately, these remarkable results are confined to a subset of patients across all malignancies including OGJ[394]. Research efforts are now being focussed on firstly acquiring a deeper understanding underpinning the treatment failure of ICB and secondly in identifying new combinations with ICB to convert non-responders to responders, expanding the benefits of ICB to a greater spectrum of patients.

Features of the TME including nutrient deprivation[104], acidosis[395] and hypoxia[396] are key contributors in generating and driving the formation of treatment resistant tumours. These characteristic features of the TME are extremely harsh and induce a considerable amount of tumour cell death[104,395,396]. However, these features promote the selection and outgrowth of resistant cancer clones, which are often resistant to current standards of care[104,395,396]. Moreover, these conditions of nutrient deprivation do not support effector T cells, which require glucose and amino acids to fulfil their energy requirements and nutritional needs and concomitantly promote the generation of pro-tumourigenic myeloid cells within the TME[104,395,396]. Acidosis and hypoxia are well characterised features of the TME and are also immunosuppressive, dampening T cell function[397,398]. These characteristic features of the TME impose profound metabolic alterations in both cancer cells and immune cells, and subsequently alter their phenotype generating ultimately treatment resistant cancer cell clones and an immunosuppressive TME conducive to neoplastic outgrowth[104]. This has led to the formation of a new field known as "immunometabolism" which relies on targeting the metabolism of immune cells to consequently enhance an anti-tumour phenotype[104]. PD-L1 ICB is an attractive therapeutic approach to improve the metabolic fitness of T cells increasing glycolysis in T cells, supporting effector T cell function and dampening glycolysis in tumour cells, freeing up more glucose in the TME for T cells[399]. However, the immunosuppressive features of the TME may also be contributing to ICB resistance in OGJ. Therefore, we sought to investigate the effect of

nutrient deprivation, hypoxia and acidosis on IC expression profiles of OGJ cells and T cells as well as characterising T cell phenotypes. Importantly, the efficacy of ICB under these hostile conditions was also assessed using OGJ patient-derived T cells to uncover potential factors contributing to ICB failure in OGJ which may explain therapeutic failure of ICB in OGJ patients and also identify factors within the TME to target to improve ICB efficacy. Overall, we found that several conditions of the hostile TME upregulated an array of ICs which may all be playing a role in driving a dysfunctional immune state in OGJ. This raises the question if such a wide range of ICs are being upregulated on T cells, then how do we next decide what is the best IC to target? How do we know for certain that we are targeting the most important IC on T cells? Should efforts be focussed on identifying the best combination of ICs to target sequentially or concomitantly? These array of experiments have really highlighted that PD-L1 is not the only IC that is being upregulated under these conditions aand therefore the poor success rates of PD-L1 ICBs may also be due to the fact that there are so many other ICs that have similar effects as PD-L1 in dampening anti-tumour immunity that are also expressed at high levels on T cells under these conditions. More fundamental research is necessary to decide what are the best ICs to target in OGJ patients before launching larger scale clinical trials. Rationale ex vivo tumour models will be essential in this regard in answering those pertinent questions that are crucial to design better clinical trials for patients. Testing the right combination of ICIs is really the next question that needs to be addressed, but clinical trials need to be designed based on robust pre-clinical data to support the validity of the combination or sequence of ICBs.

Glucose deprivation, serum deprivation, hypoxia and acidosis all had profound effects on the IC expression profile of OGJ patient-derived T cells. A range of ICs were significantly upregulated on the surface of T cells which may contribute to T cell dysfunction. LAG-3, TIGIT and A2aR have been implicated in promoting a regulatory T cell phenotype and pre-clinical studies have demonstrated that blockade of these ICs enhanced anti-tumour immunity and promoted tumour regression in murine studies[218,400]. This body of work demonstrates that hostile features of the OGJ TME create exploitable targets that could be harnessed with the use of novel ICBs targeting A2aR, TIGIT and LAG-3 in combination with conventional ICBs that target the PD-1/PD-L1 and CTLA-4 axes in T cells. ICB successfully decreased IL-10 production by T cells under severe acidic conditions and although, ICB increased IFN-γ production by T cells under moderately acidic conditions this effect was abrogated under severe acidic conditions highlighting the ability of acidosis to potentially limit ICB efficacy.

Collectively, these findings support a rationale for administering oral neutralizing buffers in conjunction with ICB in OGJ patients to limit the immunosuppressive effects of tumour acidosis on the efficacy of ICB. Pre-clinical murine studies reported significant success in co-administering oral neutralizing buffers with ICB to boost the efficacy of ICB[248].

In addition, it was interesting to find that PD-1 and TIGIT ICs were highly expressed on the surface of normal oesophageal epithelial cells and PD-L1, PD-L2, TIM-3, LAG-3, CD160 and A2aR were expressed at very low levels this does suggest that PD-1 and TIGIT may play a more dominant role in regulating homeostasis in the oesophagus and perhaps may also play a more prominent role in restraining anti-tumour immunity in OGJ tumours and driving immune dysfunction. If this is the case, it provides a rationale for targeting PD-1 and TIGIT in OGJ patients. The downregulation of PD-1 and TIGIT across the normal-BO-OGJ disease sequence which may reflect a loss of immune regulation and homeostasis. This might suggest that PD-1 and TIGIT play an important role in restraining pro-inflammatory responses in the oesophagus given that the progression to BO is an inflammatory driven process. Ligation of PD-1 and TIGIT to their respective ligands PD-L1[256] and poliovirus receptor[257] on the surface of dendritic cells promotes a regulatory dendritic cell phenotype that consequently dampens inflammatory responses. Similarly, ligation of PD-1 to PD-L1 on the surface of T cells promotes a regulatory phenotype[258]. In addition, ligation of TIGIT to poliovirus receptor on the surface of macrophages induces an M2 anti-inflammatory phenotype which would help resolve pathogenic inflammation[259]. Therefore, the decrease in PD-1 and TIGIT expression in the early stages of metaplastic disease on the surface of oesophageal epithelial cells may facilitate the generation of pathogenic inflammation that plays a key role in promoting the conversion of BO to OGJ. Preventing the loss of PD-1 and TIGIT on the surface of oesophageal epithelial cells may attenuate the progression to BO offering potential novel therapeutics for preventing BO development and ultimately reducing the incidence of OGJ. However, more research needs to be conducted to truly answer these questions.

OGJ is an exemplar model of an obesity-associated malignancy which arises in a background of inflammation mediated by the secretion of factors from visceral adipose tissue contributing to systemic low grade inflammation[401]. An increase in intra-abdominal pressure attributed to an increase in visceral adiposity forces caustic gastric contents including bile acid into the lower part of the oesophagus[83]. This induces recurring direct DNA damage in the epithelial cells lining the oesophagus. The chronic inflammation in the lower part of the oesophagus, mediated by infiltration of pro-inflammatory immune cells, collectively induces neoplastic

changes in epithelial cells and creates a tumour permissive niche within the oesophagus to promote tumour development, progression and treatment resistance[83]. However, although the obese visceral fat releases soluble inflammatory mediators into the circulation to create systemic tumour-promoting inflammation, it is now emerging in melanoma and lung cancer that individuals with a high body mass index respond better to ICBs[402]. Mechanistic understandings underpinning this phenomenon were uncovered by Tang *et al.*, who demonstrated that obese mice with tumours harboured T cells that exhibited a more dysfunctional phenotype compared with lean mice with tumours[100]. Additionally, PD-1 was expressed at significantly higher levels in these obese mice, which the authors suggested may be due to leptin-induced upregulation of PD-1 on the surface of T cells[100]. Leptin is a satiety hormone and is highly abundant in obese visceral fat and important hormone that regulates biological processes in the adipose tissue[403]. The authors highlighted that obesity drives T cells into a more dysfunctional phenotype whilst creating a therapeutic vulnerability that can be harnessed by ICB to boost anti-tumour immunity in obese individuals[100]. Therefore, we hypothesised that the secretome from visceral adipose tissue of OGJ patients would upregulate ICs on the surface of T cells. Increasing T cell activation and production of pro-inflammatory cytokines would lead to an increased rate of T cell exhaustion and dysfunction over time and thus create a therapeutic niche for harnessing anti-cancer immunity with the use of ICB. Interestingly, we found that adipose conditioned media (ACM) from OGJ patients increased IC expression and increased the frequency of pro-inflammatory Th1-like, Th1/17-like and Th17-like cell phenotypes. The addition of ICB in the presence of ACM decreased the production of pro-inflammatory tumour-promoting cytokines IL-17 and TNF-α which have been reported to drive malignant progression[404]. However, ICB decreased IL-10 production by T cells in the absence of ACM and while this effect was maintained by $CD8^+$ T cells in the presence of ACM, this effect was lost in $CD4^+$ T cells in the presence of the ACM. Collectively, this highlights the ability of ACM to curtail the efficacy of ICB and may highlight potential mechanisms of resistance to therapeutic ICB in obese OGJ patients.

Chemotherapy in particular is emerging as a valuable therapeutic agent to convert a ‘cold’ non-inflamed TME into a ‘hot’ inflamed TME which typically responds better to ICB[163]. However, not all chemotherapies have the ability to convert a ‘cold’ tumour into a ‘hot’ tumour and little research has been done to evaluate the immunostimulatory potential of first-line chemotherapy agents used for treating OGJ patients. Therefore, an important and clinically relevant aim of this body of work was to assess the immunostimulatory and immunoinhibitory effects of first-

line chemotherapy agents. The findings suggested that the chemotherapies that comprise the FLOT and CROSS regimens were immunostimulatory, demonstrated by the release of DAMPs following treatment with the combination regimens or single agent chemotherapies that comprise these regimens. Furthermore, these first-line chemotherapy regimens also upregulated co-stimulatory markers ICOS and CD69 on the surface of OGJ patient derived T cells, as well as increasing the secretion of pro-inflammatory cytokines IFN-γ and TNF-α. Collectively, these findings indicated that FLOT and CROSS have the potential to convert a 'cold' non-inflamed TME into a 'hot' inflamed TME via the generation of pro-inflammatory cytokines and may synergise with ICB. The addition of ICB to immunostimulatory chemotherapy regimens has the potential to synergise firstly by converting a 'cold' TME into a 'hot' TME via introduction of DNA damage and subsequent non-synonymous mutations giving rise to neo-antigens, which can recruit tumour antigen-specific T cells to the TME[163]. Secondly the addition of ICB prevents exhaustion of this newly-induced anti-tumour immune response but also reinvigorates any pre-existing anti-tumour immunity[405]. Findings from the CheckMate 649 trial help support this hypothesis in OGJ patients in which combining nivolumab with first-line chemotherapy regimens was superior than either agent alone and improved clinical end points for OGJ patients[406]. This current study also demonstrated that ICB was more effective in enhancing lymphocyte-mediated cytolysis of OGJ cells in the presence of post-FLOT and post-CROSS CT tumour cell secretome, which may likely be due to the presence of DAMPS which could be enhancing T cell activation and cytolysis via upregulating co-stimulatory molecules such as CD69 on the surface of T cells promoting T cell activation. To further support this hypothesis, we also demonstrated that FLOT tumour cell conditioned media enhanced the cytotoxic potential of T cells, demonstrated by an increase in CD107a on the surface of $CD8^+$ T cells. Overall, these findings highlighted that both FLOT and CROSS CT chemotherapy regimens synergised with ICB promoting lymphocyte-mediated killing of OGJ cells increasing T cell activation and would be ideal first-line chemotherapy regimens that could benefit from the addition of an ICB to prevent exhaustion of induced anti-tumour immunity by these regimens.

Furthermore, the results from this study demonstrated that FLOT and CROSS chemotherapy regimens upregulated inhibitory IC ligands and receptors on the surface of both OGJ cells and T cells highlighting a link between chemotherapy and immune resistance in the context of OGJ. This link was also identified in breast cancer wherein paclitaxel, etoposide and 5-fluorouracil upregulated PD-L1 on the surface of breast cancer cells, which induced T cell apoptosis[406].

These findings also offer important clinical insights and guidance into the optimal timing and scheduling of ICB with current standards of care. The findings in this study demonstrate that first-line chemotherapy regimens are creating a therapeutic niche in OGJ patients upregulating the target of a range of ICBs, which could be therapeutically exploited by administering ICB with concomitant chemotherapy regimens. The chemotherapy-induced upregulation of ICs on OGJ cells and T cells may have detrimental effects on the generation and amplitude of anti-tumour immunity however, chemotherapy is creating a highly exploitable therapeutic target via this upregulation of ICs to harness anti-tumour immunity. Although both FLOT and CROSS CT regimens upregulated ICs on the surface of T cells there was no significant difference between their effects. However, 5-FU and FLOT had a more substantial effect in upregulating ICs in particular PD-L1 on the surface of OGJ cells. This may be a beneficial effect as it creates a therapeutic target for ICBs. In addition, tumour cells upregulating these ICs may depend more so on these tumour cell-intrinsic IC signalling pathways and may become 'addicted' and dependent on their pro-survival effects. Therefore, blocking these ICs may reduce the survival of tumour cells and enhanced chemotherapy toxicity. Collectively, these results support a rationale for combining chemotherapy with ICB to upregulate the targets of ICBs in particular PD-L1 whilst also stimulating T cell activation and lymphocyte-mediated killing. However, further research needs to be conducted to appropriately identify which IC or ICs to target in combination with FLOT as this regimen increased the expression of a range of ICs on T cells and OGJ cells. Simply targeting the IC that was increased the most may not be the most rationale or scientific method for identify the best IC to target in combination with chemotherapy to achieve the greatest amount of synergism.

Our study also profiled IC expression on the surface of OGJ tumour cells *in vitro* and *ex vivo* and found that OGJ cells express a wide range of IC receptors, which typically are thought to be expressed predominantly by T cells. This phenomenon goes against the central dogma that IC ligands are only expressed on tumour cells and antigen presenting cells, and their cognate receptors expressed only on T cells[407]. PD-1, TIGIT, LAG-3 A2aR and TIM-3 were expressed at low levels on the surface of OGJ cells. Other studies have reported similar findings in different solid malignancies in which PD-1, A2aR, TIGIT and TIM-3 were identified on the surface of melanoma, pancreatic, lung, head and neck, colorectal and gastric cancers[175,176,202,203]. In addition, immune-independent roles for IC receptors and ligands have been identified across a range of solid tumours, whereby ICs expressed on tumour cells promote a range of hallmarks of cancer via tumour cell-intrinsic signalling via increasing

tumour cell proliferation, metabolism, DNA repair, chemoresistance, metastasis and cancer-stemness[163,175,176,202,203]. Our findings identified for the first time that ICs also exhibit novel immune-independent functions in promoting various cancer hallmarks such as proliferation, metabolism, DNA repair and cancer stemness in OGJ cells. The findings from this study demonstrated that A2aR, PD-1 and PD-L1 promoted OGJ cell proliferation and viability. Similar findings were reported for A2aR signalling in gastric cancer[408], PD-1 signalling in pancreatic cancer[237] and PD-L1 signalling in lung cancer[409]. In addition, we demonstrated that blockade of A2aR, PD-1 or PD-L1 signalling alone induced apoptosis and increased the cytotoxicity of FLOT chemotherapy in OGJ cells. In support of our findings indicating an immune-independent synergy between ICB and chemotherapy, PD-1 blockade and PD-L1 blockade enhanced the toxicity of 5-FU and cisplatin in gastric and lung cancer cells, respectively. We also demonstrated that PD-1 blockade or PD-L1 blockade decreased the expression of cancer stem-like marker ALDH in OGJ cells. This is supported by reports in the literature which have identified a role for the PD-1/PD-L1 axis in promoting a cancer stem-like phenotype in lung cancer cells via signalling through the STT3-β-catenin pathway[328].

Additionally, PD-1 and PD-L1 blockade decreased the expression of DNA repair genes in OGJ cells alone and in combination with the FLOT chemotherapy regimen in this study. Complementary studies in the literature reported that PD-1 and PD-L1 signalling regulated DNA damage response signalling and repair of damaged DNA via regulating activation of DNA damage response elements and expression of DNA repair machinery[181,341,350–352]. These findings reveal mechanistic understandings underpinning the immune-independent functions of ICB, whereby ICB decreases the survival of OGJ cells alone and in combination with FLOT chemotherapy regimens.

TIGIT blockade and PD-1 blockade also decreased proliferation, anti-apoptotic factor expression and induced apoptosis in OGJ cells. However, under glucose deprivation and hypoxia PD-1 signalling enhanced the survival of OGJ cells, which may be explained by the promotion of a metabolic phenotype in OGJ cells via PD-1 blockade. PD-1 blockade upregulated the surface expression of GLUT1 and increased basal respiration and glycolytic reserve, which may confer OGJ cells with a more metabolically fit phenotype to survive the harsh conditions of glucose deprivation and hypoxia. Importantly, these mechanistic and functional experiments put forward a new immune-independent hypothesis for explaining PD-1 ICB resistance in hypoxic and glucose deprived tumours. It is well-established that hypoxic and glucose-deprived tumours are inhospitable environments for anti-tumour T cells and is a

key contributor to immune suppression in which anti-tumour T cells are skewed under these conditions to a more tumour-promoting regulatory T cell phenotype[104,397].

This body of work investigated the direct effects of first-line chemotherapy regimens on IC expression on T cells and OGJ cells, however, within the tumour microenvironment there are a wide range of cell types and soluble factors which may ultimately result in a different effect on IC upregulation or downregulation and it will be important for future studies to take into account the multicellular effects on IC expression and efficacy of ICB.

7.2 Conclusion

Collectively this body of work highlights a therapeutic rationale for combining ICB with concomitant chemotherapy to not just enhance anti-tumour immunity but to also suppress various immune-independent hallmarks of cancer and to achieve synergistic responses in OGJ to ultimately boost the efficacy first-line chemotherapy regimens in OGJ. The immunosuppressive features of the TME including nutrient deprivation, hypoxia and acidosis and visceral adipose tissue secretome in the context of OGJ is also demonstrated whereby these features upregulate inhibitory IC expression on the surface of T cells creating a therapeutic vulnerability that could be exploited with the use of ICB to harness anti-cancer immunity. However, the ability of acidosis to curtail the efficacy of ICB is also depicted underlining a rationale to use oral neutralization buffers to improve the clinical success of ICB for treating OGJ patients.

7.3 Future directions

This research has identified a number of areas for future work and is an important starting point to further develop this emerging field investigating novel immune-independent functions of ICs in OGJ, with important translational implications for other solid malignancies. This body of work has identified that IC receptors are also expressed on the surface of OGJ cells and possess novel immune-independent functions through tumour-cell intrinsic signalling whereby a range of hallmarks of cancer are enhanced including proliferation, DNA repair, metabolism, stem-like marker expression and chemoresistance. This body of work was carried out using *in vitro* models and *ex vivo* tumour biopsies and although this is important to answer specific research questions under tightly controlled conditions it does not factor in the different soluble and cellular mediators within the tumour microenvironment and how this might affect the function of tumour cell-intrinsic signalling of ICs in OGJ cells.

ICs are expressed on a wide range of immune cell types not just T cells. It has been postulated that the effects of PD-1 blockade are mediated by the inhibition of PD-1 on myeloid cells not just T cells[410]. Therefore, future studies should involve investigating the effects of neoadjuvant chemo(radio)therapy regimens and ICBs on these cell types and which ICBs may be the best to use with first-line conventional regimens to synergistically boost anti-tumour immunity. Future work using multicellular organoids, organ-on-a-chip technology and tumour biopsies as models to recapitulate the complex tumour microenvironment of OGJ tumours to identify how different ICBs in various combinations with other ICBs and/or chemotherapies alter immune cell and tumour cell phenotypes and function will be necessary. A deeper interrogation of the changes occurring across these cell types using transcriptomics and proteomics will be important to discern how important the novel immune-independent functions and immune-dependent functions of ICs are in the clinical success of ICBs. It could potentially be the case where immune-independent IC signalling may be more important in promoting tumourigenesis in certain patients but in other patients immune-dependent IC signalling may play a more prominent role in promoting tumour survival. However, it is quite likely that both immune-independent and immune-dependent functions of ICs work in tandem to determine tumour progression.

A an important limitation of this research that should be addressed through further work within the group and across the research field is use of more appropriate tumour models. For example, the use of more complex models to better recapitulate the architecture of the TME such as patient-derived tumour organoids (PDOTS) which retain both myeloid and lymphoid cells of the patients tumour and can be grown for up to 6 days in a microfluidics device mimicking blood flow and fluidic pressure that is present within the TME. These models have been useful for testing ICBs in murine and patient tumour biopsy samples. In addition, using more high throughput technologies that can garner a greater amount of information about the TME and would be superior to that of flow cytometry. CODEX technology which depicts both the spatial and phenotypic information of the cells that comprise the TME, and would be very useful in this scenario to elucidate the spatial organisation of cells within the TME i.e. tumour core and the IC expression and cellular phenotype. Tumour organoids would also help capture the heterogenous nature of OGJ and would be useful for confirming the data generated using cell lines in this study.

Furthermore, this body of work has identified a wide range of ICs on the surface of T cells in OGJ patients. However, the precise function of these ICs is unknown in cancer, several of these

ICs including TIM-3, LAG-3 and TIGIT have been identified as important ICs in promoting Treg development. However, it remains to be determined if particular ICs play a more prominent role in driving immune dysfunction in particular tumour types depending on the organ as it has been suggested that ICs have tissue specialized functions. Given that PD-1 and TIGIT ICs were highly expressed on the surface of normal oesophageal epithelial cells and PD-L1, PD-L2, TIM-3, LAG-3, CD160 and A2aR were expressed at very low levels this does suggest that PD-1 and TIGIT may play a more dominant role in regulating homeostasis in the oesophagus and perhaps may also play a more prominent role in restraining anti-tumour immunity in OGJ tumours and driving immune dysfunction. If this is the case, it provides a rationale for targeting PD-1 and TIGIT in OGJ patients. However, more research needs to be conducted to truly answer these questions. In addition, it would be very interesting to profile ICs on the surface of healthy tissues throughout the GI tract and within other organs outside the GI tract to identify the IC expression profile of normal healthy tissue and if specific ICs might play more specialised roles in maintaining homeostasis in site specific organs, which is a very interesting hypothesis with important clinical and therapeutic implications.

Furthermore, first-line FLOT and CROSS CT chemotherapy regimens significantly upregulated a range of ICs on T cells as well as OGJ cells *in vitro*, an important clinical question is what ICs are the most appropriate to target in combination with these regimens. In addition, it would be important to determine if these chemotherapies also upregulate ICs on T cells and OGJ cells in patients after each cycle of chemotherapy. A question which still remains unanswered due to logistics of tumour sampling which currently is limited to time of diagnosis and 6 weeks after the last cycle of chemotherapy. Longitudinal profiling of the tumour, perhaps using the Cytosponge technology which comes in the form of a capsule attached to a long string. The patient swallows the capsule while holding onto the string in their hand and once the sponge reaches the top of the stomach and bottom of the oesophagus it opens and using the string the sponge can be pulled up the patient's oesophagus and out their mouth. This allows the sponge to capture cells including immune cells, normal cells and tumour cells non-invasively from the oesophagus. This technology has been very useful in monitoring the progression of BO in clinical trials and would also be very useful in the research field for obtaining longitudinal tumour biopsy sampling after each cycle of chemotherapy for research purposes as well as clinical decision making. Targeting each IC that is upregulated is not feasible due to financial toxicity and immune-related adverse events. Therefore, it is essential to firstly identify what function this wide range of ICs have on T cells and OGJ cells in the

absence and presence of chemotherapy treatment using *ex vivo* and *in vitro* models to gain a deeper insight into functional mechanisms. It may likely be the case where there is some over-lapping functions between ICs on T cells and OGJ cells, as the immune system is a complex network with several inbuilt mechanisms of redundancy to maintain homeostasis.

This body of work also demonstrated that the visceral adipose tissue secretome upregulated specific ICs on the surface of Th1-like, Th1/17-like, Th17-like and Treg cells. To acquire a deeper understanding of how the adipose tissue secretome is affecting T cell phenotypes and potentially driving T cell dysfunction and subsequent exhaustion, it will be important to identify the function of each IC in T cell subset phenotypes. It is also important to determine if the alteration in IC expression profiles reflects a change in T cell phenotype as well as playing a role in skewing and maintaining a particular T cell phenotype. This body of work also identified a subset of patients whose visceral adipose tissue secretome promoted OGJ cell proliferation and a separate sub-cohort that decreased OGJ cell proliferation. It is unclear what was different between these cohorts, as on a clinical level treatment response, tumour stage or obesity status did not discern these effects. Identification of these soluble factors could help identify novel therapeutics to abrogate the tumour-promoting effects of the visceral adipose tissue secretome.

References

1. Lin, Z. *et al.* In vivo antigen-driven plasmablast enrichment in combination with antigen-specific cell sorting to facilitate the isolation of rare monoclonal antibodies from human B cells. *Nat. Protoc.* **9**, 1563–1577 (2014).
2. Ferlay, J. *et al.* Cancer incidence and mortality worldwide: Sources, methods and major patterns in GLOBOCAN 2012. *Int. J. Cancer* **136**, E359–E386 (2015).
3. Pennathur M. K.; Jobe, B. A.; Luketich, J. D., A. . G. Oesophageal carcinoma. *Lancet* **381**, 400–412 (2013).
4. Shi J. B., W. J. . G. Molecular mechanisms of chemoresistance in gastric cancer. *World J Gastrointest Oncol* **8**, 673–681 (2016).
5. Hu, B. *et al.* Gastric cancer: Classification, histology and application of molecular pathology. *J. Gastrointest. Oncol.* **3**, 251–61 (2012).
6. Chen, Q., Zhuang, H. & Liu, Y. The association between obesity factor and esophageal caner. *J. Gastrointest. Oncol.* **3**, 226–31 (2012).

7. Lee, M.-J., Wu, Y. & Fried, S. K. Adipose tissue heterogeneity: implication of depot differences in adipose tissue for obesity complications. *Mol. Aspects Med.* **34**, 1–11 (2013).
8. Donohoe, C. L., O'Farrell, N. J., Doyle, S. L. & Reynolds, J. V. The role of obesity in gastrointestinal cancer: evidence and opinion. *Therap. Adv. Gastroenterol.* **7**, 38–50 (2014).
9. Al-Batran J. T.; Hofheinz, R.; Homann, N.; Rethwisch, V.; Probst, S.; Stoehlmacher, J.; Clemens, M. R.; Mahlberg, R.; Fritz, M.; Seipelt, G.; Sievert, M.; Pauligk, C.; Atmaca, A.; Jager, E., S. E. . H. Biweekly fluorouracil, leucovorin, oxaliplatin, and docetaxel (FLOT) for patients with metastatic adenocarcinoma of the stomach or esophagogastric junction: a phase II trial of the Arbeitsgemeinschaft Internistische Onkologie. *Ann Oncol* **19**, 1882–1887 (2008).
10. Donlon, N. E. *et al.* FLOT-regimen Chemotherapy and Transthoracic en bloc Resection for Esophageal and Junctional Adenocarcinoma. *Ann. Surg.* (9000).
11. Longley D. P.; Johnston, P. G., D. B. . H. 5-fluorouracil: mechanisms of action and clinical strategies. *Nat Rev Cancer* **3**, 330–338 (2003).
12. van Heijl J. J.; Koppert, L. B.; van Berge Henegouwen, M. I.; Muller, K.; Steyerberg, E. W.; van Dekken, H.; Wijnhoven, B. P.; Tilanus, H. W.; Richel, D. J.; Busch, O. R.; Bartelsman, J. F.; Koning, C. C.; Offerhaus, G. J.; van der Gaast, A., M. . van L. Neoadjuvant chemoradiation followed by surgery versus surgery alone for patients with adenocarcinoma or squamous cell carcinoma of the esophagus (CROSS). *BMC Surg* **8**, 21 (2008).
13. Longley, D. B., Harkin, D. P. & Johnston, P. G. 5-Fluorouracil: mechanisms of action and clinical strategies. *Nat. Rev. Cancer* **3**, 330–338 (2003).
14. Rustum, Y. M. Biochemical Rationale for the 5-Fluorouracil Leucovorin Combination and Update of Clinical Experience. *J. Chemother.* **2**, 5–11 (1990).
15. Espinosa, M. *et al.* Oxaliplatin activity in head and neck cancer cell lines. *Cancer Chemother. Pharmacol.* **55**, 301–305 (2005).
16. Amiri, M. *et al.* Cytotoxicity of carboplatin on human glioblastoma cells is reduced by the concomitant exposure to an extremely low-frequency electromagnetic field (50 Hz, 70 G). *Electromagn. Biol. Med.* **37**, 138–145 (2018).
17. Herbst, R. S. & Khuri, F. R. Mode of action of docetaxel – a basis for combination with novel anticancer agents. *Cancer Treat. Rev.* **29**, 407–415 (2003).

18. Wanderley, C. W. *et al.* Paclitaxel Reduces Tumor Growth by Reprogramming Tumor-Associated Macrophages to an M1 Profile in a TLR4-Dependent Manner. *Cancer Res.* **78**, 5891 LP – 5900 (2018).
19. Bang E.; Feyereislova, A.; Chung, H. C.; Shen, L.; Sawaki, A.; Lordick, F.; Ohtsu, A.; Omuro, Y.; Satoh, T.; Aprile, G.; Kulikov, E.; Hill, J.; Lehle, M.; Ruschoff, J.; Kang, Y. K., Y. J. . V. C. Trastuzumab in combination with chemotherapy versus chemotherapy alone for treatment of HER2-positive advanced gastric or gastro-oesophageal junction cancer (ToGA): a phase 3, open-label, randomised controlled trial. *Lancet* **376**, 687–697 (2010).
20. Donahue F. C.; Li, Z.; Schomas, D. A.; Allen, M. S.; Cassivi, S. D.; Jatoi, A.; Miller, R. C.; Wigle, D. A.; Shen, K. R.; Deschamps, C., J. M. . N. Complete Pathologic Response After Neoadjuvant Chemoradiotherapy for Esophageal Cancer Is Associated With Enhanced Survival. *Ann Thorac Surg* **87**, 392–399 (2009).
21. Pardoll, D. M. The blockade of immune checkpoints in cancer immunotherapy. *Nat. Rev. Cancer* **12**, 252–264 (2012).
22. Ehrlich, P. Ueber den jetzigen Stand der Karzinomforschung | Nederlands Tijdschrift voor Geneeskunde. *Ned. Tijdschr. Geneeskd* **5**, 273–290 (1909).
23. Ostrand-Rosenberg, S. Immune surveillance: a balance between protumor and antitumor immunity. *Curr. Opin. Genet. Dev.* **18**, 11–8 (2008).
24. Schreiber, R. D., Old, L. J. & Smyth, M. J. Cancer Immunoediting: Integrating Immunity's Roles in Cancer Suppression and Promotion. *Science (80-.).* **331**, 1565–1570 (2011).
25. Beatty, G. L. & Gladney, W. L. Immune escape mechanisms as a guide for cancer immunotherapy. *Clin. Cancer Res.* **21**, 687–92 (2015).
26. Dunn, G. P., Bruce, A. T., Ikeda, H., Old, L. J. & Schreiber, R. D. Cancer immunoediting: from immunosurveillance to tumor escape. *Nat. Immunol.* **3**, 991–998 (2002).
27. Coulie, P. G., Van den Eynde, B. J., van der Bruggen, P. & Boon, T. Tumour antigens recognized by T lymphocytes: at the core of cancer immunotherapy. *Nat. Rev. Cancer* **14**, 135–146 (2014).
28. Schreiber, R. D., Old, L. J. & Smyth, M. J. Cancer Immunoediting: Integrating Immunity's Roles in Cancer Suppression and Promotion. *Science (80-.).* **331**, 1565–1570 (2011).

29. Mellman, I., Coukos, G. & Dranoff, G. Cancer immunotherapy comes of age. *Nature* **480**, 480–489 (2011).
30. Mbongue, J. C. *et al.* The Role of Indoleamine 2, 3-Dioxygenase in Immune Suppression and Autoimmunity. *Vaccines* **3**, 703–29 (2015).
31. Kim, J. M. & Chen, D. S. Immune escape to PD-L1/PD-1 blockade: seven steps to success (or failure). *Ann. Oncol.* **27**, 1492–1504 (2016).
32. Wilson, E. B. *et al.* Human tumour immune evasion via TGF-β blocks NK cell activation but not survival allowing therapeutic restoration of anti-tumour activity. *PLoS One* **6**, e22842 (2011).
33. Thomas, D. A. & Massagué, J. TGF-β directly targets cytotoxic T cell functions during tumor evasion of immune surveillance. *Cancer Cell* **8**, 369–380 (2005).
34. Munn, D. H. & Mellor, A. L. Indoleamine 2,3 dioxygenase and metabolic control of immune responses. *Trends Immunol.* **34**, 137–143 (2013).
35. Griffioen, A. W., Damen, C. A., Blijham, G. H. & Groenewegen, G. Tumor angiogenesis is accompanied by a decreased inflammatory response of tumor-associated endothelium. *Blood* **88**, 667–73 (1996).
36. Griffioen, A. W., Damen, C. A., Martinotti, S., Blijham, G. H. & Groenewegen, G. Endothelial intercellular adhesion molecule-1 expression is suppressed in human malignancies: the role of angiogenic factors. *Cancer Res.* **56**, 1111–17 (1996).
37. Motz, G. T. *et al.* Tumor endothelium FasL establishes a selective immune barrier promoting tolerance in tumors. *Nat. Med.* **20**, 607–615 (2014).
38. O'Connell, J. Fas ligand and the fate of antitumour cytotoxic T lymphocytes. *Immunology* **105**, 263–6 (2002).
39. Bennett, M. W. *et al.* Expression of Fas ligand by human gastric adenocarcinomas: a potential mechanism of immune escape in stomach cancer.
40. Zhu, J. *et al.* Resistance to cancer immunotherapy mediated by apoptosis of tumor-infiltrating lymphocytes. *Nat. Commun.* **8**, 1404 (2017).
41. Kazama, H. *et al.* Induction of Immunological Tolerance by Apoptotic Cells Requires Caspase-Dependent Oxidation of High-Mobility Group Box-1 Protein. *Immunity* **29**, 21–32 (2008).
42. Groh, V., Wu, J., Yee, C. & Spies, T. Tumour-derived soluble MIC ligands impair expression of NKG2D and T-cell activation. *Nature* **419**, 734–738 (2002).
43. Rabinovich, G. A., Gabrilovich, D. & Sotomayor, E. M. Immunosuppressive strategies

that are mediated by tumor cells. *Annu. Rev. Immunol.* **25**, 267–96 (2007).

44. Quatromoni, J. G. & Eruslanov, E. Tumor-associated macrophages: function, phenotype, and link to prognosis in human lung cancer. *Am. J. Transl. Res.* **4**, 376–89 (2012).
45. Umansky, V., Blattner, C., Gebhardt, C. & Utikal, J. The Role of Myeloid-Derived Suppressor Cells (MDSC) in Cancer Progression. *Vaccines* **4**, (2016).
46. Dilek, N., Vuillefroy de Silly, R., Blancho, G. & Vanhove, B. Myeloid-derived suppressor cells: mechanisms of action and recent advances in their role in transplant tolerance. *Front. Immunol.* **3**, 208 (2012).
47. Hanahan, D. & Weinberg, R. A. Hallmarks of Cancer: The Next Generation. *Cell* **144**, 646–674 (2011).
48. Haabeth, O. A. W. *et al.* How Do CD4(+) T Cells Detect and Eliminate Tumor Cells That Either Lack or Express MHC Class II Molecules? *Front. Immunol.* **5**, 174 (2014).
49. Murphy, T. L. & Murphy, K. M. Dendritic cells in cancer immunology. *Cell. Mol. Immunol.* **19**, 3–13 (2022).
50. Van De Vyver, A. J. *et al.* Predicting Tumor Killing and T-Cell Activation by T-Cell Bispecific Antibodies as a Function of Target Expression: Combining In Vitro Experiments with Systems Modeling. *Mol. Cancer Ther.* **20**, 357–366 (2021).
51. Swain, S. L. T-Cell Subsets: Who does the polarizing? *Curr. Biol.* **5**, 849–851 (1995).
52. Ohue, Y. & Nishikawa, H. Regulatory T (Treg) cells in cancer: Can Treg cells be a new therapeutic target? *Cancer Sci.* **110**, 2080–2089 (2019).
53. Guéry, L. & Hugues, S. Th17 Cell Plasticity and Functions in Cancer Immunity. *Biomed Res. Int.* **2015**, 314620 (2015).
54. Chen, L. & Flies, D. B. Molecular mechanisms of T cell co-stimulation and co-inhibition. *Nat. Rev. Immunol.* **13**, 227–242 (2013).
55. Macián, F. *et al.* Transcriptional mechanisms underlying lymphocyte tolerance. *Cell* **109**, 719–31 (2002).
56. Śledzińska, A., Menger, L., Bergerhoff, K., Peggs, K. S. & Quezada, S. A. Negative immune checkpoints on T lymphocytes and their relevance to cancer immunotherapy. *Mol. Oncol.* **9**, 1936–65 (2015).
57. Baumeister, S. H., Freeman, G. J., Dranoff, G. & Sharpe, A. H. Coinhibitory Pathways in Immunotherapy for Cancer. *Annu. Rev. Immunol* **34**, 539–73 (2016).
58. Ma Q.; Wang, M.; Li, X.; Zhang, Y., K. . J. Research progress and clinical application

of predictive biomarker for immune checkpoint inhibitors. *Expert Rev Mol Diagn* **19**, 517–529 (2019).

59. Wei J. H.; Cogdill, A. P.; Zhao, Y.; Anang, N. A. S.; Andrews, M. C.; Sharma, P.; Wang, J.; Wargo, J. A.; Pe'er, D.; Allison, J. P., S. C. . L. Distinct Cellular Mechanisms Underlie Anti-CTLA-4 and Anti-PD-1 Checkpoint Blockade. *Cell* **170**, 1120-1133.e17 (2017).
60. Sahin M.; Alese, O.; Shaib, W.; Lesinski, G. B.; El-Rayes, B.; Wu, C., I. H. . A. Immune checkpoint inhibitors for the treatment of MSI-H/MMR-D colorectal cancer and a perspective on resistance mechanisms. *Br J Cancer* **121**, 809–818 (2019).
61. Crisci R.; Mele, S.; Vitale, P.; Ronga, G.; De Filippi, R.; Berretta, M.; Rossi, P.; Pinto, A., S. . D. F. Overview of Targeted Drugs for Mature B-Cell Non-hodgkin Lymphomas. *Front Oncol* **9**, 443 (2019).
62. Madden M. K., K. . K. Immune Checkpoint Inhibitors in Lung Cancer and Melanoma. *Semin Oncol Nurs* **35**, 150932 (2019).
63. Fashoyin-Aje M.; Chen, H.; He, K.; Veeraraghavan, J.; Goldberg, K. B.; Keegan, P.; McKee, A. E.; Pazdur, R., L. . D. FDA Approval Summary: Pembrolizumab for Recurrent Locally Advanced or Metastatic Gastric or Gastroesophageal Junction Adenocarcinoma Expressing PD-L1. *Oncologist* **24**, 103–109 (2019).
64. Shah, M. A. *et al.* Efficacy and Safety of Pembrolizumab for Heavily Pretreated Patients With Advanced, Metastatic Adenocarcinoma or Squamous Cell Carcinoma of the Esophagus: The Phase 2 KEYNOTE-180 Study. *JAMA Oncol.* **5**, 546–550 (2019).
65. Chen, C. *et al.* Efficacy and safety of immune checkpoint inhibitors in advanced gastric or gastroesophageal junction cancer: a systematic review and meta-analysis. *Oncoimmunology* **8**, e1581547 (2019).
66. van der Woude, L. L., Gorris, M. A. J., Halilovic, A., Figdor, C. G. & de Vries, I. J. M. Migrating into the Tumor: a Roadmap for T Cells. *Trends in Cancer* **3**, 797–808 (2017).
67. van der Woude M. A. J.; Halilovic, A.; Figdor, C. G.; de Vries, I. J. M., L. L. . G. Migrating into the Tumor: a Roadmap for T Cells. *Trends Cancer* **3**, 797–808 (2017).
68. Apetoh F.; Tesniere, A.; Obeid, M.; Ortiz, C.; Criollo, A.; Mignot, G.; Maiuri, M. C.; Ullrich, E.; Saulnier, P.; Yang, H.; Amigorena, S.; Ryffel, B.; Barrat, F. J.; Saftig, P.; Levi, F.; Lidereau, R.; Nogues, C.; Mira, J. P.; Chompret, A.; Joulin, V.; C, L. . G. Toll-like receptor 4-dependent contribution of the immune system to anticancer

chemotherapy and radiotherapy. *Nat Med* **13**, 1050–1059 (2007).

69. Koyama E. A.; Li, Y. Y.; Herter-Sprie, G. S.; Buczkowski, K. A.; Richards, W. G.; Gandhi, L.; Redig, A. J.; Rodig, S. J.; Asahina, H.; Jones, R. E.; Kulkarni, M. M.; Kuraguchi, M.; Palakurthi, S.; Fecci, P. E.; Johnson, B. E.; Janne, P. A.; Engelman, J., S. . A. Adaptive resistance to therapeutic PD-1 blockade is associated with upregulation of alternative immune checkpoints. *Nat Commun* **7**, 10501 (2016).
70. Kato, K. *et al.* Pembrolizumab in previously treated metastatic esophageal cancer: Longer term follow-up from the phase 2 KEYNOTE-180 Study. *J. Clin. Oncol.* **37**, 4032 (2019).
71. Kim, S.-B. *et al.* 124O - KEYNOTE-181: Pembrolizumab vs chemotherapy in patients (pts) with advanced/metastatic adenocarcinoma (AC) or squamous cell carcinoma (SCC) of the esophagus as second-line (2L) therapy. *Ann. Oncol.* **30**, ix42–ix43 (2019).
72. Shitara, K. *et al.* Pembrolizumab versus paclitaxel for previously treated, advanced gastric or gastro-oesophageal junction cancer (KEYNOTE-061): a randomised, open-label, controlled, phase 3 trial. *Lancet* **392**, 123–133 (2018).
73. Kim, S. T. *et al.* Comprehensive molecular characterization of clinical responses to PD-1 inhibition in metastatic gastric cancer. *Nat. Med.* **24**, 1449–1458 (2018).
74. Rha, S. Y. *et al.* Targeting HER2 in combination with anti-PD-1 and chemotherapy confers a significant tumor shrinkage of gastric cancer: A multi-institutional phase Ib/II trial of first-line triplet regimen (pembrolizumab, trastuzumab, chemotherapy) for HER2-positive advan. *J. Clin. Oncol.* **38**, 3081 (2020).
75. Chung, H. C. *et al.* 125O - Pembrolizumab + chemotherapy for advanced G/GEJ adenocarcinoma (GC): The phase III KEYNOTE-062 study. *Ann. Oncol.* **30**, ix43–ix44 (2019).
76. Moehler, M. H. *et al.* Results of the JAVELIN Gastric 100 phase 3 trial: avelumab maintenance following first-line (1L) chemotherapy (CTx) vs continuation of CTx for HER2− advanced gastric or gastroesophageal junction cancer (GC/GEJC). *J. Clin. Oncol.* **38**, 278 (2020).
77. Bang, Y.-J. *et al.* Phase III, randomised trial of avelumab versus physicians choice of chemotherapy as third-line treatment of patients with advanced gastric or gastro-oesophageal junction cancer: primary analysis of JAVELIN Gastric 300. *Ann. Oncol.* **29**, 2052–2060 (2018).

78. Janjigian, Y. Y. *et al.* Checkmate 649: A randomized, multicenter, open-label, phase 3 study of nivolumab (Nivo) plus ipilimumab (Ipi) versus oxaliplatin plus fluoropyrimidine in patients (Pts) with previously untreated advanced or metastatic gastric (G) or gastroesophageal junct. *J. Clin. Oncol.* **35**, TPS213–TPS213 (2017).
79. Shah, M. A. *et al.* A phase II, open-label, randomized study to evaluate the efficacy and safety of GS-5745 combined with nivolumab versus nivolumab alone in subjects with unresectable or recurrent gastric or gastroesophageal junction adenocarcinoma. *J. Clin. Oncol.* **35**, TPS4141–TPS4141 (2017).
80. Kelly, R. J. *et al.* Safety and Efficacy of Durvalumab and Tremelimumab Alone or in Combination in Patients with Advanced Gastric and Gastroesophageal Junction Adenocarcinoma. *Clin. Cancer Res.* **26**, 846 LP – 854 (2020).
81. O'Sullivan, J., Lysaght, J., Donohoe, C. L. & Reynolds, J. V. Obesity and gastrointestinal cancer: the interrelationship of adipose and tumour microenvironments. *Nat. Rev. Gastroenterol. Hepatol.* **15**, 699–714 (2018).
82. Quail, D. F. & Dannenberg, A. J. The obese adipose tissue microenvironment in cancer development and progression. *Nat. Rev. Endocrinol.* **15**, 139–154 (2019).
83. Davern, M. *et al.* The tumour immune microenvironment in oesophageal cancer. *Br. J. Cancer* (2021). doi:10.1038/s41416-021-01331-y
84. Anaparthy, R. & Sharma, P. Progression of Barrett oesophagus: role of endoscopic and histological predictors. *Nat. Rev. Gastroenterol. Hepatol.* **11**, 525–534 (2014).
85. Dumas, J.-F. & Brisson, L. Interaction between adipose tissue and cancer cells: role for cancer progression. *Cancer Metastasis Rev.* **40**, 31–46 (2021).
86. Engin, A. B., Engin, A. & Gonul, I. I. The effect of adipocyte–macrophage crosstalk in obesity-related breast cancer. *J. Mol. Endocrinol.* **62**, R201–R222
87. Divella, R., De Luca, R., Abbate, I., Naglieri, E. & Daniele, A. Obesity and cancer: the role of adipose tissue and adipo-cytokines-induced chronic inflammation. *J. Cancer* **7**, 2346–2359 (2016).
88. Mendonça, F. & Soares, R. Obesity and cancer phenotype: Is angiogenesis a missed link? *Life Sci.* **139**, 16–23 (2015).
89. Incio, J. *et al.* Obesity-Induced Inflammation and Desmoplasia Promote Pancreatic Cancer Progression and Resistance to Chemotherapy. *Cancer Discov.* **6**, 852–869 (2016).
90. Kern, L. *et al.* Obesity-Induced TNFα and IL-6 Signaling: The Missing Link between

Obesity and Inflammation—Driven Liver and Colorectal Cancers. *Cancers* **11**, (2019).

91. Lin, E. W., Karakasheva, T. A., Hicks, P. D., Bass, A. J. & Rustgi, A. K. The tumor microenvironment in esophageal cancer. *Oncogene* **35**, 5337–5349 (2016).
92. Zhao, Z.-F. *et al.* Interleukin-6 as a potential molecular target in esophageal squamous cell carcinoma. *Oncol. Lett.* **11**, 925–932 (2016).
93. Howard, J. M. *et al.* Associations between leptin and adiponectin receptor upregulation, visceral obesity and tumour stage in oesophageal and junctional adenocarcinoma. *Br. J. Surg.* **97**, 1020–1027 (2010).
94. Park, J. & Scherer, P. E. Leptin and cancer: from cancer stem cells to metastasis. *Endocr. Relat. Cancer* **18**, C25–C29 (2011).
95. Howard, J. M., Pidgeon, G. P. & Reynolds, J. V. Leptin and gastro-intestinal malignancies. *Obes. Rev.* **11**, 863–874 (2010).
96. Huang, F.-L. & Yu, S.-J. Esophageal cancer: Risk factors, genetic association, and treatment. *Asian J. Surg.* **41**, 210–215 (2018).
97. Darvin, P., Toor, S. M., Sasidharan Nair, V. & Elkord, E. Immune checkpoint inhibitors: recent progress and potential biomarkers. *Exp. Mol. Med.* **50**, 1–11 (2018).
98. Power, R., Lowery, M. A., Reynolds, J. V & Dunne, M. R. The Cancer-Immune Set Point in Oesophageal Cancer . *Frontiers in Oncology* **10**, 891 (2020).
99. Donnelly, D. *et al.* The complex relationship between body mass index and response to immune checkpoint inhibition in metastatic melanoma patients. *J. Immunother. Cancer* **7**, 222 (2019).
100. Wang, Z. *et al.* Paradoxical effects of obesity on T cell function during tumor progression and PD-1 checkpoint blockade. *Nat. Med.* **25**, 141–151 (2019).
101. King, R. *et al.* Hypoxia and its impact on the tumour microenvironment of gastroesophageal cancers. *World J. Gastrointest. Oncol.* **13**, 312–331 (2021).
102. Munn, D. H. & Bronte, V. Immune suppressive mechanisms in the tumor microenvironment. *Curr. Opin. Immunol.* **39**, 1–6 (2016).
103. Gajewski, T. F., Meng, Y. & Harlin, H. Immune Suppression in the Tumor Microenvironment. *J. Immunother.* **29**, (2006).
104. DePeaux, K. & Delgoffe, G. M. Metabolic barriers to cancer immunotherapy. *Nat. Rev. Immunol.* (2021). doi:10.1038/s41577-021-00541-y
105. Guo, C. *et al.* Chapter Four - Immunometabolism: A new target for improving cancer

immunotherapy. in *Immunotherapy of Cancer* (eds. Wang, X.-Y. & Fisher, P. B. B. T.-A. in C. R.) **143**, 195–253 (Academic Press, 2019).

106. Park, H.-R. *et al.* Effect on Tumor Cells of Blocking Survival Response to Glucose Deprivation. *JNCI J. Natl. Cancer Inst.* **96**, 1300–1310 (2004).
107. Li, Y., Wu, Y. & Hu, Y. Metabolites in the Tumor Microenvironment Reprogram Functions of Immune Effector Cells Through Epigenetic Modifications . *Frontiers in Immunology* **12**, 1017 (2021).
108. Warburg, O., Wind, F. & Negelein, E. THE METABOLISM OF TUMORS IN THE BODY . *J. Gen. Physiol.* **8**, 519–530 (1927).
109. Mondanelli, G. *et al.* A Relay Pathway between Arginine and Tryptophan Metabolism Confers Immunosuppressive Properties on Dendritic Cells. *Immunity* **46**, 233–244 (2017).
110. Yin, Z. *et al.* Targeting T cell metabolism in the tumor microenvironment: an anti-cancer therapeutic strategy. *J. Exp. Clin. Cancer Res.* **38**, 403 (2019).
111. MacPherson, S., Kilgour, M. & Lum, J. J. Understanding lymphocyte metabolism for use in cancer immunotherapy. *FEBS J.* **285**, 2567–2578 (2018).
112. Villa, M., O'Sullivan, D. & Pearce, E. L. Glucose makes T_{reg} lose their temper. *Cancer Cell* **39**, 460–462 (2021).
113. Giannone, G. *et al.* Immuno-Metabolism and Microenvironment in Cancer: Key Players for Immunotherapy. *International Journal of Molecular Sciences* **21**, (2020).
114. Mockler, M. B., Conroy, M. J. & Lysaght, J. Targeting T Cell Immunometabolism for Cancer Immunotherapy; Understanding the Impact of the Tumor Microenvironment . *Frontiers in Oncology* **4**, 107 (2014).
115. Kazemi, M. H. *et al.* Immune and metabolic checkpoints blockade: Dual wielding against tumors. *Int. Immunopharmacol.* **94**, 107461 (2021).
116. McDonald, D. M. & Baluk, P. Significance of Blood Vessel Leakiness in Cancer. *Cancer Res.* **62**, 5381 LP – 5385 (2002).
117. Facciabene, A. *et al.* Tumour hypoxia promotes tolerance and angiogenesis via CCL28 and Treg cells. *Nature* **475**, 226–230 (2011).
118. Schornack, P. A. & Gillies, R. J. Contributions of Cell Metabolism and H+ Diffusion to the Acidic pH of Tumors. *Neoplasia* **5**, 135–145 (2003).
119. Riva, C., Chauvin, C., Pison, C. & Leverve, X. Cellular physiology and molecular events in hypoxia-induced apoptosis. *Anticancer Res.* **18**, 4729–4736 (1998).

120. Wojtkowiak, J. W. *et al.* Chronic Autophagy Is a Cellular Adaptation to Tumor Acidic pH Microenvironments. *Cancer Res.* **72**, 3938 LP – 3947 (2012).
121. Moellering, R. E. *et al.* Acid treatment of melanoma cells selects for invasive phenotypes. *Clin. Exp. Metastasis* **25**, 411–425 (2008).
122. Marino, M. L. *et al.* Autophagy Is a Protective Mechanism for Human Melanoma Cells under Acidic Stress *. *J. Biol. Chem.* **287**, 30664–30676 (2012).
123. Erra Díaz, F., Dantas, E. & Geffner, J. Unravelling the Interplay between Extracellular Acidosis and Immune Cells. *Mediators Inflamm.* **2018**, 1218297 (2018).
124. Fischer, K. *et al.* Inhibitory effect of tumor cell-derived lactic acid on human T cells. *Blood* **109**, 3812–9 (2007).
125. Calcinotto, A. *et al.* Modulation of Microenvironment Acidity Reverses Anergy in Human and Murine Tumor-Infiltrating T Lymphocytes. *Cancer Res.* **72**, 2746 LP – 2756 (2012).
126. Gonzalez-Cao, M. *et al.* Tumor mutational burden as predictive factor of response to immunotherapy. *Transl. lung cancer Res.* **7**, S358–S361 (2018).
127. Folprecht, G. Tumor mutational burden as a new biomarker for PD-1 antibody treatment in gastric cancer. *Cancer Commun.* **39**, 74 (2019).
128. Wang, F. *et al.* Safety, efficacy and tumor mutational burden as a biomarker of overall survival benefit in chemo-refractory gastric cancer treated with toripalimab, a PD-1 antibody in phase Ib/II clinical trial NCT02915432. *Ann. Oncol.* **30**, 1479–1486 (2019).
129. Christensen, S. *et al.* 5-Fluorouracil treatment induces characteristic T>G mutations in human cancer. *Nat. Commun.* **10**, 4571 (2019).
130. Galon D., J. . B. Approaches to treat immune hot, altered and cold tumours with combination immunotherapies. *Nat Rev Drug Discov* **18**, 197–218 (2019).
131. Nars R., M. S. . K. Immunomodulatory effects of low dose chemotherapy and perspectives of its combination with immunotherapy. *Int J Cancer* **132**, 2471–2478 (2013).
132. Shurin, G. V, Tourkova, I. L., Kaneno, R. & Shurin, M. R. Chemotherapeutic Agents in Noncytotoxic Concentrations Increase Antigen Presentation by Dendritic Cells via an IL-12-Dependent Mechanism. *J. Immunol.* **183**, 137 LP – 144 (2009).
133. Ma, Y. *et al.* Anticancer Chemotherapy-Induced Intratumoral Recruitment and Differentiation of Antigen-Presenting Cells. *Immunity* **38**, 729–741 (2013).

134. Ma, Y. *et al.* CCL2/CCR2-Dependent Recruitment of Functional Antigen-Presenting Cells into Tumors upon Chemotherapy. *Cancer Res.* **74**, 436 LP – 445 (2014).
135. Rasmussen A., L. . A. Chemotherapy-induced immunosuppression. *Env. Heal. Perspect* **43**, 21–25 (1982).
136. Moehler, M. H. *et al.* CheckMate 649: A randomized, multicenter, open-label, phase III study of nivolumab (NIVO) + ipilimumab (IPI) or nivo + chemotherapy (CTX) versus CTX alone in patients with previously untreated advanced (Adv) gastric (G) or gastroesophageal junction (GEJ) . *J. Clin. Oncol.* **36**, TPS192–TPS192 (2018).
137. Wang, Y.-J., Fletcher, R., Yu, J. & Zhang, L. Immunogenic effects of chemotherapy-induced tumor cell death. *Genes Dis.* **5**, 194–203 (2018).
138. Lim W.; Cheng, C.; Descallar, J.; Ng, W.; Solomon, M.; Bokey, L.; Wong, K.; Lee, M. T.; de Souza, P.; Shin, J. S.; Lee, C. S., S. H. . C. Effect of neoadjuvant chemoradiation on tumor-infiltrating/associated lymphocytes in locally advanced rectal cancers. *Anticancer Res* **34**, 6505–6513 (2014).
139. Vincent G.; Chalmin, F.; Ladoire, S.; Bruchard, M.; Chevriaux, A.; Martin, F.; Apetoh, L.; Rebe, C.; Ghiringhelli, F., J. . M. 5-Fluorouracil selectively kills tumor-associated myeloid-derived suppressor cells resulting in enhanced T cell-dependent antitumor immunity. *Cancer Res* **70**, 3052–3061 (2010).
140. Galetto S.; Forno, S.; Moro, F.; Mussa, A.; Matera, L., A. . B. Drug- and cell-mediated antitumor cytotoxicities modulate cross-presentation of tumor antigens by myeloid dendritic cells. *Anticancer Drugs* **14**, 833–843 (2003).
141. Wang R.; Yu, J.; Zhang, L., Y. J. . F. Immunogenic effects of chemotherapy-induced tumor cell death. *Genes Dis* **5**, 194–203 (2018).
142. Li X. F.; Wang, L. P.; Xu, Y. J.; Huang, L.; Zhang, T. F.; Liu, J. Y.; Li, F.; Zhang, Z.; Yue, D. L.; Wang, F.; Zhang, B.; Zhang, Y., J. Y. . D. Selective depletion of regulatory T cell subsets by docetaxel treatment in patients with nonsmall cell lung cancer. *J Immunol Res* **2014**, 286170 (2014).
143. Tanaka H.; Mizumoto, N.; Takashima, A., H. . M. Classification of chemotherapeutic agents based on their differential in vitro impacts on dendritic cells. *Cancer Res* **69**, 6978–6986 (2009).
144. Emens G., L. A. . M. The interplay of immunotherapy and chemotherapy: harnessing potential synergies. *Cancer Immunol Res* **3**, 436–443 (2015).
145. Popovic E. M.; Zaidi, N., A. . J. Emerging strategies for combination checkpoint

modulators in cancer immunotherapy. *J Clin Invest* **128**, 3209–3218 (2018).

146. Song L.; Wang, Y.; Liu, Q.; Goodwin, T. J.; Li, J.; Dorosheva, O.; Liu, T.; Liu, R.; Huang, L., W. . S. Synergistic and low adverse effect cancer immunotherapy by immunogenic chemotherapy and locally expressed PD-L1 trap. *Nat Commun* **9**, 2237 (2018).
147. Emens, L. A. & Middleton, G. The Interplay of Immunotherapy and Chemotherapy: Harnessing Potential Synergies. *Cancer Immunol. Res.* **3**, 436–443 (2015).
148. Martins O.; Galluzzi, L.; Senovilla, L.; Schlemmer, F.; Adjemian, S.; Menger, L.; Michaud, M.; Zitvogel, L.; Kroemer, G., I. . K. Surface-exposed calreticulin in the interaction between dying cells and phagocytes. *Ann N Y Acad Sci* **1209**, 77–82 (2010).
149. Pawaria, S. & Binder, R. J. CD91-dependent programming of T-helper cell responses following heat shock protein immunization. *Nat. Commun.* **2**, 521 (2011).
150. Sun L.; Li, T.; Chen, S.; Song, J.; Li, D., F. . C. Oxaliplatin induces immunogenic cells death and enhances therapeutic efficacy of checkpoint inhibitor in a model of murine lung carcinoma. *J Recept Signal Transduct Res* **39**, 208–214 (2019).
151. Haruna M.; Iwahori, K.; Kanazawa, T.; Yamamoto, Y.; Goto, K.; Kawashima, A.; Morimoto-Okazawa, A.; Funaki, S.; Shintani, Y.; Kumanogoh, A.; Wada, H., M. . H. Docetaxel Upregulates HMGB1 Levels in Non-small Cell Lung Cancer. *Biol Pharm Bull* **43**, 399–403 (2020).
152. Zitvogel L.; Ghiringhelli, F.; Kroemer, G., L. . A. Immunological aspects of cancer chemotherapy. *Nat Rev Immunol* **8**, 59–73 (2008).
153. Bracci G.; Sistigu, A.; Belardelli, F., L. . S. Immune-based mechanisms of cytotoxic chemotherapy: implications for the design of novel and rationale-based combined treatments against cancer. *Cell Death Differ* **21**, 15–25 (2014).
154. Pan D.; Huang, J.; Wang, R.; Feng, B.; Song, H.; Chen, L., B. . C. HMGB1-mediated autophagy promotes docetaxel resistance in human lung adenocarcinoma. *Mol Cancer* **13**, 165 (2014).
155. Cottone A.; Gualteroni, C.; Perrotta, C.; Bianchi, M. E.; Rovere-Querini, P.; Manfredi, A. A., L. . C. 5-Fluorouracil causes leukocytes attraction in the peritoneal cavity by activating autophagy and HMGB1 release in colon carcinoma cells. *Int J Cancer* **136**, 1381–1389 (2015).
156. Lau, T.-S., Chan, L. K.-Y., Man, G. C.-W. & Kwong, J. Abstract 1232: Paclitaxel induces immunogenic cell death in ovarian cancer via TLR4-independent and

dependent pathways. *Cancer Res.* **79**, 1232 LP – 1232 (2019).

157. Tesniere T.; Kepp, O.; Apetoh, L.; Ghiringhelli, F.; Zitvogel, L.; Kroemer, G., A. . P. Molecular characteristics of immunogenic cancer cell death. *Cell Death Differ* **15**, 3–12 (2008).
158. Murshid, A., Gong, J. & Calderwood, S. K. The role of heat shock proteins in antigen cross presentation. *Front. Immunol.* **3**, 63 (2012).
159. Wang, C.-J., Lam, W., Bussom, S., Chang, H.-M. & Cheng, Y.-C. TREX1 acts in degrading damaged DNA from drug-treated tumor cells. *DNA Repair (Amst).* **8**, 1179–1189 (2009).
160. House P.; Lai, J.; Chen, A. X. Y.; Oliver, A. J.; Teo, Z. L.; Todd, K. L.; Henderson, M. A.; Giuffrida, L.; Petley, E. V.; Sek, K.; Mardiana, S.; Gide, T. N.; Quek, C.; Scolyer, R. A.; Long, G. V.; Wilmott, J. S.; Loi, S.; Darcy, P. K.; Beavis, P. A., I. G. . S. Macrophage-Derived CXCL9 and CXCL10 Are Required for Antitumor Immune Responses Following Immune Checkpoint Blockade. *Clin Cancer Res* **26**, 487–504 (2020).
161. Lohard N.; Maillet, L.; Gautier, F.; Fetiveau, A.; Lasla, H.; Nguyen, F.; Vuillier, C.; Dumont, A.; Moreau-Aubry, A.; Frapin, M.; David, L.; Loussouarn, D.; Kerdraon, O.; Campone, M.; Jezequel, P.; Juin, P. P.; Barille-Nion, S., S. . B. STING-dependent paracriny shapes apoptotic priming of breast tumors in response to anti-mitotic treatment. *Nat Commun* **11**, 259 (2020).
162. Siew S. Y.; Yew, H. C.; Lim, S. W.; Ng, Y. C.; Lew, S. M.; Seetoh, W. G.; Seow, S. V.; Koh, H. L., Y. Y. . N. Oxaliplatin regulates expression of stress ligands in ovarian cancer cells and modulates their susceptibility to natural killer cell-mediated cytotoxicity. *Int Immunol* **27**, 621–632 (2015).
163. Davern, M. & Lysaght, J. Cooperation between chemotherapy and immunotherapy in gastroesophageal cancers. *Cancer Lett.* (2020). doi:https://doi.org/10.1016/j.canlet.2020.09.014
164. Zeng, D. *et al.* Tumor Microenvironment Characterization in Gastric Cancer Identifies Prognostic and Immunotherapeutically Relevant Gene Signatures. *Cancer Immunol. Res.* **7**, 737 LP – 750 (2019).
165. Katoh, H. *et al.* Immunogenetic Profiling for Gastric Cancers Identifies Sulfated Glycosaminoglycans as Major and Functional B Cell Antigens in Human Malignancies. *Cell Rep.* **20**, 1073–1087 (2017).

166. Alexandrov, L. B. *et al.* Signatures of mutational processes in human cancer. *Nature* **500**, 415–421 (2013).

167. Dulak, A. M. *et al.* Exome and whole-genome sequencing of esophageal adenocarcinoma identifies recurrent driver events and mutational complexity. *Nat. Genet.* **45**, 478–486 (2013).

168. Secrier, M. *et al.* Mutational signatures in esophageal adenocarcinoma define etiologically distinct subgroups with therapeutic relevance. *Nat. Genet.* **48**, 1131–1141 (2016).

169. Secrier, M. *et al.* Correction: Corrigendum: Mutational signatures in esophageal adenocarcinoma define etiologically distinct subgroups with therapeutic relevance. *Nat. Genet.* **49**, 317 (2017).

170. Grasso, C. S. *et al.* Genetic Mechanisms of Immune Evasion in Colorectal Cancer. *Cancer Discov.* **8**, 730 LP – 749 (2018).

171. Zhang, P., Su, D.-M., Liang, M. & Fu, J. Chemopreventive agents induce programmed death-1-ligand 1 (PD-L1) surface expression in breast cancer cells and promote PD-L1-mediated T cell apoptosis. *Mol. Immunol.* **45**, 1470–1476 (2008).

172. Tran C. T.; Xiao, R.; Moore, E.; Davis, R.; Park, S. J.; Spielbauer, K.; Van Waes, C.; Schmitt, N. C., L. . A. Cisplatin Alters Antitumor Immunity and Synergizes with PD-1/PD-L1 Inhibition in Head and Neck Squamous Cell Carcinoma. *Cancer Immunol Res* **5**, 1141–1151 (2017).

173. Grabosch M.; Zeng, F.; Ma, T.; Zhang, L.; Ross, M.; Brozick, J.; Fang, Y.; Tseng, G.; Kim, E.; Gambotto, A.; Elishaev, E.; P. Edwards R; Vlad, A. M., S. . B. Cisplatin-induced immune modulation in ovarian cancer mouse models with distinct inflammation profiles. *Oncogene* **38**, 2380–2393 (2019).

174. Van Der Kraak, L. *et al.* 5-Fluorouracil upregulates cell surface B7-H1 (PD-L1) expression in gastrointestinal cancers. *J. Immunother. Cancer* **4**, 65 (2016).

175. Sato A.; Yasuhara, T.; Permata, T. B. M.; Hagiwara, Y.; Isono, M.; Nuryadi, E.; Sekine, R.; Oike, T.; Kakoti, S.; Yoshimoto, Y.; Held, K. D.; Suzuki, Y.; Kono, K.; Miyagawa, K.; Nakano, T.; Shibata, A., H. . N. DNA double-strand break repair pathway regulates PD-L1 expression in cancer cells. *Nat Commun* **8**, 1751 (2017).

176. Permata Y.; Sato, H.; Yasuhara, T.; Oike, T.; Gondhowiardjo, S.; Held, K. D.; Nakano, T.; Shibata, A., T. B. M. . H. Base excision repair regulates PD-L1 expression in cancer cells. *Oncogene* **38**, 4452–4466 (2019).

177. Ng J.; Tao, L.; Lam, A. K.; Chan, K. W.; Ko, J. M. Y.; Yu, V. Z.; Wong, M.; Li, B.; Lung, M. L., H. Y. . L. Chemotherapeutic Treatments Increase PD-L1 Expression in Esophageal Squamous Cell Carcinoma through EGFR/ERK Activation. *Transl Oncol* **11**, 1323–1333 (2018).

178. Fournel, L. *et al.* Cisplatin increases PD-L1 expression and optimizes immune check-point blockade in non-small cell lung cancer. *Cancer Lett.* **464**, 5–14 (2019).

179. David, J. M. *et al.* A novel bifunctional anti-PD-L1/TGF-β Trap fusion protein (M7824) efficiently reverts mesenchymalization of human lung cancer cells. *Oncoimmunology* **6**, e1349589 (2017).

180. Chang, C.-H. *et al.* Metabolic Competition in the Tumor Microenvironment Is a Driver of Cancer Progression. *Cell* **162**, 1229–41 (2015).

181. Sato, H. *et al.* DNA double-strand break repair pathway regulates PD-L1 expression in cancer cells. *Nat. Commun.* **8**, 1751 (2017).

182. Kleffel, S. *et al.* Melanoma Cell-Intrinsic PD-1 Receptor Functions Promote Tumor Growth. *Cell* **162**, 1242–56 (2015).

183. Wang, Y. *et al.* PD-L1 induces epithelial-to-mesenchymal transition via activating SREBP-1c in renal cell carcinoma. *Med. Oncol.* **32**, 212 (2015).

184. Kollmann, D. *et al.* Expression of Programmed Cell Death Protein 1 by Tumor-Infiltrating Lymphocytes and Tumor Cells is Associated with Advanced Tumor Stage in Patients with Esophageal Adenocarcinoma. *Ann. Surg. Oncol.* **24**, 2698–2706 (2017).

185. Gao, M. *et al.* Direct therapeutic targeting of immune checkpoint PD-1 in pancreatic cancer. *Br. J. Cancer* **120**, 88–96 (2019).

186. Yan, F. *et al.* Elevated Cellular PD1/PD-L1 Expression Confers Acquired Resistance to Cisplatin in Small Cell Lung Cancer Cells. *PLoS One* **11**, e0162925 (2016).

187. Cao, Y. *et al.* Tim-3 expression in cervical cancer promotes tumor metastasis. *PLoS One* **8**, e53834–e53834 (2013).

188. Jiang, J. *et al.* Decreased galectin-9 and increased Tim-3 expression are related to poor prognosis in gastric cancer. *PLoS One* **8**, e81799 (2013).

189. Mulati, K. *et al.* VISTA expressed in tumour cells regulates T cell function. *Br. J. Cancer* **120**, 115–127 (2019).

190. Villarroel-Espindola, F. *et al.* Spatially Resolved and Quantitative Analysis of VISTA/PD-1H as a Novel Immunotherapy Target in Human Non–Small Cell Lung

Cancer. *Clin. Cancer Res.* **24**, 1562–1573 (2018).

191. Zhou, X.-M. *et al.* Intrinsic Expression of Immune Checkpoint Molecule TIGIT Could Help Tumor Growth in vivo by Suppressing the Function of NK and CD8+ T Cells. *Front. Immunol.* **9**, 2821 (2018).
192. Kleffel, S. *et al.* Melanoma Cell-Intrinsic PD-1 Receptor Functions Promote Tumor Growth. *Cell* **162**, 1242–56 (2015).
193. Wu, S.-G. *et al.* Patterns of Distant Metastasis Between Histological Types in Esophageal Cancer . *Frontiers in Oncology* **8**, 302 (2018).
194. Shi Z.; Miao, J.; Du, S.; Ai, S.; Xu, E.; Feng, M.; Song, J.; Guan, W., L. . W. Adenosine interaction with adenosine receptor A2a promotes gastric cancer metastasis by enhancing PI3K-AKT-mTOR signaling. *Mol Biol Cell* **30**, 2527–2534 (2019).
195. Wang, T. *et al.* Cancer stem cell targeted therapy: progress amid controversies. *Oncotarget* **6**, 44191–206 (2015).
196. Gaurav Shukla, Amit Kumar Srivastava, Rahul Patidar, P. K. and R. S. Therapeutic Potential, Challenges and Future Perspective of Cancer Stem Cells in Translational Oncology:A Critical Review | BenthamScience. *Curr. Stem Cell Res. Ther.* **11**, (2016).
197. Schatton, T. *et al.* Modulation of T-Cell Activation by Malignant Melanoma Initiating Cells. *Cancer Res.* **70**, 697–708 (2010).
198. Peitzsch A.; Pantel, K.; Dubrovska, A., C. . T. Cancer stem cells: The root of tumor recurrence and metastases. *Semin Cancer Biol* **44**, 10–24 (2017).
199. Schatton M. H., T. . F. Antitumor Immunity and Cancer Stem Cells. *Ann N Y Acad Sci* **1176**, 154–169 (2009).
200. Hsu, J.-M. *et al.* STT3-dependent PD-L1 accumulation on cancer stem cells promotes immune evasion. *Nat. Commun.* **9**, 1908 (2018).
201. Yan, F. *et al.* Elevated Cellular PD1/PD-L1 Expression Confers Acquired Resistance to Cisplatin in Small Cell Lung Cancer Cells. *PLoS One* **11**, e0162925 (2016).
202. Liu, N. *et al.* Programmed death 1 induces cell chemoresistance to 5-fluorouracil in gastric cancer cell lines. *Transl. Cancer Res.* **5**, 781–788 (2016).
203. Tu B.; Zhang, Y.; Zhang, C.; Kahila, M.; Nowsheen, S.; Yin, P.; Yuan, J.; Pei, H.; Li, H.; Yu, J.; Song, Z.; Zhou, Q.; Zhao, F.; Liu, J.; Dong, H.; Mutter, R. W.; Lou, Z., X. . Q. PD-L1 (B7-H1) Competes with the RNA Exosome to Regulate the DNA Damage Response and Can Be Targeted to Sensitize to Radiation or Chemotherapy. *Mol Cell* **74**, 1215-1226.e4 (2019).

204. Yan A. B.; Finnes, H.; Markovic, S. N.; Park, S.; Dronca, R. S.; Dong, H., Y. . K. Combining Immune Checkpoint Inhibitors With Conventional Cancer Therapy. *Front Immunol* **9**, (2018).

205. Borghaei H, Langer CJ, Gadgeel S, Papadimitrakopoulou VA, Patnaik A, Powell SF, et al. Updated results from KEYNOTE-021 cohort G: a randomized, phase 2 study of pemetrexed and carboplatin (PC) with or without pembrolizumab (pembro) as first-line therapy for advanced nonsquamous NSCLC. (2020).

206. van den Ende, T. *et al.* A phase II feasibility trial of neoadjuvant chemoradiotherapy combined with atezolizumab for resectable esophageal adenocarcinoma: The PERFECT trial. *J. Clin. Oncol.* **37**, 4045 (2019).

207. Fuchs, C. S. *et al.* Preliminary safety data from KEYNOTE-059: Pembrolizumab plus 5-fluorouracil (5-FU) and cisplatin for first-line treatment of advanced gastric cancer. *J. Clin. Oncol.* **34**, 4037 (2016).

208. Zong, Y. *et al.* Immunotherapy : Open Access Identification of Co-inhibitory Receptors PD-1 and TIM-3 on T Cells from Gastric Cancer Patients. **1**, 1–9 (2015).

209. Buchbinder A., E. I. . D. CTLA-4 and PD-1 Pathways: Similarities, Differences, and Implications of Their Inhibition. *Am J Clin Oncol* **39**, 98–106 (2016).

210. Ise, W. *et al.* CTLA-4 suppresses the pathogenicity of self antigen–specific T cells by cell-intrinsic and cell-extrinsic mechanisms. *Nat. Immunol.* **11**, 129–135 (2010).

211. Qureshi, O. S. *et al.* Trans-Endocytosis of CD80 and CD86: A Molecular Basis for the Cell-Extrinsic Function of CTLA-4. *Science (80-.).* **332**, 600–603 (2011).

212. Holmgaard, R. B., Zamarin, D., Munn, D. H., Wolchok, J. D. & Allison, J. P. Indoleamine 2,3-dioxygenase is a critical resistance mechanism in antitumor T cell immunotherapy targeting CTLA-4. *J. Exp. Med.* **210**, 1389–402 (2013).

213. Robert, L. *et al.* CTLA4 Blockade Broadens the Peripheral T-Cell Receptor Repertoire. *Clin. Cancer Res.* **20**, 2424–2432 (2014).

214. Koehn, B. H. *et al.* PD-1-Dependent Mechanisms Maintain Peripheral Tolerance of Donor-Reactive CD8⁺ T Cells to Transplanted Tissue. *J. Immunol.* **181**, 5313 LP – 5322 (2008).

215. Isoyama, S. *et al.* Cancer immunotherapy with PI3K and PD-1 dual-blockade via optimal modulation of T cell activation signal. *J. Immunother. Cancer* **9**, e002279 (2021).

216. Blank, C. & Mackensen, A. Contribution of the PD-L1/PD-1 pathway to T-cell

exhaustion: an update on implications for chronic infections and tumor evasion. *Cancer Immunol. Immunother.* **56**, 739–745 (2007).

217. Tomita T.; Kimura, G.; Inoue, T.; Wakumoto, Y.; Yao, M.; Sugiyama, T.; Oya, M.; Fujii, Y.; Obara, W.; Motzer, R. J.; Uemura, H., Y. . K. Nivolumab plus ipilimumab versus sunitinib in previously untreated advanced renal-cell carcinoma: analysis of Japanese patients in CheckMate 214 with extended follow-up. *Jpn J Clin Oncol* **50**, 12–19 (2020).
218. Anderson N.; Kuchroo, V. K., A. C. . J. Lag-3, Tim-3, and TIGIT: Co-inhibitory Receptors with Specialized Functions in Immune Regulation. *Immunity* **44**, 989–1004 (2016).
219. Qi, X. *et al.* Wilms' tumor 1 (WT1) expression and prognosis in solid cancer patients: a systematic review and meta-analysis. *Sci. Rep.* **5**, 8924 (2015).
220. Lu J.; Cui, P.; Liu, T.; Piao, C.; Xu, X.; Zhang, Q.; Xiao, M.; Liu, X.; Wang, Y.; Yang, L., X. . L. Co-inhibition of TIGIT, PD1, and Tim3 reverses dysfunction of Wilms tumor protein-1 (WT1)-specific CD8+ T lymphocytes after dendritic cell vaccination in gastric cancer. *Am J Cancer Res* **8**, 1564–1575 (2018).
221. Xie J.; Cheng, S.; Zheng, L.; Ji, F.; Yang, L.; Zhang, Y.; Ji, H., J. . W. Expression of immune checkpoints in T cells of esophageal cancer patients. in *Oncotarget* **7**, 63669–63678 (2016).
222. Woo, S.-R. *et al.* Immune inhibitory molecules LAG-3 and PD-1 synergistically regulate T-cell function to promote tumoral immune escape. *Cancer Res.* **72**, 917–27 (2012).
223. Bristol-Myers Squibb. Bristol-Myers Squibb - Anti-LAG-3 (BMS-986016) in Combination with Opdivo (nivolumab) Showed Activity in Patients with Melanoma Who Were Relapsed or Refractory to Anti-PD-1/PD-L1 Therapy. (2017). Available at: https://investors.bms.com/iframes/press-releases/press-release-details/2017/Anti-LAG-3-BMS-986016-in-Combination-with-Opdivo-nivolumab-Showed-Activity-in-Patients-with-Melanoma-Who-Were-Relapsed-or-Refractory-to-Anti-PD-1PD-L1-Therapy/default.aspx. (Accessed: 3rd November 2017)
224. Yu X.; Zhang, Y.; Ying, J.; Zhang, W.; Zhong, Q.; Zhou, A.; Zeng, Y., Y. . M. Changes in Expression of Multiple Checkpoint Molecules and Infiltration of Tumor Immune Cells after Neoadjuvant Chemotherapy in Gastric Cancer. in *J Cancer* **10**, 2754–2763 (2019).

225. Kobayashi, T. *et al.* Pituitary dysfunction induced by immune checkpoint inhibitors is associated with better overall survival in both malignant melanoma and non-small cell lung carcinoma: a prospective study. *J. Immunother. Cancer* **8**, e000779 (2020).
226. Martins, F. *et al.* Adverse effects of immune-checkpoint inhibitors: epidemiology, management and surveillance. *Nat. Rev. Clin. Oncol.* **16**, 563–580 (2019).
227. Almutairi, A. R., McBride, A., Slack, M., Erstad, B. L. & Abraham, I. Potential Immune-Related Adverse Events Associated With Monotherapy and Combination Therapy of Ipilimumab, Nivolumab, and Pembrolizumab for Advanced Melanoma: A Systematic Review and Meta-Analysis . *Frontiers in Oncology* **10**, 91 (2020).
228. Wu, H. *et al.* T-cells produce acidic niches in lymph nodes to suppress their own effector functions. *Nat. Commun.* **11**, 4113 (2020).
229. Davern, M. *et al.* Chemotherapy regimens induce inhibitory immune checkpoint protein expression on stem-like and senescent-like oesophageal adenocarcinoma cells. *Transl. Oncol.* **14**, 101062 (2021).
230. Ding, G. *et al.* IFN-γ down-regulates the PD-1 expression and assist nivolumab in PD-1-blockade effect on CD8+ T-lymphocytes in pancreatic cancer. *BMC Cancer* **19**, 1053 (2019).
231. Kimchi, E. T. *et al.* Progression of Barrett's Metaplasia to Adenocarcinoma Is Associated with the Suppression of the Transcriptional Programs of Epidermal Differentiation. *Cancer Res.* **65**, 3146 LP – 3154 (2005).
232. Cao, Y. *et al.* Tim-3 expression in cervical cancer promotes tumor metastasis. *PLoS One* **8**, e53834 (2013).
233. Cao, Y. *et al.* Tim-3 expression in cervical cancer promotes tumor metastasis. *PLoS One* **8**, e53834 (2013).
234. Buckley, A. M. *et al.* Real-time metabolic profiling of oesophageal tumours reveals an altered metabolic phenotype to different oxygen tensions and to treatment with Pyrazinib. *Sci. Rep.* **10**, 12105 (2020).
235. Yu, Y. *et al.* Glucose metabolism involved in PD-L1-mediated immune escape in the malignant kidney tumour microenvironment. *Cell Death Discov.* **7**, 15 (2021).
236. Kim, S. *et al.* Programmed cell death ligand-1-mediated enhancement of hexokinase 2 expression is inversely related to T-cell effector gene expression in non-small-cell lung cancer. *J. Exp. Clin. Cancer Res.* **38**, 462 (2019).
237. Pu, N. *et al.* Cell-intrinsic PD-1 promotes proliferation in pancreatic cancer by

targeting CYR61/CTGF via the hippo pathway. *Cancer Lett.* **460**, 42–53 (2019).

238. Singer, K., Cheng, W.-C., Kreutz, M., Ho, P.-C. & Siska, P. J. Immunometabolism in cancer at a glance. *Dis. Model. & Mech.* **11**, dmm034272 (2018).
239. Terrén, I., Orrantia, A., Vitallé, J., Zenarruzabeitia, O. & Borrego, F. NK Cell Metabolism and Tumor Microenvironment . *Frontiers in Immunology* **10**, 2278 (2019).
240. Gabrilovich, D. I. Myeloid-Derived Suppressor Cells. *Cancer Immunol. Res.* **5**, 3–8 (2017).
241. Ashby, B. S. pH STUDIES IN HUMAN MALIGNANT TUMOURS. *Lancet* **288**, 312–315 (1966).
242. Vaupel, P., Kallinowski, F. & Okunieff, P. Blood Flow, Oxygen and Nutrient Supply, and Metabolic Microenvironment of Human Tumors: A Review. *Cancer Res.* **49**, 6449 LP – 6465 (1989).
243. Ibrahim-Hashim, A. & Estrella, V. Acidosis and cancer: from mechanism to neutralization. *Cancer Metastasis Rev.* **38**, 149–155 (2019).
244. Hayes, C., Donohoe, C. L., Davern, M. & Donlon, N. E. The oncogenic and clinical implications of lactate induced immunosuppression in the tumour microenvironment. *Cancer Lett.* **500**, 75–86 (2021).
245. Vermeulen, M. *et al.* Acidosis Improves Uptake of Antigens and MHC Class I-Restricted Presentation by Dendritic Cells. *J. Immunol.* **172**, 3196 LP – 3204 (2004).
246. Martínez, D. *et al.* Extracellular Acidosis Triggers the Maturation of Human Dendritic Cells and the Production of IL-12. *J. Immunol.* **179**, 1950 LP – 1959 (2007).
247. Tong, J. *et al.* Acid-Sensing Ion Channels Contribute to the Effect of Acidosis on the Function of Dendritic Cells. *J. Immunol.* **186**, 3686 LP – 3692 (2011).
248. Pilon-Thomas, S. *et al.* Neutralization of Tumor Acidity Improves Antitumor Responses to Immunotherapy. *Cancer Res.* **76**, 1381 LP – 1390 (2016).
249. Bellone, M. *et al.* The acidity of the tumor microenvironment is a mechanism of immune escape that can be overcome by proton pump inhibitors. *Oncoimmunology* **2**, e22058 (2013).
250. Muz, B., de la Puente, P., Azab, F. & Azab, A. K. The role of hypoxia in cancer progression, angiogenesis, metastasis, and resistance to therapy. *Hypoxia (Auckland, N.Z.)* **3**, 83–92 (2015).
251. Zhu, Z.-J. *et al.* Hypoxia induces chemoresistance of esophageal cancer cells to

cisplatin through regulating the lncRNA-EMS/miR-758-3p/WTAP axis. *Aging (Albany. NY).* **13**, 17155–17176 (2021).

252. Donlon, N. E. *et al.* Adverse Biology in Adenocarcinoma of the Esophagus and Esophagogastric Junction Impacts Survival and Response to Neoadjuvant Therapy Independent of Anatomic Subtype. *Ann. Surg.* **272**, (2020).
253. Chang, C.-H. *et al.* Metabolic Competition in the Tumor Microenvironment Is a Driver of Cancer Progression. *Cell* **162**, 1229–41 (2015).
254. Zhai, Y., Moosavi, R. & Chen, M. Immune Checkpoints, a Novel Class of Therapeutic Targets for Autoimmune Diseases . *Frontiers in Immunology* **12**, 815 (2021).
255. Kapoor, H., Lohani, K. R., Lee, T. H., Agrawal, D. K. & Mittal, S. K. Animal Models of Barrett's Esophagus and Esophageal Adenocarcinoma–Past, Present, and Future. *Clin. Transl. Sci.* **8**, 841–847 (2015).
256. Oh, S. A. *et al.* PD-L1 expression by dendritic cells is a key regulator of T-cell immunity in cancer. *Nat. Cancer* **1**, 681–691 (2020).
257. Yu, X. *et al.* The surface protein TIGIT suppresses T cell activation by promoting the generation of mature immunoregulatory dendritic cells. *Nat. Immunol.* **10**, 48–57 (2009).
258. Fanelli, G. *et al.* PD-L1 signaling on human memory CD4+ T cells induces a regulatory phenotype. *PLoS biology* **19**, e3001199 (2021).
259. Chen, X. *et al.* TIGIT negatively regulates inflammation by altering macrophage phenotype. *Immunobiology* **221**, 48–55 (2016).
260. Augustin, R. C., Delgoffe, G. M. & Najjar, Y. G. Characteristics of the Tumor Microenvironment That Influence Immune Cell Functions: Hypoxia, Oxidative Stress, Metabolic Alterations. *Cancers (Basel).* **12**, 3802 (2020).
261. Kleffel, S. *et al.* Melanoma Cell-Intrinsic PD-1 Receptor Functions Promote Tumor Growth. *Cell* **162**, 1242–1256 (2015).
262. Liotti, F. *et al.* PD-1 blockade delays tumor growth by inhibiting an intrinsic SHP2/Ras/MAPK signalling in thyroid cancer cells. *J. Exp. Clin. Cancer Res.* **40**, 22 (2021).
263. Yao, H., Wang, H., Li, C., Fang, J.-Y. & Xu, J. Cancer Cell-Intrinsic PD-1 and Implications in Combinatorial Immunotherapy . *Frontiers in Immunology* **9**, 1774 (2018).
264. Li, H. *et al.* Programmed cell death-1 (PD-1) checkpoint blockade in combination with

a mammalian target of rapamycin inhibitor restrains hepatocellular carcinoma growth induced by hepatoma cell-intrinsic PD-1. *Hepatology* **66**, 1920–1933 (2017).

265. Tomita, M. *et al.* Anti PD-1 treatment increases [18F]FDG uptake by cancer cells in a mouse B16F10 melanoma model. *EJNMMI Res.* **8**, 82 (2018).
266. Jiang, M. *et al.* A clinically acceptable strategy for sensitizing anti-PD-1 treatment by hypoxia relief. *J. Control. Release* **335**, 408–419 (2021).
267. Cham, C. M., Driessens, G., O'Keefe, J. P. & Gajewski, T. F. Glucose deprivation inhibits multiple key gene expression events and effector functions in CD8+ T cells. *Eur. J. Immunol.* **38**, 2438–2450 (2008).
268. Cohen, S., Danzaki, K. & MacIver, N. J. Nutritional effects on T-cell immunometabolism. *Eur. J. Immunol.* **47**, 225–235 (2017).
269. Patsoukis, N. *et al.* PD-1 alters T-cell metabolic reprogramming by inhibiting glycolysis and promoting lipolysis and fatty acid oxidation. *Nat. Commun.* **6**, 6692 (2015).
270. Raud, B. *et al.* Etomoxir Actions on Regulatory and Memory T Cells Are Independent of Cpt1a-Mediated Fatty Acid Oxidation. *Cell Metab.* **28**, 504-515.e7 (2018).
271. Lin, R. *et al.* Fatty Acid Oxidation Controls CD8⁺ Tissue-Resident Memory T-cell Survival in Gastric Adenocarcinoma. *Cancer Immunol. Res.* **8**, 479 LP – 492 (2020).
272. Sobhani, N. *et al.* CTLA-4 in Regulatory T Cells for Cancer Immunotherapy. *Cancers* **13**, (2021).
273. Sharma, A. *et al.* Anti-CTLA-4 Immunotherapy Does Not Deplete FOXP3+ Regulatory T Cells (Tregs) in Human Cancers. *Clin. Cancer Res.* **25**, 1233 LP – 1238 (2019).
274. Chang, C. H. *et al.* Metabolic Competition in the Tumor Microenvironment Is a Driver of Cancer Progression. *Cell* **162**, 1229–1241 (2015).
275. Naing, A. *et al.* CD8+ T cell stimulation with pegylated recombinant human IL-10 in the patient with advanced solid tumors - a Phase I study. *J. Immunother. Cancer* **3**, P204–P204 (2015).
276. Lee, J. B., Ha, S.-J. & Kim, H. R. Clinical Insights Into Novel Immune Checkpoint Inhibitors . *Frontiers in Pharmacology* **12**, 1074 (2021).
277. Braun, D. A. *et al.* Beyond conventional immune-checkpoint inhibition — novel immunotherapies for renal cell carcinoma. *Nat. Rev. Clin. Oncol.* **18**, 199–214 (2021).

278. Romio, M. *et al.* Extracellular purine metabolism and signaling of CD73-derived adenosine in murine Treg and Teff cells. *Am. J. Physiol. Physiol.* **301**, C530–C539 (2011).
279. Ma, S.-R. *et al.* Blockade of adenosine A2A receptor enhances CD8+ T cells response and decreases regulatory T cells in head and neck squamous cell carcinoma. *Mol. Cancer* **16**, 99 (2017).
280. Grosso, J. F. *et al.* LAG-3 regulates CD8+ T cell accumulation and effector function in murine self- and tumor-tolerance systems. *J. Clin. Invest.* **117**, 3383–3392 (2007).
281. Gandhi, M. K. *et al.* Expression of LAG-3 by tumor-infiltrating lymphocytes is coincident with the suppression of latent membrane antigen–specific CD8+ T-cell function in Hodgkin lymphoma patients. *Blood* **108**, 2280–2289 (2006).
282. Camisaschi, C. *et al.* LAG-3 Expression Defines a Subset of CD4+CD25highFoxp3+ Regulatory T Cells That Are Expanded at Tumor Sites. *J. Immunol.* **184**, 6545 LP – 6551 (2010).
283. Ascierto, P. A. *et al.* Efficacy of BMS-986016, a monoclonal antibody that targets lymphocyte activation gene-3 (LAG-3), in combination with nivolumab in pts with melanoma who progressed during prior anti–PD-1/PD-L1 therapy (mel prior IO) in all-comer and biomarker-enrich. *Ann. Oncol.* **28**, v611–v612 (2017).
284. Mocellin, S. & Nitti, D. CTLA-4 blockade and the renaissance of cancer immunotherapy. *Biochim. Biophys. Acta - Rev. Cancer* **1836**, 187–196 (2013).
285. Acharya, N., Sabatos-Peyton, C. & Anderson, A. C. Tim-3 finds its place in the cancer immunotherapy landscape. *J. Immunother. Cancer* **8**, e000911 (2020).
286. Deng, W.-W. *et al.* LAG-3 confers poor prognosis and its blockade reshapes antitumor response in head and neck squamous cell carcinoma. *Oncoimmunology* **5**, e1239005 (2016).
287. Saleh, R. & Elkord, E. Acquired resistance to cancer immunotherapy: Role of tumor-mediated immunosuppression. *Semin. Cancer Biol.* **65**, 13–27 (2020).
288. Chihara, N. *et al.* Induction and transcriptional regulation of the co-inhibitory gene module in T cells. *Nature* **558**, 454–459 (2018).
289. Anderson, A. C., Joller, N. & Kuchroo, V. K. Lag-3, Tim-3, and TIGIT: Co-inhibitory Receptors with Specialized Functions in Immune Regulation. *Immunity* **44**, 989–1004 (2016).
290. Sakuishi, K. *et al.* Targeting Tim-3 and PD-1 pathways to reverse T cell exhaustion

and restore anti-tumor immunity. *J. Exp. Med.* **207**, 2187–2194 (2010).

291. Ngiow, S. F. *et al.* Anti-TIM3 Antibody Promotes T Cell IFN-γ–Mediated Antitumor Immunity and Suppresses Established Tumors. *Cancer Res.* **71**, 3540 LP – 3551 (2011).
292. Zhou, Q. *et al.* Coexpression of Tim-3 and PD-1 identifies a CD8+ T-cell exhaustion phenotype in mice with disseminated acute myelogenous leukemia. *Blood* **117**, 4501–4510 (2011).
293. Fourcade Z.; Benallaoua, M.; Guillaume, P.; Luescher, I. F.; Sander, C.; Kirkwood, J. M.; Kuchroo, V.; Zarour, H. M., J. . S. Upregulation of Tim-3 and PD-1 expression is associated with tumor antigen–specific CD8+ T cell dysfunction in melanoma patients. in *J Exp Med* **207**, 2175–2186 (2010).
294. Li, N., Jilisihan, B., Wang, W., Tang, Y. & Keyoumu, S. Soluble LAG3 acts as a potential prognostic marker of gastric cancer and its positive correlation with CD8+T cell frequency and secretion of IL-12 and INF-γ in peripheral blood. *Cancer Biomarkers* **23**, 341–351 (2018).
295. Fougeray, S., Brignone, C. & Triebel, F. A soluble LAG-3 protein as an immunopotentiator for therapeutic vaccines: Preclinical evaluation of IMP321. *Vaccine* **24**, 5426–5433 (2006).
296. Végran, F., Boidot, R., Michiels, C., Sonveaux, P. & Feron, O. Lactate Influx through the Endothelial Cell Monocarboxylate Transporter MCT1 Supports an NF-κB/IL-8 Pathway that Drives Tumor Angiogenesis. *Cancer Res.* **71**, 2550 LP – 2560 (2011).
297. Ruan, G.-X. & Kazlauskas, A. Lactate Engages Receptor Tyrosine Kinases Axl, Tie2, and Vascular Endothelial Growth Factor Receptor 2 to Activate Phosphoinositide 3-Kinase/Akt and Promote Angiogenesis *. *J. Biol. Chem.* **288**, 21161–21172 (2013).
298. Nowicki-Osuch, K. *et al.* Molecular phenotyping reveals the identity of Barrett's esophagus and its malignant transition. *Science (80-.).* **373**, 760 LP – 767 (2021).
299. Donlon, N. E. *et al.* Radiation and Immunotherapy in Upper Gastrointestinal Cancers: The Current State of Play. *International Journal of Molecular Sciences* **22**, (2021).
300. Joshi, S. S., Maron, S. B. & Catenacci, D. V. Pembrolizumab for treatment of advanced gastric and gastroesophageal junction adenocarcinoma. *Future Oncol.* **14**, 417–430 (2018).
301. Kroemer, M. *et al.* Investigation of the prognostic value of CD4 T cell subsets expanded from tumor-infiltrating lymphocytes of colorectal cancer liver metastases. *J.*

Immunother. Cancer **8**, e001478 (2020).

302. Pardoll, D. M. The blockade of immune checkpoints in cancer immunotherapy. *Nat. Rev. Cancer* **12**, 252–264 (2012).
303. Hintzen, R. Q., de Jong, R., Lens, S. M. A. & van Lier, R. W. CD27: marker and mediator of T-cell activation? *Immunol. Today* **15**, 307–311 (1994).
304. Razmara, M., Hilliard, B., Ziarani, A. K., Chen, Y. H. & Tykocinski, M. L. CTLA-4·Ig converts naive CD4+CD25− T cells into CD4+CD25+ regulatory T cells. *Int. Immunol.* **20**, 471–483 (2008).
305. Walker, L. S. K. Treg and CTLA-4: Two intertwining pathways to immune tolerance. *J. Autoimmun.* **45**, 49–57 (2013).
306. Amarnath, S. *et al.* The PDL1-PD1 Axis Converts Human T_H1 Cells into Regulatory T Cells. *Sci. Transl. Med.* **3**, 111ra120 LP-111ra120 (2011).
307. Peinado, H. *et al.* Pre-metastatic niches: organ-specific homes for metastases. *Nat. Rev. Cancer* **17**, 302–317 (2017).
308. Hung, K. *et al.* The Central Role of CD4+ T Cells in the Antitumor Immune Response . *J. Exp. Med.* **188**, 2357–2368 (1998).
309. Wang, W. *et al.* miR-100 maintains phenotype of tumor-associated macrophages by targeting mTOR to promote tumor metastasis via Stat5a/IL-1ra pathway in mouse breast cancer. *Oncogenesis* **7**, 97 (2018).
310. Apte, R. N. & Voronov, E. Immunotherapeutic approaches of IL-1 neutralization in the tumor microenvironment. *J. Leukoc. Biol.* **102**, 293–306 (2017).
311. Cruceriu, D., Baldasici, O., Balacescu, O. & Berindan-Neagoe, I. The dual role of tumor necrosis factor-alpha (TNF-α) in breast cancer: molecular insights and therapeutic approaches. *Cell. Oncol.* **43**, 1–18 (2020).
312. Vieira, S. M. *et al.* A crucial role for TNF-α in mediating neutrophil influx induced by endogenously generated or exogenous chemokines, KC/CXCL1 and LIX/CXCL5. *Br. J. Pharmacol.* **158**, 779–789 (2009).
313. Parameswaran, N. & Patial, S. Tumor necrosis factor-α signaling in macrophages. *Crit. Rev. Eukaryot. Gene Expr.* **20**, 87–103 (2010).
314. O'Sullivan J.; Donohoe, C. L.; Reynolds, J. V., J. . L. Obesity and gastrointestinal cancer: the interrelationship of adipose and tumour microenvironments. *Nat Rev Gastroenterol Hepatol* **15**, 699–714 (2018).

315. Vitiello, G. A. & Miller, G. Targeting the interleukin-17 immune axis for cancer immunotherapy. *J. Exp. Med.* **217**, (2019).
316. Lu, L. *et al.* IL-17A promotes migration and tumor killing capability of B cells in esophageal squamous cell carcinoma. *Oncotarget; Vol 7, No 16* (2016).
317. Benevides, L. *et al.* IL17 Promotes Mammary Tumor Progression by Changing the Behavior of Tumor Cells and Eliciting Tumorigenic Neutrophils Recruitment. *Cancer Res.* **75**, 3788 LP – 3799 (2015).
318. Holzheimer, R. (René) & Mannick, J. A. *Surgical treatment : evidence-based and problem-oriented*. (Zuckschwerdt, 2001).
319. Bancewicz, J. *et al.* Surgical resection with or without preoperative chemotherapy in oesophageal cancer: a randomised controlled trial. *Lancet* **359**, 1727–1733 (2002).
320. Klevebro, F. *et al.* A randomized clinical trial of neoadjuvant chemotherapy versus neoadjuvant chemoradiotherapy for cancer of the oesophagus or gastro-oesophageal junction. *Ann. Oncol.* **27**, 660–667 (2016).
321. Cunningham, D. *et al.* Perioperative Chemotherapy versus Surgery Alone for Resectable Gastroesophageal Cancer. *N. Engl. J. Med.* **355**, 11–20 (2006).
322. van Heijl, M. *et al.* Neoadjuvant chemoradiation followed by surgery versus surgery alone for patients with adenocarcinoma or squamous cell carcinoma of the esophagus (CROSS). *BMC Surg.* **8**, 21 (2008).
323. Villanueva, L. *et al.* Total neoadjuvant chemotherapy with FLOT scheme in resectable adenocarcinoma of the gastro-oesophageal junction or gastric adenocarcinoma: Impact on pathological complete response and safety. *Ecancermedicalscience* **15**, 1–10 (2020).
324. Galluzzi, L., Buqué, A., Kepp, O., Zitvogel, L. & Kroemer, G. Immunogenic cell death in cancer and infectious disease. *Nat. Rev. Immunol.* **17**, 97–111 (2017).
325. Serrano-del Valle, A., Anel, A., Naval, J. & Marzo, I. Immunogenic Cell Death and Immunotherapy of Multiple Myeloma . *Frontiers in Cell and Developmental Biology* **7**, 50 (2019).
326. Kroemer, G., Galluzzi, L., Kepp, O. & Zitvogel, L. Immunogenic Cell Death in Cancer Therapy. *Annu. Rev. Immunol.* **31**, 51–72 (2013).
327. Kollmann, D. *et al.* Expression of Programmed Cell Death Protein 1 by Tumor-Infiltrating Lymphocytes and Tumor Cells is Associated with Advanced Tumor Stage in Patients with Esophageal Adenocarcinoma. *Ann. Surg. Oncol.* **24**, 2698–2706

(2017).

328. Hsu W.; Hsu, Y. H.; Chan, L. C.; Yu, W. H.; Cha, J. H.; Chen, C. T.; Liao, H. W.; Kuo, C. W.; Khoo, K. H.; Hsu, J. L.; Li, C. W.; Lim, S. O.; Chang, S. S.; Chen, Y. C.; Ren, G. X.; Hung, M. C., J. M. . X. STT3-dependent PD-L1 accumulation on cancer stem cells promotes immune evasion. *Nat Commun* **9**, 1908 (2018).
329. Ma X.; Zhou, Q.; Liu, J.; Yang, X.; Zhang, D.; Yang, S.; Du, Y.; Li, H.; Su, C., B. . D. Use of aspirin in the prevention of colorectal cancer through TIGIT-CD155 pathway. *J Cell Mol Med* **23**, 4514–4522 (2019).
330. Raniszewska, A., Polubiec-Kownacka, M., Rutkowska, E. & Domagala-Kulawik, J. PD-L1 Expression on Lung Cancer Stem Cells in Metastatic Lymph Nodes Aspirates. *Stem Cell Rev. Reports* **15**, 324–330 (2019).
331. Sato, H. *et al.* DNA double-strand break repair pathway regulates PD-L1 expression in cancer cells. *Nat. Commun.* **8**, 1751 (2017).
332. Fournel Z.; Stadler, N.; Damotte, D.; Lococo, F.; Boulle, G.; Segal-Bendirdjian, E.; Bobbio, A.; Icard, P.; Tredaniel, J.; Alifano, M.; Forgez, P., L. . W. Cisplatin increases PD-L1 expression and optimizes immune check-point blockade in non-small cell lung cancer. *Cancer Lett* **464**, 5–14 (2019).
333. Van Der Kraak G.; Ramanan, K.; Kaltenmeier, C.; Zhang, L.; Normolle, D. P.; Freeman, G. J.; Tang, D.; Nason, K. S.; Davison, J. M.; Luketich, J. D.; Dhupar, R.; Lotze, M. T., L. . G. 5-Fluorouracil upregulates cell surface B7-H1 (PD-L1) expression in gastrointestinal cancers. in *J Immunother Cancer* **4**, (2016).
334. Wang, Q.-E. DNA damage responses in cancer stem cells: Implications for cancer therapeutic strategies. *World J. Biol. Chem.* **6**, 57–64 (2015).
335. Reya, T., Morrison, S. J., Clarke, M. F. & Weissman, I. L. Stem cells, cancer and cancer stem cells. *Nature* **414**, 105–111 (2001).
336. Lynam-Lennon S.; Sommerville, G.; Bibby, B. A.; Ffrench, B.; Quinn, J.; Gasch, C.; O'Leary, J. J.; Gallagher, M. F.; Reynolds, J. V.; Maher, S. G., N. . H. MicroRNA-17 is downregulated in esophageal adenocarcinoma cancer stem-like cells and promotes a radioresistant phenotype. in *Oncotarget* **8**, 11400–11413 (2017).
337. Cai, Y. *et al.* Elimination of senescent cells by β-galactosidase-targeted prodrug attenuates inflammation and restores physical function in aged mice. *Cell Res.* **30**, 574–589 (2020).
338. Dai, C. Y. & Enders, G. H. p16INK4a can initiate an autonomous senescence program.

Oncogene **19**, 1613–1622 (2000).

339. Kleffel C.; Barthel, S. R.; Mueller, H.; Schlapbach, C.; Guenova, E.; Elco, C. P.; Lee, N.; Juneja, V. R.; Zhan, Q.; Lian, C. G.; Thomi, R.; Hoetzenecker, W.; Cozzio, A.; Dummer, R.; Mihm, M. C., Jr.; Flaherty, K. T.; Frank, M. H.; Murphy, G. F.; Sharpe, S. . P. Melanoma Cell-Intrinsic PD-1 Receptor Functions Promote Tumor Growth. *Cell* **162**, 1242–1256 (2015).
340. Ozawa, N. *et al.* PD-L1 upregulation is associated with activation of the DNA double-strand break repair pathway in patients with colitic cancer. *Sci. Rep.* **11**, 13077 (2021).
341. Tu, X. *et al.* PD-L1 (B7-H1) Competes with the RNA Exosome to Regulate the DNA Damage Response and Can Be Targeted to Sensitize to Radiation or Chemotherapy. *Mol. Cell* **74**, 1215-1226.e4 (2019).
342. Lynam-Lennon, N. *et al.* MicroRNA-31 modulates tumour sensitivity to radiation in oesophageal adenocarcinoma. *J. Mol. Med.* **90**, 1449–1458 (2012).
343. Gupta, H. B. *et al.* Tumor cell-intrinsic PD-L1 promotes tumor-initiating cell generation and functions in melanoma and ovarian cancer. *Signal Transduct. Target. Ther.* **1**, 16030 (2016).
344. Kollmann D.; Jedamzik, J.; Chang, Y. T.; Jomrich, G.; Paireder, M.; Kristo, I.; Kazakov, D.; Michal, M.; Cozzio, A.; Hoetzenecker, W.; Schatton, T.; Asari, R.; Preusser, M.; Guenova, E.; Schoppmann, S. F., D. . I. Expression of Programmed Cell Death Protein 1 by Tumor-Infiltrating Lymphocytes and Tumor Cells is Associated with Advanced Tumor Stage in Patients with Esophageal Adenocarcinoma. *Ann Surg Oncol* **24**, 2698–2706 (2017).
345. Sun, F. *et al.* Oxaliplatin induces immunogenic cells death and enhances therapeutic efficacy of checkpoint inhibitor in a model of murine lung carcinoma. *J. Recept. Signal Transduct.* **39**, 208–214 (2019).
346. Woo, J., Cohen, S. A. & Grim, J. E. Targeted therapy in gastroesophageal cancers: past, present and future. *Gastroenterol. Rep.* **3**, 316–29 (2015).
347. Stutvoet, T. S. *et al.* MAPK pathway activity plays a key role in PD-L1 expression of lung adenocarcinoma cells. *J. Pathol.* **249**, 52–64 (2019).
348. Degirmenci, U., Wang, M. & Hu, J. Targeting Aberrant RAS/RAF/MEK/ERK Signaling for Cancer Therapy. *Cells* **9**, (2020).
349. Ebert, P. J. R. *et al.* MAP Kinase Inhibition Promotes T Cell and Anti-tumor Activity in Combination with PD-L1 Checkpoint Blockade. *Immunity* **44**, 609–621 (2016).

350. Permata, T. B. M. *et al.* Base excision repair regulates PD-L1 expression in cancer cells. *Oncogene* **38**, 4452–4466 (2019).
351. Sato, H., Jeggo, P. A. & Shibata, A. Regulation of programmed death-ligand 1 expression in response to DNA damage in cancer cells: Implications for precision medicine. *Cancer Sci.* **110**, 3415–3423 (2019).
352. Meng, X., Yang, S. & Camp, V. J. A. The Interplay Between the DNA Damage Response, RNA Processing and Extracellular Vesicles . *Frontiers in Oncology* **9**, 1538 (2020).
353. Mah, L.-J., El-Osta, A. & Karagiannis, T. C. γH2AX: a sensitive molecular marker of DNA damage and repair. *Leukemia* **24**, 679–686 (2010).
354. Martinez-Balibrea, E. *et al.* Tumor-Related Molecular Mechanisms of Oxaliplatin Resistance. *Mol. Cancer Ther.* **14**, 1767 LP – 1776 (2015).
355. Pienta, K. J. Preclinical mechanisms of action of docetaxel and docetaxel combinations in prostate cancer. *Semin. Oncol.* **28**, 3–7 (2001).
356. Zhong, F., Cheng, X., Sun, S. & Zhou, J. Transcriptional activation of PD-L1 by Sox2 contributes to the proliferation of hepatocellular carcinoma cells. *Oncol. Rep.* **37**, 3061–3067 (2017).
357. Al-Batran, S.-E. *et al.* Perioperative chemotherapy with fluorouracil plus leucovorin, oxaliplatin, and docetaxel versus fluorouracil or capecitabine plus cisplatin and epirubicin for locally advanced, resectable gastric or gastro-oesophageal junction adenocarcinoma (FLOT4): a ra. *Lancet* **393**, 1948–1957 (2019).
358. Pfirschke C.; Rickelt, S.; Cortez-Retamozo, V.; Garris, C.; Pucci, F.; Yamazaki, T.; Poirier-Colame, V.; Newton, A.; Redouane, Y.; Lin, Y. J.; Wojtkiewicz, G.; Iwamoto, Y.; Mino-Kenudson, M.; Huynh, T. G.; Hynes, R. O.; Freeman, G. J.; Kroemer, G.; Zitvo, C. . E. Immunogenic Chemotherapy Sensitizes Tumors to Checkpoint Blockade Therapy. *Immunity* **44**, 343–354 (2016).
359. Lin T. A.; Hicks, P. D.; Bass, A. J.; Rustgi, A. K., E. W. . K. The Tumor Microenvironment in Esophageal Cancer. *Oncogene* **35**, 5337–5349 (2016).
360. Haabeth, O. A. W. *et al.* CD4+ T-cell–Mediated Rejection of MHC Class II–Positive Tumor Cells Is Dependent on Antigen Secretion and Indirect Presentation on Host APCs. *Cancer Res.* **78**, 4573 LP – 4585 (2018).
361. Metzger, T. C. *et al.* ICOS Promotes the Function of CD4⁺ Effector T Cells during Anti-OX40–Mediated Tumor Rejection. *Cancer Res.* **76**, 3684

LP – 3689 (2016).

362. Maldonado, A. *et al.* Decreased effector memory CD45RA+ CD62L- CD8+ T cells and increased central memory CD45RA- CD62L+ CD8+ T cells in peripheral blood of rheumatoid arthritis patients. *Arthritis Res Ther* **5**, R91 (2003).
363. van Sandick, J. W. *et al.* Lymphocyte subsets and T h 1/T h 2 immune responses in patients with adenocarcinoma of the oesophagus or oesophagogastric junction: relation to pTNM stage and clinical outcome. *Cancer Immunol. Immunother.* **52**, 617–624 (2003).
364. Qin, S. *et al.* Novel immune checkpoint targets: moving beyond PD-1 and CTLA-4. *Mol. Cancer* **18**, 155 (2019).
365. Koyama, S. *et al.* Adaptive resistance to therapeutic PD-1 blockade is associated with upregulation of alternative immune checkpoints. *Nat. Commun.* **7**, 10501 (2016).
366. Humphries, M. P. *et al.* The adaptive immune and immune checkpoint landscape of neoadjuvant treated esophageal adenocarcinoma using digital pathology quantitation. *BMC Cancer* **20**, 500 (2020).
367. Pietilä, E. A. *et al.* Co-evolution of matrisome and adaptive adhesion dynamics drives ovarian cancer chemoresistance. *Nat. Commun.* **12**, 3904 (2021).
368. Keung, E. Z., Ukponmwan, E. U., Cogdill, A. P. & Wargo, J. A. The Rationale and Emerging Use of Neoadjuvant Immune Checkpoint Blockade for Solid Malignancies. *Ann. Surg. Oncol.* **25**, 1814–1827 (2018).
369. Lin, E. W., Karakasheva, T. A., Hicks, P. D., Bass, A. J. & Rustgi, A. K. The tumor microenvironment in esophageal cancer. *Oncogene* **35**, 5337–5349 (2016).
370. Nolte, M. A., Van Olffen, R. W., Van Gisbergen, K. P. J. M. & Van Lier, R. A. W. Timing and tuning of CD27–CD70 interactions: the impact of signal strength in setting the balance between adaptive responses and immunopathology. *Immunol. Rev.* **229**, 216–231 (2009).
371. Matter, M., Odermatt, B., Yagita, H., Nuoffer, J.-M. & Ochsenbein, A. F. Elimination of chronic viral infection by blocking CD27 signaling . *J. Exp. Med.* **203**, 2145–2155 (2006).
372. Borst, J., Hendriks, J. & Xiao, Y. CD27 and CD70 in T cell and B cell activation. *Curr. Opin. Immunol.* **17**, 275–281 (2005).
373. Peperzak, V., Xiao, Y., Veraar, E. A. M. & Borst, J. CD27 sustains survival of CTLs in virus-infected nonlymphoid tissue in mice by inducing autocrine IL-2 production. *J.*

Clin. Invest. **120**, 168–178 (2010).

374. Claus, C. *et al.* CD27 Signaling Increases the Frequency of Regulatory T Cells and Promotes Tumor Growth. *Cancer Res.* **72**, 3664 LP – 3676 (2012).
375. French, R. R. *et al.* Eradication of lymphoma by CD8 T cells following anti-CD40 monoclonal antibody therapy is critically dependent on CD27 costimulation. *Blood* **109**, 4810–4815 (2007).
376. Wischhusen, J. *et al.* Identification of CD70-mediated Apoptosis of Immune Effector Cells as a Novel Immune Escape Pathway of Human Glioblastoma. *Cancer Res.* **62**, 2592 LP – 2599 (2002).
377. Yang, Z.-Z., Novak, A. J., Ziesmer, S. C., Witzig, T. E. & Ansell, S. M. CD70+ non-Hodgkin lymphoma B cells induce Foxp3 expression and regulatory function in intratumoral CD4+CD25− T cells. *Blood* **110**, 2537–2544 (2007).
378. Roberts, D. J. *et al.* Control of established melanoma by CD27 stimulation is associated with enhanced effector function and persistence, and reduced PD-1 expression of tumor infiltrating CD8(+) T cells. *J. Immunother.* **33**, 769–779 (2010).
379. Arens, R. *et al.* Tumor Rejection Induced by CD70-mediated Quantitative and Qualitative Effects on Effector CD8+ T Cell Formation . *J. Exp. Med.* **199**, 1595–1605 (2004).
380. Keller, A. M., Schildknecht, A., Xiao, Y., van den Broek, M. & Borst, J. Expression of Costimulatory Ligand CD70 on Steady-State Dendritic Cells Breaks $CD8^+$ T Cell Tolerance and Permits Effective Immunity. *Immunity* **29**, 934–946 (2008).
381. BORREGO, ROBERTSON, RITZ, PEÑA & SOLANA. CD69 is a stimulatory receptor for natural killer cell and its cytotoxic effect is blocked by CD94 inhibitory receptor. *Immunology* **97**, 159–165 (1999).
382. Rudd, C. E. & Schneider, H. Unifying concepts in CD28, ICOS and CTLA4 co-receptor signalling. *Nat. Rev. Immunol.* **3**, 544–556 (2003).
383. Hutloff, A. *et al.* ICOS is an inducible T-cell co-stimulator structurally and functionally related to CD28. *Nature* **397**, 263–266 (1999).
384. Ng Tang, D. *et al.* Increased frequency of ICOS+ CD4 T cells as a pharmacodynamic biomarker for anti-CTLA-4 therapy. *Cancer Immunol. Res.* **1**, 229–234 (2013).
385. Xiao, Z., Mayer, A. T., Nobashi, T. W. & Gambhir, S. S. ICOS Is an Indicator of T-cell–Mediated Response to Cancer Immunotherapy. *Cancer Res.* **80**, 3023 LP – 3032 (2020).

386. Galon, J. & Bruni, D. Approaches to treat immune hot, altered and cold tumours with combination immunotherapies. *Nat. Rev. Drug Discov.* **18**, 197–218 (2019).
387. Somasundaram, A., Socinski, M. A. & Villaruz, L. C. Immune checkpoint blockade in lung cancer. *Discov. Med.* **22**, 55–65 (2016).
388. Okadome, K. *et al.* Prognostic and clinical impact of PD-L2 and PD-L1 expression in a cohort of 437 oesophageal cancers. *Br. J. Cancer* **122**, 1535–1543 (2020).
389. Malek, T. R. The main function of IL-2 is to promote the development of T regulatory cells. *J. Leukoc. Biol.* **74**, 961–965 (2003).
390. Li, J.-Y. *et al.* Selective Depletion of Regulatory T Cell Subsets by Docetaxel Treatment in Patients with Nonsmall Cell Lung Cancer. *J. Immunol. Res.* **2014**, 286170 (2014).
391. Chan, O. T. M. & Yang, L.-X. The immunological effects of taxanes. *Cancer Immunol. Immunother.* **49**, 181–185 (2000).
392. Yonemura N.; Kawamura, T.; Tsukiyama, G.; Bandou, E.; Sakamoto, N.; Tsubosa, Y.; Sato, H., Y. . K. Treatment results of adenocarcinoma of the gastroesophageal junction. *Hepatogastroenterology* **55**, 475–481 (2008).
393. Goode E. C., E. F. . S. Immunotherapy for Gastroesophageal Cancer. in *J Clin Med* **5**, (2016).
394. Chuang, J., Chao, J., Hendifar, A., Klempner, S. J. & Gong, J. Checkpoint inhibition in advanced gastroesophageal cancer: clinical trial data, molecular subtyping, predictive biomarkers, and the potential of combination therapies. *Transl. Gastroenterol. Hepatol.* **4**, 63 (2019).
395. Boedtkjer, E. & Pedersen, S. F. The Acidic Tumor Microenvironment as a Driver of Cancer. *Annu. Rev. Physiol.* **82**, 103–126 (2020).
396. Tao, R. *et al.* Hypoxia imaging in upper gastrointestinal tumors and application to radiation therapy. *J. Gastrointest. Oncol.* **9**, 1044–1053 (2018).
397. Sitkovsky, M. V. T regulatory cells: hypoxia-adenosinergic suppression and re-direction of the immune response. *Trends Immunol.* **30**, 102–108 (2009).
398. Feng, L., Dong, Z., Tao, D., Zhang, Y. & Liu, Z. The acidic tumor microenvironment: a target for smart cancer nano-theranostics. *Natl. Sci. Rev.* **5**, 269–286 (2018).
399. Wong, W. Metabolic competition between tumors and T cells. *Sci. Signal.* **8**, ec281 LP-ec281 (2015).
400. Zarek, P. E. *et al.* A2A receptor signaling promotes peripheral tolerance by inducing

T-cell anergy and the generation of adaptive regulatory T cells. *Blood* **111**, 251–259 (2008).

401. Mongan, A. M. *et al.* Visceral obesity stimulates anaphase bridge formation and spindle assembly checkpoint dysregulation in radioresistant oesophageal adenocarcinoma. *Clin. Transl. Oncol.* **18**, 632–640 (2016).
402. McQuade, J. L. *et al.* Association of body-mass index and outcomes in patients with metastatic melanoma treated with targeted therapy, immunotherapy, or chemotherapy: a retrospective, multicohort analysis. *Lancet Oncol.* **19**, 310–322 (2018).
403. Ronnemaa, T., Karonen, S.-L., Rissanen, A., Koskenvuo, M. & Koivisto, V. A. Relation between Plasma Leptin Levels and Measures of Body Fat in Identical Twins Discordant for Obesity. *Ann. Intern. Med.* **126**, 26–31 (1997).
404. Balkwill, F. TNF-α in promotion and progression of cancer. *Cancer Metastasis Rev.* **25**, 409 (2006).
405. Nowak, A. K., Robinson, B. W. S. & Lake, R. A. Synergy between Chemotherapy and Immunotherapy in the Treatment of Established Murine Solid Tumors. *Cancer Res.* **63**, 4490 LP – 4496 (2003).
406. Janjigian, Y. Y. *et al.* First-line nivolumab plus chemotherapy versus chemotherapy alone for advanced gastric, gastro-oesophageal junction, and oesophageal adenocarcinoma (CheckMate 649): a randomised, open-label, phase 3 trial. *Lancet* **398**, 27–40 (2021).
407. Pardoll, D. M. The blockade of immune checkpoints in cancer immunotherapy. *Nat. Rev. Cancer* **12**, 252–64 (2012).
408. Shi, L. *et al.* Adenosine interaction with adenosine receptor A2a promotes gastric cancer metastasis by enhancing PI3K–AKT–mTOR signaling. *Mol. Biol. Cell* **30**, 2527–2534 (2019).
409. Castello, A., Rossi, S., Toschi, L., Mansi, L. & Lopci, E. Soluble PD-L1 in NSCLC Patients Treated with Checkpoint Inhibitors and Its Correlation with Metabolic Parameters. *Cancers (Basel).* **12**, 1373 (2020).
410. Yu, G.-T. *et al.* PD-1 blockade attenuates immunosuppressive myeloid cells due to inhibition of CD47/SIRPα axis in HPV negative head and neck squamous cell carcinoma. *Oncotarget; Vol 6, No 39* (2015).

Appendix

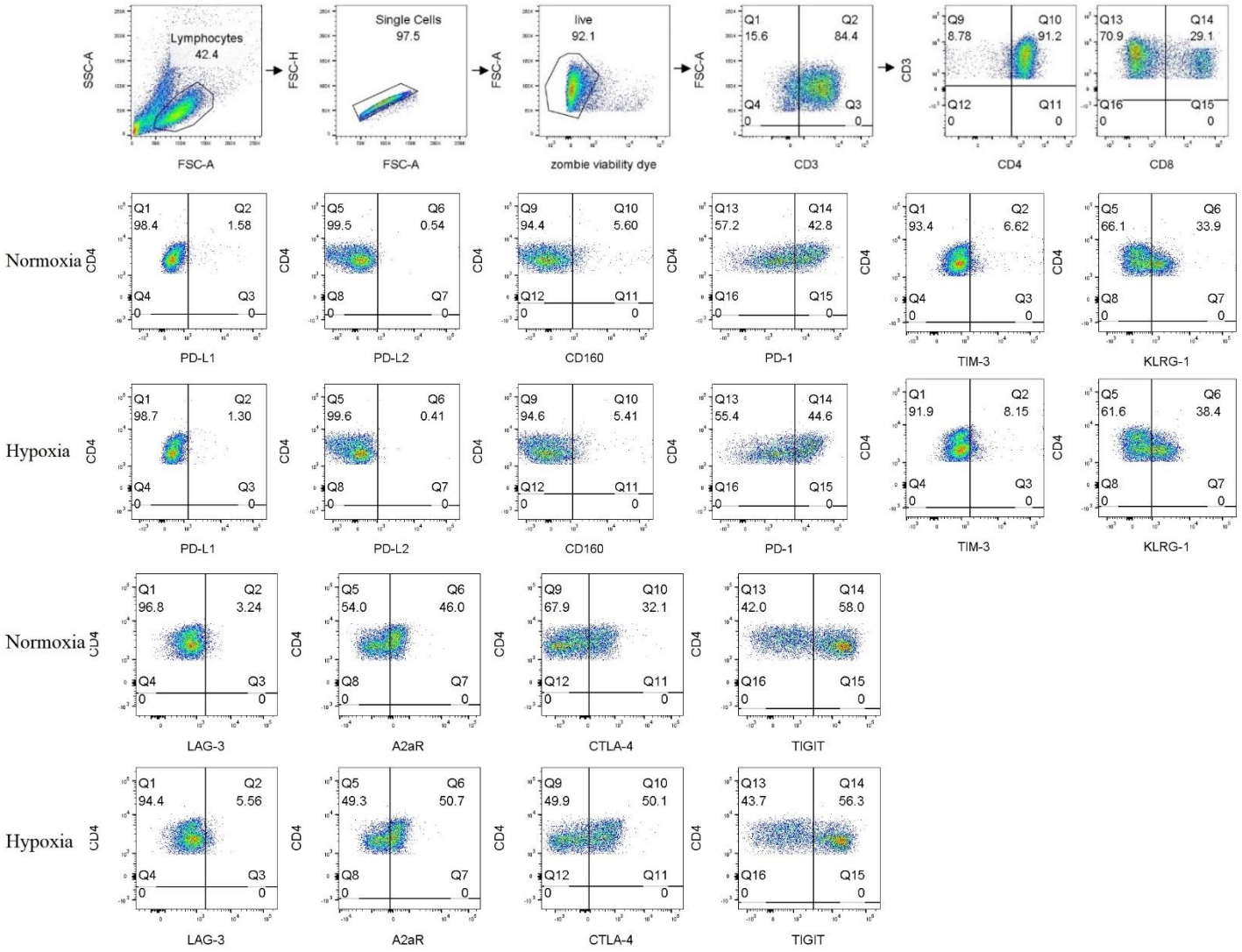

Figure A3.1: Gating strategy and representative dot plots for assessing expression of ICs on T cells surfaces under nutrient deprivation and hypoxia by flow cytometry. Gate 1 is the lymphocyte gate which included all cells in the FSC versus SSCA plot, doublet cells were then excluded using FSC-H versus FSC-A plot, dead cells were excluded using zombie viability dye. The surface expression of PD-L1, PD-L2, CD160, PD-1, TIM-3, KLRG-1, LAG-3, A2aR, CTLA-4 and TIGIT was assessed on $CD3^+CD4^+$ cells and $CD3^+CD8^+$ cells. Representative dot plots are shown for each gated on $CD3^+CD4^+$ cells following 48h culture of PBMCs under normoxia and hypoxia.

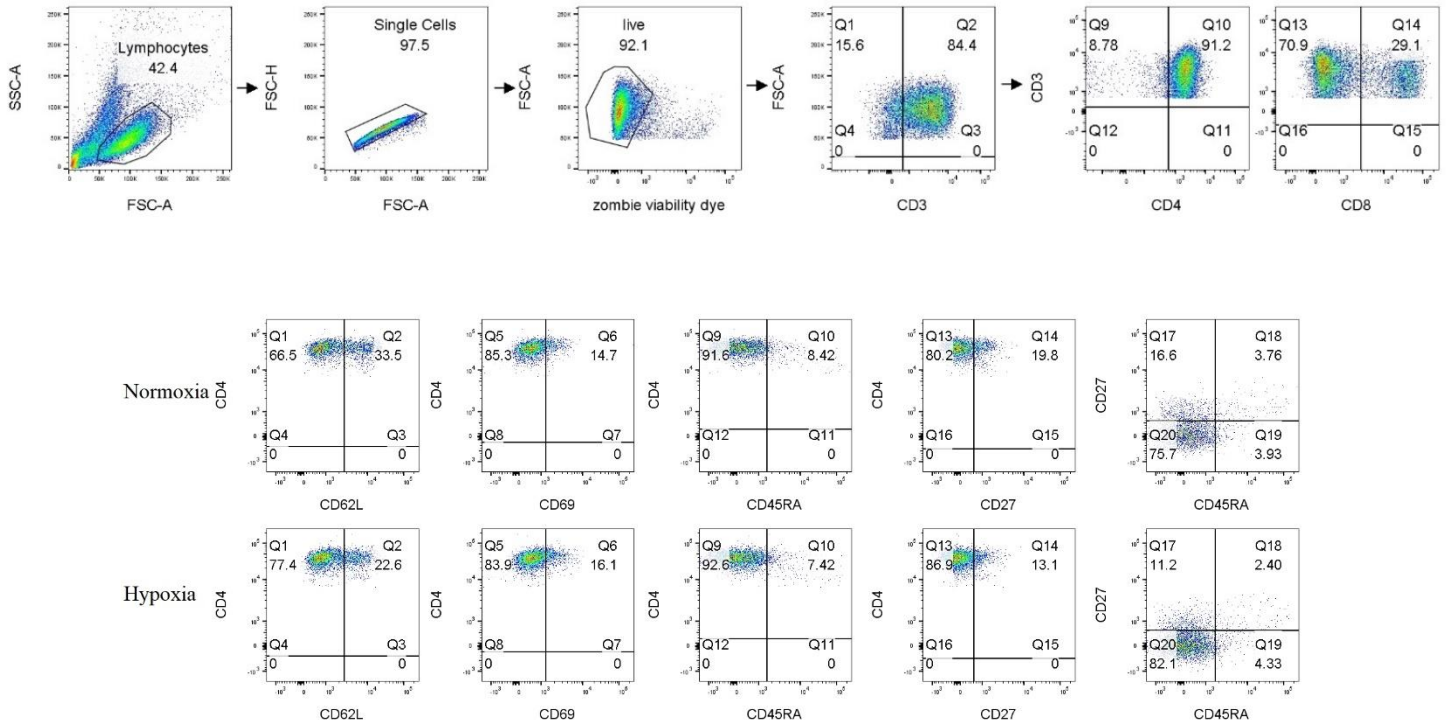

Figure A3.2: Gating strategy and representative dot plots for assessing expression of T cell activation markers and T cell differentiation states under nutrient deprivation and hypoxia by flow cytometry. Gate 1 is the lymphocyte gate and included all cells in the FSC versus SSCA plot, doublet cells were then excluded using FSC-H versus FSC-A plot, dead cells were excluded using zombie viability dye. The surface expression of CD62L, CD69, CD45RA and CD27 as well as T cell differentiation states was assessed on $CD3^+CD4^+$ cells and $CD3^+CD8^+$ cells. Representative dot plots are shown for each marker gated on $CD3^+CD4^+$ cells following 48h PBMCs under normoxia and hypoxia. Representative dot plots also shown depicting viable naïve ($CD27^+CD45RA^+$), central memory ($CD27^+CD45RA^-$), effector memory ($CD27^-CD45RA^-$) and terminally differentiated effector memory ($CD27^-CD45RA^+$) $CD3^+CD4^+$ cells.

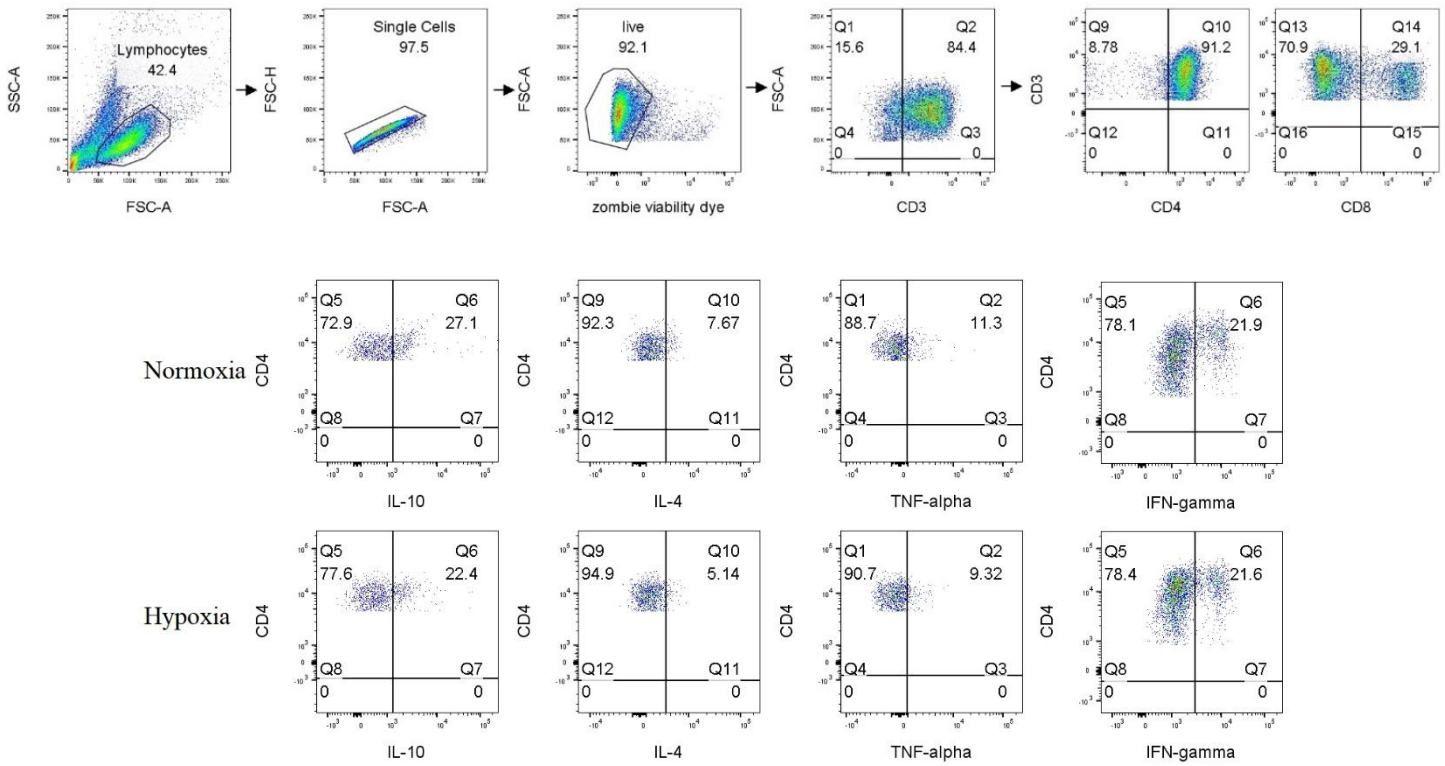

Figure A3.3: Gating strategy and representative dot plots for assessing cytokine production by T cells under nutrient deprivation and hypoxia by flow cytometry. Gate 1 is the lymphocyte gate and included all cells in the FSC versus SSCA plot, doublet cells were then excluded using FSC-H versus FSC-A plot, dead cells were excluded using zombie aqua viability marker. The intracellular surface expression of IL-10, IL-4, TNF-α, and IFN-γ was assessed on $CD3^+CD4^+$ cells and $CD3^+CD8^+$ cells. Representative dot plots are shown for IL-10, IL-4, TNF-α, and IFN-γ gated on $CD3^+CD4^+$ cells following 48h culture of PBMCs under normoxia and hypoxia.

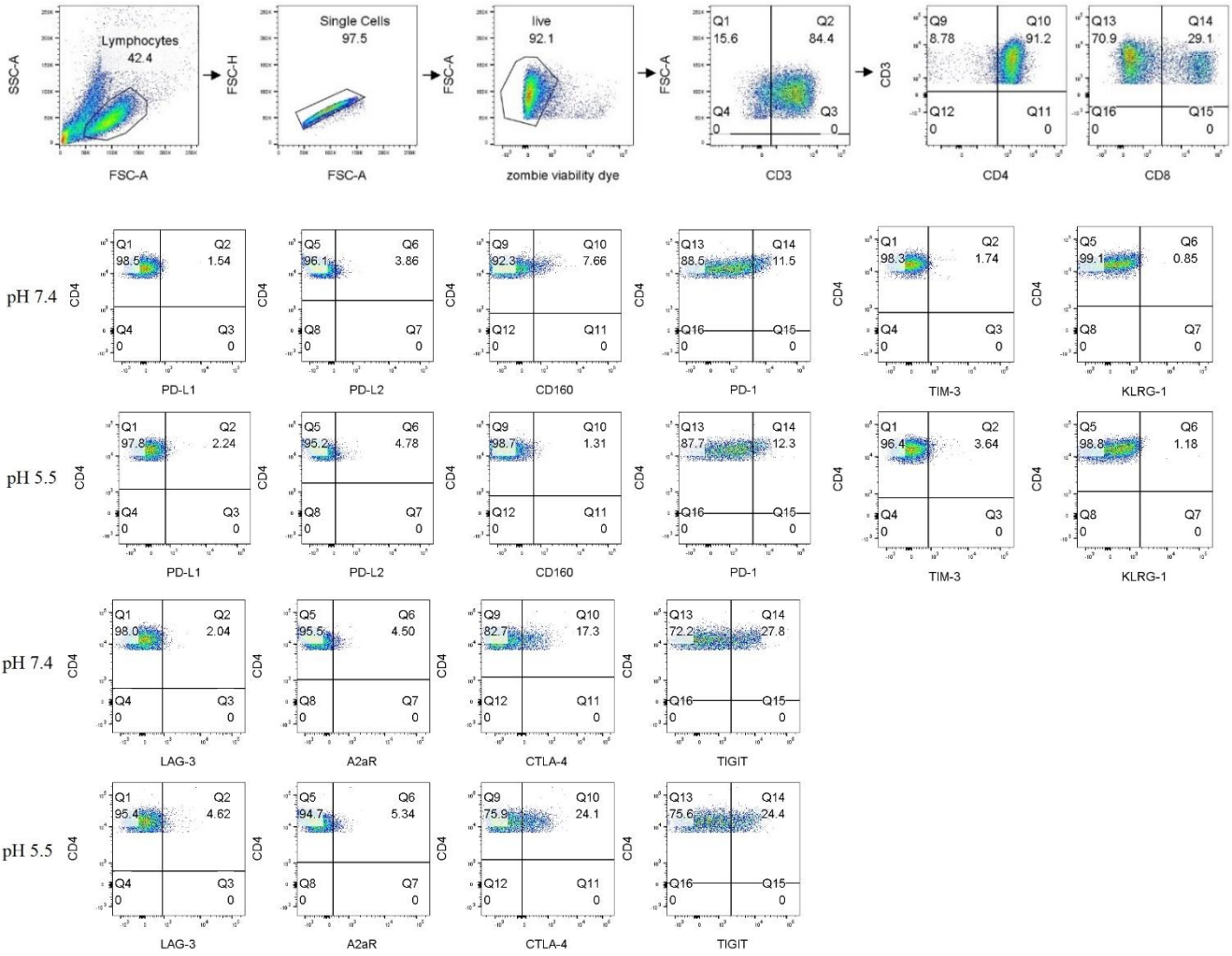

Figure A3.4: Gating strategy for assessing expression of ICs on T cell surfaces under acidic conditions by flow cytometry. Gate 1 included all cells in the FSC versus SSCA plot, doublet cells were then excluded using FSC-H versus FSC-A plot, dead cells were excluded using zombie viability dye. The surface expression of PD-L1, PD-L2, CD160, PD-1, TIM-3, KLRG-1, LAG-3, A2aR, CTLA-4 and TIGIT was assessed on $CD3^+CD4^+$ cells and $CD3^+CD8^+$ cells. Representative dot plots are shown for each gated on $CD3^+CD4^+$ cells following 48h culture of PBMCs in pH 7.4 cRPMI and pH 5.5 cRPMI.

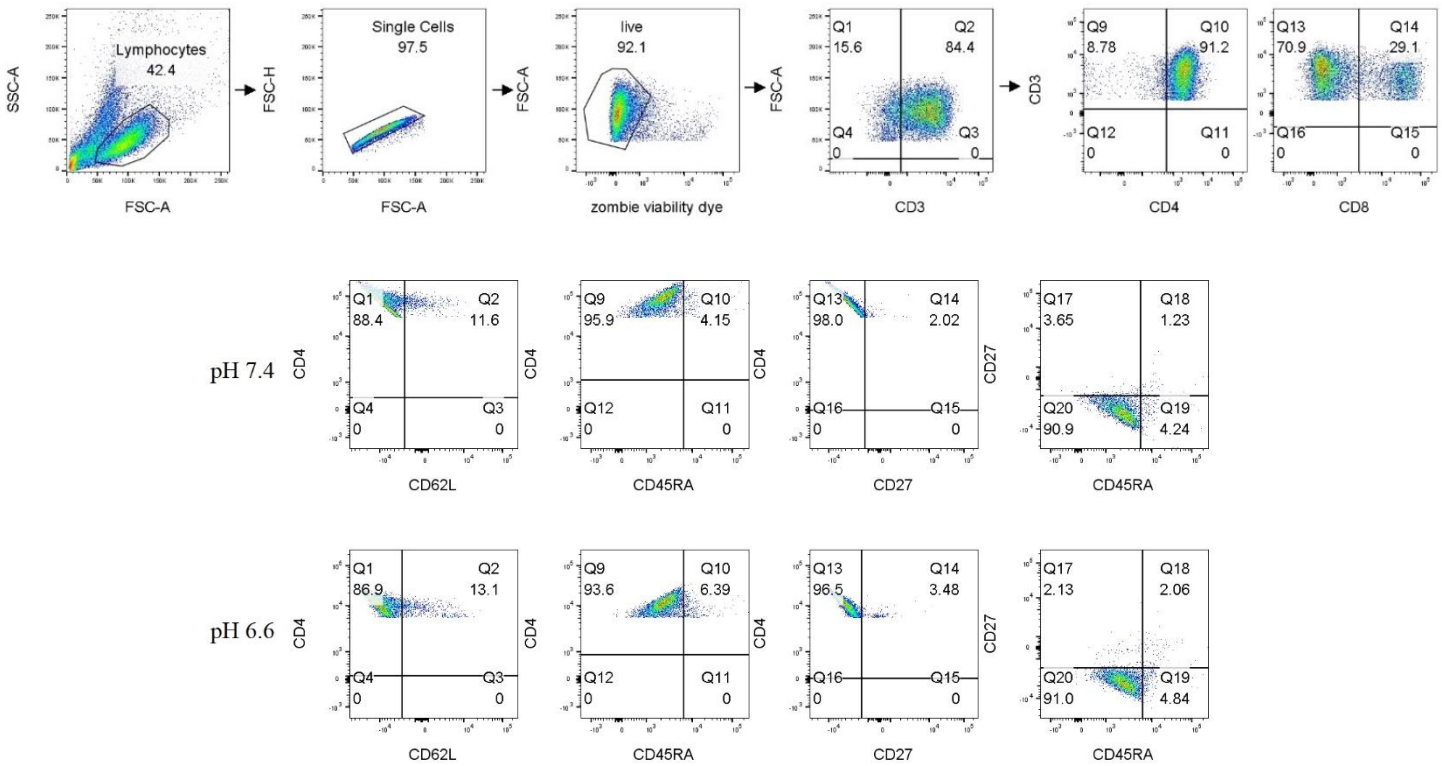

Figure A3.5: Gating strategy and representative dot plots for assessing expression of T cell activation markers and T cell differentiation states under acidic conditions by flow cytometry. Gate 1 included all cells in the FSC versus SSCA plot, doublet cells were then excluded using FSC-H versus FSC-A plot, dead cells were excluded using zombie viability dye. The surface expression of CD62L, CD69, CD45RA and CD27 as well as T cell differentiation states was assessed on $CD3^+CD4^+$ cells and $CD3^+CD8^+$ cells. Representative dot plots are shown for each marker gated on $CD3^+CD4^+$ cells following 48h culture of PBMCs in pH 7.4 cRPMI and pH 5.5 cRPMI. Representative dot plots also shown depicting viable naïve ($CD27^+CD45RA^+$), central memory ($CD27^+CD45RA^-$), effector memory ($CD27^-CD45RA^-$) and terminally differentiated effector memory ($CD27^-CD45RA^+$) $CD3^+CD4^+$ cells.

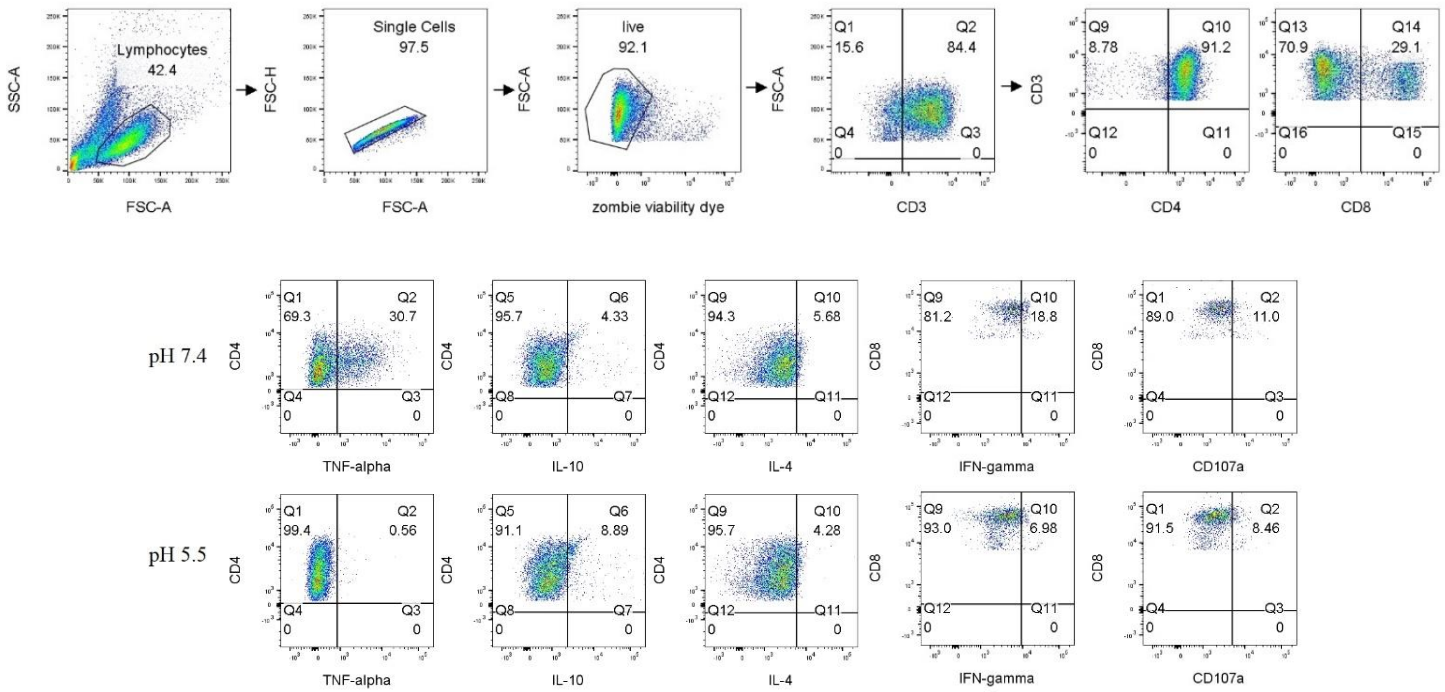

Figure A3.6: Gating strategy and representative dot plots for assessing cytokine production by T cells under acidic conditions by flow cytometry. Gate 1 included all cells in the FSC versus SSCA plot, doublet cells were then excluded using FSC-H versus FSC-A plot, dead cells were excluded using zombie aqua viability marker. The intracellular surface expression of IFN-γ, TNF-α, IL-4 and IL-10 was assessed on $CD3^+CD4^+$ cells and $CD3^+CD8^+$ cells. Representative dot plots are shown for IFN-γ, TNF-α, IL-4 and IL-10 gated on $CD3^+CD4^+$ cells and for CD107a gated on $CD3^+CD8^+$ cells following 48h culture of PBMCs in pH 7.4 cRPMI and pH 5.5 cRPMI.

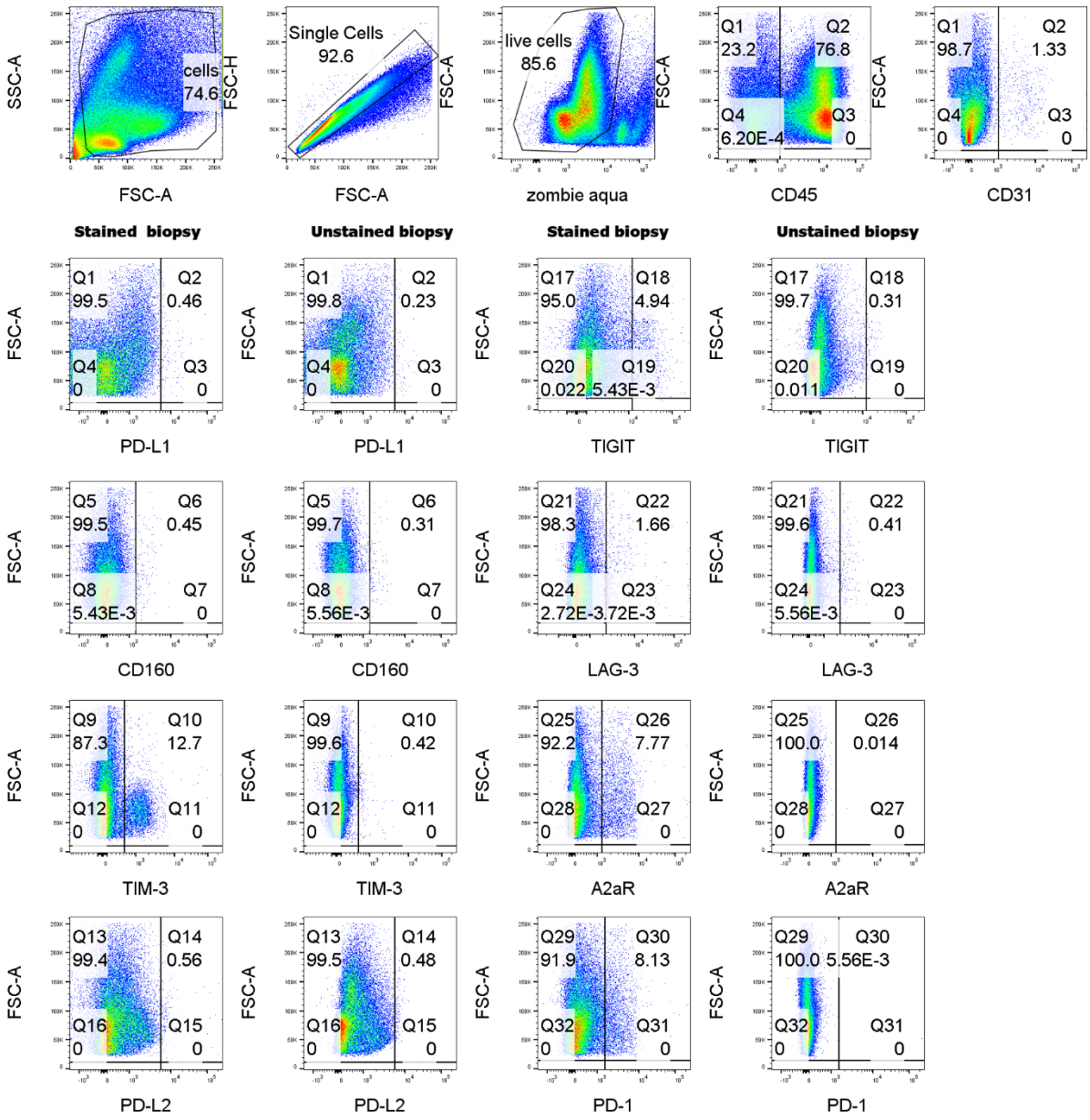

Figure A5.1: Gating strategy for assessing expression of IC ligands and receptors on the surface of OGJ cells in tumour tissue biopsies. Gate 1 included all cells in the FSC versus SSCA plot, doublet cells were then excluded using FSC-H versus FSC-A plot, dead cells were excluded using zombie aqua viability marker, immune cells were excluded using CD45 marker and endothelial cells were then excluded using CD31 marker. The surface expression of inhibitory IC ligands was then assessed on this live, doublet excluded and CD45-CD31- population characterised as OGJ cells as previously reported21. Representative dot plots are shown for stained and unstained digested tumour tissue biopsy sample for PD-L1, PD-L2, CD160, PD-1, TIGIT, TIM-3, LAG-3 and A2aR ICs.

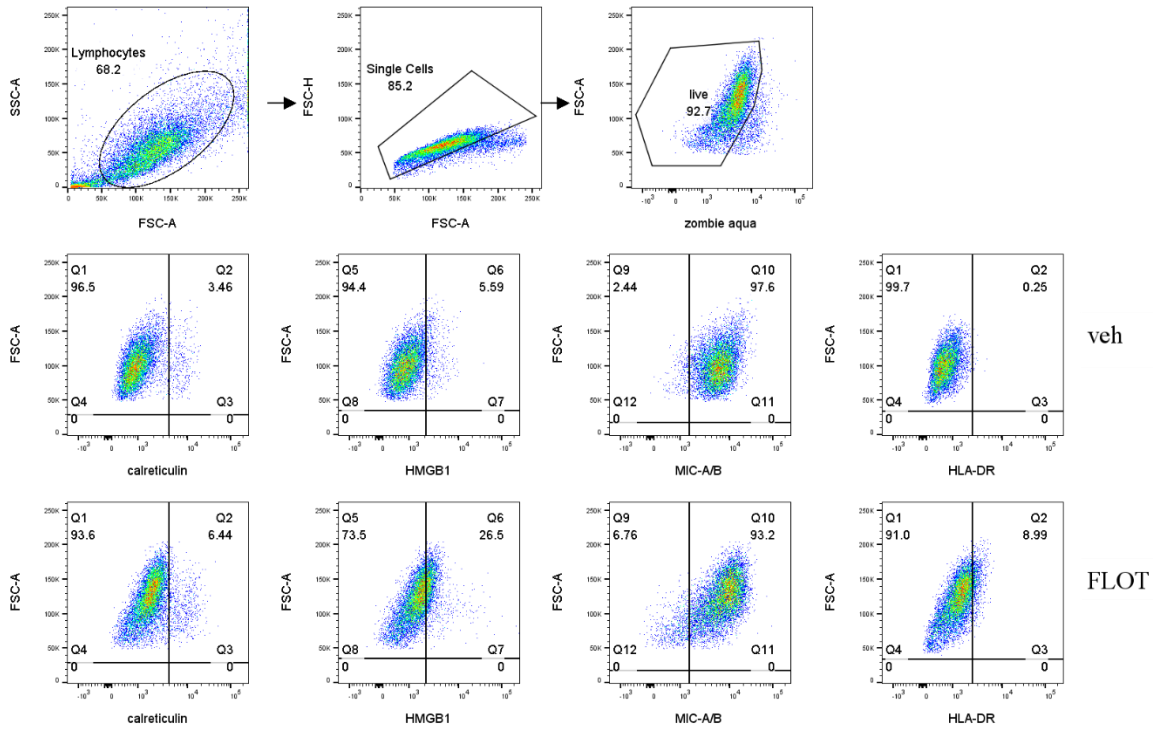

Figure A6.1: Gating strategy for assessing expression of DAMPs on the surface of OGJ cells by flow cytometry. Gate 1 included all cells in the FSC versus SSCA plot, doublet cells were then excluded using FSC-H versus FSC-A plot, dead cells were excluded using zombie aqua viability marker. The surface expression of calreticulin, HMGB1, MIC-A/B and HLA-DR on OGJ cells was then assessed on this live, doublet excluded population. Representative dot plots are shown for veh and FLOT treated OE33 cells *in vitro*.

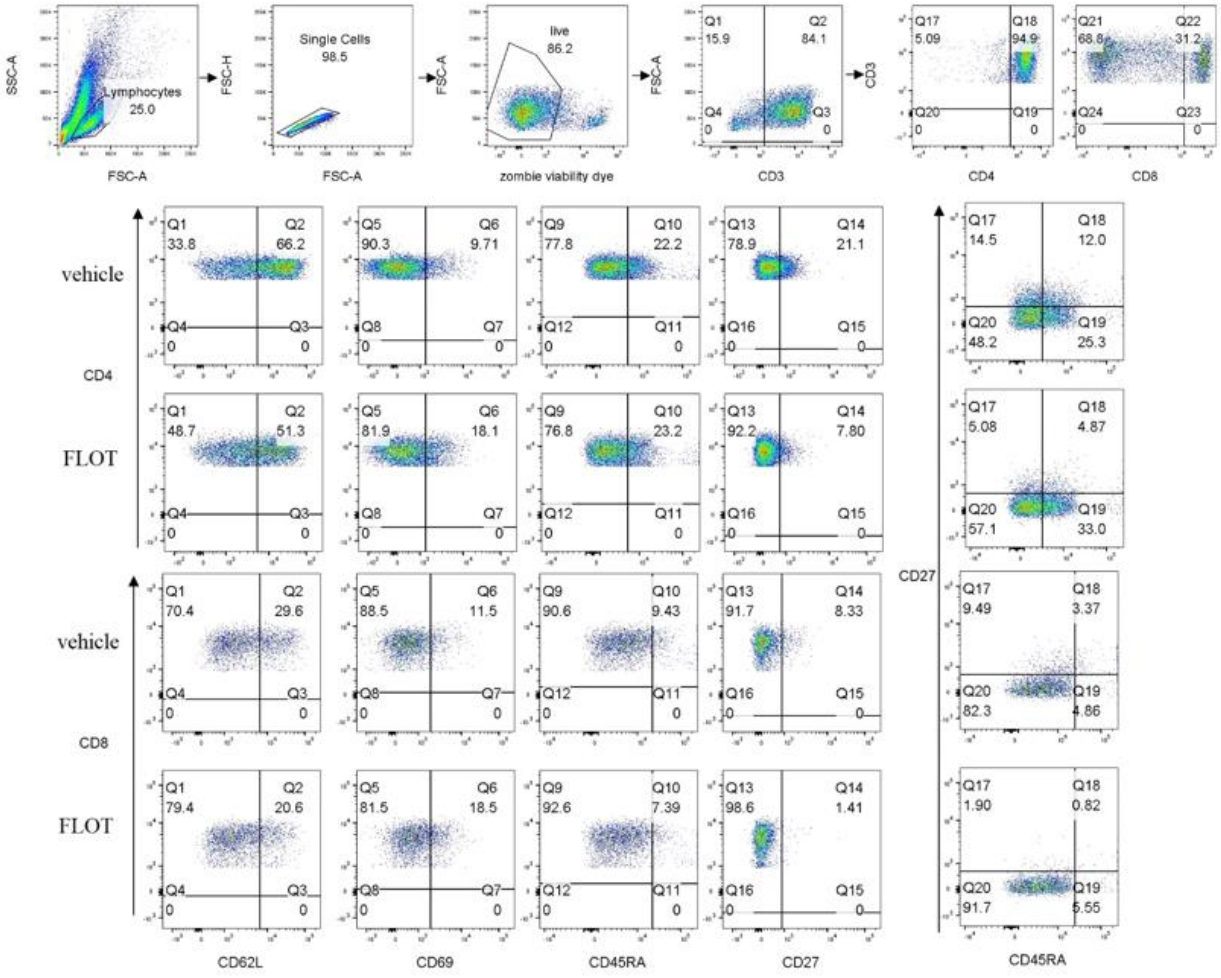

Figure A6.2: Gating strategy for assessing expression of T cell activation markers and T cell differentiation states by flow cytometry. Gate 1 included all cells in the FSC versus SSCA plot, doublet cells were then excluded using FSC-H versus FSC-A plot, dead cells were excluded using zombie viability dye. The surface expression of CD27, CD69 and CD62L as well as T cell differentiation states was assessed on $CD3^+CD4^+$ cells and $CD3^+CD8^+$ cells. Representative dot plots are shown for each marker gated on $CD3^+CD4^+$ cells following treatment with vehicle control or FLOT chemotherapy regimen for 48h. Representative dot plots also shown depicting viable naïve ($CD27^+CD45RA^+$), central memory ($CD27^+CD45RA^-$), effector memory ($CD27^-CD45RA^-$) and terminally differentiated effector memory ($CD27^-CD45RA^+$) $CD3^+CD4^+$ cells.

A

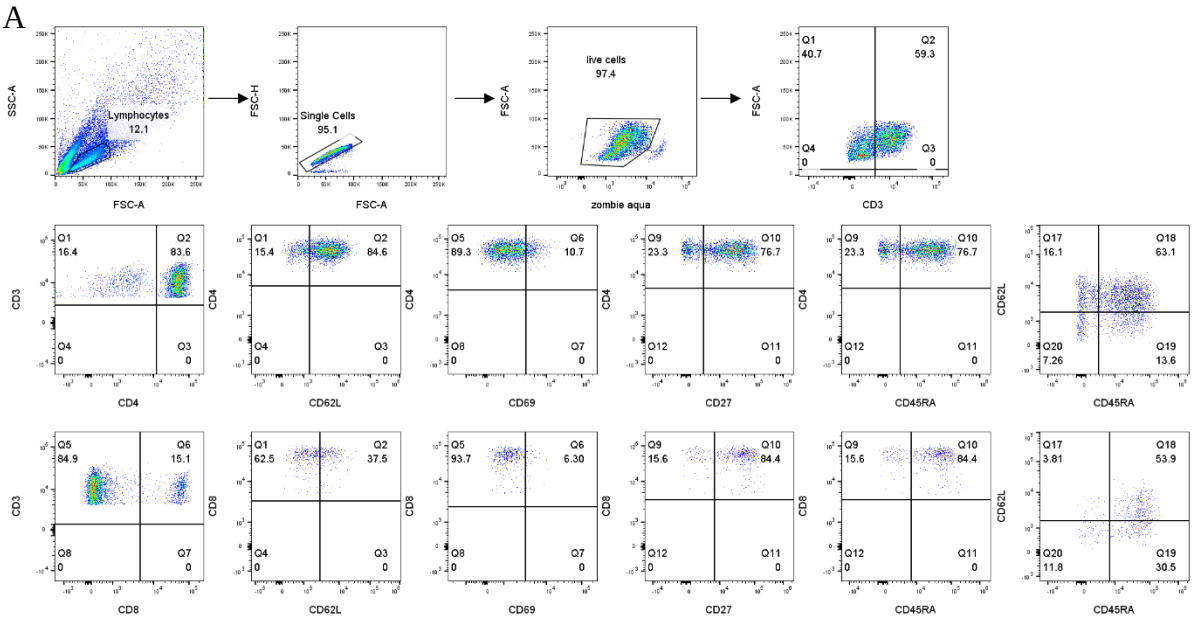

B

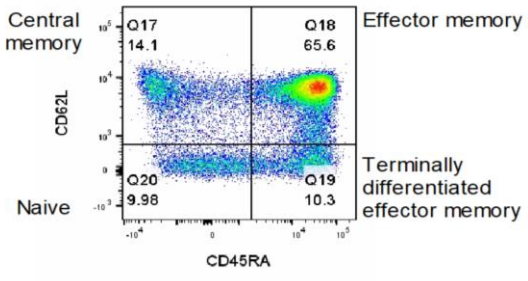

Figure A6.3: Gating strategy for assessing expression of activation markers on T cells surfaces and T cell differentiation states by flow cytometry. Gate 1 included all cells in the FSC versus SSCA plot, doublet cells were then excluded using FSC-H versus FSC-A plot, dead cells were excluded using zombie aqua viability marker. The surface expression of CD62L, CD69, CD27 and CD45RA was assessed on $CD3^{+}CD4^{+}$ cells and $CD3^{+}CD8^{+}$ cells. The percentage of $CD3^{+}CD4^{+}$ cells and $CD3^{+}CD8^{+}$ cells co-expressing $CD45RA^{+}CD62L^{+}$ (naïve T cells), $CD45RA^{-}CD62L^{+}$, (central memory T cells), $CD45RA^{-}CD62L^{-}$ (effector memory T cells) and $CD45RA^{+}CD62L^{-}$ (terminally differentiated effector memory T cells) was also assessed by flow cytometry (A). Representative dot plots are shown for each marker. Representative dot plot showing the characterisation of naïve, central memory, effector memory and terminally differentiated T cells following treatment with TCM (B).

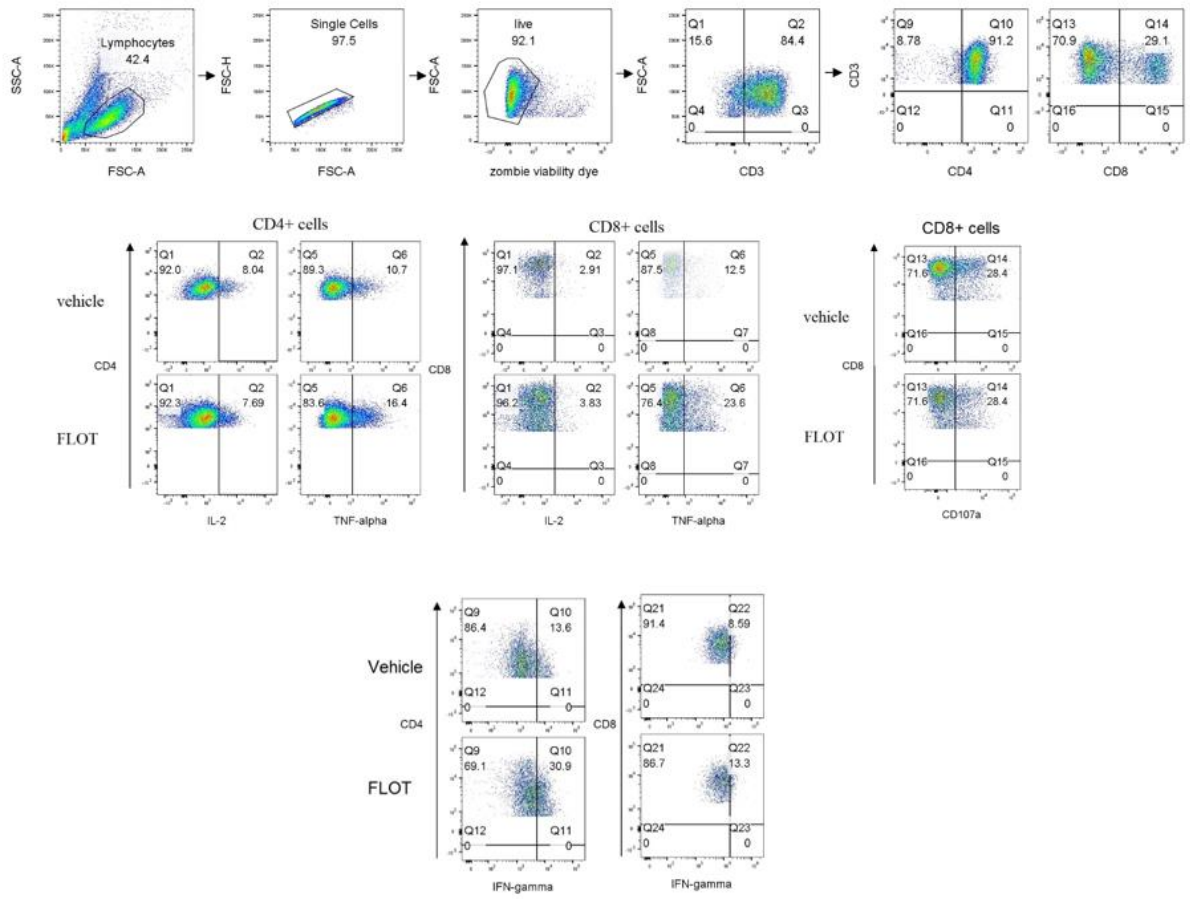

Figure A6.4: Gating strategy for assessing direct effects of FLOT and CROSS CT on cytokine production by T cells by flow cytometry. Gate 1 included all cells in the FSC versus SSCA plot, doublet cells were then excluded using FSC-H versus FSC-A plot, dead cells were excluded using zombie aqua viability marker. The intracellular surface expression of IFN-γ, TNF-α and IL-2 was assessed on $CD3^+CD4^+$ cells and $CD3^+CD8^+$ cells. Representative dot plots are shown for IL-2, TNF-α and IFN-γ gated on $CD4^+$ cells and $CD8^+$ cells for and CD107a gated on $CD3^+CD8^+$ cells following treatment with vehicle control or FLOT chemotherapy regimen for 48h.

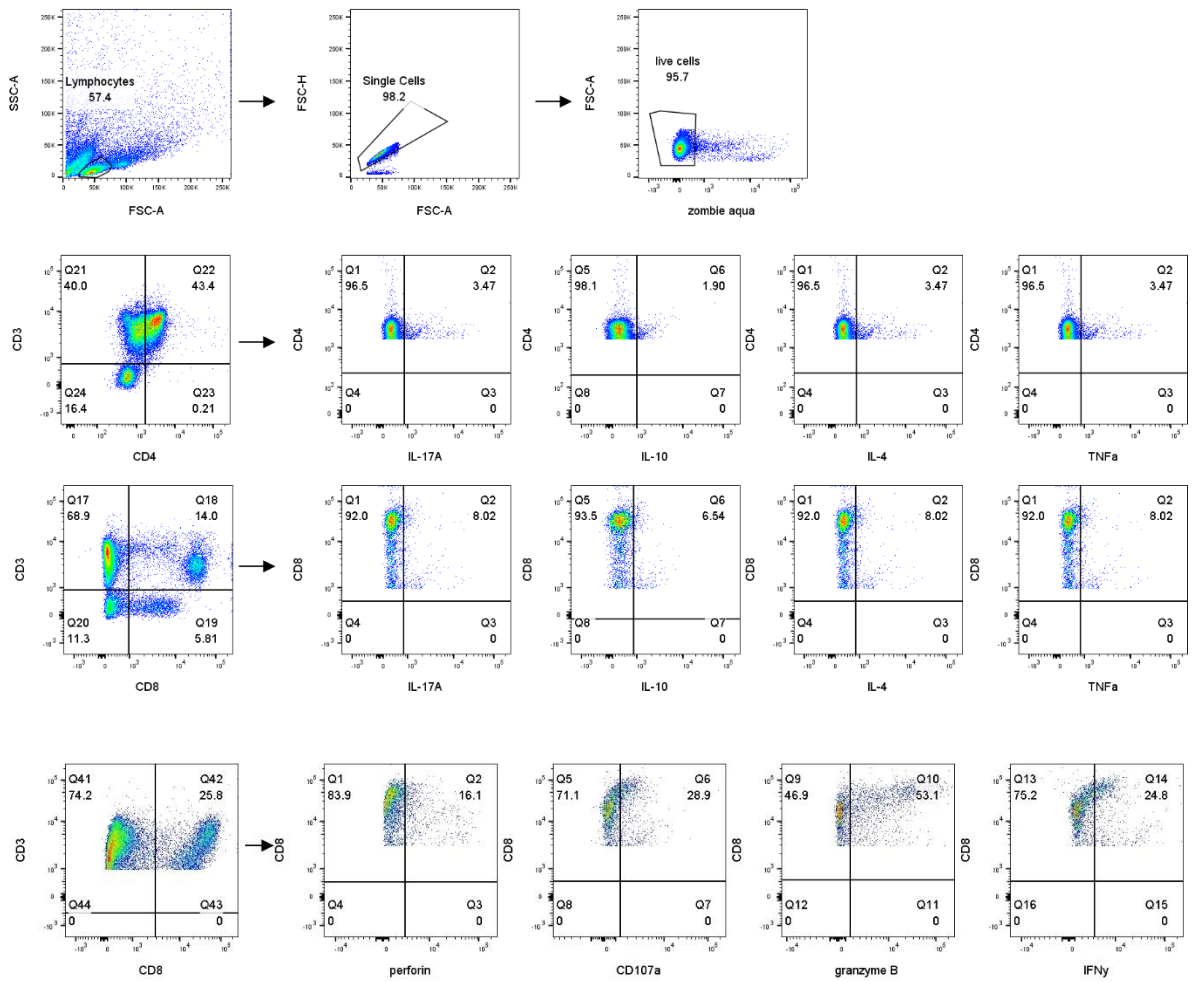

Figure A6.5: Gating strategy for assessing effect of conditioned media from post-FLOT and post-CROSS CT tumour cell conditioned media on cytokine production by T cells by flow cytometry. Gate 1 included all cells in the FSC versus SSCA plot, doublet cells were then excluded using FSC-H versus FSC-A plot, dead cells were excluded using zombie aqua viability marker. The intracellular surface expression of IL-17A, IL-10, IL-4 and TNF-α was assessed in $CD3^+CD4^+$ cells and $CD3^+CD8^+$ cells. Intracellular perforin expression, extracellular CD107a expression and intracellular granzyme B and IFN-γ was assessed on $CD3^+CD8^+$ cells by flow cytometry. Representative dot plots are shown for each marker.

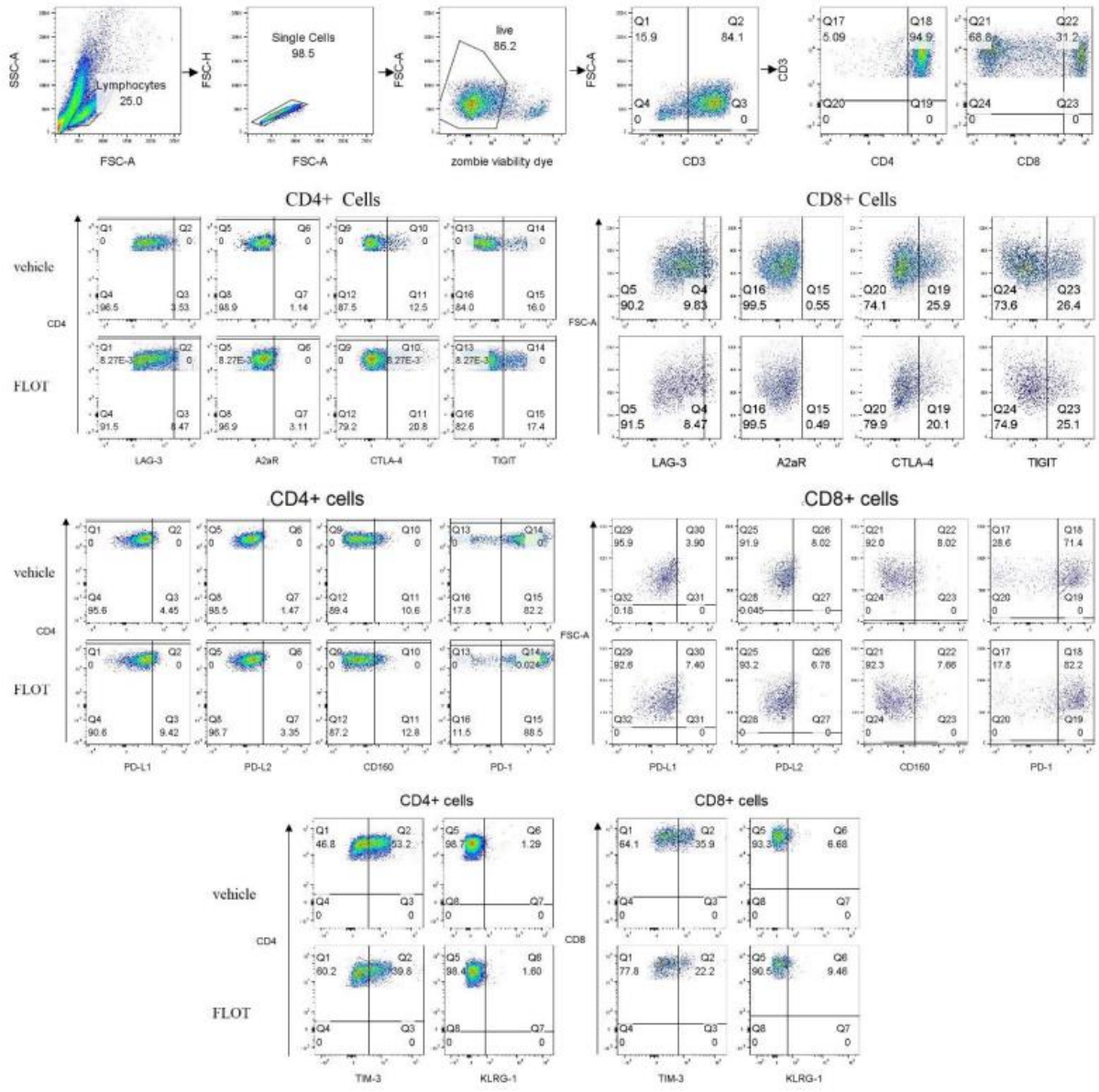

Figure A6.6: Gating strategy for assessing direct effects of FLOT and CROSS CT on the expression of ICs on T cells surfaces by flow cytometry. Gate 1 included all cells in the FSC versus SSCA plot, doublet cells were then excluded using FSC-H versus FSC-A plot, dead cells were excluded using zombie viability dye. The surface expression of PD-L1, PD-L2, CD160, PD-1, TIM-3, LAG-3, A2aR, CTLA-4 and TIGIT was assessed on $CD3^+CD4^+$ cells and $CD3^+CD8^+$ cells. Representative dot plots are shown for each IC gated on $CD4^+$ cells and $CD3^+$ cells following treatment with vehicle control or FLOT chemotherapy regimen for 48h.